



University of Sussex

A University of Sussex DPhil thesis

Available online via Sussex Research Online:

<http://sro.sussex.ac.uk/>

This thesis is protected by copyright which belongs to the author.

This thesis cannot be reproduced or quoted extensively from without first obtaining permission in writing from the Author

The content must not be changed in any way or sold commercially in any format or medium without the formal permission of the Author

When referring to this work, full bibliographic details including the author, title, awarding institution and date of the thesis must be given

Please visit Sussex Research Online for more information and further details

University of Sussex

Synthesis and reactions of β -diketiminato heavy group 14 metal
alkoxides and phosphanides

Eric Chi Yan Tam

Submitted in accordance with the requirements for the degree of
Doctor of Philosophy (PhD)

School of Life Sciences
Department of Chemistry
September 2012

*This thesis is dedicated to my mother and father,
for their love, patience and support
and
in loving memory of my beloved grandmother*

I hereby declare that this thesis has not been and will not be, submitted in whole or in part to another University for the award of any other degree.

Eric. C.Y. Tam

UNIVERSITY OF SUSSEX

ERIC CHI YAN TAM

SUBMITTED FOR THE DEGREE OF DOCTOR OF PHILOSOPHY (PhD)

SYNTHESIS AND REACTIONS OF β -DIKETIMINATO HEAVY GROUP 14
METAL ALKOXIDES AND PHOSPHANIDESSUMMARY

Some low-valent, three-coordinated β -diketiminato heavy group 14 metal complexes have been synthesised and their reactions examined. Initially, our attention is focused on several β -diketiminatolead(II) alkoxides. The lead(II) alkoxides show different basic and nucleophilic reactivities from transition metal analogues. For example, the reaction between the lead(II) *tert*-butoxide and methyl iodide proceeds only under forcing conditions to give the lead(II) iodide and methyl *tert*-butyl ether. However, facile reversible carbon dioxide insertion into the lead-oxygen bond is observed.

To investigate the steric effect of the bulky β -diketiminato ligand, compounds with various aromatic groups attached to nitrogen have been made. When either $[(\text{BDI}_{\text{Ph}})\text{PbCl}]$ ($\text{BDI}_{\text{Ph}} = [\text{HC}\{\text{C}(\text{Me})\text{N}(\text{C}_6\text{H}_5)\}_2]^-$) or $[(\text{BDI}_{\text{IPP}})\text{PbCl}]$ ($\text{BDI}_{\text{IPP}} = [\text{HC}\{\text{C}(\text{Me})\text{N}(4\text{-}^i\text{PrC}_6\text{H}_4)\}_2]^-$) was treated with potassium *tert*-butoxide, the reactions gave the unexpected bis[β -diketiminato]lead(II) complexes. However, treatment of $[(\text{BDI}_{\text{DMP}})\text{PbCl}]$ ($\text{BDI}_{\text{DMP}} = [\text{HC}\{\text{C}(\text{Me})\text{N}(2,6\text{-Me}_2\text{C}_6\text{H}_3)\}_2]^-$) with AgOTf led to the expected β -diketiminatolead(II) triflate. These results suggest that the *ortho*-substituent on the *N*-aryl groups in the β -diketiminato ligand plays an important role in influencing the formation of bis[β -diketiminato]lead(II) complexes.

A series of β -diketiminato heavy group 14 metal phosphanides was synthesised. The phosphorus is pyramidally coordinated in the compounds containing diphenyl- or dicyclohexylphosphanido ligands. In contrast, the geometry at phosphorus is planar in the germanium(II) and tin(II) bis(trimethylsilyl)phosphanides. The phosphorus in the lead(II) bis(trimethylsilyl)phosphanide is pyramidally coordinated. The observed conformations may be explained by the steric congestion from the β -diketiminato ligand

III

and electronic effects in the phosphanido ligand. Reactions of the phosphanido complexes with one equivalent of elemental chalcogen give phosphinochalcogenoito complexes. Further reaction with elemental chalcogen gives phosphinodichalcogenoato complexes. In contrast, treatment of the germanium(II) dicyclohexylphosphanide with elemental chalcogen leads to the formation of germanium(IV) chalcogenide. The presence of NMR-active nuclei in these complexes makes possible detailed spectroscopic analysis.

Acknowledgements

Over the past four years leading to this work, I can say, without regret, that it has been a lifetime experience. However, this journey would not be going as smoothly without the people who are around to offer their assistance and support.

First of all, I would like to say a very special thank you to my supervisor, Dr. J. Robin Fulton, who gave me guidance and support throughout my research. It is not only her input and numerous simulating discussions on the research, which drive success in our investigations, but also her understandings and advises in helping me to develop personal skills in the research environments. More importantly, her trusts and believes in giving me an opportunity to pursue a doctorate degree in chemistry. For that, I am truly appreciated.

I would also like to say a sincerely thank you to our collaborators, Dr. Martyn P. Coles and Dr. J. David Smith, for the stimulating discussions on the phosphanide project. Furthermore, I would like to thank David for his helpful comments on the thesis. I would also like to express my appreciation to Dr. John Spencer and Prof. Malcolm Heggie for their help with the PhD program.

X-ray crystallography and various spectroscopic analysis had played crucial roles in my research. I would like to thank Dr. Martyn P. Coles and Dr. Peter B. Hitchcock for X-ray crystallography, Dr. Iain J. Day for NMR spectroscopy and Dr. Alaa Abdul-Sada for mass spectroscopy, for their help and input into the research. I would also like to express my gratitude to Dr. David Apperley and EPSRC National Solid-state NMR Research Service to provide solid-state NMR spectroscopic analysis.

To all of my colleagues in the Fulton group, in especially Lisa Harris, Dr. Morgan J. Taylor, Dr. Lorenzo Ferro and Dr. Nick C. Johnstone, it has been a fabulous experience to work as a team with you all. For all the fun, research discussions and of course our Friday Swan sessions, it will always be in my mind. Thank you very much all!

I would like to express my appreciation to the University of Sussex Graduate Teaching Assistance (GTA) for my funding during my doctorate study.

Last but not least, I would also like to express my deepest gratitude to Grecia García García for your support, your encouragement and your time throughout the past years. I would like to say thank you to Rosa Martha Jiménez Barrera for letting me to know you. Finally, I would like to say a big thank you to my sister, Elsa W. T. Tam (FCCA), Jason C. S. Lam, Dodo Wong, Simon S.W. Lai, Serena M. T. Poon (LLB.), and Dr. Wesley T.K. Chan for all of your supports and listening through some difficult time during my doctorate study. And of course to all those who I have not mentioned, you will never be forgotten.

Brighton would not be the same for me without any of you.

Table of Contents

Declaration.....	I
Summary	II
Acknowledgments.....	IV
Contents	VI
Abbreviations	XI
Nomenclature	XIV
List of compounds.....	XVI
List of Figures	XVIII
List of Schemes	XXVI
List of Tables	XXIX
Synthesis and reactions of β-diketiminato heavy group 14 metal alkoxides and phosphanides	1
1. Introduction.....	2
1.1 History. Environmental and health implications of lead chemistry	2
1.2 Low-valent heavy group 14 metal complexes.....	2
1.3 β-Diketiminato (BDI) ligands	6
1.4 Examples of β-diketiminatometal complexes. Applications and reactions	11
1.5 β-Diketiminato heavy group 14 metal complexes.....	17
2. Lead(II) alkoxide complexes and their reactivities	23
2.1 Chapter remarks.....	23
2.2 Introduction	26
2.2.1 Lead(II)-induced hydrolysis of RNA	26
2.2.2 Transition metal hydroxide, alkoxide and aryloxide complexes	28
2.2.3 Heavy group 14 metal alkoxide complexes.....	32
2.2.4 β -Diketiminatometal alkoxides and aryloxides	35
2.2.5 β -Diketiminato heavy group 14 metal alkoxides and aryloxides	37

2.3 Results and discussion	42
2.3.1 Synthesis of β -diketiminatolead(II) alkoxides	42
2.3.2 Reactivity of β -diketiminatolead(II) alkoxides	46
2.3.2.1 Basicity	46
2.3.2.2 Nucleophilicity	47
2.3.2.3 Reaction with an unsaturated electrophile	48
2.3.2.4 Ligand coordination	52
2.3.2.5 Reactions with CO ₂	53
2.3.2.6 Reactions with other heterocumulenes	57
2.3.3 Mechanism of CO ₂ insertion into the lead(II) alkoxides 3 and 4	58
2.4 Conclusions	60
3. Structure and characteristics of lead(II) complexes with various β-diketiminato ligands	61
3.1 Introduction	61
3.1.1 Metal complexes with less bulky β -diketiminato ligands than BDI _{DIPP}	61
3.1.2 Four-coordinate lead(II) complexes	66
3.1.3 Other bis(β -diketiminato)metal complexes	68
3.2 Results and discussion	72
3.2.1 Synthesis of β -diketiminates 19–21	72
3.2.2 Synthesis of β -diketiminatolead(II) chlorides 22–24	72
3.2.3 Reactions of the β -diketiminatolead(II) chlorides 22–24	80
3.2.4 Reactions of the bis[β -diketiminato]lead(II) complexes 25 and 26	95
3.3 Conclusions	100
4. β-Diketiminato heavy group 14 metal phosphanides and their reactions with elemental chalcogens	101
4.1 Introduction	101
4.1.1 Overview of metal phosphanido complexes	101
4.1.2 Nature of the M–P bond in metal phosphanido complexes	107
4.1.3 Previous examples of β -diketiminato heavy group 14 metal phosphanides	111

VIII

4.1.4	Complexes containing heavy group 14 metal-phosphorus multiple bond.....	113
4.1.5	Heavy group 14 metal phosphanido complexes	115
4.1.6	Reactions of heavy group 14 metal complexes with elemental chalcogens	118
4.1.7	Reactions of metal phosphanido complexes and related compounds with elemental chalcogens.....	121
4.2	Results and discussion	129
4.2.1	Synthesis of β -diketiminato heavy group 14 metal diphenylphosphanides 33–35	129
4.2.2	X-ray crystal structures of the β -diketiminato heavy group 14 metal diphenylphosphanides 33–35	133
4.2.3	NMR spectra of the β -diketiminato heavy group 14 metal diphenylphosphanides 33–35	139
4.2.3.1	The β -diketiminatogermanium(II) diphenylphosphanide 33	140
4.2.3.2	The β -diketiminatotin(II) diphenylphosphanide 34	143
4.2.3.3	The β -diketiminatolead(II) diphenylphosphanide 35	145
4.2.4	Synthesis of β -diketiminato heavy group 14 metal dicyclohexylphosphanides 36–38	147
4.2.5	X-ray crystal structures of the β -diketiminato heavy group 14 metal dicyclohexylphosphanides 36–38	147
4.2.6	NMR spectra of the β -diketiminato heavy group 14 metal dicyclohexylphosphanides 36–38	154
4.2.6.1	The β -diketiminatogermanium(II) dicyclohexylphosphanide 36	155
4.2.6.2	The β -diketiminatotin(II) dicyclohexylphosphanide 37	156
4.2.6.3	The β -diketiminatolead(II) dicyclohexylphosphanide 38	160
4.2.7	Synthesis of β -diketiminato heavy group 14 metal bis(trimethylsilyl)phosphanides 40–42	163
4.2.8	X-ray crystal structures of the β -diketiminato heavy group 14 metal bis(trimethylsilyl)phosphanides 40–42	164
4.2.9	NMR spectra of the β -diketiminato heavy group 14 metal bis(trimethylsilyl)phosphanides 40–42	169
4.2.9.1	The β -diketiminatogermanium(II) bis(trimethylsilyl)phosphanide 40	170
4.2.9.2	The β -diketiminatotin(II) bis(trimethylsilyl)phosphanide 41	173
4.2.9.3	The β -diketiminatolead(II) bis(trimethylsilyl)phosphanide 42	182

4.2.10 Synthesis of the lead(II) bis(trimethylsilyl)phosphanides containing other β -diketiminato ligands.....	188
4.3 Summary	192
4.4 Reactions of the β-diketiminato heavy group 14 metal phosphanides with elemental chalcogens.....	196
4.4.1 Reactions of the β -diketiminato heavy group 14 metal dicyclohexylphosphanides 36–38 with elemental selenium.....	196
4.4.2 Synthesis of β -diketiminatotin(II) and -lead(II) dicyclohexylphosphinoselenoite 46 and 47	197
4.4.3 X-ray crystal structures of [(BDI _{DIPP})MSePCy ₂] (46 , M = Sn and 47 , M = Pb).....	199
4.4.4 NMR spectra of [(BDI _{DIPP})MSePCy ₂] (46 , M = Sn and 47 , M = Pb).....	205
4.4.4.1 The β -diketiminatotin(II) dicyclohexylphosphinoselenoite 46	205
4.4.4.2 The β -diketiminatolead(II) dicyclohexylphosphinoselenoite 47	209
4.4.5 Synthesis of β -diketiminato heavy group 14 metal dicyclohexylphosphinodiselenoates 48–50	209
4.4.6 X-ray crystal structures of [(BDI _{DIPP})MSeP(Se)Cy ₂] (48 , M = Ge; 49 , M = Sn; and 50 , M = Pb)	210
4.4.7 NMR spectra of [(BDI _{DIPP})MSeP(Se)Cy ₂] (48 , M = Ge; 49 , M = Sn; and 50 , M = Pb)	218
4.4.7.1 The β -diketiminatogermanium(II) dicyclohexylphosphinodiselenoate 48	219
4.4.7.2 The β -diketiminatotin(II) dicyclohexylphosphinodiselenoate 49	221
4.4.7.3 The β -diketiminatolead(II) dicyclohexylphosphinodiselenoate 50	226
4.4.8 Synthesis of β -diketiminatogermanium(IV) selenide (51)	227
4.4.9 X-ray crystal structure of [(BDI _{DIPP})Ge(Se)PCy ₂] (51)	228
4.4.10 NMR spectra of [(BDI _{DIPP})Ge(Se)PCy ₂] (51)	231
4.4.11 Synthesis of β -diketiminato heavy group 14 metal dicyclohexylphosphinodithioates 52–53	232
4.4.12 X-ray crystal structures of [(BDI _{DIPP})MSP(S)Cy ₂] (52 , M = Sn; and 53 , M = Pb) ..	233
4.4.13 NMR spectra of [(BDI _{DIPP})MSP(S)Cy ₂] (52 , M = Sn; and 53 , M = Pb).....	240
4.4.13.1 The β -diketiminatotin(II) dicyclohexylphosphinodithioate 52	240
4.4.13.2 The β -diketiminatolead(II) dicyclohexylphosphinodithioate 53	241

4.4.14	Synthesis of β -diketiminatogermanium(IV) sulfide 54	241
4.4.15	X-ray crystal structure of [(BDI _{DIPP})Ge(S)PCy ₂] (54)	242
4.4.16	NMR spectra of [(BDI _{DIPP})Ge(S)PCy ₂] (54)	245
4.4.17	Synthesis of [(BDI _{DIPP})SnSeP(S)Cy ₂] (55).....	246
4.4.18	Reactions of the β -diketiminato heavy group 14 metal bis(trimethylsilyl)phosphanides with elemental selenium.....	248
4.4.19	X-ray crystal structure of [(BDI _{DIPP})Ge(Se)P(SiMe ₃) ₂] (56).....	249
4.4.20	NMR spectra of [(BDI _{DIPP})Ge(Se)P(SiMe ₃) ₂] (56)	253
4.4.21	Synthesis of β -diketiminatotin(II) trimethylsilylselenide (57)	253
4.4.22	X-ray crystal structure of [(BDI _{DIPP})SnSeSiMe ₃] (57).....	254
4.4.23	NMR spectra of [(BDI _{DIPP})SnSeSiMe ₃] (57).....	257
4.5	Conclusions	258
5.	Experimental	260
5.1	General methods and procedures.....	260
5.2	Experimental procedures for Chapter 2	261
5.3	Experimental procedures for Chapter 3	269
5.4	Experimental procedures for Chapter 4	275
6.	References	293
Appendix 1.	Publications	310
Appendix 2.	X-ray crystal structure of [(BDI _{DIPP})Sn ⁿ Bu] (39).....	333
Appendix 3.	Synthesis of β -diketiminatolead(II) triflate 58	336
Appendix 4.	Calculations of the free energy of activation from variable-temperature NMR spectroscopic studies	341
Appendix 5.	X-ray crystallographic data	346
Appendix 6.	References for appendices.....	537

Abbreviations

(br)	Broad signal
(m)	Multiplet
(s)	Sharp signal
°	Degree(s)
°C	Degree Celsius
Å	Angstrom
abs coeff	Absorption coefficient
Ac	Acetate
Anal. Calcd.	Analytical calculated
Ar	Aryl
avg.	Average
BDI	β-Diketiminato
bipy	2,2'-Bipyridine
C ₆ D ₆	Deuterated benzene
CCl ₄	Carbon tetrachloride
CDCl ₃	Deuterated chloroform
CO ₂	Carbon dioxide
Conc.	Concentrated
Cp	Cyclopentadienyl
CS ₂	Carbon disulfide
Cy	Cyclohexyl
d	Doublet
d-septet	Doublet of septets
D.I.	Deionised
D ₂ O	Deuterated water
DCM	Dichloromethane
dd	Doublet of doublets
decomp.	Decomposition
deg	Degree(s)
DEPT	Distortionless enhancement by polarization transfer
DFT	Density functional theory
DIPP	2,6-Diisopropylphenyl
dL	Decilitre
DME	1,2-Dimethoxyethane
DMP	2,6-Dimethylphenyl
DMSO	Dimethyl sulfoxide
DOP	Degree of pyramidalisation
ECYT	Eric. C.Y. Tam

XII

EI-MS	Electron impact mass spectrometry
eq	Number of molar equivalents
Et	Ethyl
ex.	Excess
EXSY	Two dimensional exchange spectroscopy
g	Gram(s)
h	Hour(s)
HCl	Hydrochloric acid
HMBC	Heteronuclear multiple-bond correlation spectroscopy
HSQC	Heteronuclear single-quantum correlation spectroscopy
Hz	Hertz
IPP	4-Isopropylphenyl
ⁱ Pr	Isopropyl
indep reflns	Independent reflections
IR	Infrared spectroscopy
<i>J</i>	Coupling constant
K	Kelvin
kJ mol^{-1}	Kilojoule per mole
LF	Dr. Lorenzo Ferro
lit.	Literature
M	Molar
<i>m</i> -	Meta-
M.p.	Melting Point
<i>m/z</i>	Mass-to-charge ratio
Me	Methyl
measd	Measured
MeOH	Methanol
mg	Milligram(s)
MHz	Megahertz
min	Minute(s)
mL	Millilitre(s)
mmol	Millimole(s)
mol	Mole(s)
mol%	Mole percentage
MS	Mass spectroscopy
<i>n</i> -BuLi	<i>n</i> -Butyllithium
NBO	Natural bond orbital
ⁿ Bu	<i>n</i> -Butyl
NCJ	Dr. Nicholas C. Johnstone
nm	Nanometre(s)

XIII

NMR	Nuclear magnetic resonance
No.	Number(s)
<i>o</i> -	Ortho-
Obs.	Observed
ORTEP	Oak Ridge thermal-ellipsoid plot program
<i>p</i> -	Para-
param	Parameters
Pg.	Page
Ph	Phenyl
phen	1,10-Phenanthroline
ppm	Parts per million
py	Pyridine
q	Quartet
reflns	Reflections
RNA	Ribonucleic acid
RT	Room temperature (usually at 25 °C)
s	Singlet
t	Triplet
^t Bu	Tertiary butyl
Tf	Trifluoromethanesulfonyl
THF	Tetrahydrofuran
THF- <i>d</i> ₈	Deuterated tetrahydrofuran
TMEDA	Tetramethylethylenediamine
TMS	Trimethylsilyl
tol	Toluene
Tol- <i>d</i> ₈	Deuterated toluene
UV/Vis	Ultraviolet-visible spectroscopy
ν	Wavenumbers (in cm ⁻¹)
VT	Variable temperature
δ	Chemical shift in ppm from specified standard
Δ	Differences
ϵ	Extinction coefficient
λ	Wavelength
λ_{max}	Wavelength of maximum absorption
μL	Microlitre
$\Sigma_{\text{bond angle}}$	Sum of bond angles

Nomenclature

In this thesis, most of the compounds are supported by a bulky β -diketiminato ligand. A series of β -diketiminato heavy group 14 metal complexes containing various substituents were synthesised. Since there are several ways of naming these compounds, the nomenclature used in this thesis is set out as below in Table i.^[1]

Table i. Nomenclature of the compounds synthesised in this thesis, where L = (BDI), M = Ge, Sn or Pb

Structure	Nomenclature	Abbreviated name
[LMCl]	β -diketiminatometal(II) chloride	metal(II) chloride
[LMBr]	β -diketiminatometal(II) bromide	metal(II) bromide
[LMI]	β -diketiminatometal(II) iodide	metal(II) iodide
[LMO ⁱ Pr]	β -diketiminatometal(II) isopropoxide	metal(II) isopropoxide
[LMO ^t Bu]	β -diketiminatometal(II) <i>tert</i> -butoxide	metal(II) <i>tert</i> -butoxide
[LMOC ₆ H ₃ ^t Bu _{2-2,4}]	β -diketiminatometal(II) 2,4- <i>tert</i> -butylaryloxide	metal(II) aryloxide
[LMOCO ₂ ⁱ Pr]	β -diketiminatometal(II) isopropoxycarbonate	metal(II) isopropoxycarbonate
[LMOCO ₂ ^t Bu]	β -diketiminatometal(II) <i>tert</i> -butoxycarbonate	metal(II) <i>tert</i> -butoxycarbonate
[LMN(Ph)CO ₂ ⁱ Pr]	β -diketiminatometal(II) carbamate	metal(II) carbamate
[LMOTf]	β -diketiminatometal(II) triflate	metal(II) triflate
[LML]	bis[β -diketiminato]metal(II)	bis[β -diketiminato]metal(II)
[LMPPh ₂]	β -diketiminatometal(II) diphenylphosphanide	metal(II) diphenylphosphanide
[LMPCy ₂]	β -diketiminatometal(II) dicyclohexylphosphanide	metal(II) dicyclohexylphosphanide
[LM ⁿ Bu]	<i>n</i> -Butyl(β -diketiminato)metal(II)	metal(II) alkyl
[LMP(SiMe ₃) ₂]	β -diketiminatometal(II) bis(trimethylsilyl)phosphanide	metal(II) bis(trimethylsilyl)phosphanide
[LMSePCy ₂]	β -diketiminatometal(II) dicyclohexylphosphinoselenoite	metal(II) dicyclohexylphosphinoselenoite
[LMSeP(Se)Cy ₂]	β -diketiminatometal(II) dicyclohexylphosphinodiselenoate	metal(II) dicyclohexylphosphinodiselenoate
[LM(Se)PCy ₂]	β -diketiminatometal(IV) selenide	metal(IV) selenide
[LMSP(S)Cy ₂]	β -diketiminatometal(II) dicyclohexylphosphinodithioate	metal(II) dicyclohexylphosphinodithioate
[LM(S)PCy ₂]	β -diketiminatometal(IV) sulfide	metal(IV) sulfide

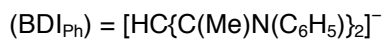
Structure	Nomenclature	Abbreviated Name
[LMSeP(S)Cy ₂]	β-diketiminatometal(II) dicyclohexylphosphinoselenothioate	metal(II) dicyclohexylphosphinoselenothioate
[LM(Se)P(SiMe ₃) ₂]	β-diketiminatometal(IV) selenide	metal(IV) selenide
[LMSeSiMe ₃]	β-diketiminatometal(II) trimethylsilylselenide	metal(II) trimethylsilylselenide

i. Leigh, G.J.; *Nomenclature of inorganic chemistry*. Blackwell Scientific Publications.: Oxford, England, 1990

List of compounds

Compound	Compound No.	Chapter
[(BDI _{DIPP})H]	1	2
[(BDI _{DIPP})PbCl]	2	2
[(BDI _{DIPP})PbO ^{<i>i</i>} Pr]	3	2
[(BDI _{DIPP})PbO ^{<i>t</i>} Bu]	4	2
[(BDI _{DIPP})PbOC(CH ₃) ₂ CH=CH ₂]	5	2
[(BDI _{DIPP})PbOMe] [#]	6	2
[(BDI _{DIPP})PbOEt] [#]	7	2
[(BDI _{DIPP})PbOCH ₂ CH=CH ₂] [#]	8	2
[(BDI _{DIPP})PbOC ₆ H ₃ ^{<i>i</i>} Bu _{2-2,4}]	9	2
[(BDI _{DIPP})PbCCPh]	10	2
[(BDI _{DIPP})PbI]	11	2
MeO ^{<i>t</i>} Bu	12	2
[C ₆ H ₅ CH=C{C(CH ₃)N(2,6- ^{<i>i</i>} Pr ₂ C ₆ H ₃) ₂ } ₂]	13	2
[(BDI _{DIPP})PbOCO ₂ ^{<i>i</i>} Pr]	14	2
[(BDI _{DIPP})PbOCO ₂ ^{<i>t</i>} Bu]	15	2
[(BDI _{DIPP})PbO*CO ₂ ^{<i>i</i>} Pr]	16	2
[(BDI _{DIPP})PbO*CO ₂ ^{<i>t</i>} Bu]	17	2
[(BDI _{DIPP})PbN(Ph)CO ₂ ^{<i>i</i>} Pr]	18	2
[(BDI _{Ph})H]	19	3
[(BDI _{IIP})H]	20	3
[(BDI _{DMP})H]	21	3
[(BDI _{Ph})PbCl]	22	3
[(BDI _{IIP})PbCl]	23	3
[(BDI _{DMP})PbCl]	24	3
[(BDI _{Ph}) ₂ Pb]	25	3
[(BDI _{IIP}) ₂ Pb]	26	3
[(BDI _{Ph})Li]	27	3
[(BDI _{DMP})PbO ^{<i>t</i>} Bu]	28	3
[(BDI _{DMP})PbOTf]	29	3
[(BDI _{IIP})PbI]	30	3
[(BDI _{DIPP})GeCl]	31	4
[(BDI _{DIPP})SnCl]	32	4
[(BDI _{DIPP})GePPh ₂]	33	4
[(BDI _{DIPP})SnPPh ₂]	34	4

Compound	Compound No.	Chapter
[(BDI _{DIPP})PbPPh ₂]	35	4
[(BDI _{DIPP})GePCy ₂]	36	4
[(BDI _{DIPP})SnPCy ₂]	37	4
[(BDI _{DIPP})PbPCy ₂]	38	4
[(BDI _{DIPP})Sn ⁿ Bu]	39	4
[(BDI _{DIPP})GeP(SiMe ₃) ₂]	40	4
[(BDI _{DIPP})SnP(SiMe ₃) ₂]	41	4
[(BDI _{DIPP})PbP(SiMe ₃) ₂]	42	4
[(BDI _{DMP})PbP(SiMe ₃) ₂]	43	4
[(BDI _{I_{PP}})PbP(SiMe ₃) ₂]	44	4
[(BDI _{Ph})PbP(SiMe ₃) ₂]	45	4
[(BDI _{DIPP})SnSePCy ₂]	46	4
[(BDI _{DIPP})PbSePCy ₂]	47	4
[(BDI _{DIPP})GeSeP(Se)Cy ₂]	48	4
[(BDI _{DIPP})SnSeP(Se)Cy ₂]	49	4
[(BDI _{DIPP})PbSeP(Se)Cy ₂]	50	4
[(BDI _{DIPP})Ge(Se)PCy ₂]	51	4
[(BDI _{DIPP})SnSP(S)Cy ₂]	52	4
[(BDI _{DIPP})PbSP(S)Cy ₂]	53	4
[(BDI _{DIPP})Ge(S)PCy ₂]	54	4
[(BDI _{DIPP})SnSeP(S)Cy ₂]	55	4
[(BDI _{DIPP})Ge(Se)P(SiMe ₃) ₂]	56	4
[(BDI _{DIPP})SnSeSiMe ₃]	57	4
[(BDI _{DIPP})PbOTf]	58	Appendix 3

Remarks:

= attempted synthesis

List of Figures

Figure 1. Structure of β -diketiminato anion $[\text{HC}\{\text{C}(\text{Me})\text{N}(2,6\text{-}i\text{-Pr}_2\text{C}_6\text{H}_3)\}_2]^-$ (BDI_{DIPP})	7
Figure 2. Examples of β -diketiminates	7
Figure 3. Iron(I) complexes, xviii and xix , with different β -diketiminato ligand	10
Figure 4. Bonding modes in metal β -diketiminates.....	11
Figure 5. Hemidirected and holodirected coordination modes in lead(II) complexes	18
Figure 6. Examples of β -diketiminato heavy group 14 metal halides xlvi – liii	20
Figure 7. Key features which encourage the lead(II)-induced hydrolytic of RNA.....	27
Figure 8. Molybdenum and rhenium hydroxide complexes lxiv and lxv	28
Figure 9. Previously reported β -diketiminatolead(II) alkoxides 3 and 4	42
Figure 10. ORTEP diagram of $[(\text{BDI}_{\text{DIPP}})\text{PbOC}(\text{CH}_3)_2\text{CH}=\text{CH}_2]$ (5). H atoms are omitted and C atoms in the <i>N</i> -aryl groups in the β -diketiminato ring are minimised for clarity. The ellipsoid probability is shown at 30%	44
Figure 11. ORTEP diagram showing the side-on view of $[(\text{BDI}_{\text{DIPP}})\text{PbOC}(\text{CH}_3)_2\text{CH}=\text{CH}_2]$ (5). H atoms are omitted and C atoms in the <i>N</i> -aryl groups in the β -diketiminato ring are minimised for clarity. The ellipsoid probability is shown at 30%	44
Figure 12. ORTEP diagram of compound 13 . The ellipsoid probability is shown at 30%.....	49
Figure 13. VT- ^1H NMR spectra (400 MHz, toluene- d_8) of $[(\text{BDI}_{\text{DIPP}})\text{PbOCO}_2^i\text{Bu}]$ (15), where A = $\gamma\text{-H}$ and B = CHMe_2	55
Figure 14. β -Diketiminato anions used in this study	61
Figure 15. Space-filling models of $[(\text{BDI}_{\text{DIPP}})\text{SnCl}]$ (xliv , top-right) and $[(\text{BDI}_{\text{Ph}})\text{SnCl}]$ (cxlv , bottom-right). The tin, chloride and nitrogen atoms are represented in purple, green and blue, respectively	62
Figure 16. Bis-lead(II) complexes	68
Figure 17. ^1H VT-NMR spectra (400 MHz, toluene- d_8) of $[(\text{BDI}_{\text{DMP}})\text{PbCl}]$ (24), where A and B are signals from <i>o</i> - CH_3 protons, C is toluene residue and D is toluene- d_8	74
Figure 18. ORTEP diagram of $[(\text{BDI}_{\text{Ph}})\text{PbCl}]$ (22). H atoms are omitted and C atoms in the β -diketiminato ring are minimised for clarity. The ellipsoid probability is shown at 30%	76
Figure 19. ORTEP diagram showing the polymeric chain of $[(\text{BDI}_{\text{Ph}})\text{PbCl}]$ (22). H atoms are omitted and C atoms in the β -diketiminato ring are minimised for clarity. The ellipsoid probability is shown at 30%	76

- Figure 20.** ORTEP diagram showing the monomeric structure of $[(BDI_{DMP})PbCl]$ (**24**). H atoms are omitted and C atoms in the β -diketiminato ring are minimised for clarity. The ellipsoid probability is shown at 30% 78
- Figure 21.** ORTEP diagram showing the dimer unit of $[(BDI_{DMP})PbCl]$ (**24**). H atoms are omitted and C atoms in the *N*-aryl groups in the β -diketiminato ring are minimised for clarity. The ellipsoid probability is shown at 30% 78
- Figure 22.** ORTEP diagram of $[(BDI_{Ph})_2Pb]$ (**25**). H atoms are omitted and C atoms in the β -diketiminato ring are minimised for clarity. The ellipsoid probability is shown at 30%. C–H $\cdots\pi$ and Pb \cdots toluene_{centre} interactions are shown by dotted lines 84
- Figure 23.** ORTEP diagram showing the side-on view of $[(BDI_{Ph})_2Pb]$ (**25**). H atoms, CH $\cdots\pi$ interactions and the solvated toluene fragment are omitted, C atoms in the *N*-aryl groups in the β -diketiminato ring are minimised for clarity. The ellipsoid probability is shown at 30% 84
- Figure 24.** ORTEP diagram of $[(BDI_{IPP})_2Pb]$ (**26**). H atoms and C atoms in the β -diketiminato ring are minimised for clarity. The ellipsoid probability is shown at 30%. C–H $\cdots\pi$ interactions are shown as dotted lines 86
- Figure 25.** ORTEP diagram showing the side-on view of $[(BDI_{IPP})_2Pb]$ (**26**). H atoms and C–H $\cdots\pi$ interactions are omitted, C atoms in the *N*-aryl groups in the β -diketiminato ring are minimised for clarity. The ellipsoid probability is shown at 30% 86
- Figure 26.** ORTEP diagram of $[(BDI_{DMP})PbO^tBu]$ (**28**). H atoms are omitted and C atoms in the β -diketiminato ring are minimised for clarity. The ellipsoid probability is shown at 30%.... 89
- Figure 27.** ORTEP diagram showing the side-on view of $[(BDI_{DMP})PbO^tBu]$ (**28**). H atoms are omitted and C atoms in the *N*-aryl groups in the β -diketiminato ring are minimised for clarity. The ellipsoid probability is shown at 30% 89
- Figure 28.** ORTEP diagram of the monomeric unit of $[(BDI_{DMP})PbOTf]$ (**29**). H atoms are omitted and C atoms in the β -diketiminato ring are minimised for clarity. The ellipsoid probability is shown at 30% 93
- Figure 29.** ORTEP diagram showing the polymeric chain of $[(BDI_{DMP})PbOTf]$ (**29**). H atoms are omitted and C atoms in the *N*-aryl groups in the β -diketiminato ring are minimised for clarity. The ellipsoid probability is shown at 30% 93
- Figure 30.** ORTEP diagram of $[(BDI_{IPP})PbI]$ (**30**). H atoms are omitted and C atoms in the β -diketiminato ring are minimised for clarity. The ellipsoid probability is shown at 30% 97
- Figure 31.** ORTEP diagram of $[(BDI_{IPP})PbI]$ (**30**) showing the polymeric chain. H atoms are omitted and C atoms in the *N*-aryl group in the β -diketiminato ring are minimised for clarity. The ellipsoid probability is shown at 30% 97
- Figure 32.** Examples of metal phosphanido complexes **ccxiv–ccxvii** 106
- Figure 33.** Hafnium phosphanido complexes **ccxviii–ccxx** and their $^{31}P\{^1H\}$ NMR resonances in C_6D_6 at room temperature 109

Figure 34. Examples of stannaphosphenes and stannaphosphines	114
Figure 35. Examples of germaphosphene	115
Figure 36. Examples of 'heavy ketones'	119
Figure 37. Heavy group 14 macrocyclic complexes with terminal chalcogenido ligand	119
Figure 38. Examples of heavy group 14 metal complexes containing phosphinodichalcogenoato and related ligands	124
Figure 39. <i>Endo</i> and <i>exo</i> conformations in β -diketiminato heavy group 14 metal complexes	131
Figure 40. $^{13}\text{C}\{^1\text{H}\}$ NMR spectrum of $[(\text{BDI}_{\text{DIPP}})\text{SnCl}]$ (32) showing the J_{CSn} ; a and a' are from CHMe_2 ; b and b' are from CHMe_2 ; c is from NCMe . The ab_2 and $\text{a'b}'_2$ indicate resonances from different pairs of isopropyl groups	132
Figure 41. Schematic view of $[(\text{BDI}_{\text{DIPP}})\text{SnCl}]$ (32) showing the relative distance between the tin atom and the isopropyl substituents. H atoms are omitted. The distances are obtained from the crystal structure data	132
Figure 42. ORTEP diagram of $[(\text{BDI}_{\text{DIPP}})\text{GePPh}_2]$ (33). H atoms are omitted and C atoms in the <i>N</i> -aryl groups in the β -diketiminato ring are minimised for clarity. The ellipsoid probability is shown at 30%	134
Figure 43. ORTEP diagram showing the side-on view of $[(\text{BDI}_{\text{DIPP}})\text{GePPh}_2]$ (33). H atoms are omitted and C atoms in the <i>N</i> -aryl groups in the β -diketiminato ring and phenyl groups are minimised for clarity. The ellipsoid probability is shown at 30%	134
Figure 44. ORTEP diagram of $[(\text{BDI}_{\text{DIPP}})\text{SnPPh}_2]$ (34). H atoms are omitted and C atoms in the <i>N</i> -aryl groups in the β -diketiminato ring are minimised for clarity. The ellipsoid probability is shown at 30%	135
Figure 45. ORTEP diagram showing the side-on view of $[(\text{BDI}_{\text{DIPP}})\text{SnPPh}_2]$ (34). H atoms are omitted and C atoms in the <i>N</i> -aryl groups in the β -diketiminato ring and the phenyl groups are minimised for clarity. The ellipsoid probability is shown at 30%	136
Figure 46. ORTEP diagram of $[(\text{BDI}_{\text{DIPP}})\text{PbPPh}_2]$ (35). H atoms are omitted and C atoms in the <i>N</i> -aryl groups in the β -diketiminato ring are minimised for clarity. The ellipsoid probability is shown at 30%	137
Figure 47. ORTEP diagram showing the side-on view of $[(\text{BDI}_{\text{DIPP}})\text{PbPPh}_2]$ (35). H atoms are omitted and C atoms in the <i>N</i> -aryl groups in the β -diketiminato ring and the phenyl groups are minimised for clarity. The ellipsoid probability is shown at 30%	137
Figure 48. ^1H NMR spectrum (400 MHz, C_6D_6) of $[(\text{BDI}_{\text{DIPP}})\text{GeCl}]$ (31 , top) and $[(\text{BDI}_{\text{DIPP}})\text{GePPh}_2]$ (33 , bottom), where A = $\gamma\text{-H}$ and B & C = CHMe_2 proton resonances	141
Figure 49. ^1H - ^{31}P HMBC NMR spectrum of $[(\text{BDI}_{\text{DIPP}})\text{GePPh}_2]$ (33) in C_6D_6 , with A = $\gamma\text{-H}$; B & C = CHMe_2 ; D & E = CHMe_2 and F = NCMe . Impurities are designated by §	141

- Figure 50.** $^{13}\text{C}\{^1\text{H}\}$ NMR spectrum of $[(\text{BDI}_{\text{DIPP}})\text{GePPh}_2]$ (**33**) showing the J_{CP} ; a and a' are from CHMe_2 ; b and b' are from CHMe_2 ; c is from NCMe . The ab_2 and $a'b'_2$ indicate resonances from different pairs of isopropyl groups..... 142
- Figure 51.** Schematic view of $[(\text{BDI}_{\text{DIPP}})\text{GePPh}_2]$ (**33**) showing the distances between the phosphorus atom and the isopropyl substituents. H atoms are omitted. The distances are obtained from the crystal structure data..... 143
- Figure 52.** $^{13}\text{C}\{^1\text{H}\}$ NMR spectrum of $[(\text{BDI}_{\text{DIPP}})\text{SnPPh}_2]$ (**34**) showing the J_{CP} and J_{CSn} ; a and a' are from CHMe_2 ; b and b' are from CHMe_2 ; c is from NCMe . The ab_2 and $a'b'_2$ indicate resonances from different pairs of isopropyl groups 144
- Figure 53.** Schematic view of $[(\text{BDI}_{\text{DIPP}})\text{SnPPh}_2]$ (**34**) showing the distances between the phosphorus or tin atom and the isopropyl substituents. H atoms are omitted. The distances are obtained from the crystal structure data..... 145
- Figure 54.** $^{13}\text{C}\{^1\text{H}\}$ NMR spectrum of $[(\text{BDI}_{\text{DIPP}})\text{PbPPh}_2]$ (**35**) showing the J_{CP} and J_{CPb} ; a and a' are from CHMe_2 ; b and b' are from CHMe_2 ; c is from NCMe . The ab_2 and $a'b'_2$ indicate resonances from different pairs of isopropyl groups 146
- Figure 55.** Schematic view of $[(\text{BDI}_{\text{DIPP}})\text{PbPPh}_2]$ (**35**) showing the distances between the phosphorus or lead atom and the isopropyl substituents. H atoms are omitted. The distances are obtained from the crystal structure data 146
- Figure 56.** ORTEP diagram of $[(\text{BDI}_{\text{DIPP}})\text{GePCy}_2]$ (**36**). H atoms are omitted and C atoms in the *N*-aryl groups in the β -diketimate ring are omitted for clarity. The ellipsoid probability is shown at 30% 148
- Figure 57.** ORTEP diagram showing the side-on view of $[(\text{BDI}_{\text{DIPP}})\text{GePCy}_2]$ (**36**). H atoms are omitted, and C atoms in the *N*-aryl groups in the β -diketimate ring and the cyclohexyl groups are minimised for clarity. The ellipsoid probability is shown at 30% 149
- Figure 58.** ORTEP diagram of $[(\text{BDI}_{\text{DIPP}})\text{SnPCy}_2]$ (**37**). H atoms are omitted and C atoms in the *N*-aryl groups in the β -diketimate ring are minimised for clarity. The ellipsoid probability is shown at 30% 150
- Figure 59.** ORTEP diagram showing the side-on view of $[(\text{BDI}_{\text{DIPP}})\text{SnPCy}_2]$ (**37**). H atoms are omitted, and C atoms in the *N*-aryl groups in the β -diketimate ring and the cyclohexyl groups are minimised for clarity. The ellipsoid probability is shown at 30% 150
- Figure 60.** ORTEP diagram of $[(\text{BDI}_{\text{DIPP}})\text{PbPCy}_2]$ (**38**). H atoms are omitted and C atoms in the *N*-aryl groups in the β -diketimate ring are minimised for clarity. The ellipsoid probability is shown at 30% 152
- Figure 61.** ORTEP diagram showing the side-on view of $[(\text{BDI}_{\text{DIPP}})\text{PbPCy}_2]$ (**38**). H atoms are omitted, C atoms in the *N*-aryl groups in the β -diketimate ring and the cyclohexyl groups are minimised for clarity. The ellipsoid probability is shown at 30% 152
- Figure 62.** VT- ^1H NMR spectra (400 MHz, toluene- d_8) of $[(\text{BDI}_{\text{DIPP}})\text{SnPCy}_2]$ (**37**) where A = $\gamma\text{-H}$; B = CHMe_2 ; and C = Cy-CH 157

- Figure 63.** VT- $^{31}\text{P}\{^1\text{H}\}$ NMR spectra (162 MHz, toluene- d_8) of $[(\text{BDI}_{\text{DIPP}})\text{SnPCy}_2]$ (**37**) where A = phosphorus resonance and B = tin satellites 158
- Figure 64.** Solid state $^{31}\text{P}\{^1\text{H}\}$ NMR spectrum (162 MHz) of $[(\text{BDI}_{\text{DIPP}})\text{SnPCy}_2]$ (**37**) 159
- Figure 65.** VT- ^1H NMR spectra (400 MHz, toluene- d_8) of $[(\text{BDI}_{\text{DIPP}})\text{PbPCy}_2]$ (**38**), where A = $\gamma\text{-H}$, B = CHMe_2 and C = Cy-CH 160
- Figure 66.** VT- $^{31}\text{P}\{^1\text{H}\}$ NMR spectra (162 MHz, toluene- d_8) of $[(\text{BDI}_{\text{DIPP}})\text{PbPCy}_2]$ (**38**) 161
- Figure 67.** $^1\text{H}\text{-}^{31}\text{P}$ HMBC NMR spectra of $[(\text{BDI}_{\text{DIPP}})\text{PbPCy}_2]$ (**38**) in toluene- d_8 at 30 °C (top) and -80 °C (bottom), where A = $\gamma\text{-H}$, B = CHMe_2 , C = CHMe_2 , D = Cy-CH and E = Cy-CH_2 162
- Figure 68.** ORTEP diagram of $[(\text{BDI}_{\text{DIPP}})\text{SnP}(\text{SiMe}_3)_2]$ (**41**). H atoms are omitted and C atoms in the *N*-aryl groups in the β -diketiminato ring are minimised for clarity. The ellipsoid probability is shown at 30% 166
- Figure 69.** ORTEP diagram showing the side-on view of $[(\text{BDI}_{\text{DIPP}})\text{SnP}(\text{SiMe}_3)_2]$ (**41**). H atoms are omitted and C atoms in the *N*-aryl groups in the β -diketiminato ring are minimised for clarity. The ellipsoid probability is shown at 30% 166
- Figure 70.** VT- ^1H NMR spectra (400 MHz, toluene- d_8) of $[(\text{BDI}_{\text{DIPP}})\text{GeP}(\text{SiMe}_3)_2]$ (**40**), where A = $\gamma\text{-H}$; B = CHMe_2 ; C = CHMe_2 ; and D & E = SiMe_3 . The unidentified contaminant is designated by \S 171
- Figure 71.** VT- $^{31}\text{P}\{^1\text{H}\}$ NMR spectra (162 MHz, toluene- d_8) of $[(\text{BDI}_{\text{DIPP}})\text{GeP}(\text{SiMe}_3)_2]$ (**40**), where A = phosphorus resonance. Impurities are designated by \S 172
- Figure 72.** VT- $^{29}\text{Si}\{^1\text{H}\}$ NMR spectra (79 MHz, toluene- d_8) of $[(\text{BDI}_{\text{DIPP}})\text{GeP}(\text{SiMe}_3)_2]$ (**40**), showing two resonances, A and B 173
- Figure 73.** VT- ^1H NMR spectra (400 MHz, toluene- d_8) of $[(\text{BDI}_{\text{DIPP}})\text{SnP}(\text{SiMe}_3)_2]$ (**41**), where A = NCMe ; B = CHMe_2 ; and C & D = SiMe_3 174
- Figure 74.** VT- $^{31}\text{P}\{^1\text{H}\}$ NMR spectra (162 MHz, toluene- d_8) of $[(\text{BDI}_{\text{DIPP}})\text{SnP}(\text{SiMe}_3)_2]$ (**41**), where A = ^{119}Sn satellite, B = ^{117}Sn satellite and C = phosphorus resonance 175
- Figure 75.** $^{13}\text{C}\{^1\text{H}\}$ NMR spectrum (100 MHz) of $[(\text{BDI}_{\text{DIPP}})\text{SnP}(\text{SiMe}_3)_2]$ (**41**) in C_6D_6 at 30 °C showing the J_{CP} and J_{CSn} ; a and a' are from CHMe_2 ; b and b' are from CHMe_2 ; c is from NCMe . The ab_2 and $\text{a'b}'_2$ indicate resonances from different pairs of isopropyl groups .. 176
- Figure 76.** Schematic view of $[(\text{BDI}_{\text{DIPP}})\text{SnP}(\text{SiMe}_3)_2]$ (**41**) showing the relative distance between the tin atom and the isopropyl substituents. H atoms are omitted. The distances are obtained from the crystal structure data 177
- Figure 77.** Schematic view of $[(\text{BDI}_{\text{DIPP}})\text{SnP}(\text{SiMe}_3)_2]$ (**41**) showing the relative distance between the phosphorus atom and the isopropyl substituents. H atoms are omitted. The distances are obtained from the crystal structure data 177
- Figure 78.** VT- $^{29}\text{Si}\{^1\text{H}\}$ NMR spectra (79 MHz, toluene- d_8) of $[(\text{BDI}_{\text{DIPP}})\text{SnP}(\text{SiMe}_3)_2]$ (**41**) showing two silicon resonances A and B 178

- Figure 79.** ^1H - ^{29}Si HMBC NMR spectra (toluene- d_8) of $[(\text{BDI}_{\text{DIPP}})\text{SnP}(\text{SiMe}_3)_2]$ (**41**) at 30 °C (top) and -80 °C (bottom), where A & B = silicon resonances; and C & D = proton resonances in SiMe_3 at -80 °C, E = silicon resonance and F = proton resonance in SiMe_3 at 30 °C 179
- Figure 80.** Solid state $^{31}\text{P}\{^1\text{H}\}$ NMR spectrum (162 MHz) of $[(\text{BDI}_{\text{DIPP}})\text{SnP}(\text{SiMe}_3)_2]$ (**41**) 180
- Figure 81.** Solid state $^{29}\text{Si}\{^1\text{H}\}$ NMR spectrum (79 MHz) of $[(\text{BDI}_{\text{DIPP}})\text{SnP}(\text{SiMe}_3)_2]$ (**41**) 181
- Figure 82.** Solid state $^{29}\text{Si}\{^{31}\text{P}\}$ NMR spectrum (79 MHz) of $[(\text{BDI}_{\text{DIPP}})\text{SnP}(\text{SiMe}_3)_2]$ (**41**) 181
- Figure 83.** VT- ^1H NMR spectra (400 MHz, toluene- d_8) of $[(\text{BDI}_{\text{DIPP}})\text{PbP}(\text{SiMe}_3)_2]$ (**42**), where A = $\gamma\text{-H}$; B = CHMe_2 ; C = toluene- d_8 ; D = NCMe ; E = CHMe_2 and F = SiMe_3 182
- Figure 84.** VT- $^{31}\text{P}\{^1\text{H}\}$ NMR spectra (162 MHz, toluene- d_8) of $[(\text{BDI}_{\text{DIPP}})\text{PbP}(\text{SiMe}_3)_2]$ (**42**), where A & B are the phosphorus resonances at -90 °C. Impurities are designated by * 184
- Figure 85.** $^{13}\text{C}\{^1\text{H}\}$ NMR spectrum (100 MHz) of $[(\text{BDI}_{\text{DIPP}})\text{PbP}(\text{SiMe}_3)_2]$ (**42**) in C_6D_6 at 30 °C, showing the J_{CP} ; a and a' are from CHMe_2 ; b and b' are from CHMe_2 ; c is from NCMe . The ab_2 and $\text{a'b}'_2$ indicate resonances from different pairs of isopropyl groups 185
- Figure 86.** Solid state $^{31}\text{P}\{^1\text{H}\}$ NMR spectrum (162 MHz) of $[(\text{BDI}_{\text{DIPP}})\text{PbP}(\text{SiMe}_3)_2]$ (**42**) 186
- Figure 87.** Solid state $^{29}\text{Si}\{^1\text{H}\}$ NMR spectrum (79 MHz) of $[(\text{BDI}_{\text{DIPP}})\text{PbP}(\text{SiMe}_3)_2]$ (**42**) 187
- Figure 88.** Solid state $^{29}\text{Si}\{^{31}\text{P}\}$ NMR spectrum (79 MHz) of $[(\text{BDI}_{\text{DIPP}})\text{PbP}(\text{SiMe}_3)_2]$ (**42**) 187
- Figure 89.** VT- ^1H NMR spectra (400 MHz, toluene- d_8) of $[(\text{BDI}_{\text{Ph}})\text{PbP}(\text{SiMe}_3)_2]$ (**45**), where A = $\gamma\text{-H}$; B = NCMe ; and C = SiMe_3 190
- Figure 90.** VT- $^{31}\text{P}\{^1\text{H}\}$ NMR spectra (162 MHz, toluene- d_8) of $[(\text{BDI}_{\text{Ph}})\text{PbP}(\text{SiMe}_3)_2]$ (**45**), where A = lead satellites and B = phosphorus resonance 191
- Figure 91.** Graphical representation of M-P bond lengths in the germanium(II) and tin(II) phosphanides $[(\text{BDI}_{\text{DIPP}})\text{MPR}_2]$ (M = Ge or Sn, R = Ph, Cy or SiMe_3) 193
- Figure 92.** Factors influencing the geometry around the phosphorus atom from the *N*-aryl substituents by (a): metal-phosphorus bond and (b): bite angle of the β -diketiminato ligand 193
- Figure 93.** ORTEP diagram of $[(\text{BDI}_{\text{DIPP}})\text{SnSePCy}_2]$ (**46**). H atoms are omitted and C atoms in the *N*-aryl groups in the β -diketiminato ring are minimised for clarity. The ellipsoid probability is shown at 30% 200
- Figure 94.** ORTEP diagram showing the side-on view of $[(\text{BDI}_{\text{DIPP}})\text{SnSePCy}_2]$ (**46**). H atoms are omitted, C atoms in the *N*-aryl groups in the β -diketiminato ring and the cyclohexyl groups are minimised for clarity. The ellipsoid probability is shown at 30% 200
- Figure 95.** ORTEP diagram of $[(\text{BDI}_{\text{DIPP}})\text{PbSePCy}_2]$ (**47**). H atoms are omitted and C atoms in the *N*-aryl groups in the β -diketiminato ring are minimised for clarity. The ellipsoid probability is shown at 30% 202

- Figure 96.** ORTEP diagram showing the side-on view of [(BDI_{DIPP})PbSePCy₂] (**47**). H atoms are omitted and C atoms in the *N*-aryl groups in the β-diketiminato ring and the cyclohexyl groups are minimised for clarity. The ellipsoid probability is shown at 30% 202
- Figure 97.** VT-¹H NMR spectra (400MHz, toluene-*d*₈) of [(BDI_{DIPP})SnSePCy₂] (**46**) where A = γ-*H*; B = CHMe₂ and C = Cy-CH 206
- Figure 98.** ³¹P{¹H} NMR spectrum (162 MHz, toluene-*d*₈) of [(BDI_{DIPP})SnSePCy₂] (**46**) with an extended acquisition time. The enhanced satellites are indicated in the diagram, and where A = phosphorus resonance. Impurities are designated by § 207
- Figure 99.** VT-³¹P{¹H} NMR spectra (162 MHz, toluene-*d*₈) of [(BDI_{DIPP})SnSePCy₂] (**46**) where A = phosphorus resonance; B = ⁷⁷Se; C = ¹¹⁷Sn; and D = ¹¹⁹Sn satellites 208
- Figure 100.** ORTEP diagram of [(BDI_{DIPP})GeSeP(Se)Cy₂] (**48**). H atoms are omitted and C atoms in the *N*-aryl groups in the β-diketiminato ring are minimised for clarity. The ellipsoid probability is shown at 30% 212
- Figure 101.** ORTEP diagram showing the side-on view of [(BDI_{DIPP})GeSeP(Se)Cy₂] (**48**). H atoms are omitted and C atoms in the *N*-aryl groups in the β-diketiminato ring and the cyclohexyl groups are minimised for clarity. The ellipsoid probability is shown at 30%... 212
- Figure 102.** ORTEP diagram of [(BDI_{DIPP})SnSeP(Se)Cy₂] (**49**). H atoms are omitted and C atoms in the *N*-aryl groups in the β-diketiminato ring are minimised for clarity. The ellipsoid probability is shown at 30% 214
- Figure 103.** ORTEP diagram showing the side-on view of [(BDI_{DIPP})SnSeP(Se)Cy₂] (**49**). H atoms are omitted and C atoms in the *N*-aryl groups in the β-diketiminato ring and the cyclohexyl groups are minimised for clarity. The ellipsoid probability is shown at 30%... 214
- Figure 104.** ORTEP diagram of [(BDI_{DIPP})PbSeP(Se)Cy₂] (**50**). H atoms are omitted and C atoms in the *N*-aryl groups in the β-diketiminato ring are minimised for clarity. The ellipsoid probability is shown at 30% 216
- Figure 105.** ORTEP diagram showing the side-on view of [(BDI_{DIPP})PbSeP(Se)Cy₂] (**50**). H atoms are omitted, C atoms in the *N*-aryl groups in the β-diketiminato ring and the cyclohexyl groups are minimised for clarity. The ellipsoid probability is shown at 30%... 216
- Figure 106.** VT-¹H NMR spectra (400 MHz, toluene-*d*₈) of [(BDI_{DIPP})SnSeP(Se)Cy₂] (**49**), where A = γ-*H*; B = CHMe₂; C = Cy-CH 221
- Figure 107.** ³¹P{¹H} NMR spectrum (162 MHz, toluene-*d*₈) of [(BDI_{DIPP})SnSeP(Se)Cy₂] (**49**) with an extended acquisition time. The enhanced satellites are indicated in the diagram and where A = phosphorus resonance. Impurities are designated by § 222
- Figure 108.** VT-³¹P{¹H} NMR spectra (162 MHz, toluene-*d*₈) of [(BDI_{DIPP})SnSeP(Se)Cy₂] (**49**) where A = phosphorus resonance; B = ⁷⁷Se; C = ¹¹⁷Sn; and D = ¹¹⁹Sn satellites 223
- Figure 109.** Solid state ⁷⁷Se NMR spectrum (79 MHz) of [(BDI_{DIPP})SnSeP(Se)Cy₂] (**49**). Impurities are designated by § 226

- Figure 110.** ORTEP diagram of $[(BDI_{DIPP})Ge(Se)PCy_2]$ (**51**). H atoms are omitted and C atoms in the *N*-aryl groups in the β -diketiminato ring are minimised for clarity. The ellipsoid probability is shown at 30% 229
- Figure 111.** ORTEP diagram showing the side-on view of $[(BDI_{DIPP})Ge(Se)PCy_2]$ (**51**). H atoms are omitted and C atoms in the *N*-aryl groups in the β -diketiminato ring and the cyclohexyl groups are minimised for clarity. The ellipsoid probability is shown at 30% 229
- Figure 112.** ORTEP diagram of $[(BDI_{DIPP})SnSP(S)Cy_2]$ (**52**). H atoms are omitted and C atoms in the *N*-aryl groups in the β -diketiminato ring are minimised for clarity. The ellipsoid probability is shown at 30% 235
- Figure 113.** ORTEP diagram showing the side-on view of $[(BDI_{DIPP})SnSP(S)Cy_2]$ (**52**). H atoms are omitted, and C atoms in the *N*-aryl groups in the β -diketiminato ring and the cyclohexyl groups are minimised for clarity. The ellipsoid probability is shown at 30% 235
- Figure 114.** ORTEP diagram of $[(BDI_{DIPP})PbSP(S)Cy_2]$ (**53**). H atoms are omitted and C atoms in the *N*-aryl groups in the β -diketiminato ring are minimised for clarity. The ellipsoid probability is shown at 30% 237
- Figure 115.** ORTEP diagram showing the side-on view of $[(BDI_{DIPP})PbSP(S)Cy_2]$ (**53**). H atoms are omitted, and C atoms in the *N*-aryl groups in the β -diketiminato ring and the cyclohexyl groups are minimised for clarity. The ellipsoid probability is shown at 30% 237
- Figure 116.** ORTEP diagram of $[(BDI_{DIPP})Ge(S)PCy_2]$ (**54**). H atoms are omitted and C atoms in the *N*-aryl groups in the β -diketiminato ring are minimised for clarity. The ellipsoid probability is shown at 30% 243
- Figure 117.** ORTEP diagram showing the side-on view of $[(BDI_{DIPP})Ge(S)PCy_2]$ (**54**). H atoms are omitted and C atoms in the *N*-aryl groups in the β -diketiminato ring and the cyclohexyl groups are minimised for clarity. The ellipsoid probability is shown at 30% 243
- Figure 118.** ORTEP diagram of $[(BDI_{DIPP})Ge(Se)P(SiMe_3)_2]$ (**56**). H atoms are omitted and C atoms in the *N*-aryl groups in the β -diketiminato ring are minimised for clarity. The ellipsoid probability is shown at 30% 250
- Figure 119.** ORTEP diagram showing the side-on view of $[(BDI_{DIPP})Ge(Se)P(SiMe_3)_2]$ (**56**). H atoms are omitted and C atoms in the *N*-aryl groups in the β -diketiminato ring are minimised for clarity. The ellipsoid probability is shown at 30% 250
- Figure 120.** ORTEP diagram of $[(BDI_{DIPP})SnSeSiMe_3]$ (**57**). H atoms are omitted and C atoms in the *N*-aryl groups in the β -diketiminato ring are minimised for clarity. The ellipsoid probability is shown at 30% 255
- Figure 121.** ORTEP diagram showing the side-on view of $[(BDI_{DIPP})SnSeSiMe_3]$ (**57**). H atoms are omitted and C atoms in the *N*-aryl groups in the β -diketiminato ring are minimised for clarity. The ellipsoid probability is shown at 30% 255

List of Schemes

Scheme 1. Synthesis of the amidinate tin(II) alkoxide x	5
Scheme 2. Synthesis of the β -diketimine xiv	8
Scheme 3. Proposed mechanism for the formation of β -diketimine xiv	8
Scheme 4. A stepwise synthetic route for the synthesis of compound xv	9
Scheme 5. Synthesis of the asymmetric β -diketimine xvi	10
Scheme 6. Synthesis of the β -diketimine xvii	10
Scheme 7. General reaction scheme for the synthesis of metal β -diketiminates	12
Scheme 8. Synthesis of the dimethyl vanadium(III) β -diketiminato xxii	12
Scheme 9. Reactions of the dimeric β -diketiminatomagnesium complex xxiv	13
Scheme 10. Synthesis of the chromium(I) β -diketiminato xxix	14
Scheme 11. Synthesis of the β -diketiminatozinc(II) isopropoxides xxxiii and xxxiv	15
Scheme 12. Polymerisation of <i>rac</i> -lactide to form heterotactic PLA with the β - diketiminatozinc(II) isopropoxides xxxiii and xxxiv	15
Scheme 13. Synthesis of the oxoborane β -diketiminato xxxviii	16
Scheme 14. Synthesis of the hydroxyphosphenium salt xli	16
Scheme 15. Synthesis and reactions of the lanthanum(III) dibromide complex xlii	17
Scheme 16. Synthesis of the β -diketiminatolead(II) amide liv	20
Scheme 17. Reactions between the β -diketiminatogermanium(II) or -tin(II) hydrides, lviii–lix , and unsaturated molecules	22
Scheme 18. Proposed mechanism of the lead(II)-induced hydrolytic cleavage of RNA	26
Scheme 19. Reactions of complexes lxiv and lxv	29
Scheme 20. Reactions of the iridium hydroxide complex lxxii	30
Scheme 21. Proposed mechanism for the formation of compound lxxxi	31
Scheme 22. Proposed mechanism for the formation of the metal hydrosulfido complexes lxxxii and lxxxiii	32
Scheme 23. Synthesis of the heavy group 14 metal alkoxide complexes lxxxvi–lxxxviii	33
Scheme 24. Synthesis of the cyclopentadienyl heterobimetallic alkoxide complexes lxxxix–xci	34

Scheme 25. Synthesis and reactions of the β -diketiminatolead(II) aryloxyde cxiii	37
Scheme 26. Synthesis of the β -diketiminatotin(II) isopropoxyde cxvi	38
Scheme 27. Synthesis of the β -diketiminatogermanium(II) aryloxides cxvvi and cxvii	39
Scheme 28. Synthesis of the β -diketiminatogermanium(II) hydroxyde cxviii	40
Scheme 29. Reactions of the β -diketiminatogermanium(II) hydroxyde cxviii	40
Scheme 30. Synthesis of the β -diketiminatolead(II) chloridy 2	42
Scheme 31. β -Diketiminatolead(II) alkoxyde 5 and the attempted syntheses of compounds 6–8	43
Scheme 32. Attempted reactions of the β -diketiminatolead(II) <i>tert</i> -butoxyde 4 with monodentate or bidentate ligands in C_6D_6	52
Scheme 33. ^{13}C -labeling study on the lead(II) carbonates 14 and 15	55
Scheme 34. Reaction of the lead(II) isopropoxy carbonate 14 with phenyl isocyanate	57
Scheme 35. Reactions of the β -diketiminatolead(II) alkoxydes with heterocumulenes	57
Scheme 36. Two pathways for carbon dioxide insertion into a M–O bond	58
Scheme 37. Proposed mechanism for the formation of compound cxlvi	65
Scheme 38. Reactions of the β -diketiminatopalladium chloridy cxlix	66
Scheme 39. Reactions of the β -diketiminatoaluminium dihydrody clii	66
Scheme 40. Synthesis of the bis[β -diketiminato]chromium(II) complex clxvi	68
Scheme 41. Proposed reaction pathway for the formation of compound clxvi	69
Scheme 42. Synthesis of the bis[β -diketiminato]palladium(II) complex cxcii	71
Scheme 43. Synthesis of the β -diketiminatolead(II) chloridy 22–24	73
Scheme 44. Synthesis of the platinum phosphanidy cci	103
Scheme 45. Reactions of the platinum phosphanidy cci	103
Scheme 46. The fluxional process in the terminal phosphanidy ligand in ccxiii	106
Scheme 47. Two different coordination modes of the phosphanidy (PR_2) ligand.....	107
Scheme 48. Synthesis of complexes ccxxii and ccxxiii	109
Scheme 49. Synthesis of the β -diketiminatogermanium(II) bis(trimethylsilyl)phosphanidy ccxxvi	111
Scheme 50. Synthesis of the heavy group 14 metal phosphanidy ccxlili–ccxlv	117
Scheme 51. Inversion process in the homoleptic tin(II) phosphanidy ccxlv	117

XXVIII

Scheme 52. General synthetic route to ‘heavy ketones’	119
Scheme 53. Resonance structures of the metal-chalcogen bond	120
Scheme 54. Proposed stepwise process in the synthesis of [(BDI _{DIPP})Ge(S)SH] (ccl)	120
Scheme 55. Reactions between metal phosphanido complexes [L _n MPPR ₂] and an excess of elemental chalcogen (E)	121
Scheme 56. Proposed Equilibrium structures in the phosphorus chalcogenido complexes [L _n MP(E)R ₂].....	121
Scheme 57. Reaction between germaphosphene cclix and elemental sulfur.....	124
Scheme 58. Synthesis of compounds cclxiii and cclxiv	125
Scheme 59. Synthesis of the tris(diselenophosphinato)indium complex	127
Scheme 60. Reactions of the platinum phosphanide cclxviii with elemental sulfur.....	128
Scheme 61. Synthesis of the β-diketiminato heavy group 14 metal chlorides.....	129
Scheme 62. Reactions of the β-diketiminatotin(II) and -lead(II) dicyclohexylphosphanides, 37 and 38 , with elemental selenium in C ₆ D ₆	197
Scheme 63. Synthesis of [(BDI _{DIPP})MSeP(Se)Cy ₂] (Cy = cyclohexyl; 48 , M = Ge; 49 , M = Sn; and 50 , M = Pb)	210
Scheme 64. Preliminary reactions between the tin(II) or lead(II) dicyclohexylphosphanides, 37 or 38 , and elemental sulfur.....	232
Scheme 65. Proposed interchangeable structures of [(BDI _{DIPP})SnSeP(S)Cy ₂] (55) in solution	248
Scheme 66. Proposed reaction pathways for the reaction between phosphanido complex and elemental chalcogen	259

List of Tables

Table 1. NBO analysis of M(II) ion in LMCl (L = (BDI _{DIPP}); M = Ge, Sn or Pb)	18
Table 2. Summary of the reactions reported in Chapter 2 and the associated primary investigator (Legend: NCJ, Dr. Nick C. Johnstone; LF, Dr. Lorenzo Ferro and ECYT, Eric C.Y. Tam).....	23
Table 3. Selected acid dissociation constants (pK _a) of hydrated metal ions	27
Table 4. Selected bond lengths (Å) and angles (deg) for [(BDI _{DIPP})PbOC(CH ₃) ₂ CH=CH ₂] (5) ...	45
Table 5. Selected crystallographic data for compound 5	45
Table 6. Selected bond lengths (Å) and angles (deg) for compound 13	50
Table 7. Selected crystallographic data for compound 13	51
Table 8. Selected bond lengths (Å) and angles (deg) for [(BDI _{Ph})PbCl] (22)	77
Table 9. Selected bond lengths (Å) and angles (deg) for [(BDI _{DMP})PbCl] (24)	79
Table 10. Selected crystallographic data for [(BDI _{Ph})PbCl] (22) and [(BDI _{DMP})PbCl] (24)	80
Table 11. Selected bond lengths (Å) and angles (deg) for [(BDI _{Ph}) ₂ Pb] (25)	85
Table 12. Selected bond lengths (Å) and angles (deg) for [(BDI _{Ipp}) ₂ Pb] (26)	87
Table 13. Selected crystallographic data for [(BDI _{Ph}) ₂ Pb] (25) and [(BDI _{Ipp}) ₂ Pb] (26).....	87
Table 14. Selected bond lengths (Å) and angles (deg) for [(BDI _{DMP})PbO ^t Bu] (28).....	90
Table 15. Selected crystallographic data for [(BDI _{DMP})PbO ^t Bu] (28)	91
Table 16. Selected bond lengths (Å) and angles (deg) for [(BDI _{DMP})PbOTf] (29)	94
Table 17. Selected crystallographic data for [(BDI _{DMP})PbOTf] (29).....	95
Table 18. Selected bond lengths (Å) and angles (deg) for [(BDI _{Ipp})PbI] (30).....	98
Table 19. Selected crystallographic data for [(BDI _{Ipp})PbI] (30)	99
Table 20. Suzuki cross-coupling reaction of bromobenzene with phenylboronic acid	105
Table 21. Physical observations of different coordination modes in metal-phosphorus bond .	108
Table 22. Selected structural data for complexes ccxxii and ccxxiii	110
Table 23. ³¹ P{ ¹ H} NMR spectroscopic and selected solid state structural data of [(BDI _{DIPP})MP(SiMe ₃) ₂] (ccxxvi , M = Ge; cxv , M = Pb) in C ₆ D ₆	113
Table 24. Selected NMR spectroscopic data for ccxxviii – ccxxxii	114
Table 25. Selected NMR spectroscopic and structural data for ccxxxiii – ccxxxv	115

Table 26. Selected NMR spectroscopic (at 298 K) and solid state structural data for ccxxxviii–ccxli	116
Table 27. Coordination modes for phosphorus chalcogenides $(-E)PR_2$	122
Table 28. Coordination modes for phosphinodichalcogenoate $(-E(E)PR_2)^-$ and related anions	123
Table 29. Selected bond lengths (Å) and angles (deg) for $[(BDI_{DIPP})MPPh_2]$ (33 , M = Ge; 34 , M = Sn; and 35 , M = Pb)	138
Table 30. Selected crystallographic data for $[(BDI_{DIPP})MPPh_2]$ (33 , M = Ge; 34 , M = Sn; and 35 , M = Pb)	139
Table 31. Selected multinuclear NMR spectroscopic data for $[(BDI_{DIPP})MPPh_2]$ (33 , M = Ge; 34 M = Sn; and 35 , M = Pb) in C_6D_6 at 30 °C	140
Table 32. Selected bond lengths (Å) and angles (deg) for $[(BDI_{DIPP})MPCy_2]$ (Cy = cyclohexyl; 36 , M = Ge; 37 , M = Sn; and 38 , M = Pb)	153
Table 33. Selected crystallographic data for $[(BDI_{DIPP})MPCy_2]$ (Cy = cyclohexyl; 36 , M = Ge; 37 , M = Sn; and 38 , M = Pb)	154
Table 34. Selected multinuclear NMR spectroscopic data for $[(BDI_{DIPP})MPCy_2]$ (Cy = cyclohexyl; 36 , M = Ge; 37 , M = Sn; and 38 , M = Pb) in C_6D_6 at 30 °C, unless specified	155
Table 35. Selected bond lengths (Å) and angles (deg) for $[(BDI_{DIPP})SnP(SiMe_3)_2]$ (41)	167
Table 36. Selected crystallographic data for $[(BDI_{DIPP})SnP(SiMe_3)_2]$ (41)	168
Table 37. Selected multinuclear NMR spectroscopic data (30 °C) for $[LMP(SiMe_3)_2]$ (L = (BDI_{DIPP}) ; 40 , M = Ge; 41 , M = Sn; and 42 , M = Pb) in C_6D_6 , unless specified	169
Table 38. Selected multinuclear NMR spectroscopic data for $[(BDI_{DMP})PbP(SiMe_3)_2]$ (43), $[(BDI_{IPP})PbP(SiMe_3)_2]$ (44) and $[(BDI_{Ph})PbP(SiMe_3)_2]$ (45)	189
Table 39. Selected bond lengths (Å) and angles (deg) for $[(BDI_{DIPP})MSePCy_2]$ (Cy = cyclohexyl; 46 , M = Sn and 47 , M = Pb)	203
Table 40. Selected crystallographic data for $[(BDI_{DIPP})MSePCy_2]$ (Cy = cyclohexyl; 46 , M = Sn and 47 , M = Pb)	204
Table 41. Selected multinuclear NMR spectroscopic data (C_6D_6 , 30 °C) for $[(BDI_{DIPP})MSePCy_2]$ (Cy = cyclohexyl; 46 , M = Sn and 47 , M = Pb)	205
Table 42. Selected bond lengths (Å) and angles (deg) for $[LMSeP(Se)Cy_2]$ (L = (BDI_{DIPP}) ; Cy = cyclohexyl; 48 , M = Ge; 49 , M = Sn; and 50 , M = Pb)	217
Table 43. Selected crystallographic data for $[LMSeP(Se)Cy_2]$ (L = (BDI_{DIPP}) ; Cy = cyclohexyl; 48 , M = Ge; 49 , M = Sn; and 50 , M = Pb)	218
Table 44. Selected multinuclear NMR spectroscopic data (30 °C) for $[LMSeP(Se)Cy_2]$ (L = (BDI_{DIPP}) ; Cy = cyclohexyl; 48 , M = Ge; 49 , M = Sn; and 50 , M = Pb)	219

Table 45. Selected multinuclear solid state NMR spectroscopic data for [(BDI _{DIPP})SnSeP(Se)Cy ₂] (49)	224
Table 46. Selected bond lengths (Å) and angles (deg) for [(BDI _{DIPP})Ge(Se)PCy ₂] (51)	230
Table 47. Selected crystallographic data for [(BDI _{DIPP})Ge(Se)PCy ₂] (51)	231
Table 48. Selected bond lengths (Å) and angles (deg) for [(BDI _{DIPP})MSP(S)Cy ₂] (Cy = cyclohexyl; 52 , M = Sn; and 53 , M = Pb)	238
Table 49. Selected crystallographic data for [(BDI _{DIPP})MSP(S)Cy ₂] (Cy = cyclohexyl; 52 , M = Sn; and 53 , M = Pb)	239
Table 50. Selected multinuclear NMR spectroscopic data (C ₆ D ₆ , 30 °C) for [(BDI _{DIPP})MSP(S)Cy ₂] (Cy = cyclohexyl; 52 , M = Sn; and 53 , M = Pb).....	240
Table 51. Selected bond lengths (Å) and angles (deg) for [(BDI _{DIPP})Ge(S)PCy ₂] (54)	244
Table 52. Selected crystallographic data for [(BDI _{DIPP})Ge(S)PCy ₂] (54)	245
Table 53. Selected multinuclear NMR spectroscopic data for [(BDI _{DIPP})SnSeP(S)Cy ₂] (55) in C ₆ D ₆ at 30 °C	247
Table 54. Selected bond lengths (Å) and angles (deg) for [(BDI _{DIPP})Ge(Se)P(SiMe ₃) ₂] (56) ...	251
Table 55. Selected crystallographic data for [(BDI _{DIPP})Ge(Se)P(SiMe ₃) ₂] (56)	252
Table 56. Selected bond lengths (Å) and angles (deg) for [(BDI _{DIPP})SnSeSiMe ₃] (57)	256
Table 57. Selected crystallographic data for [(BDI _{DIPP})SnSeSiMe ₃] (57)	257

**Synthesis and reactions of β -diketiminato heavy group 14
metal alkoxides and phosphanides**

1. Introduction

1.1 History. Environmental and health implications of lead chemistry

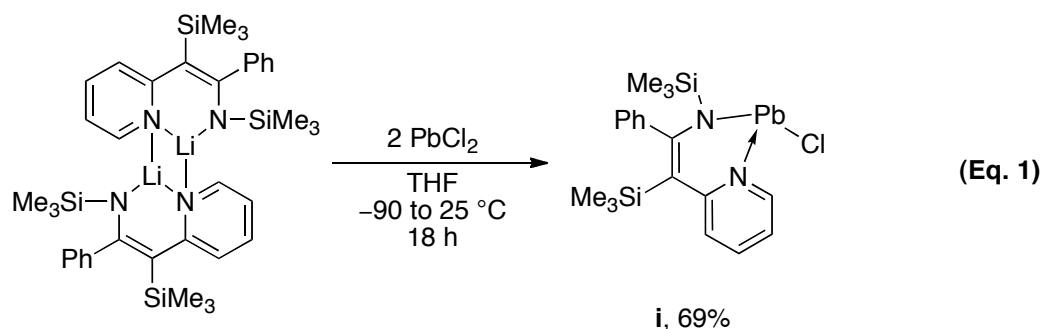
Metallic lead has been used by humans since at least 6500 BC.^[1] It is ideal for applications such as water pipes, coatings and paint.^[2-4] In the modern era, the use of tetraethyllead as an anti-knocking additive in gasoline to improve automotive engine performance and the huge demand for lead-acid batteries led to persistent growth in lead consumption.^[5-6] According to a report published by the United States Geological Survey, more than 8.6 million tones of lead were consumed worldwide in 2008.^[7]

The extensive use of lead gives cause for concern over human health. One of the biggest sources of lead pollution is emission from automotive vehicle exhausts onto roadside soil in the form of lead bromidechloride (PbBrCl).^[5, 8-11] The lead enters into the ecosystem and the food chain, which results in a rise of blood lead levels in human beings.^[2] Lead is mostly accumulated in the skeleton, and is slowly released to other parts of the body.^[12] Since lead can affect the central nervous system, early symptoms of lead poisoning include headaches, restlessness and memory loss. In severe cases, reduced consciousness and death may occur.^[12-13] High concentrations of lead in children may also cause reading disability, hyperactive behaviour, and lower academic achievement.^[14-16] International efforts to introduce unleaded gasoline and tighten controls in lead contamination in food have significantly reduced the average blood lead level to the Centre for Disease Control's recommendation of 10 $\mu\text{g}/\text{dL}$ in the developed world.^[17-18] However, lead pollution remains as a health concern in the developing world. For instance, China has become the centre of the international lead market in the past 15 years.^[19-21]

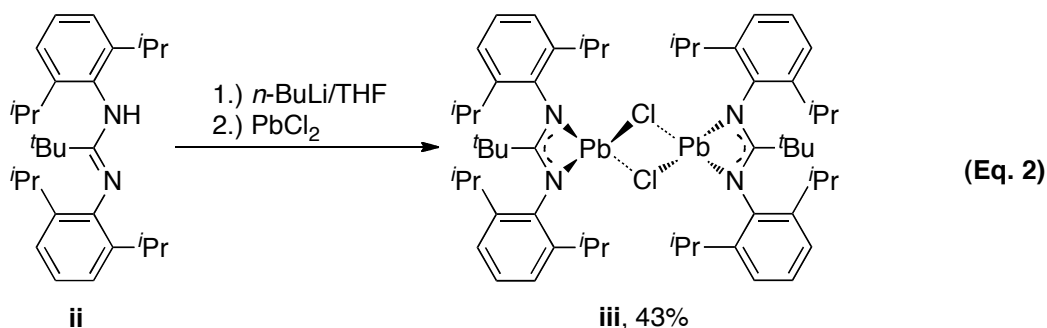
1.2 Low-valent heavy group 14 metal complexes

Since the chemistry of heavy group 14 metals, germanium, tin and lead, is relatively less studied, we decided to investigate the reactivities of some low-valent heavy group 14 metal complexes. Over the years, a lot of effort has been devoted to the search for supporting ligands.^[22-24] As the focus of these studies is on the chemistry of metal-oxygen or -phosphorus bonds, the metal centre needs to be stabilised by a mono-anionic

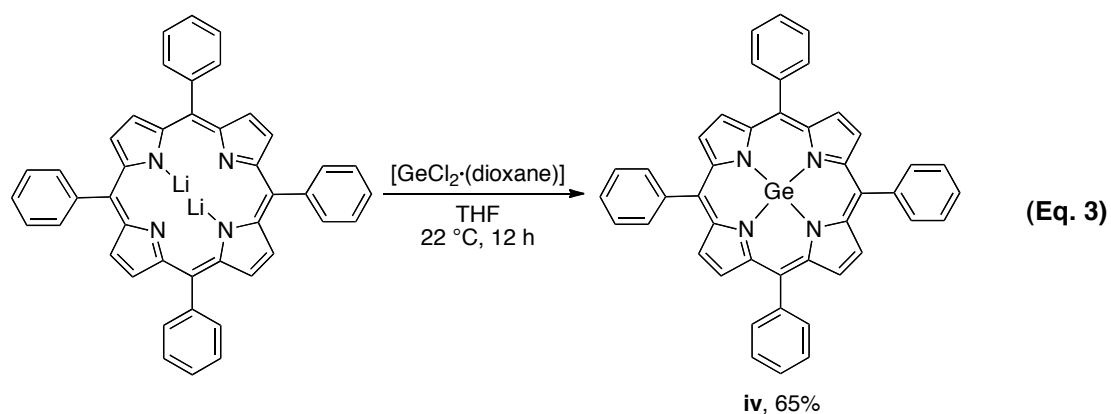
ligand. For example, Leung *et al.* reported the synthesis of a lead(II) complex supported by a pyridyl-1-azaallyl ligand.^[25] Treatment of the pyridyl-1-azaallyllithium compound $[\text{Li}\{\text{N}(\text{SiMe}_3)\text{C}(\text{Ph})\text{C}(\text{SiMe}_3)(\text{C}_5\text{H}_4\text{N}-2)\}]_2$ with two equivalents of lead dichloride gave the lead(II) chloride complex **i** in 69% yield (equation 1).



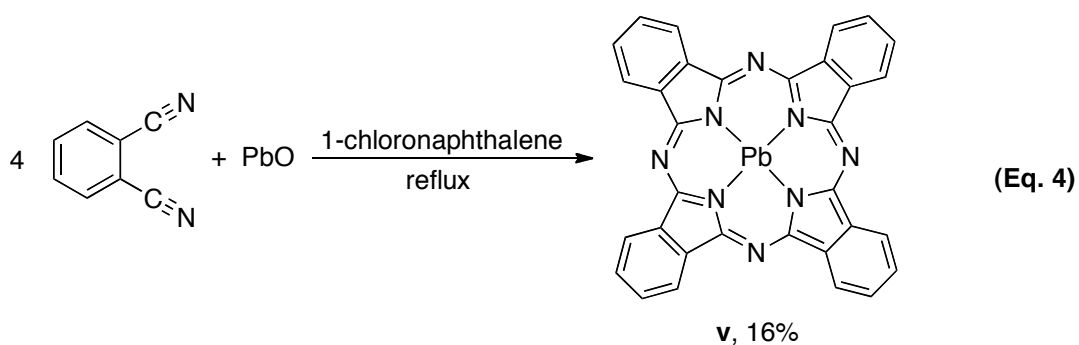
A bulky ligand is also required to protect the heavy group 14 metal ions from dimerisation, oligomerisation, or polymerisation. One example of a dimeric lead(II) complex is illustrated in equation 2.^[26] The amidinato ligand **ii** was lithiated and treated with lead dichloride to form the lead(II) dimer **iii**.



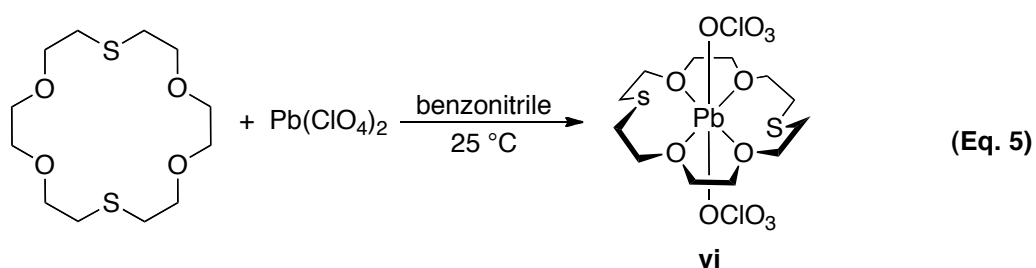
Cyclic ligands have been used extensively in applications such as molecular recognition and catalysis.^[27-29] Vaid *et al.* synthesised the germanium(II) porphyrin complex **iv** in moderate yield by treatment of the lithiated ligand with one equivalent of $[\text{GeCl}_2 \cdot (\text{dioxane})]$ in THF (equation 3).^[30]



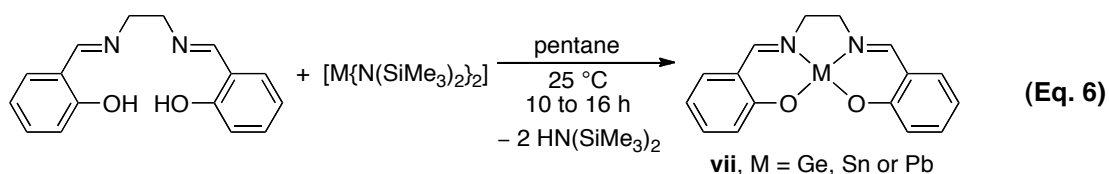
In contrast, the phthalocyanine ligand in the lead(II) compound **v** was generated *in situ* by refluxing four equivalents of phthalonitrile with PbO in the presence of 1-chloronaphthalene to give the lead(II) complex **v** (equation 4).^[31-32]



Other cyclic ligands, such as crown ethers or other multidentate ligands, can be used to stabilise low-valent heavy group 14 metal centres. For example, treatment of $\text{Pb}(\text{ClO}_4)_2$ with 1,10-dithia-18-crown-6 in benzonitrile in a 1:1 ratio gave the lead(II) complex **vi**, which showed a distorted octahedral geometry around the lead atom, with the two $(\text{OCIO}_3)^-$ anions occupying axial positions (equation 5).^[33]

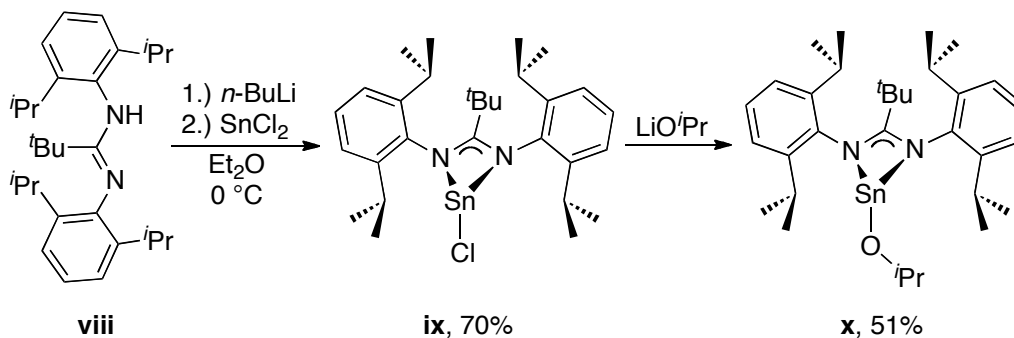


The use of the tetradentate Schiff base salen (*N,N'*-bis(salicylaldehyde)ethylenediamine) ligands has also been explored. Barrau *et al.* synthesised a series of salen complexes with germanium(II), tin(II) or lead(II) ions.^[34] Treatment of H₂salen with the corresponding bis[bis(trimethylsilyl)amino]metal in pentane at room temperature gave the metal complexes **vii** (equation 6). These were stable under dry oxygen in the solid state. Unfortunately, they were insoluble in non-polar or aprotic solvents, which hindered their purification.



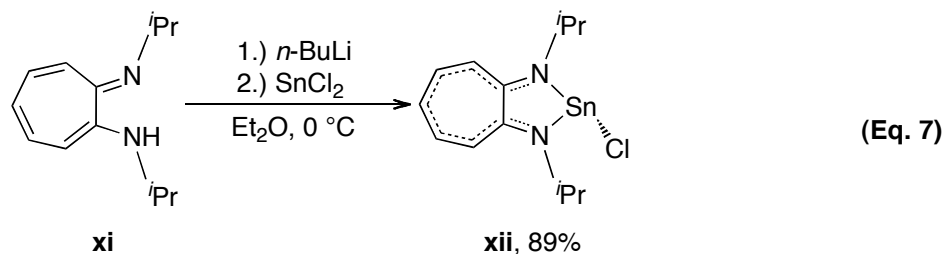
The use of amidinato ligands has been extensively explored in the last 20 years. This type of ligand contains a conjugated π -system and acts as a Lewis base for various metal ions.^[35] Gibson *et al.* synthesised a series of three-coordinate tin(II) complexes supported by an amidinato ligand.^[36] After lithiation of amidine **viii** with *n*-BuLi, the addition of tin dichloride gave the three-coordinate tin(II) chloride complex **ix** in 70 % yield. Reaction of compound **ix** with lithium isopropoxide gave the tin(II) isopropoxide complex **x** (Scheme 1). X-ray crystallography showed that these tin(II) complexes adopted a distorted pyramidal coordination geometry at the metal centre.

Scheme 1. Synthesis of the amidinate tin(II) alkoxide **x**^[36]



A similar conjugated π -system is found in the aminotroponiminato ligand, which contains a delocalised C₇N₂M ring. Synthesis of the tin(II) chloride complex **xii** was achieved by lithiation of the aminotroponimine **xi** with *n*-BuLi, followed by the addition

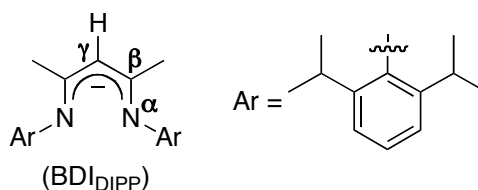
of tin dichloride at 0 °C in diethyl ether (equation 7).^[37] The solid state structure showed an intermolecular Sn···Cl interaction (3.558 Å).



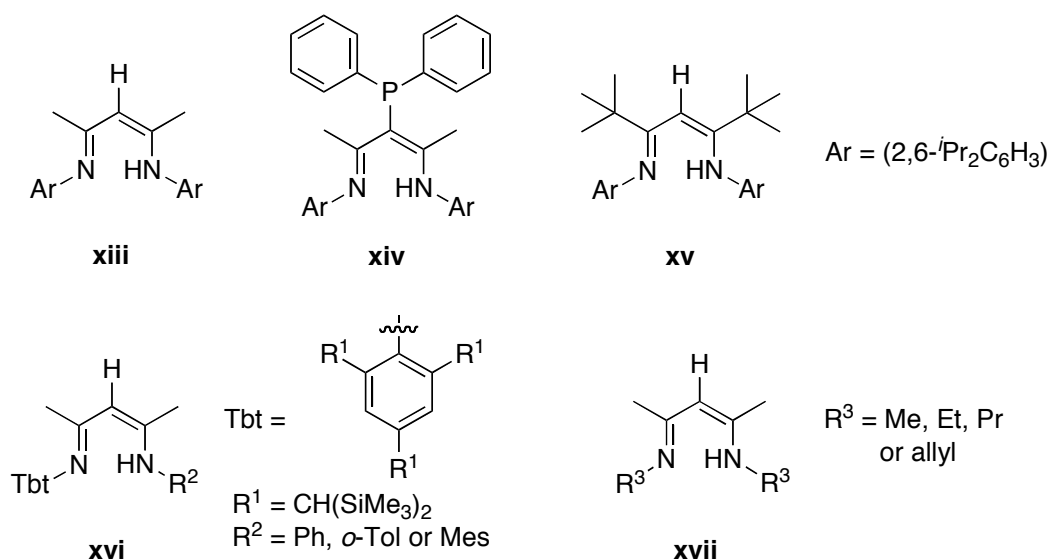
The previous section demonstrates that low-valent heavy group 14 metal complexes can be synthesised. Although the conjugated ligand systems (Scheme 1 and equation 7) can be used for the synthesis of heavy group 14 metal complexes containing terminal alkoxide or phosphanido ligands, they suffer several structural and synthetic drawbacks. First, with amidinato ligands, dimeric metal complexes are commonly obtained. Coles *et al.* suggested that a bulky substituent at the amidinate carbon might prevent dimer formation by forcing the nitrogen substituents towards the metal ion, thus providing additional steric protection for the metal ion.^[38] To the best of our knowledge, no known mono lead(II) amidinato complex has been reported, even with a bulky substituent, such as dicyclohexylamide, on the amidinate carbon.^[26] Secondly, compounds containing the aminotroponiminato ligand are extremely sensitive to air and moisture, suggesting that the highly delocalised heterocyclic ring may not provide enough steric protection for the heavy group 14 metal ion.^[39] No aminotroponiminato lead(II) complex has been reported.

1.3 β -Diketiminato (BDI) ligands

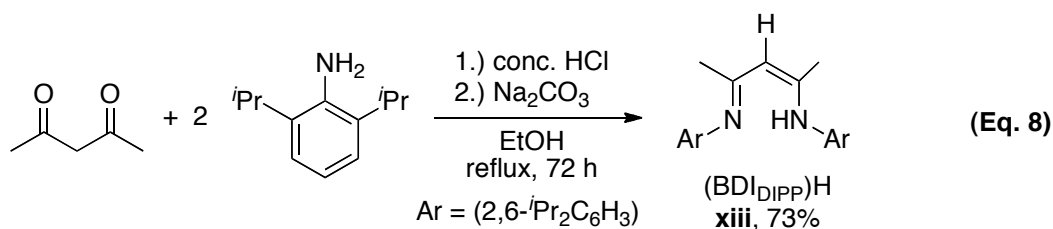
To synthesise heavy group 14 metal complexes with enhanced steric protection and synthetic flexibility, we utilised the bulky β -diketiminato anion $[\text{HC}\{\text{C}(\text{Me})\text{N}(2,6\text{-}i\text{Pr}_2\text{C}_6\text{H}_3)\}_2]^-$ (BDI_{DIPP}), which incorporates two 2,6-diisopropylbenzene groups, to stabilise an array of three-coordinate heavy group 14 metal complexes (Figure 1).^[40]

Figure 1. Structure of β -diketiminate anion $[\text{HC}(\text{C}(\text{Me})\text{N}(2,6\text{-}^i\text{Pr}_2\text{C}_6\text{H}_3))_2]^-$ (BDI_{DIPP})

One of the greatest advantages of the β -diketiminate framework is the ease with which the substituents on the α -nitrogen and β and/or γ carbon atoms may be modified. Thus can be used to fine-tune the structural and/or electronic properties of the β -diketiminate anion. Some examples are given in Figure 2.

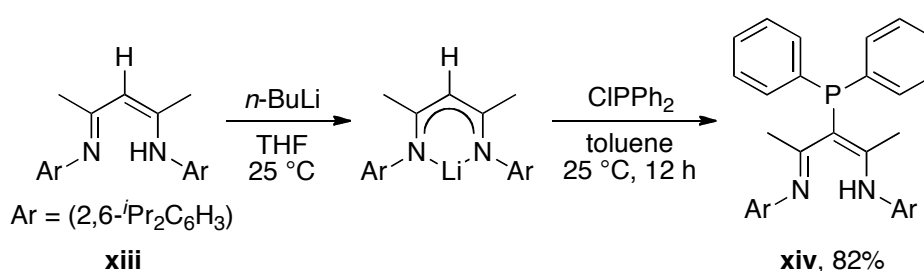
Figure 2. Examples of β -diketimines^[41-45]

The general synthetic route to $(\text{BDI}_{\text{DIPP}})\text{H}$ (**xiii**) is a one-pot reaction involving treatment of 2,4-pentanedione with two equivalents of 2,6-diisopropylaniline in ethanol (equation 8).^[41] Compound **xiii** can be stored under ambient conditions for several months with no sign of decomposition.

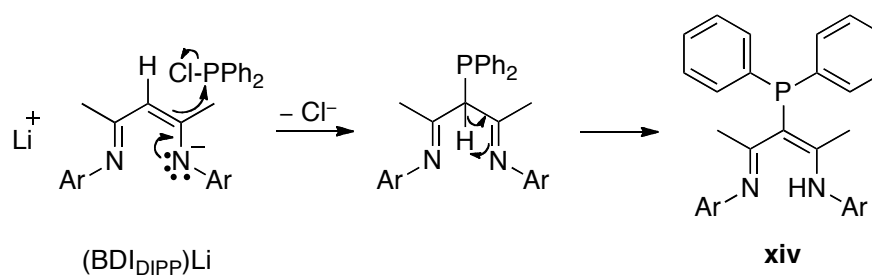


The β -diketimines can also be synthesised in other ways; some are presented here. Treatment of compound **xiii** with *n*-BuLi, followed by the addition of chlorodiphenylphosphine gives the β -diketimine **xiv** (Scheme 2).^[42] Burford *et al.* proposed that the reaction proceeds *via* nucleophilic attack by the C–C π -electrons in the delocalised β -diketiminate ring on the phosphorus atom in chlorodiphenylphosphine. This is followed by a proton migration to give compound **xiv** in 82 % yield (Scheme 3).^[42]

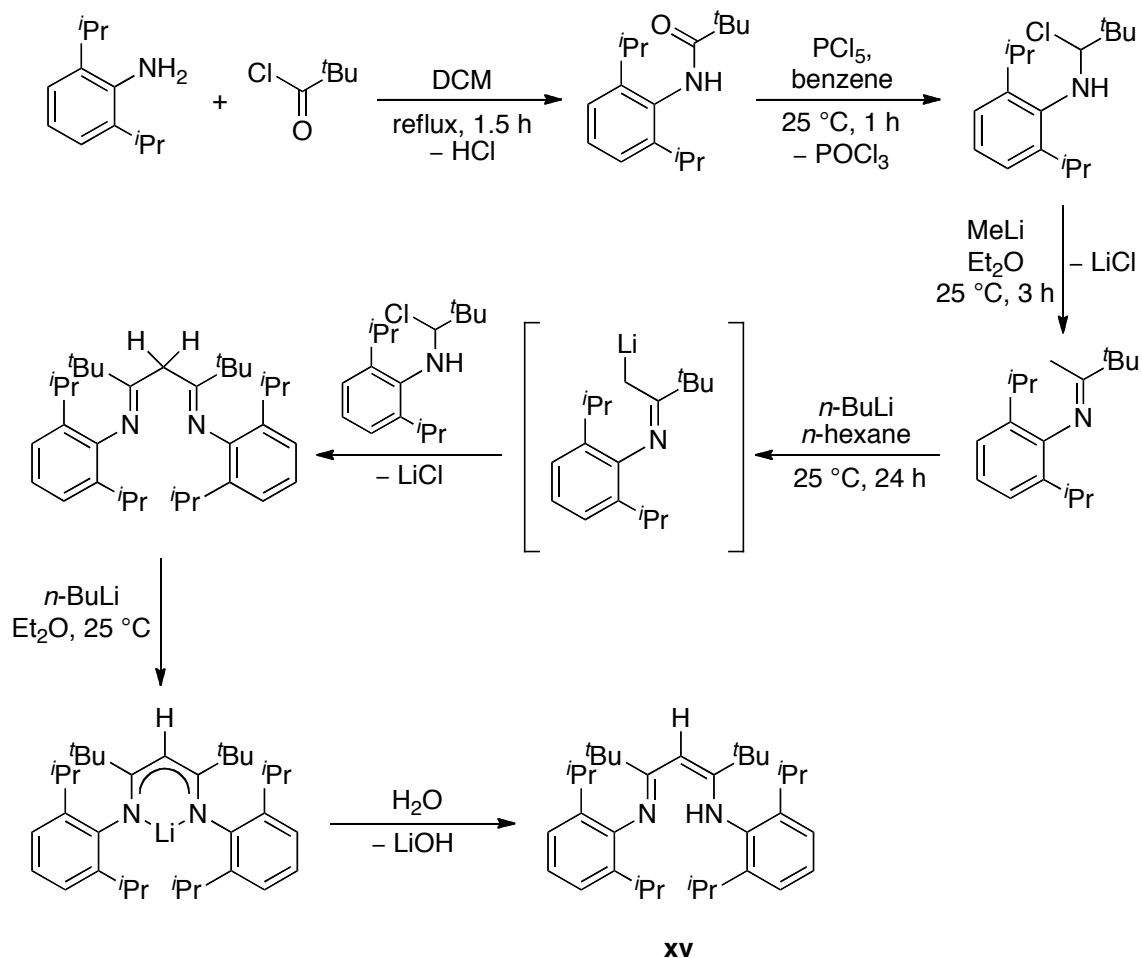
Scheme 2. Synthesis of the β -diketimine **xiv**^[42]



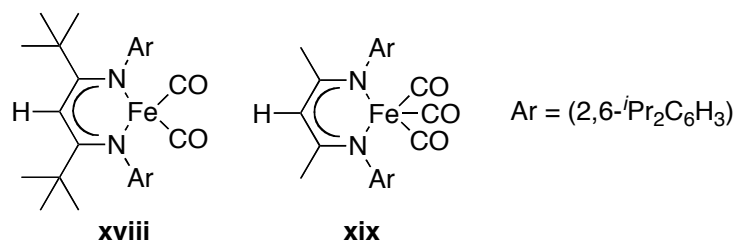
Scheme 3. Proposed mechanism for the formation of β -diketimine **xiv**^[42]



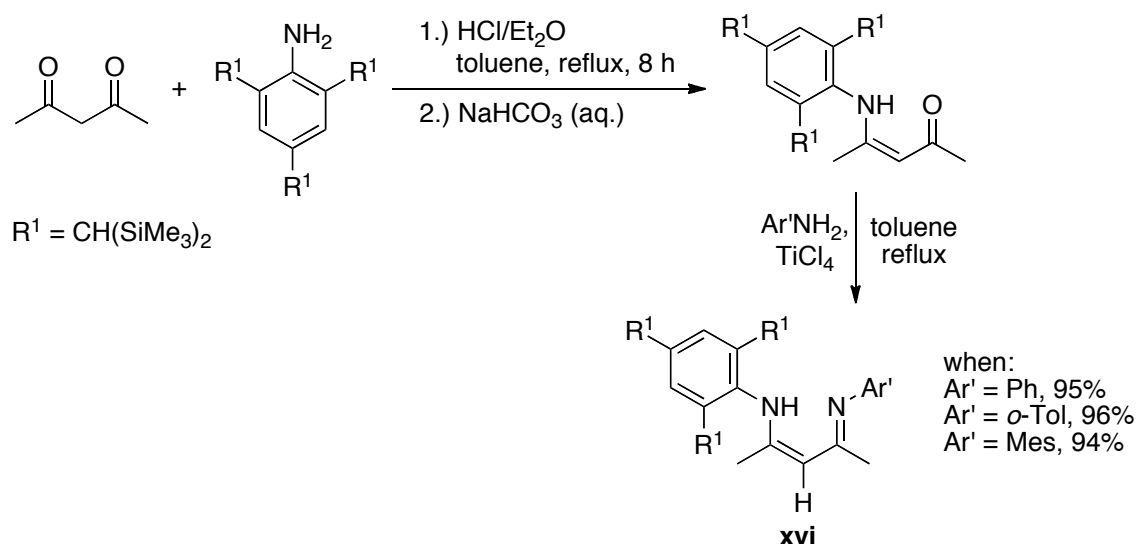
Unlike the one-pot synthesis discussed previously, an alternative stepwise synthetic route may be required when a bulky substituent is present at the β -C atom.^[46] This type of synthetic route can also be used to synthesise asymmetrically substituted diimines. Synthesis of the β -diketimine **xv** is illustrated in Scheme 4.^[43]

Scheme 4. A stepwise synthetic route for the synthesis of compound **xv**^[43]

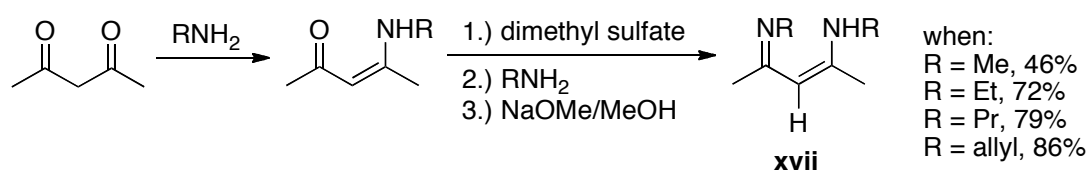
The bulky substituents, such as the *tert*-butyl group in compound **xv**, on the β -C atom force the substituents on the α -N atom towards the metal centre to enhance steric crowding. This effect was demonstrated by Holland *et al.* in their study of low-coordinate iron(I) complexes.^[47] In the presence of an excess of CO, a novel four-coordinate iron(I) complex **xviii** was obtained when a *tert*-butyl group was present at the β -C position, whereas a five-coordinate iron(I) complex **xix** was formed when a methyl group was present (Figure 3).

Figure 3. Iron(I) complexes, **xviii** and **xix**, with different β -diketiminato ligand^[47]

Tokitoh *et al.* developed the use of TiCl₄ as acid catalyst to facilitate the condensation reaction between amines and sterically hindered carbonyl groups (Scheme 5).^[44] The β -diketimine **xvi** was synthesised in near quantitative yield in the final step under reflux.

Scheme 5. Synthesis of the asymmetric β -diketimine **xvi**^[44]

With a less bulky substituent on the α -N atom, an effective and solvent-free synthesis was demonstrated by Bradley *et al.*^[45] The presence of dimethyl sulfate, which acted as a strong electrophile, activated oxygen as the leaving group. As a result, the carbonyl group was converted into an imino group to give the β -diketimine **xvii** (Scheme 6).

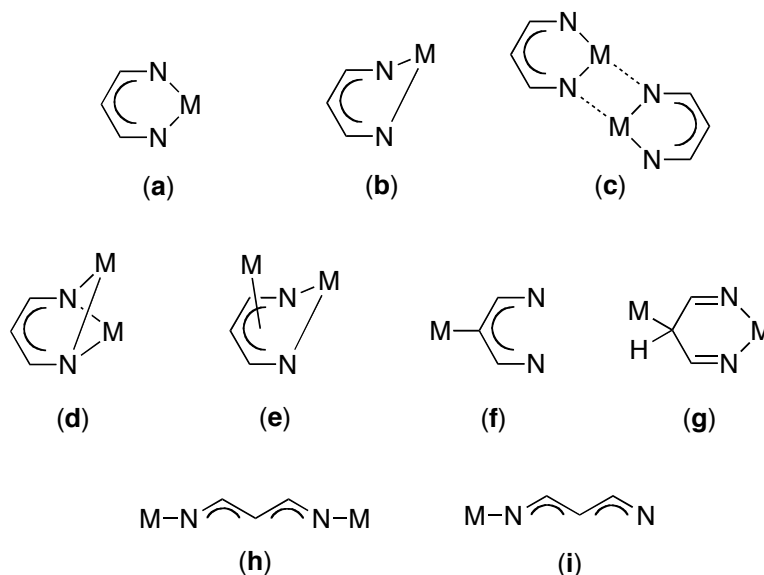
Scheme 6. Synthesis of the β -diketimine **xvii**^[45]

1.4 Examples of β -diketiminatometal complexes. Applications and reactions

The previous section demonstrated that β -diketiminates can be synthesised with functionality to meet a variety of specific requirements. Some important examples are examined.

A review by Lappert *et al.* summarised the various bonding modes observed in metal β -diketiminates (Figure 4).^[48] Mode (a) and (b) are the common binding modes. In mode (c), two metal β -diketiminates form a binuclear complex. Another metal ion can also be coordinated to the two nitrogen atoms in the β -diketiminato backbone as observed in mode (d). In mode (e), there is a π -interaction between a second metal ion and the delocalised NCCCN fragment in the β -diketiminato framework. Alternatively, a metal ion may be bound to the γ -C of the β -diketiminato ring as shown in modes (f) and (g). In modes (h) and (i), the β -diketiminato acts as a terminal ligand in which metal atoms coordinate to nitrogen.

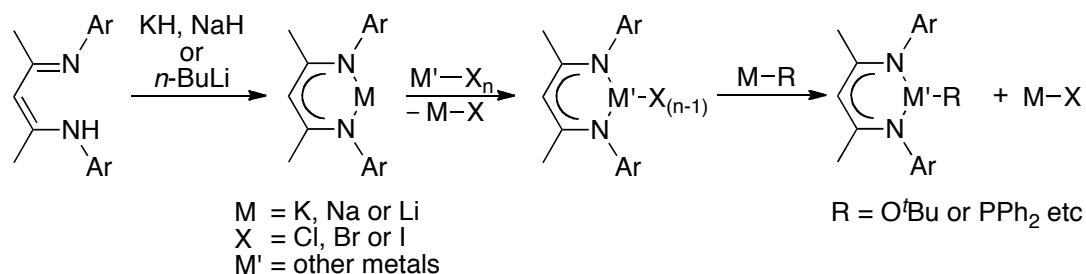
Figure 4. Bonding modes in metal β -diketiminates^[48]



Alkali metal β -diketiminates are important precursors in the synthesis of β -diketiminates of other metals (Scheme 7). For example, alkali metal β -diketiminates can be used as ligand transfer reagents, in the presence of metal precursors such as metal halides.^[48] The β -diketiminatometal halide can react further with various alkali metal

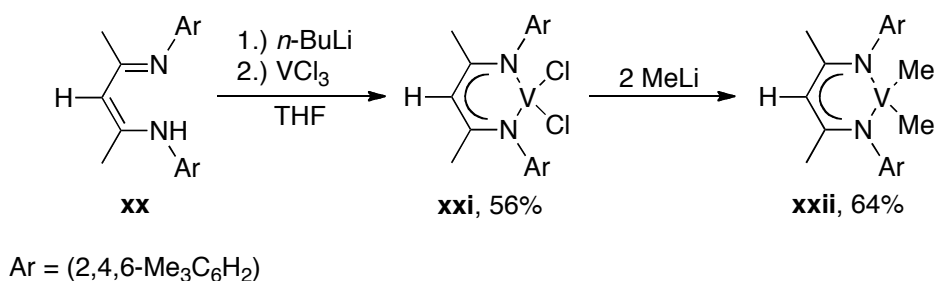
salts, such as potassium *tert*-butoxide or lithium diphenylphosphanide, to attach another functional group to the metal.

Scheme 7. General reaction scheme for the synthesis of metal β -diketiminates

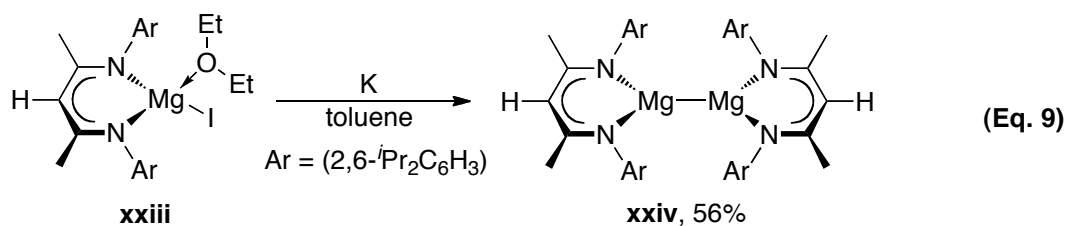


This methodology can be demonstrated by the synthesis of $[\text{HC}\{\text{C}(\text{CH}_3)\text{N}(2,4,6\text{-Me}_3\text{C}_6\text{H}_2)\}_2\text{VMe}_2]$ (**xxii**).^[43] Treatment of the β -diketimine **xx** with *n*-BuLi; followed by the addition of vanadium trichloride gave the vanadium(III) β -diketimate complex **xxi**. Further reaction with two equivalents of methyllithium gave the dimethyl vanadium(III) complex **xxii**.

Scheme 8. Synthesis of the dimethyl vanadium(III) β -diketimate **xxii**^[43]

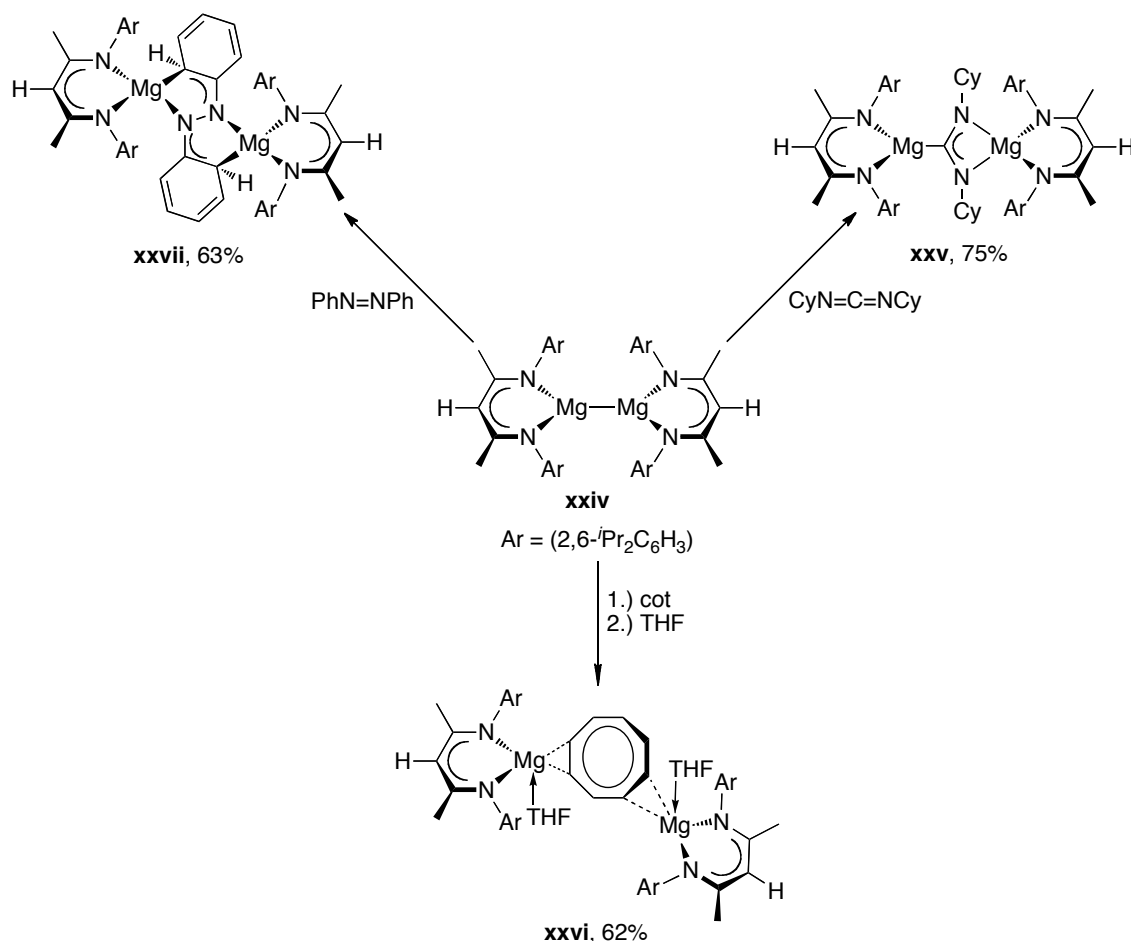


Alkaline earth metals form compounds in which the metal is in oxidation state +2. However, Stasch *et al.* utilised the β -diketiminato ligand to stabilise the Mg_2^{2+} fragment in complex **xxiv**.^[49] The compound $[\text{Mg}(\text{BDI}_{\text{DIPP}})]_2$ (**xxiv**) was generated in 56% yield by treatment of the β -diketiminatomagnesium iodide **xxiii** with potassium metal in toluene (equation 9). An X-ray crystallographic study revealed that the coordination at magnesium centre was planar and a long Mg–Mg bond (2.8457(8) Å) was present.



The reactions of the dimeric magnesium complex **xxiv** were investigated (Scheme 9).^[49-50] The complex **xxiv** doubly reduced the carbodiimide (CyN=C=NCy) to form the complex **xxv**. Similarly, compound **xxiv** reacted with cyclooctatetraene (cot) or azobenzene (PhN=NPh) to form the products, **xxvi** and **xxvii**, respectively.

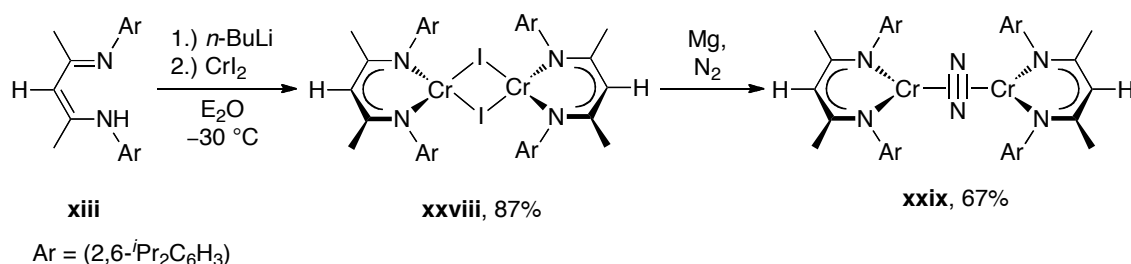
Scheme 9. Reactions of the dimeric β -diketiminatomagnesium complex **xxiv**.^[49-50]



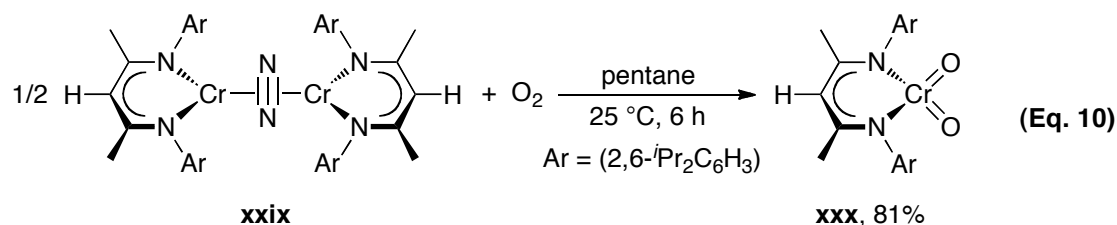
Transition metals supported by β -diketiminato ligands have been extensively explored over the last decade. Theopold *et al.* synthesised the dinuclear chromium(II) iodide [(BDI_{DIPP})Cr(μ -I)]₂ (**xxviii**) by treatment of the β -diketimine **xiii** with *n*-BuLi, followed

by the addition of chromium diiodide.^[51] Further reaction of compound **xxviii** with dry N₂ (1 atm) in the presence of Mg turnings gave [$\{(\text{BDI}_{\text{DIPP}})\text{Cr}\}_2(\mu\text{-N}_2)$] (**xxix**) in good yield (Scheme 10). The compound **xxix** is the only known chromium(I) complex featuring a side-on bonding of N₂.

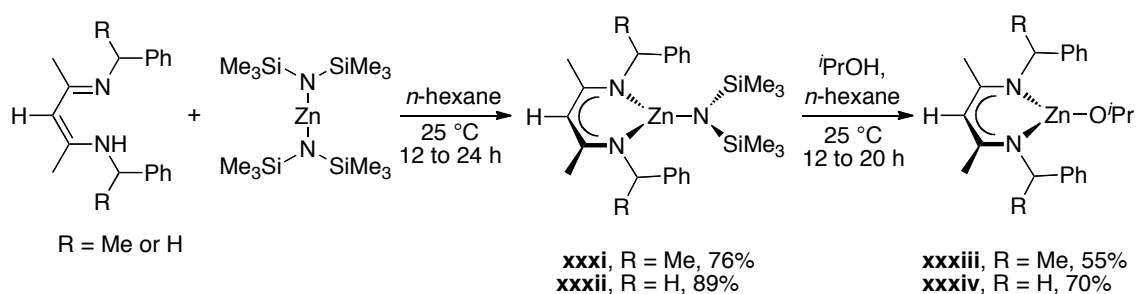
Scheme 10. Synthesis of the chromium(I) β -diketiminato **xxix**^[51]



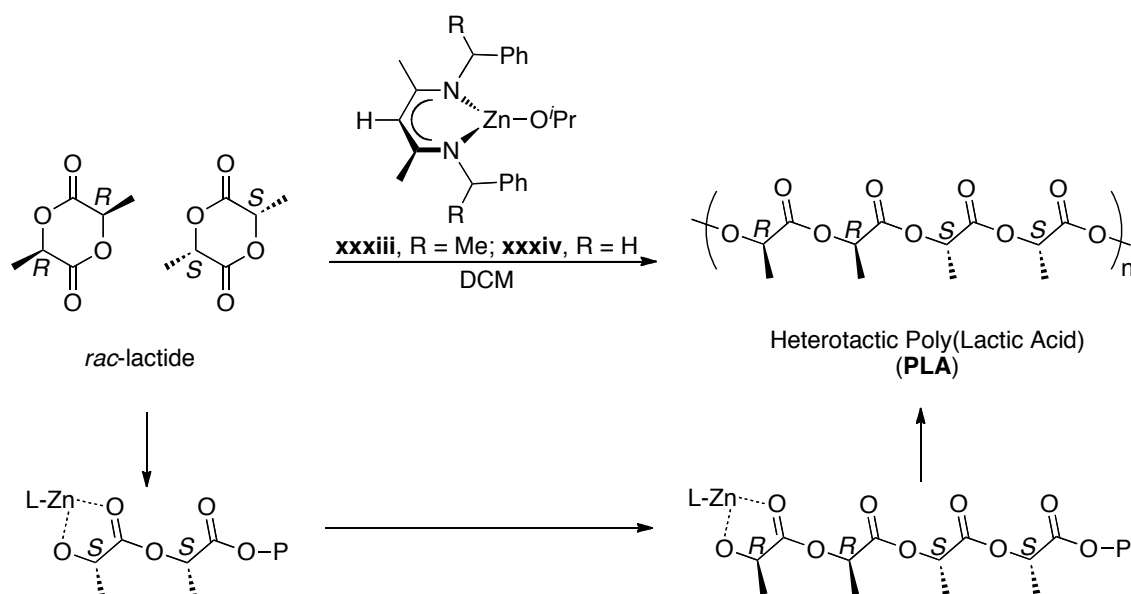
The work on compound **xxix** suggests that the N₂ ligand can be replaced by various π -acids or removed by oxidation. For example, a four-electron oxidative addition of dioxygen to the chromium(I) centre was observed when complex **xxix** was treated with dioxygen to give $[(\text{BDI}_{\text{DIPP}})\text{Cr}(\text{O})_2]$ (**xxx**) in good yield (equation 10).



Recently, Schaper *et al.* reported the use of a chiral zinc(II) β -diketiminato to promote polymerisation of *rac*-lactide to form the polylactide (PLA) (Scheme 12).^[52] The catalysts **xxxiii** and **xxxiv** were synthesised by treatment of the corresponding β -diketiminatozinc(II) amides, **xxxi** and **xxxii**, respectively, with isopropanol (Scheme 11).

Scheme 11. Synthesis of the β -diketiminatozinc(II) isopropoxides **xxxiii** and **xxxiv**^[52]

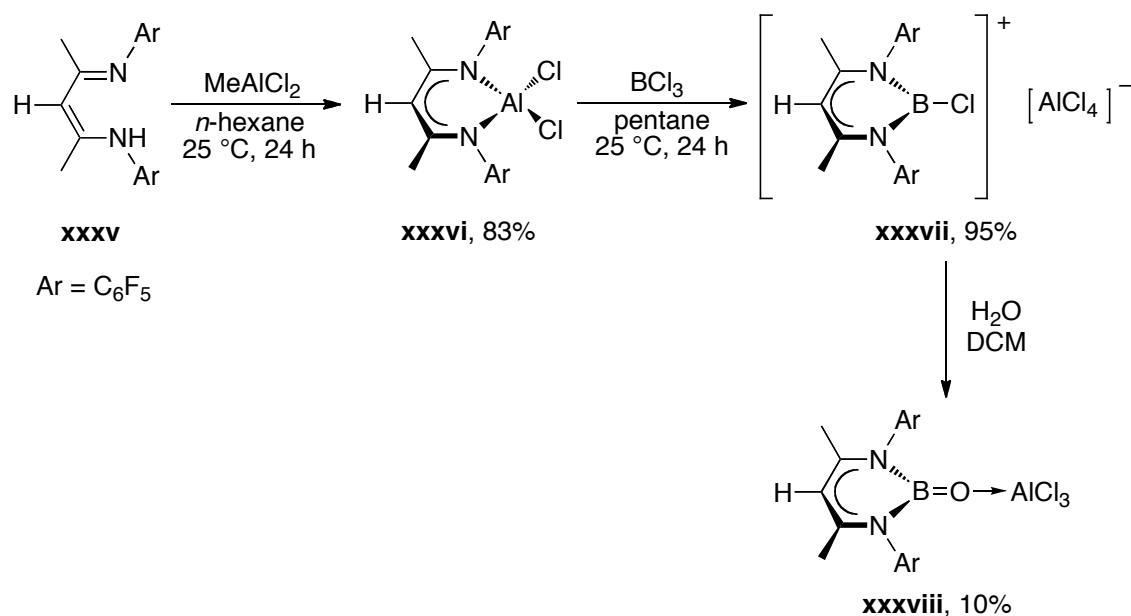
They are active initiators in the polymerisation of *rac*-lactide in dichloromethane (DCM). Both complexes demonstrated a strong preference for inserting *RR*- and *SS*-enantiomers in an alternating manner to form heterotactic PLA as the major product (Scheme 12).^[52-53]

Scheme 12. Polymerisation of *rac*-lactide to form heterotactic PLA with the β -diketiminatozinc(II) isopropoxides **xxxiii** and **xxxiv**^[52-53]

β -Diketiminato ligands have also been used to support the p-block main group elements. As heavy group 14 metal β -diketiminates will be examined in detail in subsequent chapters, our focus here will be on group 13 and 15 compounds. Recently, Cowley *et al.* reported the first synthesis of an oxoborane *via* an ion exchange reaction.^[54] Treatment of β -diketimine **xxxv** with MeAlCl_2 gave the aluminium(III) dichloride complex **xxxvi** in good yield. Further treatment with BCl_3 gave the salt $[\text{HC}\{\text{C}(\text{Me})\text{N}(\text{C}_6\text{F}_5)\}_2\text{BCl}]^+[\text{AlCl}_4]^-$ (**xxxvii**) in almost quantitative yield. Further

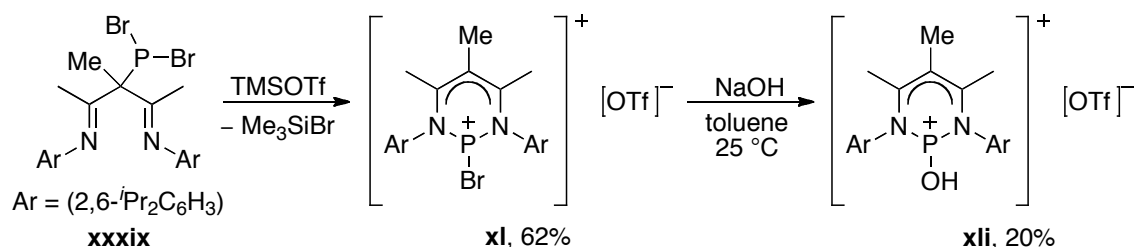
reaction with one equivalent of H₂O gave the AlCl₃ adduct of the oxoborane **xxxviii** (Scheme 13).

Scheme 13. Synthesis of the oxoborane β -diketiminato **xxxviii**^[54]



Cowley *et al.* also reported the β -diketiminatophosphenium salts **xl** and **xli**.^[55] The reaction between compound **xxxix** and trimethylsilyl triflate (TMSOTf) resulted in Me₃SiBr elimination to give the boromophosphenium salt **xl** (Scheme 14). The ³¹P{¹H} NMR spectrum of **xl** showed a singlet at δ_P 102.2 ppm. X-ray crystallographic study showed that the geometry at phosphorus was pyramidal. Treatment of compound **xl** with NaOH in toluene gave the hydroxyphosphenium salt **xli** (Scheme 14).^[56]

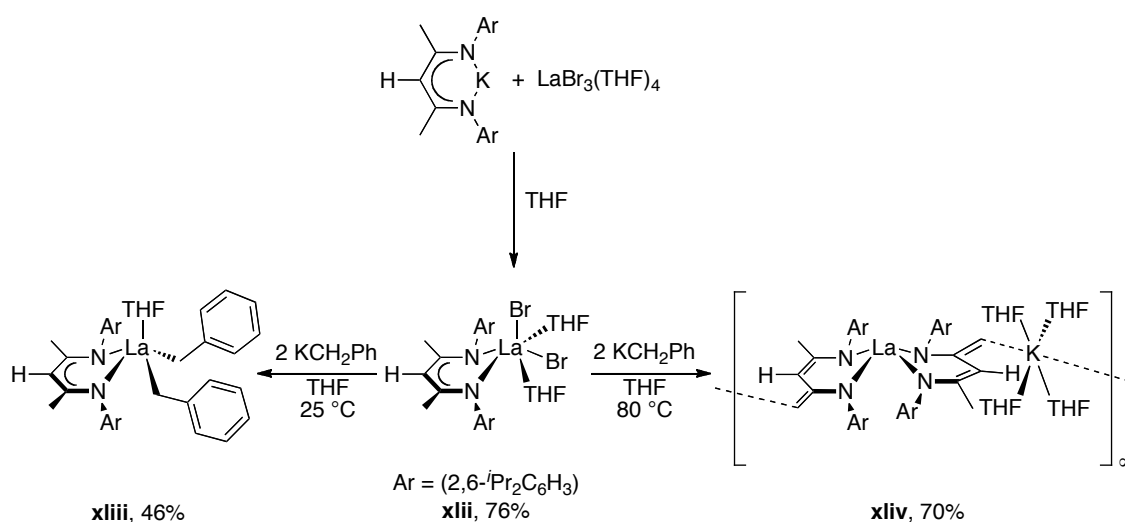
Scheme 14. Synthesis of the hydroxyphosphenium salt **xli**^[56]



The β -diketiminato ligand has also been used in lanthanide chemistry. Hessen *et al.* synthesised the β -diketiminatolanthanum(III) dibromide **xlii** by treatment of the potassium β -diketiminato with LaBr₃(THF)₄ (Scheme 15).^[57] Further reaction of

compound **xlii** with two equivalents of KCH_2Ph at room temperature led to dibenzyl β -diketiminatolanthanum(III) **xliii** in 46% yield. However, when the latter reaction was performed at 80°C , a coordination polymer of $\{[\mu\text{-}\eta^2\text{:}\eta^1\text{-ArNC(Me)CHC(CH}_2\text{)NAr}]_2\text{La}[\text{K}(\text{THF})_4]\}_\infty$ (**xliv**, $\text{Ar} = (2,6\text{-}^i\text{Pr}_2\text{C}_6\text{H}_3)$) was observed. The authors suggested that the formation of compound **xliv** could be explained by deprotonation of the methyl substituents in the NCCCN ring of **xliii** by the benzyl groups attached to the lanthanum.

Scheme 15. Synthesis and reactions of the lanthanum(III) dibromide complex **xlii**^[57]



In summary, β -diketiminato ligands have been used extensively in supporting various metal ions. The sterically bulky and electron-rich properties of the β -diketiminato ligands have enabled chemists to probe unusual oxidation states, rare coordination environments, and reactivities towards small molecules.

1.5 β -Diketiminato heavy group 14 metal complexes

Before discussion of heavy group 14 metal β -diketiminates, some general comments on the elements are necessary. Divalent lead has an electronic configuration of $[\text{Xe}]4f^{14}5d^{10}6s^2$. The electrons in the 6s orbital do not hybridise with those of the 6p orbital to a significant extent due to relativistic contraction and energetic stabilisation of the 6s orbital.^[58] Hence, the pair of electrons in the lead(II) ion remains in the 6s orbital and is described as “inert”.^[1, 59-60] The amount of 6s and 6p orbital mixing can be calculated.^[61-63] The NBO analysis performed by our group to investigate the

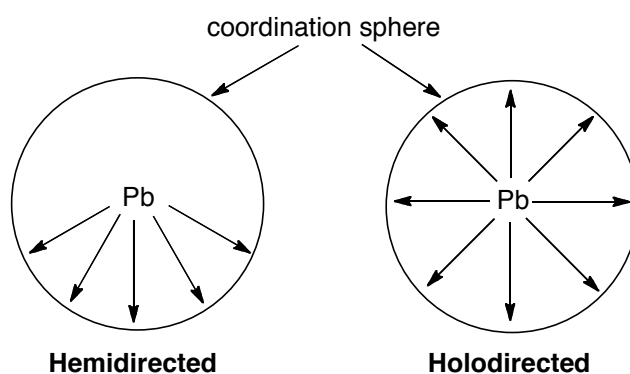
hybridisation of the heavy group 14 metal lone pair in the compounds [(BDI_{DIPP})MCl] (M = Ge, Sn or Pb) suggests that the lone pair has an s-character ranging from 82–92% with the corresponding p-contribution between 8–18% (Table 1).^[62] The metal lone pair is present in hybridised orbitals ($sp^{0.23}$ for Ge, $sp^{0.16}$ for Sn and $sp^{0.09}$ for Pb).

Table 1. NBO analysis of M(II) ion in LMCl (L = (BDI_{DIPP}); M = Ge, Sn or Pb)^[62]

	Natural electron configuration	Lone pair NBO on M	Hybridisation
LGeCl	Ge: 4s(1.68) 4p(1.23) 5p(0.01)	s[81.58%] p 0.23 [18.42%]	$sp^{0.23}$
LSnCl	Sn: 5s(1.75) 5p(0.98)	s[86.09%] p 0.16 [13.91%]	$sp^{0.16}$
LPbCl	Pb: 6s(1.85) 6p(0.86) 7p(0.01)	s[91.79%] p 0.09 [8.21%]	$sp^{0.09}$

The directionality of this lone pair of electrons has been debated over the years. Glusker *et al.* examined the effect of this lone pair of electrons on the geometry of the ligands coordination around the lead(II) centre.^[61] They divided the structures of lead(II) complexes into two categories, namely *hemidirected*, where the ligands coordinate only at one side of the lead(II) ion; or *holodirected*, where the ligands coordinate anywhere around the lead(II) ion (Figure 5).

Figure 5. Hemidirected and holodirected coordination modes in lead(II) complexes^[61]

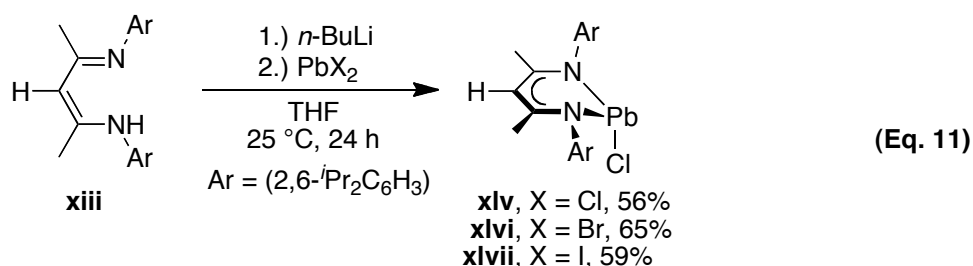


The coordination at a lead(II) centre may also be described by the coordination number. Glusker *et al.* suggested that in the hemidirected case, the coordination number is < 6 , whereas in the case of holodirected coordination, a higher coordination number (> 8) is

required.^[61, 64] In this classification, β -diketiminatolead(II) complexes with coordination number 3 are hemidirected with the lone pair of electrons in the 6s orbital playing little part in the bonding.

β -Diketiminato ligands have been used to support the heavy group 14 metal centres, germanium, tin and lead, in their +2 oxidation state. Since complexes containing terminal alkoxide or phosphanido ligands will be examined in subsequent chapters, other examples, such as β -diketiminato heavy group 14 metal amide or alkyl complexes, will be illustrated in this section.

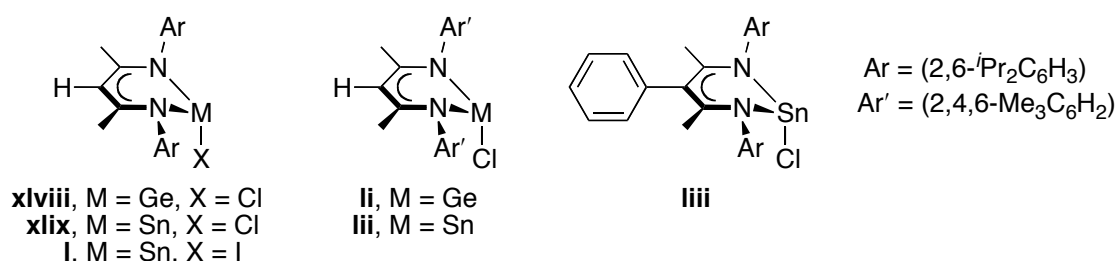
β -Diketiminato heavy group 14 metal halides are one of the key precursors for the synthesis of other novel heavy group 14 metal complexes. Our group synthesised the first three-coordinate β -diketiminatolead(II) halides **xliv**–**xlvi** (equation 11).^[62] Treatment of β -diketimine **xiii** with *n*-BuLi generated [(BDI_{DIPP})Li]. Addition of the corresponding lead dihalide gave [(BDI_{DIPP})PbX] (**xliv**, X = Cl, **xlvi**, X = Br and **xlvi**, X = I) in good yields. The ¹H NMR spectra of these complexes revealed two important signatures: the singlet ($\delta_{\text{H}} \sim 4.9$ ppm) assigned to the γ -CH, and two septets ($\delta_{\text{H}} \sim 3.0$ – 4.0 ppm) assigned to the tertiary protons in the isopropyl group (CHMe₂) of the *N*-aryl substituents in the β -diketimate ring. All the β -diketiminatolead(II) halides adopted a pyramidal geometry around the metal centre as shown by solid state structure determinations.



Other β -diketiminato heavy group 14 metal halides were synthesised using a similar synthetic methodology. Some examples are illustrated in Figure 6.^[65-69] Roesky and Power synthesised various β -diketiminatogermanium(II) and -tin(II) halides **xlvi**–**l**.^[65-67] Other examples of germanium(II) and tin(II) halide complexes containing various β -diketiminato ligands, are also known. For instance, Dias *et al.* reported the use of $[\text{HC}\{\text{C}(\text{Me})\text{N}(2,4,6\text{-Me}_3\text{C}_6\text{H}_2)\}_2]^-$ to stabilise the germanium(II) and tin(II) chloride

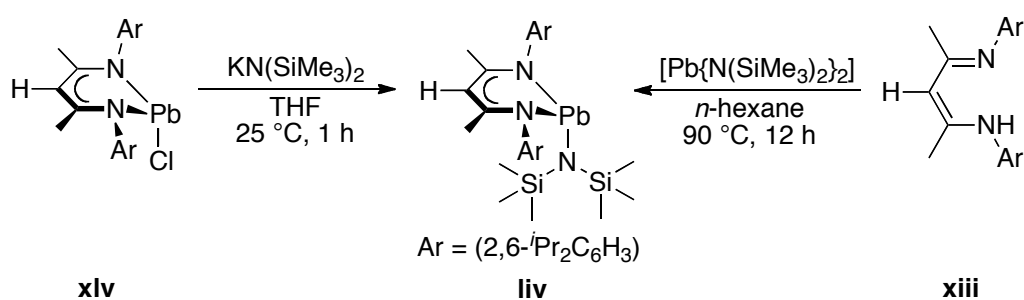
complexes, **li** and **lii**, and Lappert *et al.* synthesised the tin(II) chloride complex **liii** containing a phenyl group on the γ -C in the β -diketiminato backbone.^[68-69]

Figure 6. Examples of β -diketiminato heavy group 14 metal halides **xlviii–liii**^[65-69]

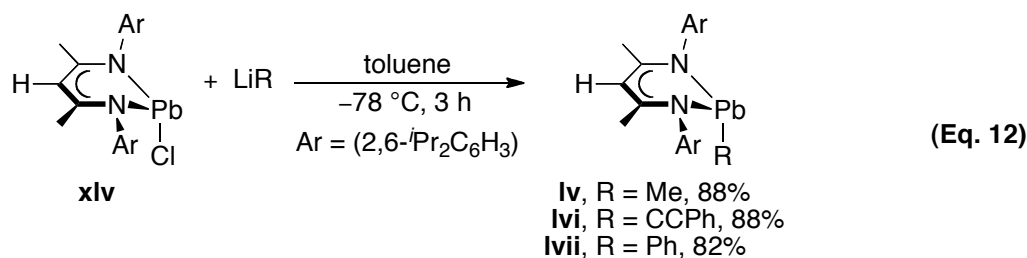


The metal-halide bond in these β -diketiminato heavy group 14 metal compounds can be further functionalised by treatment with various alkali metal salts, such as potassium alkoxide or lithium phosphanide. For example, our group reported the synthesis of β -diketiminatolead(II) amide **liv**.^[62] Treatment of the lead(II) chloride **xlv** with one equivalent of KN(SiMe₃)₂ at room temperature gave [(BDI_{DIPP})PbN(SiMe₃)₂] (**liv**) (Scheme 16). Alternatively, this compound could be obtained when the β -diketimine **xliii** was treated directly with [Pb{N(SiMe₃)₂}₂] under reflux in *n*-hexane.

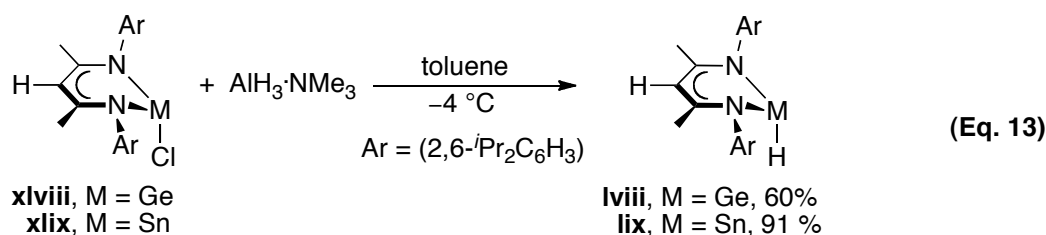
Scheme 16. Synthesis of the β -diketiminatolead(II) amide **liv**^[62]



Several β -diketiminatolead(II) alkyls were synthesised by a similar synthetic strategy.^[70] Treatment of the β -diketiminatolead(II) chloride **xlv** with the appropriate lithium alkyl at -78 °C gave the β -diketiminatolead(II) alkyls **lv–lvii** in good yields (equation 12). Compounds **lv** and **lvi** were sensitive to air and moisture; however complex **lvii** could be exposed to air for a short time without decomposition.

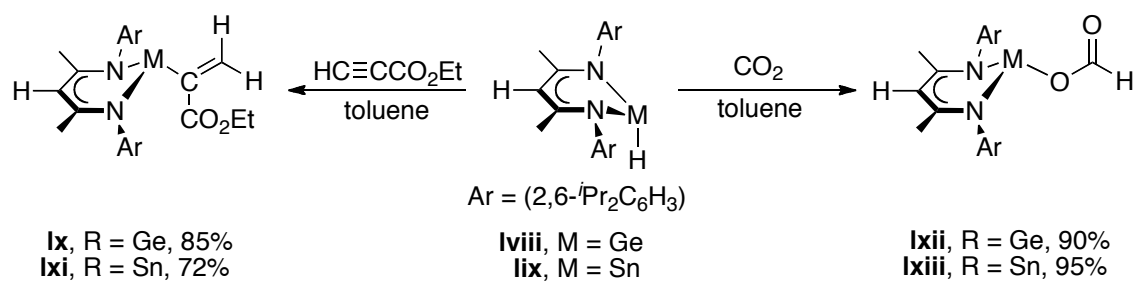


β -Diketiminatogermanium(II) and -tin(II) hydrides **lviii** and **lix** were recently reported by Roesky *et al.*^[71] Treatment of the β -diketiminatogermanium(II) or -tin(II) chlorides, **xlvi** or **xlvii**, with $\text{AlH}_3 \cdot \text{NMe}_3$ gave the corresponding β -diketiminatogermanium(II) and -tin(II) hydrides **lviii** and **lix** in good yields (equation 13). The germanium(II) hydride **lviii** was stable at room temperature, whereas the tin(II) hydride **lix** must be stored at low temperature. In the ^1H NMR spectra, the hydride proton resonances were at δ_{H} 8.08 and 13.83 ppm for compounds **lviii** and **lix**, respectively. The β -diketiminatolead(II) hydride has not yet been reported.



The reactions between the germanium(II) or tin(II) hydrides, **lviii** or **lix**, and alkynes resulted in a 1,2-proton transfer from the terminal hydride to the carbon-carbon triple bond to give compounds **lx** and **lxi** (Scheme 17).^[72-75] The reactions between the metal hydride complexes and carbon dioxide were also reported. Treatment of compounds **lviii** or **lix** with carbon dioxide gave the β -diketiminato heavy group 14 metal formates, **lxii** or **lxiii**, in good yields.^[75]

Scheme 17. Reactions between the β -diketiminatogermanium(II) or -tin(II) hydrides, **Iviii–lix**, and unsaturated molecules^[72-75]



β -Diketiminato heavy group 14 metal complexes with terminal alkoxide or phosphanido ligands will be discussed in subsequent chapters.

2. Lead(II) alkoxide complexes and their reactivities

2.1 Chapter remarks

This chapter describes a concurrent work by the author (ECYT), Dr. Nicholas C. Johnstone (NCJ) and Dr. Lorenzo Ferro (LF) on the synthesis and reactions of the β -diketiminatolead(II) alkoxides **3** and **4**. To indicate the overlap between the collaborators, the primary investigator of each reaction is indicated in Table 2. The experimental results will be discussed in detail.

Table 2. Summary of the reactions reported in Chapter 2 and the associated primary investigator (Legend: NCJ, Dr. Nick C. Johnstone; LF, Dr. Lorenzo Ferro and ECYT, Eric C.Y. Tam)

Pg.	Caption	Reactions/Compounds	Primary Investigator
42	Scheme 30	<p>1 $\xrightarrow[25\text{ }^\circ\text{C, 45 min}]{n\text{-BuLi, THF}}$ $\xrightarrow[25\text{ }^\circ\text{C, 20 h}]{\text{PbCl}_2}$ 2, 79%</p> <p>Ar = (2,6-$\text{Pr}_2\text{C}_6\text{H}_3$)</p>	NCJ
42	Figure 9	<p>3 4 Ar = (2,6-$\text{Pr}_2\text{C}_6\text{H}_3$)</p>	NCJ
43	Scheme 31	<p>6, R² = Me 7, R² = Et 8, R² = CH₂CHCH₂</p> <p>2 $\xrightarrow[25\text{ }^\circ\text{C, 20 h}]{\text{NaOR}^2}$ 6, 7, 8</p> <p>2 $\xrightarrow[25\text{ }^\circ\text{C, 20 h}]{\text{NaOR}^1}$ 5, R¹ = C(CH₃)₂CH=CH₂, 87%</p> <p>Ar = (2,6-$\text{Pr}_2\text{C}_6\text{H}_3$)</p>	ECYT
46	Eq. 32	<p>3, R = Pr 4, R = tBu</p> <p>Ar = (2,6-$\text{Pr}_2\text{C}_6\text{H}_3$) 9</p>	ECYT
46	Eq. 33	<p>3 or 4 C₆D₆ $\xrightarrow[25\text{ to }40\text{ }^\circ\text{C, 3 days}]{} \text{Product}$</p>	ECYT

Pg.	Caption	Reactions/Compounds	Primary Investigator
47	Eq. 34	<p> $\text{3, R} = \textit{i}\text{Pr}$ $\text{4, R} = \textit{t}\text{Bu}$ </p>	ECYT
47	Eq. 35	<p> 4 11, 41\% 12 </p>	ECYT
48	Eq. 36	<p> 4 $\text{Ar} = (2,6\text{-}^i\text{Pr}_2\text{C}_6\text{H}_3)$ $\text{X} = \text{Br or Cl}$ </p>	ECYT
48	Eq. 37	<p> 4 13, 60\% </p>	ECYT
52	Scheme 32	<p> $\text{4, R} = \textit{i}\text{Bu}$ </p>	ECYT
53	Eq. 38	<p> $\text{3, R} = \textit{i}\text{Pr}$ $\text{14, R} = \textit{i}\text{Pr}$ </p>	NCJ

Pg.	Caption	Reactions/Compounds	Primary Investigator
53	Eq. 38	<p>4, R = ^tBu</p> <p>Ar = (2,6-ⁱPr₂C₆H₃)</p> <p>15, R = ^tBu</p>	ECYT
55	Scheme 33	<p>3, R = ⁱPr</p> <p>Ar = (2,6-ⁱPr₂C₆H₃)</p> <p>14, R = ⁱPr</p> <p>16, R = ⁱPr</p>	NCJ
55	Scheme 33	<p>4, R = ^tBu</p> <p>Ar = (2,6-ⁱPr₂C₆H₃)</p> <p>15, R = ^tBu</p> <p>17, R = ^tBu</p>	ECYT
56	Eq. 39	<p>15</p> <p>3</p> <p>14</p> <p>4</p> <p>Ar = (2,6-ⁱPr₂C₆H₃)</p> <p>L = (BDI)_{DIPP}</p>	ECYT
57	Scheme 34	<p>3</p> <p>14</p> <p>18</p> <p>Ar = (2,6-ⁱPr₂C₆H₃)</p>	ECYT
57	Scheme 35	<p>R = ⁱPr or ^tBu</p> <p>Ar = (2,6-ⁱPr₂C₆H₃)</p> <p>R = ^tBu</p>	ECYT
57	Scheme 35	<p>Ar = (2,6-ⁱPr₂C₆H₃)</p> <p>18, R = ⁱPr, 53%* (* work by NCJ)</p>	NCJ

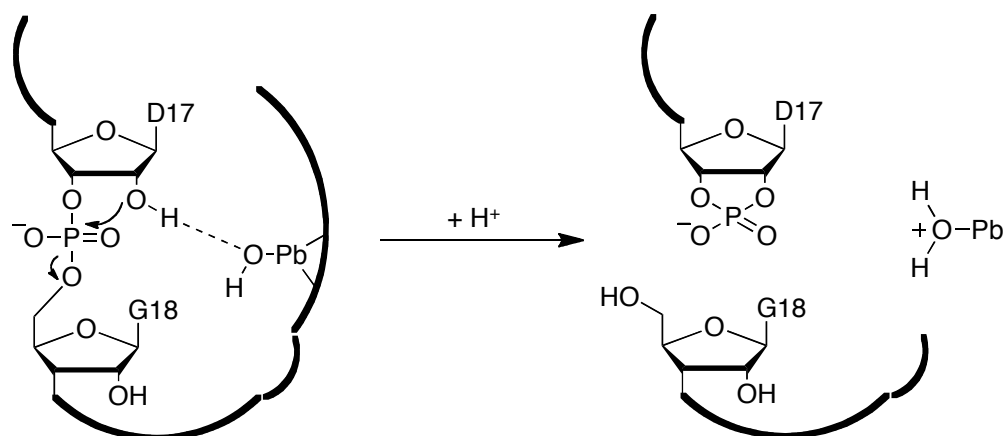
2.2 Introduction

2.2.1 Lead(II)-induced hydrolysis of RNA

Although the chemistry of transition metal alkoxide complexes has been extensively explored, the reactivities of lead(II) analogues have been less well studied. As mobile lead(II) compounds have deleterious effects on human health due to the lead(II)-induced cleavage of RNA, the biological system is briefly discussed.

Generally, RNA cleavage occurs in loops or bulges, presumably allowing the lead to coordinate to one strand in order to access and cleave the opposite strand.^[76] Klug *et al.* proposed a mechanistic pathway for lead(II)-induced hydrolytic cleavage of the sugar-phosphate in yeast phenylalanine RNA (Scheme 18).^[77] In this system, the major cleavage site is between residues D17 and G18. Initially, a lead(II)-hydroxide deprotonates the proximal 2'-OH of ribose D17 in the backbone. The deprotonated alcohol then undergoes an intramolecular nucleophilic attack at the phosphate in residue G18, resulting in cleavage between the residues D17 and G18.^[78]

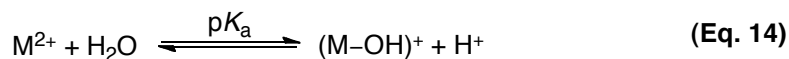
Scheme 18. Proposed mechanism of the lead(II)-induced hydrolytic cleavage of RNA^[77-78]



Other metal ions, including manganese(II), cobalt(II), or zinc(II), have exhibited similar reactivity.^[79-80] However, Farakas *et al.* showed that lead(II) ion is far more efficient in inducing cleavage, in terms of reaction time, than other metal ions.^[80] This may attribute to the low pK_a value of hydrated lead(II) in aqueous solution ($pK_a = 7.71$, equation 14).^[81] In contrast to the other hydrated metal ions which have higher pK_a

values, significant concentration of $(\text{Pb-OH})^+$ can be formed at physiological pH (Table 3).^[82]

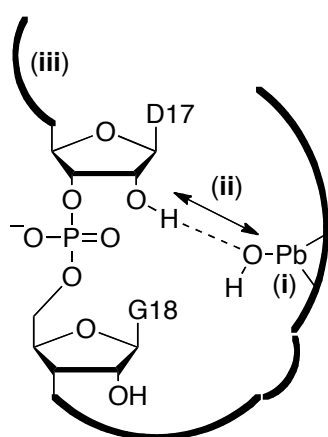
Table 3. Selected acid dissociation constants (pK_a) of hydrated metal ions^[82]



M^{2+}	pK_a
Pb^{2+}	7.71
Zn^{2+}	8.96
Co^{2+}	10.20
Mn^{2+}	10.59

There are two other aspects which contribute to the lead(II)-induced hydrolysis of RNA (Figure 7).^[77, 82] First, the lead(II)-bonded hydroxyl group is in a favourable orientation at approximately 6 Å from the proximal 2'-OH group in the D17 residue. Secondly, the region around the D17 residue is sufficiently flexible to allow the reacting atom to adopt a favourable orientation.^[83]

Figure 7. Key features which encourage the lead(II)-induced hydrolytic of RNA^[77, 82-83]



Legend:

- (i): Lead(II) has $pK_a = 7.71$, which leads to the formation of $\text{Pb}^{2+}\text{-OH}$ at neutral pH
- (ii): $\text{Pb-O}\cdots\text{H-O}$ distance (ca. 6.0 Å) is short enough for the deprotonation to occur
- (iii): The flexibility of the region around D17 residue allows it to adopt a favourable orientation for the reaction to occur

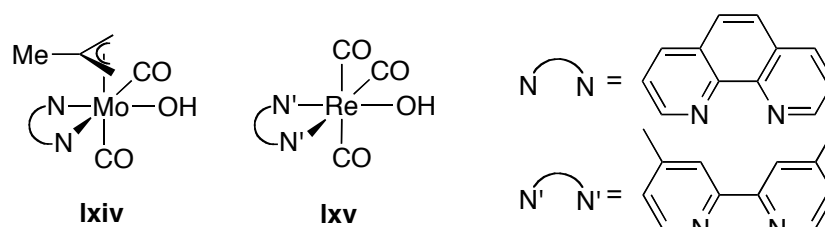
From a biological perspective, lead(II) hydroxides are important intermediates. However, only biochemical mechanistic studies have been performed on the lead(II)-induced RNA hydrolysis; molecular studies on the lead(II) hydroxide complexes have not been made. Hence, there is limited knowledge on the actual reactivity of lead(II)

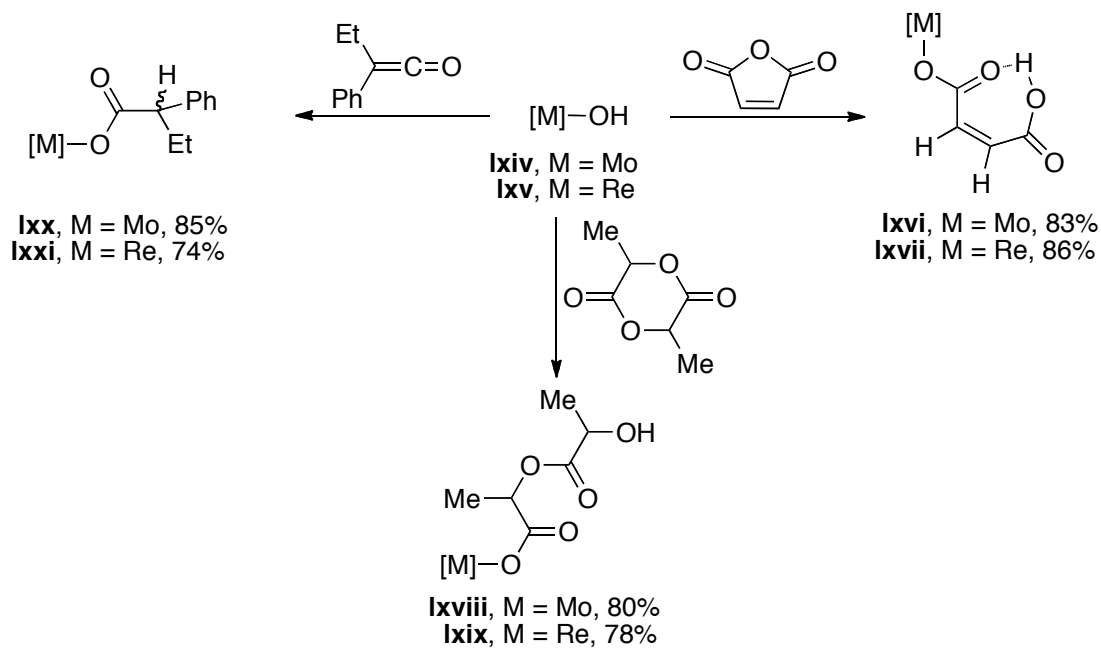
hydroxide complexes. In fact, this is due to the lack of soluble divalent lead hydroxide complexes. Thus we decided to investigate the chemistry of divalent lead alkoxides in order to further understand the chemistry of the Pb–O bond, and perhaps gain insight into the mechanism of lead(II)-induced RNA cleavage.

2.2.2 Transition metal hydroxide, alkoxide and aryloxide complexes

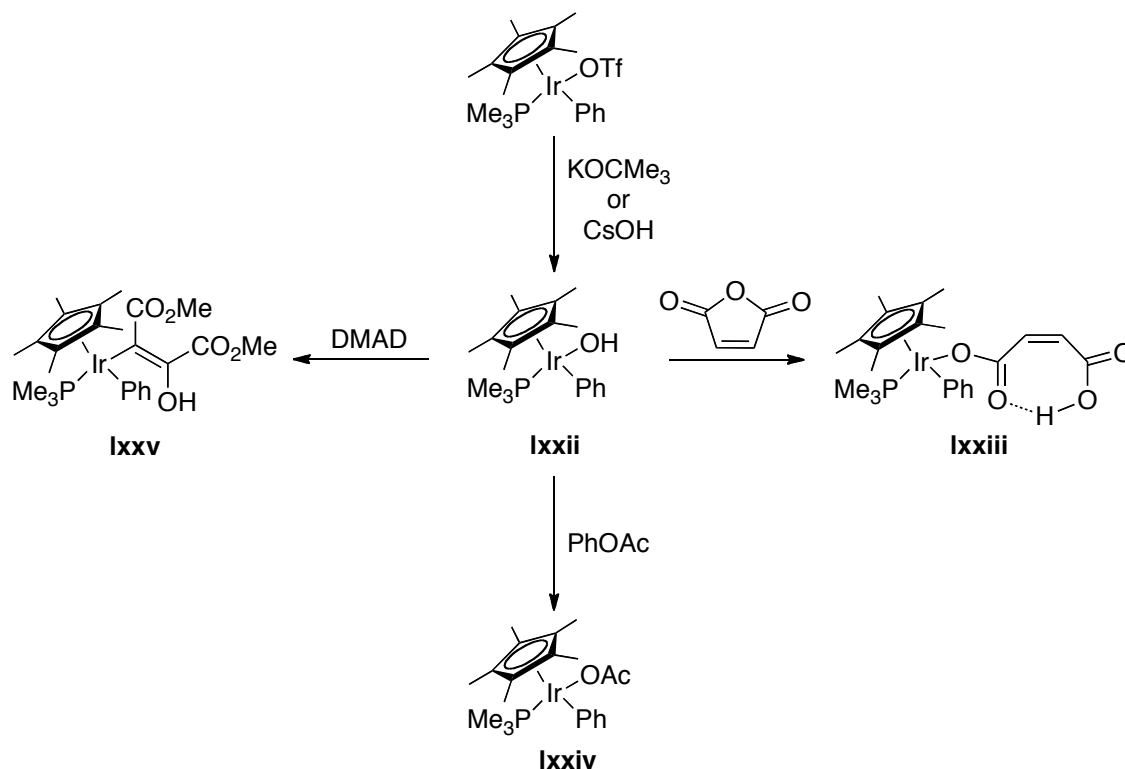
There have been a number of studies on the chemistry of transition metal alkoxide and aryloxide complexes. Pérez *et al.* reported a series of molybdenum and rhenium hydroxide complexes, which act as nucleophiles towards organic molecules (Figure 8 and Scheme 19).^[84] Complexes **lxiv** and **lxv** both reacted with maleic anhydride to give the ring-opened products **lxvi** and **lxvii**. Similarly, metal complexes **lxviii** and **lxix** containing lactyl-lactato as ligand were formed when the hydroxide complexes **lxiv** and **lxv** reacted with *rac*-lactide. Treatment of the hydroxide complexes **lxiv** and **lxv** with phenyl(ethyl)ketene gave compounds **lxx** and **lxxi** *via* insertion of the ketene into the O–H bond.

Figure 8. Molybdenum and rhenium hydroxide complexes **lxiv** and **lxv**^[84]

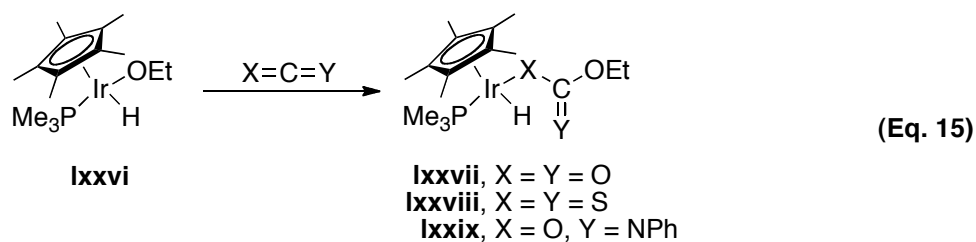


Scheme 19. Reactions of complexes **ixiv** and **ixv**^[84]

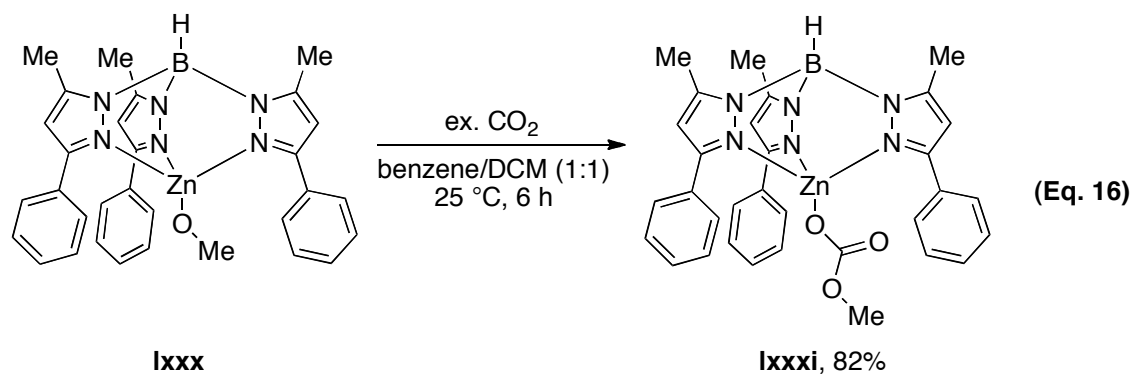
Similar reactions were observed in a series of low-valent metal hydroxides.^[85-86] For instance, Bergman *et al.* synthesised a coordinatively saturated iridium hydroxide complex $[\text{Cp}^*(\text{PMe}_3)\text{Ir}(\text{Ph})\text{OH}]$ (**ixxii**, $\text{Cp}^* = 1,2,3,4,5\text{-pentamethylcyclopentadienyl}$) (Scheme 20).^[87] Treatment of compound **ixxii** with maleic anhydride or phenyl acetate gave the corresponding hydrogen maleate complex **ixxiii** and acetate complex **ixxiv**, respectively. The hydroxide complex **ixxii** reacted with dimethyl acetylenedicarboxylate (DMAD) to give the insertion product **ixxv**.

Scheme 20. Reactions of the iridium hydroxide complex **Ixxii**^[87]

Insertion of heterocumulenes, for example carbon dioxide and carbon disulfide, into metal-oxygen bonds in metal alkoxide complexes is well known. This is demonstrated by Bergman's iridium alkoxide complex **Ixxvi**, which reacts with various heterocumulenes, including carbon dioxide, carbon disulfide and phenyl isocyanate, to give the insertion products **Ixxvii–Ixxix** (Equation 15).^[88]

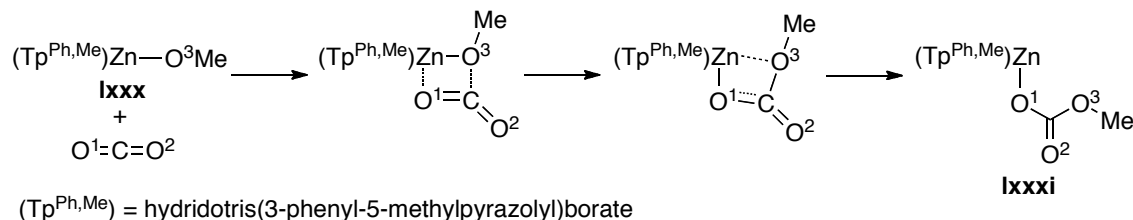


Vahrenkamp *et al.* reported the insertion of carbon dioxide into a metal-oxygen bond.^[89] Treatment of the pyrazolylborate zinc alkoxide complex $[(\text{Tp}^{\text{Ph,Me}})\text{ZnOMe}]$ (**Ixxx**, $(\text{Tp}^{\text{Ph,Me}}) = \text{hydridotris}(3\text{-phenyl-5-methylpyrazolyl})\text{borate}$) with an excess of carbon dioxide at room temperature gave $[(\text{Tp}^{\text{Ph,Me}})\text{ZnOCO}_2\text{Me}]$ (**Ixxxi**) in good yield (equation 16).

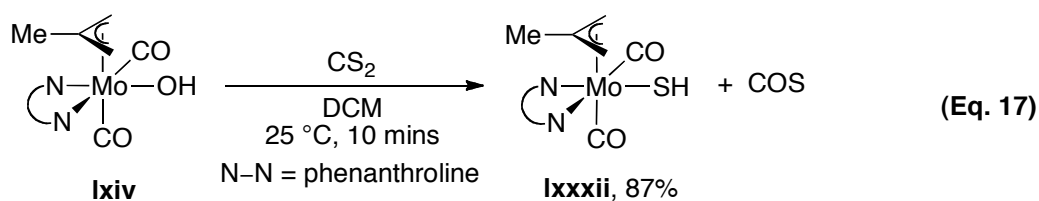


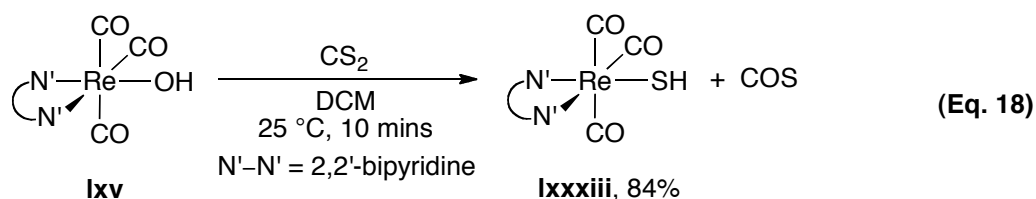
A proposed mechanism for the formation of **Ixxxi** is illustrated in Scheme 21.^[89-90] Initially, the oxygen from the alkoxide ligand interacts with the carbon in carbon dioxide and the zinc ion is weakly coordinated to O1, leading to the formation of a four-membered Zn–O–C–O ring. This is followed by the formation of the C–O3 bond and weakening of the C=O1 bond. The final step involves the formation of a new Zn–O1 bond and breaking of the Zn–O3 bond to give the complex **Ixxxi**.

Scheme 21. Proposed mechanism for the formation of compound **Ixxxi**^[89-90]



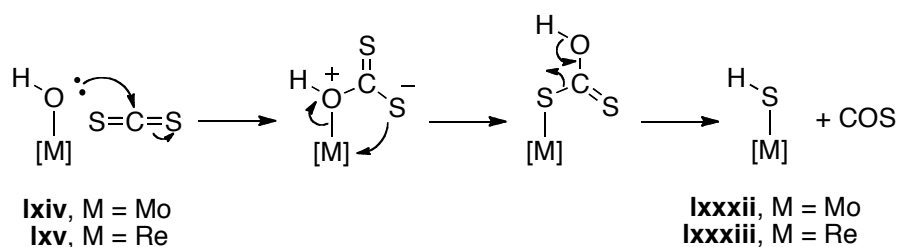
Pérez *et al.* reported an unusual reaction between the molybdenum or rhenium hydroxide complexes **Ixiv** or **Ixv** and carbon disulfide.^[91] Treatment of the compounds **Ixiv** or **Ixv** with one equivalent of carbon disulfide gave the hydrosulfide metal complexes **Ixxxii** and **Ixxxiii**, as well as carbonyl sulfide as by-product (equations 17 and 18). The ¹H NMR spectra of compounds **Ixxxii** and **Ixxxiii** showed singlets at δ_{H} –0.60 and –2.43 ppm, respectively, assigned to the proton in the S–H group.





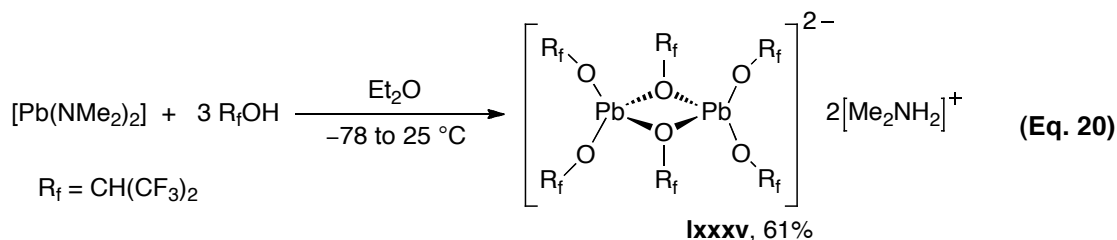
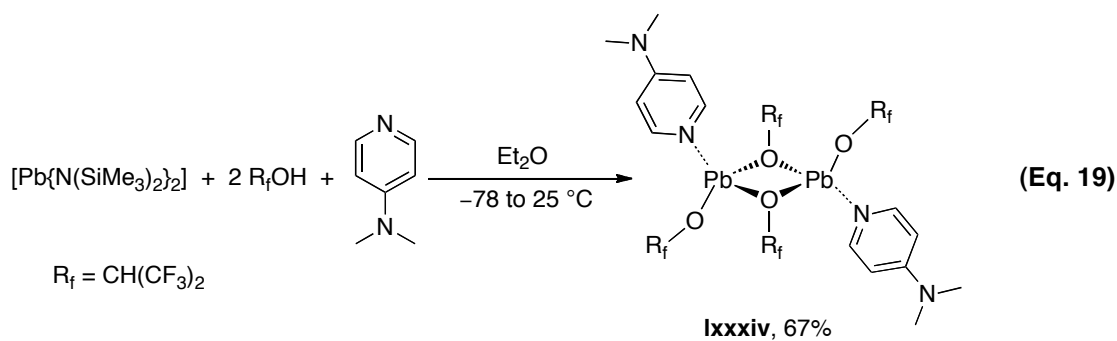
It was suggested that the formation of the metal hydrosulfido complexes **Ixxxii** and **Ixxxiii** were initiated by nucleophilic attack of the hydroxyl oxygen atom on to the electrophilic carbon atom of carbon disulfide (Scheme 22).^[92] The resulting zwitterionic intermediate underwent rearrangement to give the final product. This mechanism was further supported by theoretical calculations.

Scheme 22. Proposed mechanism for the formation of the metal hydrosulfido complexes **Ixxxii** and **Ixxxiii**^[92]



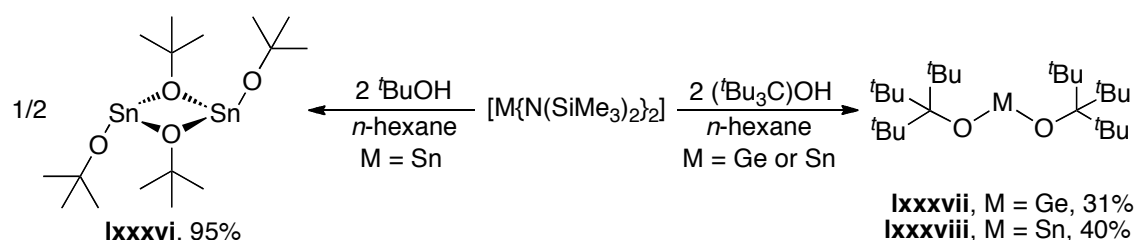
2.2.3 Heavy group 14 metal alkoxide complexes

Examples of heavy group 14 metal complexes containing terminal alkoxides are rare. Hoffman *et al.* reported that treatment of $[\text{Pb}\{\text{N}(\text{SiMe}_3)_2\}_2]$ with hexafluoroisopropanol (R_fOH) and 4-(dimethylamino)pyridine ($p\text{-Me}_2\text{NC}_5\text{H}_4\text{N}$) gave the neutral lead dimer $[\text{Pb}(\mu\text{-OR}_f)(\text{OR}_f)(p\text{-Me}_2\text{NC}_5\text{H}_4\text{N})_2]$ (**Ixxxiv**, $\text{R}_f = \text{CH}(\text{CF}_3)_2$) (equation 19)^[93]. In contrast, treatment of $[\text{Pb}(\text{NMe}_2)_2]$ with R_fOH gave the salt $[\{\text{Pb}(\mu\text{-OR}_f)(\text{OR}_f)_2\}_2][\text{Me}_2\text{NH}_2]_2$ (**Ixxxv**) containing a dimeric anion (equation 20). The solid state structures of these compounds showed weak intermolecular interaction between the lead atom and the terminal alkoxide in the neighbouring unit ($\text{Pb-O}' = 2.716(6)$ Å in **Ixxxiv**, and $2.659(5)$ Å in **Ixxxv**).



Lappert *et al.* synthesised a dimeric tin(II) alkoxide $[\text{Sn}(\text{O}^t\text{Bu})(\mu\text{-O}^t\text{Bu})_2]$ (**Ixxxvi**) by treatment of $[\text{Sn}\{\text{N}(\text{SiMe}_3)_2\}_2]$ with two equivalents of *tert*-butanol (Scheme 23).^[94] X-ray crystallographic study showed that the dimeric complex had a four-membered, almost planar Sn_2O_2 ring with the terminal *tert*-butoxide groups in *trans*-configuration. As with other three-coordinate divalent tin and germanium complexes (*vide infra*), the ligands were coordinated with a pyramidal geometry around the metal centres. The monomeric two-coordinate germanium(II) and tin(II) alkoxide complexes **Ixxxvii** and **Ixxxviii** were obtained by the use of bulkier (tri-*tert*-butyl)methoxide substituents. These monomeric complexes adopted a V-shaped geometry around the metal centre, for instance the O–Ge–O bond angle in compound **Ixxxvii** was $85.9(4)^\circ$.

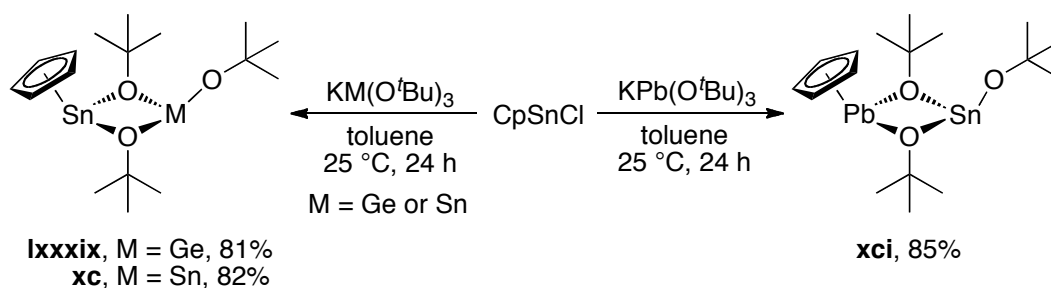
Scheme 23. Synthesis of the heavy group 14 metal alkoxide complexes **Ixxxvi–Ixxxviii**^[94]



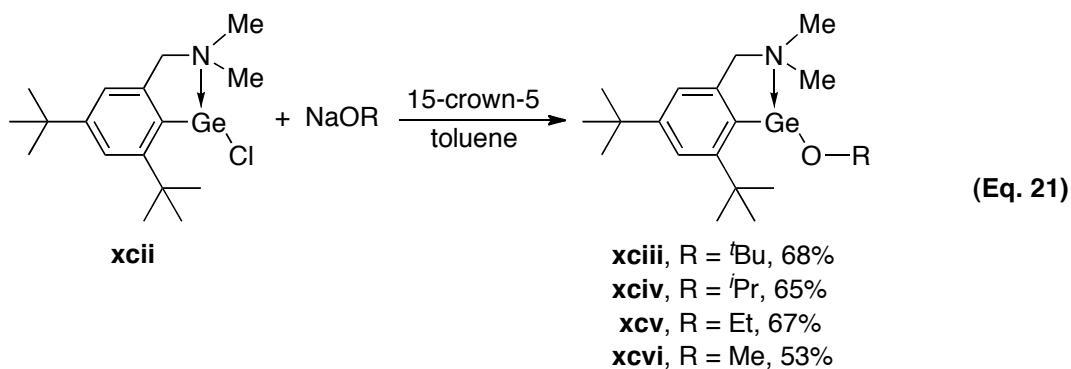
A series of cyclopentadienyl heterobimetallic alkoxide complexes was synthesised by Veith and co-workers.^[95-96] Treatment of CpSnCl (Cp = cyclopentadienyl) with $\text{KM}(\text{O}^t\text{Bu})_3$ (M = Ge or Sn) at room temperature gave the heterobimetallic alkoxide

complexes $[\text{CpSn}(\mu\text{-O}^t\text{Bu})_2\text{M}(\text{O}^t\text{Bu})]$ (**lxxxix**, $\text{M} = \text{Ge}$ and **xc**, $\text{M} = \text{Sn}$) (Scheme 24). However, when CpSnCl was treated with $\text{KPb}(\text{O}^t\text{Bu})_3$ under the same conditions, the cyclopentadienyl group was transferred from tin to lead to give $[\text{CpPb}(\mu\text{-O}^t\text{Bu})_2\text{Sn}(\text{O}^t\text{Bu})]$ (**xcj**).^[96] The solid state structures of these complexes were reported. Like Lappert's dimeric tin(II) alkoxide **lxxxvi** (Scheme 23, Page 33), compounds **lxxxix** and **xc** have nearly planar M_2O_2 rings. However, the terminal ligands adopt a *cis*-configuration with respect to the ring. The geometry around the metal centres is pyramidal.

Scheme 24. Synthesis of the cyclopentadienyl heterobimetallic alkoxide complexes **lxxxix–xcj**^[95–96]

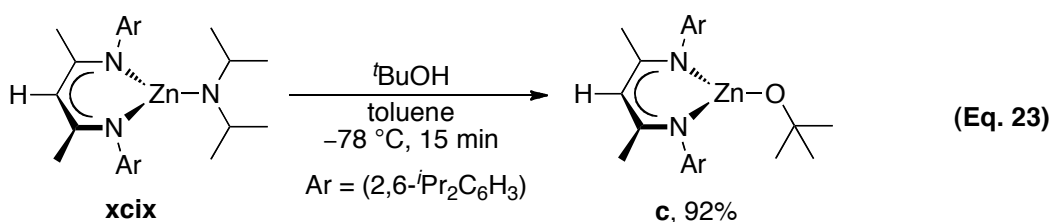
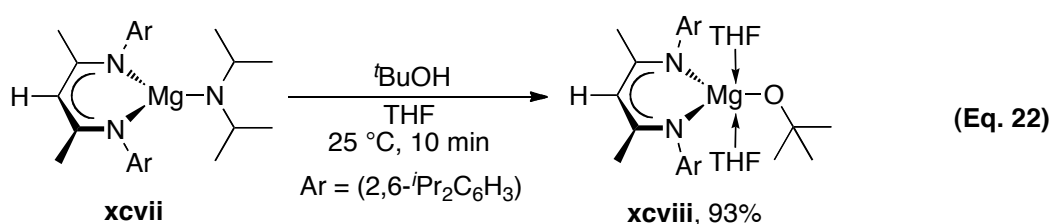


Jutzi *et al.* reported the use of 2,4-di-*tert*-butyl-6[(dimethylamino)methyl]phenyl ligand to stabilise a series of germanium(II) alkoxide complexes.^[97] Treatment of the germanium(II) chloride complex **xcii** with an excess of the sodium alkoxide in the presence of 15-crown-5 gave the germanium(II) alkoxide complexes **xciii–xcvi** in good yields (equation 21). The solid state structures of these compounds showed that a three-coordinate germanium atom was present, with an additional $\text{N} \rightarrow \text{Ge}$ dative bond.

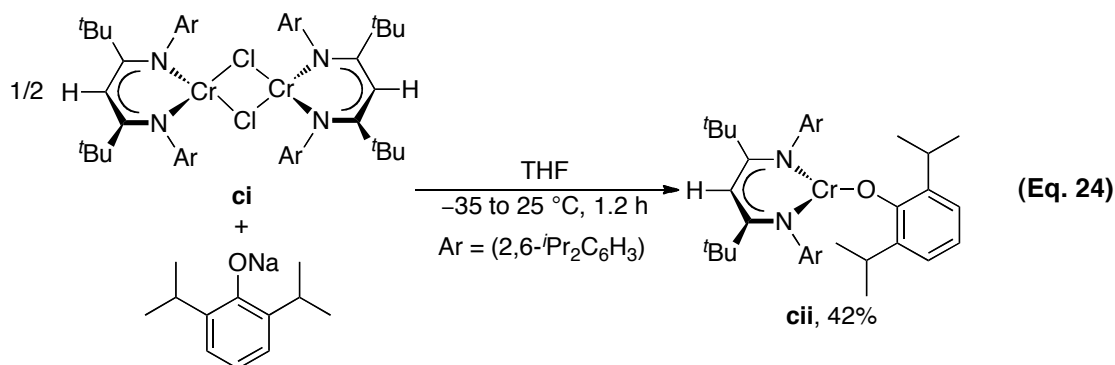


2.2.4 β -Diketiminato metal alkoxides and aryloxides

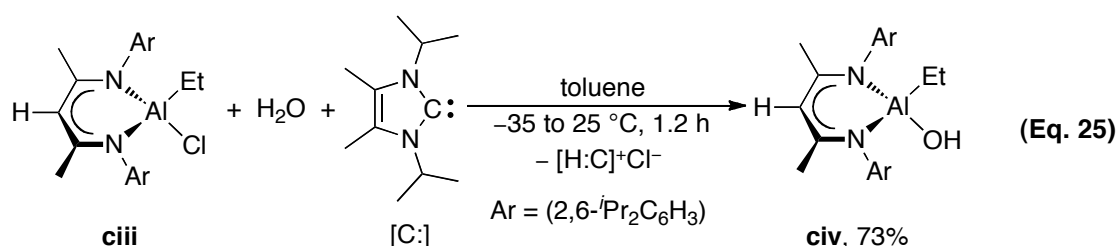
The use of β -diketiminato ligand $[\text{HC}\{\text{C}(\text{Me})\text{N}(2,6\text{-}^i\text{Pr}_2\text{C}_6\text{H}_3)\}_2]^-$ (BDI_{DIPP}) in supporting terminal M–O bond has been explored with both transition metals and some main group metals. However, the reactivity of these β -diketiminato metal alkoxides and aryloxides has not been examined extensively. Chisholm *et al.* reported the synthesis of β -diketiminato magnesium(II) and -zinc(II) isopropoxides.^[98] Treatment of the β -diketiminato metal amides **xcvii** and **xcix** with *tert*-butanol gave the corresponding metal isopropoxide complexes **xcviii** and **c**, in near quantitative yields (equations 22 and 23).



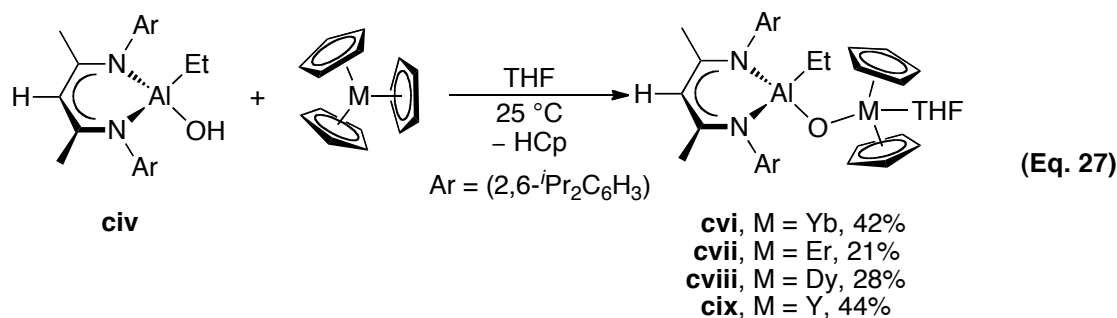
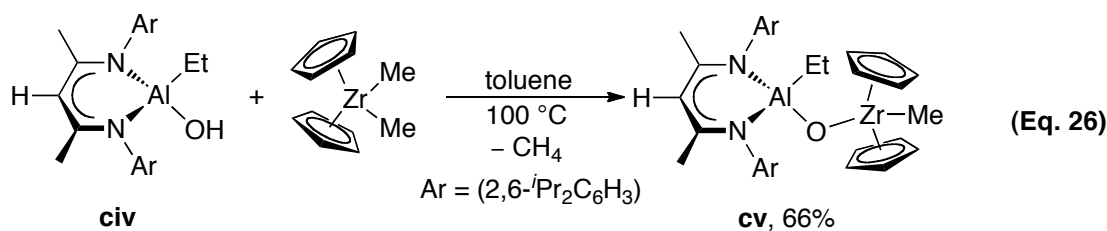
A three-coordinate β -diketiminatochromium(II) aryloxide **cii** was synthesised by Mindiola *et al.*^[99] Treatment of the dimeric β -diketiminatochromium(II) chloride **ci** with $[\text{NaOC}_6\text{H}_3^i\text{Pr}_2\text{-2,6}]$ in THF gave the monomeric β -diketiminatochromium(II) aryloxide **cii** (equation 24). No further reaction of the aryloxide **cii** was reported.



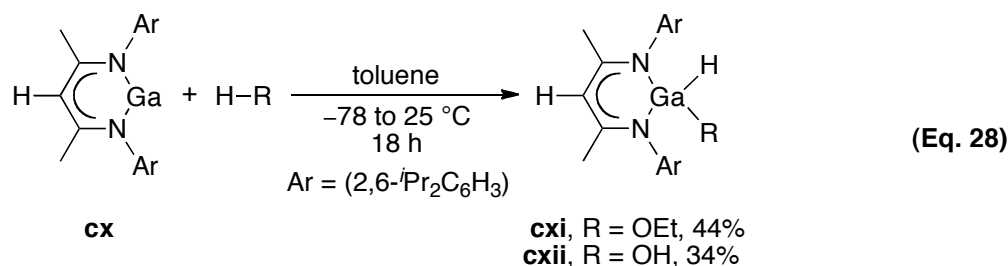
The chemistry of the β -diketiminatoaluminium(III) hydroxide **civ** has been explored.^[100-101] The β -diketiminatoaluminium(III) hydroxide **civ** was synthesised by treatment of $[(\text{BDI}_{\text{DIPP}})\text{AlEt}(\text{Cl})]$ (**ciii**) with water in the presence of 1,3-diisopropyl-4,5-dimethylimidazol-2-ylidene $[\text{C}:]$, which acted as an HCl acceptor (equation 25). The solid state structure of **civ** showed that the coordination geometry at aluminium was tetrahedral. The ^1H NMR spectrum showed a single resonance at δ_{H} 0.63 ppm, assigned to the hydroxyl proton.



Reaction of compound **civ** with Cp_2ZrMe_2 (Cp = cyclopentadienyl) gave the μ -O bridged heterobimetallic oxide complex $[(\text{BDI}_{\text{DIPP}})\text{AlEt}(\mu\text{-O})\text{ZrMeCp}_2]$ (**cv**) with evolution of methane (equation 26). Similarly, treatment of compound **civ** with one equivalent of various rare earth metal derivatives of Cp_3M (M = Yb, Er, Dy or Y) in THF gave the heterobimetallic oxo-bridged complexes **cvi**–**cix** with elimination of cyclopentadiene (HCp) (equation 27).



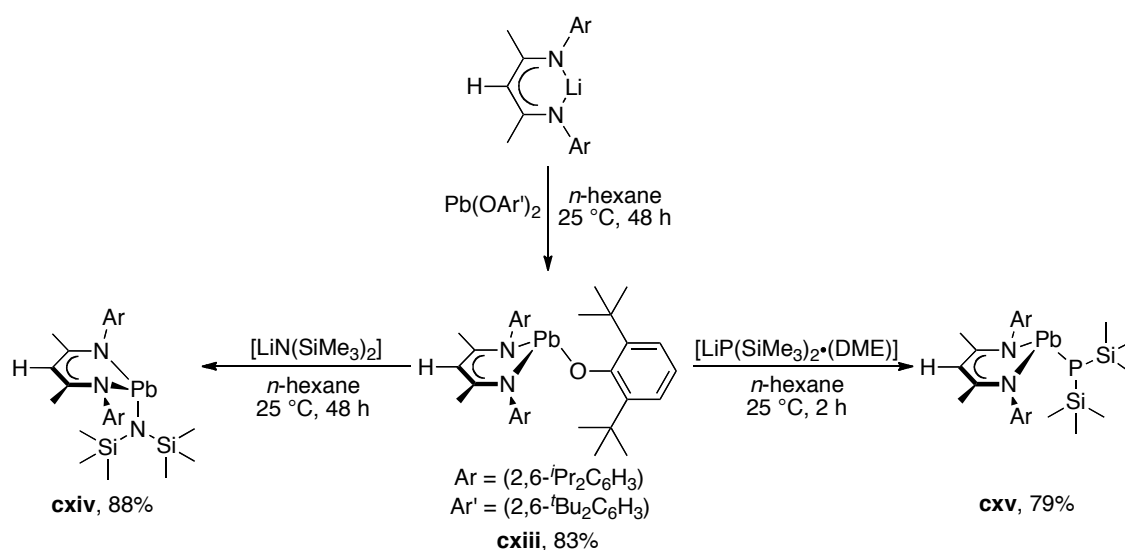
Linti *et al.* reported the synthesis of the β -diketiminatogallium(III) alkoxide **cx**i and hydroxide **cx**ii.^[102] These compounds were accessible *via* the facile oxidative addition of ethanol or water to the β -diketiminatogallium(I) complex **cx** to form [(BDI_{DIPP})GaH(OEt)] (**cx**i) and [(BDI_{DIPP})GaH(OH)] (**cx**ii), respectively. An X-ray crystallographic study on compound **cx**i showed that the ligands were coordinated in a distorted tetrahedral geometry around the gallium atom.



2.2.5 β -Diketiminato heavy group 14 metal alkoxides and aryloxides

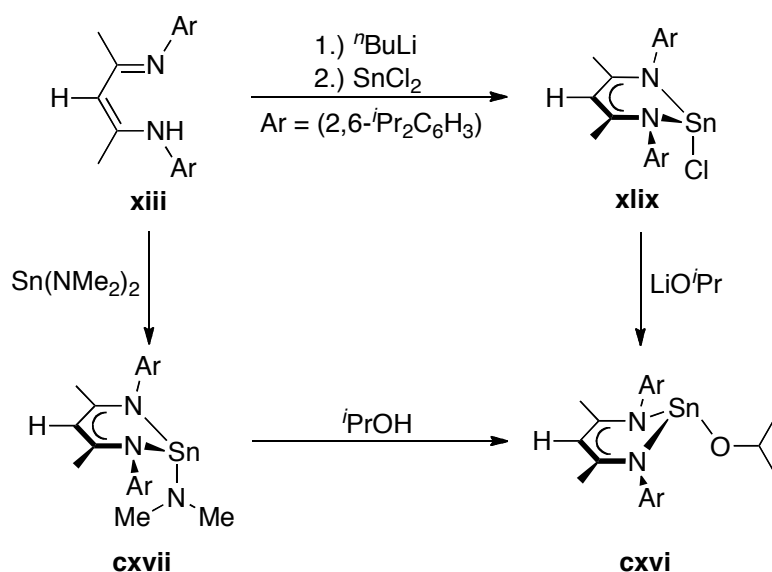
Examples of β -diketiminato heavy group 14 metal alkoxides and aryloxides are rare and their reactions have not been explored extensively. Driess *et al.* reported the synthesis of the β -diketiminatolead(II) aryloxide **cx**iii by treatment of the lithium β -diketimate with lead diphenolate (Scheme 25).^[103] Subsequent reactions of the lead(II) aryloxide **cx**iii with [LiN(SiMe₃)₂] or [LiP(SiMe₃)₂·(DME)] (DME = 1,2-dimethoxyethane) gave the corresponding lead(II) amide **cx**iv or phosphanide **cx**v complexes.

Scheme 25. Synthesis and reactions of the β -diketiminatolead(II) aryloxide **cx**iii^[103]

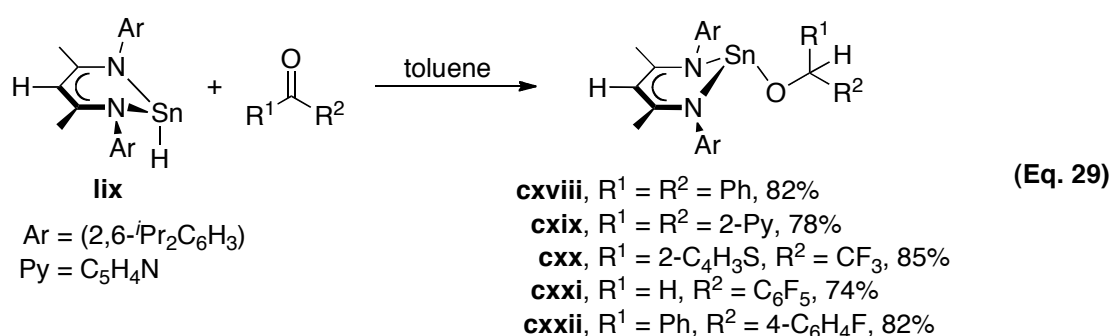


Gibson *et al.* reported the synthesis of the β -diketiminatotin(II) isopropoxide **cxvi**.^[40] Treatment of the β -diketiminatotin(II) chloride **xliv** with lithium isopropoxide gave [(BDI_{DIPP})SnO^{*i*}Pr] (**cxvi**) (Scheme 26). The complex was also accessible by the alcoholysis of the β -diketiminatotin(II) amide **cxvii** with isopropyl alcohol.

Scheme 26. Synthesis of the β -diketiminatotin(II) isopropoxide **cxvi**^[40]

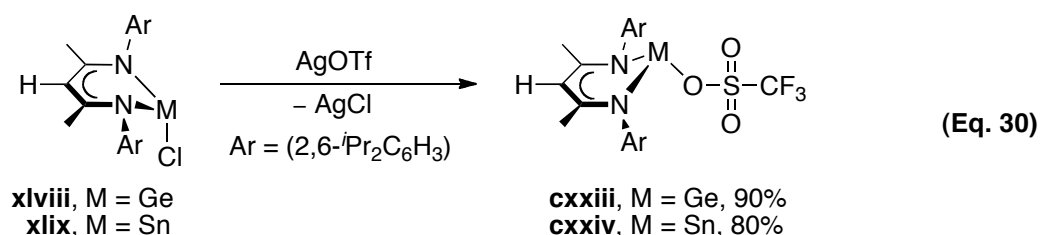


Roesky *et al.* synthesised a series of β -diketiminatotin(II) alkoxides **cxviii–cxxxii** via nucleophilic hydride addition to the carbonyl carbon of ketones.^[73, 104] For instance, treatment of the β -diketiminatotin(II) hydride **lix** with ketones gave the β -diketiminatotin(II) alkoxides **cxviii–cxxxii** in good yields (equation 29).



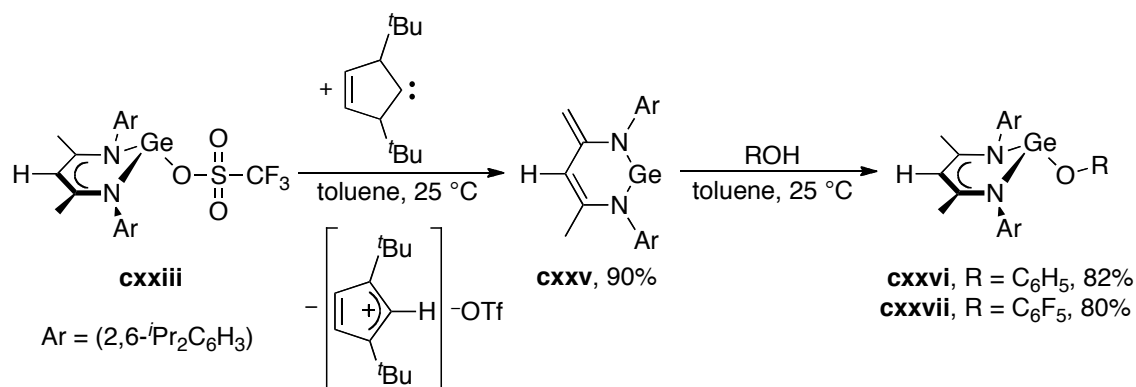
The β -diketiminatogermanium(II) and -tin(II) complexes containing a terminal triflate ligand were synthesised by Roesky *et al.*^[65, 105] Treatment of the β -diketiminatometal chlorides **xlvi** or **xliv** with silver trifluoromethanesulfonate gave the monomeric

compounds [(BDI_{DIPP})M(OTf)] (**cxiii**, M = Ge; **cxiv**, M = Sn) in good yields with elimination of silver chloride (equation 30).



The reaction of the germanium(II) triflate **cxiii** was explored.^[105] Addition of 1,3-di-*tert*-butylimidazol-2-ylidene led to the formation of the cyclogermylene **cxv**, in which one of the backbone methyl groups was deprotonated, so that both *N*-aryl nitrogen atoms were bound to the metal centre as anionic ligands (Scheme 27).^[106] Treatment of the cyclogermylene **cxv** with phenol or pentafluorophenol led to the formation of the germanium(II) aryloxides **cxvi** and **cxvii** in good yields.

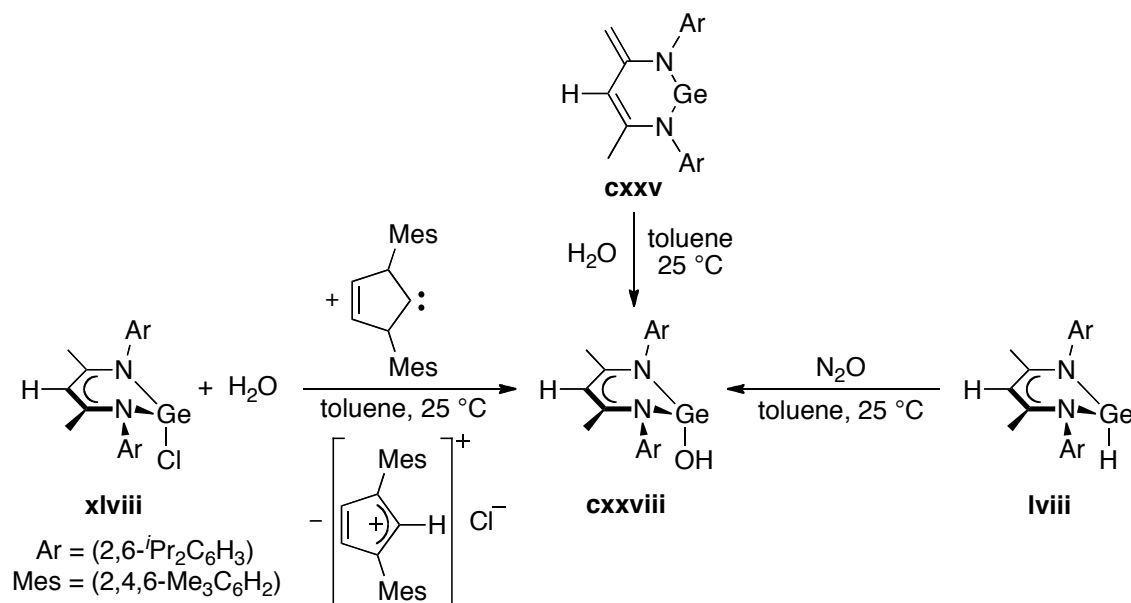
Scheme 27. Synthesis of the β-diketiminatogermanium(II) aryloxides **cxvi** and **cxvii**^[105]



Metal hydroxide complexes are generally rare and difficult to synthesise. However, Roesky *et al.* did manage to synthesise the β-diketiminatogermanium(II) hydroxide **cxviii** *via* hydrolysis of organohalogermanes.^[107] Treatment of the β-diketiminatogermanium(II) chloride **xlvi** with degassed water in the presence of 1,3-dimesitylimidazol-2-ylidene gave [(BDI_{DIPP})GeOH] (**cxviii**) (Scheme 28). Alternatively, the hydroxide complex **cxviii** was synthesised *via* a reaction between the β-diketiminatogermanium(II) hydride **lviii** and nitrous oxide.^[108] The germanium(II) hydroxide **cxviii** was also accessible *via* the reaction between cyclogermylene **cxv**

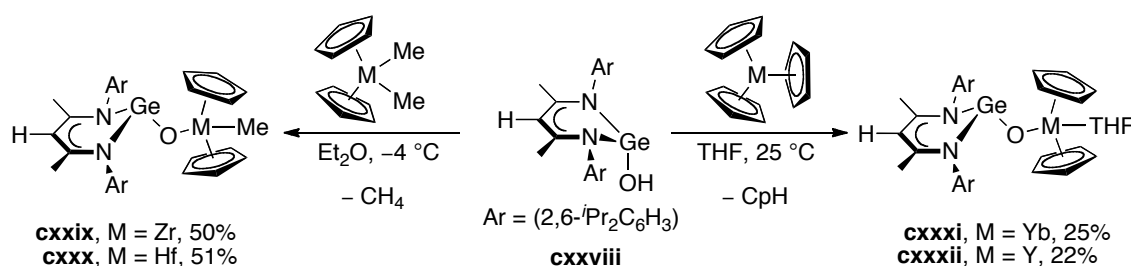
and water at room temperature.^[105] The ^1H NMR spectrum of the germanium(II) hydroxide **cxxviii** showed a singlet at δ_{H} 1.65 ppm, assigned to the terminal hydroxyl proton.^[108] An X-ray crystallographic study on the germanium(II) hydroxide **cxxviii** revealed that the complex existed as a dimer in the solid state.

Scheme 28. Synthesis of the β -diketiminatogermanium(II) hydroxide **cxxviii**^[105, 107-108]

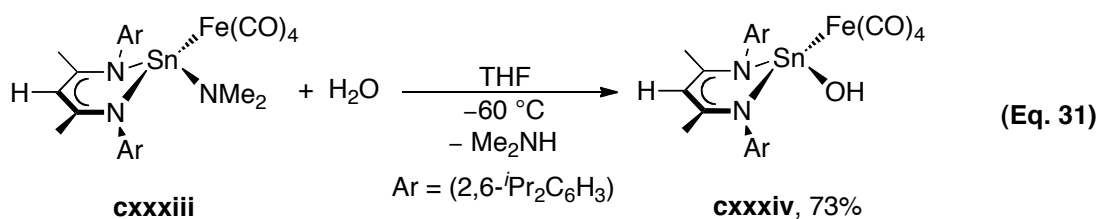


Treatment of the germanium(II) hydroxide **cxxviii** with Cp₂MMe₂ (Cp = cyclopentadienyl, M = Zr or Hf) gave the heterobimetallic oxide complexes **cxxix** and **cxxx** (Scheme 29).^[109-110] The ^1H NMR spectra of **cxxix** and **cxxx** showed single resonances at δ_{H} 5.39 and 5.33 ppm, respectively, for the protons in the Cp group. The ligands were coordinated in a tetrahedral geometry around the transition metal centre as shown by the solid state structures. Similarly, when compound **cxxviii** was treated with Cp₃M (M = Yb and Y), the heterobimetallic complexes **cxxxi** and **cxxxii**, possessing a germanium-oxygen-lanthanide linkage, were obtained (Scheme 29).

Scheme 29. Reactions of the β -diketiminatogermanium(II) hydroxide **cxxviii**^[109-110]



The synthesis of the β -diketiminatotin(II) hydroxide was more complex. Attempts were made to make it by treatment of the β -diketiminatotin(II) chloride **xlix** with water, in the presence of an N-heterocyclic carbene.^[111] Unfortunately, this reaction led to the β -diketimine **xiii** and an intractable mixture. However, by protecting the tin centre with a bulky Lewis acid $[\text{Fe}(\text{CO})_4]$, the monomeric β -diketiminatotin(II) hydroxide **cxxxiv** was synthesised by addition of one equivalent of degassed water to the tin(II) amido precursor $[(\text{BDI}_{\text{DIPP}})\text{Sn}(\text{NMe}_2)\text{Fe}(\text{CO})_4]$ (**cxxxiii**) (equation 31). A single resonance at δ_{H} 1.66ppm was ascribed to the hydroxyl proton in the ^1H NMR spectrum of compound **cxxxiv**. An X-ray crystallographic study revealed that **cxxxiv** was monomeric and that the ligands were coordinated in a distorted tetrahedral geometry around the tin centre.



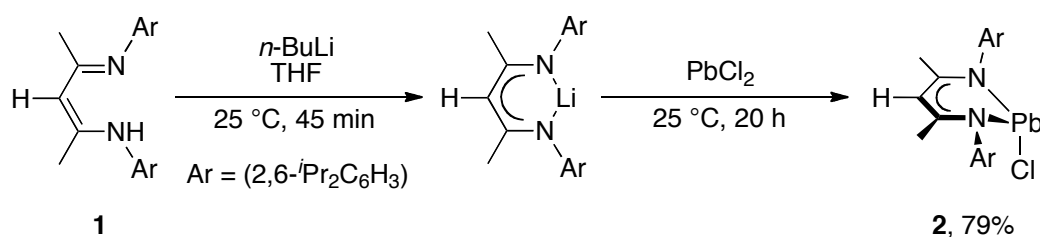
In summary, the bulky β -diketiminato ligand provides steric protection for the heavy group 14 metal centres to make possible the synthesis of a variety of alkoxide complexes. But little work has been done on their reactions.^[112] Prior to our studies, β -diketiminatolead(II) alkoxides were unknown, thus making both the synthesis and reactivity studies of such complexes an attractive area of research.

2.3 Results and discussion

2.3.1 Synthesis of β -diketiminatolead(II) alkoxides

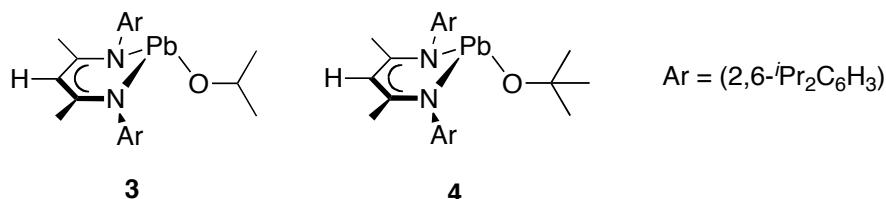
The β -diketimine, (BDI_{DIPP})H (**1**), and β -diketiminatolead(II) chloride [(BDI_{DIPP})PbCl] (**2**) were synthesised according to the literature procedures.^[41, 62] The β -diketimine **1** was lithiated and added to a THF slurry of lead dichloride to give the lead(II) chloride **2** (Scheme 30).

Scheme 30. Synthesis of the β -diketiminatolead(II) chloride **2**^[62]



The β -diketiminatolead(II) isopropoxide **3** and *tert*-butoxide **4** were synthesised previously by Dr. Nicholas C. Johnstone (NCJ) (Figure 9), but little information about their reactions was obtained.^[113] In the first part of this chapter, the synthesis and characterisation of a third alkoxide is described. In the second part, the information at present available on the reactivity of this class of compounds is brought together and compared with those obtained previously on transition metal analogues. Contributions from individuals are shown in Table 2 (Page 23).

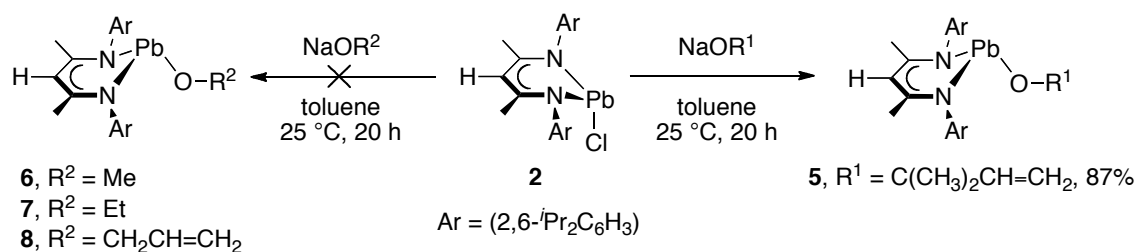
Figure 9. Previously reported β -diketiminatolead(II) alkoxides **3** and **4**^[113-114]



The newly synthesised β -diketiminatolead(II) alkoxide [(BDI_{DIPP})PbOC(CH₃)₂CH=CH₂] (**5**) is accessible by treatment of the lead(II) chloride **2** with sodium 2-methyl-3-but-3-ene-2-oxide in toluene at room temperature (Scheme 31). The ¹H NMR spectrum shows three doublets of doublets centred at δ_{H} 5.70, 4.59 and

4.53 ppm with a ratio of 1:1:1, as well as a singlet at δ_{H} 0.95 ppm, with an intensity of 6 protons, for the $-\text{OC}(\text{CH}_3)_2\text{CH}=\text{CH}_2$ fragment. A single lead resonance is found at δ_{Pb} 1685 ppm in the ^{207}Pb NMR spectrum. This is downfield from that of the parent lead(II) chloride **2** (δ_{Pb} 1413 ppm).^[70] Elemental analysis is in good agreement with the calculated values. In contrast, syntheses of the lead(II) complexes of primary alkoxides **6–8** were not successful (Scheme 31). Such reactions led to an intractable mixture, including the β -diketimine **1**. This decomposition may be due to the inability of the less bulky primary alkoxide substituents to stabilise the low-coordinated lead atom.

Scheme 31. β -Diketiminatolead(II) alkoxide **5** and the attempted syntheses of compounds **6–8**



Yellow single crystals of $[(\text{BDI}_{\text{DIPP}})\text{PbOC}(\text{CH}_3)_2\text{CH}=\text{CH}_2]$ (**5**) were obtained by recrystallisation from toluene at $-30\text{ }^\circ\text{C}$. ORTEP drawings of **5** are shown in Figures 10 and 11. Selected bond lengths and angles are given in Table 4, and selected crystallographic data in Table 5. The ligands are coordinated in a pyramidal geometry around the metal centre with the sum of bond angles 266° . The lead atom is displaced from the mean NCCCN plane in the β -diketimate ring by 0.874 \AA . The Pb–O bond distance ($2.150(2)\text{ \AA}$) in **5** is similar to those found in $[(\text{BDI}_{\text{DIPP}})\text{PbO}^i\text{Pr}]$ (**3**, Pb–O = $2.135(3)\text{ \AA}$) and $[(\text{BDI}_{\text{DIPP}})\text{PbO}^t\text{Bu}]$ (**4**, Pb–O = $2.126(3)\text{ \AA}$).^[114] The Pb–O–C(16) bond angle ($115.4(2)^\circ$) in compound **5** is also similar to those in complexes **3** and **4** (Pb–O–C = $118.0(2)^\circ$ and $121.4(2)^\circ$, respectively).^[114]

Figure 10. ORTEP diagram of $[(\text{BDI}_{\text{DIPP}})\text{PbOC}(\text{CH}_3)_2\text{CH}=\text{CH}_2]$ (**5**). H atoms are omitted and C atoms in the *N*-aryl groups in the β -diketiminato ring are minimised for clarity. The ellipsoid probability is shown at 30%

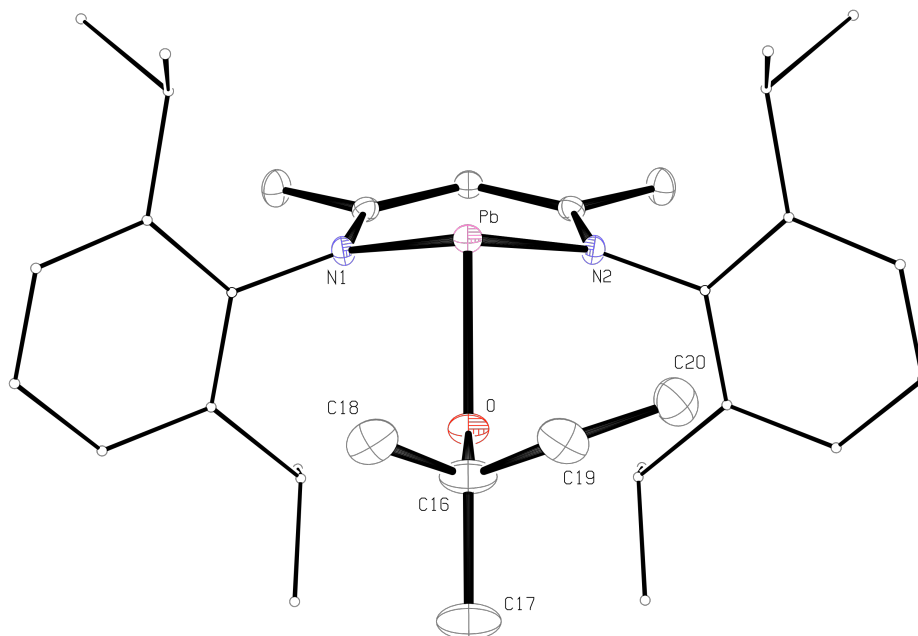


Figure 11. ORTEP diagram showing the side-on view of $[(\text{BDI}_{\text{DIPP}})\text{PbOC}(\text{CH}_3)_2\text{CH}=\text{CH}_2]$ (**5**). H atoms are omitted and C atoms in the *N*-aryl groups in the β -diketiminato ring are minimised for clarity. The ellipsoid probability is shown at 30%

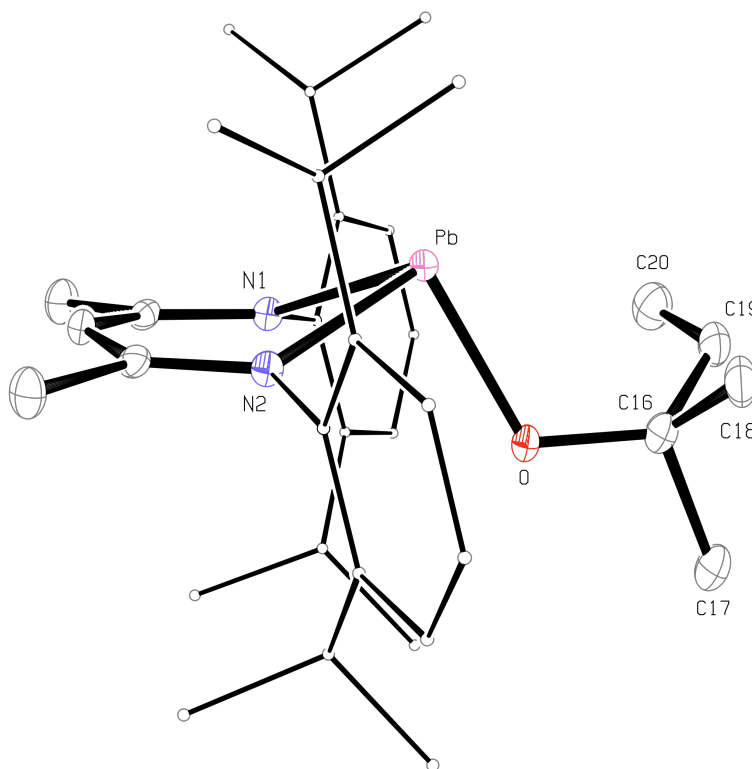


Table 4. Selected bond lengths (Å) and angles (deg) for [(BDI_{DIPP})PbOC(CH₃)₂CH=CH₂] (**5**)

Pb–N(1)	2.3151(16)	N(1)–Pb–N(2i)	80.13(8)
Pb–N(2)	2.315(2)	N(1)–Pb–O	92.87(6)
Pb–O	2.150(2)	N(2)–Pb–O	92.87(7)
O–C(16)	1.404(4)	Pb–O–C(16)	115.4(2)
C(16)–C(19)	1.398(10)	C(16)–C(19)–C(20)	121.9(7)
C(19)–C(20)	1.318(9)		
Pb–NCCCN _{plane}	0.874	NCCCN _{plane} –NPbN _{plane}	29.2
		Σ bond angle around Pb	266
		DOP of Pb (%) ^a	105

^a Degree of pyramidalisation (DOP, %) = [(360 – Σ_{bond angle}) / 0.9]^[115] When a DOP is 100%, it is equivalent to a sum of bond angles of 270°, whereas a DOP of 0% indicates a planar geometry at the central atom; Symmetry transformation used to generate equivalent atoms: (i) *x*, –*y* + 1/2, *z*

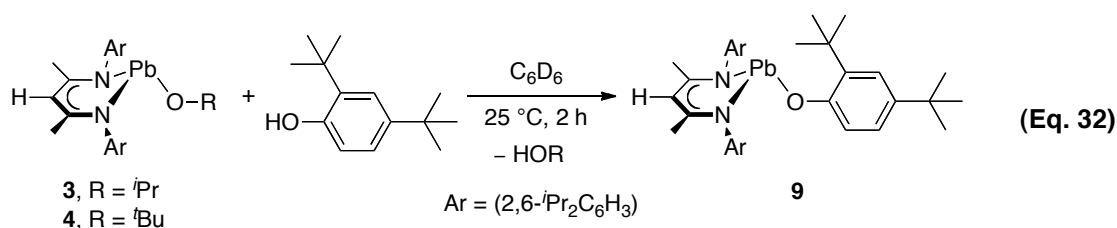
Table 5. Selected crystallographic data for compound **5**

[(BDI _{DIPP})PbOC(CH ₃) ₂ CH=CH ₂] (5)	
chemical formula	C ₃₄ H ₅₀ N ₂ OPb
molecular mass	709.95
temperature (K)	173(2)
wavelength (Å)	0.71073
crystal system	orthorhombic
space group	<i>Pnma</i>
<i>a</i> (Å)	16.7481(2)
<i>b</i> (Å)	21.1755(3)
<i>c</i> (Å)	9.3249(1)
<i>α</i> (deg)	90
<i>β</i> (deg)	90
<i>γ</i> (deg)	90
<i>V</i> (Å ³)	3307.07(7)
<i>Z</i>	4
ρ_{calcd} (Mg m ⁻³)	1.43
θ range (deg)	3.41–27.47
abs coeff (mm ⁻¹)	5.13
measd/indep reflns/ <i>R</i> (int)	48 777/3866/0.052
reflns with <i>I</i> > 2 σ (<i>I</i>)	3608
data/restraints/param	3866/0/194
goodness of fit on <i>F</i> ²	0.913
final <i>R</i> indices [<i>I</i> > 2 σ (<i>I</i>)]	<i>R</i> 1 = 0.019, <i>wR</i> 2 = 0.051
<i>R</i> indices (all data)	<i>R</i> 1 = 0.021, <i>wR</i> 2 = 0.052
largest diff peak and hole (e Å ⁻³)	0.65 and –1.46

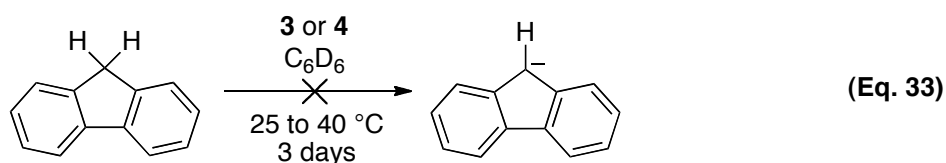
2.3.2 Reactivity of β -diketiminatolead(II) alkoxides

2.3.2.1 Basicity

Transition metal alkoxides have highly polarized M–O bonds. This is exemplified in the case of ruthenium-hydroxides, which can reversibly deprotonate toluene ($pK_a = 43$ in DMSO).^[86, 116] Hence, we decided to investigate the basicity of our lead(II) alkoxide complexes by exposing them to a range of acids. Treatment of the β -diketiminatolead(II) alkoxide [(BDI_{DIPP})PbO^{*i*}Pr] (**3**) or [(BDI_{DIPP})PbO^{*t*}Bu] (**4**) with 2,4-di-*tert*-butylphenol results in alcohol exchange to form the β -diketiminatolead(II) aryloxide **9** (equation 32). However, decomposition of compound **9** occurs in the presence of free isopropanol or *tert*-butanol to form the β -diketimine **1** and a white precipitate, possibly [Pb(OR)(μ -OR)]₂ (R = ^{*i*}Pr or ^{*t*}Bu), after 24 hours. The ¹H NMR spectrum of the resulting aryloxide **9** is the same as that found previously.^[117]

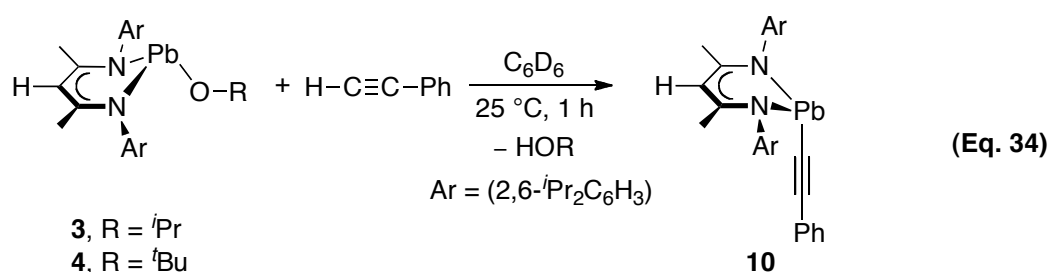


Fluorene is easily deprotonated at the C-9 position to form a stable aromatic fluorenyl anion, as shown by its relatively low pK_a in DMSO ($pK_a = 22.6$).^[118-119] However, treatment of the alkoxides **3** or **4** with one equivalent of fluorene does not give evidence for the formation of the fluorenyl anion, even at 40°C for three days, suggesting that the alkoxides have a relatively low basicity (equation 33).



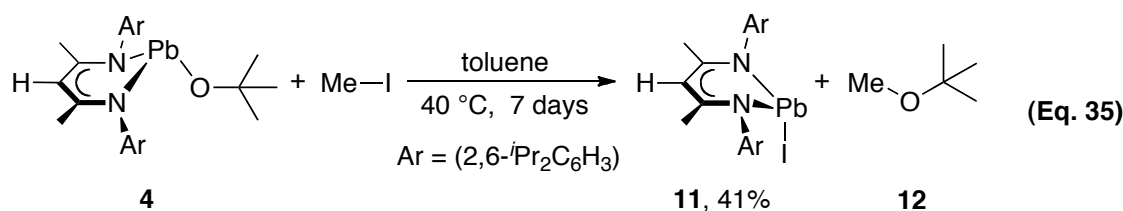
Treatment of the β -diketiminatolead(II) alkoxide **3** or **4** with phenylacetylene in toluene gives the ligand exchange product [(BDI_{DIPP})PbCCPh] (**10**) (equation 34). The ¹H NMR spectrum of the mixture reveals a singlet at δ_{H} 4.88 ppm, assigned to the γ -H, and two

septets at δ_{H} 4.09 and 3.30 ppm, assigned to the tertiary protons of the isopropyl groups (CHMe_2) in the β -diketiminato ring. Depending on the starting alkoxide, proton resonances assigned to isopropanol (δ_{H} 4.09 and 1.21 ppm) or *tert*-butanol (δ_{H} 1.42 ppm) are found, indicating the presence of free alcohol. The β -diketimine **1** and insoluble white precipitates are also observed, probably from reaction of the free alcohol with either reactants or product. During our studies, Roesky *et al.* generated compound **10** by treatment of the β -diketiminatolead(II) chloride **2** with LiCCPh in toluene.^[70] The NMR spectroscopic data for Roesky's compound are in good agreement with those we obtained.

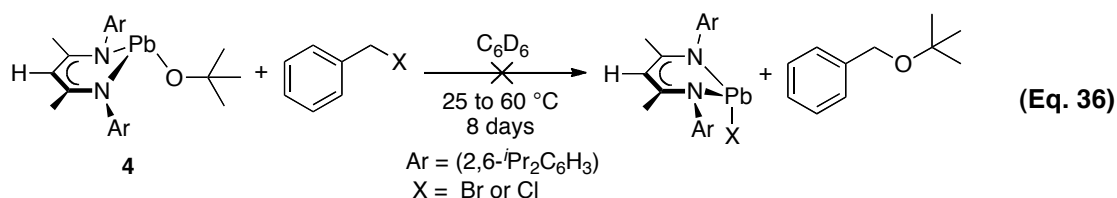


2.3.2.2 Nucleophilicity

Transition metal alkoxides generally react readily with aliphatic electrophiles, exemplifying their nucleophilicity.^[86] Hence, in a small scale study in an NMR tube, we treated alkoxide **4** with methyl iodide. No reaction was observed at room temperature. However, after seven days at 40 °C, conversion to the expected nucleophilic substituted products, the known β -diketiminatolead(II) iodide [(BDI_{DIPP})PbI] (**11**) and methyl *tert*-butyl ether **12**, were observed (equation 35).^[62] The photosensitive lead(II) iodide **11** was obtained in 41% yield when the reaction was performed on a larger scale. The NMR spectroscopic data for this compound are consistent with those reported in the literature.^[62]

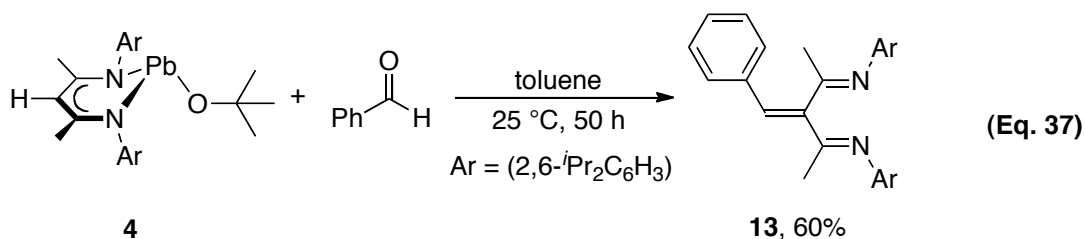


However, treatment of the lead(II) *tert*-butoxide **4** with benzyl bromide or chloride gave an intractable mixture of products (equation 36). The small scale NMR study did not show any evidence for the formation of the β -diketiminatolead(II) halide or benzyl-*tert*-butyl ether.



2.3.2.3 Reaction with an unsaturated electrophile

The reaction of the β -diketiminatolead(II) *tert*-butoxide **4** with an unsaturated electrophile was also examined. Addition of benzaldehyde to the lead(II) *tert*-butoxide **4** resulted in the formation of a white precipitate, and two compounds in a 1:1 ratio. One was identified as β -diketimine **1**. The second was separated by washing the crude product with pentane. An X-ray crystallographic study showed that it was the diimine **13** (equation 37).



Single crystals of **13** were obtained by recrystallisation from THF at -30 °C. ORTEP drawing of **13** is shown in Figure 12. Selected bond lengths and angles are given in Table 6, and selected crystallographic data in Table 7. The C(2)–C(30) bond length is 1.337(2) Å, similar to the C=C bond distance (1.379(2) Å) in Mair's β -triketimine [ArN(H)C(CH₃)C{C(CH₃)NAr}₂] (Ar = (2-*i*PrC₆H₄)).^[120] Both N(2)–C(3) (1.273(2) Å) and N(1)–C(1) (1.281(2) Å) in **13** are shorter than the N–C bond lengths (1.318(3) and 1.341(3) Å) in the β -diketimine **1**, indicating that formal N=C double bonds are present.^[121] The bond distances for C(1)–C(2) and C(2)–C(3), 1.486(2) and 1.508(2) Å respectively, are in the range for C–C single bonds.^[122] Dihedral angles:

$C(6)-N(1)-C(1)-C(2) = -176.9(1)^\circ$, $N(1)-C(1)-C(2)-C(30) = -178.7(1)^\circ$, and $C(1)-C(2)-C(30)-C(31) = -176.3(1)^\circ$; as well as bond lengths: $C(1)-C(2) = 1.486(2)$ Å and $C(2)-C(30) = 1.508(2)$ Å show that there is conjugation between one of the imine groups and the $C(2)-C(30)$ double bond, but not the other.

Figure 12. ORTEP diagram of compound **13**. The ellipsoid probability is shown at 30%

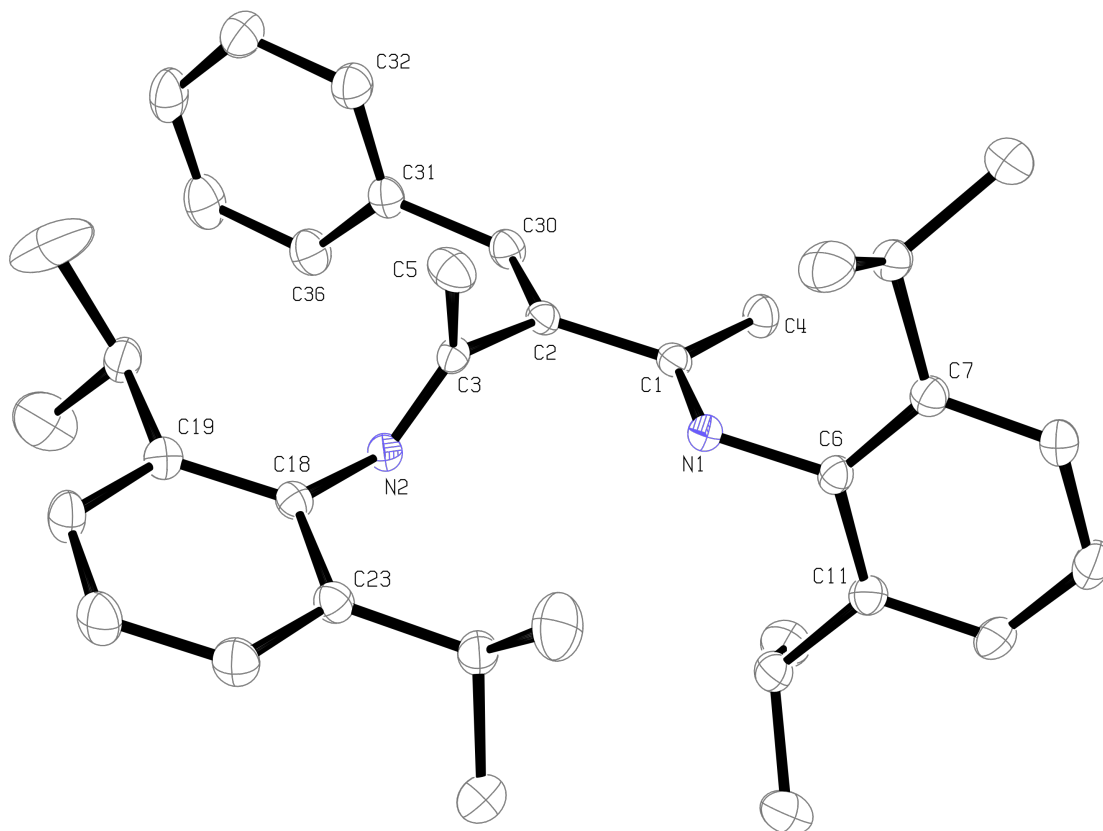


Table 6. Selected bond lengths (Å) and angles (deg) for compound **13**

<i>Bond lengths (Å)</i>			
N(1)–C(1)	1.281(2)	C(2)–C(3)	1.508(2)
N(2)–C(3)	1.273(2)	C(1)–C(4)	1.507(2)
N(1)–C(6)	1.431(2)	C(3)–C(5)	1.501(2)
N(2)–C(18)	1.433(2)	C(2)–C(30)	1.337(2)
C(1)–C(2)	1.486(2)	C(30)–C(31)	1.487(2)
<i>Bond angles (deg)</i>			
C(1)–N(1)–C(6)	121.12(12)	N(2)–C(3)–C(2)	117.74(13)
C(3)–N(2)–C(18)	120.49(13)	C(1)–C(2)–C(3)	116.31(12)
N(1)–C(1)–C(2)	117.47(13)	C(2)–C(30)–C(31)	127.10(14)
N(1)–C(1)–C(4)	124.38(13)	C(1)–C(2)–C(30)	121.66(13)
N(2)–C(3)–C(5)	126.13(14)	C(3)–C(2)–C(30)	121.97(13)
<i>Dihedral angles (deg)</i>			
C(11)–C(6)–N(1)–C(1)	–100.6(2)	N(1)–C(1)–C(2)–C(3)	4.2(2)
C(6)–N(1)–C(1)–C(2)	–176.9(1)	C(23)–C(18)–N(2)–C(3)	–93.2(2)
N(1)–C(1)–C(2)–C(30)	–178.7(1)	C(18)–N(2)–C(3)–C(2)	178.0(1)
C(1)–C(2)–C(30)–C(31)	–176.3(1)	N(2)–C(3)–C(2)–C(30)	85.8(2)
C(2)–C(30)–C(31)–C(32)	85.1(2)	C(3)–C(2)–C(30)–C(31)	0.6(2)
N(2)–C(3)–C(2)–C(1)	–97.1(2)		

Table 7. Selected crystallographic data for compound **13**

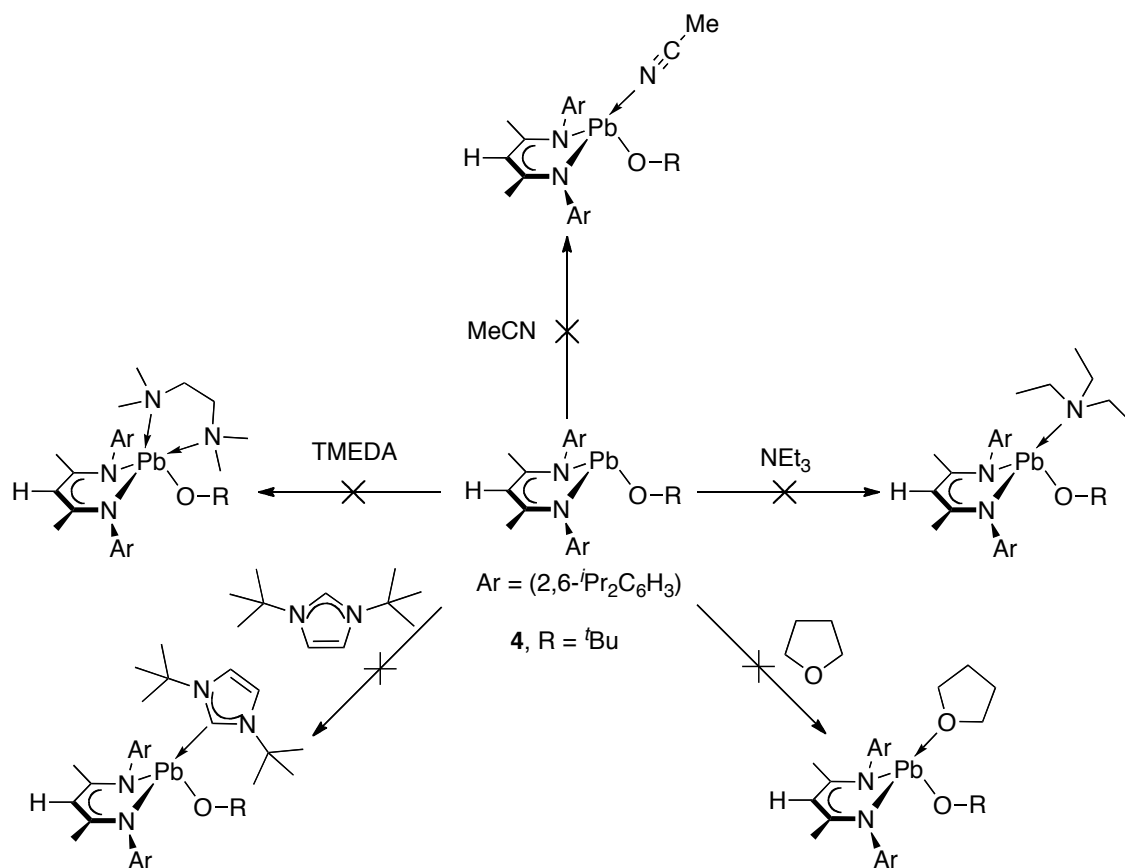
[PhCH=C{C(CH ₃)N(2,6- <i>i</i> -Pr ₂ C ₆ H ₃)} ₂] (13)	
chemical formula	C ₃₆ H ₄₆ N ₂
molecular mass	506.75
temperature (K)	173(2)
wavelength (Å)	0.71073
crystal system	monoclinic
space group	<i>P</i> 2 ₁ / <i>c</i> (No. 14)
<i>a</i> (Å)	13.2095(3)
<i>b</i> (Å)	8.8710(2)
<i>c</i> (Å)	26.1615(5)
<i>α</i> (deg)	90
<i>β</i> (deg)	91.691(1)
<i>γ</i> (deg)	90
<i>V</i> (Å ³)	3064.31(11)
<i>Z</i>	4
ρ_{calcd} (Mg m ⁻³)	1.10
θ range (deg)	3.42–26.02
abs coeff (mm ⁻¹)	0.06
measd/indep reflns/ <i>R</i> (int)	20 035/5950/0.048
reflns with <i>I</i> > 2 σ (<i>I</i>)	4443
data/restraints/param	5950/0/353
goodness of fit on <i>F</i> ²	1.008
final <i>R</i> indices [<i>I</i> > 2 σ (<i>I</i>)]	<i>R</i> 1 = 0.051, <i>wR</i> 2 = 0.120
<i>R</i> indices (all data)	<i>R</i> 1 = 0.074, <i>wR</i> 2 = 0.134
largest diff peak and hole (e Å ⁻³)	0.19 and -0.23

The ¹H NMR spectrum of the diimine **13** showed two septets at δ_{H} 2.83 and 2.67 ppm, assigned to the tertiary isopropyl protons (CHMe₂), as well as four doublets centred at δ_{H} 1.14, 1.13, 0.95 and 0.82 ppm, assigned to the methyl protons in the isopropyl substituents (CHMe₂) in the *N*-aryl groups. The four doublets are consistent with a structure, in which the two *N*-aryl substituents are inequivalent in solution. The methyl groups within each isopropyl group are also inequivalent. As there is no further separation of the isopropyl resonances, there appears to be no restricted rotation about the *N*-aryl bond.

2.3.2.4 Ligand coordination

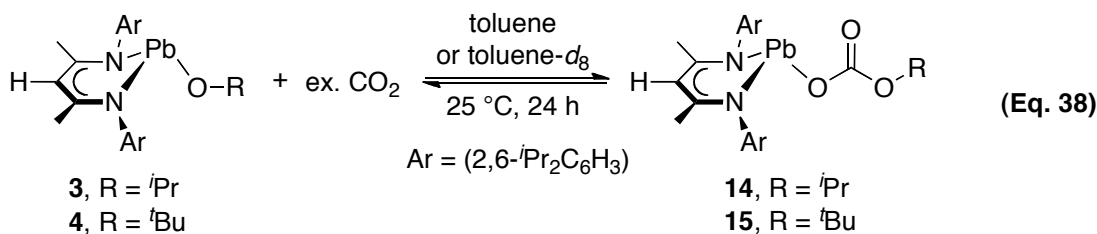
In the insertion of CO₂ into the metal-oxygen bond, it is sometimes claimed that the initial step involves the coordination of CO₂ to the metal centre (Scheme 36, Page 58).^[123-125] In order to investigate whether this is likely in the case of the β -diketiminatolead(II) alkoxides, we looked in a series of NMR experiments at the interactions of the lead(II) *tert*-butoxide **4** with some monodentate and bidentate ligands (Scheme 32). No evidence of coordination was observed when acetonitrile, THF, or 1,3-di-*tert*-butylimidazol-2-ylidene was added to the lead(II) *tert*-butoxide **4**. Similarly, upon addition of the bidentate ligand, tetramethylethylenediamine (TMEDA), the ¹H NMR spectrum did not show any changes of the chemical shifts for either TMEDA (δ_{H} 2.36 and 2.12 ppm) or the lead(II) *tert*-butoxide **4** (δ_{H} 4.57 ppm for γ -H; δ_{H} 3.83 and 3.12 ppm for CHMe₂). Furthermore, crystallisation of **4** from a 1:1 mixture of *n*-hexane and acetonitrile solution resulted in the formation of pure, unsolvated crystals.

Scheme 32. Attempted reactions of the β -diketiminatolead(II) *tert*-butoxide **4** with monodentate or bidentate ligands in C₆D₆



2.3.2.5 Reactions with CO₂

Concurrent work with NCJ in our group showed that treatment of the β -diketiminatolead(II) isopropoxide **3** with an excess of CO₂ gave the isolable β -diketiminatolead(II) isopropoxycarbonate [(BDI_{DIPP})PbOCO₂^{*i*}Pr] (**14**) (equation 38).^[113] An X-ray crystallographic study by NCJ confirmed its connectivity.^[114] The ¹H NMR spectrum of the carbonate **14** showed a broad resonance at δ_{H} 3.33 ppm for the tertiary CHMe₂ proton in the terminal carbonate ligand. The characteristic carbonyl resonance (δ_{C} 160.9 ppm) was shown in the ¹³C{¹H} NMR spectrum. The ²⁰⁷Pb NMR spectrum, acquired by NCJ, showed a single resonance at δ_{Pb} 809 ppm which is upfield from that in the lead(II) isopropoxide **3** (δ_{Pb} 1500 ppm).^[114] A carbonyl stretching absorption was observed at 1695 cm⁻¹ in the IR spectrum in CCl₄ as solvent.^[114] The formation of the lead(II) isopropoxycarbonate **14** appeared to be irreversible, as reduction in pressure did not lead to the formation of the parent lead(II) isopropoxide **3**. However, when ¹³CO₂ was added to a solution of **14**, the resonance at δ_{C} 160.9 ppm in the ¹³C{¹H} NMR spectrum increased in intensity, indicating that ¹³CO₂ was exchanging into **14**.

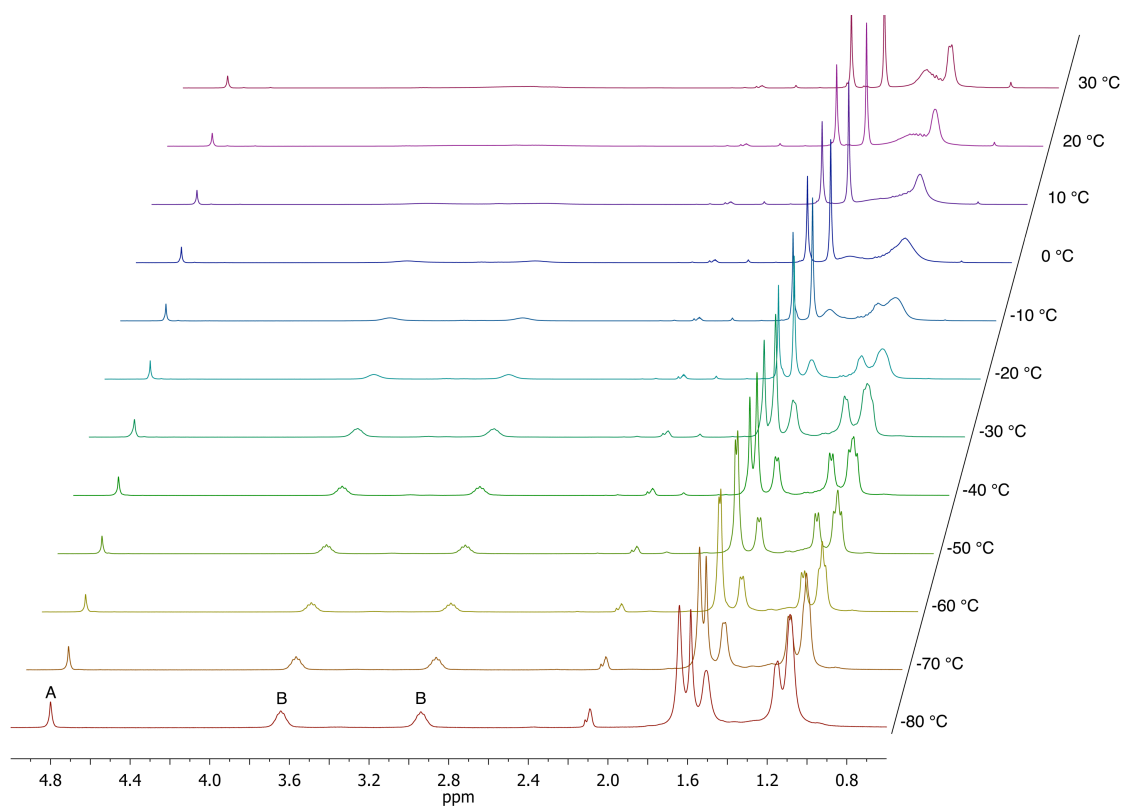


The insertion of CO₂ into the lead(II) *tert*-butoxide **4** is described in this thesis. Treatment of **4** with an excess of carbon dioxide gives the corresponding carbonate [(BDI_{DIPP})PbOCO₂^{*t*}Bu] (**15**) at room temperature (equation 38). Formation of compound **15** is shown by a singlet at δ_{C} 160.3 ppm in the ¹³C{¹H} NMR spectrum and by an absorption at 1731 cm⁻¹ in the IR spectrum in CCl₄ as solvent, which is indicative of the carbonyl functionality.^[126-128] In contrast to the isopropoxycarbonate **14**, the β -diketiminatolead(II) *tert*-butoxycarbonate **15** was converted into the parent lead(II) *tert*-butoxide **4**, when the pressure of the CO₂ atmosphere was reduced. Furthermore, we were unable to isolate the lead(II) *tert*-butoxycarbonate **15** from the reaction. This is partially due to loss of CO₂ and degradation to an intractable white solid, even at -30

°C in solution (equation 38). The lead(II) *tert*-butoxycarbonate **15** shows a resonance at δ_{Pb} 817 ppm in the ^{207}Pb NMR spectrum, upfield from the lead(II) *tert*-butoxide **4** (δ_{Pb} 1713 ppm).

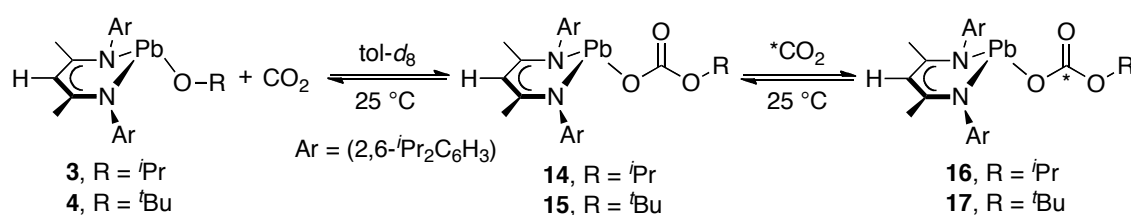
The ^1H NMR spectrum of the lead(II) *tert*-butoxycarbonate **15** shows a singlet at δ_{H} 4.78 ppm assigned to the γ -*H*, as well as a broad resonance at δ_{H} 3.32 ppm assigned to the tertiary isopropyl protons of the *N*-aryl group (CHMe_2). In addition, two resonances at δ_{H} 1.27 and 1.14 ppm are assigned to the methyl protons in the isopropyl group (CHMe_2). The broadness of the CHMe_2 resonance suggests that rotation about the *N*-aryl bond in **15** at room temperature is faster than that in the parent alkoxide **4**, possibly due to a reduced crowding around the metal centre. The spectrum of the lead(II) *tert*-butoxide **4** shows two septets at δ_{H} 3.84 and 3.14 ppm assigned to the CHMe_2 resonances, and four doublets centred at δ_{H} 1.66, 1.26, 1.21 and 1.16 ppm, assigned to the CHMe_2 resonances at room temperature, indicating that rotation is restricted about the *N*-aryl bond on the NMR timescale in the alkoxide **4**.^[62, 114] To investigate whether rotation would be restricted in the carbonate **15**, a variable temperature (VT) ^1H NMR study of **15** in toluene- d_8 showed that upon gradually decreasing the temperature, the broad tertiary isopropyl proton resonance (CHMe_2) became even broader at 20 °C and on further cooling separated into two broad resonances at δ_{H} 3.64 and 2.94 ppm with $\Delta\delta_{\text{H}}$ 280 Hz at -80 °C (Figure 13). However, we were unable to measure the barrier of rotation about the *N*-aryl bond. The facile decomposition of **15** at high temperature prevented measurement of the upper coalescence temperature.

Figure 13. VT- ^1H NMR spectra (400 MHz, toluene- d_8) of $[(\text{BDI}_{\text{DIPP}})\text{PbOCO}_2^t\text{Bu}]$ (**15**), where A = $\gamma\text{-H}$ and B = CHMe_2

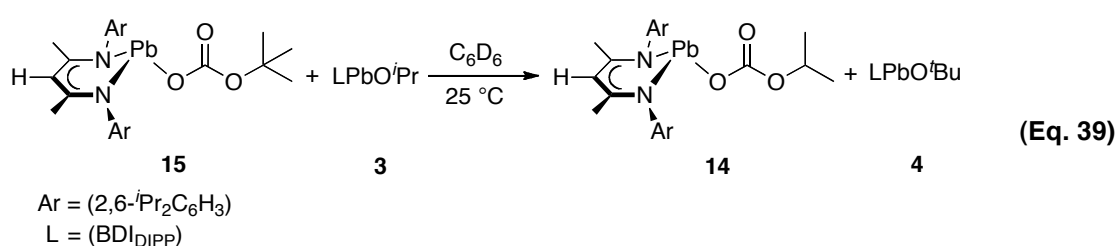


The lead(II) *tert*-butoxycarbonate **15** was generated *in situ* by the addition of one equivalent of CO_2 to the lead(II) *tert*-butoxide **4**, and its formation was confirmed by ^1H NMR spectroscopy (Scheme 33). Then one equivalent of $^{13}\text{CO}_2$ was added. The $^{13}\text{C}\{^1\text{H}\}$ NMR spectrum of the mixture revealed that the carbonyl resonance at δ_{C} 160.3 ppm had increased in intensity. The *tert*-butoxycarbonate **15** thus behaved like the isopropoxycarbonate **14** (studied by NCJ), to give the corresponding carbonate **17**.^[114] Several attempts were made to determine the rate of $^{13}\text{CO}_2$ exchange by ^{13}C -EXSY experiments, but we were unable to obtain reproducible data.

Scheme 33. ^{13}C -labeling study on the lead(II) carbonates **14** and **15**



The relative stabilities of the carbonates **14** and **15** were further investigated by a competition study between the two lead(II) alkoxides and carbon dioxide. The lead(II) *tert*-butoxycarbonate **15** was generated *in situ* and one equivalent of the lead(II) isopropoxide **3** was added (equation 39). The ^1H NMR spectrum of this mixture showed complete conversion to the lead(II) isopropoxycarbonate **14** and the lead(II) *tert*-butoxide **4** after 24 hours at room temperature. There was no indication of the presence of the lead(II) isopropoxide **3** in solution. This suggested that $[(\text{BDI}_{\text{DIPP}})\text{PbOCO}_2^i\text{Pr}]$ (**14**) was formed preferentially.

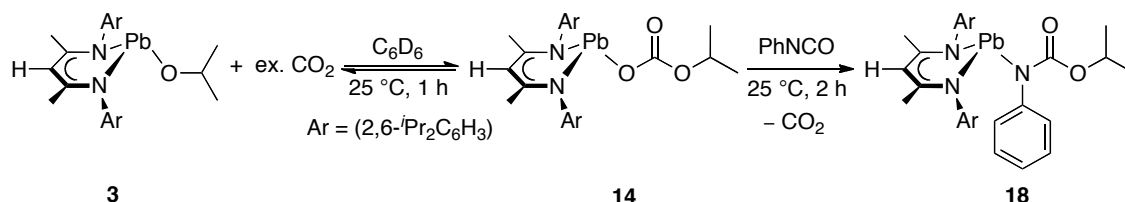


This result can be attributed to both steric and electronic factors. First, the bulk of both of the β -diketiminato and the *tert*-butoxide ligands in $[(\text{BDI}_{\text{DIPP}})\text{PbO}^t\text{Bu}]$ (**4**) may make the oxygen atom less available for coordination with carbon dioxide, than that in the lead(II) isopropoxide $[(\text{BDI}_{\text{DIPP}})\text{PbO}^i\text{Pr}]$ (**3**).^[128] Secondly, work by Bryndza and co-workers on a series of late transition metal complexes showed that there is a correlation between the stability of the transition metal alkoxide and the basicity of its corresponding alcohol; the metal alkoxide is more stable when the $\text{p}K_{\text{a}}$ of the corresponding alcohol is higher.^[129] If the lead(II) alkoxides show a similar trend, we can expect the lead(II) *tert*-butoxide **4** to be more stable than the lead(II) isopropoxide **3**, based on the $\text{p}K_{\text{a}}$ of the corresponding alcohols (*c.f.* $\text{p}K_{\text{a}}$ of *tert*-butanol in DMSO = 32.2; $\text{p}K_{\text{a}}$ of isopropanol in DMSO = 30.2).^[130-132] Further evidence for this hypothesis was gained by a combined experimental and theoretical study on the isostructural tin system (performed by Dr. Lorenzo Ferro (LF) in collaboration with Dr. Hazel Cox).^[128]

The reaction between the lead(II) isopropoxycarbonate **14** and phenyl isocyanate was also investigated. The carbonate **14** was generated *in situ* and treated with phenyl isocyanate in C_6D_6 to give almost exclusive formation of the known lead(II) carbamate $[(\text{BDI}_{\text{DIPP}})\text{PbN}(\text{Ph})\text{CO}_2^i\text{Pr}]$ (**18**) after 2 hours at room temperature (Scheme 34). The ^1H

NMR spectrum of compound **18** is identical to that in the literature.^[114] This suggests that there is a thermodynamic preference for the formation of the lead(II) carbamate **18**.

Scheme 34. Reaction of the lead(II) isopropoxycarbonate **14** with phenyl isocyanate

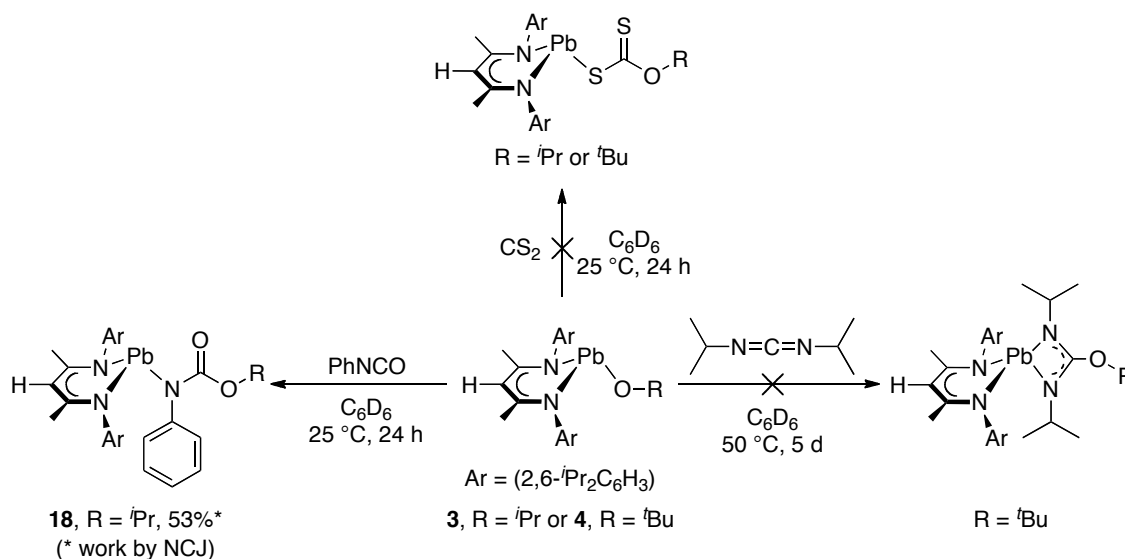


2.3.2.6 Reactions with other heterocumulenes

Although the clean insertion of carbon disulfide into transition metal-oxygen bonds has been reported in literature, treatment of the lead(II) alkoxides **3** or **4** with carbon disulfide resulted in the formation of an intractable mixture of products (Scheme 35).^[88, 126, 133] No reaction was observed when the lead(II) *tert*-butoxide **4** was treated with *N,N'*-diisopropylcarbodiimide in C₆D₆.

Work by NCJ showed that treatment of the lead(II) isopropoxide **3** with phenyl isocyanate in toluene gave the isolable insertion product, the lead(II) carbamate **18**, in 53% yield.^[114] However, the analogous reaction between the lead(II) *tert*-butoxide **4** and phenyl isocyanate gave an intractable mixture.

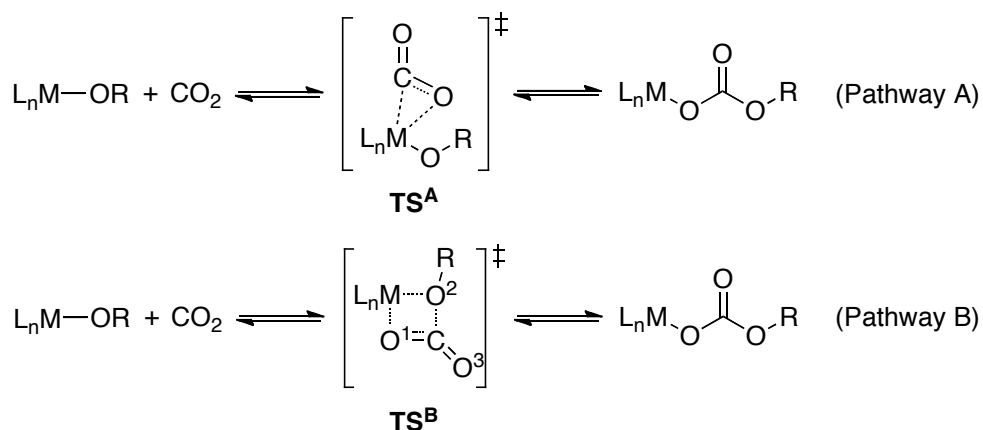
Scheme 35. Reactions of the β -diketiminatolead(II) alkoxides with heterocumulenes



2.3.3 Mechanism of CO₂ insertion into the lead(II) alkoxides **3** and **4**

The results described above show that the insertion of CO₂ into the Pb–O bond in our lead(II) alkoxides is reversible. In his mechanistic study of the tin analogues, LF considered that the initial coordination of carbon dioxide can proceed *via* two different pathways (Scheme 36).^[128] First, due to the minimal reactivity with aliphatic electrophiles, a reaction pathway that avoided a nucleophilic attack by the oxygen atom was examined. It was postulated that the carbon dioxide coordinated to the metal centre in η^2 -fashion to form a three-membered M–C–O cyclic transition state (**TS^A**, pathway A). This led to insertion of carbon dioxide into the M–O bond. The second pathway was the traditional nucleophilic pathway, in which the lone pair on the oxygen from the metal alkoxide interacted with CO₂ to form a four-membered transition state (**TS^B**), leading to the formation of a new C–O₂ bond, and weakening of the C=O₁ bond. This is followed by the formation of a new M–O₁ bond and breaking of the M–O₂ bond to form the metal carbonate complex (pathway B).

Scheme 36. Two pathways for carbon dioxide insertion into a M–O bond^[128]



A study by LF using density functional theory (DFT) showed that the energy of the transition state **TS^A** for the β -diketiminatotin(II) isopropoxide in pathway A is $\Delta G^\ddagger = 237.0 \text{ kJ mol}^{-1}$, significantly higher than the transition state **TS^B** in pathway B ($\Delta G^\ddagger = 69.5 \text{ kJ mol}^{-1}$).^[128] Furthermore, the pathway from **TS^A** to the final carbonate was not found. My experimental results show that the reluctance of the lead centre to coordinate various monodentate or bidentate ligands also suggests that the initial coordination of CO₂ to the metal centre, as in pathway A, is unlikely (Section 2.3.2.4, Page 52).

The reactions between the β -diketiminatolead(II) alkoxides, **3** and **4**, and aliphatic electrophiles are generally slow or give an intractable mixture, for example the reaction of the lead(II) *tert*-butoxide **4** with methyl iodide only proceeds under forcing conditions. This is in contrast to the reactions of transition metal alkoxides. For example, the oxygen of the alkoxide ligand in Pérez's rhenium alkoxide $[\text{Re}(\text{OMe})(\text{CO})_3(\text{bipy})]$ (bipy = 2,2'-bipyridine) behaves as a nucleophilic centre, which reacts with methyl iodide to give $[\text{Re}(\text{I})(\text{CO})_3(\text{bipy})]$ and dimethyl ether.^[133] The rhenium alkoxide also reacts with CS_2 to give the corresponding insertion product $[\text{Re}\{\text{SC}(\text{S})\text{OMe}\}(\text{CO})_3(\text{bipy})]$. More importantly, Vahrenkamp's pyrazolylborate-zinc methoxide complex $[(\text{Tp}^{\text{Ph,Me}})\text{ZnOMe}]$ ($(\text{Tp}^{\text{Ph,Me}} = \text{hydridotris}(3\text{-phenyl-5-methylpyrazolyl})\text{borate})$) acts as a nucleophile and reacts readily with methyl iodide to give the corresponding zinc iodide and dimethyl ether.^[89] However, the zinc complex only reacts with CO_2 under forcing conditions. Several variables, such as differences in the Lewis acidity of the metal centre and the steric hindrance from the ligands around the metal, prevent direct comparisons between the lead(II) alkoxides, **3** and **4**, and Vahrenkamp's zinc alkoxide. However, based on the experimental results reported in this thesis, it is reasonable to suggest that the oxygen atom in the lead(II) alkoxides **3** and **4** is only weakly nucleophilic.

2.4 Conclusions

β -Diketiminatolead(II) alkoxides were synthesised and their reactions towards various organic substrates were examined. The experimental results reported demonstrate that the oxygen in the alkoxide ligand in the lead(II) alkoxides **3** and **4** is neither basic nor nucleophilic towards the organic substrates tested. Although insertion of CO₂ into the Pb–O bond is observed in both the lead(II) isopropoxide **3** and the *tert*-butoxide **4** to form the corresponding carbonates **14** and **15**, we were unable to study the kinetics of these reactions with CO₂ in greater detail as the reactions were too fast. Subsequent studies by LF on the isostructural tin system proved to be more fruitful because the tin system reacted a lot slower with CO₂, and the equilibrium between the tin alkoxides and the corresponding carbonates could be measured using an atmosphere of CO₂.^[128] A similar trend with regards to the different alkoxides was observed in the tin system. The differences in the reactivity with CO₂ are attributed to a combination of steric and electronic effects. Our failure to observe coordination of an additional ligand to the lead centre in the alkoxide **4** supports our hypothesis that insertion of CO₂ into the Pb–O bond proceeds *via* a four-membered transition state, as for the tin analogues.

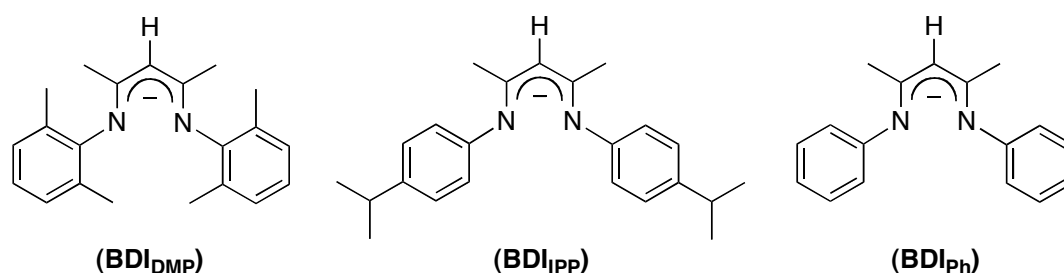
3. Structure and characteristics of lead(II) complexes with various β -diketiminato ligands

3.1 Introduction

3.1.1 Metal complexes with less bulky β -diketiminato ligands than BDI_{DIPP}

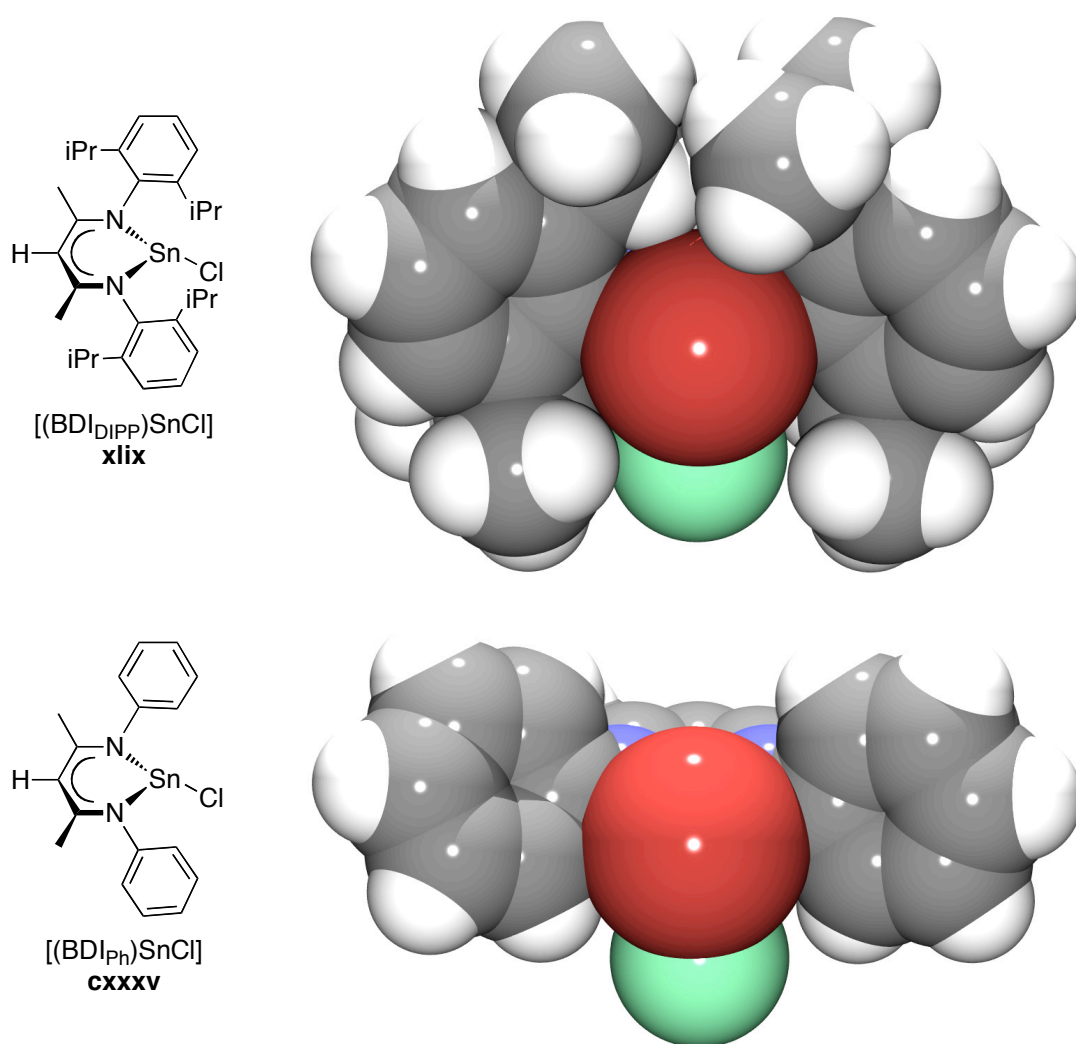
In recent years, the use of β -diketiminato ligands to stabilise various metal centres has expanded rapidly across the periodic table.^[48] The variety of possible substitution patterns, as described in Chapter 1, to accommodate different metal ions is one of the major advantages of this ligand system. The β -diketiminato anion with a bulky *N*-aryl substituent $[\text{HC}\{\text{C}(\text{Me})\text{N}(2,6\text{-}^i\text{Pr}_2\text{C}_6\text{H}_3)\}_2]^-$ (BDI_{DIPP}) has been widely used to support heavy group 14 metal ions.^[62, 70, 112, 114, 117, 134] The advantage of the (BDI_{DIPP}) ligand is that the isopropyl groups are thought to provide enough bulk to prevent coordination of more than one ligand to the metal centre. To the best of our knowledge, the only other example of a compound with β -diketiminato ligand, other than (BDI_{DIPP}), attached to lead is $[(\text{BDI}_{\text{TMS}})_2\text{Pb}]$ ($\text{BDI}_{\text{TMS}} = [\text{HC}\{\text{C}(\text{Me})\text{N}(\text{SiMe}_3)\}_2]^-$), in which the (BDI_{TMS}) ligand is smaller, so that two β -diketiminato ligands may be bound to the metal centre.^[135] There are a few examples of monomeric germanium(II) and tin(II) complexes, supported by β -diketiminato ligands with less sterically demanding *N*-aryl groups, such as $[\text{CH}\{\text{C}(\text{Me})\text{N}(\text{C}_6\text{H}_5)\}_2\text{GeR}]$ ($\text{R} = \text{Me}$ or Cl) and $[\text{CH}\{\text{C}(\text{Me})\text{N}(2,6\text{-CH}_2\text{C}_6\text{H}_3)\}_2\text{SnO}^i\text{Pr}]$.^[40, 136-137] We wished to examine the influence of the *N*-aryl group in the β -diketiminato ligand on the coordination geometry and chemistry of the lead(II) complexes. Hence, we focused our attention on the synthesis of complexes containing less sterically demanding β -diketiminato ligands: $[\text{HC}\{\text{C}(\text{Me})\text{N}(2,6\text{-Me}_2\text{C}_6\text{H}_3)\}_2\text{CH}]^-$ (BDI_{DMP}), $[\text{HC}\{\text{C}(\text{Me})\text{N}(4\text{-}^i\text{PrC}_6\text{H}_4)\}_2]^-$ (BDI_{IPP}) and $[\text{HC}\{\text{C}(\text{Me})\text{N}(\text{C}_6\text{H}_5)\}_2]^-$ (BDI_{Ph}) (Figure 14).

Figure 14. β -Diketiminato anions used in this study



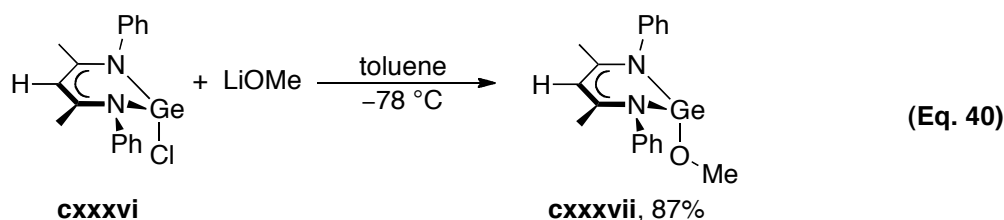
The effects of substituents at the *ortho*-position of the *N*-aryl groups in the β -diketiminato framework are illustrated by the space-filling models of two β -diketiminatotin(II) chlorides **xliv** and **cxxxv** (Figure 15).^[65, 136] The space-filling model of [(BDI_{DIPP})SnCl] (**xliv**) shows that the tin(II) centre is partly surrounded by the isopropyl groups of the *N*-aryl substituents. However, the tin(II) centre in [(BDI_{Ph})SnCl] (**cxxxv**) is more exposed than that in complex **xliv**.

Figure 15. Space-filling models of [(BDI_{DIPP})SnCl] (**xliv**, top-right) and [(BDI_{Ph})SnCl] (**cxxxv**, bottom-right).^[65, 136] The tin, chloride and nitrogen atoms are represented in purple, green and blue, respectively

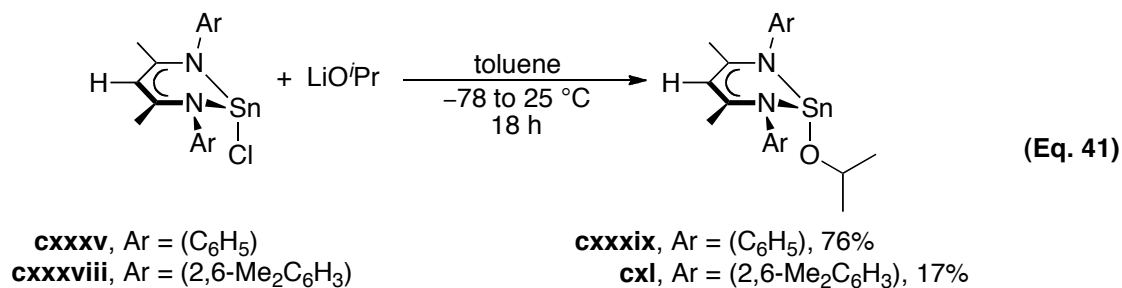


The (BDI_{Ph}) anion has also been used to generate germanium(II) complexes. Barrau and co-workers reported the synthesis of [(BDI_{Ph})GeOMe] (**cxxxvii**) by treatment of the β -

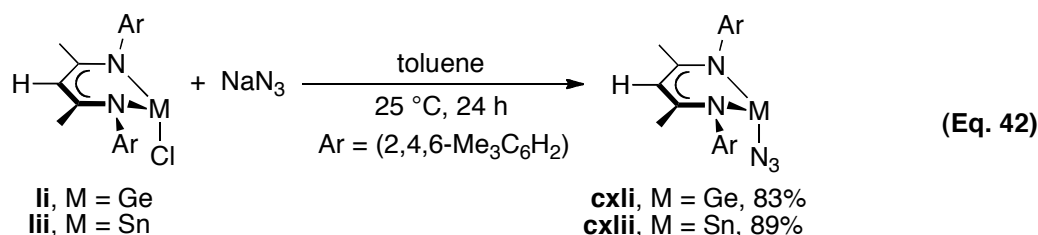
diketiminatogermanium(II) chloride [(BDI_{Ph})GeCl] (**cxxxvi**) with lithium methoxide (equation 40).^[137] The solid state structure of compound **cxxxvii** was not reported.



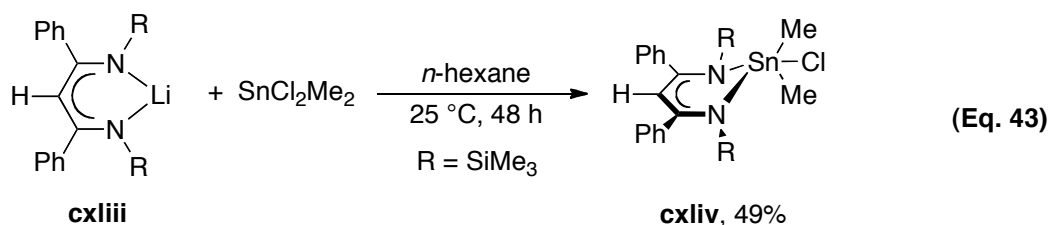
Gibson *et al.* synthesised the β -diketiminatotin(II) alkoxides **cxxxix** and **cxl**.^[40] Treatment of the β -diketiminatotin(II) chlorides, **cxxxv** or **cxxxviii**, with lithium isopropoxide gave the tin(II) isopropoxides **cxxxix** or **cxl** (equation 41). [(BDI_{Ph})SnO^{*i*}Pr] (**cxxxix**) was isolated as a yellow solid in good yield, whereas [(BDI_{DMP})SnO^{*i*}Pr] (**cxl**) was obtained as an impure oil. However, washing the crude product with cold heptane gave pure **cxl** in 17% yield. An X-ray crystallographic study showed the geometry around the tin centre was pyramidal. The solid state structure of [(BDI_{Ph})SnO^{*i*}Pr] (**cxxxix**) has not been reported.



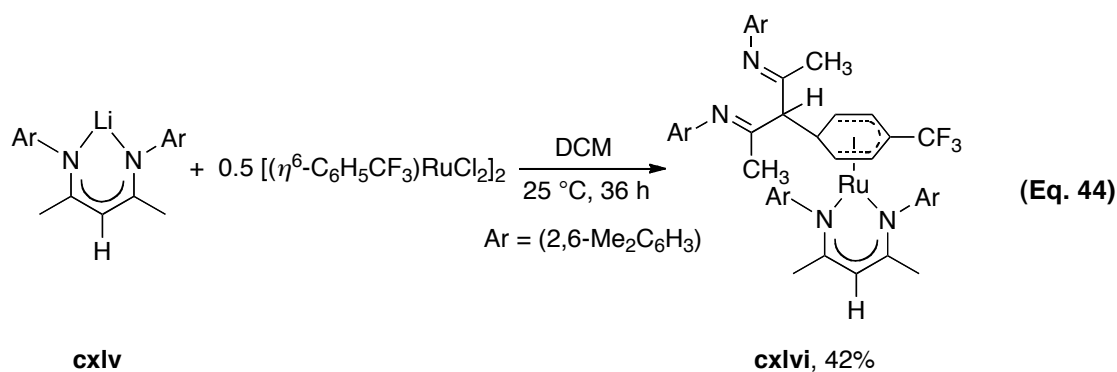
Dias *et al.* described the germanium(II) and tin(II) azide complexes **cxli** and **cxlii**, supported by [HC{C(Me)N(2,4,6-Me₃C₆H₂)}₂]⁻ (BDI_{TMP}) anion.^[68] Treatment of the β -diketiminatometal chlorides **li** or **lii** with sodium azide gave the corresponding metal azide complexes [(BDI_{TMP})MN₃] (**cxli**, M = Ge; **cxlii**, M = Sn) (equation 42). The IR spectra of these azide complexes showed N₃ asymmetric stretching vibrations at ~2060 cm⁻¹. The X-ray crystallographic studies showed the azide group was almost linear with the N–N–N bond angle 176.3(6)° for **cxli** and 176.0(7)° for **cxlii**.



Lappert *et al.* reported a five-coordinate tin(IV) β -diketiminato complex **cxliv** formed upon addition of lithium β -diketiminato **cxliii** to SnCl_2Me_2 (equation 43).^[138] The solid state structural analysis showed that the ligands were coordinated in a distorted bipyramidal geometry around the metal centre, with chloride and one of the nitrogen atoms occupying axial positions.

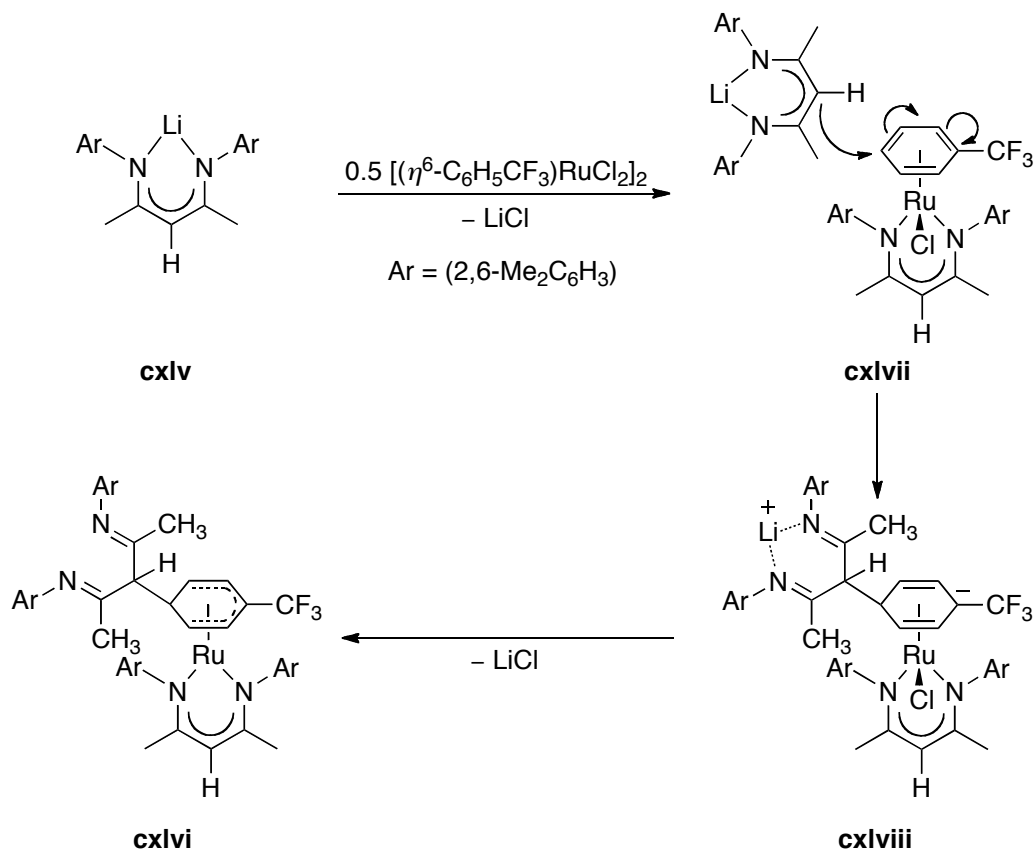


Examples of compounds of transition and other main group metals coordinated to β -diketiminato ligands containing less sterically demanding *N*-aryl groups than those in (BDI_{DIPP}) are known. Treatment of the lithium β -diketiminato **cxlv** with $[(\eta^6\text{-C}_6\text{H}_5\text{CF}_3)\text{RuCl}_2]_2$ gave the unexpected product **cxlvi** (equation 44).^[139] X-ray structural analysis showed that the γ -carbon of the β -diimine ligand was bound to the *para*-position of the η^6 -arene fragment to give a η^5 -cyclohexadienyl ligand that was coordinated to the ruthenium centre.

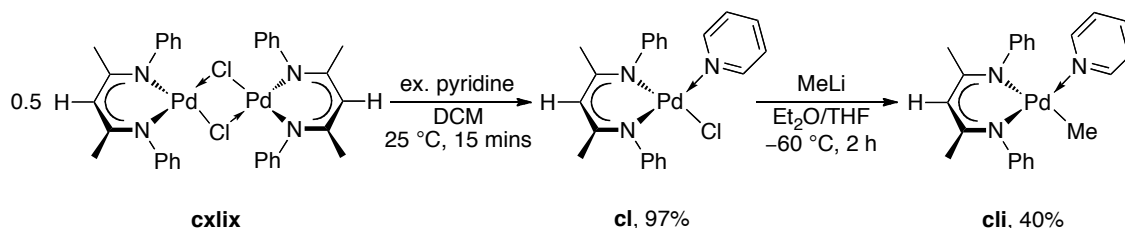


It was suggested that the formation of compound **cxlvi** was initiated by nucleophilic attack of the γ -carbon in the lithium β -diketiminato on the coordinated η^6 -arene fragment of the ruthenium complex **cxlvii**. The final step involved the elimination of lithium chloride from compound **cxlviii** to give complex **cxlvi** (Scheme 37).

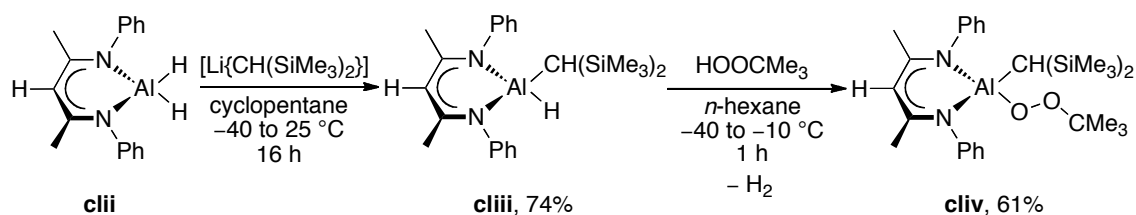
Scheme 37. Proposed mechanism for the formation of compound **cxlvi**^[139]



Song *et al.* reported the synthesis of some mononuclear palladium β -diketiminato complexes.^[140] Treatment of the dimeric β -diketiminatopalladium chloride **cxlix** with an excess of pyridine gave the monomeric palladium complex **cl** in near quantitative yield (Scheme 38). Further reaction with methyllithium gave the palladium alkyl complex **cli**. The direct reaction of the dimeric β -diketiminatopalladium chloride **cxlix** with methyllithium led to the formation of palladium metal and an intractable mixture of products.

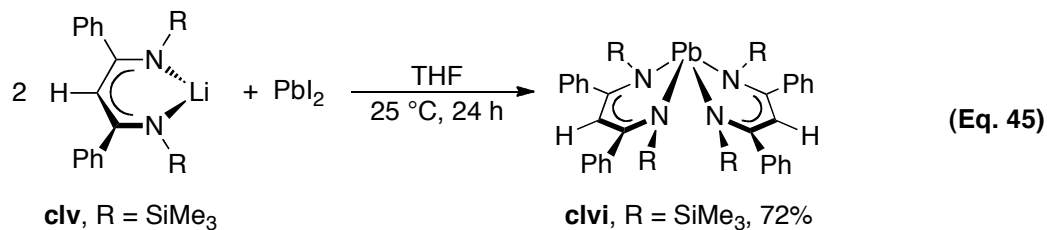
Scheme 38. Reactions of the β -diketiminatopalladium chloride **cxlix**^[140]

Uhl *et al.* reported the synthesis of the β -diketiminatoaluminium alkyl peroxide **cliv**.^[141] Treatment of the dihydride **clii** with $[\text{Li}\{\text{CH}(\text{SiMe}_3)_2\}]$ in cyclopentane gave the aluminium alkyl complex $[(\text{BDI}_{\text{Ph}})\text{Al}(\text{H})\text{CH}(\text{SiMe}_3)_2]$ (**cliii**) in good yield (Scheme 39). Further reaction with *tert*-butyl hydrogen peroxide in *n*-hexane gave compound **cliv**, with evolution of H_2 gas. This aluminium complex is a rare example of a compound with both a reducing Al–C function and an oxidising peroxy group in close proximity in a single molecule.

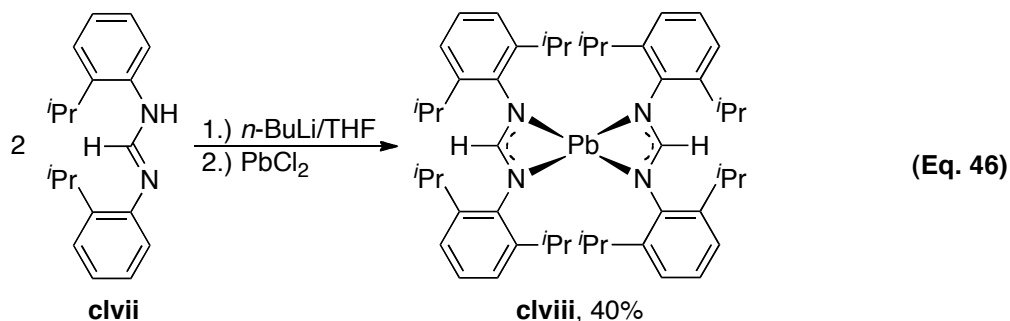
Scheme 39. Reactions of the β -diketiminatoaluminium dihydride **clii**^[141]

3.1.2 Four-coordinate lead(II) complexes

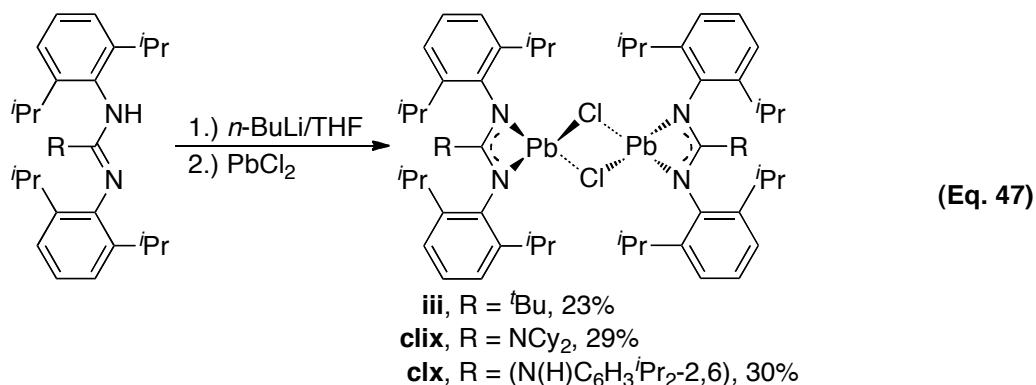
Despite several attempts, the synthesis of $[(\text{BDI}_{\text{DIPP}})_2\text{Pb}]$ has not been successful.^[62] To the best of our knowledge, Lappert *et al.* reported the only bis(β -diketiminato) heavy group 14 metal complex.^[135] Treatment of lead diiodide with two equivalents of lithium β -diketiminato **clv** gave the bis[β -diketiminato]lead(II) **clvi** in 72% yield (equation 45). Formation of this compound is possible, presumably because the SiMe_3 groups are smaller than the 2,6-diisopropylphenyl groups in $(\text{BDI}_{\text{DIPP}})$. The structural analysis of the complex showed that the two β -diketiminato ligands were on one side of the central lead atom. The N–Pb–N bond angles indicated a distorted disphenoidal coordination geometry at lead.^[142]



Other bidentate ligand systems are known to form bis-complexes with lead. Treatment of amidine **clvii** with *n*-BuLi, followed by the addition of one equivalent of lead dichloride gave the complex **clviii** (equation 46).^[26] The solid state structure showed that the ligands were coordinated in a pseudo-bipyramidal geometry around the lead centre with one vacant site, similar to that observed in **civi**.

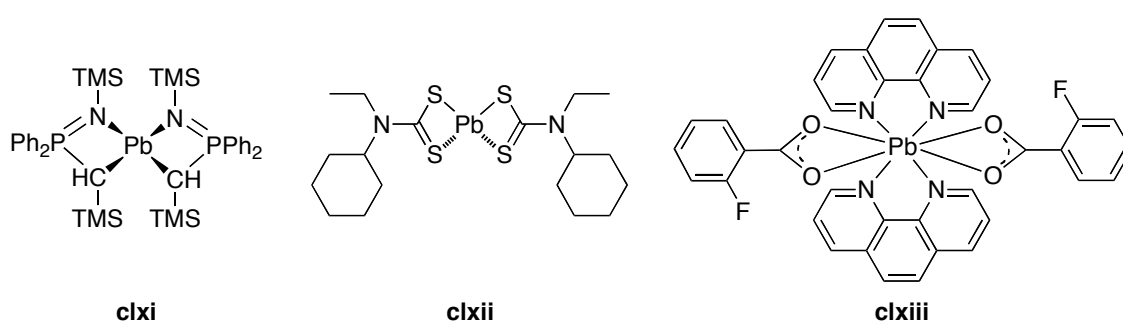


When the proton on the amidinate backbone was changed to a bulkier group, such as *tert*-butyl, or when a guanidinato ligand was used, then only one bidentate ligand could coordinate to lead. Treatment of amidines or guanidines with lead dichloride under the same conditions gave the dimeric lead(II) chlorides **iii**, **clix** and **clx** (equation 47). These dimers were the sole products observed from these reactions even when the ratio of the reagents was varied.^[143]



Bis-lead(II) complexes were obtained with other ligand systems (Figure 16).^[144-146] Compound **clxi** was accessible from the reaction between $[\text{Li}\{\text{CH}(\text{SiMe}_3)\text{P}(\text{Ph})_2=\text{NSiMe}_2\}]$ and lead dichloride in a 2:1 ratio. The synthesis of **clxii** involved the reaction between *N*-ethylcyclohexylamine and lead dichloride in the presence of an excess of carbon disulfide. The octa-coordinate lead(II) complex **clxiii** was synthesised by treatment of PbCO_3 with 1,10-phenanthroline and 2-fluorobenzoic acid. The X-ray structural analyses of compounds **clxi** and **clxii** showed that the ligands were coordinated in a hemidirected coordination mode (Figure 5, Page 18) with a pseudo-bipyramidal geometry around the lead centre.^[61] In contrast, the four bidentate ligands in **clxiii** adopted a holodirected coordination mode around the lead centre.^[61]

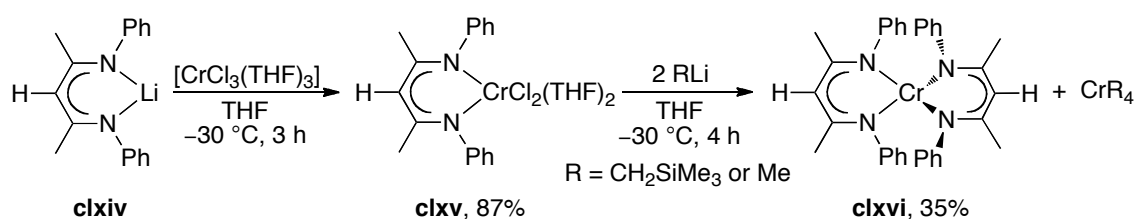
Figure 16. Bis-lead(II) complexes^[144-146]



3.1.3 Other bis(β -diketiminato)metal complexes

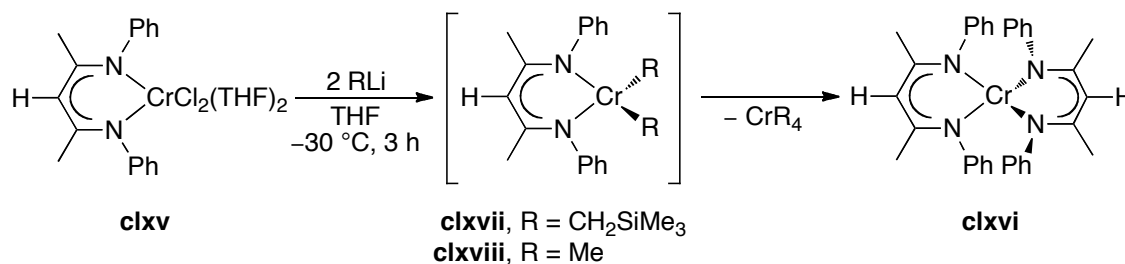
A variety of metal centres have been able to support by more than one β -diketiminato ligand. For instance, treatment of $[\text{CrCl}_3(\text{THF})_3]$ with lithium β -diketiminato **clxiv** gave the β -diketiminatochromium(III) dichloride **clxv**.^[147] Further reaction with lithium alkyls, for example $\text{Me}_3\text{SiCH}_2\text{Li}$ or MeLi , gave the unexpected bis[β -diketiminato]chromium(II) complex **clxvi** and a homoleptic chromium(IV) alkyl, either $\text{Cr}(\text{CH}_2\text{SiMe}_3)_4$ or CrMe_4 , respectively, as a by-product (Scheme 40).

Scheme 40. Synthesis of the bis[β -diketiminato]chromium(II) complex **clxvi**^[147]

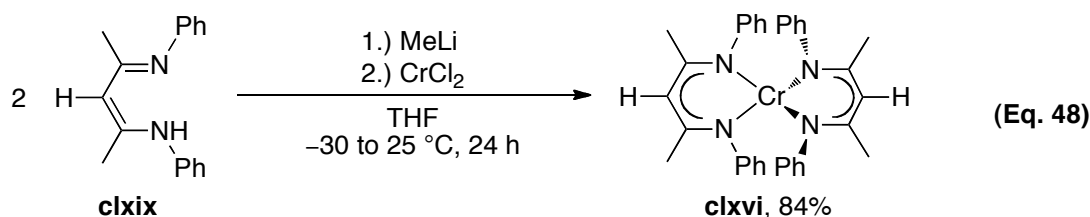


Theopold *et al.* suggested that the unstable β -diketiminatochromium(III) alkyl $[(\text{BDI}_{\text{Ph}})\text{CrR}_2]$ (**clxvii**, $\text{R} = \text{CH}_2\text{SiMe}_3$; **clxviii**, $\text{R} = \text{Me}$), disproportionated to give bis[β -diketiminato]chromium(II) **clxvi** and the chromium(IV) alkyl (CrR_4) (Scheme 41).^[147]

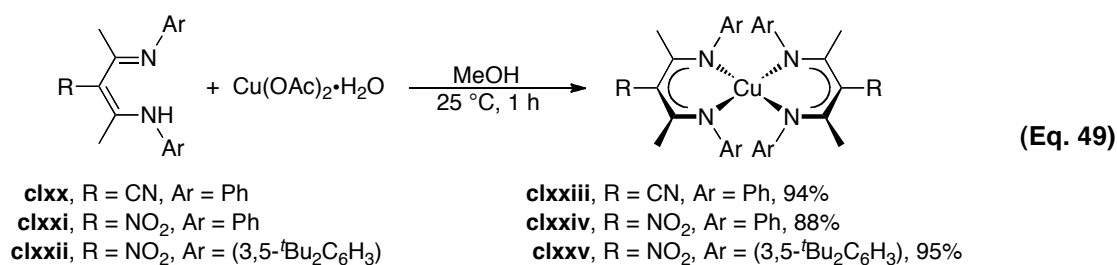
Scheme 41. Proposed reaction pathway for the formation of compound **clxvi**^[147]



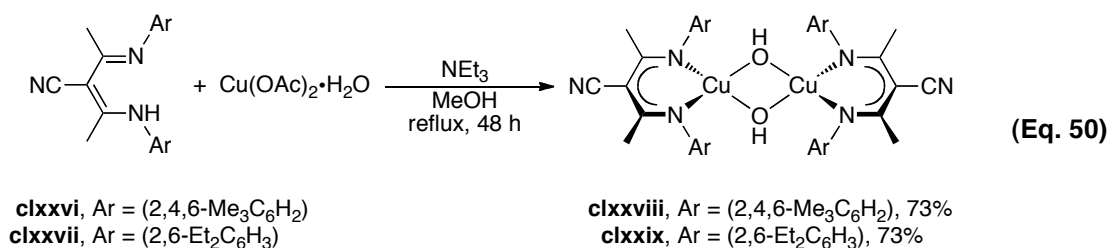
Alternatively, the bis[β -diketiminato]chromium(II) complex **clxvi** was accessible in 84% yield by lithiation of the β -diketimine **clxix** with methyllithium, followed by addition of chromium dichloride in THF (equation 48).



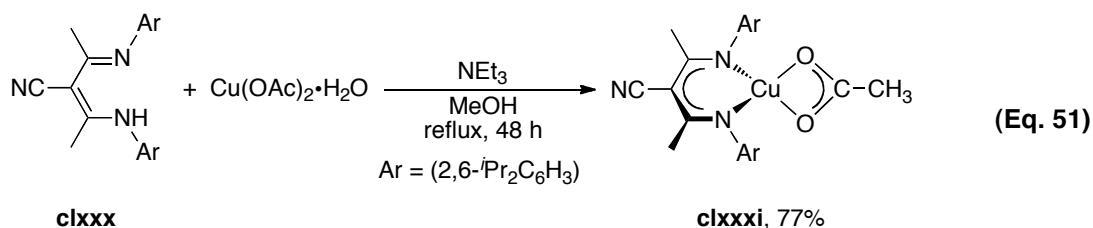
Itoh *et al.* reported a study on the role of *N*-substituents in the β -diketiminato ligand in the control of the formation of some copper(II) complexes.^[148] Treatment of β -diketimines **clxx–clxxii** with cupric acetate in methanol gave the bis[β -diketiminato]copper(II) complexes **clxxiii–clxxv** under ambient conditions (equation 49). The β -diketiminato ligands are coordinated in a distorted tetrahedral geometry around the metal centre.



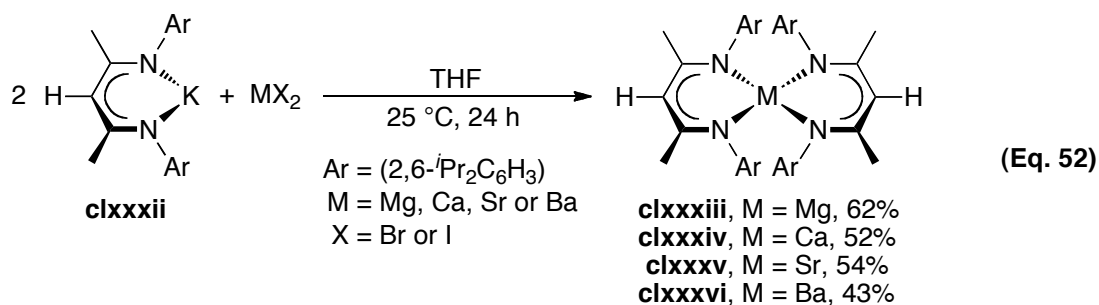
The steric effects of the *ortho*-substituents in the *N*-aryl group were also examined.^[148] Treatment of β -diketimines **clxxvi** and **clxxvii** with cupric acetate gave the corresponding di(μ -hydroxo)dicopper(II) complexes **clxxviii** and **clxxix** (equation 50).



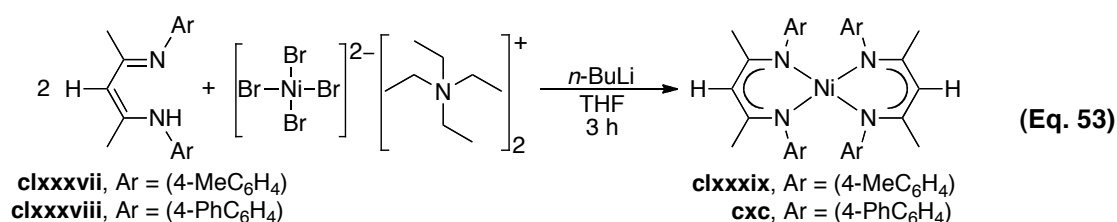
Treatment of cupric acetate with the β -diketimine **clxxx** in the presence of triethylamine gave the monomeric β -diketiminatocopper(II) acetate **clxxxii** in 77% yield (equation 51).^[148] This complex showed a distorted square planar geometry around the metal centre with the acetate fragment coordinated in a bidentate fashion.



A series of bis(β -diketiminato) alkaline-earth metal complexes were synthesised by Harder.^[149] Treatment of the alkaline-earth metal diiodide or dibromide with two equivalents of the potassium β -diketimate **clxxxii** gave the corresponding bis(β -diketiminato)metal complexes **clxxxiii–clxxxvi** in good yields (equation 52). X-ray crystallographic studies showed that the ligands were coordinated in a distorted tetrahedral geometry around the metal centre. The average C–N–C bond angle between the aryl group and the β -diketimate backbone increased down the group, with **clxxxiii**, M = Mg (115.1(2)°) < **clxxxiv**, M = Ca (117.6(1)°) < **clxxxv**, M = Sr (118.5(2)°) < **clxxxvi**, M = Ba (119.0(2)°). This finding was attributed to the increase in ionic radii down the group (*c.f.* Mg²⁺, 0.57 Å; Ca²⁺, 1.00 Å; Sr²⁺, 1.18 Å; Ba²⁺, 1.35 Å), which relieved crowding around the metal.^[150] C–H \cdots π interactions between the isopropyl group from one ligand and the aromatic ring from another ligand were observed. Similar observations were found in other bis(β -diketiminato)metal complexes.^[151-152]

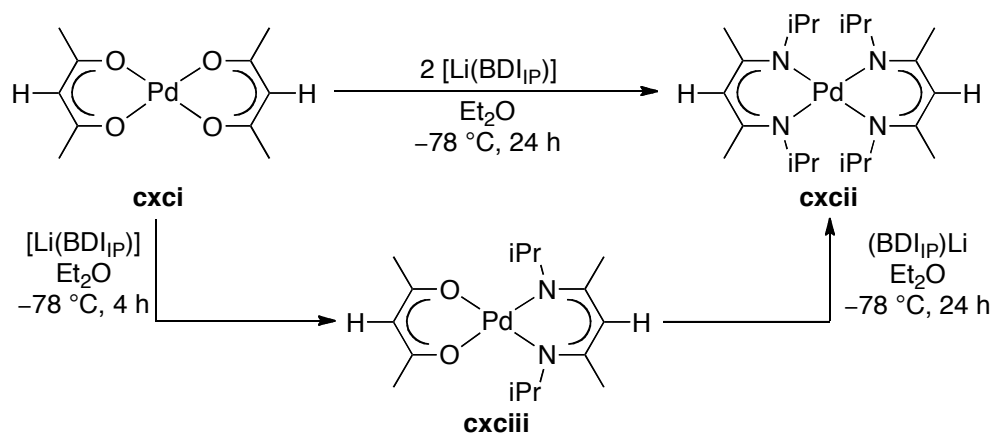


Lithiation of β -diketimines, **clxxxvii** or **clxxxviii**, followed by addition of tetraethylammonium tetrabromonickelate gave the bis[β -diketiminato]nickel(II) complexes **clxxxix** or **cx** (equation 53).^[153]



Treatment of [Pd(acac)₂] (acac = acetylacetonate) (**cxci**) with two equivalents of [Li(BDI_{IP})] (BDI_{IP} = [HC{C(Me)N(*i*Pr)}₂]⁻) in an one-pot reaction gave [Pd(BDI_{IP})₂] (**cxcii**) (Scheme 42).^[154] Treatment of [Pd(acac)₂] (**cxci**) with one equivalent of the lithium β -diketiminato in diethyl ether gave [Pd(BDI_{IP})(acac)] (**cxciiii**), and addition of more lithium β -diketiminato gave **cxcii**, indicating that the one-pot reaction proceeded in a stepwise manner.

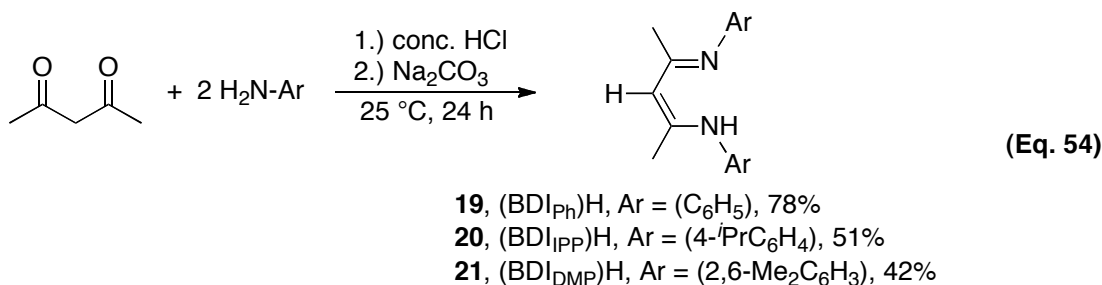
Scheme 42. Synthesis of the bis[β -diketiminato]palladium(II) complex **cxcii**^[154]



3.2 Results and discussion

3.2.1 Synthesis of β -diketimines **19–21**

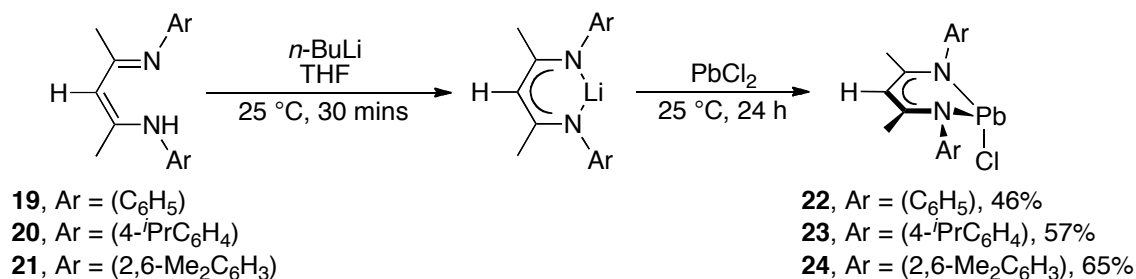
The condensation of acetylacetone with 2,6-diisopropylaniline in the presence of concentrated hydrochloric acid and ethanol under reflux reliably gave (BDI_{DIPP})H (**1**) in good yield.^[41] However, this approach gave poor yields of other substituted anilines. Good yields of (BDI_{Ph})H (**19**), (BDI_{Ipp})H (**20**) and (BDI_{DMP})H (**21**) (78%, 51% and 42%, respectively) were obtained from reactions in concentrated hydrochloric acid at room temperature (equation 54).^[155-156]



β -Diketimines **19** and **21** were obtained as white solids that were purified by washing with cold methanol. In contrast, (BDI_{Ipp})H (**20**) was obtained as a viscous brown oil. The ¹H NMR spectrum of the oil showed very few impurities; hence it was used without further treatment. The known compounds **19** and **21**, and the newly synthesised β -diketimine **20**, were characterised by ¹H and ¹³C{¹H} NMR spectroscopy.^[155-156] The ¹H NMR spectra show two distinctive singlet resonances, assigned to the N-H ($\delta_H \sim 12.7$ ppm) and the γ -H ($\delta_H \sim 4.8$ ppm) protons. In (BDI_{Ipp})H (**20**), the tertiary proton of the isopropyl group (CHMe₂) is shown by a septet at δ_H 2.87 ppm with an integration of two protons. A downfield resonance at approximately δ_C 160 ppm is assigned to the β -C in these compounds. This is consistent with the signal at δ_C 161.4 ppm in the β -diketimine (BDI_{DIPP})H (**1**).^[41]

3.2.2 Synthesis of β -diketiminatolead(II) chlorides **22–24**

The β -diketiminatolead(II) chlorides **22–24** were synthesised in moderate yield (46–65%) by lithiation of the β -diketimines **19–21** with *n*-BuLi, followed by addition of the generated lithium β -diketimate to a THF slurry of lead dichloride (Scheme 43).

Scheme 43. Synthesis of the β -diketiminatolead(II) chlorides **22–24**

The lead(II) chlorides **22–24** are sensitive to air, moisture and light. [(BDI_{Ph})PbCl] (**22**) and [(BDI_{IPP})PbCl] (**23**) are virtually insoluble in common aromatic or non-polar organic solvents, but are readily soluble in chlorinated solvents. Hence, purification can be conveniently achieved by washing with pentane, which removes the undesired lithium β -diketimate and β -diketimine from the crude solid. [(BDI_{DMP})PbCl] (**24**) is more soluble in common aprotic organic solvents, so purification is achieved by washing the crude solid with cold pentane and recrystallisation from a concentrated toluene solution at $-30\text{ }^{\circ}\text{C}$.

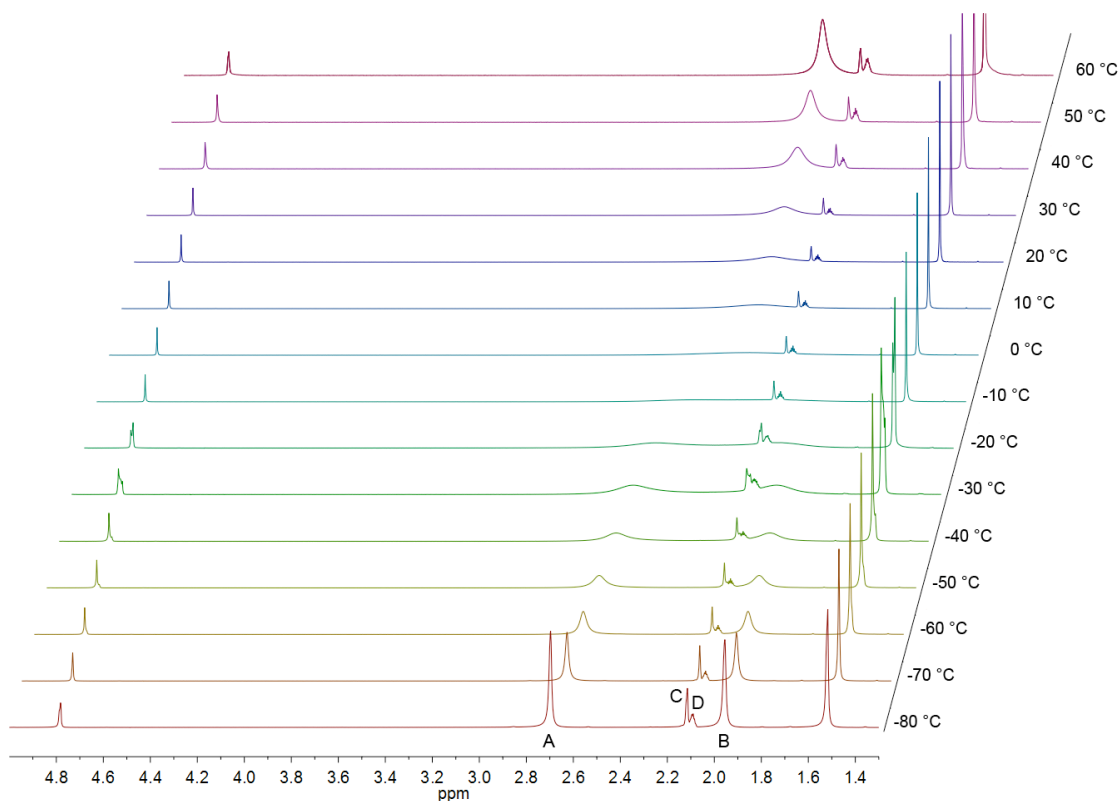
These compounds were characterised by multinuclear NMR spectroscopy and elemental analyses. The proton resonance for the γ -H in the β -diketimate backbone is at δ_{H} 4.74, 4.77 and 4.83 ppm for compounds **22**, **23** and **24**, respectively. These values are similar to those in the β -diketimine counterparts ($\delta_{\text{H}} \sim 4.8$ ppm). In compound **23**, a septet centred at δ_{H} 2.68 ppm ($^3J_{\text{HH}} = 7.2$ Hz) is assigned to the tertiary proton in the isopropyl group (CHMe₂).

The ¹H NMR spectrum of [(BDI_{DMP})PbCl] (**24**) displays a broad resonance at δ_{H} 2.31 ppm, assigned to the protons in the methyl group at the *ortho*-position of the *N*-substituted aryl fragment (*o*-CH₃) in the β -diketimate ring. The broad signal is indicative of restricted rotation about the *N*-aryl bond and is in contrast to the sharp singlet resonances observed for the protons in the *ortho*-methyl groups (*o*-CH₃) in two previously reported β -diketiminato heavy group 14 metal chlorides [(BDI_{TMP})MCl] (BDI_{TMP} = [HC{C(Me)N(2,4,6-Me₃C₆H₂)}₂]⁻; M = Ge or Sn).^[46, 68, 98] However, the broad signal for the *ortho*-methyl substituents (*o*-CH₃) in the ¹H NMR spectrum of the β -diketiminatomagnesium(II) iodide [(BDI_{TMP})MgI(THF)] is similar to that in

compound **24**.^[157] No explanation was provided for the broadness of the resonance in the magnesium compound.

The restricted rotation about the *N*-aryl bond in [(BDI_{DMP})PbCl] (**24**) was investigated by a variable-temperature (VT) ¹H-NMR spectroscopic study (Figure 17). With decreasing temperature, the *ortho*-methyl proton resonance (*o*-CH₃) becomes broad and it is resolved into two singlets at δ_{H} 2.66 and 1.96 ppm ($\Delta\delta_{\text{H}}$ 296 Hz) at -80 °C. At 60 °C, sharpening of the signal at δ_{H} 2.28 ppm indicates the approach to the fast-exchange limit. From the coalescence temperature (-10 °C), the barrier of N–C bond rotation is estimated to be $\Delta G^{\ddagger} = 49.9$ kJ mol⁻¹ (Appendix 4, Page 341).^[158] All the resonances separate into two uneven doublets from -20 to -30 °C, but further investigation indicates that this is due to an unresolved shimming problem of the NMR instrument, currently under investigation by Dr. Iain J. Day, the NMR specialist at the University of Sussex.^[159]

Figure 17. ¹H VT-NMR spectra (400 MHz, toluene-*d*₈) of [(BDI_{DMP})PbCl] (**24**), where A and B are signals from *o*-CH₃ protons, C is toluene residue and D is toluene-*d*₈



The γ -C resonance is found at δ_C 100.5, 105.4 and 103.7 ppm for the β -diketiminatolead(II) chlorides **22**, **23** and **24** respectively, i.e. downfield from signals in the parent β -diketiminines (δ_C 97.6, 97.1 and 93.6 for (BDI_{Ph})H (**19**), (BDI_{IPP})H (**20**) and (BDI_{DMP})H (**21**), respectively). This suggests that the electrons in the NCCCN framework are delocalised in the β -diketiminato ligand. A single lead resonance at δ_{Pb} 1228, 1220 and 1388 ppm for **22**, **23** and **24** respectively, is found in their ^{207}Pb NMR spectra. These resonances may be compared to that for [(BDI_{DIPP})PbCl] (**2**, δ_{Pb} 1413 ppm).^[70] Elemental analyses of these compounds are in good agreement with the calculated values.

The poor solubility in common organic solvents and extreme air- and moisture-sensitive of [(BDI_{Ph})PbCl] (**22**) and [(BDI_{IPP})PbCl] (**23**) made the isolation of single crystals for X-ray crystallographic studies difficult. Although single crystals of compounds **22** and **23** could be obtained from concentrated dichloromethane solutions at $-30\text{ }^\circ\text{C}$, none of these crystals (despite being obtained from several different samples) gave well-defined diffraction patterns. This may be due to immediate decomposition upon removal of crystals from the mother liquor. However, single crystals of [(BDI_{Ph})PbCl] (**22**) were adventitiously obtained after 48 hours from a NMR tube fitted with a Young's tap and containing C_6D_6 as solvent at room temperature. Single crystals of [(BDI_{DMP})PbCl] (**24**) were obtained by recrystallisation from a concentrated solution in toluene at $-30\text{ }^\circ\text{C}$.

ORTEP drawings of [(BDI_{Ph})PbCl] (**22**) are shown in Figures 18 and 19. Selected bond lengths and bond angles are given in Table 8; and selected crystallographic data in Table 10. The geometry around the lead atom is pyramidal with the sum of bond angles around the metal centre 261.0° . This is similar to that in other β -diketiminatolead(II) halides; for example in [(BDI_{DIPP})PbCl] (**2**), the sum of bond angles around the metal centre is 267.2° .^[62] The Pb–Cl bond length is 2.8081(11) Å, which is significantly longer than the Pb–Cl bond lengths in [(BDI_{DIPP})PbCl] (**2**) (2.5653(7) Å), Smith's [PbCl{C(SiMe₃)₂(SiMe₂C₅H₄N-2)}] (2.647(3) Å) and Leung's [Pb{N(SiMe₃)C(Ph)C(SiMe₃)(C₅H₄N-2)}Cl] (2.599(3) Å).^[25, 62, 160] The lead atom in [(BDI_{Ph})PbCl] (**22**) is only 0.112 Å from the mean NCCCN plane of the β -diketiminato ring. In contrast, the lead atom in [(BDI_{DIPP})PbCl] (**2**) is 0.683 Å from the mean NCCCN plane of the β -diketiminato ring and in other tri-coordinated β -

diketiminatolead(II) complexes, it is approximately 0.25–1.25 Å.^[70, 103, 114] The electrons of the *N*-aryl substituents are not delocalised into the NCCCN ring in the β-diketiminato ligand, as shown by the dihedral angles (C(7)–C(6)–N(1)–Pb = –56.2(5)° and C(17)–C(12)–N(2)–Pb = –49.6(5)°). The solid state structure of compound **22** comprises of a ‘polymeric-chain’ (Figure 19). The Pb–Cl' bond length (2.9928 (11) Å) is longer than the Pb–Cl bond length (2.8081(11) Å) within a monomeric unit. The Cl–Pb–Cl' and Pb–Cl–Pb' bond angles are 167.42(2) Å and 120.00(4) Å, respectively.

Figure 18. ORTEP diagram of [(BDI_{Ph})PbCl] (**22**). H atoms are omitted and C atoms in the β-diketiminato ring are minimised for clarity. The ellipsoid probability is shown at 30%

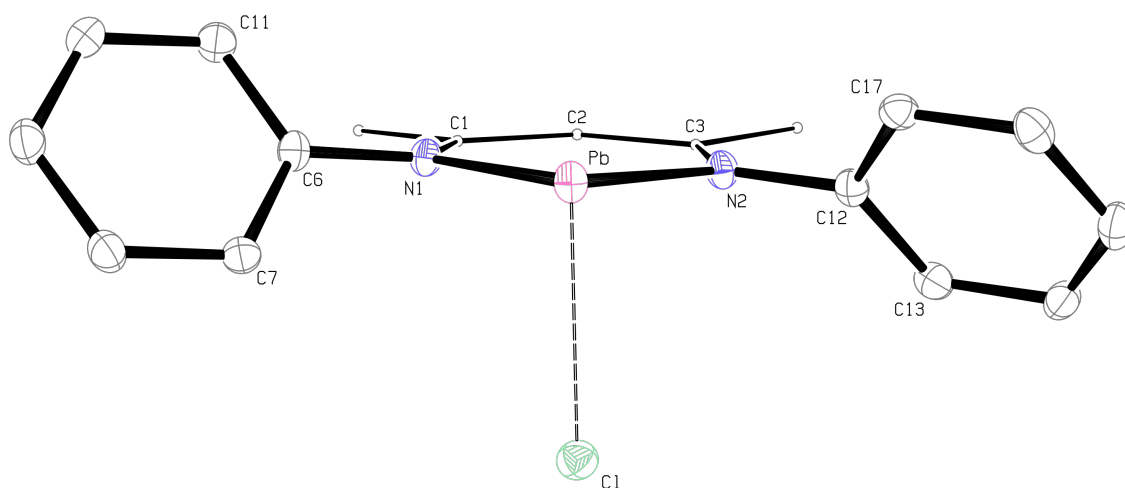


Figure 19. ORTEP diagram showing the polymeric chain of [(BDI_{Ph})PbCl] (**22**). H atoms are omitted and C atoms in the β-diketiminato ring are minimised for clarity. The ellipsoid probability is shown at 30%

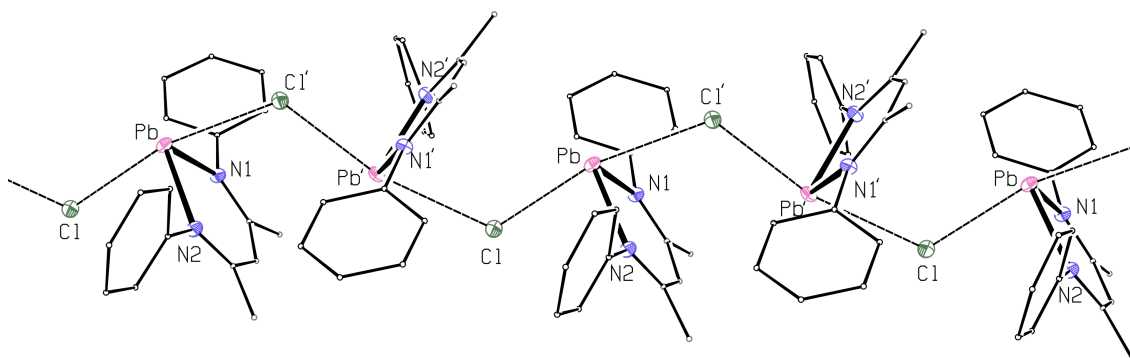


Table 8. Selected bond lengths (Å) and angles (deg) for [(BDI_{Ph})PbCl] (**22**)

<i>Bond lengths (Å)</i>			
Pb–N(1)	2.279(3)	Pb–Cl(i)'	2.9928(11)
Pb–N(2)	2.285(4)	N(1)–C(1)	1.328(5)
N(1)–C(6)	1.425(5)	N(2)–C(3)	1.332(5)
N(2)–C(12)	1.419(5)	C(1)–C(2)	1.399(6)
Pb–Cl	2.8081(11)	C(2)–C(3)	1.402(6)
Pb–NCCCN _{plane}	0.112		
<i>Bond angles (deg)</i>			
N(1)–Pb–Cl	90.52(9)	N(2)–Pb–Cl(i)'	83.40(9)
N(2)–Pb–Cl	85.78(9)	Cl–Pb–Cl(i) ^a	167.42(2)
N(1)–Pb–N(2)	84.68(12)	N(1)–C(1)–C(2)	125.1(4)
Pb–Cl–Pb(ii)'	120.00(4)	N(2)–C(3)–C(2)	124.1(4)
N(1)–Pb–Cl(i)'	82.10(9)	C(1)–C(2)–C(3)	132.7(4)
Σ bond angle around Pb	261.0	NCCCN _{plane} –NPbN _{plane}	3.8
DOP (%) ^a	110		
<i>Dihedral angles (deg)</i>			
C(7)–C(6)–N(1)–Pb	–56.2(5)	C(17)–C(12)–N(2)–Pb	–49.6(5)

^a Degree of pyramidalisation (DOP, %) = [(360 – Σ_{bond angles}) / 0.9]^[115] When a DOP is 100%, it is equivalent to a sum of bond angles of 270°, whereas a DOP of 0% indicates a planar geometry at the central atom; Symmetry transformation used to generate equivalent atoms: (i) –x + 1/2, y – 1/2, –z + 1/2; (ii) –x + 1/2, y + 1/2, –z + 1/2

ORTEP drawings of [(BDI_{DMP})PbCl] (**24**) are shown in Figures 20 and 21. Selected bond lengths and angles are given in Table 9, and selected crystallographic data in Table 10. The ligands are coordinated in a pyramidal geometry around the lead atom with the sum of bond angles 272.3°. The metal centre is 0.110 Å from the mean plane of NCCCN in the β-diketiminato ring. The electrons of the *N*-aryl substituents are not delocalised on to the NCCCN ring in the β-diketiminato ligand as shown by the dihedral angles (C(11)–C(6)–N(1)–Pb = 78.3(4)°, C(19)–C(14)–N(2)–Pb = –83.3(4)°). The Pb–Cl bond distance (2.5757(11) Å) is similar to that in [(BDI_{DIPP})PbCl] (**2**) (2.5653(7) Å)^[62]. The structure in the solid state is dimeric; the lead atom in any one molecule interacts with an aryl group from a neighbouring unit, with the Pb⋯aryl_{centre} distance 3.486 Å (dotted lines in Figure 21). The reported distances for η⁶-interaction between divalent lead and arene rings fall in the range of 2.85–3.83 Å.^[161-163] Although a relatively close interaction has been observed in [(η⁶-1,2-Me₂C₆H₄)Pb(AlCl₄)₂] (Pb⋯(η⁶-aryl) = 2.858 Å), longer range interactions (Pb⋯aryl_{centre} = 3.06–3.83 Å) are

more common and generally only observed in the solid state.^[161-162] The weaker $\text{Pb}\cdots\text{aryl}_{\text{centre}}$ interaction in the lead(II) chloride **24** may be attributed to crowding from the β -diketiminato ligand.

Figure 20. ORTEP diagram showing the monomeric structure of $[(\text{BDI}_{\text{DMP}})\text{PbCl}]$ (**24**). H atoms are omitted and C atoms in the β -diketiminato ring are minimised for clarity. The ellipsoid probability is shown at 30%

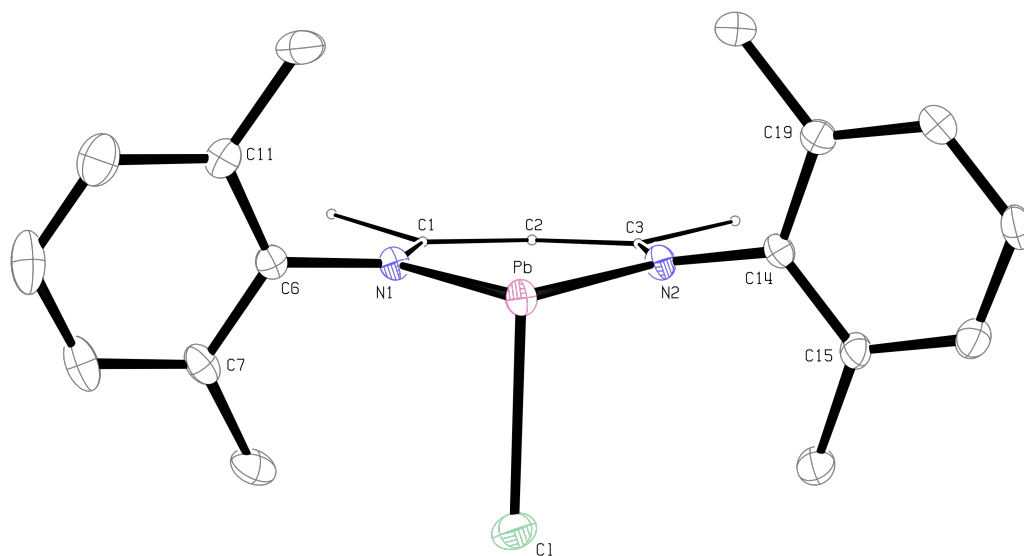


Figure 21. ORTEP diagram showing the dimer unit of $[(\text{BDI}_{\text{DMP}})\text{PbCl}]$ (**24**). H atoms are omitted and C atoms in the *N*-aryl groups in the β -diketiminato ring are minimised for clarity. The ellipsoid probability is shown at 30%

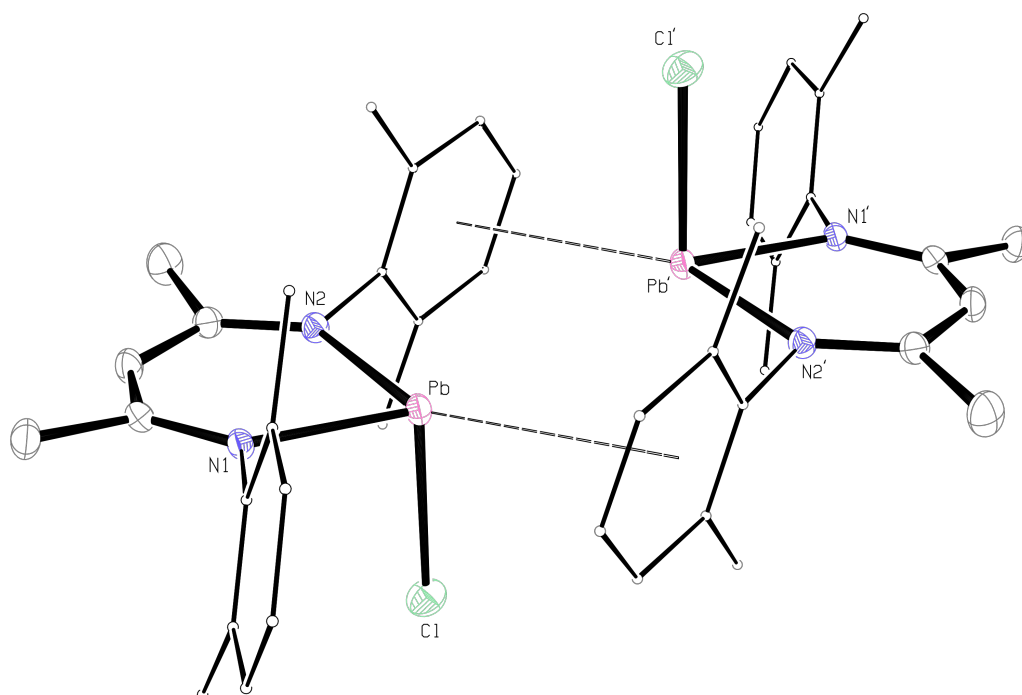


Table 9. Selected bond lengths (Å) and angles (deg) for [(BDI_{DMP})PbCl] (**24**)

<i>Bond lengths (Å)</i>			
Pb–N(1)	2.288(3)	N(1)–C(1)	1.325(5)
Pb–N(2)	2.306(3)	N(2)–C(3)	1.334(5)
Pb–Cl	2.5757(11)	C(1)–C(2)	1.408(6)
N(1)–C(6)	1.439(5)	C(2)–C(3)	1.397(6)
N(2)–C(14)	1.429(5)		
Pb–NCCCN _{plane}	0.110	Pb–Aryl _{centre}	3.486
<i>Bond angles (deg)</i>			
N(1)–Pb–Cl	93.49(8)	N(1)–C(1)–C(2)	124.7(4)
N(2)–Pb–Cl	96.29(9)	N(2)–C(3)–C(2)	124.7(4)
N(1)–Pb–N(2)	82.56(12)	C(1)–C(2)–C(3)	130.8(4)
Σ bond angle around Pb	272.3	NCCCN _{plane} –NPbN _{plane}	3.4
DOP (%) ^a	97.4		
<i>Dihedral angles (deg)</i>			
C(11)–C(6)–N(1)–Pb	78.3(4)	C(19)–C(14)–N(2)–Pb	–83.3(4)

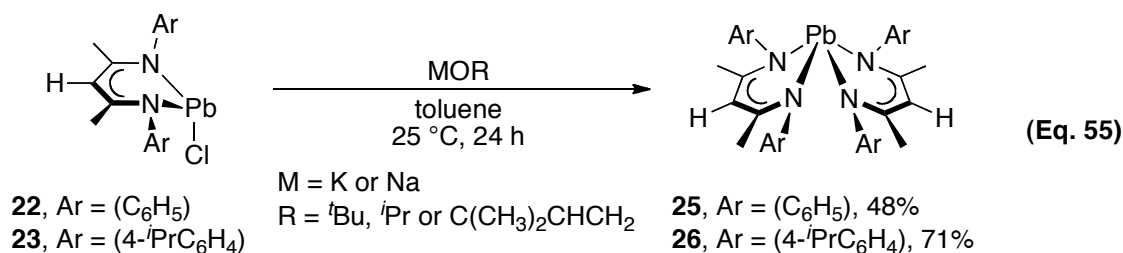
^a Degree of pyramidalisation (DOP, %) = [(360 – Σ_{bond angle}) / 0.9]^[115] When a DOP is 100%, it is equivalent to a sum of bond angles of 270°, whereas a DOP of 0% indicates a planar geometry at the central atom

Table 10. Selected crystallographic data for [(BDI_{Ph})PbCl] (**22**) and [(BDI_{DMP})PbCl] (**24**)

	[(BDI _{Ph})PbCl] (22)	[(BDI _{DMP})PbCl] (24)
chemical formula	C ₁₇ H ₁₇ ClN ₂ Pb, 0.5(C ₇ H ₈)	2(C ₂₁ H ₂₅ ClN ₂ Pb), C ₇ H ₈
molecular mass	538.03	1188.28
temperature (K)	173(2)	173(2)
wavelength (Å)	0.71073	0.71073
crystal system	monoclinic	triclinic
space group	<i>C</i> 2/ <i>c</i> (No. 15)	<i>P</i> $\bar{1}$ (No. 2)
<i>a</i> (Å)	23.4501(5)	8.3126(3)
<i>b</i> (Å)	10.0070(2)	12.5001(4)
<i>c</i> (Å)	16.7676(4)	12.9418(4)
α (deg)	90	112.537(2)
β (deg)	106.434(1)	94.850(2)
γ (deg)	90	104.513(1)
<i>V</i> (Å ³)	3774.02(14)	1177.65(7)
<i>Z</i>	8	1
ρ_{calcd} (Mg m ⁻³)	1.89	1.68
θ range (deg)	3.40–27.10	3.40–26.76
abs coeff (mm ⁻¹)	9.09	7.289
measd/indep reflns/ <i>R</i> (int)	29 205/4164/0.061	15 979/4989/0.056
reflns with $I > 2\sigma(I)$	3591	4563
data/restraints/param	4164/0/206	4989/0/239
goodness of fit on F^2	1.009	1.038
final <i>R</i> indices [$I > 2\sigma(I)$]	<i>R</i> 1 = 0.027, <i>wR</i> 2 = 0.056	<i>R</i> 1 = 0.027, <i>wR</i> 2 = 0.060
<i>R</i> indices (all data)	<i>R</i> 1 = 0.037, <i>wR</i> 2 = 0.059	<i>R</i> 1 = 0.032, <i>wR</i> 2 = 0.062
largest diff peak and hole (e Å ⁻³)	1.95 and -0.94	1.77 and -1.03

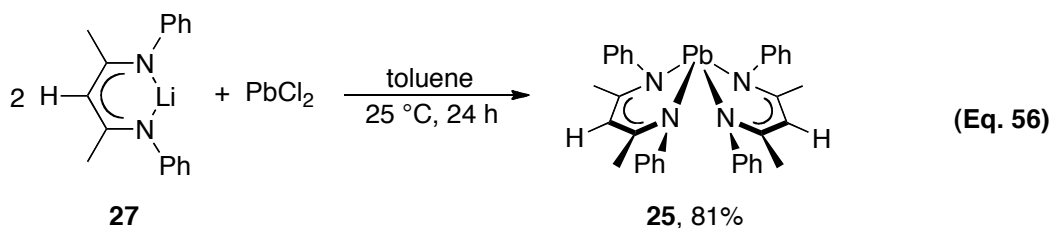
3.2.3 Reactions of the β -diketiminatolead(II) chlorides **22–24**

Initially, we attempted to synthesise a series of β -diketiminatolead(II) alkoxides containing a range of substituents in the β -diketiminato ring. However, treatment of [(BDI_{Ph})PbCl] (**22**) or [(BDI_{IPP})PbCl] (**23**) with potassium *tert*-butoxide at room temperature did not give the corresponding lead(II) *tert*-butoxides. Instead, the bis[β -diketiminato]lead(II) complexes [(BDI_{Ph})₂Pb] (**25**) and [(BDI_{IPP})₂Pb] (**26**), together with an unidentified white precipitate, were obtained (equation 55).



In a ¹H NMR study of the reaction between [(BDI_{Ph})PbCl] (**22**) and potassium *tert*-butoxide, a singlet at δ_H 1.39 ppm was observed. This resonance was not observed in the isolated bis[β-diketiminato]lead(II) complex **25**. It can be tentatively assigned to [Pb(μ-Cl)(*O*^tBu)]₂, but we were unable to verify this by isolating a pure sample. Although the compound is not known, Buhro's [Pb₃(μ-*O*^tBu)₆] shows a single resonance at δ_H 1.43 ppm, which may be compared to that in our product.^[164] Bis[β-diketiminato]lead(II) complexes **25** and **26** are formed as described in equation 55, with potassium *tert*-butoxide, potassium isopropoxide or sodium 2-methyl-3-buten-2-oxide. However, treatment of [(BDI_{Ph})PbCl] (**22**) with potassium methoxide did not give the bis[β-diketiminato]lead(II) complex **25**, instead a white precipitate and β-diketimine **19** were obtained.

[(BDI_{Ph})₂Pb] (**25**) is also accessible *via* treatment of lead dichloride with two equivalents of lithium β-diketimate [(BDI_{Ph})Li] (**27**) at room temperature (equation 56). The ¹H and ¹³C{¹H} NMR spectra of the product were identical to those of the product from equation 55. This finding contrasts with those from previous attempts to synthesise [(BDI_{DIPP})₂Pb] by treatment of lead dichloride with two equivalents of [(BDI_{DIPP})Li].^[62] This suggests that substituents at the *ortho*-position of the *N*-aryl fragments cause congestion between neighbouring β-diketiminato ligands and prevent the formation of [(BDI_{DIPP})₂Pb].



The bis[β -diketiminato]lead(II) complexes **25** and **26** are soluble in common aprotic organic solvents. They are stable in the solid state and can be stored in an inert environment at -30 °C for several weeks without decomposition. Both complexes were characterised by multinuclear NMR spectroscopy, elemental analyses and X-ray crystallography. The ^1H NMR spectrum of $[(\text{BDI}_{\text{Ph}})_2\text{Pb}]$ (**25**) shows resonances at δ_{H} 4.85 and 1.85 ppm for the γ -*H* and β -*Me* protons in the β -diketiminato ligand. The $^{13}\text{C}\{^1\text{H}\}$ NMR spectrum shows resonances at δ_{C} 162.2 and 100.7 ppm for the β -*Me* and γ -*C* carbon atoms, respectively. These results show that the two β -diketiminato ligands are equivalent in solution. Similar observations can be found in Lappert's $[(^{\text{Ph}}\text{BDI}_{\text{TMS}})_2\text{Pb}]$ ($^{\text{Ph}}\text{BDI}_{\text{TMS}} = [\text{HC}\{\text{C}(\text{C}_6\text{H}_5)\text{N}(\text{SiMe}_3)\}_2]^-$), as well as in other bis(β -diketiminato) transition metal complexes, such as Schulz's $[(\text{BDI}_{\text{TMP}})_2\text{Zn}]$ ($\text{BDI}_{\text{TMP}} = [\text{HC}\{\text{C}(\text{Me})\text{N}(2,4,6\text{-Me}_3\text{C}_6\text{H}_2)\}_2]^-$) and Song's $[(\text{BDI}_{\text{Ph}})_2\text{Pd}]$.^[165-166] The resonance at δ_{Pb} 454 ppm in the ^{207}Pb NMR spectrum of $[(\text{BDI}_{\text{Ph}})_2\text{Pb}]$ (**25**) is considerably upfield from that in the lead(II) chloride $[(\text{BDI}_{\text{Ph}})\text{PbCl}]$ (**22**, δ_{Pb} 1228 ppm).

Similarly, the ^1H NMR spectrum of $[(\text{BDI}_{\text{IPP}})_2\text{Pb}]$ (**26**) shows signals at δ_{H} 4.90 and 1.92 ppm, for the γ -*H* and β -*Me* protons respectively, in the β -diketiminato ligand. The $^{13}\text{C}\{^1\text{H}\}$ NMR spectrum shows resonances at δ_{C} 162.2 and 103.4 ppm for β -*Me* and γ -*C* carbon atoms, respectively. These resonances may be compared to those found in the NMR spectra of $[(\text{BDI}_{\text{Ph}})_2\text{Pb}]$ (**25**). The isopropyl groups at the *para*-position of the *N*-substituted aryl fragments in compound **26** give a septet at δ_{H} 2.76 ppm and a doublet at δ_{H} 1.19 ppm assigned to the tertiary (CHMe_2) and methyl (CHMe_2) isopropyl protons, respectively. This finding is similar to that in Roesky's bis[β -diketiminato]zinc(II) complex $[(\text{BDI}_{\text{MOP}})_2\text{Zn}]$ ($\text{BDI}_{\text{MOP}} = [\text{HC}\{\text{C}(\text{Me})\text{N}(4\text{-(MeO)C}_6\text{H}_4)\}_2]^-$), which shows the *para*-methoxy substituents of the *N*-substituted aryl fragments are chemically equivalent.^[167] Signals at δ_{C} 34.4 and 24.9 ppm are observed for the tertiary (CHMe_2) and methyl (CHMe_2) isopropyl carbons in the $^{13}\text{C}\{^1\text{H}\}$ NMR spectrum of $[(\text{BDI}_{\text{IPP}})_2\text{Pb}]$ (**26**). The lead resonance at δ_{Pb} 476 ppm is obtained from the ^{207}Pb NMR spectrum; the shift is similar to that from $[(\text{BDI}_{\text{Ph}})_2\text{Pb}]$ (**25**, δ_{Pb} 454 ppm).

Single crystals of $[(\text{BDI}_{\text{Ph}})_2\text{Pb}]$ (**25**) were obtained by recrystallisation from toluene at -30 °C. ORTEP drawings of $[(\text{BDI}_{\text{Ph}})_2\text{Pb}]$ (**25**) are shown in Figures 22 and 23. Selected bond lengths and angles are given in Table 11, and selected crystallographic

data in Table 13. The ligands are arranged in a distorted disphenoidal geometry around the metal centre.^[142] Both Pb–N(1) (2.482(3) Å) and Pb–N(4) (2.466(3) Å) are longer than Pb–N(2) (2.363(3) Å) and Pb–N(3) (2.338(3) Å). In addition, the N(1)–Pb–N(4) bond angle (151.05(11)°) is significantly wider than the N(2)–Pb–N(3) bond angle (89.87(11)°). The coordination is similar to that in Lappert's [(^{Ph}BDI_{TMS})₂Pb] (^{Ph}BDI_{TMS} = [HC{C(C₆H₅)N(SiMe₃)}₂]), in which there are two different Pb–N bond lengths (*ca.* 2.609 and 2.313 Å) and N–Pb–N bond angles of 166.20(10)° and 93.87(10)°.^[135] Density functional theory calculations on four-coordinate gas-phase lead(II) complexes performed by Glusker *et al.* suggest that the longer Pb–N bonds (avg. 2.620 Å) associated with wider N–Pb–N angles (avg. 156.8°) have more s-character than the shorter Pb–N bonds (avg. 2.446 Å) with smaller N–Pb–N angles (avg. 91.6°).^[61] In [(BDI_{Ph})₂Pb] (**25**), one of the ligands does not lie directly below the other one (Figure 23). This asymmetry is shown in differences in Pb–N bond lengths and N–Pb–N bond angles. In addition, there may be weak C–H⋯π interactions between the *ortho*-hydrogen of the *N*-substituted aryl group and the aryl ring from the other ligand (dotted lines in Figure 22).^[168] Two C–H⋯π interactions, with distances of C(11)–H(1)⋯aryl_{centre} = 2.632 Å and C(34)–H(34)⋯aryl_{centre} = 2.647 Å, are within the range reported for C–H⋯π distances (< 2.90 Å), for example in Harder's [(BDI_{DIPP})₂Ca] (avg. C–H⋯aryl_{centre} = 2.696 Å) and [(BDI_{DIPP})₂Sr] (avg. C–H⋯aryl_{centre} = 2.761 Å).^[149] Furthermore, the lead atom is weakly solvated with a toluene molecule which coordinates in η⁶-fashion with the metal centre (Pb⋯toluene_{centre} = 3.616 Å) in [(BDI_{Ph})₂Pb] (**25**). This is slightly longer than that observed in [(BDI_{DMP})PbCl] (**24**) (3.486 Å), but within the range of other reported Pb⋯aryl_{centre} interactions (3.06–3.83 Å).^[161, 163]

Figure 22. ORTEP diagram of $[(\text{BDI}_{\text{Ph}})_2\text{Pb}]$ (**25**). H atoms are omitted and C atoms in the β -diketiminato ring are minimised for clarity. The ellipsoid probability is shown at 30%. C–H $\cdots\pi$ and Pb \cdots toluene_{centre} interactions are shown by dotted lines

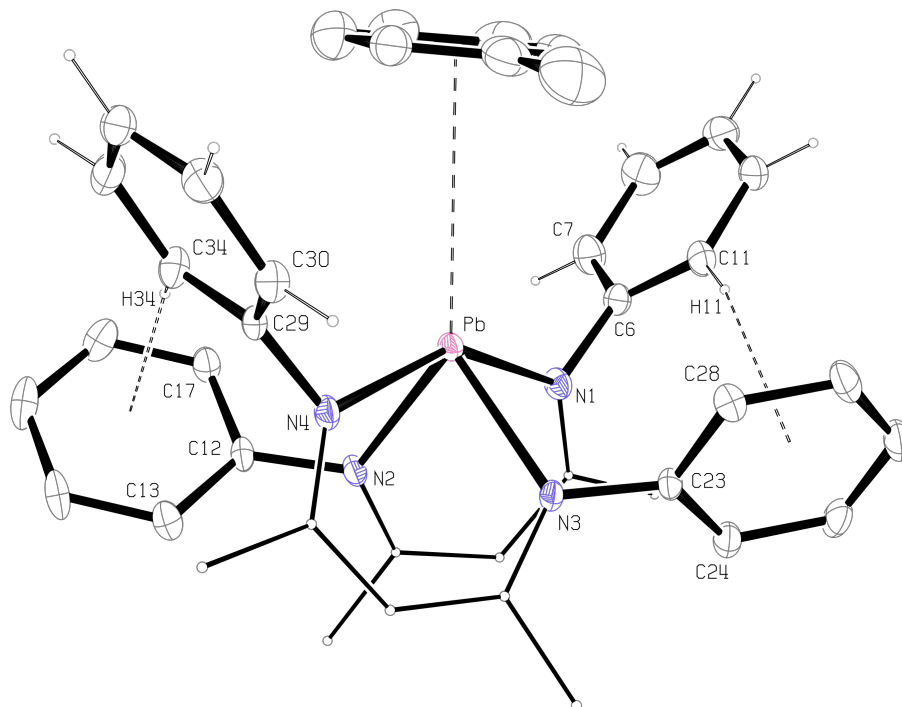


Figure 23. ORTEP diagram showing the side-on view of $[(\text{BDI}_{\text{Ph}})_2\text{Pb}]$ (**25**). H atoms, CH $\cdots\pi$ interactions and the solvated toluene fragment are omitted, C atoms in the *N*-aryl groups in the β -diketiminato ring are minimised for clarity. The ellipsoid probability is shown at 30%

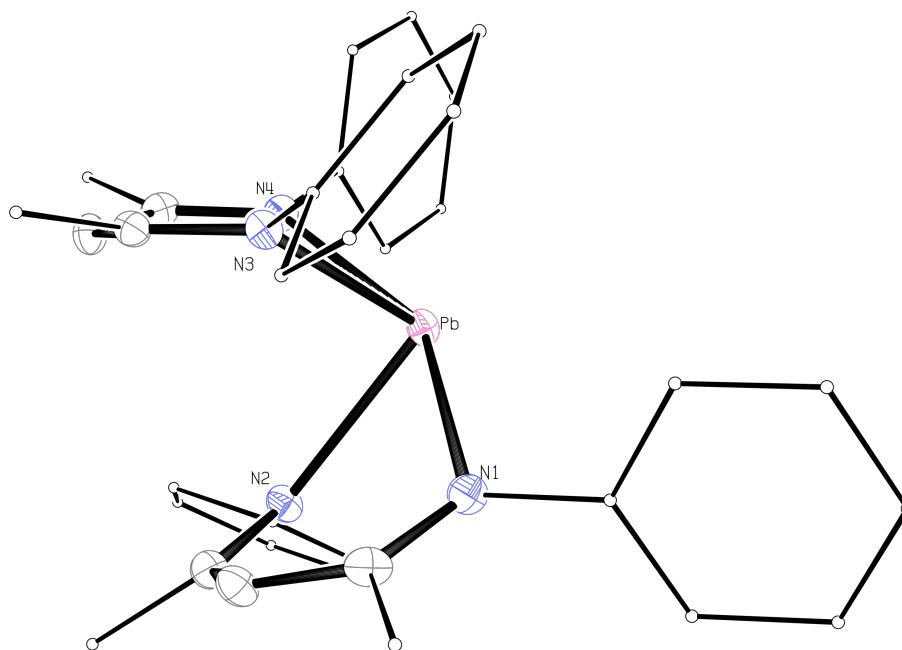


Table 11. Selected bond lengths (Å) and angles (deg) for [(BDI_{Ph})₂Pb] (**25**)

<i>Bond lengths (Å)</i>			
Pb–N(1)	2.482(3)	Pb–N(3)	2.338(3)
Pb–N(2)	2.363(3)	Pb–N(4)	2.466(3)
C(11)–H(11)⋯aryl _{centre}	2.632	Pb–Aryl _{toluene}	3.616
C(34)–H(34)⋯aryl _{centre}	2.647		
<i>Bond angles (deg)</i>			
N(1)–Pb–N(2)	73.44(10)	N(1)–Pb–N(4)	151.05(11)
N(3)–Pb–N(4)	75.40(10)	N(2)–Pb–N(3)	89.87(11)
N(1)–Pb–N(3)	85.01(10)	N(2)–Pb–N(4)	85.22(10)
<i>Dihedral angles (deg)</i>			
C(11)–C(6)–N(1)–Pb	64.9(5)	C(28)–C(23)–N(3)–Pb	72.1(4)
C(17)–C(12)–N(2)–Pb	71.7(4)	C(34)–C(29)–N(4)–Pb	64.0(4)

ORTEP drawings of [(BDI_{IPP})₂Pb] (**26**) are shown in Figures 24 and 25. Selected bond lengths and angles are given in Table 12, and selected crystallographic data in Table 13. The bis[β-diketiminato]lead(II) complexes **25** and **26** share some common structural features. The ligands are coordinated in a distorted disphenoidal geometry around the metal centre.^[142] Likewise, the two mean NCCCN planes of the β-diketiminato ligands are not parallel (Figure 25). Two different sets of bond lengths are found. Pb–N(2) (2.446(4) Å) and Pb–N(3) (2.456(5) Å) are longer than both Pb–N(1) (2.333(4) Å) and Pb–N(4) (2.348(4) Å). N(2)–Pb–N(3) (155.86(12)°) is significantly wider than N(1)–Pb–N(4) (90.33(13)°). Two C–H⋯π interactions, C(16)–H(16)⋯aryl_{centre} (2.553 Å) and C(34)–H(34)⋯aryl_{centre} (2.790 Å) are found (dotted lines in Figure 24). These distances are similar to the C–H⋯π interactions found in [(BDI_{Ph})₂Pb] (**25**) (avg. C–H⋯aryl_{centre} = 2.640 Å). There is no solvated toluene in [(BDI_{IPP})₂Pb] (**26**), possibly because the isopropyl groups at the *para*-position in the *N*-substituted aryl groups hinder access to the metal atom.

Figure 24. ORTEP diagram of $[(BDI_{IPP})_2Pb]$ (**26**). H atoms and C atoms in the β -diketiminato ring are minimised for clarity. The ellipsoid probability is shown at 30%. C–H $\cdots\pi$ interactions are shown as dotted lines

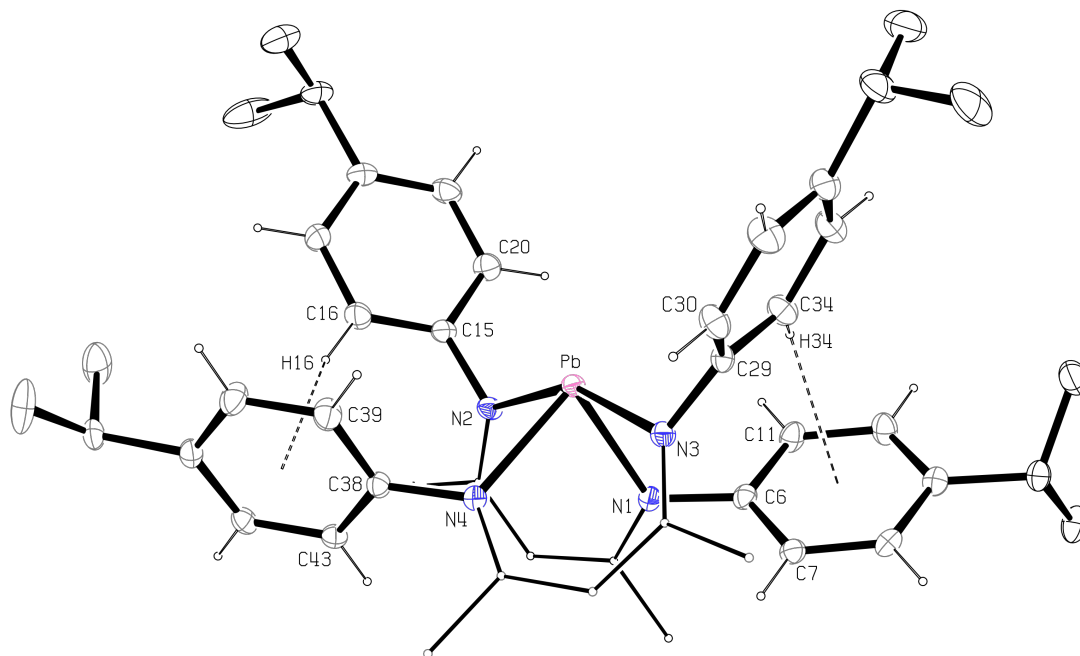


Figure 25. ORTEP diagram showing the side-on view of $[(BDI_{IPP})_2Pb]$ (**26**). H atoms and C–H $\cdots\pi$ interactions are omitted, C atoms in the *N*-aryl groups in the β -diketiminato ring are minimised for clarity. The ellipsoid probability is shown at 30%

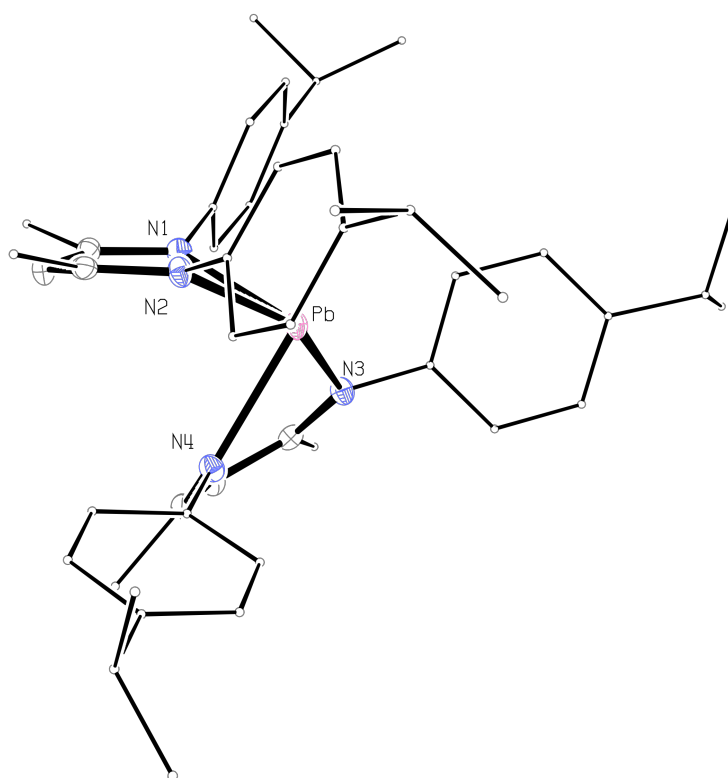


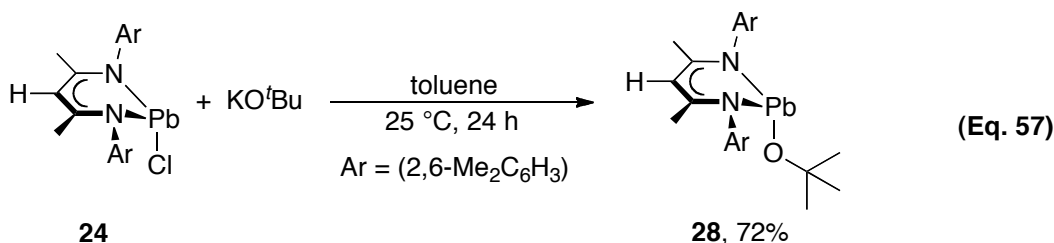
Table 12. Selected bond lengths (Å) and angles (deg) for [(BDI_{IPP})₂Pb] (**26**)

<i>Bond lengths (Å)</i>			
Pb–N(1)	2.333(4)	Pb–N(3)	2.456(5)
Pb–N(2)	2.446(4)	Pb–N(4)	2.348(4)
C(16)–H(16)⋯aryl _{centre}	2.553	C(34)–H(34)⋯aryl _{centre}	2.790
<i>Bond angles (deg)</i>			
N(1)–Pb–N(2)	75.10(13)	N(1)–Pb–N(4)	90.33(13)
N(3)–Pb–N(4)	76.71(13)	N(1)–Pb–N(3)	87.03(13)
N(2)–Pb–N(3)	155.86(12)	N(2)–Pb–N(4)	87.13(13)
<i>Dihedral angles (deg)</i>			
C(7)–C(6)–N(1)–Pb	94.6(5)	C(34)–C(29)–N(3)–Pb	–51.9(5)
C(20)–C(15)–N(2)–Pb	83.2(5)	C(39)–C(38)–N(4)–Pb	–74.7(5)

Table 13. Selected crystallographic data for [(BDI_{Ph})₂Pb] (**25**) and [(BDI_{IPP})₂Pb] (**26**)

	[(BDI _{Ph}) ₂ Pb] (25)	[(BDI _{IPP}) ₂ Pb] (26)
chemical formula	C ₃₄ H ₃₄ N ₄ Pb, C ₇ H ₈	C ₄₆ H ₅₈ N ₄ Pb
molecular mass	798.01	874.15
temperature (K)	173(2)	173(2)
wavelength (Å)	0.71073	0.71073
crystal system	triclinic	triclinic
space group	$P\bar{1}$ (No. 2)	$P\bar{1}$ (No. 2)
<i>a</i> (Å)	10.3923(2)	10.9335(3)
<i>b</i> (Å)	11.5345(4)	12.1290(2)
<i>c</i> (Å)	17.0319(5)	16.9989(4)
α (deg)	104.310(1)	85.690(2)
β (deg)	96.037(2)	73.900(1)
γ (deg)	113.289(2)	74.641(1)
<i>V</i> (Å ³)	1769.24(9)	2088.50(8)
<i>Z</i>	2	2
ρ_{calcd} (Mg m ⁻³)	1.50	1.39
θ range (deg)	3.49–27.09	3.42–26.72
abs coeff (mm ⁻¹)	4.80	4.07
measd/indep reflns/ <i>R</i> (int)	31 069/7797/0.0548	30 694/8825/0.051
reflns with $I > 2\sigma(I)$	7106	8166
data/restraints/param	7797/0/420	8825/0/464
goodness of fit on F^2	0.837	1.210
final <i>R</i> indices [$I > 2\sigma(I)$]	<i>R</i> 1 = 0.029, <i>wR</i> 2 = 0.069	<i>R</i> 1 = 0.034, <i>wR</i> 2 = 0.079
<i>R</i> indices (all data)	<i>R</i> 1 = 0.037, <i>wR</i> 2 = 0.073	<i>R</i> 1 = 0.039, <i>wR</i> 2 = 0.080
largest diff peak and hole (e Å ⁻³)	0.91 and –1.44	1.12 and –1.49

Treatment of [(BDI_{DMP})PbCl] (**24**) with potassium *tert*-butoxide at room temperature gives the β -diketiminatolead(II) alkoxide [(BDI_{DMP})PbO^{*t*}Bu] (**28**) in good yield (equation 57). There is no evidence for the formation of the bis[β -diketiminato]lead(II) complex [(BDI_{DMP})₂Pb].



The β -diketiminatolead(II) *tert*-butoxide **28** is soluble in common aprotic organic solvents, such as toluene and *n*-hexane. It has a characteristic singlet at δ_{H} 1.05 ppm in the ¹H NMR spectrum, assigned to the protons in the terminal *tert*-butoxide ligand. The chemical shift is similar to that found in [(BDI_{DIPP})PbO^{*t*}Bu] (**4**, δ_{H} 0.88 ppm).^[114] Two singlets of equal intensity at δ_{H} 2.67 and 2.16 ppm in the ¹H NMR spectrum, and at δ_{C} 20.5 and 19.2 ppm in the ¹³C{¹H} NMR spectrum, are assigned to the methyl groups at the *ortho*-position of the *N*-substituted aryl fragment. This suggests that the barrier of rotation about the *N*-aryl bond is higher than that observed in [(BDI_{DMP})PbCl] (**24**). The ²⁰⁷Pb NMR spectrum of the β -diketiminatolead(II) *tert*-butoxide **28** shows a single resonance at δ_{Pb} 1513 ppm, in the range found in other β -diketiminatolead(II) alkoxides ($\delta_{\text{Pb}} \sim 1500\text{--}1700$ ppm).^[114, 117]

Single crystals of [(BDI_{DMP})PbO^{*t*}Bu] (**28**) were obtained by recrystallisation from toluene at -30 °C. ORTEP drawings of **28** are shown in Figures 26 and 27. Selected bond lengths and angles are given in Table 14, and selected crystallographic data in Table 15. The ligands are coordinated in a pyramidal geometry around the lead atom with the sum of bond angles 267.4° . However, the lead atom lies close to the mean NCCCN plane of the β -diketiminato ring (Pb–NCCCN_{plane} = 0.001 Å). This contrasts with the previously reported [(BDI_{DIPP})PbO^{*t*}Pr] (**3**, Pb–NCCCN_{plane} = 0.907 Å) and [(BDI_{DIPP})PbO^{*t*}Bu] (**4**, Pb–NCCCN_{plane} = 1.021 Å), which may reflect relief of crowding from the *N*-substituted aryl fragments.^[114] This provides additional space to accommodate the lead atom in the NCCCN fragment of the β -diketiminato ligand. The

Table 14. Selected bond lengths (Å) and angles (deg) for [(BDI_{DMP})PbO^tBu] (**28**)

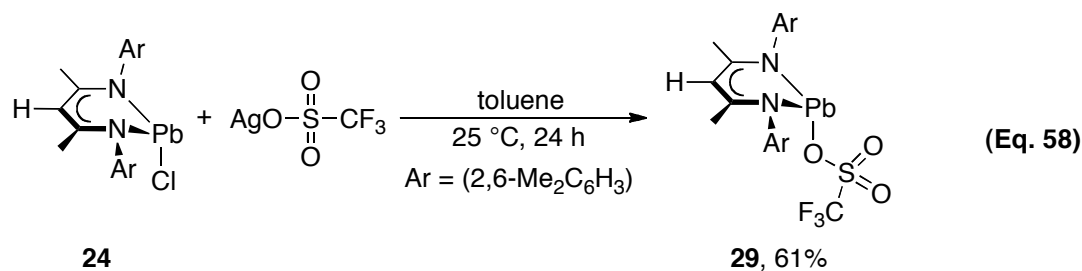
<i>Bond lengths (Å)</i>			
Pb–N(1)	2.311(3)	N(2)–C(14)	1.429(5)
Pb–N(2)	2.322(3)	N(1)–C(1)	1.329(5)
Pb–O	2.154(3)	N(2)–C(3)	1.323(5)
O–C(22)	1.426(5)	C(1)–C(2)	1.396(6)
N(1)–C(6)	1.441(5)	C(2)–C(3)	1.404(6)
Pb–NCCCN _{plane}	0.001		
<i>Bond angles (deg)</i>			
N(1)–Pb–N(2)	81.32(11)	N(1)–C(1)–C(2)	124.5(4)
N(1)–Pb–O	94.17(11)	N(2)–C(3)–C(2)	124.9(4)
N(2)–Pb–O	91.92(11)	C(1)–C(2)–C(3)	131.0(4)
Pb–O–C(22)	121.2(2)		
Σ bond angle around Pb	267.4	NCCCN _{plane} –NPbN _{plane}	0.3
DOP (%) ^a	103		
<i>Dihedral angles (deg)</i>			
C(11)–C(6)–N(1)–Pb	84.7(5)	C(19)–C(14)–N(2)–Pb	–80.7(4)

^a Degree of pyramidalisation (DOP, %) = [(360 – Σ_{bond angle}) / 0.9]^[115] When a DOP is 100%, it is equivalent to a sum of bond angles of 270°, whereas a DOP of 0% indicates a planar geometry at the central atom

Table 15. Selected crystallographic data for [(BDI_{DMP})PbO^tBu] (**28**)

[(BDI _{DMP})PbO ^t Bu] (28)	
chemical formula	C ₂₅ H ₃₄ N ₂ OPb
molecular mass	585.73
temperature (K)	173(2)
wavelength (Å)	0.71073
crystal system	triclinic
space group	<i>P</i> $\bar{1}$ (No. 2)
<i>a</i> (Å)	12.0429(4)
<i>b</i> (Å)	12.2155(4)
<i>c</i> (Å)	18.6440(5)
α (deg)	70.951(2)
β (deg)	73.482(2)
γ (deg)	88.626(1)
<i>V</i> (Å ³)	2478.36(13)
<i>Z</i>	4
ρ_{calcd} (Mg m ⁻³)	1.57
θ range (deg)	3.44–26.76
abs coeff (mm ⁻¹)	6.824
measd/indep reflns/ <i>R</i> (int)	30 981/10 379/0.057
reflns with <i>I</i> > 2 σ (<i>I</i>)	8521
data/restraints/param	10 379/0/535
goodness of fit on <i>F</i> ²	1.000
final <i>R</i> indices [<i>I</i> > 2 σ (<i>I</i>)]	<i>R</i> 1 = 0.030, <i>wR</i> 2 = 0.067
<i>R</i> indices (all data)	<i>R</i> 1 = 0.042, <i>wR</i> 2 = 0.072
largest diff peak and hole (e Å ⁻³)	0.73 and -1.62

Treatment of [(BDI_{DMP})PbCl] (**24**) with silver trifluoromethanesulfonate (AgOTf) in toluene at room temperature gives the β -diketiminatolead(II) triflate [(BDI_{DMP})PbOTf] (**29**) in 61% yield (equation 58).



The ^1H NMR spectrum of the lead(II) triflate **29** in CDCl_3 shows singlets at δ_{H} 5.14 and 2.26 ppm respectively for the γ -*H* and the *ortho*-methyl protons (*o*- CH_3) in the *N*-substituted aryl groups. This indicates that the methyl fragments are chemically equivalent and the rotation about the *N*-aryl bond is not restricted. A single resonance at δ_{C} 124.5 ppm (CDCl_3) assigned to the carbon in the CF_3 group is found in the $^{13}\text{C}\{^1\text{H}\}$ NMR spectrum. This shift may be compared to that in Driess' $[(\text{BDI}_{\text{DIPP}})\text{GeOTf}]$ (CF_3 : δ_{C} 120.9 ppm in C_6D_6).^[105, 134] A single resonance at δ_{F} -78.0 ppm (CDCl_3) is found in the ^{19}F NMR spectrum of compound **29**, which may be compared to that in Roesky's $[(\text{BDI}_{\text{DIPP}})\text{PbOTf}]$ (CF_3 : δ_{F} -76.5 ppm in C_6D_6).^[70] The ^{207}Pb NMR spectrum of **29** shows a single resonance at δ_{Pb} 1154 ppm (CDCl_3).

Single crystals of $[(\text{BDI}_{\text{DMP}})\text{PbOTf}]$ (**29**) were obtained by recrystallisation from THF at $-30\text{ }^\circ\text{C}$. ORTEP drawings of **29** are shown in Figures 28 and 29. Selected bond lengths and angles are given in Table 16, and selected crystallographic data in Table 17. The ligands are coordinated in a pyramidal geometry around the lead atom with the sum of bond angles 262.7° . The lattice of **29** comprises a polymeric chain with a triflate fragment bridging between the monomeric units (Figure 29). The $\text{Pb}-\text{O}(2)'$ bond distance (2.733(3) Å) and the $\text{O}(1)-\text{Pb}-\text{O}(2)'$ bond angle ($165.50(9)^\circ$) are similar to those in Roesky's $[(\text{BDI}_{\text{DIPP}})\text{PbOTf}]$, in which the average $\text{Pb}-\text{O}'$ bond distance is 2.624 Å and the average $\text{O}-\text{Pb}-\text{O}'$ bond angle 168.2° .^[70] In the monomeric unit of compound **29**, the $\text{Pb}-\text{O}(1)$ bond length (2.593(3) Å) is significantly longer than the $\text{Pb}-\text{O}$ bond distance found in $[(\text{BDI}_{\text{DIPP}})\text{PbOC}(\text{CH}_3)_2\text{CHCH}_2]$ (**8**, $\text{Pb}-\text{O} = 2.150(2)$ Å) and $[(\text{BDI}_{\text{DMP}})\text{PbO}^t\text{Bu}]$ (**28**, $\text{Pb}-\text{O} = 2.154(3)$ Å). This is consistent with the view that the lead(II) triflates are more ionic than the lead(II) alkoxides, i.e. the triflate is a better leaving group.^[70]

Figure 28. ORTEP diagram of the monomeric unit of [(BDI_{DMP})PbOTf] (**29**). H atoms are omitted and C atoms in the β -diketiminato ring are minimised for clarity. The ellipsoid probability is shown at 30%

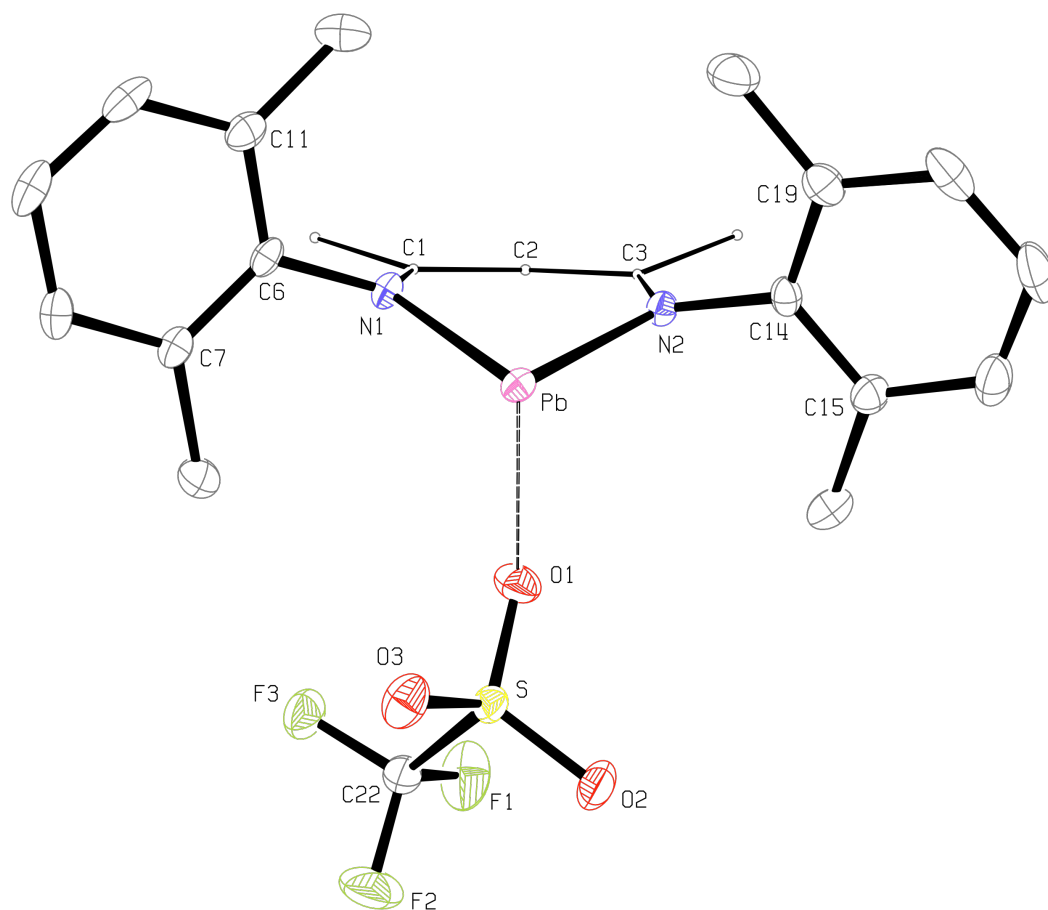


Figure 29. ORTEP diagram showing the polymeric chain of [(BDI_{DMP})PbOTf] (**29**). H atoms are omitted and C atoms in the *N*-aryl groups in the β -diketiminato ring are minimised for clarity. The ellipsoid probability is shown at 30%

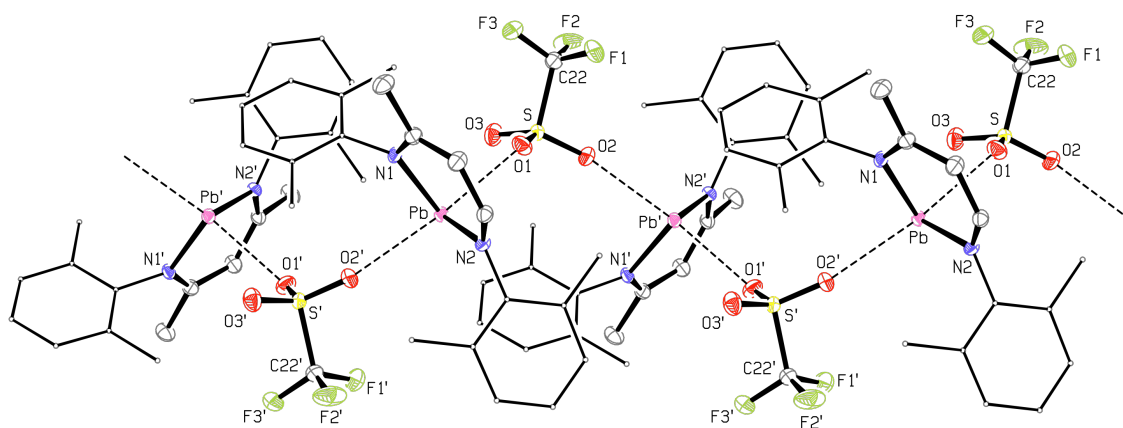


Table 16. Selected bond lengths (Å) and angles (deg) for [(BDI_{DMP})PbOTf] (**29**)

<i>Bond lengths (Å)</i>			
Pb–N(1)	2.266(3)	C(22)–F(1)	1.337(5)
Pb–N(2)	2.282(3)	C(22)–F(2)	1.313(5)
Pb–O(1)	2.593(3)	C(22)–F(3)	1.319(4)
Pb–O(2i)'	2.733(3)	N(1)–C(1)	1.335(4)
S(1)–O(1)	1.458(3)	N(2)–C(3)	1.330(4)
S(1)–O(2)	1.432(3)	C(1)–C(2)	1.397(5)
S(1)–O(3)	1.430(3)	C(2)–C(3)	1.403(5)
Pb–NCCCN _{plane}	0.606		
<i>Bond angles (deg)</i>			
N(1)–Pb–N(2)	82.88(10)	O(1)–S(1)–O(3)	113.94(18)
N(1)–Pb–O(1)	91.94(10)	O(1)–S(1)–C(22)	102.88(18)
N(2)–Pb–O(1)	87.90(9)	S(1)–C(22)–F(1)	110.8(3)
N(1)–Pb–O(2i)'	91.86(10)	F(1)–C(22)–F(2)	108.5(4)
N(2)–Pb–O(2i)'	106.45(10)	N(1)–C(1)–C(2)	124.9(3)
O(1)–Pb–O(2i)'	165.50(9)	N(2)–C(3)–C(2)	125.2(3)
Pb–O(1)–S(1)	118.10(15)	C(1)–C(2)–C(3)	129.3(3)
O(1)–S(1)–O(2i)	114.25(18)		
Σ bond angle around Pb	262.7	NCCCN _{plane} –NPbN _{plane}	20.4
DOP of Pb (%) ^a	108		
<i>Dihedral angles (deg)</i>			
C(11)–C(6)–N(1)–Pb	99.3(4)	C(19)–C(14)–N(2)–Pb	–86.9(4)

^a Degree of pyramidalisation (DOP, %) = [(360 – Σ_{bond angle}) / 0.9]^[115] When a DOP is 100%, it is equivalent to a sum of bond angles of 270°, whereas a DOP of 0% indicates a planar geometry at the central atom; Symmetry transformations used to generate equivalent atoms: (i) –x + 1, y + 1/2, –z + 1/2

Table 17. Selected crystallographic data for [(BDI_{DMP})PbOTf] (**29**)

[(BDI _{DMP})PbOTf] (29)	
chemical formula	C ₂₂ H ₂₅ F ₃ N ₂ O ₃ PbS
molecular mass	661.69
temperature (K)	173(2)
wavelength (Å)	0.71073
crystal system	monoclinic
space group	<i>P</i> 2 ₁ / <i>c</i> (No. 14)
<i>a</i> (Å)	11.4124(2)
<i>b</i> (Å)	11.5990(3)
<i>c</i> (Å)	20.5159(6)
<i>α</i> (deg)	90
<i>β</i> (deg)	117.144(2)
<i>γ</i> (deg)	90
<i>V</i> (Å ³)	2416.63(10)
<i>Z</i>	4
ρ_{calcd} (Mg m ⁻³)	1.82
θ range (deg)	3.49–26.72
abs coeff (mm ⁻¹)	7.116
measd/indep reflns/ <i>R</i> (int)	25 271/5100/0.056
reflns with <i>I</i> > 2 σ (<i>I</i>)	4472
data/restraints/param	5100/0/295
goodness of fit on <i>F</i> ²	1.046
final <i>R</i> indices [<i>I</i> > 2 σ (<i>I</i>)]	<i>R</i> 1 = 0.028, <i>wR</i> 2 = 0.053
<i>R</i> indices (all data)	<i>R</i> 1 = 0.031, <i>wR</i> 2 = 0.055
largest diff peak and hole (e Å ⁻³)	0.54 and –1.05

3.2.4 Reactions of the bis[β -diketiminato]lead(II) complexes **25** and **26**

Further ¹H NMR reactivity studies were performed on the bis[β -diketiminato]lead(II) complexes **25** and **26**. Our primary objective was to probe functionality of the lone pair on the lead atom. Initially, we attempted to convert [(BDI_{Ph})₂Pb] (**25**) to the corresponding β -diketiminatolead(II) alkoxide by treatment with potassium *tert*-butoxide. Although we seemingly obtained a mixture of intractable products in C₆D₆, the work-up of the reaction by washing the isolated solid with cold pentane revealed two major products. The absence of the imine resonance (δ_{H} 12.69 ppm) in the ¹H NMR spectrum suggested that neither of these components was the β -diketimine **19**. One of the components was identified as the bis[β -diketiminato]lead(II) complex **25** with

resonances at δ_{H} 4.85 and 1.85 ppm assigned respectively to the γ -*H* and β -*Me* protons in the β -diketiminato ring, identical with those obtained previously. The ^1H NMR spectrum of the remaining product suggested the presence of the lead(II) *tert*-butoxide $[(\text{BDI}_{\text{Ph}})\text{PbO}^t\text{Bu}]$ with resonances at δ_{H} 4.71, 1.78 and 1.34 ppm assigned respectively to the γ -*H*, β -*Me* and *O*^{*t*}*Bu* protons, with proton integration ratio of 1:6:9. Unfortunately, a pure sample could not be isolated despite several attempts, for example by washing the residue with various organic solvents or by cooling the solution to -30 °C. Furthermore, a mixture, including the starting bis[β -diketiminato]lead(II) complex **25**, was observed even after a prolonged period of time. For example, a mixture of **25** and the other product was found in a 1.3:1 ratio after 5 days at 40 °C.

Preliminary studies on the reaction of the bis[β -diketiminato]lead(II) complexes with electrophiles were investigated. When $[(\text{BDI}_{\text{Ph}})_2\text{Pb}]$ (**25**) was treated with methyl trifluoromethanesulfonate, an intractable mixture was observed. Treatment of $[(\text{BDI}_{\text{IPP}})_2\text{Pb}]$ (**26**) with methyl iodide in C_6D_6 gave an intractable mixture at room temperature. However, single crystals were obtained adventitiously from the mixture at room temperature.

An X-ray crystallographic study revealed that the product is $[(\text{BDI}_{\text{IPP}})\text{PbI}]$ (**30**) as illustrated in Figures 30 and 31. Selected bond lengths and angles are given in Table 18, and selected crystallographic data in Table 19. Ligands are coordinated in a pyramidal geometry around the lead atom with the sum of bond angles 263.9° . The lead atom deviates from the mean NCCCN plane of the β -diketiminato ring by a distance of 0.229 Å, in contrast to $[(\text{BDI}_{\text{DIPP}})\text{PbI}]$ (**11**, $\text{Pb-NCCCN}_{\text{plane}} = 0.846$ Å).^[62] The difference can be explained by the reduced crowding around the metal centre due to the absence of *ortho*-substituents on the *N*-substituted aryl groups. The lead(II) iodide **30** has a polymeric structure, with Pb–I bonds comprising the polymeric chain. Each lead atom is bound to two iodide atoms, with one Pb–I bond (3.1928(3) Å) shorter than the other Pb–I' bond (3.5079(4) Å). Both Pb–I bond lengths are longer than those found in $[(\text{BDI}_{\text{DIPP}})\text{PbI}]$ (**11**, $\text{Pb-I} = 2.9531(5)$ Å) and Filippou's $[\{\text{Pb}(2,6\text{-Trip}_2\text{C}_6\text{H}_3)\text{I}\}_2]$ (Trip = (2,4,6-*t*Pr₃C₆H₂), avg. $\text{Pb-I} = 3.1132$ Å).^[62, 169] Furthermore, the Pb–I bonds in **30** are also longer than the sum of covalent radii of lead and iodine (2.58 Å), indicating the bonding has a strong electrostatic component.^[122]

Figure 30. ORTEP diagram of $[(BDI_{IPP})PbI]$ (**30**). H atoms are omitted and C atoms in the β -diketiminato ring are minimised for clarity. The ellipsoid probability is shown at 30%

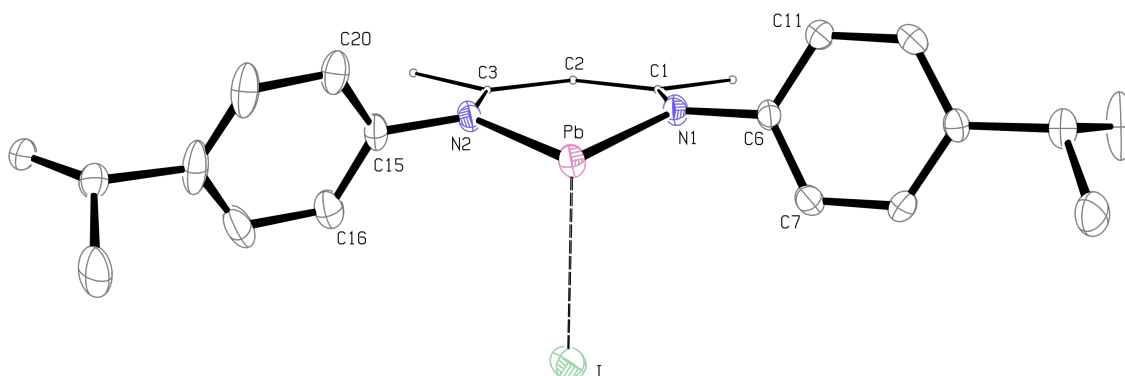


Figure 31. ORTEP diagram of $[(BDI_{IPP})PbI]$ (**30**) showing the polymeric chain. H atoms are omitted and C atoms in the N -aryl group in the β -diketiminato ring are minimised for clarity. The ellipsoid probability is shown at 30%

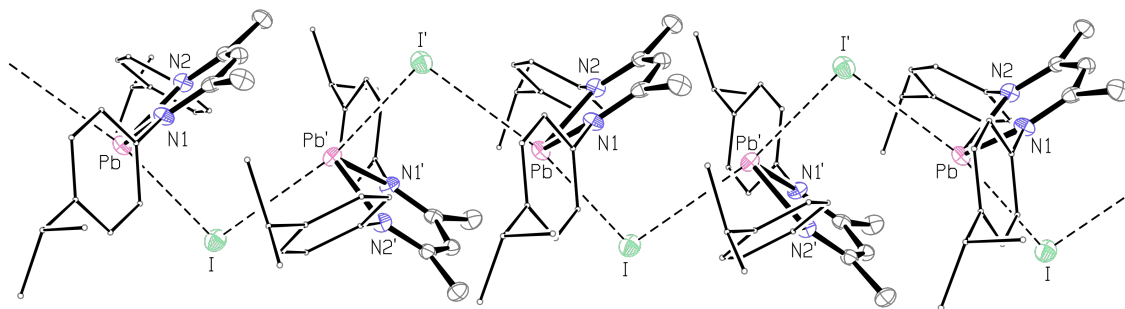


Table 18. Selected bond lengths (Å) and angles (deg) for [(BDI_{IPP})PbI] (**30**)

<i>Bond lengths (Å)</i>			
Pb–N(1)	2.284(3)	Pb–I'	3.5079(4)
Pb–N(2)	2.275(3)	N(1)–C(1)	1.324(5)
N(1)–C(6)	1.431(5)	N(2)–C(3)	1.335(5)
N(2)–C(15)	1.437(5)	C(1)–C(2)	1.404(6)
Pb–I	3.1928(3)	C(2)–C(3)	1.411(5)
Pb–NCCCN _{plane}	0.229		
<i>Bond angles (deg)</i>			
N(1)–Pb–N(2)	83.11(11)	N(2)–Pb–I'	97.49(8)
N(1)–Pb–I	92.28(8)	N(1)–C(1)–C(2)	124.9(4)
N(2)–Pb–I	88.47(8)	N(2)–C(3)–C(2)	124.0(4)
I–Pb–I'	167.809(9)	C(1)–C(2)–C(3)	131.0(4)
N(1)–Pb–I'	98.97(9)		
Σ bond angle around Pb	263.9	NCCCN _{plane} –NPbN _{plane}	7.7
DOP (%) ^a	107		
<i>Dihedral angles (deg)</i>			
C(7)–C(6)–N(1)–Pb	65.5(4)	C(20)–C(15)–N(2)–Pb	73.4(4)

^a Degree of pyramidalisation (DOP, %) = $[(360 - \sum_{\text{bond angles}})/0.9]$ [115] When a DOP is 100%, it is equivalent to a sum of bond angles of 270°, whereas a DOP of 0% indicates a planar geometry at the central atom; Symmetry transformation used to generate equivalent atoms: (i) $-x + 1/2, y + 1/2, -z + 1/2$

Table 19. Selected crystallographic data for [(BDI_{IPP})PbI] (**30**)

[(BDI _{IPP})PbI] (30)	
chemical formula	C ₂₃ H ₂₉ IN ₂ Pb, C ₆ D ₆
molecular mass	745.69
temperature (K)	173(2)
wavelength (Å)	0.71073
crystal system	monoclinic
space group	<i>C</i> 2/ <i>c</i>
<i>a</i> (Å)	28.2581(5)
<i>b</i> (Å)	9.9106(2)
<i>c</i> (Å)	20.1416(3)
<i>α</i> (deg)	90
<i>β</i> (deg)	90.889(1)
<i>γ</i> (deg)	90
<i>V</i> (Å ³)	5640.07(17)
<i>Z</i>	8
ρ_{calcd} (Mg m ⁻³)	1.76
θ range (deg)	3.50–27.10
abs coeff (mm ⁻¹)	7.10
measd/indep reflns/ <i>R</i> (int)	44 103/6196/0.074
data/restraints/param	6196/78/328
goodness of fit on <i>F</i> ²	1.084
final <i>R</i> indices [<i>I</i> > 2 σ (<i>I</i>)]	<i>R</i> 1 = 0.031, <i>wR</i> 2 = 0.056
<i>R</i> indices (all data)	<i>R</i> 1 = 0.045, <i>wR</i> 2 = 0.059
largest diff peak and hole (e Å ⁻³)	0.72 and –0.87

3.3 Conclusions

We have synthesised some lead(II) complexes containing a series of β -diketiminato ligands. X-ray crystallographic studies on $[(\text{BDI}_{\text{Ph}})\text{PbCl}]$ (**22**) and $[(\text{BDI}_{\text{IPP}})\text{PbI}]$ (**30**) show both structures are polymeric, whereas a dimeric structure is found for $[(\text{BDI}_{\text{DMP}})\text{PbCl}]$ (**24**) in the solid state. These results contrast with other β -diketiminato heavy group 14 metal halides, such as Fulton's $[(\text{BDI}_{\text{DIPP}})\text{PbX}]$ (X = Cl, Br or I) and Barrau's $[(\text{BDI}_{\text{Ph}})\text{MCl}]$ (M = Ge or Sn), in which well-defined molecular species are apparent.^[62, 136-137]

Although previous work demonstrated that treatment of $[(\text{BDI}_{\text{DIPP}})\text{PbCl}]$ (**2**) with potassium alkoxides gave the corresponding β -diketiminatolead(II) alkoxides, the analogous reactions of $[(\text{BDI}_{\text{Ph}})\text{PbCl}]$ (**22**) or $[(\text{BDI}_{\text{IPP}})\text{PbCl}]$ (**23**) led to the formation of homoleptic bis[β -diketiminato]lead(II) complexes **25** and **26**. These results are consistent with those proposed by Itoh, who suggested that the steric influence of substituents at the *ortho*-position of the *N*-substituted aryl group played an important role in controlling the formation of monomeric or dimeric β -diketiminatocopper(II) complexes (equations 49–51, Page 69–70).^[148]

Preliminary studies on the reactions of the bis[β -diketiminato]lead(II) complexes **25** and **26** with aliphatic electrophiles are intriguing. At present, we do not have any evidence to suggest that the lead atom is the primary reaction centre for these reactions, which proceeded with substitution rather than oxidative addition. Further studies are ongoing to understand the reactions of the bis[β -diketiminato]lead(II) complexes **25** and **26** with other organic substrates and the reaction mechanism involved.

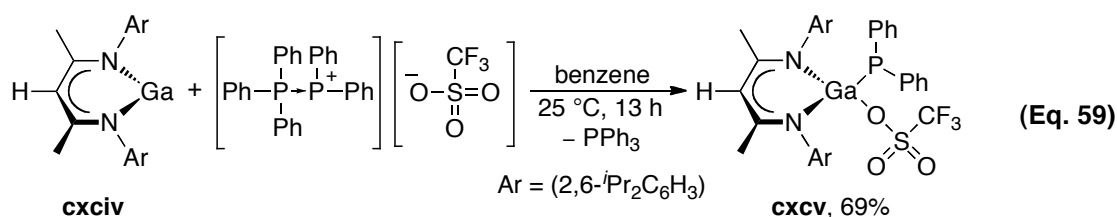
4. β -Diketiminato heavy group 14 metal phosphanides and their reactions with elemental chalcogens

4.1 Introduction

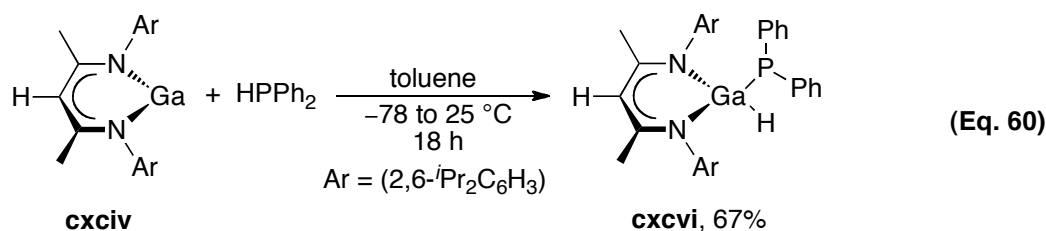
4.1.1 Overview of metal phosphanido complexes

Several β -diketiminato heavy group 14 metal complexes with terminal ligands, such as amides, alkyls and alkynes have been synthesised.^[67, 70, 170] In this chapter, we discuss the synthesis and chemistry of β -diketiminato heavy group 14 metal phosphanides.

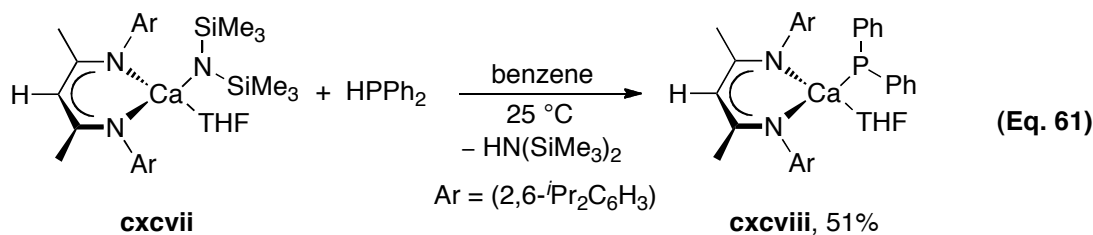
Over the years, applications of metal phosphanides have rapidly expanded in areas such as catalysis and nanotechnology.^[171-175] Examples of β -diketiminato metal phosphanides are however extremely rare and the chemistry of these compounds has been little studied. To the best of our knowledge, only β -diketiminato calcium and -gallium phosphanides are described in the literature, besides derivatives of heavy group 14 metals.^[102, 176-177] Burford *et al.* reported the first β -diketiminato gallium phosphanide **cxcv**.^[176] Treatment of [(BDI_{DIPP})Ga] (**cxiv**) with pentaphenylphosphinophosphenium triflate gave the gallium phosphanido complex **cxcv** in 69% yield (equation 59). An X-ray crystallographic study revealed a pyramidal geometry around the phosphorus atom. The ³¹P{¹H} NMR spectrum showed a singlet at δ_P -57 ppm.



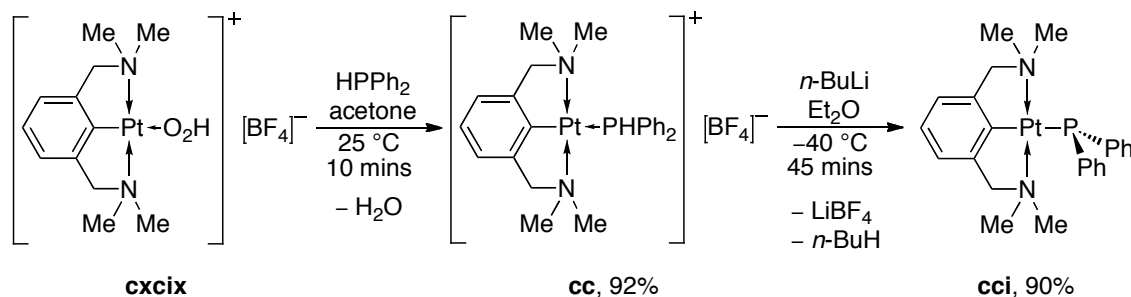
Linti *et al.* reported a similar β -diketiminato gallium phosphanide **cxvii**.^[102] Oxidative addition of diphenylphosphine to the Ga(I) compound [(BDI_{DIPP})Ga] (**cxiv**) gave the gallium phosphanide **cxvii** in moderate yield (equation 60). An X-ray crystallographic study showed that the ligands were coordinated in a pyramidal geometry around the phosphorus atom. A singlet at δ_P -61 ppm was found in the ³¹P{¹H} NMR spectrum.



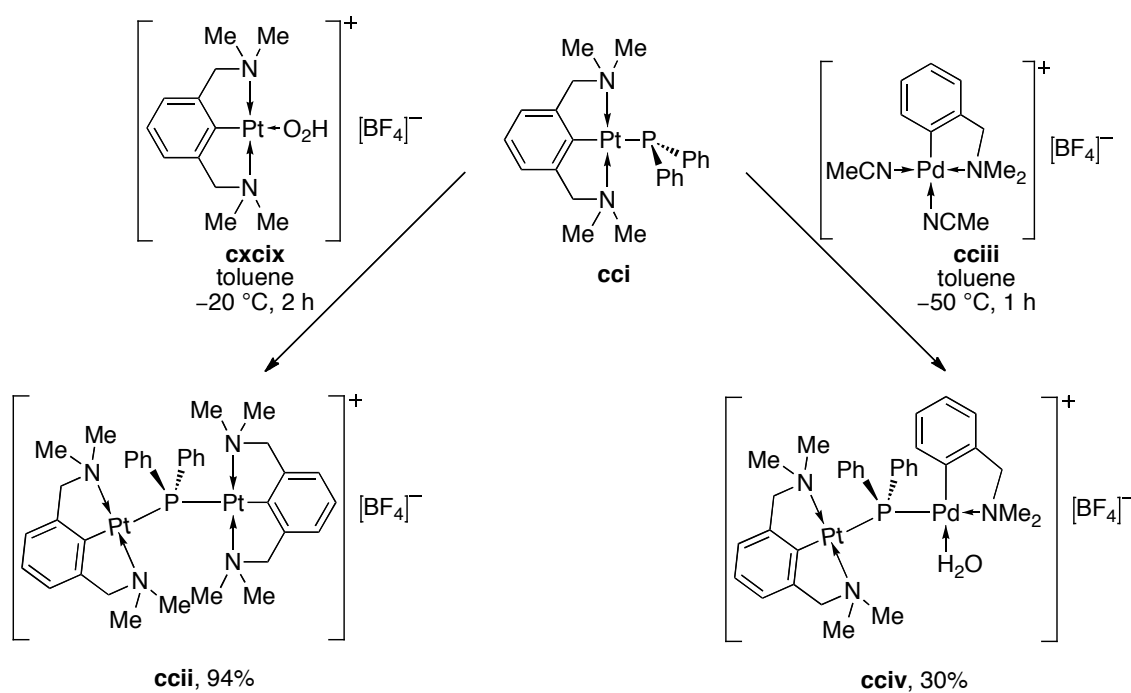
Hill and co-workers synthesised the β -diketiminatocalcium(II) phosphanide **cxcviii** *via* ligand exchange between [(BDI_{DIPP})CaN(SiMe₃)₂(THF)] (**cxcvii**) and diphenylphosphine in benzene (equation 61).^[177] The calcium(II) phosphanide **cxcviii** decomposed in solution and was thermally sensitive. The solid state structure of **cxcviii** was found to be similar to those of the gallium phosphanides **cxcv** and **cxcvi**, with a pyramidal geometry around the phosphorus atom. A singlet at $\delta_{\text{P}} -21.3$ ppm was found in the ³¹P{¹H} NMR spectrum.



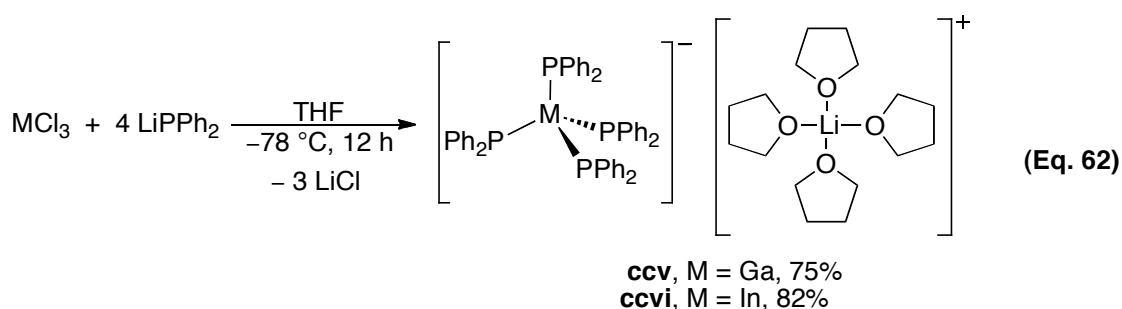
A number of derivatives containing related ligand systems have been reported. Van Koten *et al.* synthesised the monomeric platinum phosphanido complex **cci** containing a tridentate aryldiaminato ligand [C₆H₃(CH₂NMe₂)_{2-2,6}], abbreviated as NCN (Scheme 44).^[178] The ionic platinum complex **cc** was synthesised by reaction between diphenylphosphine and complex **ccix**. The geometry around the phosphorus atom in the diphenylphosphine fragment of complex **cc** was tetrahedral. The ³¹P{¹H} NMR spectrum showed a singlet at $\delta_{\text{P}} 5.2$ ppm with platinum satellites (¹J_{Pt} = 2028 Hz). Treatment of complex **cc** with *n*-BuLi at -40 °C gave the highly air sensitive platinum phosphanido complex **cci** (Scheme 44). The phosphorus was pyramidally coordinated in the phosphanido complex **cci**. The ³¹P{¹H} NMR spectrum of complex **cci** showed a singlet at $\delta_{\text{P}} 0.11$ ppm with platinum satellites (¹J_{Pt} = 1305 Hz).

Scheme 44. Synthesis of the platinum phosphanide **cci**^[178]

Further work showed that the uncoordinated lone pair of electrons on the phosphorus atom in **cci** was nucleophilic towards electrophiles (Scheme 45). Treatment of the platinum phosphanide **cci** with the parent ionic platinum complex **cxcix** gave the dinuclear diphenylphosphanido-bridged complex $[(\text{NCN})\text{Pt}(\mu\text{-PPh}_2)\text{Pt}(\text{NCN})][\text{BF}_4]$ (**ccii**). Similarly, treatment of the platinum phosphanide **cci** with $[\text{Pd}(\text{C}_6\text{H}_4\text{CH}_2\text{NMe}_2)_2(\text{NCMe})_2][\text{BF}_4]$ (**cciii**) gave the dinuclear complex $[\text{Pt}(\text{NCN})(\mu\text{-PPh}_2)\text{Pd}(\text{C}_6\text{H}_4\text{CH}_2\text{NMe}_2)_2(\text{H}_2\text{O})][\text{BF}_4]$ (**cciv**) in 30% yield. The authors suggested that the H_2O found in the solid state structure of **cciv** was due to the presence of water in the polar solvent used during work-up and crystallisation.

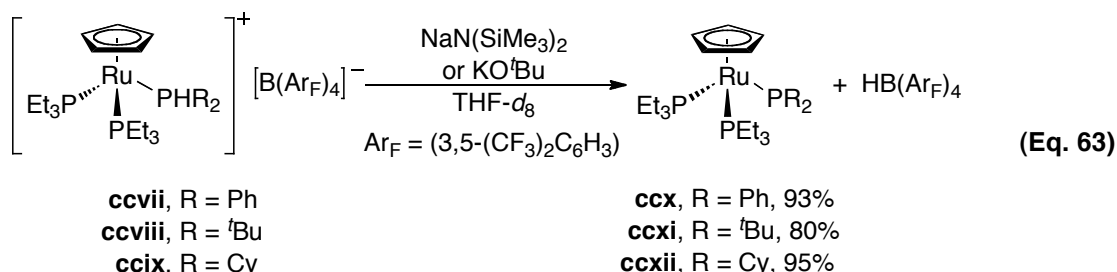
Scheme 45. Reactions of the platinum phosphanide **cci**^[178]

Cowley *et al.* synthesised the first perphosphanido gallates and indates.^[179] Treatment of MCl_3 with four equivalents of lithium diphenylphosphanide gave the ate complexes $[M(PPh_2)_4][Li(THF)_4]$ (**ccv**, $M = Ga$; **ccvi**, $M = In$) in good yields (equation 62). The authors suggested that the size of the phosphanido ligand played an important role in stabilising these anionic complexes, since the maximum number of coordinated phosphanido groups around the gallium or indium centre was three when bulky groups, such as P^tBu_2 , were used.^[180] However, when gallium or indium trichloride was treated with three equivalents of lithium diphenylphosphanide, an intractable oligomeric product was obtained. X-ray crystallographic studies on complexes **ccv** and **ccvi** revealed that the four phosphanido ligands were coordinated with a tetrahedral geometry around the metal centre, while the geometry at phosphorus was pyramidal. The M–P bond lengths (**ccv**, avg. Ga–P = 2.409 Å; **ccvi**, avg. In–P = 2.576 Å) were as found elsewhere for M–P single bonds. The $^{31}P\{^1H\}$ NMR spectra of complexes **ccv** and **ccvi** showed singlets at δ_P –33.4 and –30.2 ppm, respectively, close to the value for lithium diphenylphosphanide (δ_P –38.5 ppm).



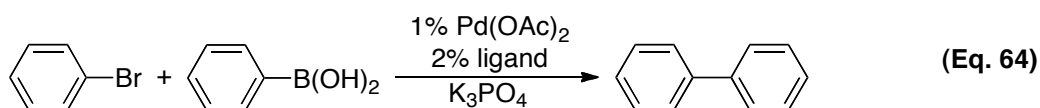
The use of metal phosphanides in catalytic reactions is of interest in both academic and industrial communities.^[181-183] Gladysz *et al.* recently reported a series of electron-rich ruthenium phosphanides, which acted as ‘ligands’ in palladium-catalysed Suzuki coupling reactions.^[184] The cationic ruthenium complexes **ccvii**–**ccix** were deprotonated with KO^tBu or $NaN(SiMe_3)_2$ to give the corresponding ruthenium phosphanides $[(\eta^5-C_5H_5)Ru(PEt_3)_2(PR_2)]$ (**ccx**, $R = Ph$; **ccxi**, $R = ^tBu$; and **ccxii**, $R = Cy$) in good yields (equation 63). However, these compounds were extremely sensitive to oxygen and decomposed to give the corresponding phosphine oxides. Resonances for the phosphorus in the phosphanido fragment were observed at δ_P 30.4 and 23.7 ppm, for compounds **ccx** and **ccxi** respectively, with two-bond coupling to the neighbouring

phosphorus in PEt_3 ($^2J_{\text{PP}} = 5$ and 4 Hz, respectively). A broad resonance ($\delta_{\text{P}} 23.7$ ppm) was found for the phosphorus in the phosphanido fragment in compound **ccxii**, but the coupling with the neighbouring phosphorus was not resolved.



A simple palladium-catalysed Suzuki cross-coupling reaction between bromobenzene and phenylboronic acid was used to investigate the ability of the ruthenium phosphanides to act as ‘ligands’ to coordinate to palladium *via* the electron-rich phosphanido group.^[185] The general conditions of the reaction are illustrated in equation 64. The results showed that the ruthenium phosphanides **ccx–ccxii** generally gave better yields ($> 90\%$) and reduced reaction time (entry 1–3, Table 20) than complexes without the phosphanido ‘ligands’ (entry 4, Table 20).

Table 20. Suzuki cross-coupling reaction of bromobenzene with phenylboronic acid^[184]

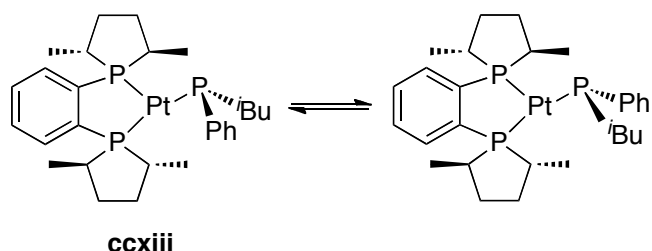


Entry	Ligand / Pd	Conversion (PhBr) (%)	Yield (by G.C.) (formation of Ph ₂ , %)	Time (h)
1	ccx / Pd(OAc) ₂	96	94	32
2	ccxi / Pd(OAc) ₂	100	96	2
3	ccxii / Pd(OAc) ₂	100	97	2
4	Pd(OAc) ₂ only	63	59	48

Other examples of metal phosphanido complexes are shown in Scheme 46 and Figure 32. Glueck *et al.* reported a platinum(II) phosphanide **ccxiii**.^[186] In solution at room temperature, the positions of the groups attached to the phosphorus were interchanged rapidly on the NMR timescale, by a process that involved a combination of inversion

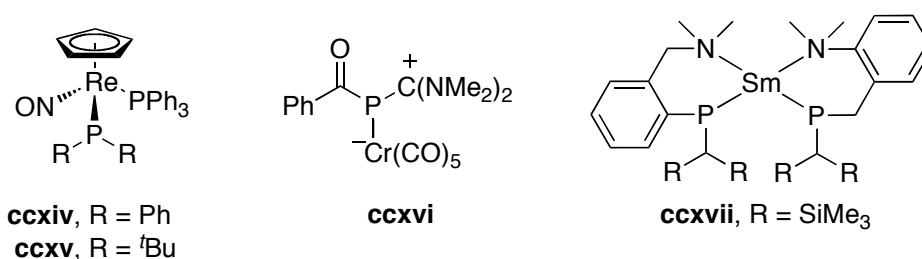
about the phosphorus atom and rotation about the Pt–P bond (Scheme 46).^[186] A VT-³¹P{¹H} NMR study showed that the barrier of this fluxional process is *ca.* 54 kJ mol⁻¹.

Scheme 46. The fluxional process in the terminal phosphanido ligand in **ccxiii**^[186]



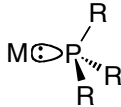
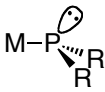
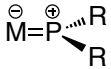
Gladysz *et al.* reported the rhenium phosphanido complexes **ccxiv** and **ccxv**, which showed the nucleophilicity of the lone pair of electrons on the phosphorus in the phosphanido ligand (Figure 32).^[187] For example, treatment of these compounds with iodosobenzene gave the corresponding phosphine oxide complexes. Weber *et al.* synthesised the chromium phosphanido complex **ccxvi** *via* a reaction between phosphalkene (PhC(O)P=C(NMe₃)₂) and [(*Z*)-cyclooctene-Cr(CO)₅] (Figure 32).^[188] There was no evidence from the solid state structure for π -conjugation between the lone pair of electrons on the phosphorus atom and the neighbouring carbonyl group. Izod *et al.* reported a rare example of a homoleptic unsolvated, alkali metal-free samarium(II) phosphanido complex **ccxvii**.^[189] An X-ray crystallographic study showed compound **ccxvii** to be monomeric in the solid state with ligands coordinated in a distorted tetrahedral geometry around the metal centre.

Figure 32. Examples of metal phosphanido complexes **ccxiv–ccxvii**^[187-189]



In summary, the lone pair of electrons on the phosphorus atom in metal phosphanido complexes is generally nucleophilic towards electrophiles, and is able to coordinate to other metal centres to form bimetallic complexes. Although the phosphorus atom is

Table 21. Physical observations of different coordination modes in metal-phosphorus bond^[191]

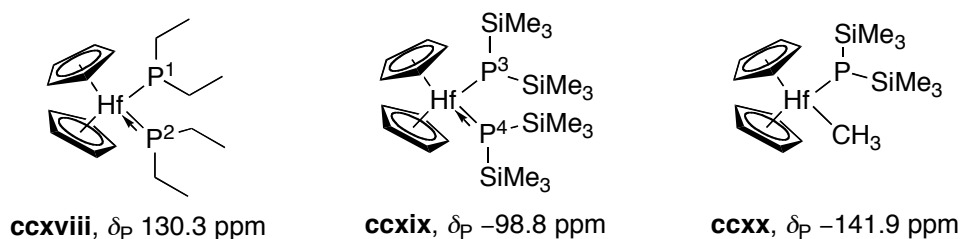
 Phosphine	 Phosphanide	 Phosphenium
PR_3	PR_2^-	PR_2^+
lone pair coordinated to M pseudotetrahedral about P	lone pair localised on P pyramidal about P long M–P bond length small M–P–R bond angle ($< 114^\circ$)	multiple M–P bond planar about P short M–P bond length large M–P–R bond angle ($\sim 130^\circ$)

Generally, the inversion barrier for PH_3 and its derivatives is higher than that for the nitrogen analogues; for instance, the inversion barrier of PH_3 is 126–147 kJ mol^{-1} , whereas the inversion barrier of NH_3 is approximately 21 kJ mol^{-1} .^[192-194] However, the presence of silyl substituents at phosphorus decreases the inversion barrier as: (a) Si–P bonds are more ionic and less strongly directional than C–P bonds; and (b) electron density from the phosphorus lone pair may be delocalised into σ^* or perhaps empty d orbitals on silicon.^[192, 195-197] The latter effect, through the π -system, is an example of ‘negative hyperconjugation’.^[198-200]

Some examples, which show various geometrical configurations at phosphorus, are described below (Figure 33). The solid state structure of the hafnium phosphanido complex **ccxviii** contained two $\text{P}(\text{C}_2\text{H}_5)_2$ ligands.^[201] The geometry about the P(1) atom in **ccxviii** was pyramidal, whereas the geometry at P(2) was planar. The Hf–P bond lengths differed by approximately 0.2 Å; Hf–P(1) = 2.682(1) Å and Hf–P(2) = 2.488(1) Å. These results indicated that one of the phosphorus lone pairs involved in the bonding with the metal centre.^[202] Similarly, the structure of the hafnium bis(trimethylsilyl)phosphanide **ccxix** showed different geometries at phosphorus, one of which had a pyramidal geometry at phosphorus, and the other one having a planar geometry at phosphorus (*c.f.* Hf–P(3) = 2.654(1) Å and Hf–P(4) = 2.553(1) Å).^[190] The $^{31}\text{P}\{^1\text{H}\}$ NMR spectrum of **ccxix** at 22 °C showed a single resonance at $\delta_{\text{P}} -98.8$ ppm in C_6D_6 , suggesting rapid exchange between the two phosphorus geometries, but separate resonances corresponding to the two geometries were not observed even at low

temperatures. In the hafnium monophosphanide **ccxx**, the geometry at phosphorus was pyramidal. The $^{31}\text{P}\{^1\text{H}\}$ NMR spectrum of **ccxx** showed a single resonance at $\delta_{\text{P}} -141.9$ ppm.

Figure 33. Hafnium phosphanido complexes **ccxviii–ccxx** and their $^{31}\text{P}\{^1\text{H}\}$ NMR resonances in C_6D_6 at room temperature^[190, 201-202]



Hillhouse *et al.* demonstrated that the phosphonium coordination mode can be supported by an electron-deficient metal centre (Scheme 48).^[203] Treatment of the dimeric nickel chloride **ccxxi** with lithium di-*tert*-butylphosphanide gave the nickel(I) phosphanide **ccxxii**. Oxidation of this compound with ferrocenium hexafluorophosphate (Cp_2FePF_6) afforded the ionic nickel(II) phosphonium complex **ccxxiii**. The X-ray crystallographic analysis revealed that the geometry at phosphorus was pyramidal in **ccxxii**, but the geometry at phosphorus was planar in **ccxxiii**. Complex **ccxxii** had a longer Ni–P bond (2.2077(12) Å) and a smaller Ni–P–C bond angle (116.7(1)°) than those in complex **ccxxiii** (Ni–P = 2.098(2) Å and Ni–P–C = 124.1(2)°) (Table 22). Unfortunately, NMR spectroscopic data were not available for **ccxxii**, which was paramagnetic. However, the diamagnetic nickel(II) phosphonium complex **ccxxiii** showed a triplet at δ_{P} 348 ppm in CD_2Cl_2 with a coupling constant of $J_{\text{PP}} = 175$ Hz.

Scheme 48. Synthesis of complexes **ccxxii** and **ccxxiii**^[203]

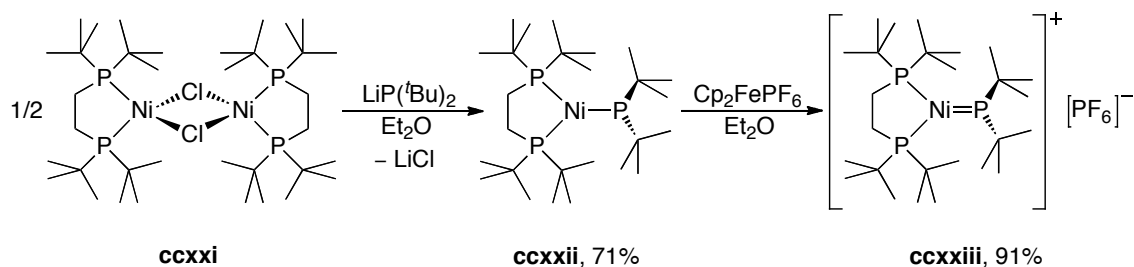
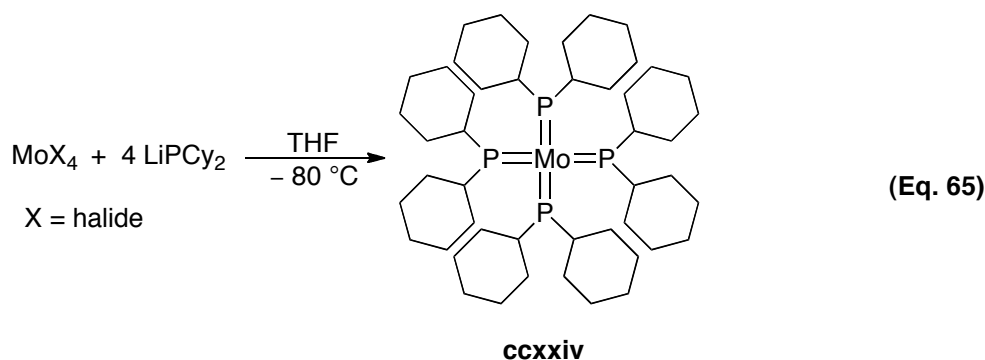


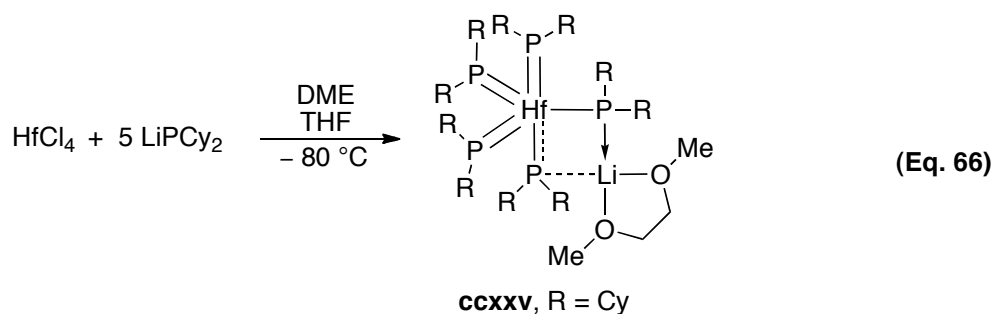
Table 22. Selected structural data for complexes **ccxxii** and **ccxxiii**^[203]

	Ni–P (Å)	Ni–P–C (deg)	Σ P _{bond angle} (deg)
ccxxii	2.2077(12)	116.7(1)	344
ccxxiii	2.098(2)	124.1(2)	360

Baker *et al.* synthesised a series of homoleptic early transition metal dicyclohexylphosphanides which featured metal-phosphorus multiple bonding.^[202] For example, treatment of molybdenum halides with four equivalents of lithium dicyclohexylphosphanide in THF at $-80\text{ }^{\circ}\text{C}$ gave $[\text{Mo}(\text{PCy}_2)_4]$ (**ccxxiv**) (equation 65). The solid state structure of **ccxxiv** showed a distorted tetrahedral geometry at the molybdenum centre and a planar geometry around the phosphorus atoms. The short Mo–P bond lengths (avg. $2.265\text{ }\text{\AA}$) and large P–Mo–P angles (avg. 123.1°) suggested that the ligands were coordinated in the phosphonium coordination mode.



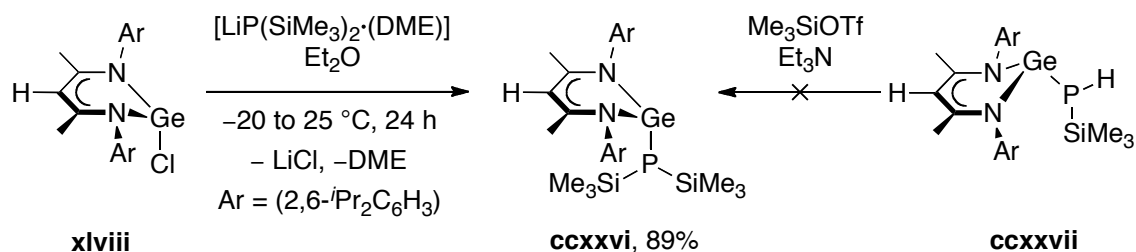
Treatment of hafnium chloride with five equivalents of lithium dicyclohexylphosphanide in the presence of 1,2-dimethoxyethane (DME) gave complex **ccxxv** (equation 66).^[202] The solid state structure showed that the phosphanido ligands were coordinated in a distorted bipyramidal geometry around the metal centre. Both pyramidal and planar geometries were found around the phosphorus centres. The average Hf–P bond length to the phosphorus with a pyramidal geometry is $2.675\text{ }\text{\AA}$ with an average Hf–P–C bond angle 119° . A shorter Hf–P bond length (avg. $2.504\text{ }\text{\AA}$) is observed to the phosphorus with a planar geometry, together with a wider Hf–P–C bond angle (avg. 125°).



4.1.3 Previous examples of β -diketiminato heavy group 14 metal phosphanides

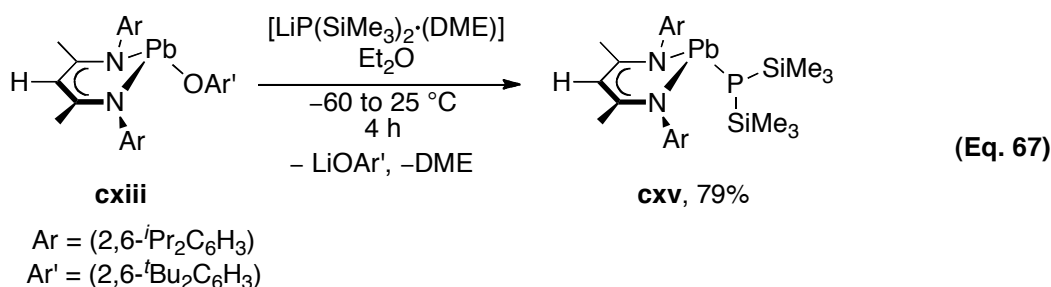
Examples of β -diketiminato heavy group 14 metal phosphanides are rare in comparison to transition metal analogues. Driess *et al.* synthesised the β -diketiminatogermanium(II) and -lead(II) phosphanides **ccxxvi** and **cxv** (Scheme 49 and equation 67).^[103, 134] Treatment of the germanium(II) chloride **xlvi** with $[\text{LiP}(\text{SiMe}_3)_2(\text{DME})]$ in diethyl ether gave the β -diketiminatogermanium(II) bis(trimethylsilyl)phosphanide **ccxxvi** in good yield (Scheme 49).^[134] However, synthesis of the phosphanide **ccxxvi** *via* treatment of $[(\text{BDI}_{\text{DIPP}})\text{GeP}(\text{H})(\text{SiMe}_3)]$ **ccxxvii** with trimethylsilyl triflate in the presence of triethylamine was not successful. An X-ray crystallographic study showed the geometry at phosphorus was planar in the germanium(II) phosphanide **ccxxvi**, and it was suggested that this reflected crowding from the bulky β -diketiminato and trimethylsilyl ligands, as well as the low inversion barrier in the bis(trimethylsilyl)phosphanido group.^[134] The $^{31}\text{P}\{^1\text{H}\}$ NMR spectrum of **ccxxvi** showed a resonance at $\delta_{\text{P}} -192.7$ ppm.

Scheme 49. Synthesis of the β -diketiminatogermanium(II) bis(trimethylsilyl)phosphanide **ccxxvi**^[134]



Treatment of the β -diketiminatolead(II) aryloxide **cxiii** with $[\text{LiP}(\text{SiMe}_3)_2(\text{DME})]$ in the presence of diethyl ether gave the lead(II) bis(trimethylsilyl)phosphanide **cxv** in 79% yield (equation 67).^[103] An X-ray crystallographic study showed the presence of

pyramidally coordinated lead and phosphorus atoms. In contrast to other three-coordinate β -diketiminato heavy group 14 metal complexes in which the C_3N_2M ring of the β -diketiminato ligand was nearly planar, the six-membered C_3N_2Pb ring in the lead(II) phosphanide **cxv** adopted a boat-shaped conformation. The angle between the mean NCCCN plane and the NPbN plane in the β -diketiminato ring was 43.9° , wider than those in other β -diketiminato heavy group 14 metal complexes, for example $[(BDI_{DIPP})PbOC(CH_3)_2CH=CH_2]$ (**5**, 29.2°) and Roesky's $[(BDI_{DIPP})SnN(SiMe_3)_2]$ (12.2°).^[67] Driess attributed these findings to the strong σ -donor ability of the phosphorus atom in the bis(trimethylsilyl)phosphanido fragment.



An upfield resonance ($\delta_P -116.6$ ppm) with a large coupling constant ($^1J_{PbP} = 2852$ Hz) was found in the $^{31}P\{^1H\}$ NMR spectrum of **cxv**. The lead resonance was found at $\delta_{Pb} -1737$ ppm in the ^{207}Pb NMR spectrum. It was suggested that these findings could be attributed to the higher 3s-contribution from the phosphorus atom in the lead-phosphorus single bond. In $[(BDI_{DIPP})PbP=Si(Ar)Si^tBu_3]$ (Ar = (2,4,6-ⁱPr₃C₆H₂)), the more electronegative P=SiR₂ fragment made the phosphorus atom a weaker σ -donor, so that the ^{207}Pb resonance was shifted to $\delta_{Pb} 1068$ ppm in the ^{207}Pb NMR spectrum.^[103]

Although the phosphorus resonances were both negative in the $^{31}P\{^1H\}$ NMR spectra of the germanium(II) and lead(II) bis(trimethylsilyl)phosphanides **ccxxvi** and **cxv** ($\delta_P -192.7$ and -116.6 ppm, respectively), the geometry around the phosphorus atom in these complexes was different (Table 23).^[103, 134] The solid state structure of the germanium(II) bis(trimethylsilyl)phosphanide **ccxxvi** showed the geometry at phosphorus was planar, with the sum of bond angles around the phosphorus atom 355.2° . However, a pyramidally coordinated phosphorus was found in the lead derivative **cxv**, with the sum of bond angles around the phosphorus atom 305.7° . It was suggested that the planar geometry at phosphorus in the germanium derivative **ccxxvi**

was due to the low inversion barrier in the bis(trimethylsilyl)phosphanide group and crowding from the β -diketiminato ligand.^[134] However, a direct comparison between the different geometries around the phosphorus atom in these complexes was not made.

Table 23. $^{31}\text{P}\{^1\text{H}\}$ NMR spectroscopic and selected solid state structural data of $[(\text{BDI}_{\text{DIPP}})\text{MP}(\text{SiMe}_3)_2]$ (**ccxxvi**, M = Ge; **cxv**, M = Pb) in C_6D_6 ^[103, 134]

	$^{31}\text{P}\{^1\text{H}\}$ (δ_{P} , ppm)	$^1J_{\text{PM}}$ (Hz)	M–P (Å)	M–P–Si (deg) ^a	Σ P _{bond} angle (deg)
ccxxvi M = Ge	–192.7	–	2.3912(8)	122.5	355.2
cxv M = Pb	–116.6	2852	2.715(2)	103.2	305.7

^a Average value

4.1.4 Complexes containing heavy group 14 metal-phosphorus multiple bond

Data from heavy group 14 metal complexes containing metal-phosphorus double bonds are summarised in Figure 34–35 and Table 24–25. Such examples are extremely rare. Escudié and co-workers synthesised the stannaphosphenes **ccxxviii** and **ccxxix**, as well as the stannaphosphine **ccxxxi** (Figure 34).^[204–205] The tin resonances in **ccxxviii** and **ccxxix** were found at δ_{Sn} 658.3 and 499.5 ppm respectively, and the phosphorus resonances at δ_{P} 204.7 and 170.7 ppm (Table 24). These complexes showed large tin-phosphorus coupling constants ($^1J_{\text{SnP}} > 2000$ Hz), which the authors suggested that these were indicative of tin-phosphorus double bonds. In contrast, the stannaphosphine **ccxxxi**, containing a Sn–P single bond, had a smaller tin-phosphorus coupling constant $^1J_{^{119}\text{SnP}} = 959$ Hz.^[204–205]

Scheer *et al.* recently reported an ionic tin complex **ccxxx** (Figure 34 and Table 24).^[206] The $^{31}\text{P}\{^1\text{H}\}$ NMR spectrum showed coupling constants assigned by the authors to $^1J_{\text{P}^{117}\text{Sn}} = 1735$ Hz and $^1J_{\text{P}^{119}\text{Sn}} = 2004$ Hz, and taken as evidence for the presence of a tin-phosphorus double bond. The published $^1J_{\text{P}^{117}\text{Sn}}:^1J_{\text{P}^{119}\text{Sn}}$ ratio (1:1.155) was not correct (the ratio should be 1:1.046), but it seemed to be clear that the coupling constant was similar to those in other stannaphosphenes.^[207] In contrast, the aryl stannylene phosphanide **ccxxxii**, containing a tin-phosphorus single bond, showed a single

resonance at $\delta_P -70.9$ ppm with a smaller phosphorus-tin coupling constant $^1J_{P^{119}Sn} = 934$ Hz. However, the solid state structures of **ccxxviii**–**ccxxxii** were not reported.

Figure 34. Examples of stannaphosphenes and stannaphosphines^[204-206]

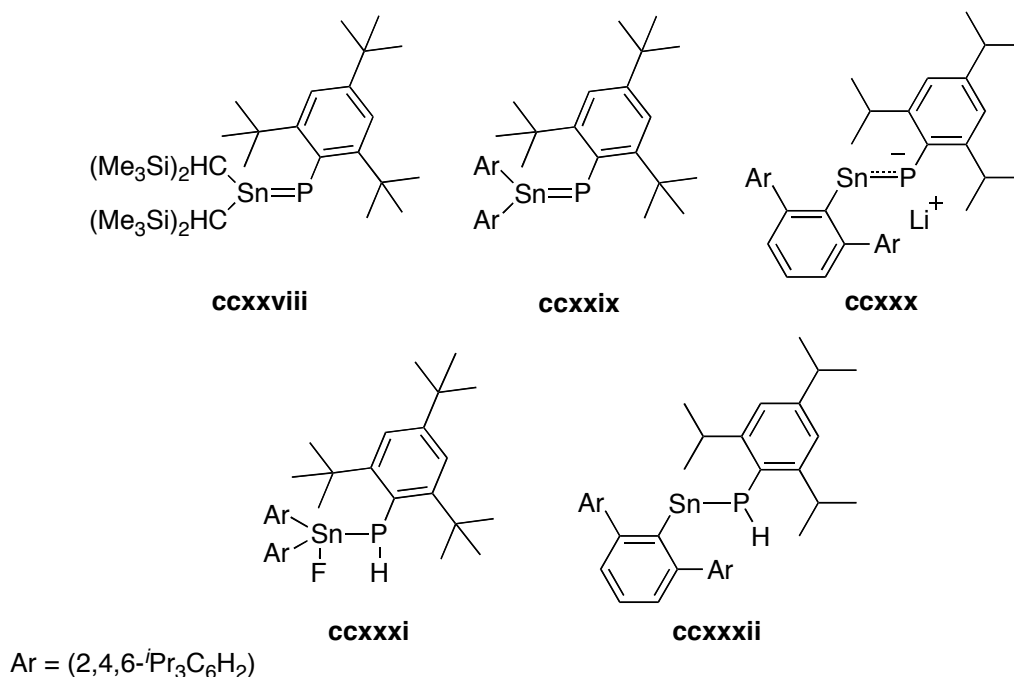


Table 24. Selected NMR spectroscopic data for **ccxxviii**–**ccxxxii**^[204-206]

	¹¹⁹ Sn (δ_{Sn} , ppm)	³¹ P{ ¹ H} (δ_P , ppm)	¹ J _{P¹¹⁹Sn} (Hz)	¹ J _{P¹¹⁷Sn} (Hz)	NMR solvent
ccxxviii	658.3	204.7	2295	2191	C ₆ D ₆
ccxxix	499.5	170.7	2208	2110	not reported
ccxxx	– ^a	229.7	2004	1735	C ₆ D ₆
ccxxxii	–34.0	–115.8	995	954	not reported
ccxxxii	– ^a	–70.9	934	– ^a	C ₆ D ₆

^a Data not reported

Several examples of germaphosphenes are known (Figure 35). The solid state structures of Escudié's germaphosphenes **ccxxxiii** and **ccxxxiv** showed respectively, Ge=P–C bond angles of 107.5(3)° and 103.1(4)° with Ge=P bond lengths of 2.183(3) and 2.143(4) Å (Table 25).^[208-209] The Ge=P bond lengths were in good agreement with the sum of covalent radii (2.12 Å) of sp² germanium (1.12 Å) and sp² phosphorus (1.00 Å), suggesting the presence of germanium-phosphorus double bonds.^[208] The solid state

structure of Sekiguchi's germaphosphene **ccxxxv** also showed a short Ge=P bond (2.175(14) Å), indicative of a germanium-phosphorus double bond.^[210] The $^{31}\text{P}\{^1\text{H}\}$ NMR spectrum of **ccxxxv** showed a single resonance at δ_{P} 416.3 ppm.

Figure 35. Examples of germaphosphene^[208-210]

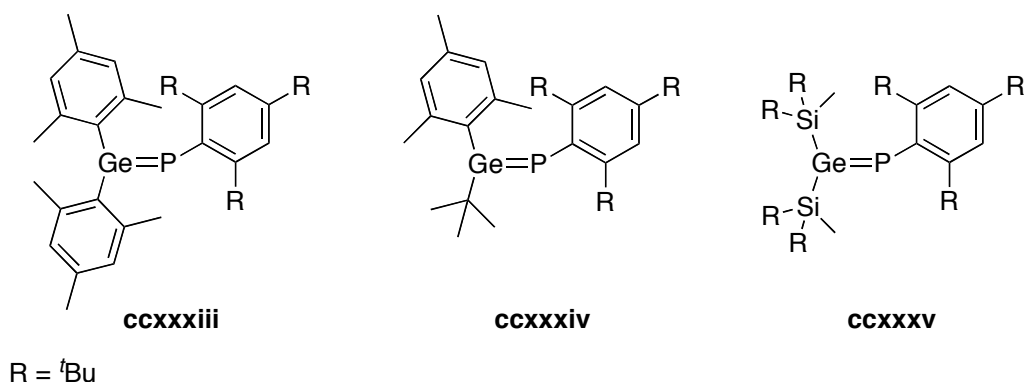


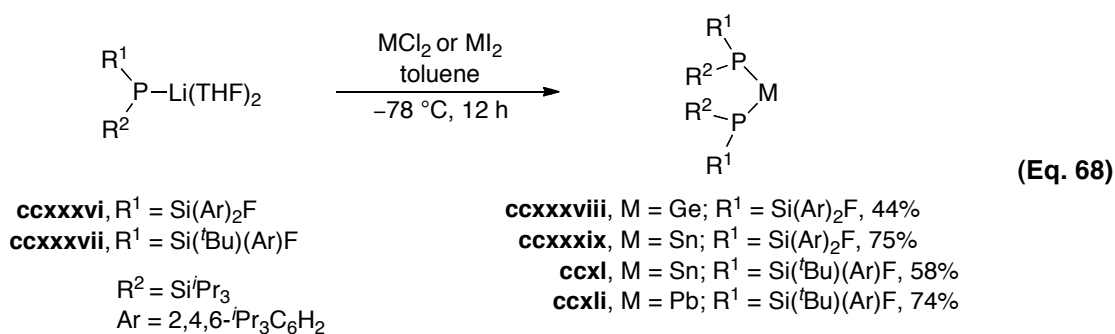
Table 25. Selected NMR spectroscopic and structural data for **ccxxxiii–ccxxxv**^[208-210]

	$^{31}\text{P}\{^1\text{H}\}$ (δ_{P} , ppm)	Ge=P (Å)	Ge=P–C (deg)	NMR solvent
ccxxxiii	– ^a	2.138(3)	107.5(3)	not reported
ccxxxiv	– ^a	2.143(4)	103.1(4)	not reported
ccxxxv	416.3	2.175(14)	109.9(16)	C ₆ D ₆

^a ^{31}P chemical shift not reported

4.1.5 Heavy group 14 metal phosphanido complexes

Several heavy group 14 metal phosphanides have been reported. Driess *et al.* synthesised a series of phosphanyl-substituted carbene analogues of heavy group 14 metal complexes.^[211] Treatment of the lithium phosphanides **ccxxxvi** or **ccxxxvii** with metal dihalide in toluene at –78 °C gave complexes **ccxxxviii–ccxli** (equation 68).



The phosphorus chemical shifts and their phosphorus-metal coupling constants of these complexes are summarised in Table 26. The germanium and tin derivatives, **ccxxxviii**, **ccxxxix** and **ccxli**, showed resonances at δ_P -62.1, -102.5 and -121.3 ppm, respectively (Table 26). The tin-phosphorus coupling constants for the tin analogues **ccxxxix** and **ccxli** were $^1J_{P^{119}Sn} = 1682$ and 1628 Hz, respectively. The $^{31}P\{^1H\}$ NMR spectrum for the lead derivative **ccxli** showed two broad resonances at δ_P -88.8 and -95.6 ppm in a 1:1 ratio with phosphorus-lead coupling constants $^1J_{PPb} = 1995$ and 1979 Hz, respectively. Although these results indicated that two diastereomers were present for the lead derivative, the authors were able to isolate only one from an X-ray crystallographic study. The geometry around the phosphorus atom was pyramidal, with an average sum of bond angles 320.9 and 320.5° for **ccxli** and **ccxli**, respectively. The ligands were coordinated in a V-shaped arrangement about the metal centre, with a P-M-P bond angle of approximately 98°. The average M-P bond length is 2.567 and 2.654 Å for the tin and lead derivatives, **ccxli** and **ccxli**, respectively.

Table 26. Selected NMR spectroscopic (at 298 K) and solid state structural data for **ccxxxviii–ccxli**^[211]

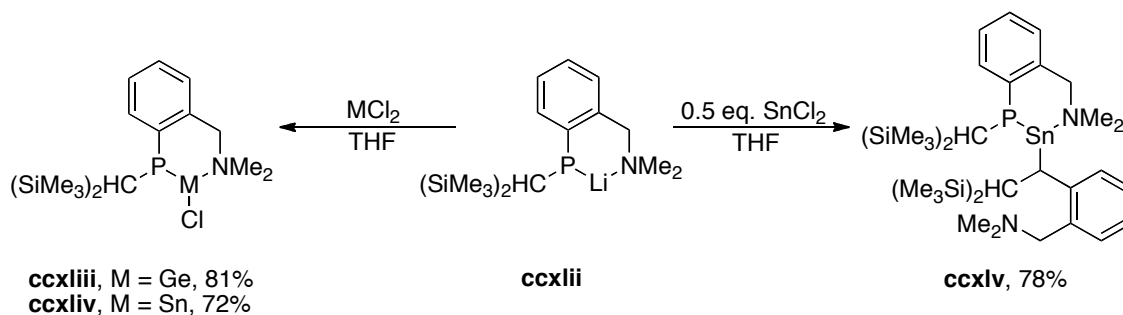
	$^{31}P\{^1H\}$ ^a (δ_P , ppm)	$^1J_{PM}$ ^a (Hz)	avg. M-P (Å)	P-M-P (deg)
ccxxxviii (M = Ge)	-62.1	N/A	- ^b	- ^b
ccxxxix (M = Sn)	-102.5	1682	- ^b	- ^b
ccxli (M = Sn)	-121.3	1628	2.567	98.78(4)
ccxli (M = Pb)	-88.8 and -95.6	1995 and 1979	2.654	97.84(4)

^a the use of NMR solvent was not specified; ^b crystallographic data not reported

Izod *et al.* reported a series of germanium(II) and tin(II) phosphanido complexes which showed dynamic behaviour in solution.^[212-213] Treatment of the lithium phosphanide **ccxlii** with one equivalent of germanium or tin dichloride gave the heteroleptic metal phosphanido complexes **ccxliii** and **ccxliv**. However, the reaction of tin dichloride with two equivalents of the lithium phosphanide **ccxlii** gave the homoleptic tin(II) phosphanide **ccxlv** (Scheme 50). In the X-ray crystallographic studies of these compounds, the pyramidal coordination at phosphorus and the Sn-P bond lengths were

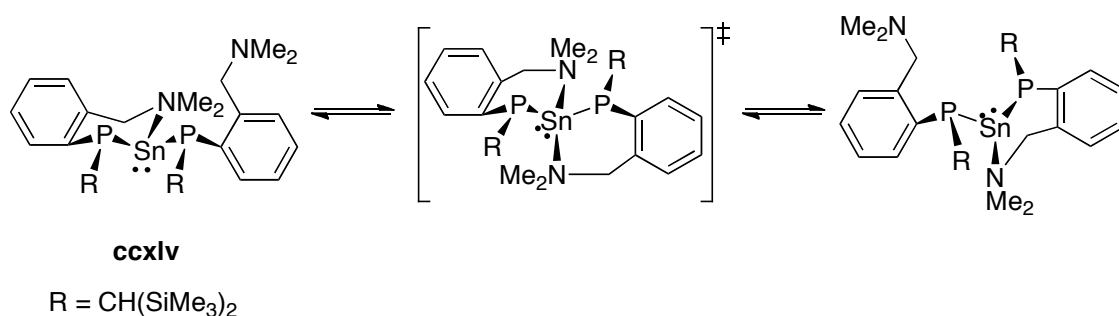
indicative of the lack of metal-phosphorus double bonds. The heteroleptic phosphanido complexes **ccxliii** and **ccxliv** decomposed on heating to give elemental metal and free phosphine [$\{(Me_3Si)_2CH\}(C_6H_4-2-CH_2NMe_2)PH$].

Scheme 50. Synthesis of the heavy group 14 metal phosphanides **ccxliii–ccxliv**^[212-213]



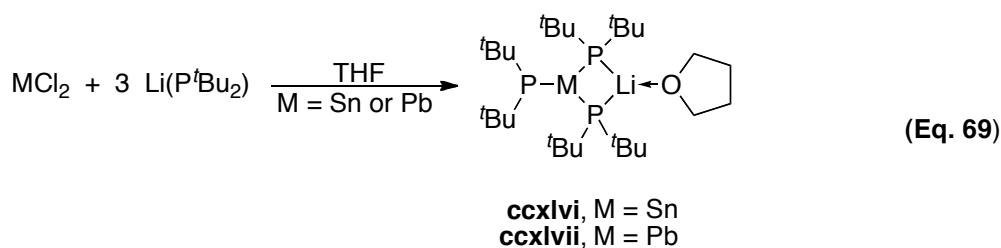
Variable-temperature $^{31}P\{^1H\}$ NMR spectra and a ^{31}P EXSY NMR experiment revealed that these complexes underwent inversion about the metal atom. An inversion was also observed in the tin(II) phosphanide **ccxliv**. The authors suggested that the inversion in **ccxliv** was *via* intramolecular exchange between the chelating and terminal phosphanido ligands (Scheme 51).

Scheme 51. Inversion process in the homoleptic tin(II) phosphanide **ccxliv**^[212-213]



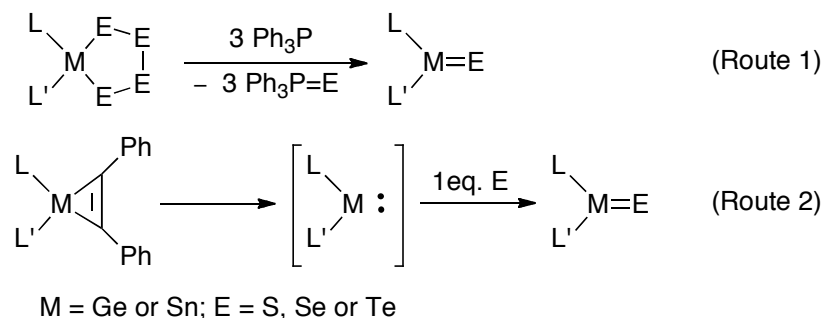
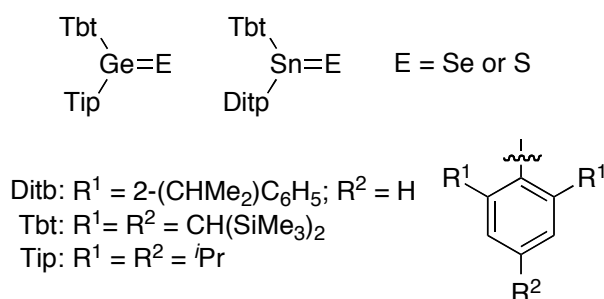
Cowley *et al.* synthesised the novel di-*tert*-butylphosphanidotin(II) and -lead(II) complexes, **ccxlvi** and **ccxlvii**, which were analogous to the heteroatom-substituted carbanions.^[214] Treatment of tin or lead dihalide with three equivalents of lithium di-*tert*-butylphosphanide in the presence of THF gave complexes **ccxlvi** and **ccxlvii**. The X-ray crystallographic studies of **ccxlvi** and **ccxlvii** showed pyramidally coordinated metal centres with the sum of bond angles around the metal centre 308.5° and 304.4°, respectively. A quartet resonance at δ_{Sn} -1310 ppm and a tin-phosphorus coupling

constant $^1J_{\text{SnP}} = 1360$ Hz was observed in the ^{119}Sn NMR spectrum of the tin derivative. The $^{31}\text{P}\{^1\text{H}\}$ NMR spectra of **ccxlv** and **ccxlvii** showed single resonances at δ_{P} 47.2 and 71.5 ppm, respectively, with tin or lead satellites (**ccxlv**, $^1J_{\text{P}^{119}\text{Sn}} = 1360$ Hz and $^1J_{\text{P}^{117}\text{Sn}} = 1300$ Hz; **ccxlvii**, $^1J_{\text{PPb}} = 1770$ Hz), suggesting that the bridging and terminal P^tBu_2 groups were exchanging positions rapidly on the NMR timescale at room temperature.

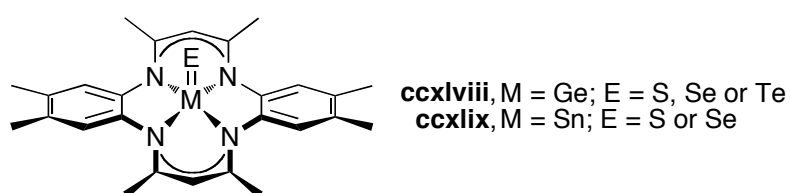


4.1.6 Reactions of heavy group 14 metal complexes with elemental chalcogens

Heavier chalcogens, selenium and tellurium, have found applications in organic synthesis, catalytic reactions, and more recently in metal-organic chemical vapour deposition (MOCVD).^[215-219] Heavier chalcogen-substituted organic compounds, such as ylides and heterocycles, have also been synthesised and compared with the analogous oxygen-substituted compounds.^[220-223] Although synthesis of the heavier chalcogen analogous of aldehydes and ketones remains challenging, Okazaki and co-workers recently reported the synthesis of ‘heavy ketones’ which contained a multiple bond between heavy group 14 and 16 elements (Figure 36).^[196, 224] Compounds of this type were accessible *via* several synthetic routes (Scheme 52), for example dechalcogenation of 1,2,3,4-tetrachalcogenametallophanes with trivalent phosphorus compounds (route 1) or chalcogenation of divalent heavy group 14 metal compounds (route 2).

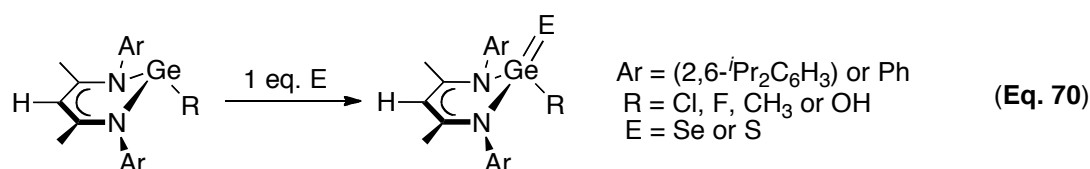
Scheme 52. General synthetic route to ‘heavy ketones’^[224]**Figure 36.** Examples of ‘heavy ketones’^[224]

Parkin *et al.* reported a series of heavy group 14 metal complexes with terminal chalcogenido ligand supported by a tetramethyldibenzotetraaza[14]annulene dianion (Me₄taa)²⁻. Oxidative addition of elemental chalcogen to heavy group 14 metal macrocycles gave complexes **ccxlviii** and **ccxlix** (Figure 37).^[225-226] The metal centre was displaced from the N₄ plane, so the macrocyclic ligand adopted a saddle-shape geometry. The metal-chalcogen interaction can be represented by the resonance structures as shown in Scheme 53. X-ray crystallographic studies indicated that the metal-chalcogen bond in these complexes could be described as an intermediate between the ⁺M–E⁻ and M=E resonance structures. For example, in [(Me₄taa)SnSe], the Sn–Se bond length was 2.394(1) Å, which was between that calculated for the Sn–Se single bond (2.57 Å) and that for the Sn=Se double bond (2.37 Å).^[226]

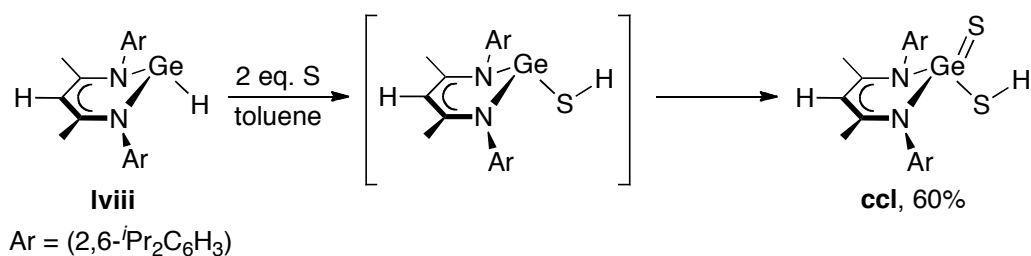
Figure 37. Heavy group 14 macrocyclic complexes with terminal chalcogenido ligand^[225-226]

Scheme 53. Resonance structures of the metal-chalcogen bond^[225-226]

Roesky *et al.* reported a series of β -diketiminatogermanium(IV) complexes containing terminal sulfido or selenido ligands by treatment of β -diketiminatogermanium(II) complexes with one equivalent of elemental chalcogen (equation 70).^[227-231] Likewise, Barrau *et al.* synthesised two similar complexes, $[(\text{BDI}_{\text{Ph}})\text{Ge}(\text{E})\text{Cl}]$ (E = Se or S), which were supported by a different β -diketiminato ligand.^[232] These complexes were accessible by chalcogenation of the parent β -diketiminatogermanium(II) chloride.



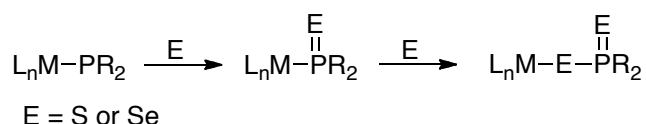
Roesky *et al.* demonstrated that the insertion may be followed by oxidative addition of elemental sulfur in the case of the β -diketiminatogermanium(II) hydride **lviii**.^[74] Treatment of **lviii** with two equivalents of elemental sulfur gave $[(\text{BDI}_{\text{DIPP}})\text{Ge}(\text{S})\text{SH}]$ (**cc1**) (Scheme 54). The solid state structure of **cc1** showed that the ligands were coordinated around the germanium(IV) centre in a distorted tetrahedral geometry. Two different Ge–S bond lengths (2.0641(4) Å and 2.2421(4) Å) were observed, which suggested the presence of Ge=S and Ge–S bonds, respectively. The authors suggested that the elemental sulfur inserted initially into the Ge–H bond, followed by oxidative addition of elemental sulfur to the germanium(II) centre to give $[(\text{BDI}_{\text{DIPP}})\text{Ge}(\text{S})\text{SH}]$ (**cc1**) in a stepwise process.

Scheme 54. Proposed stepwise process in the synthesis of $[(\text{BDI}_{\text{DIPP}})\text{Ge}(\text{S})\text{SH}]$ (**cc1**)^[74]

4.1.7 Reactions of metal phosphanido complexes and related compounds with elemental chalcogens

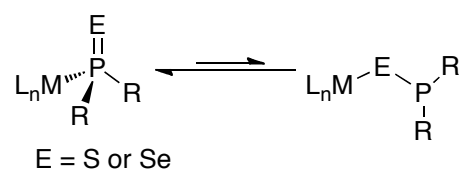
Reactions between phosphorus and elemental chalcogens (E) have been observed in a variety of transition metal complexes (Scheme 55).^[233-234] Initially, the phosphanido fragment is oxidised by a chalcogen to form a pentavalent phosphorus chalcogenide $[L_nMP(E)R_2]$. In the presence of excess elemental chalcogen, chalcogen is inserted into the metal-phosphorus bond to form the metal phosphinodichalcogenoate $[L_nMEP(E)R_2]$.

Scheme 55. Reactions between metal phosphanido complexes $[L_nMPR_2]$ and an excess of elemental chalcogen (E)^[233-234]



It was suggested that the pentavalent phosphorus chalcogenides $[L_nMP(E)R_2]$ is in equilibrium with the metal phosphinochalcogenoite $[L_nMEPR_2]$ as illustrated in Scheme 56.^[233] However, there has been no systematic study to substantiate this suggestion.

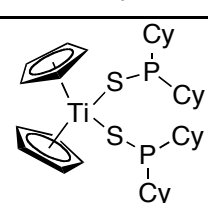
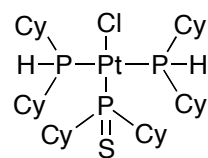
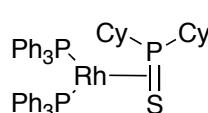
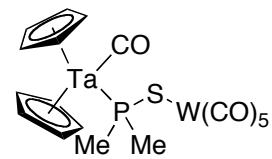
Scheme 56. Proposed Equilibrium structures in the phosphorus chalcogenido complexes $[L_nMP(E)R_2]$ ^[233]



Several coordination modes have been reported for the organophosphorus chalcogenido derivatives (Table 27).^[233, 235] Mode (a) involves a direct chalcogen coordination at the metal centre, as for example in Stephan's titanium(IV) complex $[Cp_2Ti(SPCy_2)_2]$ (**ccli**, Cp = cyclopentadienyl).^[236] In mode (b), a chalcogen-phosphorus double bond is formed and the metal centre is directly coordinated to the phosphorus atom, as illustrated in Mastroilli's platinum complex **cclii**.^[234] The P–E bond can also be coordinated to the metal centre in η^2 -fashion (mode (c)). This coordination mode can be illustrated in complex **ccliii**, which features a side-on interaction between rhodium

metal centre and the $R_2P=S$ group.^[237] The phosphorus-chalcogen fragment can also act as a bridge between the two metal centres as shown in mode (d) and illustrated in Moise's tantalum complex **ccliv**.^[238]

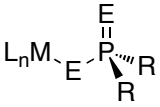
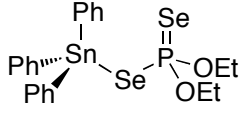
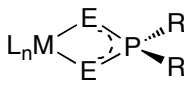
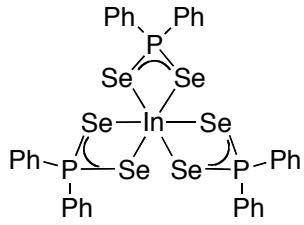
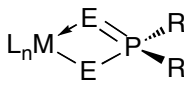
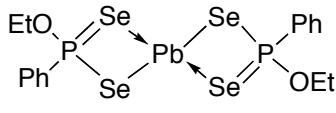
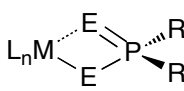
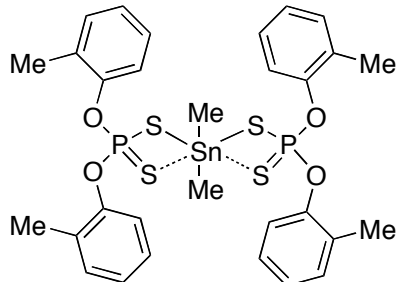
Table 27. Coordination modes for phosphorus chalcogenides $-(E)PR_2$

Coordination Mode	Examples	Ref.
$L_nM-E \cdots \begin{array}{c} \diagup \\ P \\ \diagdown \\ R \end{array}$ monodentate coordination (via chalcogen) (a)	 ccli	[236]
$L_nM \begin{array}{c} \diagup \\ E \\ \diagdown \\ P \\ \diagdown \\ R \end{array}$ monodentate coordination (via phosphorus) (b)	 ccli	[234]
$ML_n \uparrow \\ E=P \begin{array}{c} \diagup \\ R \\ \diagdown \\ R \end{array}$ η^2 -coordination (c)	 ccliii	[237]
$L_nM-E \cdots \begin{array}{c} M'L_n' \\ \diagup \\ P \\ \diagdown \\ R \end{array}$ bridging coordination (d)	 ccliv	[238]

Similarly, four different coordination modes are known for phosphinodichalcogenoato complexes $[L_nMEP(E)R_2]$ (Table 28).^[239-244] In the phosphinodichalcogenoate complex **cclv**, the ligand is monodentate and the phosphorus-chalcogen double bond does not participate in coordination with the metal centre (mode (e)). The delocalised E-M-E fragment in mode (f) acts as an isobidentate ligand. The chalcogen can participate in

non-covalent interactions with the metal centre, such as dative bonding in mode (g) or secondary interaction in mode (h). This latter interaction is described as a “semi-bonding interaction”, that is the M–E distance is between the sum of the covalent radii and the van der Waals radii of the two atoms.

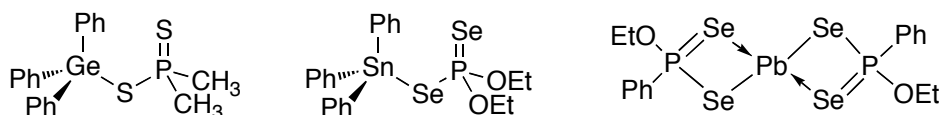
Table 28. Coordination modes for phosphinodichalcogenoate ($-E(E)PR_2^-$) and related anions

Coordination Mode	Examples	Ref.
 <p>Monodentate coordination (e)</p>	 <p>cclv</p>	[245]
 <p>Isobidentate coordination (f)</p>	 <p>cclvi</p>	[246]
 <p>Anisobidentate coordination (dative bonding) (g)</p>	 <p>cclvii</p>	[247]
 <p>Anisobidentate coordination (secondary bonding) (h)</p>	 <p>cclviii</p>	[248]

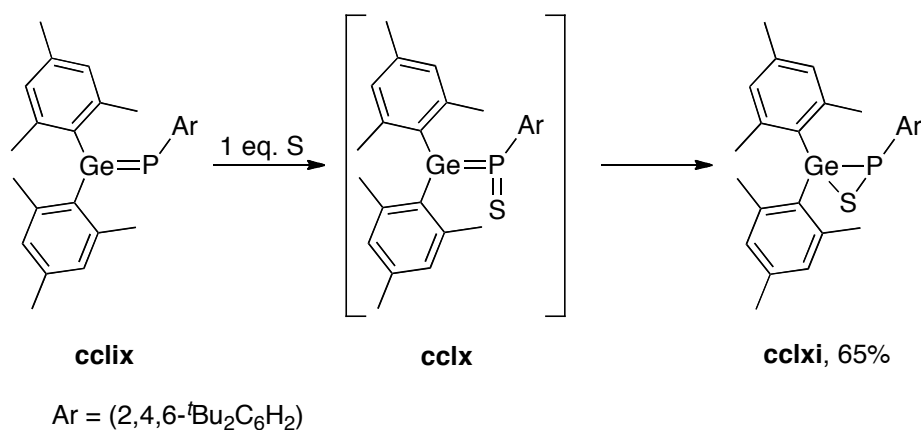
Although various heavy group 14 metal complexes containing phosphinodichalcogenoate ligands are known, the syntheses of these complexes often involve treatment of heavy group 14 metal precursors with lithium or ammonium salts of phosphinodichalcogenoates (Figure 38).^[245, 247, 249] The germathiaphosphirane **cclxi**

was obtained by treatment of the germaphosphene **cclix** with one equivalent of elemental sulfur (Scheme 57).^[250] Escudié *et al.* suggested that the formation of **cclxi** was possibly *via* the germaphosphene sulfide intermediate **cclx**. However, attempts to isolate and characterise this intermediate were not successful.

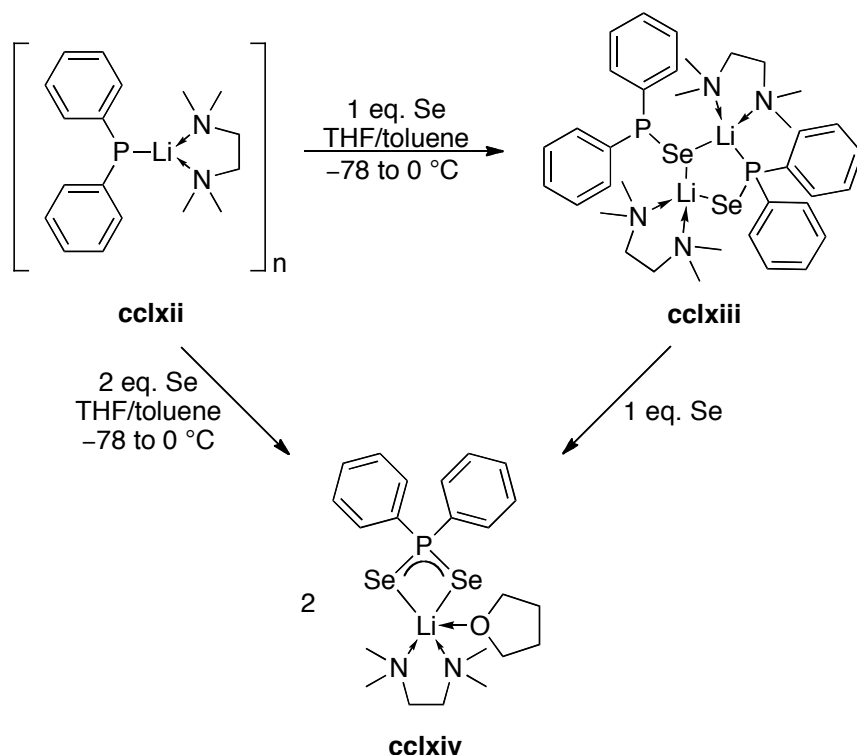
Figure 38. Examples of heavy group 14 metal complexes containing phosphinodichalcogenoato and related ligands^[245, 247, 249]



Scheme 57. Reaction between germaphosphene **cclix** and elemental sulfur^[250]



Several reactions between other main group or transition metal phosphanido complexes and elemental chalcogens have been described. Davies *et al.* reported a series of anionic selenophosphorus ligands by insertion of elemental selenium into Li–P bonds.^[251] Treatment of the lithium diphenylphosphanide **cclxii** in the presence of tetramethylethylenediamine (TMEDA) with elemental selenium gave the insertion product [Ph₂PSeLi·TMEDA]₂ (**cclxiii**) (Scheme 58). Further oxidation with another equivalent of elemental selenium afforded the lithium diselenophosphinato complex **cclxiv**. The complex **cclxiv** was also accessible by treatment of the lithium diphenylphosphanide **cclxii** with two equivalents of elemental selenium (Scheme 58).

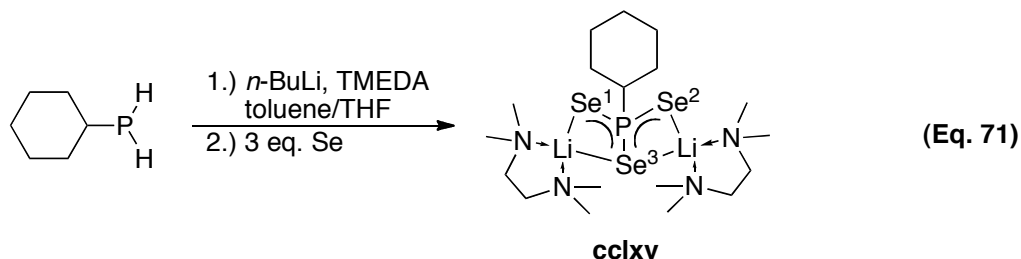
Scheme 58. Synthesis of compounds **cclxiii** and **cclxiv**^[251]

A solid state structural analysis showed that the dimeric lithium selenophosphinite **cclxiii** contained a five-membered P–Se–Li–Se–Li ring. The selenophosphinite ligands were coordinated in two different binding modes: (a) end-on bridging, which the selenium atom was bound to two lithium atoms with P–Se = 2.233(1) Å; and (b) side-on bridging in which the selenium atom was bound to lithium, and phosphorus to the other lithium atom with P–Se = 2.200(8) Å. Both P–Se bond lengths were consistent with phosphorus-selenium single bonds. A single phosphorus resonance (δ_{P} 5.1 ppm) with $^1J_{\text{PSe}} = 316$ Hz was found at room temperature in the $^{31}\text{P}\{^1\text{H}\}$ NMR spectrum. However, at -70 °C, two phosphorus resonances (δ_{P} 3.8 and 4.8 ppm) reflected the different coordination modes of the selenophosphinato ligands. These results suggested that interconversion between the coordination modes is rapid on the NMR timescale at room temperature.

The solid state structure of the lithium diselenophosphinato complex **cclxiv** showed the P–Se bond distances were 2.141(1) and 2.147(1) Å, i.e. between those of phosphorus-selenium single and double bonds, indicating that the electron were delocalised in the

PSe₂ unit.^[251] A single resonance at δ_P 20.7 ppm with phosphorus-selenium coupling ($^1J_{PSe} = 585$ Hz) was found in the $^{31}P\{^1H\}$ NMR spectrum.

Treatment of cyclohexylphosphine with two equivalents of *n*-BuLi in the presence of TMEDA, followed by the addition of three equivalents of elemental selenium gave the dilithium triselenophosphonate **cclxv** (equation 71).

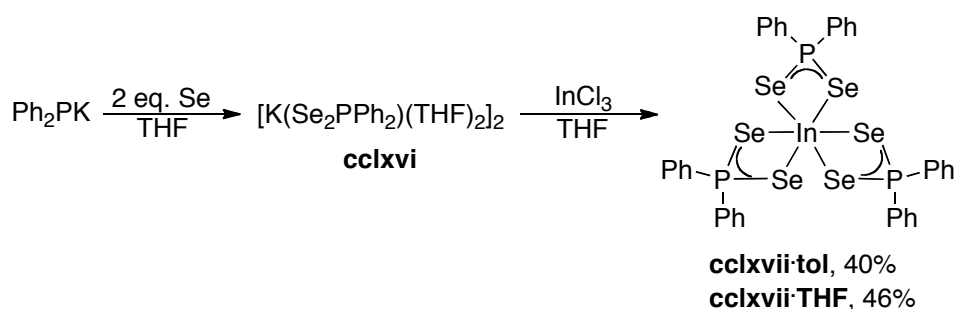


The solid state structure of **cclxv** showed the ligands were coordinated with a distorted tetrahedral geometry around the phosphorus atom. Two different P–Se bond lengths were obtained, with the P–Se¹ and P–Se² bonds (avg. 2.17 Å) shorter than the P–Se³ bond (2.206(1) Å). As in the lithium diselenophosphinate **cclxiv**, the P–Se bond lengths in **cclxv** were indicative of electron delocalisation in the PSe₃ unit. The $^{31}P\{^1H\}$ NMR spectrum showed a single resonance at δ_P 7.27 ppm with selenium satellites ($^1J_{PSe} = 477$ Hz).

The indium complex **cclxvii**, supported by seleno-phosphorus ligands has also been described.^[246] Treatment of potassium diphenylphosphanide with two equivalents of elemental selenium gave the potassium diselenophosphinate **cclxvi**. Further treatment with indium trichloride gave the tris(diselenophosphinato)indium **cclxvii** (Scheme 59). Single crystals of **cclxvii** were obtained from a THF/toluene solution to give **cclxvii·THF** or from toluene, in the absence of THF, to give **cclxvii·tol**. Both solid state structures showed that the metal centre had a distorted octahedral geometry, with the diselenophosphinato ligands coordinated in a nearly isobidentate manner, forming four-membered Se–P–Se–In chelate rings. The average P–Se bond lengths (P–Se = 2.174 Å in **cclxvii·THF** and P–Se = 2.175 Å in **cclxvii·tol**) were between those expected for P–Se single (2.26 Å) and double (2.06 Å) bonds, suggesting that the electrons in the Se–P–Se unit were delocalised.^[246] The crystal packing revealed that the molecule formed weak dimers with intermolecular Se···Se interactions. In **cclxvii·tol**, the Se···Se

contact distances ranged from 3.5340(14) to 3.7958(14) Å. However in **cclxvii**·THF, only one Se···Se contact distance (3.8145(14) Å) fell within the sum of the van der Waals radii (4.0 Å).^[246] The $^{31}\text{P}\{^1\text{H}\}$ NMR spectra of these tris(diselenophosphinato)indium complexes **cclxvii**·tol and **cclxvii**·THF showed a single resonance at δ_{P} 23.6 ppm with phosphorus-selenium coupling ($^1J_{\text{PSe}} \sim 648$ Hz).

Scheme 59. Synthesis of the tris(diselenophosphinato)indium complex^[246]



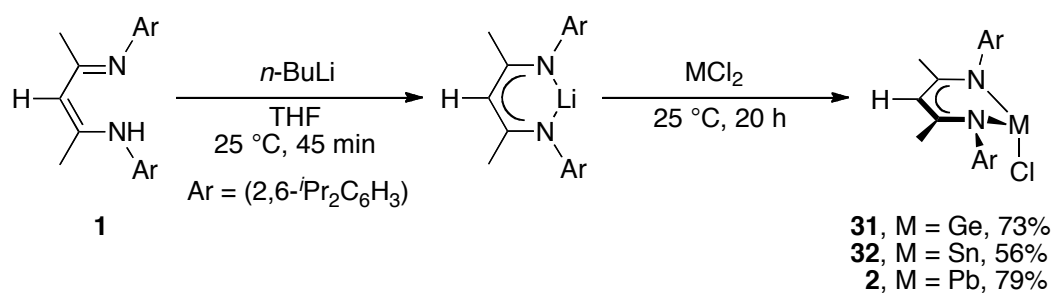
Mastrorilli *et al.* reported a platinum phosphanido complex which underwent sulfuration in a stepwise manner (Scheme 60).^[234] Treatment of the platinum phosphanide **cclxviii** with one equivalent of elemental sulfur gave the platinum thiophosphinito complex **cclii**. Further treatment with one equivalent of elemental sulfur led to the dithiophosphinatoplatinum complex **cclxix**. The $^{31}\text{P}\{^1\text{H}\}$ NMR spectrum of **cclxix** showed two resonances at δ_{P} 2.0 ppm ($^1J_{\text{PPt}} = 3048$ Hz) and 136.6 ppm ($^2J_{\text{PPt}} = 151$ Hz), assigned respectively to the monodentate PHCy_2 and the bidentate $\text{SP}(\text{S})\text{Cy}_2$ ligands. In the presence of 1,8-diazabicycloundec-7-ene (DBU), which acted as a proton scavenger, compound **cclxix** reacted further with one equivalent of elemental sulfur to give compound **cclxx**. The $^{31}\text{P}\{^1\text{H}\}$ NMR spectrum showed three signals at δ_{P} 38.9 ppm ($^1J_{\text{PPt}} = 3977$ Hz), 48.4 ppm ($^1J_{\text{PPt}} = 2977$ Hz) and 127.2 ppm ($^1J_{\text{PPt}} = 137$ Hz), assigned to the PHCy_2 , $\text{P}(\text{S})\text{Cy}_2$ and S_2PCy_2 ligands, respectively. Treatment of compound **cclxx** with one equivalent of elemental sulfur gave the bis(dithiophosphinato)platinumphosphine complex **cclxxi**. The solid state structure of this compound showed one of the S_2PCy_2 groups acted as a monodentate ligand, and the other was bound to the metal centre *via* both sulfur atoms. The $^{31}\text{P}\{^1\text{H}\}$ NMR spectrum of **cclxxi** showed three resonances at δ_{P} 2.5 ppm ($^1J_{\text{PPt}} = 355$ Hz), 81.8 ppm and 124.8 ppm ($^2J_{\text{PPt}} = 195$ Hz), assigned to the PHCy_2 , monodentate S_2PCy_2 and bidentate S_2PCy_2 ligands, respectively.

4.2 Results and discussion

4.2.1 Synthesis of β -diketiminato heavy group 14 metal diphenylphosphanides **33–35**

The β -diketiminato heavy group 14 metal chlorides were synthesised according to the literature procedures.^[62, 65] Treatment of the β -diketimine **1** with *n*-BuLi, followed by addition of the generated lithium β -diketiminato to a THF slurry of metal dichloride gave the β -diketiminato heavy group 14 metal chlorides [(BDI_{DIPP})MCl] (**31**, M = Ge; **32**, M = Sn; and **2**, M = Pb) in 56–79% yields (Scheme 61).

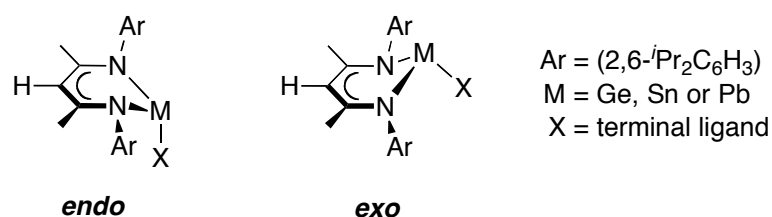
Scheme 61. Synthesis of the β -diketiminato heavy group 14 metal chlorides^[62, 65]



NMR spectroscopic analyses of these β -diketiminato heavy group 14 metal chlorides show several peaks attributed to the isopropyl groups.^[62, 65] For example, the ¹H NMR spectrum of the tin(II) chloride **32** shows two septets (δ_{H} 3.96 and 3.13 ppm) assigned to the tertiary isopropyl protons (*CHMe*₂) and four doublets centred at δ_{H} 1.45, 1.23, 1.20 and 1.07 ppm, assigned to the isopropyl methyl protons (*CHMe*₂) in the *N*-aryl groups in the β -diketiminato ligand. The results suggest: (a) that the methyl groups within each isopropyl group are inequivalent as expected from the chirality of the fragment to which the isopropyl group is attached; and (b) that the isopropyl groups at the 2- and 6-positions of each aryl group (Ar) are inequivalent due to restricted rotation about the *N*-aryl bond. Since all of the compounds described in this chapter show an approximate plane of symmetry bisecting the β -diketiminato ligand (*vide infra*), it is likely that the environments of the *N*-aryl groups on either side of this plane are the same in solution. There are thus two *CHMe*₂ resonances and four *CHMe*₂ resonances. The isopropyl groups on the same side as the terminal ligand are described as ‘adjacent’ and those on the other side as ‘opposite’ (Figure 41, Page 132).

A close inspection of the $^{13}\text{C}\{^1\text{H}\}$ NMR spectrum of the tin(II) chloride **32** revealed previously unreported couplings between the tin atom and the tertiary isopropyl carbons (CHMe_2) or the isopropyl methyl carbons (CHMe_2) as unresolved $^{117/119}\text{Sn}$ satellites. In this thesis, the number of bonds between the coupling nuclei is indicated by the superscript in the symbol J . For example, in the tin(II) chloride **32**, the coupling between the tertiary isopropyl carbon (CHMe_2) and the tin atoms, which are separated by four bonds, is indicated as $^4J_{\text{CSn}}$. Considering that there is a 4- or 5-bond separation between the carbon and tin atoms, we expect through-bond coupling to be weak. The carbon-tin coupling constant (J_{CSn}) varies between each resonance (*vide infra*), hence we assign these couplings as through-space. Previous examples of $\{^{19}\text{F}-^{19}\text{F}\}$, $\{^1\text{H}-^{19}\text{F}\}$, $\{^1\text{H}-^1\text{H}\}$, $\{^{15}\text{N}-^{19}\text{F}\}$, $\{^{31}\text{P}-^{31}\text{P}\}$, and recently $\{^{19}\text{F}-^{117/119}\text{Sn}\}$ and $\{^{19}\text{F}-^{207}\text{Pb}\}$ through-space couplings are known.^[252-257] The β -diketiminato tin(II) chloride **32** is the first example of a compound showing $\{^{13}\text{C}-^{117/119}\text{Sn}\}$ through-space coupling ($^4J_{\text{CSn}}$ and $^5J_{\text{CSn}}$, Figure 40, Page 132). It demonstrates that this phenomenon may be observed even with insensitive carbon-13 nuclei.

Before discussion of through-space coupling in the tin(II) chloride **32**, a brief examination on the conformations of the β -diketiminato heavy group 14 metal complexes in the solid state is necessary. Two conformations are observed (Figure 39).^[170] In the *endo* conformation, the metal (M) and the terminal ligand (X) are on the same side of the mean NCCCN plane of the β -diketiminato ligand. The terminal ligand lies between the two *N*-aryl groups, with the M–X bond at approximately 90° to the mean NCCCN plane. In the *exo* conformation, the metal (M) lies above the mean NCCCN plane (i.e. on the ‘opposite’ side in Figure 41, Page 132), and the terminal ligand points away from the (BDI_{DIPP})M core. The conformation adopted seems to depend on the interaction between the terminal ligand and the *N*-aryl groups in the β -diketiminato ligand. The *endo* conformation is preferred when the ligand, for example halide or methyl, can be accommodated between the *N*-aryl groups or when it can adopt a planar geometry, such as $\text{N}(\text{SiMe}_3)_2$.^[62, 67, 170] When a larger ligand, such as *tert*-butoxide, is present, the *exo* conformation may be adopted to avoid congestion from the *N*-aryl groups in the β -diketiminato ligand. Although *endo* and *exo* conformations are observed in the solid state structures, solution phase spectroscopic measurements have not, to date, differentiated between them.

Figure 39. *Endo* and *exo* conformations in β -diketiminato heavy group 14 metal complexes^[170]

Through-space coupling requires the nuclei to be in close proximity.^[255-256] The $^{13}\text{C}\{^1\text{H}\}$ NMR spectrum of the tin(II) chloride **32** shows resonances at δ_{C} 29.6 ppm with coupling $^4J_{\text{CSn}} = 20$ Hz, assigned to tertiary isopropyl carbon (CHMe_2), and at δ_{C} 25.2 ppm with coupling $^5J_{\text{CSn}} = 13$ Hz, assigned to methyl carbons in the isopropyl groups (CHMe_2) (Figure 40). Within the resolution of the NMR instrument, only resonances from one isopropyl group (**ab**₂, Figure 40) couple to the tin atom as observed in the $^{13}\text{C}\{^1\text{H}\}$ NMR spectrum. In the solid state, the tin(II) chloride **32** adopts an *endo* conformation (Figure 41).^[65] The detection of through-space coupling between the tin and some, but not all, of the isopropyl carbon nuclei suggests that the average structure in solution is similar to that in the solid, with restricted rotation about Sn–N or N–C bonds.

Figure 40. $^{13}\text{C}\{^1\text{H}\}$ NMR spectrum of $[(\text{BDI}_{\text{DIPP}})\text{SnCl}]$ (**32**) showing the J_{CSn} ; **a** and **a'** are from CHMe_2 ; **b** and **b'** are from CHMe_2 ; **c** is from NCMe . The **ab**₂ and **a'b'**₂ indicate resonances from different pairs of isopropyl groups

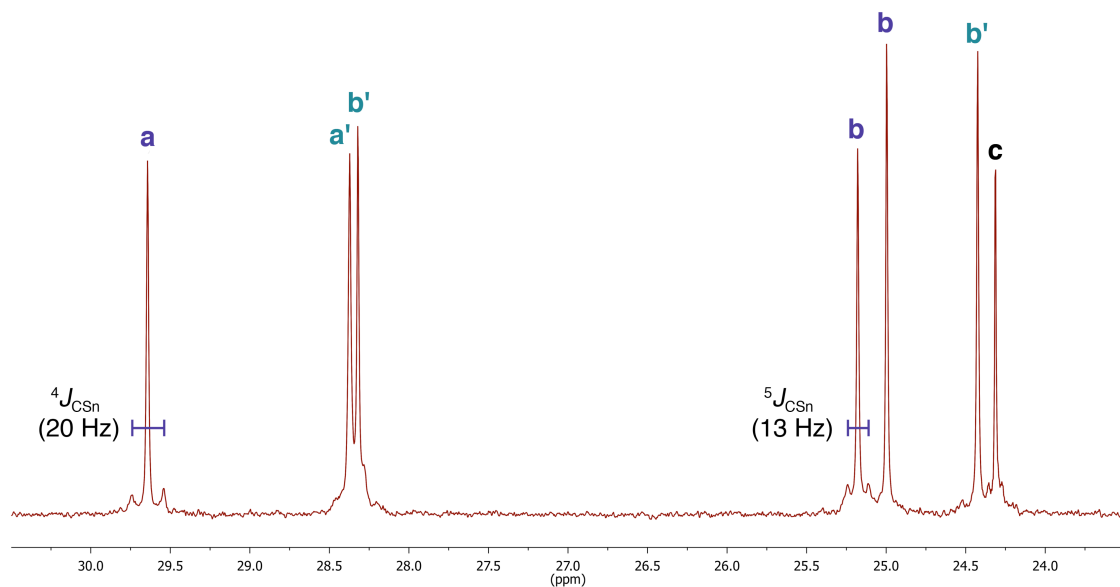
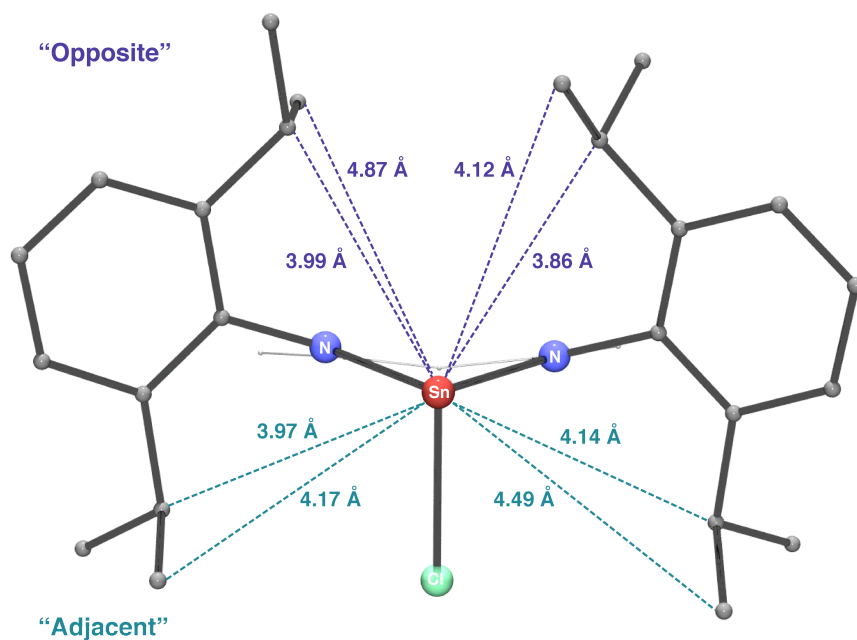
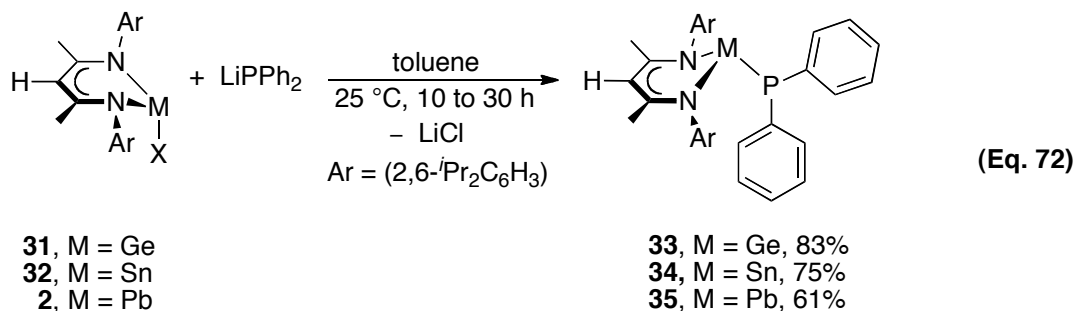


Figure 41. Schematic view of $[(\text{BDI}_{\text{DIPP}})\text{SnCl}]$ (**32**) showing the relative distance between the tin atom and the isopropyl substituents. H atoms are omitted. The distances are obtained from the crystal structure data^[65]



Treatment of the β -diketiminato heavy group 14 metal chlorides **31**, **32** and **2** with lithium diphenylphosphanide at room temperature gave the β -diketiminato heavy group 14 metal diphenylphosphanides $[(\text{BDI}_{\text{DIPP}})\text{MPPh}_2]$ (**33**, $\text{M} = \text{Ge}$; **34**, $\text{M} = \text{Sn}$; and **35**, M

= Pb) (equation 72). [(BDI_{DIPP})GePPh₂] (**33**) was obtained after 30 hours as an indigo-coloured solid in 83% yield. Roesky *et al.* reported the germanium derivative **33** about the time this thesis was submitted.^[258] The tin analogue [(BDI_{DIPP})SnPPh₂] (**34**) was obtained after 18 hours as a deep purple solid in 75% yield. The lead derivative [(BDI_{DIPP})PbPPh₂] (**35**) required the least reaction time (10 hours) and was obtained as deep red solids in 61% yield. These compounds, particularly the lead derivative **35**, are extremely reactive towards air, moisture and light. Metallic precipitates were formed after 24 hours when the lead(II) derivative **35** was allowed to stand in toluene at room temperature. The diphenylphosphanido complexes are soluble in aprotic organic solvents such as benzene or toluene. The elemental analyses of these compounds are in good agreement with the calculated values.



4.2.2 X-ray crystal structures of the β -diketiminato heavy group 14 metal diphenylphosphanides **33–35**

Single crystals of the solvent-free germanium derivative [(BDI_{DIPP})GePPh₂] (**33**) were obtained by recrystallisation from a concentrated *n*-hexane solution at -30 °C. ORTEP drawings of compound **33** are shown in Figures 42 and 43. Selected bond lengths and angles are listed in Table 29, and selected crystallographic data in Table 30. The geometry around the germanium atom is pyramidal with the sum of the bond angles around the metal centre 286.7° . The phosphorus atom is also pyramidally coordinated with the sum of bond angles 300.0° . If the two phenyl groups are discounted, there is an approximate plane of symmetry passing through the atoms C(2), Ge, and P, bisecting the β -diketiminato ring (Table 29). The germanium(II) diphenylphosphanide **33** has a long Ge–P bond ($2.4760(6)$ Å) compared with other Ge^(II)–PR₂ bond lengths, for example in DuMont's [Ge(P^{*i*}Pr₂)(μ -P^{*i*}Pr₂)]₂ (terminal Ge–P = $2.398(1)$ Å), Izod's [[{Me₃Si}₂CH}(Ph)P]₂Ge]₂·Et₂O (Ge–P = $2.4151(13)$ Å) and [[{Me₃Si}₂CH}(C₆H₄-2-

$\text{CH}_2\text{NMe}_2\text{P}]_2\text{Ge}]$ ($\text{Ge-P} = 2.4114(4) \text{ \AA}$).^[213, 259-260] Our unit cell parameters for **33** are in good agreement with those reported in Roesky's recent publication.^[258]

Figure 42. ORTEP diagram of $[(\text{BDI}_{\text{DIPP}})\text{GePPh}_2]$ (**33**). H atoms are omitted and C atoms in the *N*-aryl groups in the β -diketiminato ring are minimised for clarity. The ellipsoid probability is shown at 30%

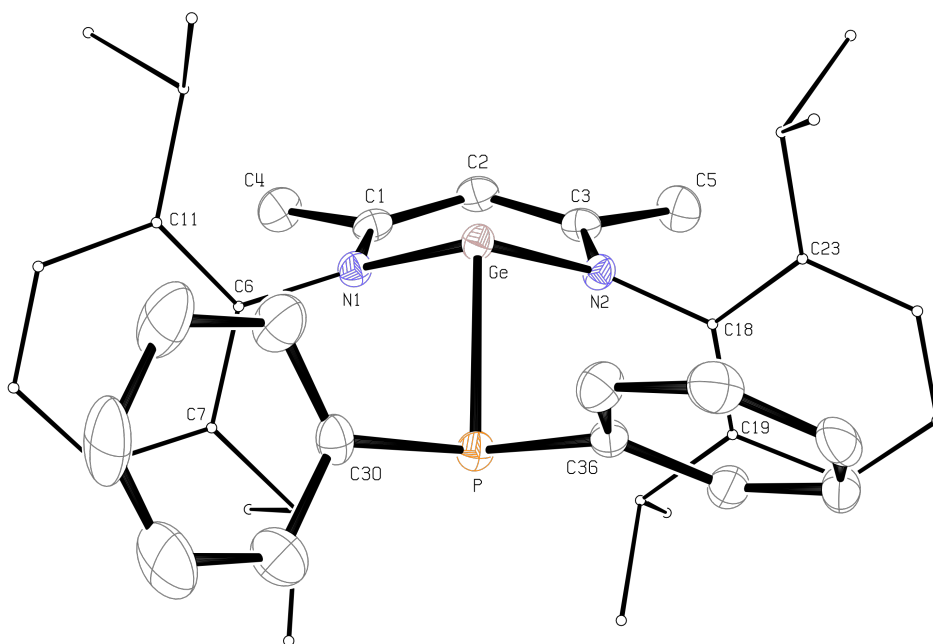
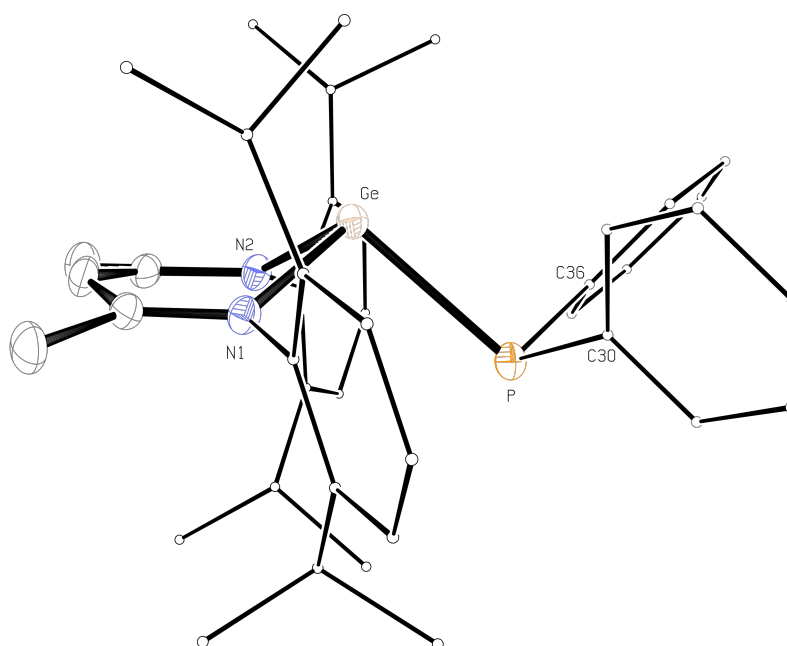


Figure 43. ORTEP diagram showing the side-on view of $[(\text{BDI}_{\text{DIPP}})\text{GePPh}_2]$ (**33**). H atoms are omitted and C atoms in the *N*-aryl groups in the β -diketiminato ring and phenyl groups are minimised for clarity. The ellipsoid probability is shown at 30%



Solvent-free single crystals of the tin(II) diphenylphosphanide $[(\text{BDI}_{\text{DIPP}})\text{SnPPh}_2]$ (**34**) were obtained by recrystallisation from a concentrated *n*-hexane solution at -30 °C. ORTEP drawings of compound **34** are shown in Figures 44 and 45. Selected bond lengths and angles are listed in Table 29, and selected crystallographic data in Table 30. The molecules of the tin(II) diphenylphosphanide **34** and the germanium derivative **33** have almost identical structure. Compound **34** adopts an *exo* conformation, with the tin atom 1.093 Å above the mean NCCCN plane of the β -diketiminato ligand. A pyramidally coordinated tin atom is found with the sum of bond angles around the metal centre 281.7° . The geometry around the phosphorus atom is also pyramidal with the sum of bond angles 295.3° . Like the germanium derivative **33**, if the phenyl groups are discounted, there is an approximate plane of symmetry passing through the atoms C(2), Sn and P, bisecting the β -diketiminato ring. The Sn–P bond length ($2.6307(9)$ Å) is similar to those in Cowley's $[\text{Li}(\text{THF})\{\text{Sn}(\text{P}^t\text{Bu}_2)_3\}]$ (Sn–P = $2.684(4)$ Å), Wang's $[\text{Sn}\{\text{P}(\text{Ph})\text{C}\{\text{C}(\text{H})\text{Ph}\}\text{P}(\text{Me})_2\text{NSiMe}_3\}_2]$ (Sn–P = $2.591(7)$ and $2.598(7)$ Å) and Izod's $[[\{(\text{Me}_3\text{Si})_2\text{CH}\}(\text{Ph})\text{P}\}_3\text{Sn}][\text{Li}(\text{THF})_4]$ (Sn–P = $2.649(2)$ Å).^[214, 260-261]

Figure 44. ORTEP diagram of $[(\text{BDI}_{\text{DIPP}})\text{SnPPh}_2]$ (**34**). H atoms are omitted and C atoms in the *N*-aryl groups in the β -diketiminato ring are minimised for clarity. The ellipsoid probability is shown at 30%

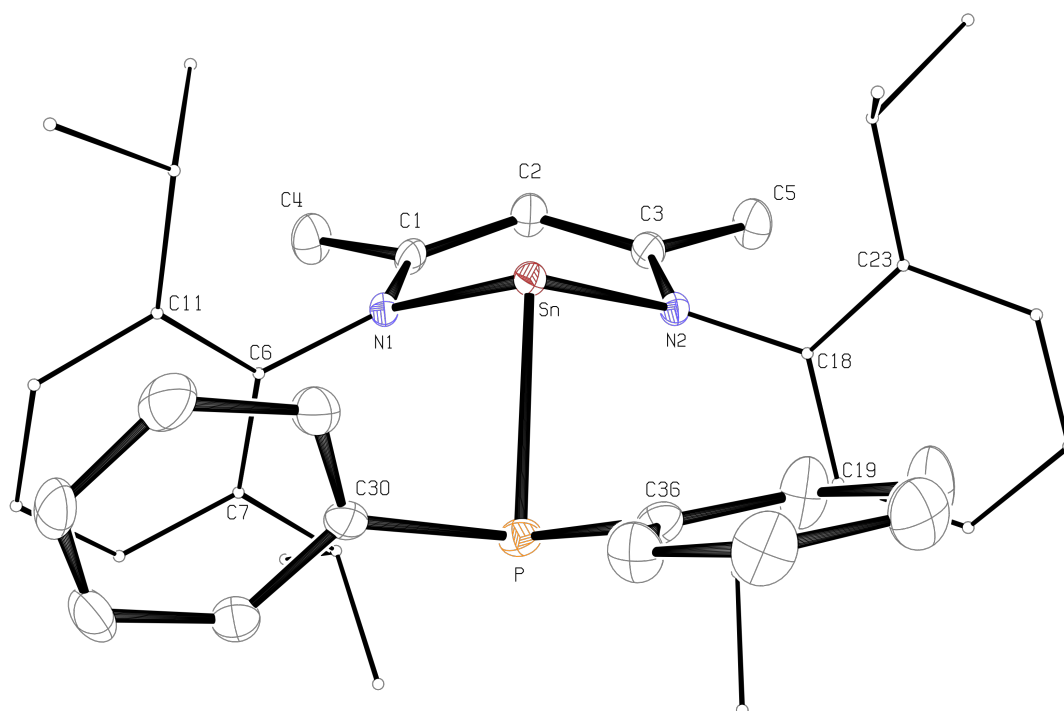
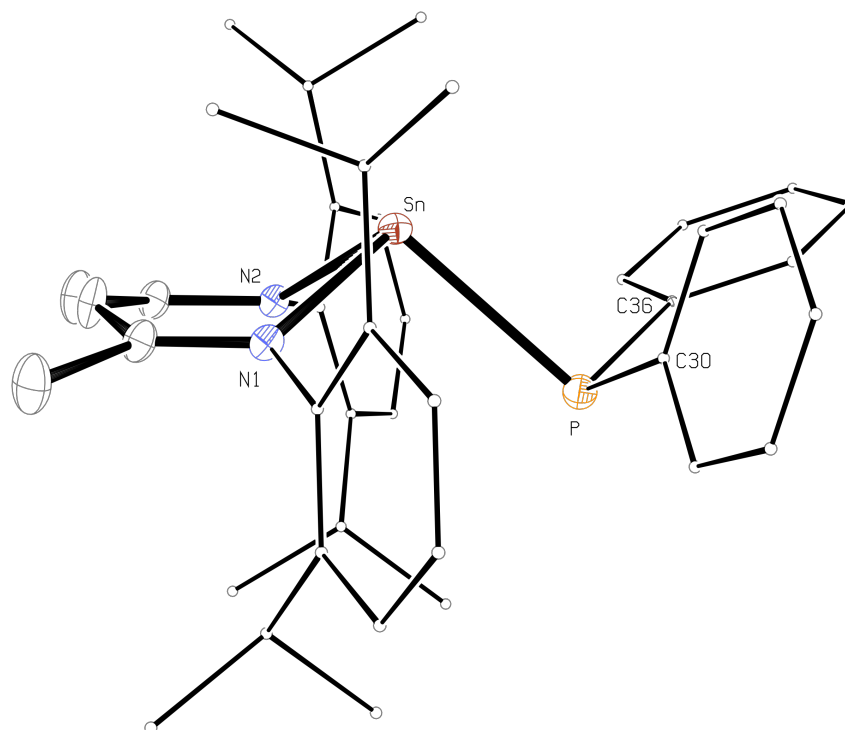


Figure 45. ORTEP diagram showing the side-on view of [(BDI_{DIPP})SnPPh₂] (**34**). H atoms are omitted and C atoms in the *N*-aryl groups in the β-diketiminato ring and the phenyl groups are minimised for clarity. The ellipsoid probability is shown at 30%



Solvent-free single crystals of [(BDI_{DIPP})PbPPh₂] (**35**) were obtained by recrystallisation from a concentrated *n*-hexane solution at -30°C . ORTEP drawings of compound **35** are shown in Figures 46 and 47. Selected bond lengths and angles are listed in Table 29, and selected crystallographic data in Table 30. The lead(II) diphenylphosphanide **35** adopts an *exo* conformation with the lead atom 1.018 \AA above the mean NCCCN plane of the β-diketiminato ligand. The lead atom is pyramidally coordinated with the sum of bond angles around the metal centre 284.4° . The sum of bond angles at the pyramidally coordinated phosphorus is 289.7° . If the two phenyl groups are discounted, there is an approximate plane of symmetry passing through the atoms C(2), P and Pb (Table 29). The Pb–P bond length ($2.720(2) \text{ \AA}$) is similar to the terminal Pb^(II)–PR₂ bond lengths in Cowley's compounds, [Li(THF){Pb(P^tBu₂)₃}] (Pb–P = $2.766(7) \text{ \AA}$) and [Pb(μ-P^tBu₂)(P^tBu₂)₂]₂ (Pb–P = $2.781(4) \text{ \AA}$).^[214, 262]

Table 29. Selected bond lengths (Å) and angles (deg) for [(BDI_{DIPP})MPPh₂] (**33**, M = Ge; **34**, M = Sn; and **35**, M = Pb)

	[(BDI _{DIPP})GePPh ₂] 33 , M = Ge	[(BDI _{DIPP})SnPPh ₂] 34 , M = Sn	[(BDI _{DIPP})PbPPh ₂] 35 , M = Pb
<i>Bond lengths (Å)</i>			
M–P	2.4760(6)	2.6307(9)	2.720(2)
M–N(1)	2.0281(19)	2.226(3)	2.324(6)
M–N(2)	2.0071(19)	2.218(3)	2.347(6)
N(1)–C(1)	1.324(3)	1.325(4)	1.303(10)
N(2)–C(3)	1.343(3)	1.335(4)	1.297(9)
C(1)–C(2)	1.395(4)	1.406(5)	1.413(11)
C(2)–C(3)	1.385(4)	1.400(6)	1.410(10)
C(1)–C(4)	1.506(3)	1.517(5)	1.530(12)
C(3)–C(5)	1.517(3)	1.516(5)	1.526(10)
P–C(30)	1.842(3)	1.841(3)	1.845(8)
P–C(36)	1.847(2)	1.843(4)	1.818(9)
M–NCCCN _{Plane}	0.936	1.093	1.018
<i>Bond angles (deg)</i>			
N(1)–M–N(2)	88.16(8)	84.06(10)	80.2(2)
N(1)–M–P	99.33(6)	97.35(7)	98.21(15)
N(2)–M–P	99.20(6)	100.32(7)	105.98(15)
M–N(1)–C(1)	119.66(16)	118.5(2)	121.2(5)
M–N(2)–C(3)	118.66(16)	117.6(2)	121.6(5)
N(1)–C(1)–C(2)	122.7(2)	124.2(3)	125.9(8)
N(2)–C(3)–C(2)	123.2(2)	124.0(3)	125.2(7)
C(1)–C(2)–C(3)	126.4(2)	128.5(3)	128.7(8)
M–P–C(30)	100.49(9)	96.12(11)	87.3(2)
M–P–C(36)	100.11(7)	97.82(11)	101.1(3)
C(30)–P–C(36)	99.38(11)	101.38(16)	101.3(4)
NCCCN _{plane} –NMN _{plane}	39.4	40.6	34.3
Σ bond angle around M	286.7	281.7	284.4
DOP of M (%)	81	87	84
Σ bond angle around P	300.0	295.3	289.7
DOP of P (%) ^a	67	72	78
<i>Dihedral angles (deg)</i>			
C(11)–C(6)–N(1)–M	78.7(3)	64.5(4)	78.7(8)
C(23)–C(18)–N(2)–M	–69.7(3)	–72.5(4)	–73.7(9)

^a Degree of pyramidalisation (DOP, %) = [(360 – Σ_{bond angle}) / 0.9]^[115] When a DOP is 100%, it is equivalent to a sum of bond angles of 270°, whereas a DOP of 0% indicates a planar geometry at the central atom

Table 30. Selected crystallographic data for [(BDI_{DIPP})MPPh₂] (**33**, M = Ge; **34**, M = Sn; and **35**, M = Pb)

	[(BDI _{DIPP})GePPh ₂] (33)	[(BDI _{DIPP})SnPPh ₂] (34)	[(BDI _{DIPP})PbPPh ₂] (35)
chemical formula	C ₄₁ H ₅₁ GeN ₂ P	C ₄₁ H ₅₁ N ₂ PSn	C ₄₁ H ₅₁ N ₂ PPb
molecular mass	675.40	721.50	810.01
temperature (K)	173(2)	173(2)	173(2)
wavelength (Å)	0.71073	0.71073	0.71073
crystal system	monoclinic	monoclinic	orthorhombic
space group	<i>P</i> 2 ₁ / <i>c</i> (No. 14)	<i>P</i> 2 ₁ (No. 4)	<i>I</i> 2 <i>cb</i> (No. 45)
<i>a</i> (Å)	17.2186(4)	11.2633(2)	15.9697(5)
<i>b</i> (Å)	12.0952(3)	12.5856(3)	18.3168(6)
<i>c</i> (Å)	18.0061(3)	12.9200(3)	25.8355(6)
<i>α</i> (deg)	90	90	90
<i>β</i> (deg)	99.289(1)	90.02	90
<i>γ</i> (deg)	90	90	90
<i>V</i> (Å ³)	3700.82(14)	1831.48(7)	7557.2(4)
<i>Z</i>	4	2	8
ρ_{calcd} (Mg m ⁻³)	1.21	1.31	1.42
θ range (deg)	3.47–27.11	3.54–27.11	3.43–27.09
abs coeff (mm ⁻¹)	0.90	0.77	4.54
measd/indep reflns/ <i>R</i> (int)	57 250/8144/0.073	29 273/8017/0.053	24 237/8198/0.081
reflns with <i>I</i> > 2 σ (<i>I</i>)	6099	7400	5814
data/restraints/param	8144/156/446	8017/1/408	8198/1/408
goodness of fit on <i>F</i> ²	1.027	1.008	0.986
final <i>R</i> indices [<i>I</i> > 2 σ (<i>I</i>)]	<i>R</i> 1 = 0.044, <i>wR</i> 2 = 0.087	<i>R</i> 1 = 0.033, <i>wR</i> 2 = 0.073	<i>R</i> 1 = 0.047, <i>wR</i> 2 = 0.085
<i>R</i> indices (all data)	<i>R</i> 1 = 0.072, <i>wR</i> 2 = 0.097	<i>R</i> 1 = 0.038, <i>wR</i> 2 = 0.076	<i>R</i> 1 = 0.086, <i>wR</i> 2 = 0.096
largest diff peak and hole (e Å ⁻³)	0.49 and -0.38	1.69 and -0.48	0.68 and -1.40

4.2.3 NMR spectra of the β -diketiminato heavy group 14 metal diphenylphosphanides **33–35**

Selected multinuclear NMR spectroscopic data for **33–35** are given in Table 31.

Table 31. Selected multinuclear NMR spectroscopic data for [(BDI_{DIPP})MPPPh₂] (**33**, M = Ge; **34**, M = Sn; and **35**, M = Pb) in C₆D₆ at 30 °C

	[(BDI _{DIPP})GePPPh ₂] (33)	[(BDI _{DIPP})SnPPPh ₂] (34)	[(BDI _{DIPP})PbPPPh ₂] (35)
	δ (ppm), J (Hz) ^a	δ (ppm), J (Hz) ^a	δ (ppm), J (Hz) ^a
¹H			
γ -H	4.75 (s)	4.71 (s)	4.59 (s)
CHMe ₂	4.15 (d-septet) ³ J _{HH} = 6.8; ⁶ J _{HP} = 0.8	4.08 (d-septet) ³ J _{HH} = 6.8; ⁶ J _{HP} = 1.2	4.04 (septet) ³ J _{HH} = 6.8
	3.24 (septet) ³ J _{HH} = 6.8	3.16 (septet) ³ J _{HH} = 6.8	3.06 (septet) ³ J _{HH} = 6.8
¹³C{¹H}			
CHMe ₂	29.7 (d) ⁵ J _{CP} = 9	29.5 (d) ⁵ J _{CP} = 6	29.4 (d) ⁵ J _{CP} = 5
	29.1 (s)	28.8 (s) ⁴ J _{CSn} = 36	28.3 (s) ⁴ J _{CPb} = 37
CHMe ₂	25.9, 25.6, 25.2 (s) 24.8 (d) ⁶ J _{CP} = 9	26.6 (d) ⁵ J _{CSn} = 43 25.6, 25.0 (s) 24.7 (d) ⁶ J _{CP} = 9	26.9 (s) 25.5 (d) ⁶ J _{CP} = 4 25.4, 25.0 (s)
³¹P{¹H}			
	-36.0 (s)	-30.8 (s) ¹ J _{P¹¹⁹Sn} = 978 ¹ J _{P¹¹⁷Sn} = 937	7.3 (s) ¹ J _{PbP} = 1130
Other Nuclei			
	-	δ (¹¹⁹ Sn) = 126 ¹ J _{P¹¹⁹SnP} = 966	δ (²⁰⁷ Pb) = 3011 ¹ J _{PbP} = 1138

^a Superscript indicates number of bonds between nuclei

4.2.3.1 The β -diketiminatogermanium(II) diphenylphosphanide **33**

The ³¹P{¹H} NMR spectrum of [(BDI_{DIPP})GePPPh₂] (**33**) shows a broad resonance at δ_P -36.0 ppm, upfield from Kornev's [Ge(NPh-NPh-PPh₂)₂] (δ_P 63.2 ppm) and Reddy's [Ph₂PC{C(Me)N(2,6-ⁱPr₂C₆H₃)}₂GeCl] (δ_P 15.2 ppm).^[263-264] The ¹H NMR spectrum of the germanium derivative **33** shows a doublet of septets centred at δ_H 4.15 ppm, assigned to one of the tertiary proton resonances in the isopropyl groups (CHMe₂) (Figure 48). The through-bond proton-proton coupling (³J_{HH} = 6.8 Hz) is further split by a through-space proton-phosphorus coupling (⁶J_{HP} = 0.8 Hz). The ¹H-³¹P Heteronuclear Multiple Bond Correlation (HMBC) NMR experiment shows correlations between the phosphorus and one of the CHMe₂ resonances (δ_H 4.15 ppm), as well as between the

phosphorus and two of the methyl proton resonances in the isopropyl groups (CHMe_2 : δ_{H} 1.70 and 1.21 ppm) (Figure 49). These findings are not reported in Roesky's recent publication or in other β -diketiminatometal phosphanides, such as Linti's $[(\text{BDI}_{\text{DIPP}})\text{Ga}(\text{H})\text{PPh}_2]$ or Burford's $[(\text{BDI}_{\text{DIPP}})\text{Ga}(\text{OTf})\text{PPh}_2]$.^[102, 176, 258]

Figure 48. ^1H NMR spectrum (400 MHz, C_6D_6) of $[(\text{BDI}_{\text{DIPP}})\text{GeCl}]$ (**31**, top) and $[(\text{BDI}_{\text{DIPP}})\text{GePPh}_2]$ (**33**, bottom), where A = γ -H and B & C = CHMe_2 proton resonances

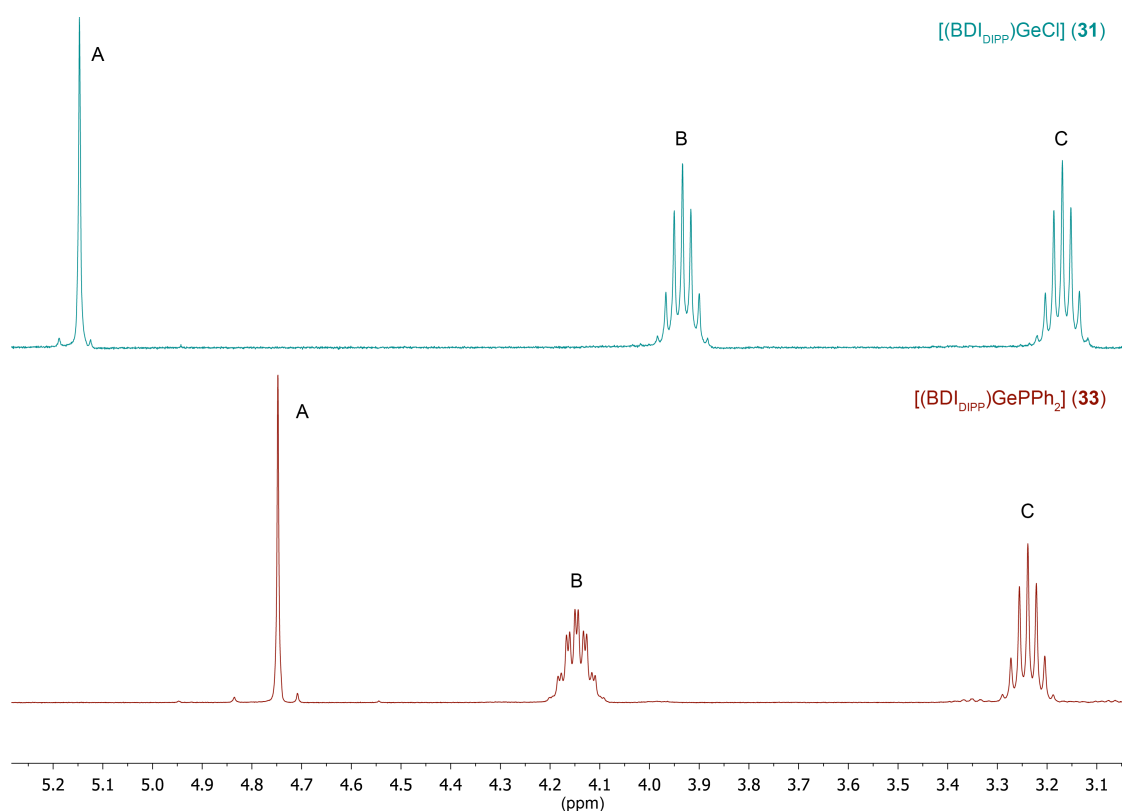
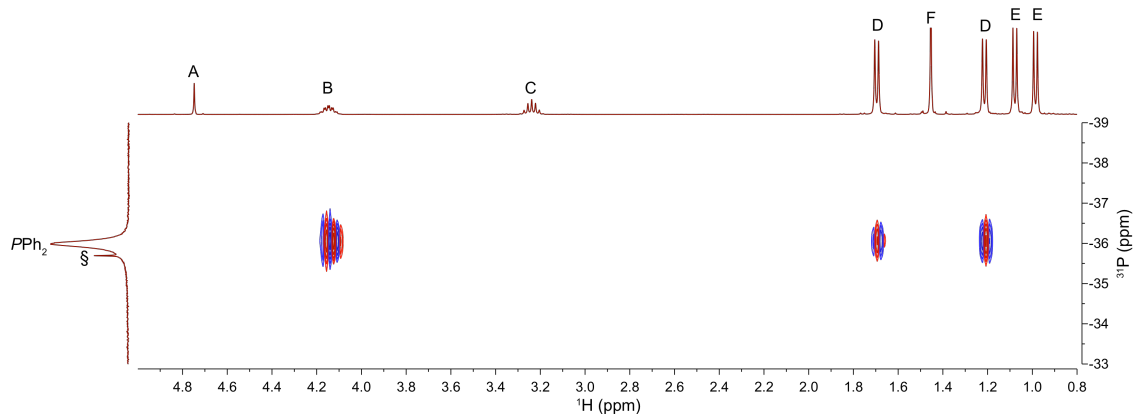


Figure 49. ^1H - ^{31}P HMBC NMR spectrum of $[(\text{BDI}_{\text{DIPP}})\text{GePPh}_2]$ (**33**) in C_6D_6 , with A = γ -H; B & C = CHMe_2 ; D & E = CHMe_2 and F = NCMe . Impurities are designated by §



The $^{13}\text{C}\{^1\text{H}\}$ NMR spectrum of $[(\text{BDI}_{\text{DIPP}})\text{GePPh}_2]$ (**33**) shows two doublets. One centred at δ_{C} 29.7 ppm is assigned to a tertiary carbon resonance in the isopropyl groups (CHMe_2) and the other centred at δ_{C} 24.8 ppm is assigned to a methyl carbon resonance in the isopropyl groups (CHMe_2) (Figure 50). The through-space carbon-phosphorus coupling is only obtained from resonances assigned to an isopropyl groups ($\mathbf{a'b'_2}$, CHMe_2 : $^5J_{\text{CP}} = 9$ Hz; CHMe_2 : $^6J_{\text{CP}} = 9$ Hz). This may be explained by the solid state structure of **33** which shows the phosphorus is closer to the ‘adjacent’ than to the ‘opposite’ isopropyl groups (Figure 51). These results indicate that the bond rotations in solution are restricted by steric interactions and that the overall conformation of **33** in solution is similar to that found in the solid state.

Figure 50. $^{13}\text{C}\{^1\text{H}\}$ NMR spectrum of $[(\text{BDI}_{\text{DIPP}})\text{GePPh}_2]$ (**33**) showing the J_{CP} ; **a** and **a'** are from CHMe_2 ; **b** and **b'** are from CHMe_2 ; **c** is from NCMe . The \mathbf{ab}_2 and $\mathbf{a'b'_2}$ indicate resonances from different pairs of isopropyl groups

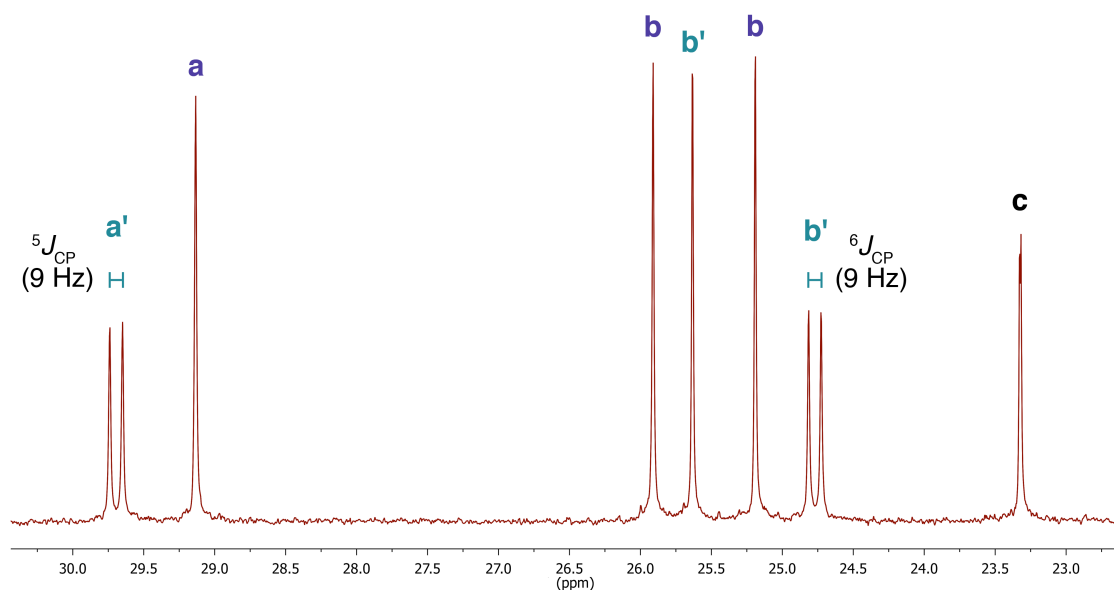
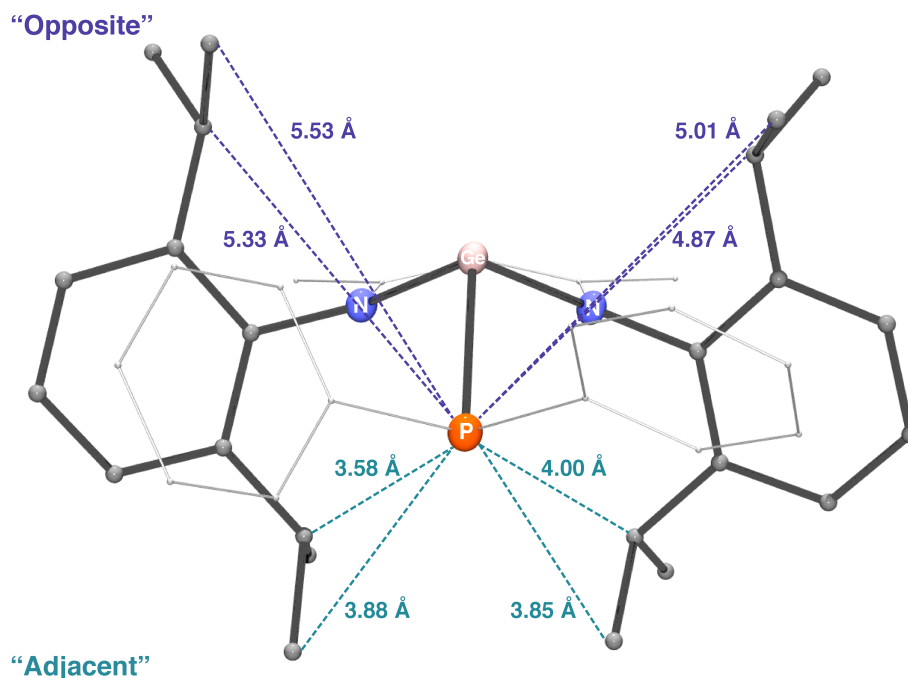


Figure 51. Schematic view of [(BDI_{DIPP})GePPh₂] (**33**) showing the distances between the phosphorus atom and the isopropyl substituents. H atoms are omitted. The distances are obtained from the crystal structure data



4.2.3.2 The β -diketiminatotin(II) diphenylphosphanide **34**

As in the germanium derivative **33**, the ^1H NMR spectrum of [(BDI_{DIPP})SnPPh₂] (**34**) shows a doublet of septets centred at δ_{H} 4.08 ppm assigned to the tertiary proton in the isopropyl group (CHMe_2) with through-bond proton-proton coupling ($^3J_{\text{HH}} = 6.8$ Hz), as well as a through-space proton-phosphorus coupling ($^6J_{\text{HP}} = 1.2$ Hz). The ^1H - ^{31}P HMBC NMR experiment shows correlations between the phosphorus (δ_{P} -30.8 ppm) and a tertiary proton resonance in the isopropyl group (CHMe_2 : δ_{H} 4.08 ppm), as well as between the phosphorus and two of the resonances assigned to the isopropyl methyl protons (CHMe_2 : δ_{H} 1.67 and 1.23 ppm). A single phosphorus resonance at δ_{P} -30.8 ppm with tin satellites ($^1J_{\text{P}^{119}\text{Sn}} = 978$ Hz and $^1J_{\text{P}^{117}\text{Sn}} = 937$ Hz) is found in the $^{31}\text{P}\{^1\text{H}\}$ NMR spectrum. The shift of the phosphorus resonance is similar to that of the germanium derivative **33** (δ_{P} -36.0 ppm) and Wang's tin(II) phosphoraniminato complex $[\text{Sn}\{\text{P}(\text{Ph})\text{C}=\text{C}(\text{H})\text{Ph}\}\text{P}(\text{Me})_2=\text{NSiMe}_3\}_2]$ (δ_{P} -42.3 ppm, $^1J_{\text{P}^{119}\text{Sn}} = 1078$ Hz).^[261]

The $^{13}\text{C}\{^1\text{H}\}$ NMR spectrum of the tin(II) diphenylphosphanide **34** shows through-space carbon-tin coupling (J_{CSn}), similar to that described for $[(\text{BDI}_{\text{DIPP}})\text{SnCl}]$ (**32**), together with through-space carbon-phosphorus coupling (J_{CP}). The tertiary carbons (CHMe_2) and those of the methyl groups (CHMe_2) in one of the isopropyl substituents couple to tin, with $^4J_{\text{CSn}} = 36$ Hz and $^5J_{\text{CSn}} = 43$ Hz, respectively (**ab**₂, Figure 52). One doublet centred at δ_{C} 29.5 ppm ($^5J_{\text{CP}} = 6$ Hz) is assigned to the tertiary carbon in the isopropyl group (CHMe_2), and one doublet centred at δ_{C} 24.7 ppm ($^6J_{\text{CP}} = 9$ Hz) is assigned to methyl carbons in the isopropyl group (CHMe_2), both showing through-space carbon-phosphorus coupling (**a'b'**₂, Figure 52). The J_{CSn} and J_{CP} couplings are obtained from separate resonances, suggesting that the tin and phosphorus atoms interact with different isopropyl groups. This can be attributed to the differences in distances between the atoms; that is the tin atom is closer to the isopropyl substituents on the ‘opposite’ side of the β -diketiminato ring, while the phosphorus atom is closer to the isopropyl substituents on the ‘adjacent’ side (Figure 53).

Figure 52. $^{13}\text{C}\{^1\text{H}\}$ NMR spectrum of $[(\text{BDI}_{\text{DIPP}})\text{SnPPh}_2]$ (**34**) showing the J_{CP} and J_{CSn} ; **a** and **a'** are from CHMe_2 ; **b** and **b'** are from CHMe_2 ; **c** is from NMe . The **ab**₂ and **a'b'**₂ indicate resonances from different pairs of isopropyl groups

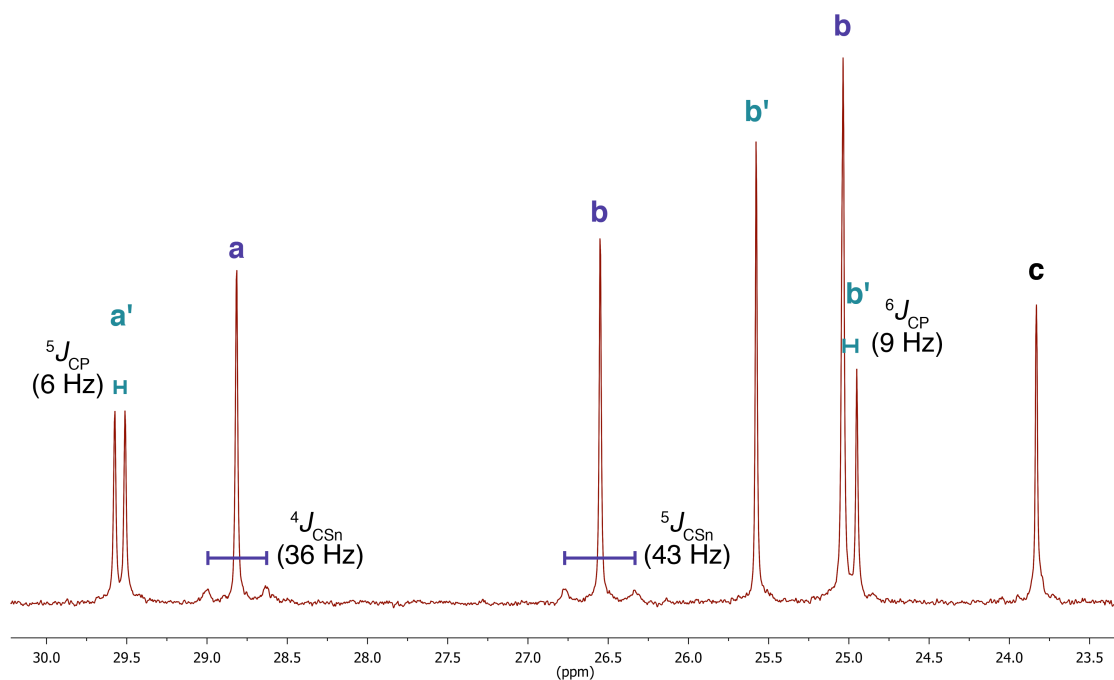
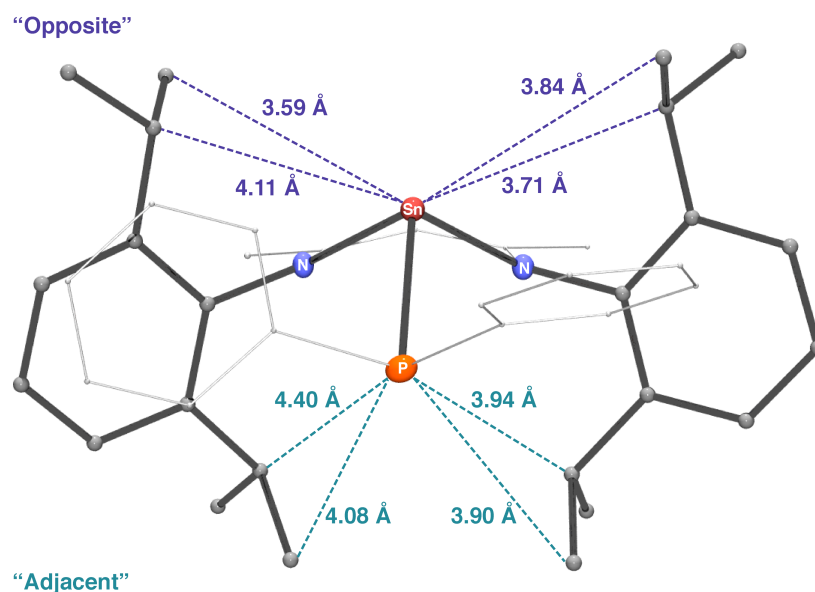


Figure 53. Schematic view of $[(\text{BDI}_{\text{DIPP}})\text{SnPPh}_2]$ (**34**) showing the distances between the phosphorus or tin atom and the isopropyl substituents. H atoms are omitted. The distances are obtained from the crystal structure data



4.2.3.3 The β -diketiminatolead(II) diphenylphosphanide **35**

The ^1H NMR spectrum of $[(\text{BDI}_{\text{DIPP}})\text{PbPPh}_2]$ (**35**) shows two septets centred at δ_{H} 4.04 and 3.06 ppm for the tertiary isopropyl protons (CHMe_2), with through-bond proton-proton coupling ($^3J_{\text{HH}} = 6.8$ Hz). Although through-space proton-phosphorus coupling (J_{HP}) is not observed in the ^1H NMR spectrum, the ^1H - ^{31}P HMBC NMR experiment shows correlations between the phosphorus atom (δ_{P} 7.3 ppm) and one of the tertiary proton resonances in the isopropyl groups (CHMe_2 : δ_{H} 4.04 ppm), as well as between the phosphorus and two methyl proton resonances in the isopropyl groups (CHMe_2 : δ_{H} 1.69 and 1.29 ppm). The lack of observed proton-phosphorus coupling in the ^1H NMR spectrum may due to a small through-space $^6J_{\text{HP}}$ coupling constant. A single phosphorus resonance (δ_{P} 7.3 ppm) with lead satellites ($^1J_{\text{PPb}} = 1130$ Hz) is shown in the $^{31}\text{P}\{^1\text{H}\}$ NMR spectrum. The phosphorus-lead coupling constant may be compared with those in Cowley's $[\text{Pb}(\mu\text{-P}^t\text{Bu}_2)(\text{P}^t\text{Bu}_2)]_2$ (terminal P^tBu_2 : δ_{P} 90.8 ppm, $^1J_{\text{PPb}} = 1100$ Hz) and Balch's $[\text{Pb}\{(\text{Ph}_2\text{P})_2\text{C}(\text{SiMe}_3)\}_2]$ (δ_{P} 21.8 ppm, $^1J_{\text{PPb}} = 1510$ Hz).^[262, 265] The ^{207}Pb NMR spectrum shows a doublet centred at δ_{Pb} 3011 ppm ($^1J_{\text{PbP}} = 1138$ Hz), downfield from the resonance in the parent lead(II) chloride **2** (δ_{Pb} 1413 ppm).^[70] The $^{13}\text{C}\{^1\text{H}\}$ NMR spectrum of **35** (Figure 54) shows through-space coupling between one of the tertiary carbon resonances (CHMe_2 (**a**): δ_{C} 28.3 ppm, $^4J_{\text{CPb}} = 37$ Hz) and lead. Through-space

carbon-phosphorus couplings (J_{CP}) are observed in another tertiary carbon resonance (CHMe_2 (**a'**): δ_C 29.4 ppm, $^5J_{CP} = 5$ Hz) and in one of the methyl carbon resonances in the isopropyl group (CHMe_2 (**b'**): δ_C 25.5 ppm, $^6J_{CP} = 4$ Hz).

Figure 54. $^{13}\text{C}\{^1\text{H}\}$ NMR spectrum of $[(\text{BDI}_{\text{DIPP}})\text{PbPPh}_2]$ (**35**) showing the J_{CP} and J_{CPb} ; **a** and **a'** are from CHMe_2 ; **b** and **b'** are from CHMe_2 ; **c** is from NCMe . The **ab**₂ and **a'b'**₂ indicate resonances from different pairs of isopropyl groups

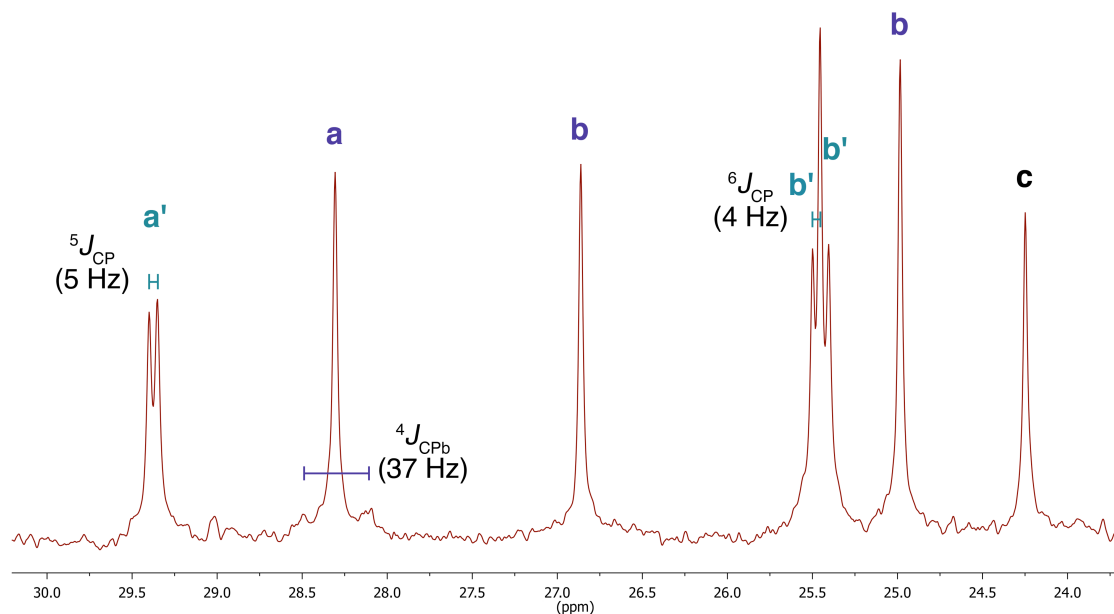
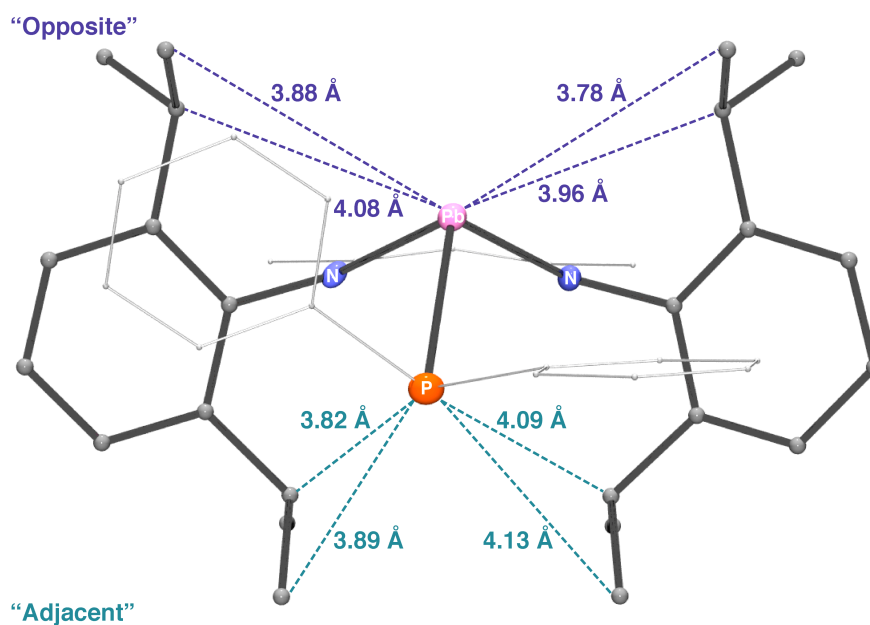
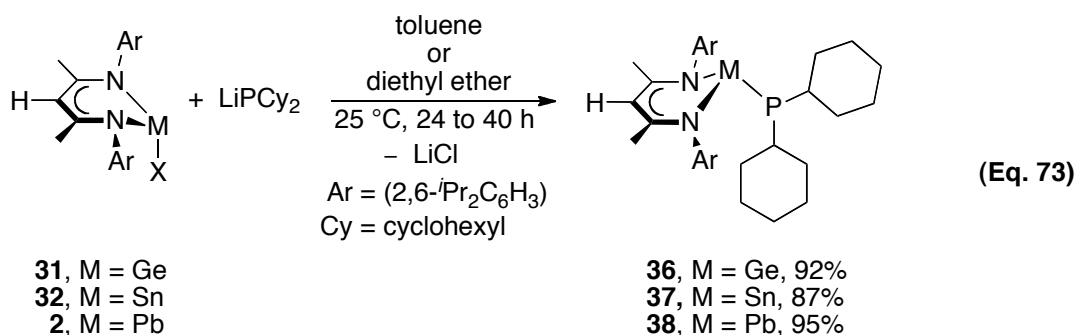


Figure 55. Schematic view of $[(\text{BDI}_{\text{DIPP}})\text{PbPPh}_2]$ (**35**) showing the distances between the phosphorus or lead atom and the isopropyl substituents. H atoms are omitted. The distances are obtained from the crystal structure data



4.2.4 Synthesis of β -diketiminato heavy group 14 metal dicyclohexylphosphanides **36–38**

Initial attempts to synthesise the β -diketiminatotin(II) dicyclohexylphosphanide **37** involved generating the lithium dicyclohexylphosphanide *in situ* by treatment of dicyclohexylphosphine with one equivalent of *n*-BuLi in *n*-hexane. The resulting mixture was immediately added to the β -diketiminatotin(II) chloride **32** in toluene. However, this approach unexpectedly led to formation of some *n*-butyl(β -diketiminato)tin(II) [(BDI_{DIPP})Sn^{*n*}Bu] (**39**), identified by X-ray crystallography (Appendix 2, Page 333). Hence, an alternative synthetic procedure was used. Lithium diphenylphosphanide was isolated as a light green solid by treatment of dicyclohexylphosphine with *n*-BuLi in *n*-hexane. Treatment of solutions of β -diketiminato heavy group 14 metal chlorides in toluene or diethyl ether with lithium dicyclohexylphosphanide at room temperature gave the β -diketiminato heavy group 14 metal dicyclohexylphosphanides **36–38** in 87–95% yields (equation 73). The dicyclohexylphosphanido complexes, especially the lead derivative **38**, are sensitive to air and moisture. Metallic precipitates are formed after several days when a toluene solution of **38** is exposed to ambient light at room temperature. Elemental analyses of these complexes are in good agreement with the calculated values.



4.2.5 X-ray crystal structures of the β -diketiminato heavy group 14 metal dicyclohexylphosphanides **36–38**

Single crystals of [(BDI_{DIPP})GePCy₂] (**36**) were obtained by recrystallisation from a concentrated *n*-hexane solution at -30°C . ORTEP drawings of the germanium(II) dicyclohexylphosphanide **36** are shown in Figures 56 and 57. Selected bond lengths and

angles are given in Table 32 and selected crystallographic data in Table 33. Compound **36** adopts an *exo* conformation, with the germanium atom 0.963 Å above the mean NCCCCN plane of the β -diketiminate ligand. The geometry at the metal centre is pyramidal, with the sum of bond angles 291.9°. The phosphorus is also pyramidally coordinated, with the sum of bond angles 298.3°. These findings are similar to those for the diphenylphosphanido analogue **33**, in which both the germanium and phosphorus atoms are pyramidally coordinated. In **36**, the Ge–P bond length is 2.4724(8) Å, which is similar to that in [(BDI_{DIPP})GePPh₂] (**33**, Ge–P = 2.4760(6) Å). The internal C–C–C bond angles in the cyclohexyl rings do not deviate significantly from the average value (111°), indicating that there is little distortion in the cyclohexyl chair conformation.

Figure 56. ORTEP diagram of [(BDI_{DIPP})GePCy₂] (**36**). H atoms are omitted and C atoms in the *N*-aryl groups in the β -diketiminate ring are omitted for clarity. The ellipsoid probability is shown at 30%

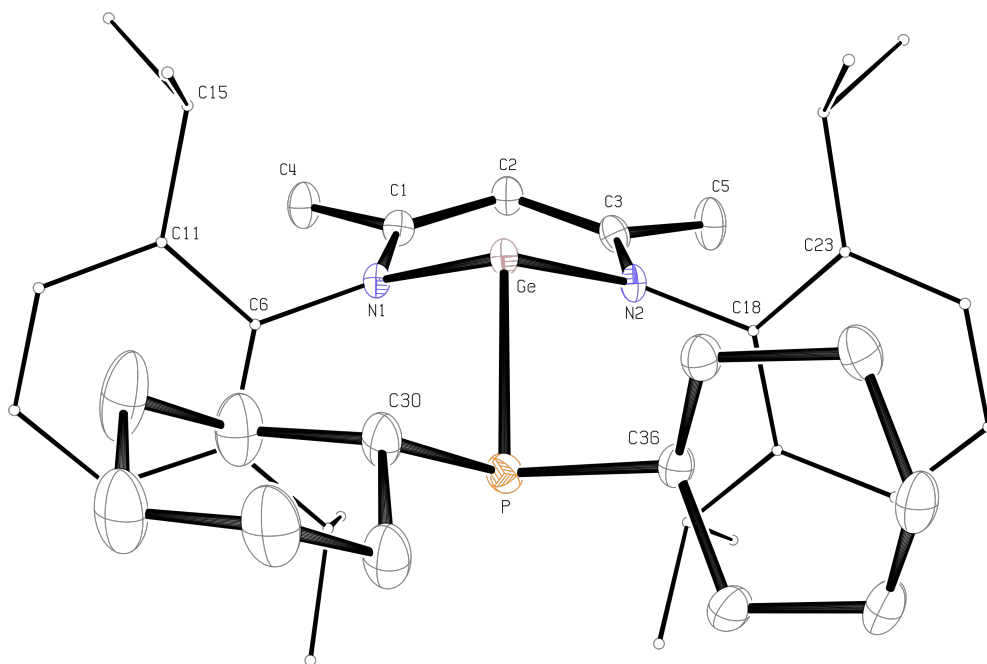
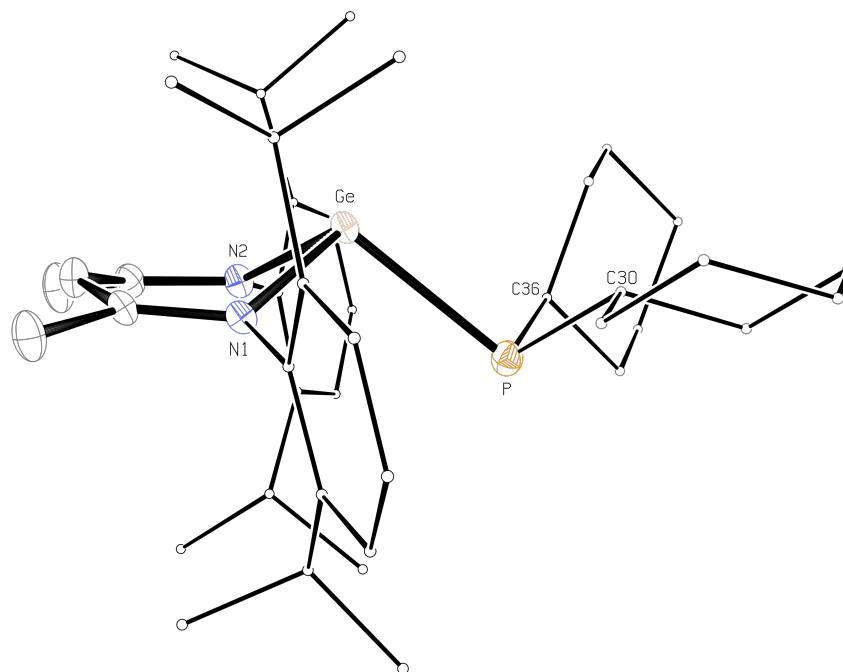


Figure 57. ORTEP diagram showing the side-on view of $[(\text{BDI}_{\text{DIPP}})\text{GePCy}_2]$ (**36**). H atoms are omitted, and C atoms in the *N*-aryl groups in the β -diketiminato ring and the cyclohexyl groups are minimised for clarity. The ellipsoid probability is shown at 30%



Single crystals of $[(\text{BDI}_{\text{DIPP}})\text{SnPCy}_2]$ (**37**) were obtained by recrystallisation from a minimum amount of toluene at $-30\text{ }^\circ\text{C}$. ORTEP drawings are shown in Figures 58 and 59. Selected bond lengths and angles are given in Table 32, and selected crystallographic data in Table 33. The tin(II) dicyclohexylphosphanide **37** adopts an *exo* conformation with the metal centre lying 1.066 \AA above the mean NCCCN plane of the β -diketiminato ligand. Delocalisation within the $\text{C}_3\text{N}_2\text{Sn}$ unit in the β -diketiminato ring is evident, but it does not extend to the *N*-aryl substituents (dihedral angles: $\text{C}(11)\text{-C}(6)\text{-N}(1)\text{-Sn} = 78.6(3)^\circ$ and $\text{C}(23)\text{-C}(18)\text{-N}(2)\text{-Sn} = -75.6(3)^\circ$). If the cyclohexyl groups are discounted, there is an approximate plane of symmetry passing through the atoms C(2), Sn and P, and bisecting the β -diketiminato ring. The tin atom is pyramidally coordinated with the sum of bond angles around the metal centre 285.8° . The geometry around the phosphorus is also pyramidal with the sum of bond angles 294.8° . The Sn–P bond distance ($2.6309(7)\text{ \AA}$) is similar to those in the tin(II) diphenylphosphanide **34** ($2.6307(9)\text{ \AA}$), Wright's $[\{\text{Sn}_2(\text{PCy})_3\}_2\text{Li}_4\cdot(\text{THF})_4]\cdot(\text{THF})_2]$ (avg. Sn–P = 2.624 \AA) and Jones' $[\{\text{Cy}_2\text{NC}(\text{NAr})_2\}\text{Sn}(\text{P}_2\text{C}_3^i\text{Bu}_3)]$ (Ar = $(2,6\text{-}^i\text{Pr}_2\text{C}_6\text{H}_3)$, Sn–P = $2.7595(17)\text{ \AA}$).^[266-267] The internal C–C–C bond angles in the cyclohexyl rings

do not deviate significantly from the average value (111°), indicating that there is little distortion in the chair conformation.

Figure 58. ORTEP diagram of $[(BDI_{DIPP})SnPCy_2]$ (**37**). H atoms are omitted and C atoms in the *N*-aryl groups in the β -diketiminato ring are minimised for clarity. The ellipsoid probability is shown at 30%

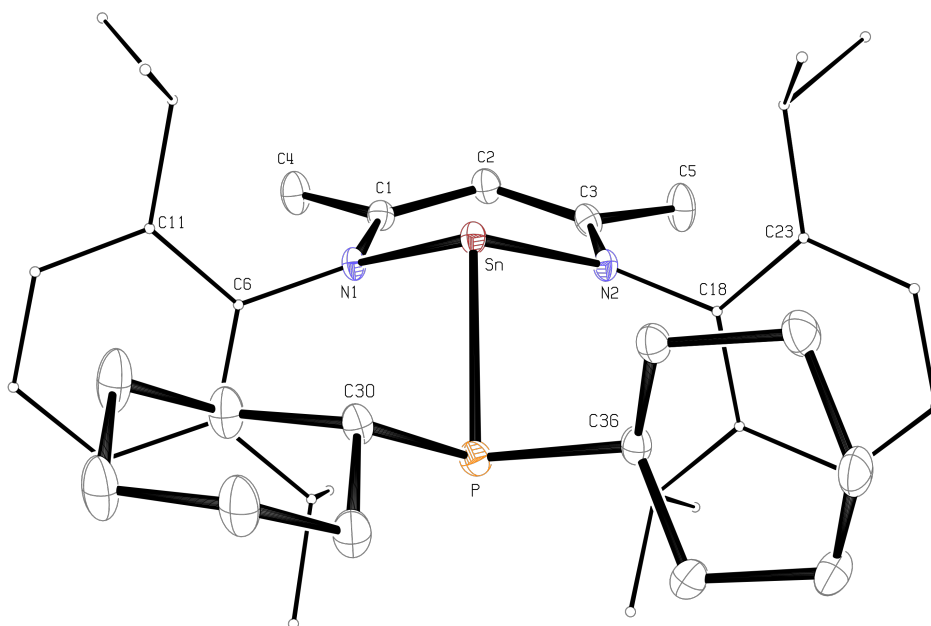
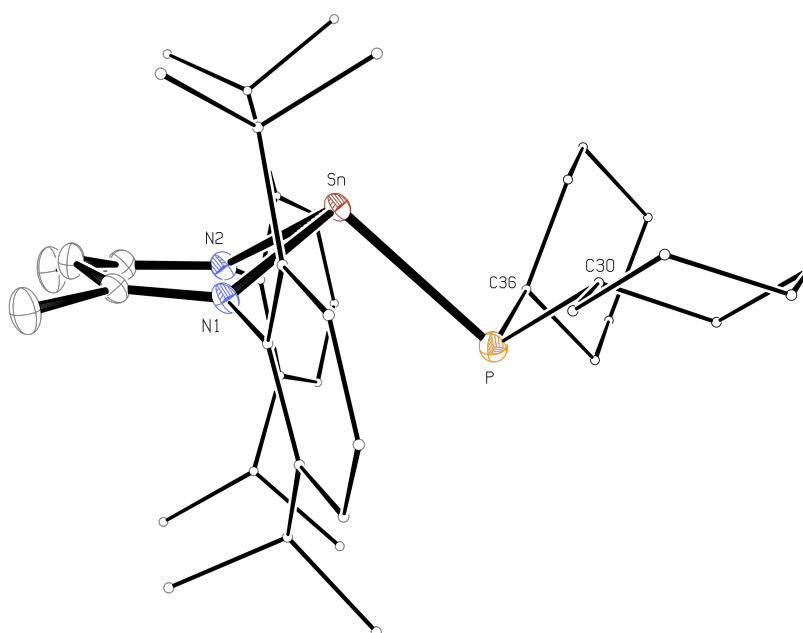


Figure 59. ORTEP diagram showing the side-on view of $[(BDI_{DIPP})SnPCy_2]$ (**37**). H atoms are omitted, and C atoms in the *N*-aryl groups in the β -diketiminato ring and the cyclohexyl groups are minimised for clarity. The ellipsoid probability is shown at 30%



Single crystals of [(BDI_{DIPP})PbPCy₂] (**38**) were obtained from toluene at -30 °C. ORTEP drawings are shown in Figures 60 and 61. Selected bond lengths and angles are given in Table 32, and selected crystallographic data in Table 33. The lead(II) dicyclohexylphosphanide **38** and the germanium and tin derivatives **36–37** are isostructural. An *exo* conformation is adopted with the lead atom 1.128 Å above the mean NCCCN plane of the β-diketiminato ligand. The lead atom is pyramidally coordinated with the sum of bond angles around the metal centre 282.1°. The phosphorus atom is also pyramidally coordinated, with the sum of bond angles around the atom 292.5°. The folding angle between the mean NCCCN plane in the β-diketiminato ring and the plane defined by the atoms N(1), Pb and N(2) is 38.7°, similar to that in Driess' [(BDI_{DIPP})PbP(SiMe₃)₂] (43.9°).^[103] The Pb–P bond distance in **38** is 2.6945(9) Å, similar to those in the lead(II) diphenylphosphanide **35** (Pb–P = 2.720(2) Å), Driess' [(BDI_{DIPP})PbP=Si(Ar)Si^tBu₃] (Ar = (2,4,6-^tPr₃C₆H₂), Pb–P = 2.671(1) Å) and Cowley's [Pb(μ-P^tBu₂)(P^tBu₂)₂] (terminal Pb–P = 2.781(4) Å).^[103, 262] The internal C–C–C bond angles in the cyclohexyl rings do not deviate significantly from the average value (111°), indicating that there is little distortion in the chair conformation.

Figure 60. ORTEP diagram of $[(\text{BDI}_{\text{DIPP}})\text{PbPCy}_2]$ (**38**). H atoms are omitted and C atoms in the *N*-aryl groups in the β -diketiminato ring are minimised for clarity. The ellipsoid probability is shown at 30%

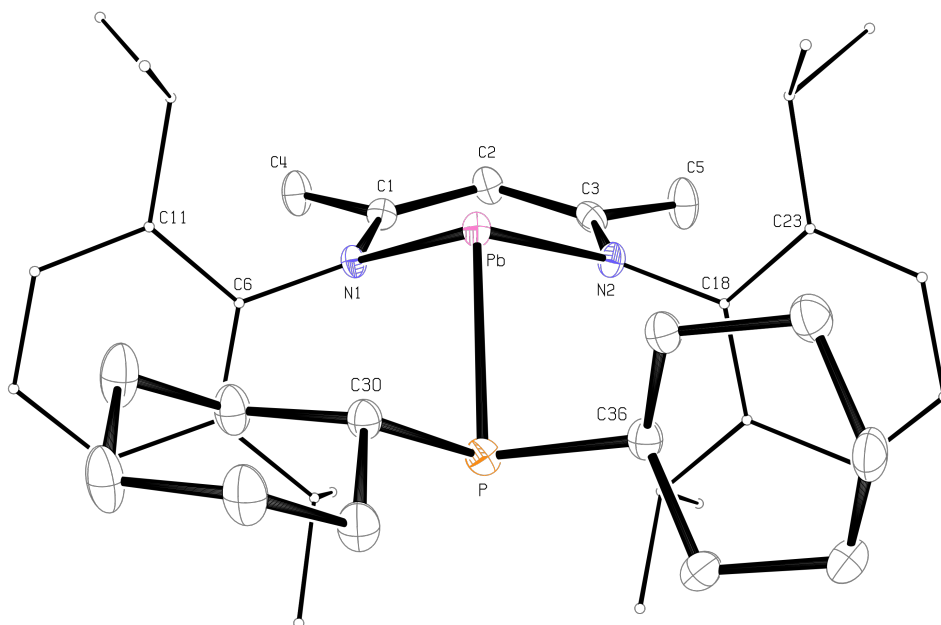


Figure 61. ORTEP diagram showing the side-on view of $[(\text{BDI}_{\text{DIPP}})\text{PbPCy}_2]$ (**38**). H atoms are omitted, C atoms in the *N*-aryl groups in the β -diketiminato ring and the cyclohexyl groups are minimised for clarity. The ellipsoid probability is shown at 30%

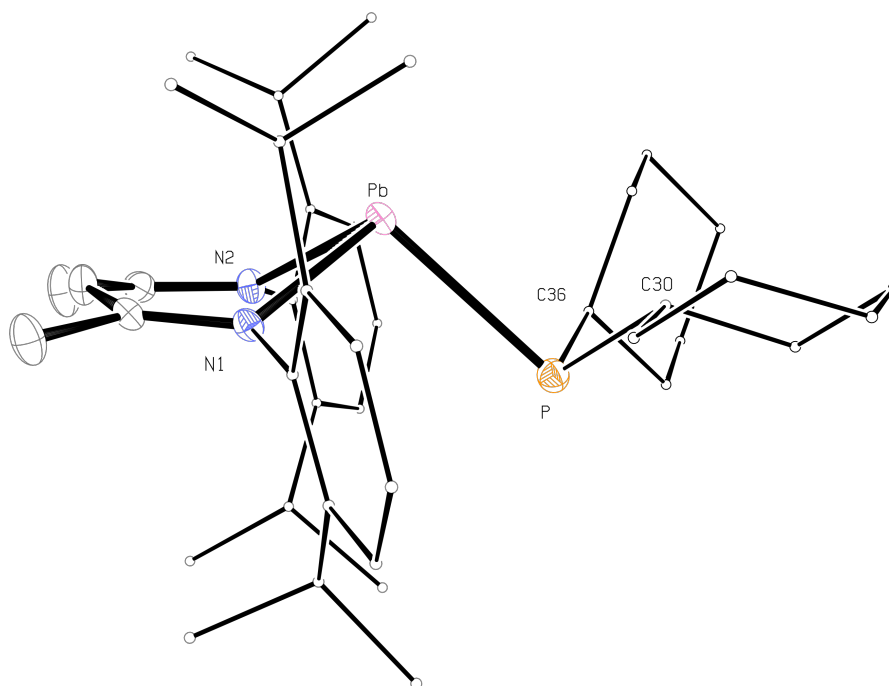


Table 32. Selected bond lengths (Å) and angles (deg) for [(BDI_{DIPP})MPCy₂] (Cy = cyclohexyl; **36**, M = Ge; **37**, M = Sn; and **38**, M = Pb)

	[(BDI _{DIPP})GePCy ₂] 36 , M = Ge	[(BDI _{DIPP})SnPCy ₂] 37 , M = Sn	[(BDI _{DIPP})PbPCy ₂] 38 , M = Pb
<i>Bond lengths (Å)</i>			
M–P	2.4724(8)	2.6309(7)	2.6945(9)
M–N(1)	2.049(2)	2.233(2)	2.342(3)
M–N(2)	2.048(2)	2.227(2)	2.326(3)
N(1)–C(1)	1.329(3)	1.328(3)	1.325(4)
N(2)–C(3)	1.328(3)	1.315(3)	1.324(4)
C(1)–C(2)	1.393(4)	1.398(4)	1.407(5)
C(2)–C(3)	1.397(4)	1.404(4)	1.408(5)
C(1)–C(4)	1.512(4)	1.512(4)	1.508(5)
C(3)–C(5)	1.509(4)	1.515(4)	1.510(5)
P–C(30)	1.900(3)	1.881(3)	1.880(3)
P–C(36)	1.889(3)	1.892(3)	1.887(3)
M–NCCCN _{Plane}	0.963	1.066	1.128
<i>Bond angles (deg)</i>			
N(1)–M–N(2)	88.05(8)	83.23(8)	80.79(9)
N(1)–M–P	102.52(6)	102.60(6)	102.03(7)
N(2)–M–P	101.35(7)	99.95(6)	99.25(7)
M–N(1)–C(1)	117.92(17)	118.50(16)	118.4(2)
M–N(2)–C(3)	119.10(18)	119.85(17)	120.3(2)
N(1)–C(1)–C(2)	123.8(2)	124.1(2)	125.0(3)
N(2)–C(3)–C(2)	123.2(2)	124.0(2)	124.2(3)
C(1)–C(2)–C(3)	126.3(3)	128.7(2)	129.7(3)
M–P–C(30)	98.12(10)	95.33(9)	93.57(11)
M–P–C(36)	97.97(9)	96.18(8)	95.17(11)
C(30)–P–C(36)	102.25(13)	103.30(12)	103.79(15)
Avg. internal angles of Cy	111	111	111
NCCCN _{plane} –NMN _{plane}	39.9	39.0	38.7
Σ bond angle around M	291.9	285.8	282.1
DOP of M (%) ^a	76	82	87
Σ bond angle around P	298.3	294.8	292.5
DOP of P (%) ^a	69	72	75
<i>Dihedral angles (deg)</i>			
C(11)–C(6)–N(1)–M	80.1(3)	78.6(3)	77.8(3)
C(23)–C(18)–N(2)–M	–76.1(3)	–75.6(3)	–74.9(4)

^a Degree of pyramidalisation (DOP, %) = [(360 – Σ_{bond angle}) / 0.9]^[115] When a DOP is 100%, it is equivalent to a sum of bond angles of 270°, whereas a DOP of 0% indicates a planar geometry at the central atom

Table 33. Selected crystallographic data for [(BDI_{DIPP})MPCy₂] (Cy = cyclohexyl; **36**, M = Ge; **37**, M = Sn; and **38**, M = Pb)

	[(BDI _{DIPP})GePCy ₂] (36)	[(BDI _{DIPP})SnPCy ₂] (37)	[(BDI _{DIPP})PbPCy ₂] (38)
chemical formula	C ₄₁ H ₆₃ GeN ₂ P	C ₄₁ H ₆₃ N ₂ PSn	C ₄₁ H ₆₃ N ₂ PPb
molecular mass	687.49	733.59	822.09
temperature (K)	173(2)	173(2)	173(2)
wavelength (Å)	0.71073	0.71073	0.71073
crystal system	monoclinic	monoclinic	monoclinic
space group	<i>P</i> 2 ₁ / <i>c</i> (No. 14)	<i>P</i> 2 ₁ / <i>c</i> (No. 14)	<i>P</i> 2 ₁ / <i>c</i> (No. 14)
<i>a</i> (Å)	10.0941(2)	9.9722(1)	9.9586(2)
<i>b</i> (Å)	23.5171(5)	23.7044(4)	23.7678(4)
<i>c</i> (Å)	17.2689(3)	17.4243(3)	17.4757(2)
<i>α</i> (deg)	90	90	90
<i>β</i> (deg)	110.600(1)	109.003(1)	108.531(1)
<i>γ</i> (deg)	90	90	90
<i>V</i> (Å ³)	3837.24(13)	3894.37(10)	3921.93(11)
<i>Z</i>	4	4	4
ρ_{calcd} (Mg m ⁻³)	1.19	1.25	1.39
θ range (deg)	3.47–26.73	3.44–27.11	3.43–27.09
abs coeff (mm ⁻¹)	0.87	0.73	4.37
measd/indep reflns/ <i>R</i> (int)	48 350/8127/0.079	57 848/8576/0.077	57 828/8624/0.068
reflns with <i>I</i> > 2 σ (<i>I</i>)	6180	6730	6904
data/restraints/param	8127/0/408	8576/0/408	8624/0/408
goodness of fit on <i>F</i> ²	0.990	1.023	1.031
final <i>R</i> indices [<i>I</i> > 2 σ (<i>I</i>)]	<i>R</i> 1 = 0.046, <i>wR</i> 2 = 0.108	<i>R</i> 1 = 0.037, <i>wR</i> 2 = 0.072	<i>R</i> 1 = 0.029, <i>wR</i> 2 = 0.054
<i>R</i> indices (all data)	<i>R</i> 1 = 0.070, <i>wR</i> 2 = 0.119	<i>R</i> 1 = 0.058, <i>wR</i> 2 = 0.079	<i>R</i> 1 = 0.047, <i>wR</i> 2 = 0.058
largest diff peak and hole (e Å ⁻³)	0.79 and -0.44	0.48 and -0.81	0.99 and -0.97

4.2.6 NMR spectra of the β -diketiminato heavy group 14 metal dicyclohexylphosphanides **36–38**

Selected multinuclear NMR spectroscopic data for **36–38** are given in Table 34.

Table 34. Selected multinuclear NMR spectroscopic data for [(BDI_{DIPP})MPCy₂] (Cy = cyclohexyl; **36**, M = Ge; **37**, M = Sn; and **38**, M = Pb) in C₆D₆ at 30 °C, unless specified

	[(BDI _{DIPP})GePCy ₂] (36)	[(BDI _{DIPP})SnPCy ₂] (37)	[(BDI _{DIPP})PbPCy ₂] (38)
	δ (ppm), J (Hz) ^a	δ (ppm), J (Hz) ^a	δ (ppm), J (Hz) ^a
¹H			
γ -H	4.73 (s)	4.72 (s)	4.61 (s)
CHMe ₂	4.08 (d-septet) ³ J _{HH} = 6.8; ⁶ J _{HP} = 2.8	3.99 (d-septet) ³ J _{HH} = 6.8; ⁶ J _{HP} = 1.6	3.95 (d-septet) ³ J _{HH} = 6.8; ⁶ J _{HP} = 0.8
	3.44 (septet) ³ J _{HH} = 6.8	3.32 (septet) ³ J _{HH} = 6.8	3.25 (septet) ³ J _{HH} = 6.8
Cy-CH	0.47 (t) ² J _{HP} = 12.8	1.00 (br)	1.00 (br)
¹³C{¹H}			
Cy-CH	35.5 (d) ¹ J _{CP} = 29	33.1 (d) ¹ J _{CP} = 28	34.4 (d) ¹ J _{CP} = 34
CHMe ₂	29.5 (d) ⁵ J _{CP} = 10	29.4 (d) ⁵ J _{CP} = 7	29.2 (d) ⁵ J _{CP} = 6
	29.2 (s)	28.4 (s)	28.3
CHMe ₂	26.3, 25.6, 25.5 (s) 24.9 (d) ⁶ J _{CP} = 11	26.7, 25.7, 25.3 (s) 25.1 (d) ⁶ J _{CP} = 10	26.9, 25.5, 25.3 (s) 25.8 (d) ⁶ J _{CP} = 11
³¹P{¹H}			
	-14.1 (s)	-15.4 (s) ¹ J _{PSn} = 953 ^c	26.9 (s) ¹ J _{PPb} = 1103
Other			
	-	$\delta(^{119}\text{Sn}) = 358$ ^b ¹ J _{SnP} = 964	$\delta(^{207}\text{Pb}) = 3981$ ¹ J _{PbP} = 1074

^aSuperscript indicates number of bonds between nuclei; ^b in toluene-*d*₆; ^c individual ¹¹⁷Sn and ¹¹⁹Sn satellites are not resolved

4.2.6.1 The β -diketiminatogermanium(II) dicyclohexylphosphanide **36**

The ¹H NMR spectrum of **36** in C₆D₆ shows a doublet of septets centred at δ_{H} 4.08 ppm, assigned to a tertiary proton resonance of the isopropyl group (CHMe₂), with through-bond proton-proton coupling ³J_{HH} = 6.8 Hz and a through-space proton-phosphorus coupling ⁶J_{HP} = 2.8 Hz. The ¹H-³¹P HMBC NMR experiment in toluene-*d*₈ shows correlations between the phosphorus resonance (δ_{P} -14.2 ppm) and the CHMe₂ resonances at δ_{H} 3.99 ppm, as well as between the phosphorus and the proton resonances at δ_{H} 1.67 and 1.22 ppm, assigned to the methyl protons in the isopropyl unit

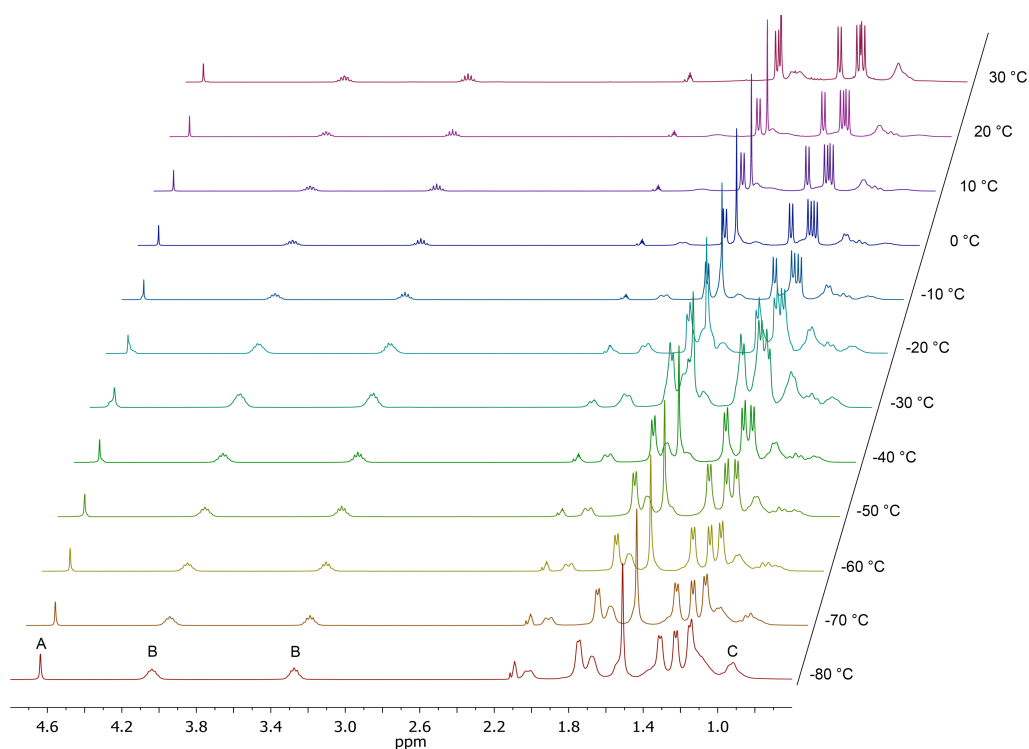
(CHMe₂). A series of multiplets ($\delta_{\text{H}} \sim 0.94\text{--}1.88$ ppm) is assigned to the CH₂ protons in the cyclohexyl groups. Similar resonances are found in other metal complexes containing dicyclohexylphosphanide substituents, such as Levason's [SnF₄{Cy₂P(CH₂)₂PCy₂}] ($\delta_{\text{H}} 1.26\text{--}2.21$ ppm) and Coles' [Ti(Cy₂PC{NCy}₂)(NMe₂)₃] ($\delta_{\text{H}} 1.24\text{--}1.70$ ppm).^[268-269] A broad triplet at $\delta_{\text{H}} 0.47$ ppm with through-bond proton-phosphorus coupling ${}^2J_{\text{HP}} = 12.8$ Hz is assigned to the tertiary CH protons in the cyclohexyl groups.

A single phosphorus resonance at $\delta_{\text{P}} -14.1$ ppm in C₆D₆ is found in the ${}^{31}\text{P}\{^1\text{H}\}$ NMR spectrum, upfield from the resonance in the diphenylphosphanide derivative **33** ($\delta_{\text{P}} -36.0$ ppm). The ${}^{13}\text{C}\{^1\text{H}\}$ NMR spectrum of the germanium(II) dicyclohexylphosphanide **36** shows through-space carbon-phosphorus coupling (J_{CP}) between the phosphorus and one of the tertiary carbon resonances (CHMe₂: $\delta_{\text{C}} 29.5$ ppm, ${}^5J_{\text{CP}} = 10$ Hz), as well as between the phosphorus and one of the methyl carbon resonances in the isopropyl group (CHMe₂: $\delta_{\text{C}} 24.9$ ppm, ${}^6J_{\text{CP}} = 11$ Hz).

4.2.6.2 The β -diketiminatotin(II) dicyclohexylphosphanide **37**

The ${}^1\text{H}$ NMR spectrum of **37** shows a doublet of septets centred at $\delta_{\text{H}} 3.99$ ppm, with through-bond proton-proton coupling ${}^3J_{\text{HH}} = 6.8$ Hz and through-space proton-phosphorus coupling ${}^6J_{\text{HP}} = 1.6$ Hz, which is assigned to one of the tertiary proton resonances (CHMe₂). As in the germanium analogue **36**, the resonances assigned to the cyclohexyl CH₂ protons are shown as multiplets ($\delta_{\text{H}} 1.00\text{--}1.54$ ppm). In an attempt to resolve the multiplet signals, a VT- ${}^1\text{H}$ NMR experiment on **37** was initiated (Figure 62). However, the resonances remained unresolved within the temperature range 30 °C to -80 °C.

Figure 62. VT- ^1H NMR spectra (400 MHz, toluene- d_8) of $[(\text{BDI}_{\text{DIPP}})\text{SnPCy}_2]$ (**37**) where A = $\gamma\text{-H}$; B = CHMe_2 ; and C = Cy-CH



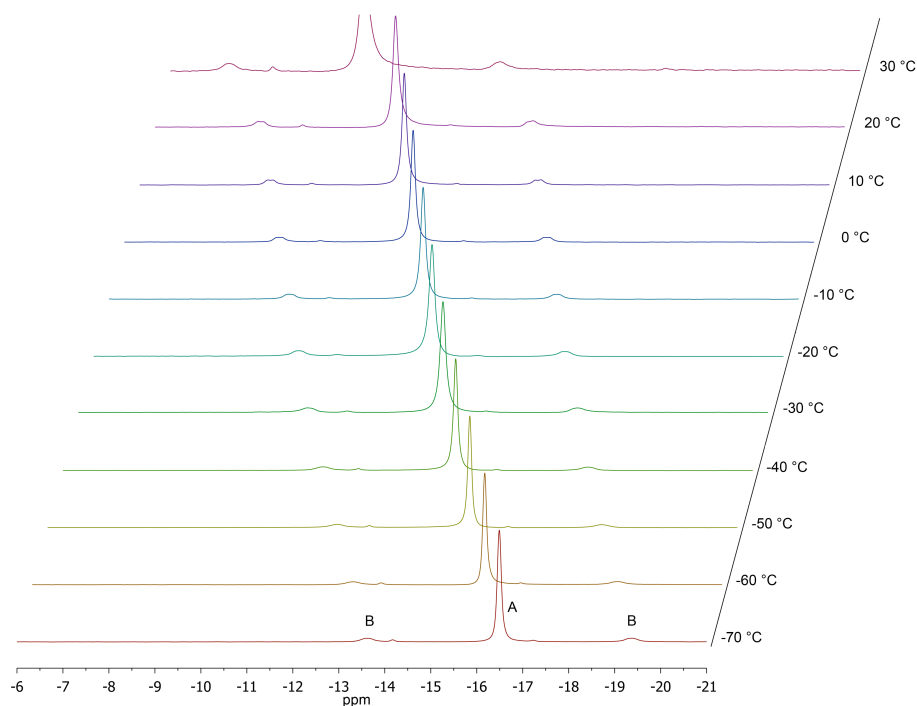
Through-space carbon-phosphorus couplings (J_{CP}) are found in the $^{13}\text{C}\{^1\text{H}\}$ NMR spectrum. Two doublets centred at δ_{C} 29.4 ppm ($^5J_{\text{CP}} = 7$ Hz) and δ_{C} 25.1 ppm ($^6J_{\text{CP}} = 10$ Hz) are assigned to a tertiary carbon (CHMe_2) resonance and a methyl carbon (CHMe_2) resonance, respectively. A doublet centred at δ_{C} 33.1 ppm ($^1J_{\text{CP}} = 28$ Hz), assigned to the tertiary CH carbon in the cyclohexyl groups, is similar to that in the germanium(II) dicyclohexylphosphanide **36** (δ_{C} 33.5 ppm, $^1J_{\text{CP}} = 29$ Hz) and Ozerov's $[(\text{PNP})\text{PdPCy}_2]$ ($\text{PNP} = [\{2\text{-P}(\text{CHMe}_2)_2\text{-4-MeC}_6\text{H}_3\}_2\text{N}]$, δ_{C} 37.4 ppm, $^2J_{\text{CP}} = 21$ Hz).^[270] The ^{119}Sn NMR spectrum of **37** in toluene- d_8 at 30 °C shows a doublet centred at δ_{Sn} 358 ppm ($^1J_{\text{SnP}} = 964$ Hz). At -80 °C, the tin signal is slightly shifted to higher field (δ_{Sn} 342 ppm, $\Delta\delta_{\text{Sn}}$ 16 ppm), with a smaller tin-phosphorus coupling constant $^1J_{\text{SnP}} = 927$ Hz ($\Delta^1J_{\text{SnP}} = 37$ Hz).

The $^{31}\text{P}\{^1\text{H}\}$ NMR spectrum of $[(\text{BDI}_{\text{DIPP}})\text{SnPCy}_2]$ (**37**) shows a single phosphorus resonance at δ_{P} -15.4 ppm with tin satellites ($^1J_{\text{PSn}} = 953$ Hz). The phosphorus-tin coupling constant is similar to that in the diphenylphosphanide analogue **34** ($^1J_{\text{P}^{119}\text{Sn}} = 978$ Hz), as well as in Scheer's $[\text{Ph}^*\text{SnP}(\text{H})\text{Trip}]$ ($\text{Ph}^* = (2,6\text{-}(\text{Trip})_2\text{C}_6\text{H}_3)$, $\text{Trip} =$

(2,4,6-*i*-Pr₃C₆H₂), $^1J_{P^{119/117}Sn} = 934$ Hz) and Escudié's [Trip₂Sn(F)P(H)Ar] (Ar = (2,4,6-*t*-Bu₃C₆H₂), $^1J_{P^{119}Sn} = 995$ Hz).^[205-206]

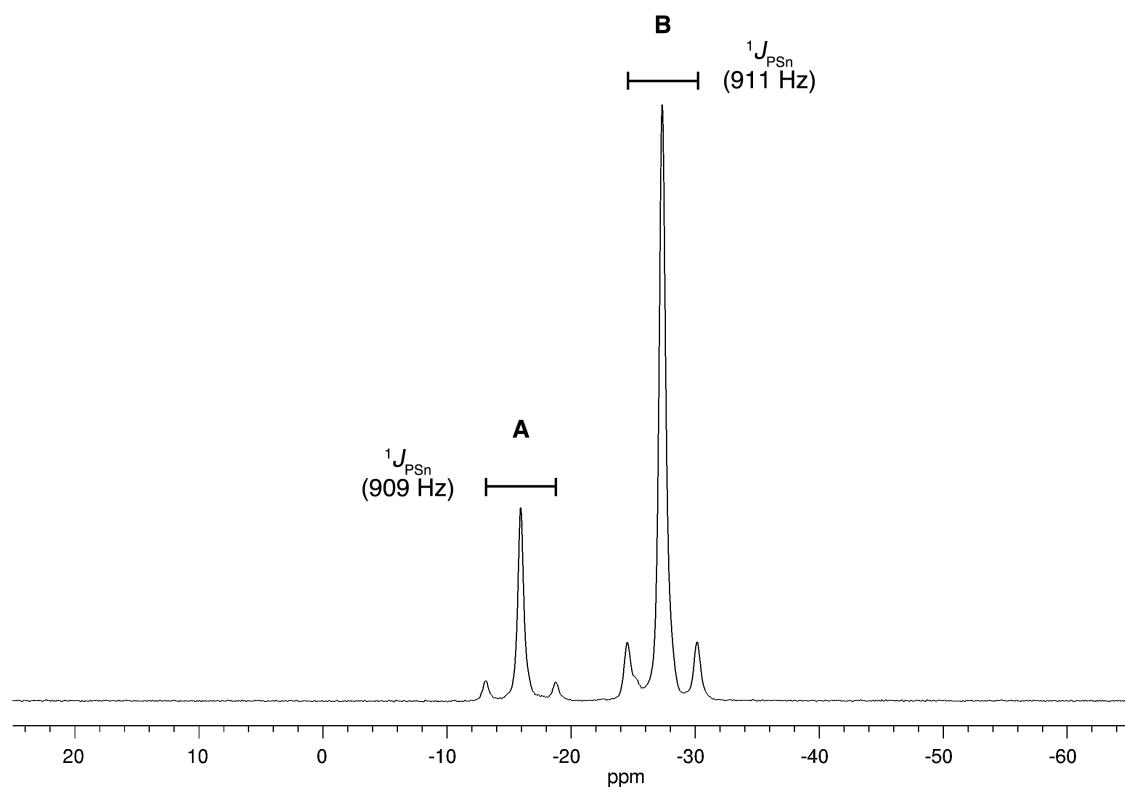
From X-ray crystallographic and NMR spectroscopic studies described in the literature, the phosphanido fragment is known to adopt both pyramidal and planar configurations (Scheme 47, Page 107). Hence, a VT- $^{31}P\{^1H\}$ NMR experiment was initiated to confirm the conformation of the tin(II) dicyclohexylphosphanide **37** in solution (Figure 63). At 30 °C, a single phosphorus resonance at $\delta_P -10.2$ ppm in toluene-*d*₈ with tin satellites ($^1J_{PSn} = 949$ Hz) is found. As the temperature is lowered to -70 °C, there is an upfield shift of the phosphorus resonance to $\delta_P -16.5$ ppm ($\Delta\delta_P$ 6.3 ppm) with a smaller phosphorus-tin coupling constant ($^1J_{PSn} = 936$ Hz, $\Delta^1J_{PSn} = 13$ Hz) is found. Such an upfield shift at low temperature has been observed previously, for example in Davies' [Ph₂PSeLi·TMEDA]₂ (from 15 °C to -70 °C, $\Delta\delta_P$ 1.2 ppm) and Izod's [{{(Me₃Si)₂CH}(C₆H₄-2-CH₂NMe₂)P}SnCl] (from 20 °C to -69 °C, $\Delta\delta_P$ 2.5 ppm).^[212, 251] There is no sign of resonance splitting or a new phosphorus resonance in the VT- $^{31}P\{^1H\}$ NMR experiment, suggesting that the geometry around the phosphorus atom found in crystalline **37** persists in solution.

Figure 63. VT- $^{31}P\{^1H\}$ NMR spectra (162 MHz, toluene-*d*₈) of [(BDI_{DIPP})SnPCy₂] (**37**) where A = phosphorus resonance and B = tin satellites



In the solid state $^{31}\text{P}\{^1\text{H}\}$ NMR spectrum of **37** at room temperature, two resonances: A ($\delta_{\text{P(solid)}} -16.0$ ppm) and B ($\delta_{\text{P(solid)}} -27.4$ ppm) are shown, with a relative intensity about 1:3 (Figure 64). There is no evidence on any correction between the two resonances. Both phosphorus-tin coupling constants (A: $^1J_{\text{PSn(solid)}} = 909$ Hz and B: $^1J_{\text{PSn(solid)}} = 911$ Hz) are similar in magnitude to that observed in solution ($^1J_{\text{PSn(solution)}} = 953$ Hz). The two phosphorus resonances observed are unexpected since the X-ray crystal structure (space group: $P2_1/c$ (No.14) and $Z = 4$) indicates that all the phosphorus environments are identical (Table 33, Page 154). We reason that the existence of both *exo* and *endo* conformations is unlikely as the phosphorus-tin coupling constants ($^1J_{\text{PSn(solid)}} \sim 900$ Hz) are similar, and consistent with those obtained for pyramidally coordinated phosphorus (Table 24, Page 114). It is possible that two polymorphs crystallised from toluene at -30 °C and that the sample used for the solid state NMR experiment was a mixture of these. Attempts to isolate crystals of the minor polymorph by visual selection under the microscope were not successful. Alternatively, this finding may attribute to the presence of an impurity in the sample used for the solid state NMR experiment. More work is necessary to explain the NMR results.

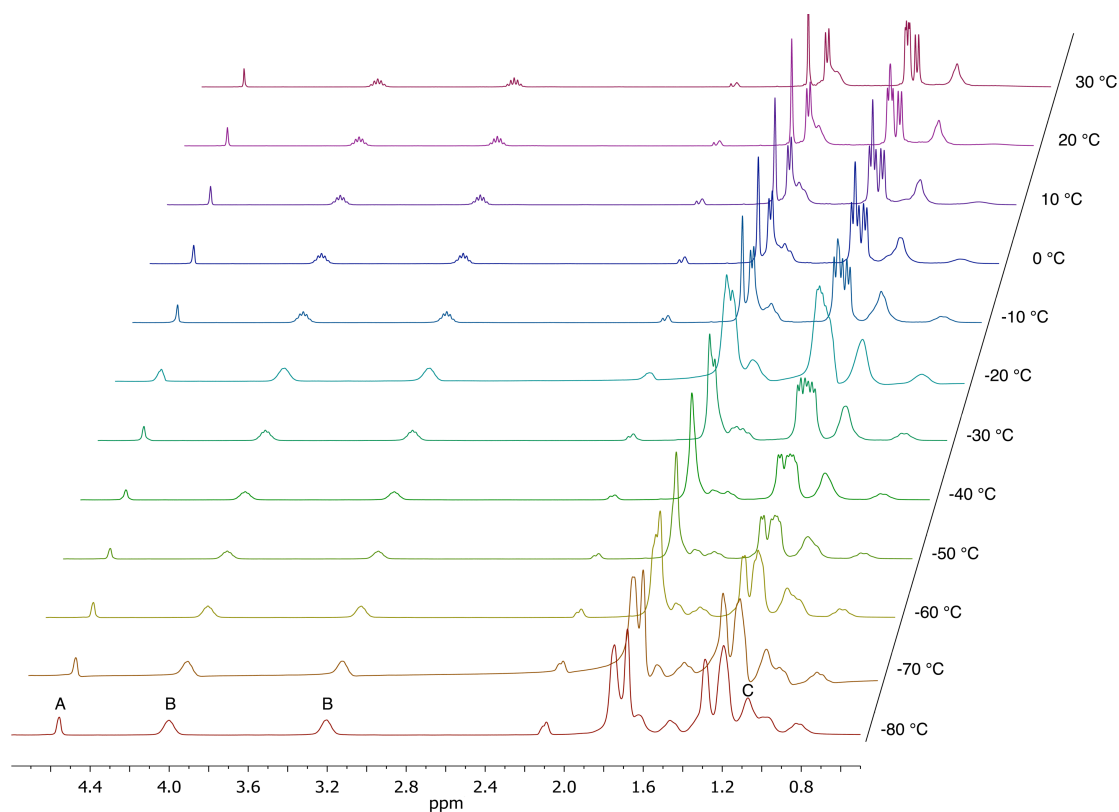
Figure 64. Solid state $^{31}\text{P}\{^1\text{H}\}$ NMR spectrum (162 MHz) of $[(\text{BDI}_{\text{DIPP}})\text{SnPCy}_2]$ (**37**)



4.2.6.3 The β -diketiminatolead(II) dicyclohexylphosphanide **38**

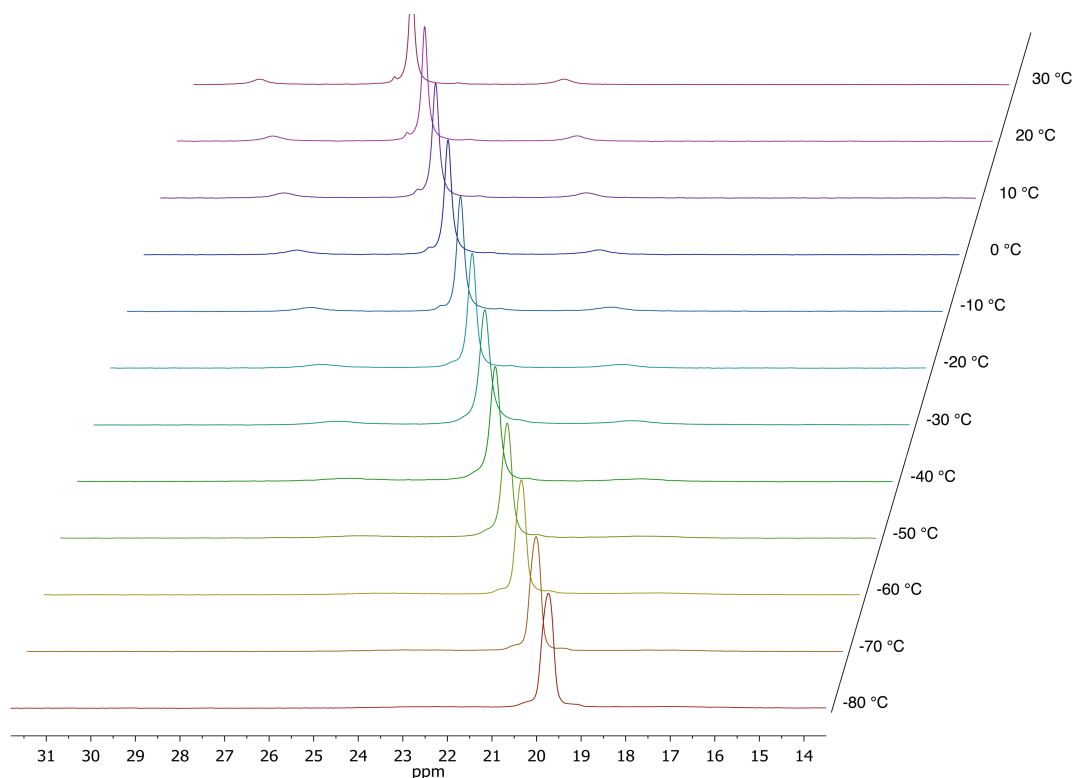
The ^1H NMR spectrum of **38** shows a doublet of septets centred at δ_{H} 3.95 ppm, assigned to a tertiary isopropyl proton (CHMe_2) resonance with through-bond proton-proton coupling ($^3J_{\text{HH}} = 6.8$ Hz) which is further split by a through-space proton-phosphorus coupling ($^6J_{\text{HP}} = 0.8$ Hz). The signal at δ_{H} 3.25 ppm, also assigned to a CHMe_2 proton, do not show any coupling to phosphorus, indicating that one of the isopropyl groups is nearer to phosphorus than the other. A broad signal at δ_{H} 1.00 ppm is assigned to the tertiary CH protons in the cyclohexyl groups. However, the two-bond proton-phosphorus coupling ($^2J_{\text{HP}}$) is not observed, probably because the signal is a little broader than usual and the value of $^2J_{\text{HP}}$ is typically small. The multiplets at δ_{H} 1.00–1.62 ppm are assigned to the CH_2 protons in the cyclohexyl groups. As in the tin derivative **37**, the multiplets in the lead(II) dicyclohexylphosphanide **38** are not resolved even at low temperature on the NMR timescale (Figure 65).

Figure 65. VT- ^1H NMR spectra (400 MHz, toluene- d_8) of $[(\text{BDI}_{\text{DIPP}})\text{PbPCy}_2]$ (**38**), where A = $\gamma\text{-H}$, B = CHMe_2 and C = Cy-CH



The $^{31}\text{P}\{^1\text{H}\}$ NMR spectrum of **38** in C_6D_6 shows a single resonance at δ_{P} 26.9 ppm with lead satellites ($^1J_{\text{PPb}} = 1103$ Hz). The phosphorus-lead coupling constant is similar to that in the lead(II) diphenylphosphanide **35** ($^1J_{\text{PPb}} = 1130$ Hz). A VT- $^{31}\text{P}\{^1\text{H}\}$ NMR experiment in toluene- d_8 shows a single resonance at δ_{P} 26.9 ppm with lead satellites ($^1J_{\text{PPb}} = 1105$ Hz) at 30 °C. The phosphorus resonance shifts upfield to δ_{P} 19.7 ppm and that the phosphorus-lead coupling constant decreases to $^1J_{\text{PPb}} = 950$ Hz ($\Delta^1J_{\text{PPb}} = 155$ Hz) at -80 °C. These findings are similar to those for the tin(II) dicyclohexylphosphanide **37**.

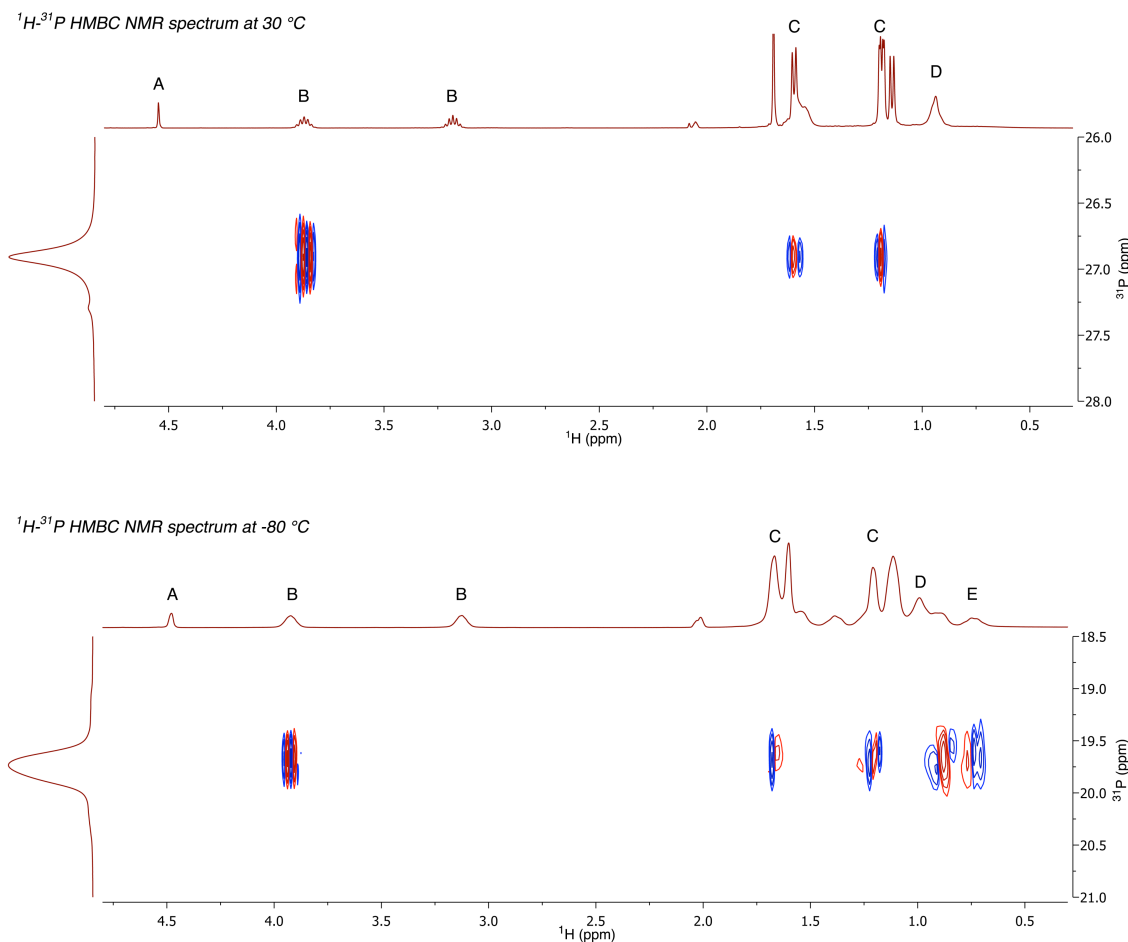
Figure 66. VT- $^{31}\text{P}\{^1\text{H}\}$ NMR spectra (162 MHz, toluene- d_8) of $[(\text{BDI}_{\text{DIPP}})\text{PbPCy}_2]$ (**38**)



A $^1\text{H}\text{-}^{31}\text{P}$ HMBC NMR experiment on the lead(II) dicyclohexylphosphanide **38** in toluene- d_8 at 30 °C shows correlations between the phosphorus signal (δ_{P} 26.9 ppm) and the isopropyl CHMe_2 signal at δ_{H} 3.90 ppm, as well as between the phosphorus and the isopropyl methyl (CHMe_2) signals at δ_{H} 1.62 and 1.20 ppm (Figure 67). At -80 °C, the $^1\text{H}\text{-}^{31}\text{P}$ HMBC NMR spectrum shows additional correlations between the phosphorus signal at δ_{P} 19.7 ppm and one of the cyclohexyl CH_2 proton signals at δ_{H} 0.71 ppm, as well as between the phosphorus and the tertiary cyclohexyl CH proton signal at δ_{H} 0.92 ppm. It is possible that at low temperature, steric interactions between the cyclohexyl

and *N*-aryl groups lead to changes in the pyramidalisation at phosphorus, giving additional detectable proton-phosphorus coupling (Figure 67) and significant changes in the observed $^1J_{\text{PbP}}$ (Figure 66, Page 161).

Figure 67. ^1H - ^{31}P HMBC NMR spectra of $[(\text{BDI}_{\text{DIP}})\text{PbPCy}_2]$ (**38**) in toluene- d_8 at 30 °C (top) and -80 °C (bottom), where A = γ -H, B = CHMe_2 , C = CHMe_2 , D = Cy-CH and E = Cy- CH_2

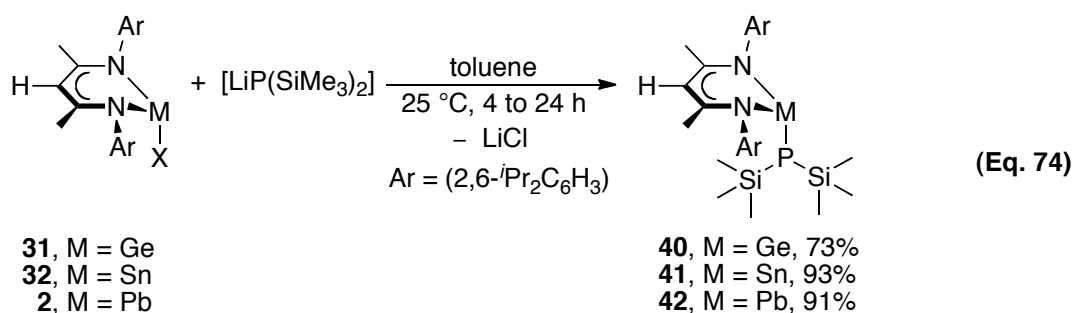


The $^{13}\text{C}\{^1\text{H}\}$ NMR spectrum of the lead(II) dicyclohexylphosphanide **38** shows through-space carbon-phosphorus couplings (J_{CP}) between the phosphorus and a tertiary isopropyl carbon signal (CHMe_2 : δ_{C} 29.2 ppm, $^5J_{\text{CP}} = 6$ Hz), as well as between the phosphorus and an isopropyl methyl carbon signal (CHMe_2 : δ_{C} 25.8 ppm, $^6J_{\text{CP}} = 11$ Hz). A doublet centred at δ_{C} 34.4 ppm ($^1J_{\text{CP}} = 34$ Hz) is assigned to the tertiary CH carbon in the cyclohexyl groups. The ^{207}Pb NMR spectrum of **38** shows a doublet centred at δ_{Pb} 3981 ppm, with lead-phosphorus coupling $^1J_{\text{PbP}} = 1074$ Hz. This resonance is downfield from the diphenylphosphanide analogue **35** (δ_{Pb} 3011 ppm).

4.2.7 Synthesis of β -diketiminato heavy group 14 metal bis(trimethylsilyl)-phosphanides **40–42**

The β -diketiminatogermanium(II) and -lead(II) bis(trimethylsilyl)phosphanides **40** and **42** have been synthesised by Driess *et al.*^[103, 134] However, the tin(II) derivative **41** has not been reported. The synthesis of the germanium(II) bis(trimethylsilyl)phosphanide **40** involved treatment of the germanium(II) chloride **31** with $[\text{LiP}(\text{SiMe}_3)_2 \cdot (\text{DME})]$ (DME = 1,2-dimethoxyethane) in diethyl ether at $-20\text{ }^\circ\text{C}$.^[134] The lead(II) derivative **42** was synthesised by treatment of the lead(II) aryloxide $[(\text{BDI}_{\text{DIPP}})\text{PbOAr}]$ (Ar = 2,6- t Bu₂C₆H₃) with $[\text{LiP}(\text{SiMe}_3)_2 \cdot (\text{DME})]$ in diethyl ether at $-60\text{ }^\circ\text{C}$.^[103]

For the β -diketiminatotin(II) bis(trimethylsilyl)phosphanide **41**, we used a methodology similar to that described previously in this thesis for the other phosphanides. The lithium bis(trimethylsilyl)phosphanide $[\text{LiP}(\text{SiMe}_3)_2]$ is isolated as a white solid from the reaction between bis(trimethylsilyl)phosphine and *n*-butyllithium in *n*-hexane at $0\text{ }^\circ\text{C}$. Treatment of the β -diketiminatotin(II) chloride **32** with $[\text{LiP}(\text{SiMe}_3)_2]$ in toluene at room temperature gives the β -diketiminatotin(II) bis(trimethylsilyl)phosphanide **41** in near quantitative yield (93%) (equation 74). The germanium(II) and lead(II) derivatives, $[(\text{BDI}_{\text{DIPP}})\text{GeP}(\text{SiMe}_3)_2]$ (**40**) and $[(\text{BDI}_{\text{DIPP}})\text{PbP}(\text{SiMe}_3)_2]$ (**42**), are made similarly in good yields (73% and 91%, respectively).



Compounds **40–42** are soluble in common aprotic organic solvents, such as toluene and *n*-hexane. These bis(trimethylsilyl)phosphanido complexes, especially the lead(II) derivative **42**, are extremely sensitive to air, moisture and light. Metallic precipitates are formed when they are allowed to stand in toluene under ambient light for 24 hours at room temperature. However, the compounds can be stored without decomposition as solids for several weeks at $-30\text{ }^\circ\text{C}$ under an inert atmosphere of dinitrogen.

Multinuclear NMR spectroscopic data of the β -diketiminatogermanium(II) and -lead(II) bis(trimethylsilyl)phosphanides **40** and **42** are similar to those reported in the literature (*vide infra*)^[103, 134] The β -diketiminatotin(II) bis(trimethylsilyl)phosphanide **41** is characterised by multinuclear NMR spectroscopy and X-ray crystallography. The elemental analysis of compound **41** is in good agreement with the calculated values.

4.2.8 X-ray crystal structures of the β -diketiminato heavy group 14 metal bis(trimethylsilyl)phosphanides **40–42**

The solid state structures of the β -diketiminatogermanium(II) and -lead(II) bis(trimethylsilyl)phosphanides **40** and **42** have already been reported, so these are discussed only briefly.^[103, 134]

The germanium(II) bis(trimethylsilyl)phosphanide **40** adopts an *endo* conformation, with the metal centre 0.551 Å below the mean NCCCN plane of the β -diketiminato ligand.^[134] The germanium centre is pyramidally coordinated with the sum of bond angles 288.6°. However, an almost planar geometry at phosphorus is found, with the sum of bond angles at phosphorus 355.2°. Scheer *et al.* recently reported a germanium(II) phosphanide [ArGeP(SiMe₃)₂] (Ar = (2,6-Trip₂C₆H₃), Trip = (2,4,6-ⁱPr₃C₆H₂)) which contains a terminal bis(trimethylsilyl)phosphanido ligand with the sum of bond angles around phosphorus 326.7°.^[206] The Ge–P bond length in **40** is 2.3912(8) Å.

Single crystals of [(BDI_{DIPP})SnP(SiMe₃)₂] (**41**) were obtained from pentane at –30 °C. ORTEP drawings are shown in Figures 68 and 69. Selected bond lengths and angles are given in Table 35, and selected crystallographic data in Table 36. The compound adopts an *endo* conformation, with the tin atom 0.595 Å below the mean NCCCN plane of the β -diketiminato ligand. The geometry around the tin atom is pyramidal with the sum of bond angles at the metal centre 282.5°. The coordination of the phosphorus is planar within experimental error, with the sum of bond angles at phosphorus 359.1°. Although previous examples of phosphorus adopting a planar geometry in transition metal chemistry have been attributed to donation of the phosphorus lone pair of electrons into empty d-orbitals on the transition metal, similar electron donation is unlikely in the heavy group 14 metal derivatives.^[190] Hence, we reason that the planar coordination

geometry at phosphorus found in the germanium(II) and tin(II) bis(trimethylsilyl)phosphanides **40** and **41** must be attributed to crowding from the β -diketiminato ligand, assisted by electronic effects associated with the trimethylsilyl groups (Section 4.1.2, Page 107). The Sn–P–Si(2) bond angle ($136.45(4)^\circ$) is wider than the remaining angles around the phosphorus (Sn–P–Si(1) = $111.29(4)^\circ$ and Si(1)–P–Si(2) = $111.32(4)^\circ$). The distortion may contribute to relief of steric strain from nearby *N*-aryl substituents. Similar distortions are found in the germanium(II) derivative **40**.^[134] Delocalisation within the C₃N₂Sn unit in the β -diketiminato ligand is evident, but it does not extend on to the *N*-aryl substituents (dihedral angles: C(11)–C(6)–N(1)–Sn = $85.4(3)^\circ$ and C(23)–C(18)–N(2)–Sn = $-87.3(3)^\circ$). Discounting the trimethylsilyl groups, there is an approximate plane of symmetry passing through the atoms C(2), Sn and P, and bisecting the β -diketiminato ring. The folding angle between the mean NCCCN plane in the β -diketiminato ligand and the plane defined by atoms N(1), Sn and N(2) is 20.9° , similar to that in the germanium(II) derivative **40** (22.1°).^[134] The Sn–P bond distance ($2.5526(7)$ Å) in the tin(II) bis(trimethylsilyl)phosphanide **41** is similar to those in Scheer's [(2,6-Trip-C₆H₃)SnP(SiMe₃)₂] (Trip = (2,4,6-*i*-Pr₃C₆H₂), Sn–P = $2.527(1)$ Å), Westerhausen's [[μ -P(SiMe₃)₂]₂SnP(SiMe₃)₂]₂Ba] (Sn–P = 2.597 Å) and Driess' [[{(*t*-Bu)F(Ar)Si} {*i*-Pr₃Si}P]₂Sn] (Ar = (2,4,6-*i*-Pr₃C₆H₂), Sn–P = $2.567(1)$ Å).^[206, 211, 271]

Figure 68. ORTEP diagram of $[(BDI_{DIPP})SnP(SiMe_3)_2]$ (**41**). H atoms are omitted and C atoms in the *N*-aryl groups in the β -diketiminato ring are minimised for clarity. The ellipsoid probability is shown at 30%

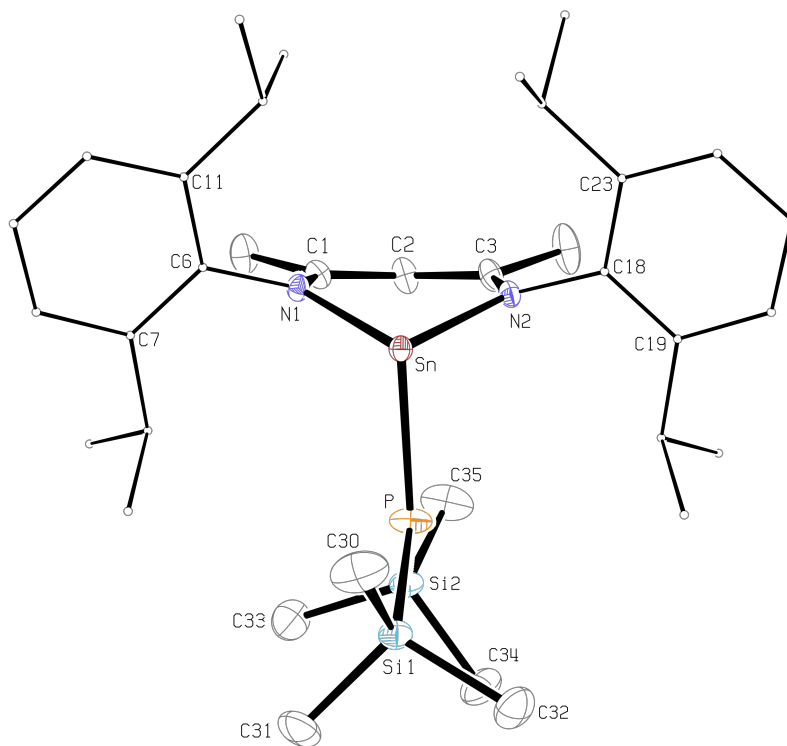


Figure 69. ORTEP diagram showing the side-on view of $[(BDI_{DIPP})SnP(SiMe_3)_2]$ (**41**). H atoms are omitted and C atoms in the *N*-aryl groups in the β -diketiminato ring are minimised for clarity. The ellipsoid probability is shown at 30%

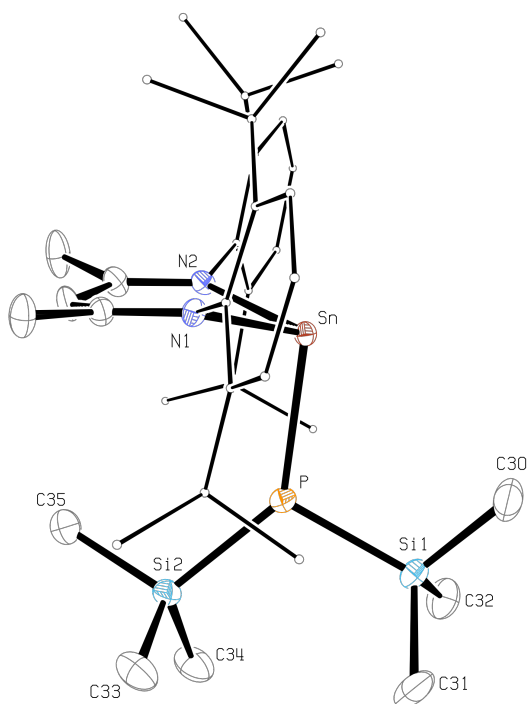


Table 35. Selected bond lengths (Å) and angles (deg) for [(BDI_{DIPP})SnP(SiMe₃)₂] (**41**)

<i>Bond lengths (Å)</i>			
Sn–N(1)	2.217(2)	C(1)–C(4)	1.514(4)
Sn–N(2)	2.2210(19)	C(3)–C(5)	1.516(4)
N(1)–C(1)	1.331(3)	Sn–P	2.5526(7)
N(2)–C(3)	1.324(3)	P–Si(1)	2.2166(10)
C(1)–C(2)	1.397(4)	P–Si(2)	2.2215(11)
C(2)–C(3)	1.404(4)		
Sn–NCCCN _{plane}	0.595		
<i>Bond angles (deg)</i>			
N(1)–Sn–N(2)	85.17(7)	N(1)–Sn–P	101.77(5)
Sn–N(1)–C(1)	124.76(17)	N(2)–Sn–P	95.55(5)
Sn–N(2)–C(3)	124.42(16)	Sn–P–Si(1)	111.29(4)
N(1)–C(1)–C(2)	124.0(2)	Sn–P–Si(2)	136.45(4)
N(2)–C(3)–C(2)	125.1(2)	Si(1)–P–Si(2)	111.32(4)
C(1)–C(2)–C(3)	129.9(2)		
Σ bond angle around Sn	282.5	Σ bond angle around P	359.1
DOP of Sn (%) ^a	86	DOP of P (%) ^a	1
NCCCN _{plane} –NSnN _{plane}	20.9		
<i>Dihedral angles (deg)</i>			
C(11)–C(6)–N(1)–Sn	85.4(3)	C(23)–C(18)–N(2)–Sn	–87.3(3)

^a Degree of pyramidalisation (DOP, %) = [(360 – Σ_{bond angle}) / 0.9]^[115] When a DOP is 100%, it is equivalent to a sum of bond angles of 270°, whereas a DOP of 0% indicates a planar geometry at the central atom

Table 36. Selected crystallographic data for [(BDI_{DIPP})SnP(SiMe₃)₂] (**41**)

[(BDI _{DIPP})SnP(SiMe ₃) ₂] (41)	
chemical formula	C ₃₅ H ₅₉ N ₂ PSi ₂ Sn
molecular mass	713.68
temperature (K)	173(2)
wavelength (Å)	0.71073
crystal system	monoclinic
space group	<i>P</i> 2 ₁ / <i>c</i> (No. 14)
<i>a</i> (Å)	12.1569(2)
<i>b</i> (Å)	15.7065(2)
<i>c</i> (Å)	23.4050(4)
<i>α</i> (deg)	90
<i>β</i> (deg)	119.547(1)
<i>γ</i> (deg)	90
<i>V</i> (Å ³)	3887.82(10)
<i>Z</i>	4
ρ_{calcd} (Mg m ⁻³)	1.22
θ range (deg)	3.48–27.10
abs coeff (mm ⁻¹)	0.78
measd/indep reflns/ <i>R</i> (int)	60 531/8547/0.076
data/restraints/param	8547/0/372
goodness of fit on <i>F</i> ²	0.991
final <i>R</i> indices [<i>I</i> > 2 σ (<i>I</i>)]	<i>R</i> 1 = 0.034, <i>wR</i> 2 = 0.070
<i>R</i> indices (all data)	<i>R</i> 1 = 0.056, <i>wR</i> 2 = 0.078
largest diff peak and hole (e Å ⁻³)	0.45 and -0.69

In contrast to the germanium(II) and tin(II) bis(trimethylsilyl)phosphanides **40** and **41**, the reported lead(II) derivative **42** adopts an *exo* conformation, with the lead atom 1.251 Å above the mean NCCCN plane of the β -diketiminato ligand.^[103] The geometry around the lead atom is pyramidal with the sum of bond angles 281.7°. The phosphorus is also pyramidally coordinated, with the sum of bond angles 305.7°. The folding angle between the mean NCCCN plane in the β -diketiminato ligand and the plane defined by the atoms N(1), Pb and N(2) is 43.9°, i.e. larger than those in the germanium(II) and tin(II) analogues **40** and **41** (22.1° and 20.9°, respectively). The Pb–P bond length is 2.715(2) Å, similar to those in the β -diketiminatolead(II) diphenylphosphanide **35** (2.720(2) Å) and dicyclohexylphosphanide **38** (2.6945(9) Å).

4.2.9 NMR spectra of the β -diketiminato heavy group 14 metal bis(trimethylsilyl)phosphanides **40–42**

Selected multinuclear NMR spectroscopic data for **40–42** are given in Table 37.

Table 37. Selected multinuclear NMR spectroscopic data (30 °C) for [LMP(SiMe₃)₂] (L = (BDI_{DIPP}); **40**, M = Ge; **41**, M = Sn; and **42**, M = Pb) in C₆D₆, unless specified

	[LGeP(SiMe ₃) ₂] (40)	[LSnP(SiMe ₃) ₂] (41)	[LPbP(SiMe ₃) ₂] (42)
	δ (ppm), J (Hz) ^a	δ (ppm), J (Hz) ^a	δ (ppm), J (Hz) ^a
¹H			
γ -H	5.06 (s)	4.95 (s)	4.75 (s)
CHMe ₂	3.90 (d-septet) ³ J _{HH} = 6.5; ⁶ J _{HP} = 1.5	3.98 (d-septet) ³ J _{HH} = 6.8; ⁶ J _{HP} = 1.6	3.92 (d-septet) ³ J _{HH} = 6.5; ⁶ J _{HP} = 1.0
	3.40 (septet) ³ J _{HH} = 6.5	3.38 (septet) ³ J _{HH} = 6.8	3.29 (septet) ³ J _{HH} = 6.5
SiMe ₃	0.44 (d) ³ J _{HP} = 5.0	0.46 (d) ³ J _{HP} = 4.4	0.30 (d) ³ J _{HP} = 4.0
¹³C{¹H}			
CHMe ₂	29.7 (d), ⁵ J _{CP} = 5 29.5 (s)	29.9 (d), ⁵ J _{CP} = 4 29.6 (s), ⁴ J _{C_{Sn}} = 21	29.0 (s) 28.4 (d), ⁵ J _{CP} = 6
CHMe ₂	28.6 (d), ⁶ J _{CP} = 5 25.6, 25.3, 25.1 (s)	28.2 (d), ⁶ J _{CP} = 5 25.5, 25.4, 25.0 (s)	28.2 (d), ⁶ J _{CP} = 5 26.1, 25.2, 25.1 (s)
SiMe ₃	6.0 (d) ² J _{CP} = 10	6.4 (d) ² J _{CP} = 11 ¹ J _{C_{Si}} = 39 ³ J _{C_{Sn}} = 60	7.5 (d) ² J _{CP} = 10
³¹P{¹H}			
	-192.8 (s) ¹ J _{PSi} = 16	-183.5 (s) ¹ J _{PSi} = 16 ¹ J _{P¹¹⁹Sn} = 2436 ¹ J _{P¹¹⁷Sn} = 2327	-116.0 (s) ¹ J _{PPb} = 2874
²⁹Si{¹H}			
	1.8 (d) ^b ¹ J _{SiP} = 17	4.0 (d) ¹ J _{SiP} = 18	7.2 (d) ¹ J _{SiP} = 36
Other			
	–	δ (¹¹⁹ Sn) = 39 ¹ J _{P¹¹⁹SnP} = 2421	δ (²⁰⁷ Pb) = -1737 ^c

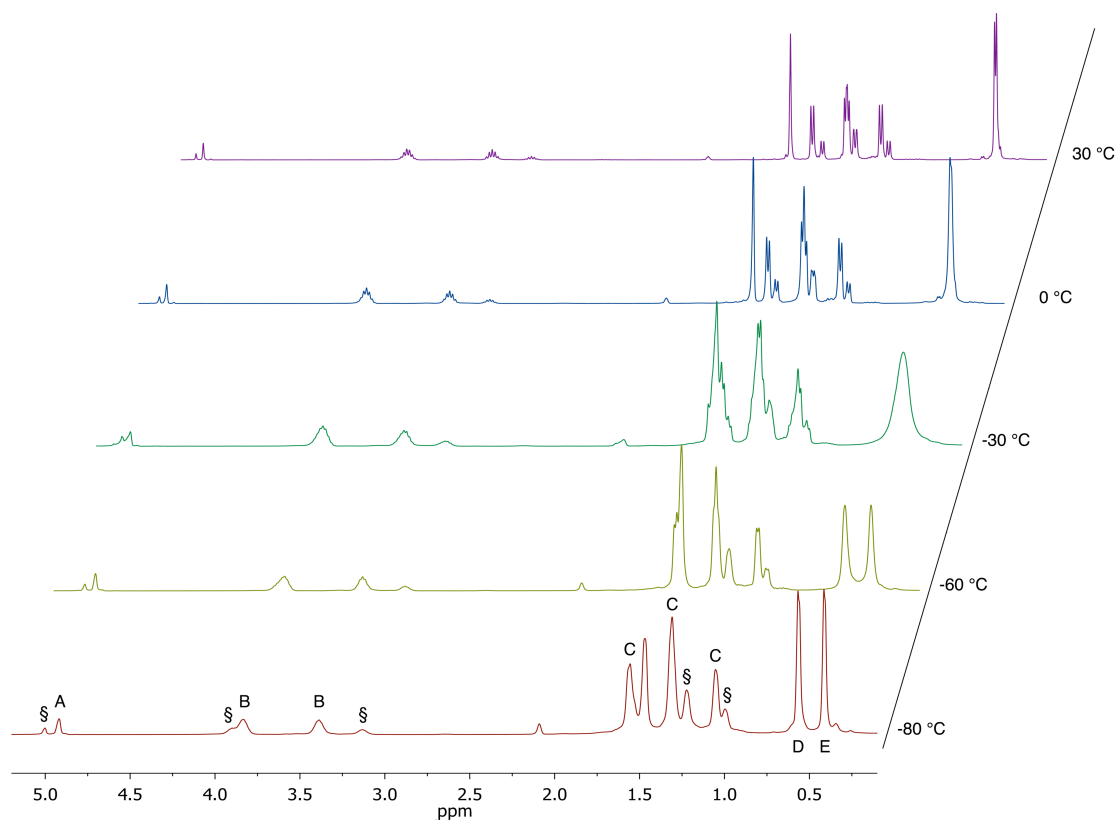
^a superscript indicates number of bonds between nuclei; ^b in toluene-*d*₆; ^c result from literature^[103]

4.2.9.1 The β -diketiminatogermanium(II) bis(trimethylsilyl)phosphanide **40**

The multinuclear NMR spectroscopic data obtained for the germanium derivative **40** are consistent with those reported in Driess' publication.^[134] As for the other β -diketiminato heavy group 14 metal phosphanides discussed in this thesis, the ^1H NMR spectrum of the germanium(II) bis(trimethylsilyl)phosphanide **40** shows a doublet of septets centred at δ_{H} 3.90 ppm, assigned to a tertiary isopropyl proton (CHMe_2) resonance, with through-bond proton-proton coupling ($^3J_{\text{HH}} = 6.5$ Hz), which is further split by through-space proton-phosphorus coupling ($^6J_{\text{HP}} = 1.5$ Hz). A doublet centred at δ_{H} 0.44 ppm is assigned to the protons in the trimethylsilyl substituents (SiMe_3), with through-bond proton-phosphorus coupling ($^2J_{\text{HP}} = 5.0$ Hz).

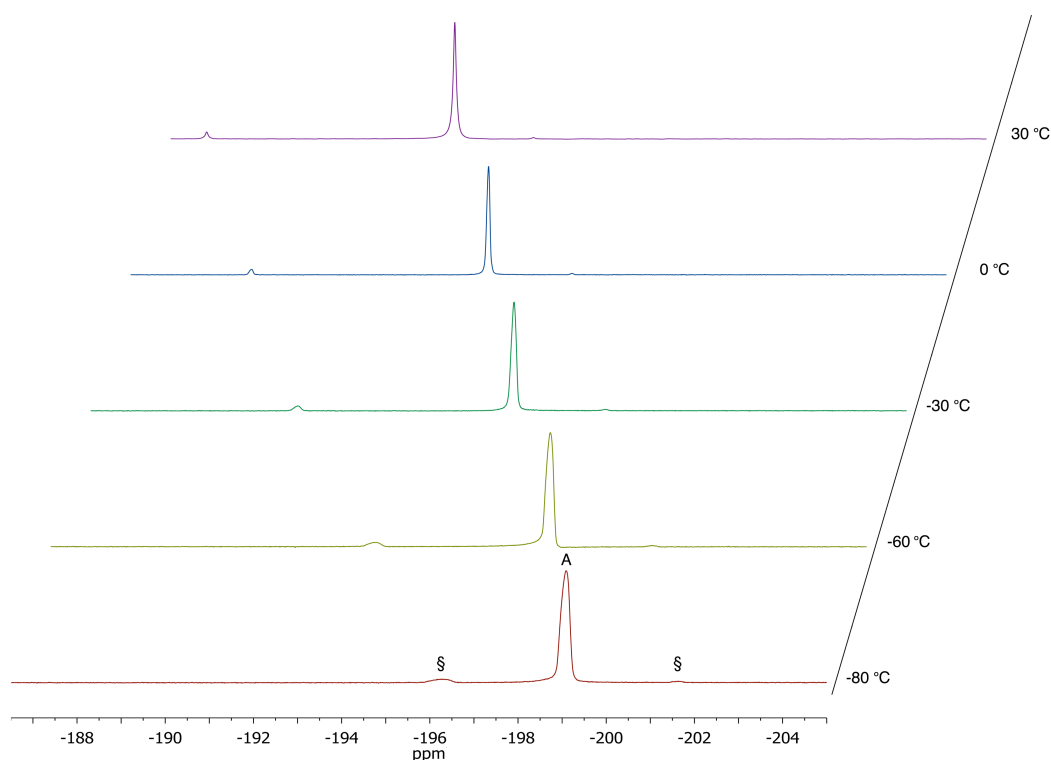
It was previously shown that in $[(\text{BDI}_{\text{DIPP}})\text{PbN}(\text{SiMe}_3)_2]$, two broad resonances in the ^1H NMR spectrum at room temperature could be assigned to the protons in the trimethylsilyl (SiMe_3) groups.^[62] These signals were split into two well-defined singlets (δ_{H} 0.46 and 0.12 ppm) at -40 °C. It was suggested that rotation about the $\text{Pb}-\text{N}_{\text{amide}}$ bond was hindered to give inequivalent trimethylsilyl groups on the NMR timescale.^[62] Given the similarity of the planar coordination geometry at phosphorus in **40** and **41**, similar behaviour is predicted for the β -diketiminatogermanium(II) and -tin(II) bis(trimethylsilyl)phosphanides **40** and **41**. The ^1H NMR spectrum of **40** recorded at 30 °C shows a doublet centred at δ_{H} 0.42 ppm in toluene- d_8 with $^3J_{\text{HP}} = 4.4$ Hz (Figure 70). This is assigned to the protons in the SiMe_3 substituents. Although the sample used in this study was contaminated with an unidentified impurity, the resonance separated into two distinct signals (δ_{H} 0.60 and 0.41 ppm) with equal intensity at -80 °C. The three-bond proton-phosphorus coupling is not resolved. From the coalescence temperature (-30 °C), the energy associated with the barrier of rotation about the $\text{Ge}-\text{P}$ bond is estimated to be 48.7 kJ mol^{-1} (Appendix 4, Page 341).

Figure 70. VT- ^1H NMR spectra (400 MHz, toluene- d_6) of $[(\text{BDI}_{\text{DIPP}})\text{GeP}(\text{SiMe}_3)_2]$ (**40**), where A = $\gamma\text{-H}$; B = CHMe_2 ; C = CHMe_2 ; and D & E = SiMe_3 . The unidentified contaminant is designated by \S



The $^{31}\text{P}\{^1\text{H}\}$ NMR spectrum of **40** shows a single resonance at $\delta_{\text{P}} -192.8$ ppm, with silicon satellites ($^1J_{\text{PSi}} = 16$ Hz). This resonance is upfield from those in $[(\text{BDI}_{\text{DIPP}})\text{GePPh}_2]$ (**33**, $\delta_{\text{P}} -36.0$ ppm), $[(\text{BDI}_{\text{DIPP}})\text{GePCy}_2]$ (**36**, $\delta_{\text{P}} -14.1$ ppm), and Scheer's $[(2,6\text{-Trip}_2\text{C}_6\text{H}_3)\text{GeP}(\text{SiMe}_3)_2]$ (Trip = $(2,4,6\text{-}^i\text{Pr}_3\text{C}_6\text{H}_2)$, $\delta_{\text{P}} -48.6$ ppm).^[206] In a VT- $^{31}\text{P}\{^1\text{H}\}$ NMR spectroscopic study, a single resonance at $\delta_{\text{P}} -192.9$ ppm in toluene- d_8 was found at 30 °C (Figure 71). With decreasing temperature, the phosphorus resonance shifted upfield to $\delta_{\text{P}} -199.1$ ppm at -80 °C. This upfield shift is also found in the VT- $^{31}\text{P}\{^1\text{H}\}$ NMR spectroscopic studies of the tin(II) and lead(II) dicyclohexylphosphanides **37** and **38** (Figure 63, Page 158; and Figure 66, Page 161). At low temperature, the $^{31}\text{P}\{^1\text{H}\}$ NMR spectrum remains as a single signal, suggesting that there is no significant change in the Ge–P bond over the temperature range investigated, and that the planar coordination geometry at phosphorus, as found in the solid state, persists in solution.

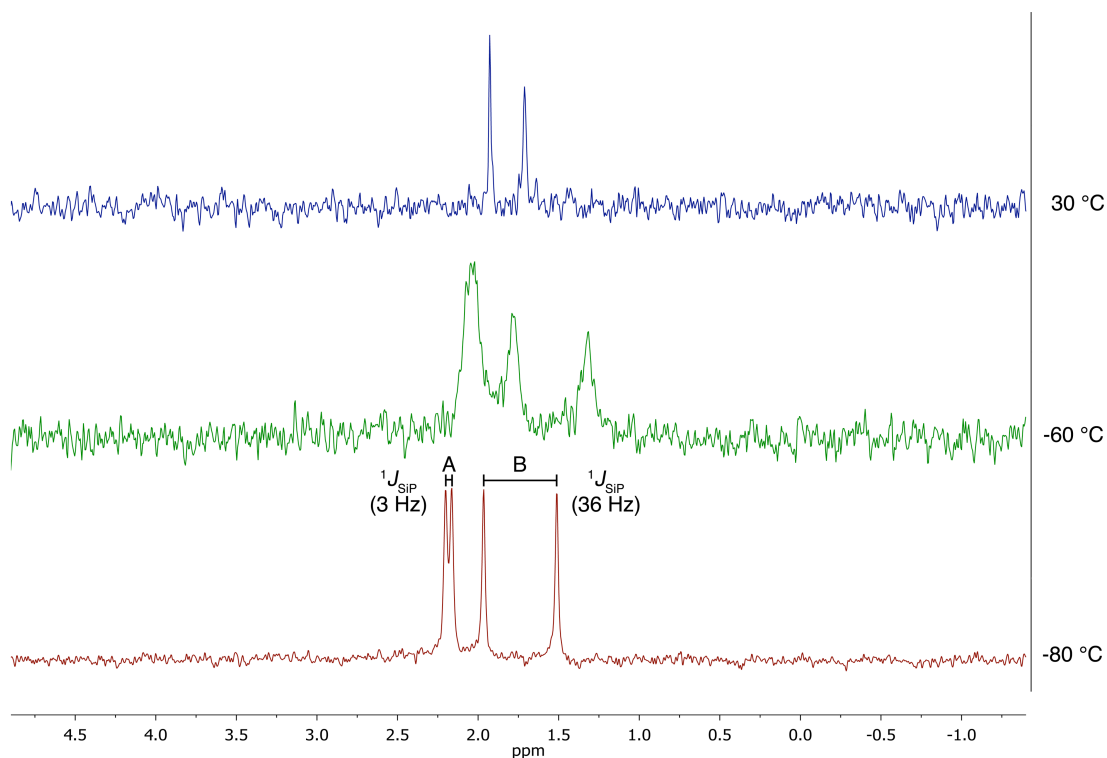
Figure 71. VT- $^{31}\text{P}\{^1\text{H}\}$ NMR spectra (162 MHz, toluene- d_8) of $[(\text{BDI}_{\text{DIPP}})\text{GeP}(\text{SiMe}_3)_2]$ (**40**), where A = phosphorus resonance. Impurities are designated by §



The $^{29}\text{Si}\{^1\text{H}\}$ NMR spectrum of **40** shows a doublet centred at δ_{Si} 1.8 ppm in toluene- d_8 , with silicon-phosphorus coupling ($^1J_{\text{SiP}} = 17$ Hz). A VT- $^{29}\text{Si}\{^1\text{H}\}$ NMR spectroscopic study shows three broad resonances at δ_{Si} 2.0, 1.8 and 1.3 ppm at -60 °C (Figure 72). When the temperature was decreased to -80 °C, the $^{29}\text{Si}\{^1\text{H}\}$ NMR spectrum shows two doublets, (A) centred at δ_{Si} 2.2 ppm and (B) centred at δ_{Si} 1.7 ppm (Figure 72). However, there is a large difference in the silicon-phosphorus coupling constants, $^1J_{\text{SiP}} = 3$ Hz in (A) and $^1J_{\text{SiP}} = 36$ Hz in (B). In the literature, a silicon-phosphorus coupling constant ($^1J_{\text{SiP}}$) of *ca.* 30 Hz can be associated with trimethylsilyl groups bound to a phosphorus with a planar coordination geometry, for example in $[(2,6\text{-Trip}_2\text{C}_6\text{H}_3)\text{SnP}(\text{SiMe}_3)_2]$ (Trip = $(2,4,6\text{-}^i\text{Pr}_3\text{C}_6\text{H}_2)$, $^1J_{\text{SiP}} = 39$ Hz) and $[\{(\text{SiMe}_3)_2\text{P}\}_2\text{Mg}\cdot 2\text{THF}]$ ($^1J_{\text{SiP}} = 33$ Hz), whereas a small $^1J_{\text{SiP}}$ is found in a dimeric structure $[\text{Mg}\{\text{P}[\text{Si}(\text{H})^i\text{Pr}_2]_2\}_2]_2$ ($^1J_{\text{SiP}} < 4$ Hz).^[206, 272-273] From the limited evidence we have, we propose that the difference in $^1J_{\text{SiP}}$ is related to the variation in bond angles around the phosphorus atom with a planar coordination geometry as shown in the solid state structure of **40** (*c.f.* Si(1)–P–Ge = $111.14(4)^\circ$, Si(2)–P–Ge = $133.93(4)^\circ$ and Si(1)–P–Si(2) = $110.13(5)^\circ$).^[134] The coalescence temperature is estimated to be at -60

°C, and the energy associated with this process is approximate to be 42.1 kJ mol⁻¹ (Appendix 4, Page 341).

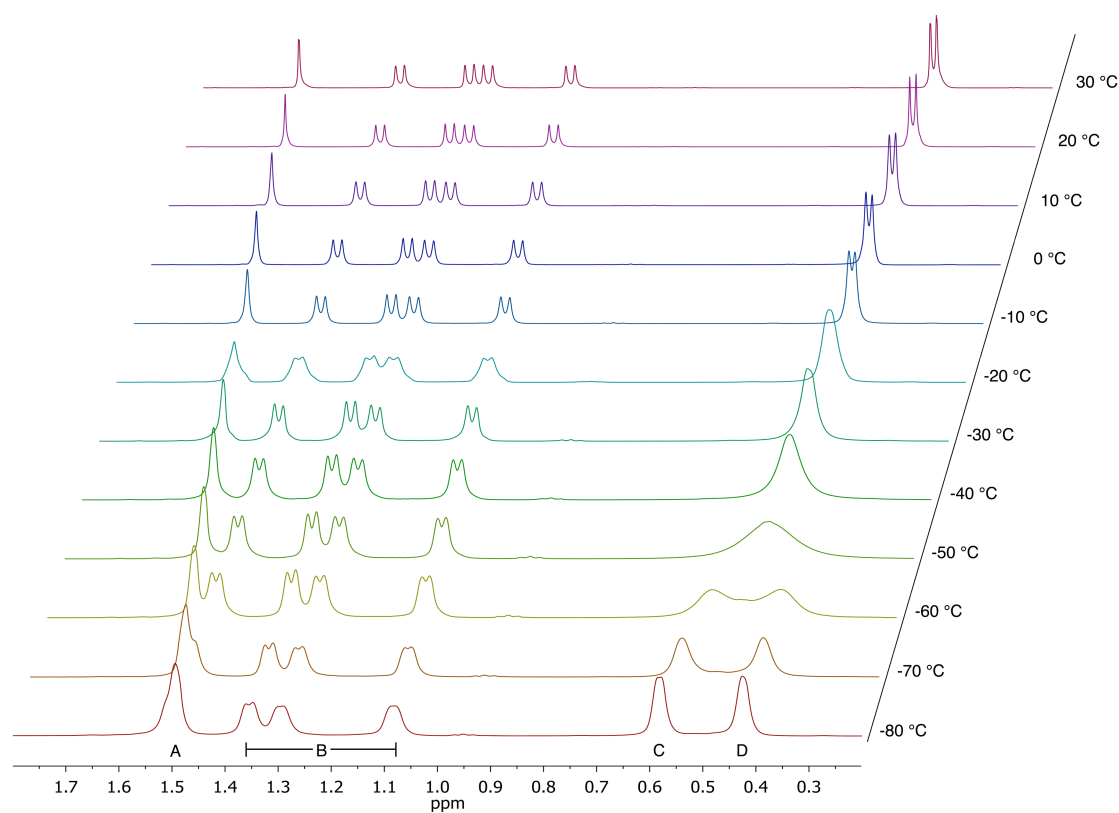
Figure 72. VT-²⁹Si{¹H} NMR spectra (79 MHz, toluene-*d*₈) of [(BDI_{DIPP})GeP(SiMe₃)₂] (**40**), showing two resonances, A and B



4.2.9.2 The β -diketiminatotin(II) bis(trimethylsilyl)phosphanide **41**

The ¹H NMR spectrum of **41** shows a doublet of septets centred at δ_{H} 3.98 ppm, assigned to a tertiary proton resonance of the isopropyl group (*CHMe*₂). This resonance shows a through-bond proton-proton coupling (³*J*_{HH} = 6.8 Hz) which is further split by a through-space proton-phosphorus coupling (⁶*J*_{HP} = 1.6 Hz). A doublet centred at δ_{H} 0.46 ppm, with proton-phosphorus coupling (³*J*_{HP} = 4.4 Hz), is assigned to the protons in the trimethylsilyl (*SiMe*₃) substituents. Hindered rotation about the Sn–P bond was investigated by a VT-¹H NMR experiment (Figure 73). With decreasing temperature, the *SiMe*₃ signal became broad at –50 °C, and resolved at –80 °C into two distinct signals, (C): δ_{H} 0.58 ppm and (D): δ_{H} 0.43 ppm, with equal intensity. These findings are similar to those observed in the germanium derivative **40**. The energy associated with the hindered rotation about the Sn–P bond is estimated to be 45.0 kJ mol⁻¹ (Appendix 4, Page 341).

Figure 73. VT- ^1H NMR spectra (400 MHz, toluene- d_8) of $[(\text{BDI}_{\text{DIPP}})\text{SnP}(\text{SiMe}_3)_2]$ (**41**), where A = NCMe; B = CHMe_2 ; and C & D = SiMe_3



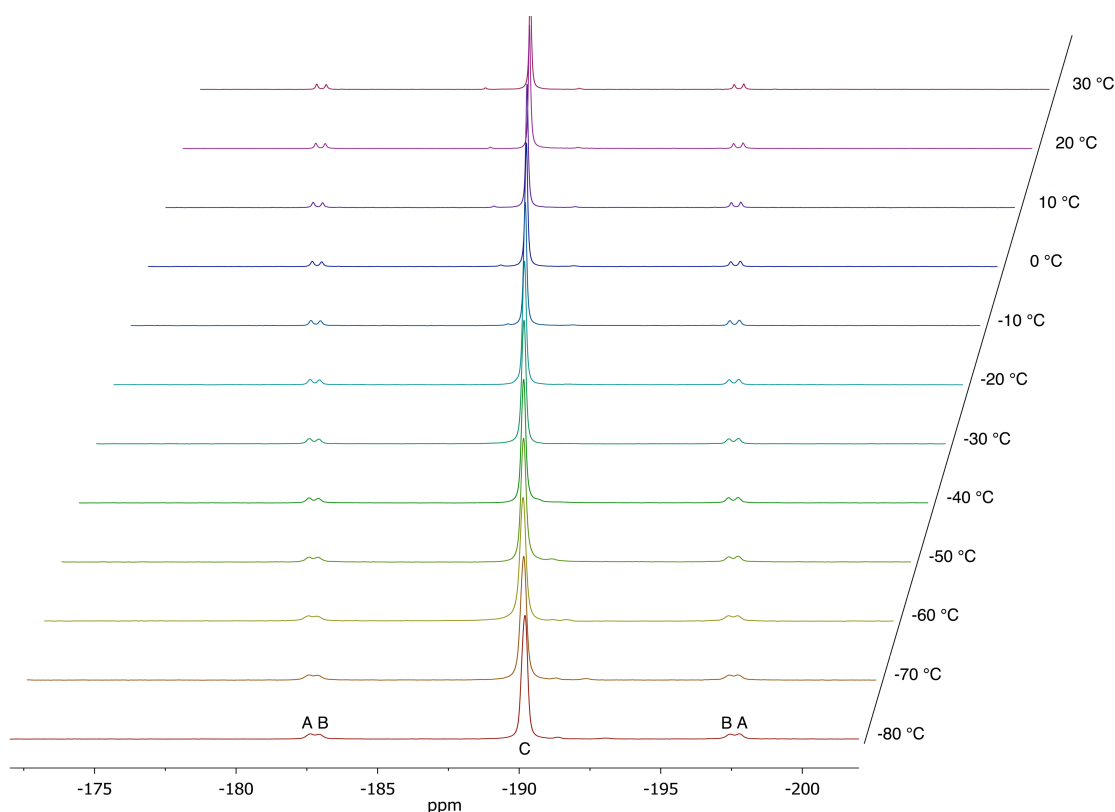
The $^31\text{P}\{^1\text{H}\}$ NMR spectrum of the tin(II) bis(trimethylsilyl)phosphanide **41** shows a single resonance at $\delta_{\text{P}} -183.5$ ppm with tin ($^1J_{\text{P}^{119}\text{Sn}} = 2436$ Hz and $^1J_{\text{P}^{117}\text{Sn}} = 2327$ Hz) and silicon satellites ($^1J_{\text{PSi}} = 16$ Hz). The phosphorus resonance of compound **41** is upfield from those in $[(\text{BDI}_{\text{DIPP}})\text{SnPPh}_2]$ (**34**, $\delta_{\text{P}} -30.8$ ppm) and $[(\text{BDI}_{\text{DIPP}})\text{SnPCy}_2]$ (**37**, $\delta_{\text{P}} -15.4$ ppm), but similar to that in Westerhausen's $[\text{R}_2\text{N}\{\text{Ca}(\mu\text{-PR}_2)_2\text{Ca}(\mu\text{-PR}_2)_2\}\text{SnPR}_2]$ ($\text{R} = \text{SiMe}_3$, $\delta_{\text{P}} -220$ ppm).^[274]

In general, the magnitude of the coupling constant 1J is dependent on the s-orbital contribution in the bond, though other factors may also be involved.^[194, 275] A large phosphorus-tin coupling constant ($^1J_{\text{PSn}} > 2000$ Hz) was previously considered as indicative of the presence of a tin-phosphorus multiple bond (Table 24, Page 114).^[204-206] However, to the best of our knowledge, solid state structure determination of a compound containing a tin-phosphorus multiple bond has not been reported. The phosphorus-tin coupling constant ($^1J_{\text{P}^{119}\text{Sn}} = 2436$ Hz) observed in the tin(II) bis(trimethylsilyl)phosphanide **41**, which contains a Sn–P single bond (Figures 68 and

69, Page 166) exceed those values reported for the stannaphosphenes (Table 24, Page 114); hence caution should be exercised when the phosphorus-tin coupling constant is used as the sole indicator of the presence of a tin-phosphorus multiple bond.

In a VT- $^{31}\text{P}\{^1\text{H}\}$ NMR experiment in toluene- d_8 , the phosphorus signal remains as a single resonance with no significant change in the phosphorus-tin coupling constant ($\Delta^1J_{\text{P}^{119}\text{Sn}} = 8 \text{ Hz}$) within the temperature range tested (30 to $-80 \text{ }^\circ\text{C}$) (Figure 74). These results suggest that the Sn–P bond does not change significantly under our experimental conditions.

Figure 74. VT- $^{31}\text{P}\{^1\text{H}\}$ NMR spectra (162 MHz, toluene- d_8) of $[(\text{BDI}_{\text{DIPP}})\text{SnP}(\text{SiMe}_3)_2]$ (**41**), where A = ^{119}Sn satellite, B = ^{117}Sn satellite and C = phosphorus resonance



The tin(II) bis(trimethylsilyl)phosphanide **41** adopts an *endo* conformation in the solid state, similar to that observed in the tin(II) chloride **32** (Figure 41, Page 132). The $^{13}\text{C}\{^1\text{H}\}$ NMR spectrum of compound **41** (Figure 75) shows through-space carbon-tin coupling in a tertiary isopropyl carbon resonance (CHMe_2 (**a**): $\delta_{\text{C}} 29.6 \text{ ppm}$, $^4J_{\text{CSn}} = 21 \text{ Hz}$), and through-space carbon-phosphorus coupling in other isopropyl resonances (CHMe_2 (**a'**): $\delta_{\text{C}} 29.9 \text{ ppm}$, $^5J_{\text{CP}} = 4 \text{ Hz}$; CHMe_2 (**b'**): $\delta_{\text{C}} 28.2 \text{ ppm}$, $^6J_{\text{CP}} = 5 \text{ Hz}$). These

results suggest that the tin and phosphorus atoms interact with different isopropyl substituents in solution. A close inspection of the solid state structure shows only the ‘adjacent’ isopropyl substituents are close enough to interact with the phosphorus (Figure 77). As in the tin(II) chloride **32**, the tin atom in the tin(II) bis(trimethylsilyl)phosphanide **41** interacts with the isopropyl substituents in the ‘opposite’ region (Figure 76). These results suggest that the overall *endo* conformation observed from the solid state is preserved in solution.

Figure 75. $^{13}\text{C}\{^1\text{H}\}$ NMR spectrum (100 MHz) of $[(\text{BDI}_{\text{DIPP}})\text{SnP}(\text{SiMe}_3)_2]$ (**41**) in C_6D_6 at 30 °C showing the J_{CP} and J_{CSn} ; **a** and **a'** are from CHMe_2 ; **b** and **b'** are from CHMe_2 ; **c** is from NCMe . The **ab**₂ and **a'b'**₂ indicate resonances from different pairs of isopropyl groups

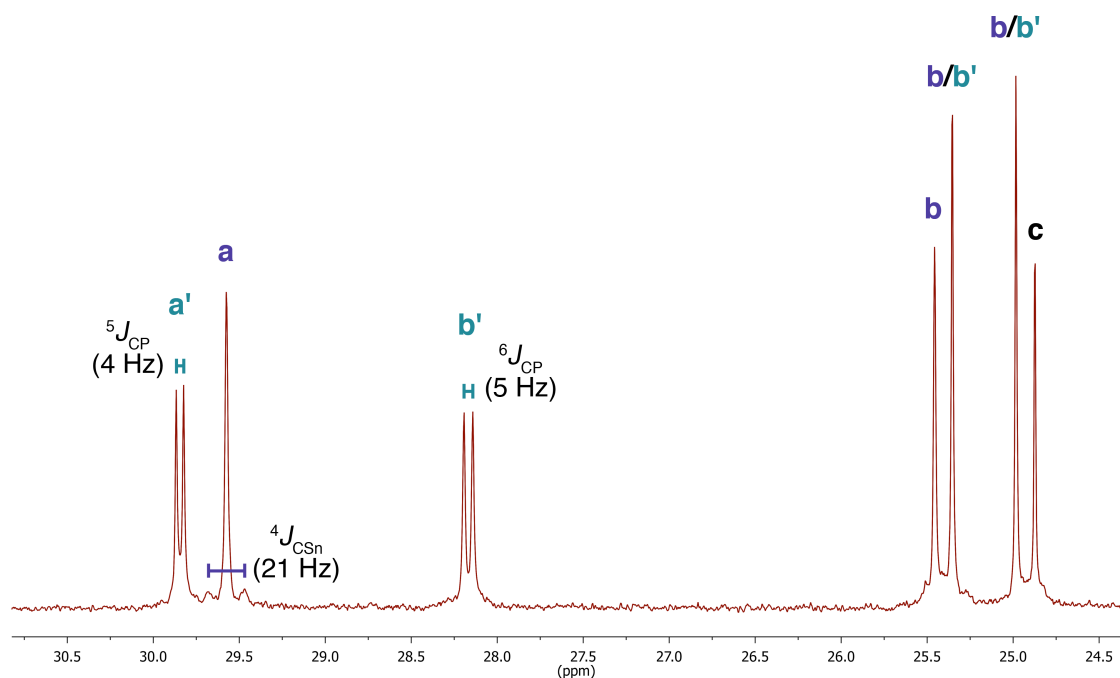


Figure 76. Schematic view of $[(\text{BDI}_{\text{DIPP}})\text{SnP}(\text{SiMe}_3)_2]$ (**41**) showing the relative distance between the tin atom and the isopropyl substituents. H atoms are omitted. The distances are obtained from the crystal structure data

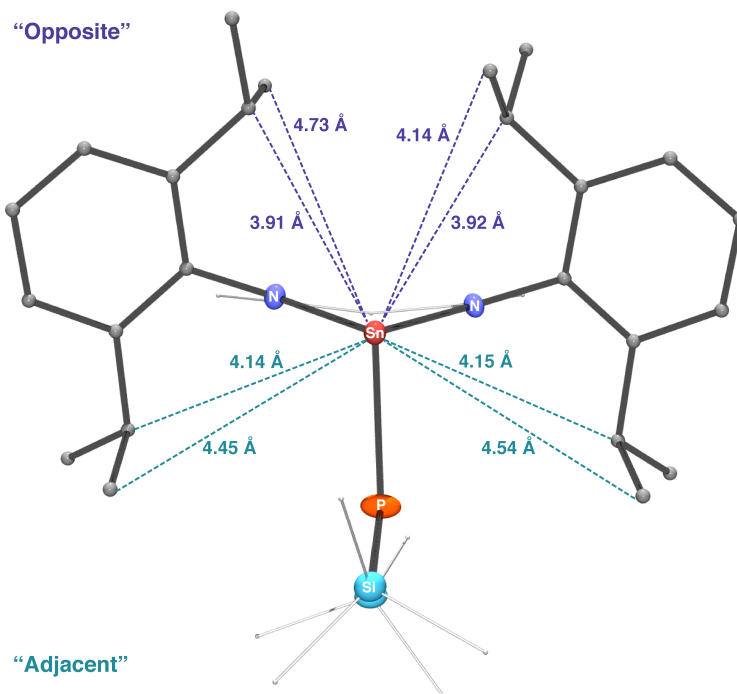
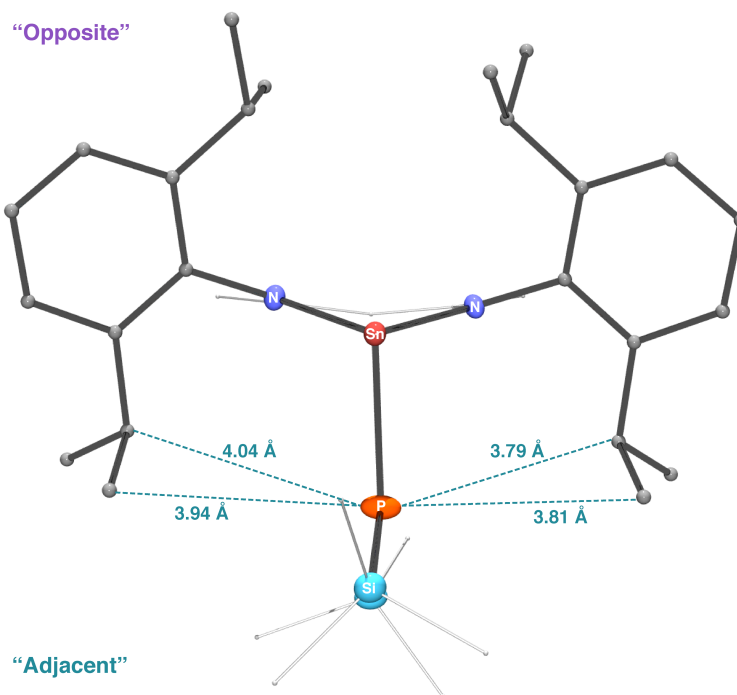


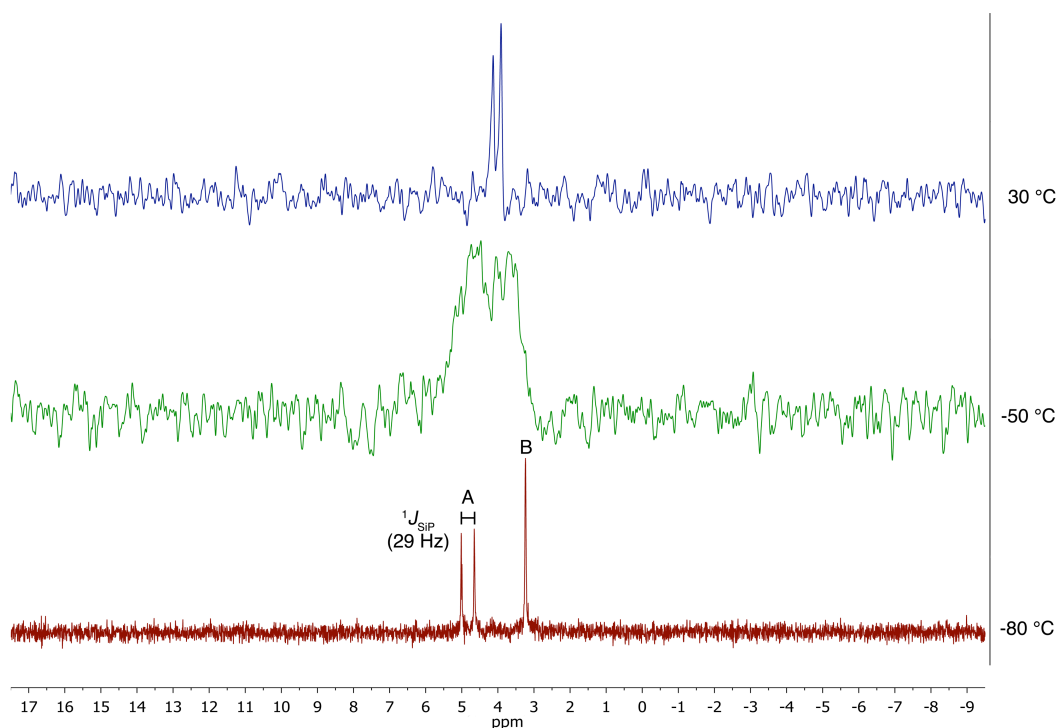
Figure 77. Schematic view of $[(\text{BDI}_{\text{DIPP}})\text{SnP}(\text{SiMe}_3)_2]$ (**41**) showing the relative distance between the phosphorus atom and the isopropyl substituents. H atoms are omitted. The distances are obtained from the crystal structure data



A doublet centred at δ_{Sn} 39 ppm with tin-phosphorus coupling ($^1J_{\text{SnP}} = 2421$ Hz) is observed in the ^{119}Sn NMR spectrum of compound **41** in C_6D_6 at 30 °C. The coupling constant $^1J_{\text{SnP}}$ is significantly larger than those observed in $[(\text{BDI}_{\text{DIPP}})\text{SnPPh}_2]$ (**34**, $^1J_{^{119}\text{SnP}} = 966$ Hz) and $[(\text{BDI}_{\text{DIPP}})\text{SnPCy}_2]$ (**37**, $^1J_{^{119}\text{SnP}} = 964$ Hz). At -80 °C, the ^{119}Sn NMR spectrum of the tin(II) bis(trimethylsilyl)phosphanide **41** in toluene- d_8 shows a doublet centred at δ_{Sn} 18 ppm with $^1J_{^{119}\text{SnP}} = 2450$ Hz.

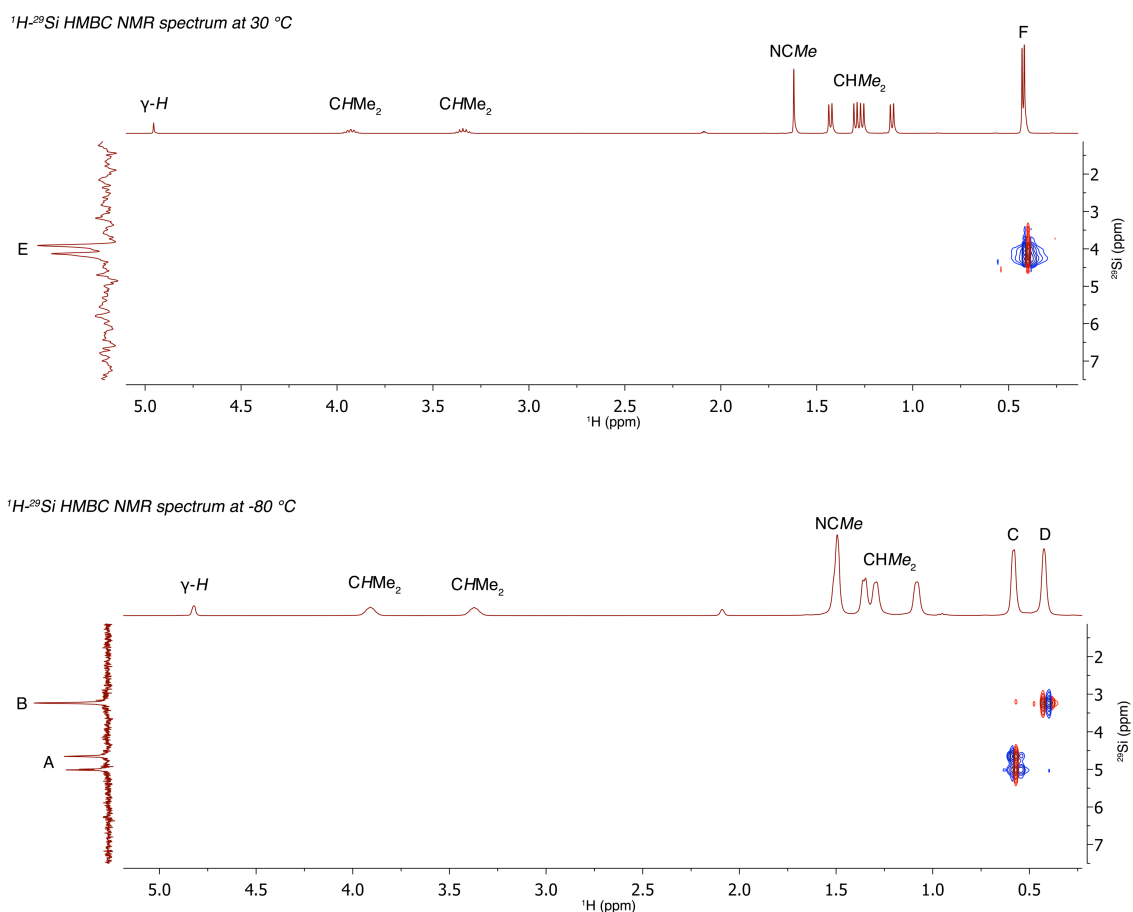
The $^{29}\text{Si}\{^1\text{H}\}$ NMR spectrum of **41** shows a doublet centred at δ_{Si} 4.0 ppm in C_6D_6 with silicon-phosphorus coupling $^1J_{\text{SiP}} = 18$ Hz. As with the germanium analogue **40**, a VT- $^{29}\text{Si}\{^1\text{H}\}$ NMR experiment shows that the silicon signal separates into two resonances, (A): at δ_{Si} 4.8 ppm and (B): at δ_{Si} 3.2 ppm, in toluene- d_8 at -80 °C (Figure 78). The resonance A is a doublet with silicon-phosphorus coupling $^1J_{\text{SiP}} = 29$ Hz, whereas the resonance B remains as a singlet. These results are consistent with the VT- ^1H NMR experiment in which the resonance assigned to the protons in the trimethylsilyl groups separates into two signals at low temperature (Figure 73, Page 174), suggesting that one silicon atom (A) couples more strongly to phosphorus than the other (B). The energy associated with this process is estimated to be 43.4 kJ mol $^{-1}$ (Appendix 4, Page 341).

Figure 78. VT- $^{29}\text{Si}\{^1\text{H}\}$ NMR spectra (79 MHz, toluene- d_8) of $[(\text{BDI}_{\text{DIPP}})\text{SnP}(\text{SiMe}_3)_2]$ (**41**) showing two silicon resonances A and B



The findings are confirmed by the ^1H - ^{29}Si HMBC NMR experiment of **41** (Figure 79). At 30 °C, the ^1H - ^{29}Si HMBC NMR spectrum shows a correlation between the silicon resonance (E: δ_{Si} 4.0 ppm) and the proton resonances of the SiMe_3 substituents (F: δ_{H} 0.43 ppm). However, at -80 °C, there are correlations between the silicon resonance A (δ_{Si} 4.8 ppm) and SiMe_3 resonance C (δ_{H} 0.58 ppm), as well as between the silicon resonance B (δ_{Si} 3.2 ppm) and the SiMe_3 resonance D (δ_{H} 0.43 ppm).

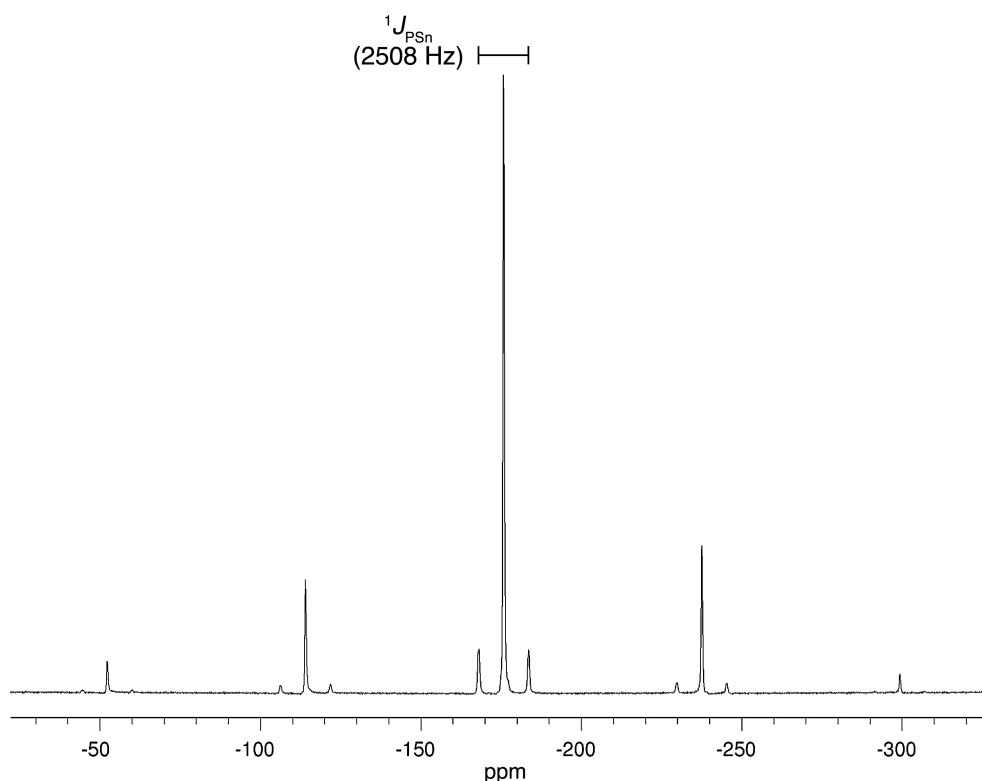
Figure 79. ^1H - ^{29}Si HMBC NMR spectra (toluene- d_6) of $[(\text{BDI}_{\text{DIPP}})\text{SnP}(\text{SiMe}_3)_2]$ (**41**) at 30 °C (top) and -80 °C (bottom), where A & B = silicon resonances; and C & D = proton resonances in SiMe_3 at -80 °C, E = silicon resonance and F = proton resonance in SiMe_3 at 30 °C



Evidence from multinuclear NMR experiments suggests that the overall conformation of the tin(II) bis(trimethylsilyl)phosphanide **41** observed in the solid state is preserved in solution. To investigate this further, a solid state $^{31}\text{P}\{^1\text{H}\}$ NMR spectrum was recorded (Figure 80). A single resonance at $\delta_{\text{P}(\text{solid})}$ -175.8 ppm was obtained with tin satellites ($^1J_{\text{PSn}(\text{solid})} = 2508$ Hz). The other signals in the spectrum are spinning

sidebands. The phosphorus-tin coupling constant obtained from the solid state spectrum is similar in magnitude to that observed in solution ($^1J_{\text{P}^{119}\text{Sn}(\text{solution})} = 2436 \text{ Hz}$), suggesting that the planar coordination geometry at phosphorus is maintained in solution.

Figure 80. Solid state $^{31}\text{P}\{^1\text{H}\}$ NMR spectrum (162 MHz) of $[(\text{BDI}_{\text{DIPP}})\text{SnP}(\text{SiMe}_3)_2]$ (**41**)



The solid state $^{29}\text{Si}\{^1\text{H}\}$ NMR spectrum of **41** (Figure 81) shows a singlet at $\delta_{\text{Si}(\text{solid})}$ 3.8 ppm and a doublet centred at $\delta_{\text{Si}(\text{solid})}$ 4.2 ppm ($^1J_{\text{SiP}(\text{solid})} = 32 \text{ Hz}$). This is consistent with the two resonances obtained from the $^{29}\text{Si}\{^1\text{H}\}$ NMR spectrum in solution at low temperature (Figure 78, Page 178). A $^{29}\text{Si}\{^{31}\text{P}\}$ NMR experiment shows that the doublet centred at $\delta_{\text{Si}(\text{solid})}$ 4.2 ppm collapses to a singlet upon irradiation (Figure 82). The significant difference in $^1J_{\text{SiP}(\text{solid})}$ for the two resonances is associated with the overall crowding from the β -diketiminato ligand. This gives differences in Sn–P–Si bond angles, resulting in different s-contribution in the P–Si bonds.

Figure 81. Solid state $^{29}\text{Si}\{^1\text{H}\}$ NMR spectrum (79 MHz) of $[(\text{BDI}_{\text{DIPP}})\text{SnP}(\text{SiMe}_3)_2]$ (**41**)

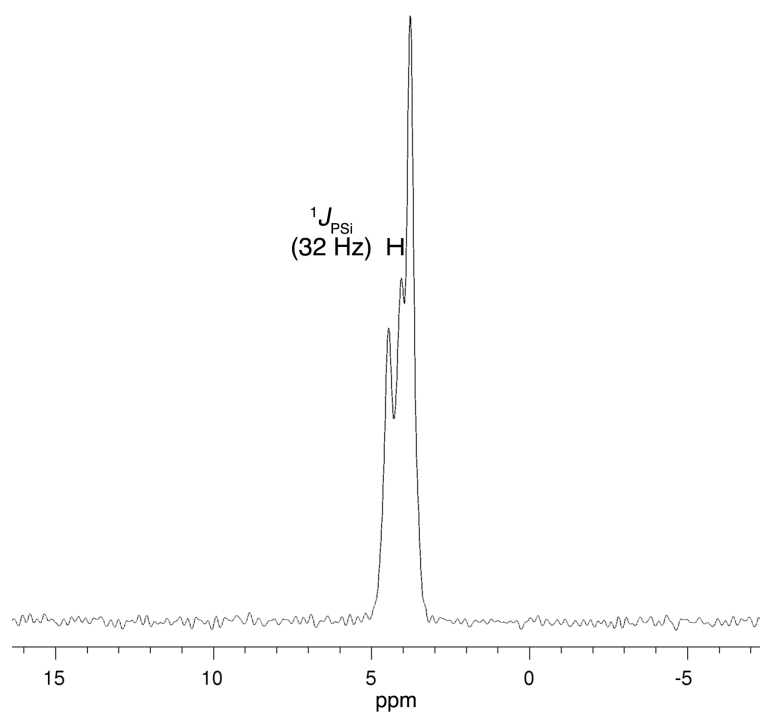
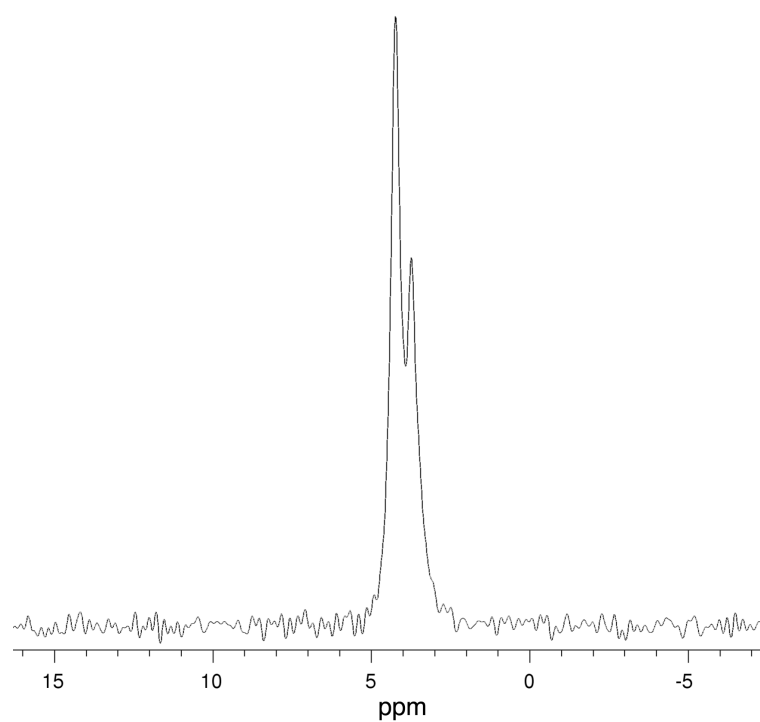


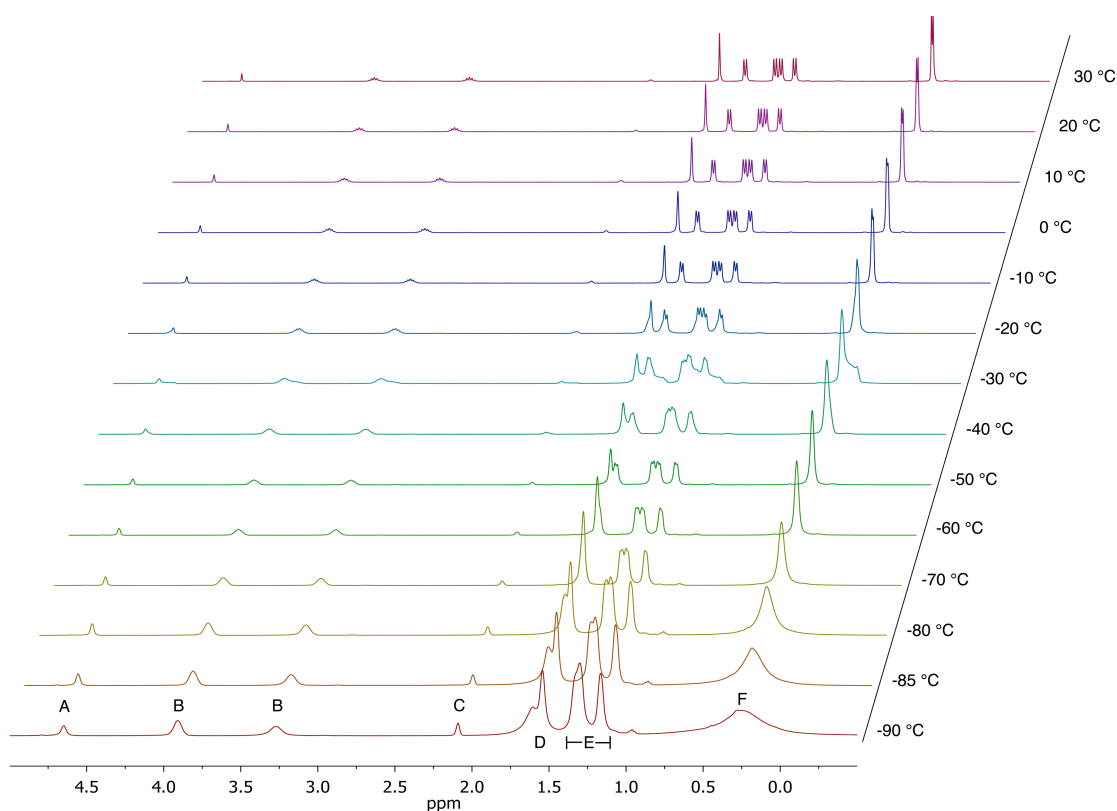
Figure 82. Solid state $^{29}\text{Si}\{^{31}\text{P}\}$ NMR spectrum (79 MHz) of $[(\text{BDI}_{\text{DIPP}})\text{SnP}(\text{SiMe}_3)_2]$ (**41**)



4.2.9.3 The β -diketiminatolead(II) bis(trimethylsilyl)phosphanide **42**

The multinuclear NMR spectroscopic data obtained for **42** are consistent with those reported in Driess' publication.^[103] The ^1H NMR spectrum shows through-space proton-phosphorus coupling to a tertiary proton resonance of the isopropyl group (CHMe_2 : δ_{H} 3.92 ppm) with $^6J_{\text{HP}} = 1.0$ Hz. A doublet centred at δ_{H} 0.30 ppm is assigned to the protons in the trimethylsilyl (SiMe_3) substituents with proton-phosphorus coupling ($^3J_{\text{HP}} = 4.0$ Hz). In a VT- ^1H NMR experiment of **42**, the resonance assigned to the SiMe_3 protons becomes broad on cooling (Figure 83). However, the broad resonance do not separate into two distinct signals at low temperature (-90 °C). The shape of the signals at -30 °C is ascribed to an unidentified shimming problem in the NMR instrument at this temperature. A similar problem was noted previously in the VT- ^1H NMR experiment of $[(\text{BDI}_{\text{DMP}})\text{PbCl}]$ (**24**) (Figure 17, Page 74).

Figure 83. VT- ^1H NMR spectra (400 MHz, toluene- d_8) of $[(\text{BDI}_{\text{DIPP}})\text{PbP}(\text{SiMe}_3)_2]$ (**42**), where A = $\gamma\text{-H}$; B = CHMe_2 ; C = toluene- d_8 ; D = NCMe ; E = CHMe_2 and F = SiMe_3

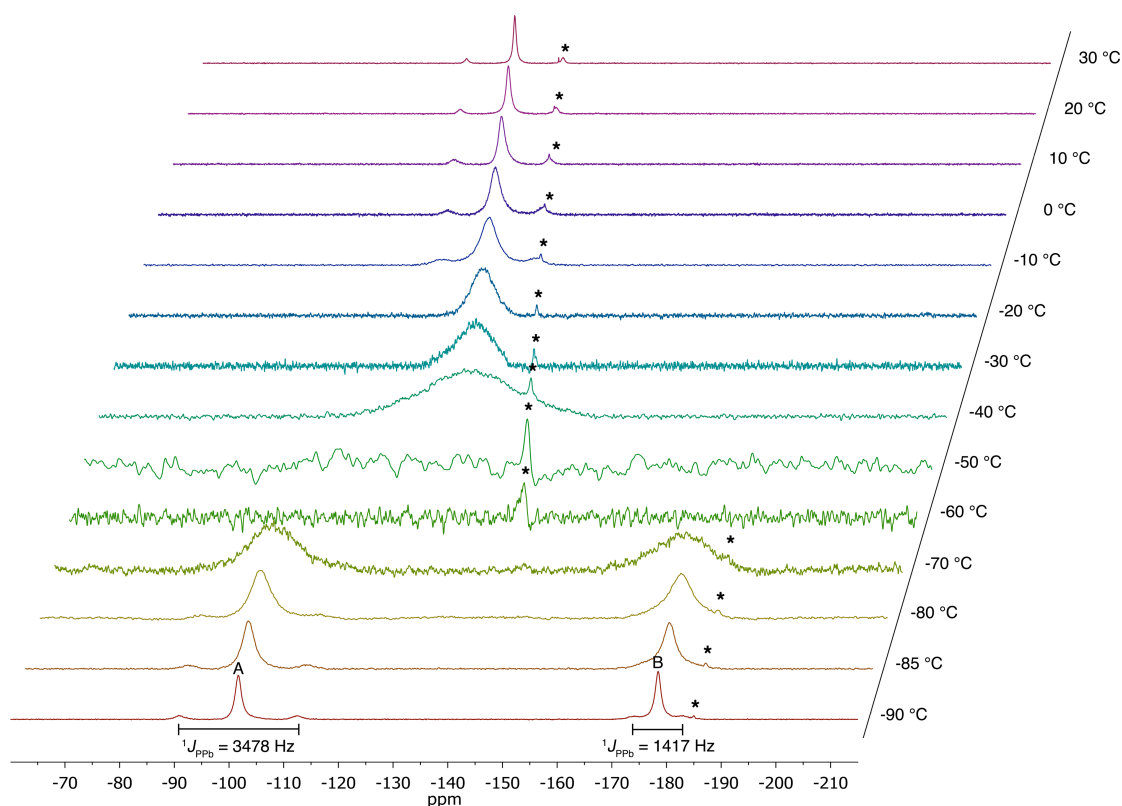


The $^3\text{P}\{^1\text{H}\}$ NMR spectrum of **42** shows a single resonance at $\delta_{\text{P}} -116.0$ ppm with lead satellites ($^1J_{\text{PPb}} = 2874$ Hz). This phosphorus-lead coupling constant ($^1J_{\text{PPb}}$) is

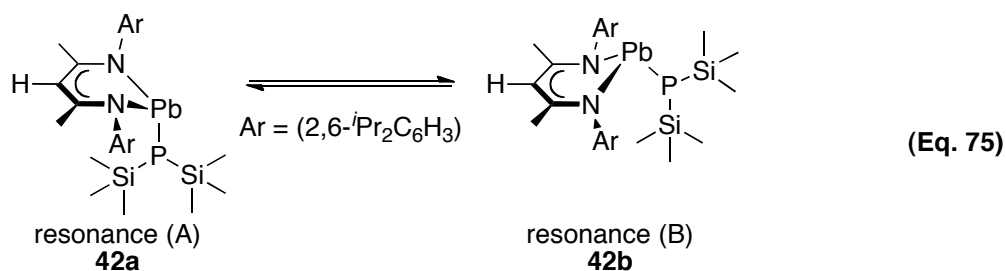
significantly larger than those in [(BDI_{DIPP})PbPPh₂] (**35**, $^1J_{\text{PPb}} = 1130$ Hz) and [(BDI_{DIPP})PbPCy₂] (**38**, $^1J_{\text{PPb}} = 1103$ Hz). In contrast to the germanium and tin analogues, **40** and **41**, the lead derivative **42** adopts an *exo* conformation, with a pyramidal coordination geometry at phosphorus in the solid state.^[103] As noted previously, the 1J coupling involving phosphorus is dependent on the s-orbital contribution in the M–P bond. Hence, the $^1J_{\text{PM}}$ coupling constant in compounds containing a pyramidal sp³ phosphorus is expected to be smaller than those with a planar sp² phosphorus. In previous work, the large phosphorus-lead coupling constant ($^1J_{\text{PPb}} = 2852$ Hz) obtained for **42** was attributed to a high 3s contribution from the phosphorus.^[103] The conformation of the germanium and tin compounds **40** and **41** are the same in the solid state as in solution. In contrast, the lead(II) bis(trimethylsilyl)phosphanide **42** shows a large phosphorus-lead coupling constant ($^1J_{\text{PPb}} = 2874$ Hz) that is not consistent with a pyramidal sp³ geometry at phosphorus ($^1J_{\text{PPb}} \sim 1000$ Hz). Hence, this compound was studied in more detail.

The VT-³¹P{¹H} NMR experiment on compound **42** in toluene-*d*₈ shows that the phosphorus signal becomes broad as the temperature is lowered to –50 °C (Figure 84). In contrast to the other systems investigated, the ³¹P{¹H} NMR spectrum recorded at –90 °C shows that the resonance separates into two with lead satellites, (A): $\delta_{\text{P}} -101.7$ ppm, $^1J_{\text{PPb}} = 3478$ Hz and (B): $\delta_{\text{P}} -178.5$ ppm, $^1J_{\text{PPb}} = 1417$ Hz. The phosphorus-lead coupling constant ($^1J_{\text{PPb}}$) observed from the resonance A is larger than that observed at 30 °C ($^1J_{\text{PPb}} = 2853$ Hz) in toluene-*d*₈. The phosphorus-lead coupling constant ($^1J_{\text{PPb}}$) at 30 °C appears to be an average from the two resonances A and B in a 7:3 ratio. To the best of our knowledge, the $^1J_{\text{PPb}}$ observed at –90 °C from our study is the largest $^1J_{\text{PPb}}$ observed hitherto: *c.f.* [Pb{Ph₂PC(H)Py}{N(SiMe₃)₂}] ($^1J_{\text{PPb}} = 2680$ Hz), [Pb{(Ph₂P)₂C(SiMe₃)₂}₂] ($^1J_{\text{PPb}} = 1510$ Hz), [Pb{P(SiMe₃)₂}₂]₂ ($^1J_{\text{PPb}} = 1264$ Hz for terminal P(SiMe₃)₂).^[265, 276-277] Although a proton-coupled ³¹P NMR spectrum was recorded at –85 °C, phosphorus-proton coupling was not observed, possibly due to broadening of the phosphorus signals at low temperature. An attempt was made to record a ¹H–³¹P HMBC NMR spectrum at –85 °C, but no measurable signal was observed.

Figure 84. VT- $^{31}\text{P}\{^1\text{H}\}$ NMR spectra (162 MHz, toluene- d_8) of $[(\text{BDI}_{\text{DIPP}})\text{PbP}(\text{SiMe}_3)_2]$ (**42**), where A & B are the phosphorus resonances at -90°C . Impurities are designated by *



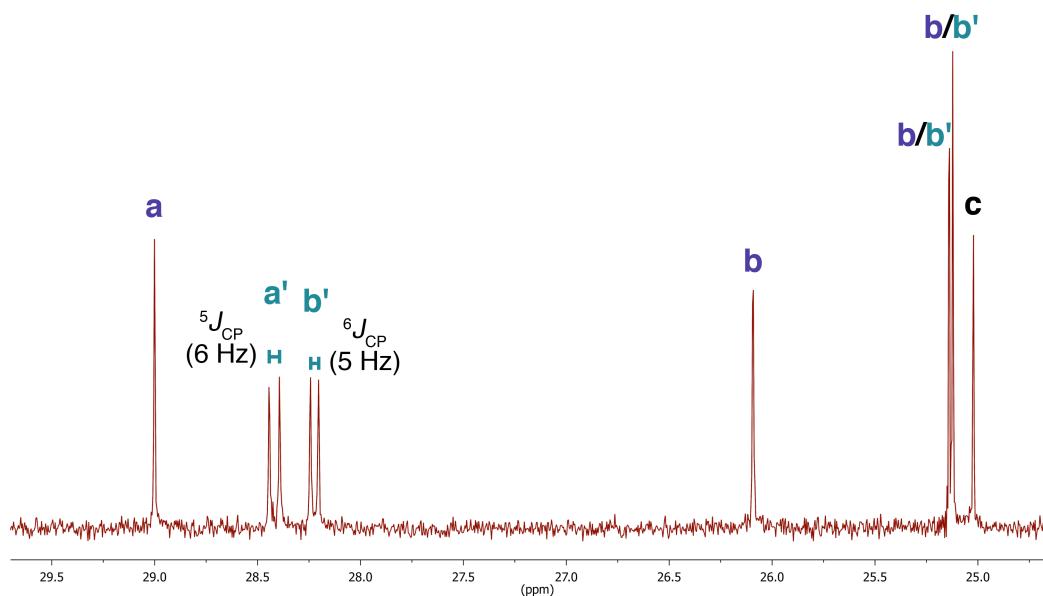
With the assumption that the magnitude of the 1J coupling involving phosphorus is dependent on the s -orbital contribution, we tentatively assign the resonance (A) to molecules in the *endo* conformation with a planar geometry at phosphorus, and the resonance (B) to molecules in the *exo* conformation with a pyramidal geometry at phosphorus (Figure 84). From the coalescence temperature (-50°C), the energy associated with the change of geometry at phosphorus is estimated to be 35.1 kJ mol^{-1} (Appendix 4, Page 341). The $^{31}\text{P}\{^1\text{H}\}$ NMR spectrum at 30°C corresponds to an equilibrium mixture of the two species, *endo* (**42a**), and *exo* (**42b**) (equation 75).



The $^{29}\text{Si}\{^1\text{H}\}$ NMR spectrum shows a doublet centred at δ_{Si} 7.2 ppm in C_6D_6 with silicon-phosphorus coupling $^1J_{\text{SiP}} = 36$ Hz. In previous examples, small silicon-phosphorus coupling constants (*c.f.* $\text{P}(\text{Si}^i\text{Pr}_3)_3$: $^1J_{\text{SiP}} = 9$ Hz) were attributed to a high ionic character in the Si–P bond.^[194] A $^{29}\text{Si}\{^1\text{H}\}$ NMR spectrum recorded at -90 °C shows a broad resonance at δ_{Si} 3.7 ppm in toluene-*d*₈.

The $^{13}\text{C}\{^1\text{H}\}$ NMR spectrum of **42** (Figure 85) shows through-space carbon-phosphorus coupling between the phosphorus and a tertiary carbon resonance of the isopropyl group (CHMe_2 (**a'**): δ_{C} 28.4 ppm, $^5J_{\text{CP}} = 6$ Hz), as well as between phosphorus and a methyl carbon resonance of the isopropyl group (CHMe_2 (**b'**): δ_{C} 28.2 ppm, $^6J_{\text{CP}} = 5$ Hz). However, the through-space carbon-lead couplings are not observed, possibly due to the noise in the baseline.

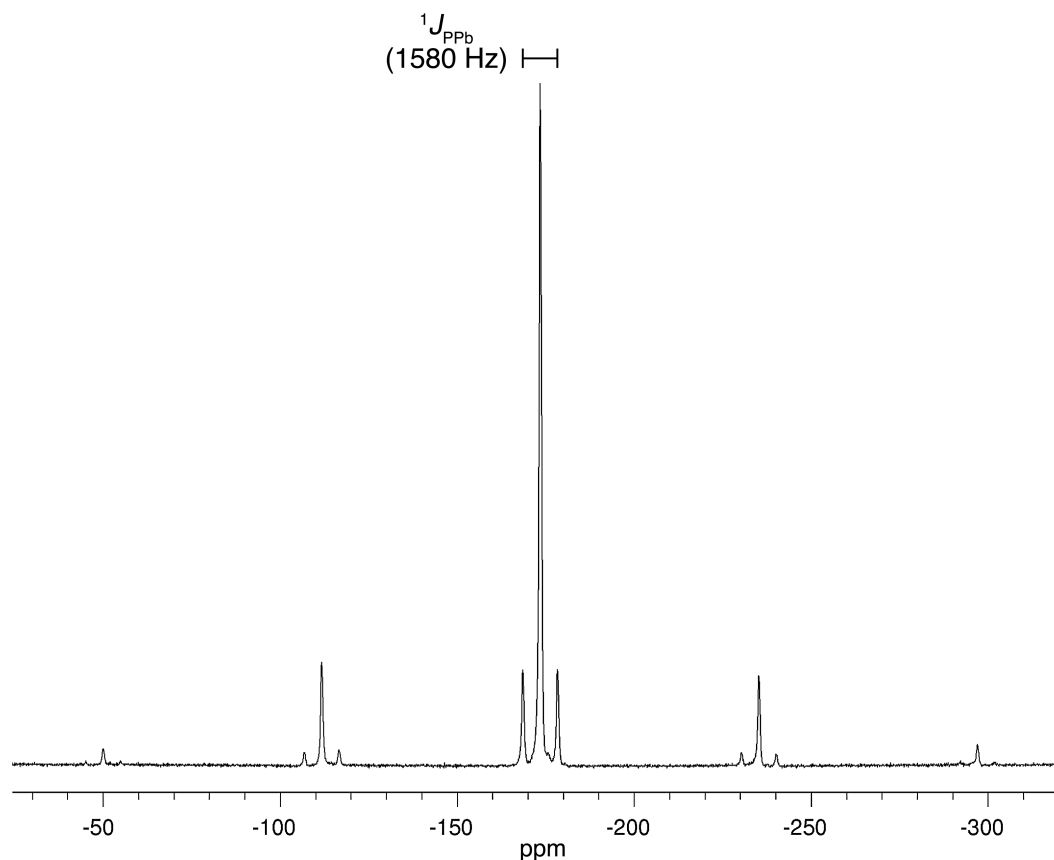
Figure 85. $^{13}\text{C}\{^1\text{H}\}$ NMR spectrum (100 MHz) of $[(\text{BDI}_{\text{DIPP}})\text{PbP}(\text{SiMe}_3)_2]$ (**42**) in C_6D_6 at 30 °C, showing the J_{CP} ; **a** and **a'** are from CHMe_2 ; **b** and **b'** are from CHMe_2 ; **c** is from NMe . The **ab**₂ and **a'b'**₂ indicate resonances from different pairs of isopropyl groups



The solid state $^{31}\text{P}\{^1\text{H}\}$ NMR spectrum of **42** (Figure 86) shows a single resonance at $\delta_{\text{P}(\text{solid})}$ -173.5 ppm with lead satellites ($^1J_{\text{PPb}(\text{solid})} = 1580$ Hz). The other signals displayed in the spectrum are spinning side-bands. This phosphorus-lead coupling constant ($^1J_{\text{PPb}}$) is significantly smaller than those observed in solution at 30 °C

($^1J_{\text{PPb(solution)}} = 2874 \text{ Hz}$), but is close to that predicted for a pyramidal geometry at phosphorus. It is thus reasonable to assign the resonance (B) ($\delta_{\text{P(solution)}} -178.5 \text{ ppm}$, $^1J_{\text{PPb(solution)}} = 1417 \text{ Hz}$, Figure 84, Page 184) at $-90 \text{ }^\circ\text{C}$ in solution to compound **42b**, with a pyramidal geometry at phosphorus (equation 75, Page 184).

Figure 86. Solid state $^{31}\text{P}\{^1\text{H}\}$ NMR spectrum (162 MHz) of $[(\text{BDI}_{\text{DIPP}})\text{PbP}(\text{SiMe}_3)_2]$ (**42**)



The solid state $^{29}\text{Si}\{^1\text{H}\}$ NMR spectrum of compound **42** (Figure 87) shows two doublets, centred at $\delta_{\text{Si(solid)}} 5.3 \text{ ppm}$ ($^1J_{\text{SiP(solid)}} = 56 \text{ Hz}$) and $\delta_{\text{Si(solid)}} 2.8 \text{ ppm}$ ($^1J_{\text{SiP(solid)}} = 49 \text{ Hz}$). These silicon resonances correspond to silicon atoms in different crystallographic environments in the solid state. The silicon-phosphorus coupling is confirmed by a solid state $^{29}\text{Si}\{^{31}\text{P}\}$ NMR experiment, which shows two singlets at $\delta_{\text{Si(solid)}} 5.2$ and 2.7 ppm (Figure 88).

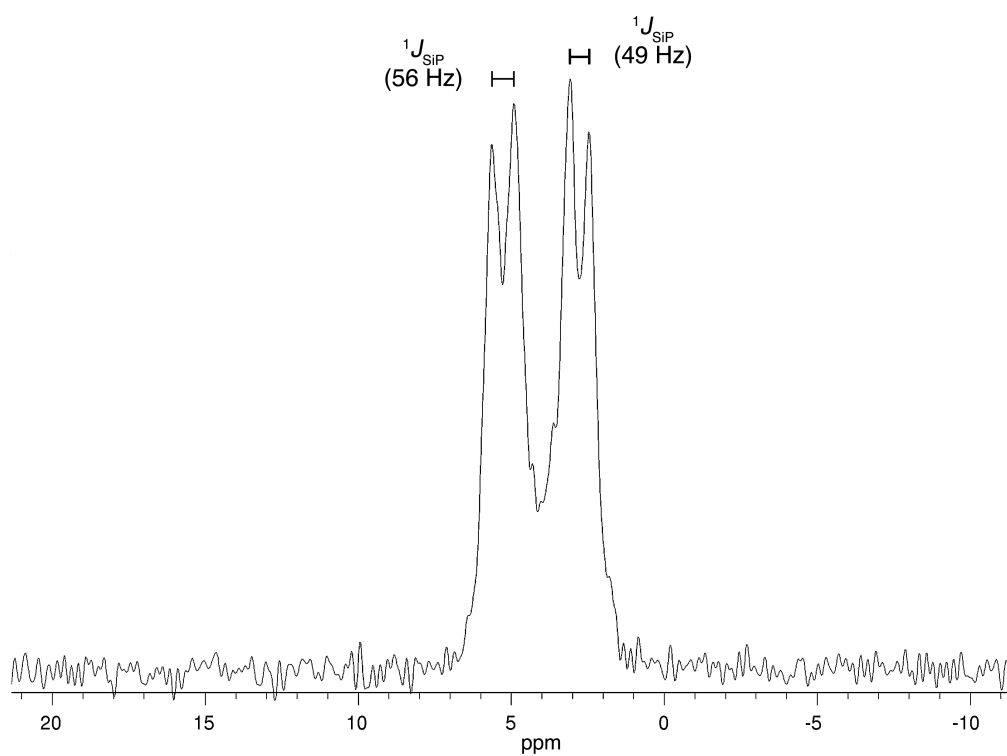
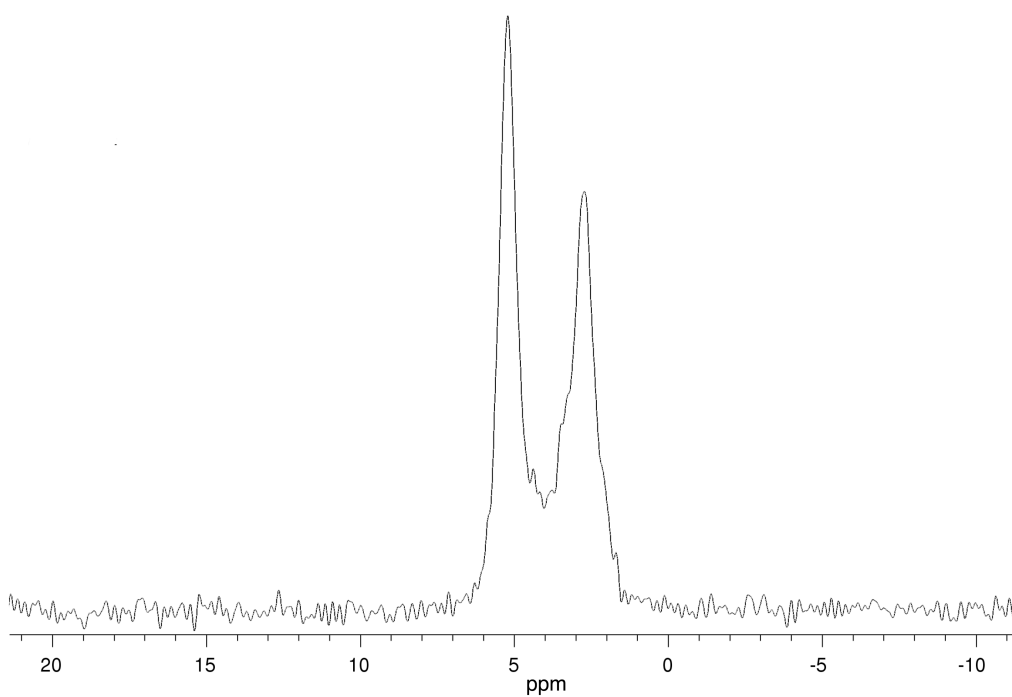
Figure 87. Solid state $^{29}\text{Si}\{^1\text{H}\}$ NMR spectrum (79 MHz) of $[(\text{BDI}_{\text{DIPP}})\text{PbP}(\text{SiMe}_3)_2]$ (**42**)**Figure 88.** Solid state $^{29}\text{Si}\{^{31}\text{P}\}$ NMR spectrum (79 MHz) of $[(\text{BDI}_{\text{DIPP}})\text{PbP}(\text{SiMe}_3)_2]$ (**42**)

Table 38. Selected multinuclear NMR spectroscopic data for [(BDI_{DMP})PbP(SiMe₃)₂] (**43**), [(BDI_{IPP})PbP(SiMe₃)₂] (**44**) and [(BDI_{Ph})PbP(SiMe₃)₂] (**45**)

	[(BDI _{DMP})PbP(SiMe ₃) ₂] (43) ^a	[(BDI _{IPP})PbP(SiMe ₃) ₂] (44) ^a	[(BDI _{Ph})PbP(SiMe ₃) ₂] (45) ^b
	δ (ppm), J (Hz)	δ (ppm), J (Hz)	δ (ppm), J (Hz)
¹H			
γ -H	4.78 (s)	4.80 (s)	4.75 (s)
SiMe ₃	0.36 (d) ³ J _{HP} = 3.6	0.51 (d) ³ J _{HP} = 3.6	0.44 (d) ³ J _{HP} = 4.0
³¹P{¹H}			
	-123.6 (s) ¹ J _{PSi} = 44 ¹ J _{PPb} = 2317	-139.9 (s) ¹ J _{PSi} = 44 ¹ J _{PPb} = 2061	-137.3 (s) ¹ J _{PSi} = 44 ¹ J _{PPb} = 2060
Other	- ^c	- ^c	δ (²⁹ Si{ ¹ H}) = 5.1 (d) ¹ J _{SiP} = 44 δ (²⁰⁷ Pb) = 2905 ¹ J _{PbP} = 2051

^a in C₆D₆; ^b in toluene-*d*₆; ^c data not available

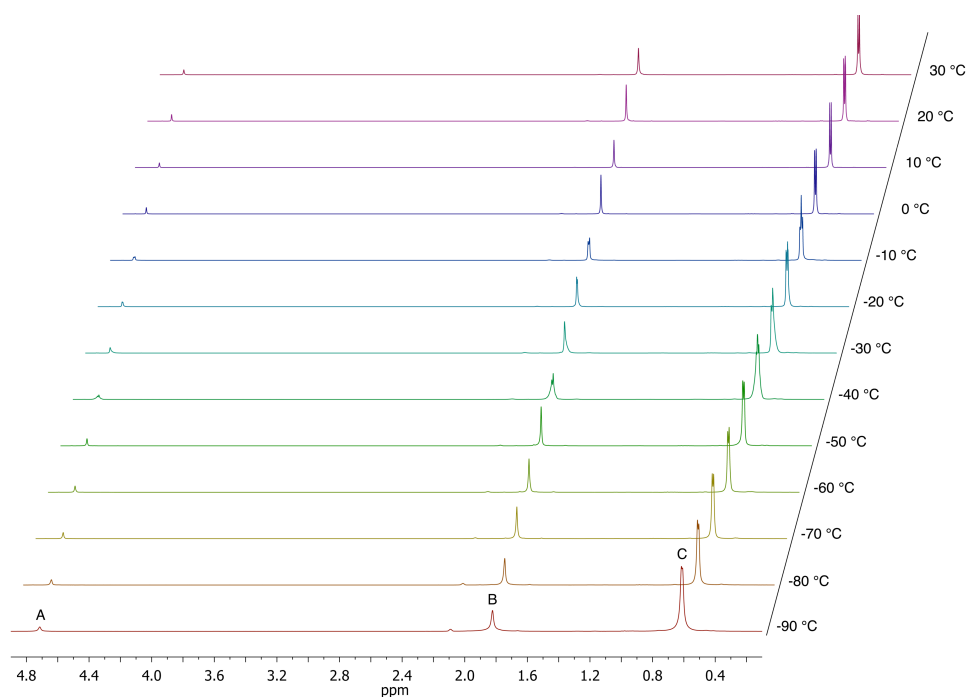
The ¹H NMR spectra of these lead(II) bis(trimethylsilyl)phosphanides **43–45** show doublets at $\delta_H \sim 0.36$ – 0.51 ppm, with proton-phosphorus coupling ³J_{HP} ~ 3.6 – 4.0 Hz, assigned to the protons in the trimethylsilyl (SiMe₃) groups. A singlet at δ_H 2.21 and 1.61 ppm is assigned to the protons in the *ortho*-methyl groups of the *N*-aryl substituents in [(BDI_{DMP})PbP(SiMe₃)₂] (**43**). For [(BDI_{IPP})PbP(SiMe₃)₂] (**44**), a septet at δ_H 2.66 ppm (³J_{HH} = 6.6 Hz), is assigned to the tertiary protons in the *para*-isopropyl groups (CHMe₂) in the *N*-aryl substituents.

The ³¹P{¹H} NMR spectrum of [(BDI_{DMP})PbP(SiMe₃)₂] (**43**) shows a single resonance at δ_P -123.6 ppm with silicon and lead satellites (¹J_{PSi} = 44 Hz and ¹J_{PPb} = 2317 Hz). A single phosphorus resonance at δ_P -139.9 ppm with silicon and lead satellites (¹J_{PSi} = 44 Hz and ¹J_{PPb} = 2061 Hz) is shown in the ³¹P{¹H} NMR spectrum of [(BDI_{IPP})PbP(SiMe₃)₂] (**44**). For [(BDI_{Ph})PbP(SiMe₃)₂] (**45**), a single resonance at δ_P -137.3 ppm with silicon and lead satellites (¹J_{PSi} = 44 Hz and ¹J_{PPb} = 2060 Hz) is shown in the ³¹P{¹H} NMR spectrum in toluene-*d*₈. The phosphorus-silicon coupling constant (¹J_{PSi}) in **45** is further confirmed by the ²⁹Si{¹H} NMR spectrum, which shows a doublet centred at δ_{Si} 5.1 ppm with ¹J_{SiP} = 44 Hz.

The decreased crowding from the *N*-aryl substituents in the β -diketiminato ligand leads to an upfield shift in the phosphorus resonance in the bis(trimethylsilyl)phosphanide derivatives: δ_P [(BDI_{DIPP})PbPR₂] (**42**) > δ_P [(BDI_{DMP})PbPR₂] (**43**) > δ_P [(BDI_IPP)PbPR₂] (**44**) (R = SiMe₃). The phosphorus-lead coupling constant ($^1J_{PbP}$) decreases with a decrease of crowding from the *N*-aryl substituents in the β -diketiminato ligand, for example in [(BDI_{DIPP})PbP(SiMe₃)₂] (**42**, $^1J_{PbP}$ = 2874 Hz) and in [(BDI_IPP)PbP(SiMe₃)₂] (**44**, $^1J_{PbP}$ = 2061 Hz). From our previous work, we predict that when the crowding from the *N*-aryl substituents in the β -diketiminato ligand is reduced, there is a preference for a pyramidal coordination geometry at phosphorus.

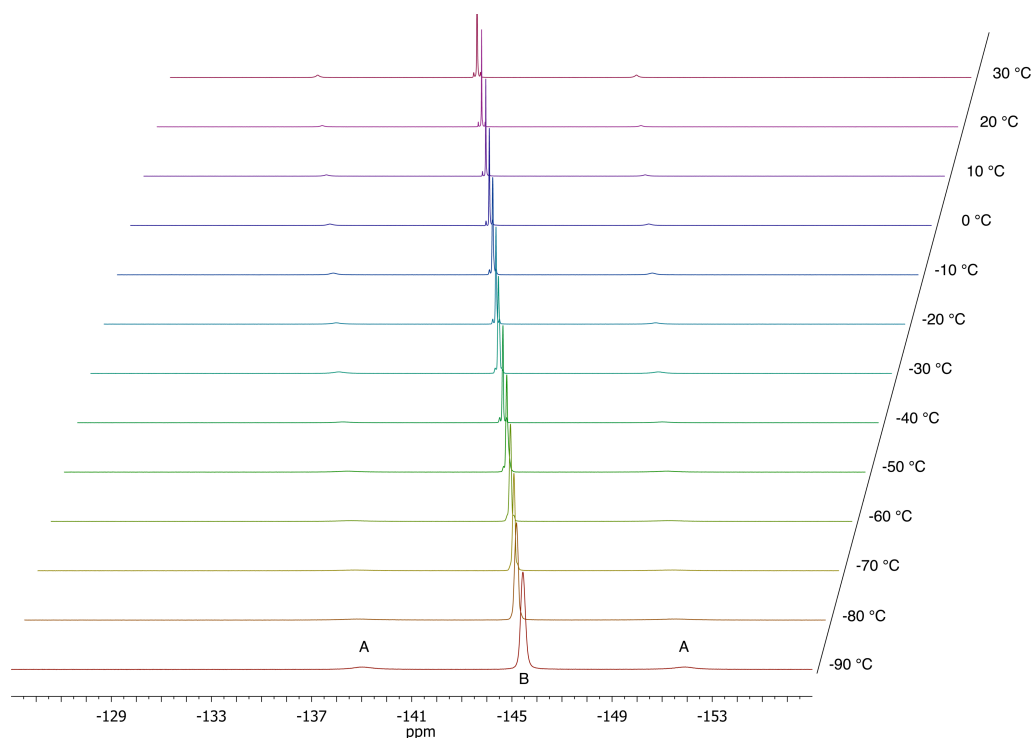
VT-¹H NMR spectra of [(BDI_{Ph})PbP(SiMe₃)₂] (**45**) are shown in Figure 89. At 30 °C, a doublet centred at δ_H 0.44 ppm with $^3J_{HP}$ = 4.0 Hz in toluene-*d*₈ is assigned to the protons in the SiMe₃ substituents. With decreasing temperature, this resonance becomes broad at -90 °C but it does not split into two distinct signals, as it does in [(BDI_{DIPP})SnP(SiMe₃)₂] (**41**) (Figure 73, Page 174). This suggests that in [(BDI_{Ph})PbP(SiMe₃)₂] (**45**), the two SiMe₃ groups are equivalent on the NMR timescale within the temperature range 30 to -90 °C, probably indicating that even at the lowest temperature, free rotation about the Pb–P bond is possible.

Figure 89. VT-¹H NMR spectra (400 MHz, toluene-*d*₈) of [(BDI_{Ph})PbP(SiMe₃)₂] (**45**), where A = γ -H; B = NCMe; and C = SiMe₃



In $[(\text{BDI}_{\text{DIPP}})\text{PbP}(\text{SiMe}_3)_2]$ (**42**), two phosphorus resonances are found at low temperature (Figure 84, Page 184), suggesting an exchange between species with a pyramidal or planar coordination geometry at phosphorus in solution. A VT- $^{31}\text{P}\{^1\text{H}\}$ NMR study on $[(\text{BDI}_{\text{Ph}})\text{PbP}(\text{SiMe}_3)_2]$ (**45**) shows a single resonance at $\delta_{\text{P}} -137.3$ ppm with silicon and lead satellites ($^1J_{\text{PSi}} = 44$ Hz and $^1J_{\text{PPb}} = 2060$ Hz) in toluene- d_8 at 30 °C (Figure 90). At -90 °C, the resonance is slightly shifted upfield to $\delta_{\text{P}} -145.4$ ppm, with lead satellites ($^1J_{\text{PPb}} = 2096$ Hz). However, the silicon satellites are not observed, due to the broadening of signals at low temperature. There is no significant change in the phosphorus-lead coupling constant ($\Delta^1J_{\text{PPb}} = 36$ Hz) within the temperature range 30 to -90 °C, suggesting that in this case, there is no equilibrium between species with planar and pyramidal geometry at phosphorus. Further work is required to establish whether the species found in solution and in the solid state are the same for **45**.

Figure 90. VT- $^{31}\text{P}\{^1\text{H}\}$ NMR spectra (162 MHz, toluene- d_8) of $[(\text{BDI}_{\text{Ph}})\text{PbP}(\text{SiMe}_3)_2]$ (**45**), where A = lead satellites and B = phosphorus resonance



4.3 Summary

A series of β -diketiminato heavy group 14 metal phosphanides [(BDI_{DIPP})MPR₂], where M is a heavy group 14 element and R is alkyl, aryl or trimethylsilyl, is synthesised. Elemental analyses are in good agreement with the calculated values. Structural and spectroscopic properties are examined. X-ray crystallographic analyses show that these complexes are monomeric in the solid state with a pyramidally coordinated metal centre, adopting either an *exo* or *endo* conformation. The germanium and tin derivatives, containing either a diphenylphosphanido (R = Ph) or dicyclohexylphosphanido (R = Cy) ligand, adopt an *exo* conformation with a pyramidal geometry at phosphorus. When R = SiMe₃, both compounds adopt an *endo* conformation with a planar geometry at phosphorus. In contrast, all the lead derivatives adopt an *exo* conformation with a pyramidally coordinated phosphorus atom.

In the literature, heavy group 14 metal complexes with terminal phosphanido ligand in less sterically congested systems feature a pyramidal geometry at phosphorus.^[214, 277] This suggests that the pyramidal geometry at phosphorus is the most stable conformation. Hence, the planar geometry around the phosphorus atom in the β -diketiminatogermanium(II) and -tin(II) bis(trimethylsilyl)phosphanides **40** and **41** may be ascribed to the steric influence from the β -diketiminato ligand. The M–P bond distances are shorter in the silyl-substituted phosphanides **40** and **41** than those in the aryl- or alkyl-substituted phosphanides within the series of germanium and tin compounds (Figure 91).^[134] This is attributed to the steric congestion from the isopropyl groups in the *N*-aryl substituents, as well as possible back donation of the lone pair electrons from phosphorus to the trimethylsilyl substituents. These factors lead to a planar configuration at the phosphorus atom. This is a reasonable explanation when comparing the geometry of the various phosphanido ligands with the same metal centre. When compounds containing different metal centres are compared, it is necessary to take account of the covalent radius of the metal: Ge–P are shorter than Sn–P bonds. This leads to the N–Ge–N bond angles in the germanium derivatives (avg. 88.80°) are wider than the N–Sn–N bond angles (avg. 84.03°), which effectively reduces the steric influence from the *ortho*-substituents in the *N*-aryl groups of the β -diketimate ring in the germanium analogues (Figure 92).

Figure 91. Graphical representation of M–P bond lengths in the germanium(II) and tin(II) phosphanides $[(\text{BDI}_{\text{DIPP}})\text{MPR}_2]$ ($\text{M} = \text{Ge}$ or Sn , $\text{R} = \text{Ph}$, Cy or SiMe_3)

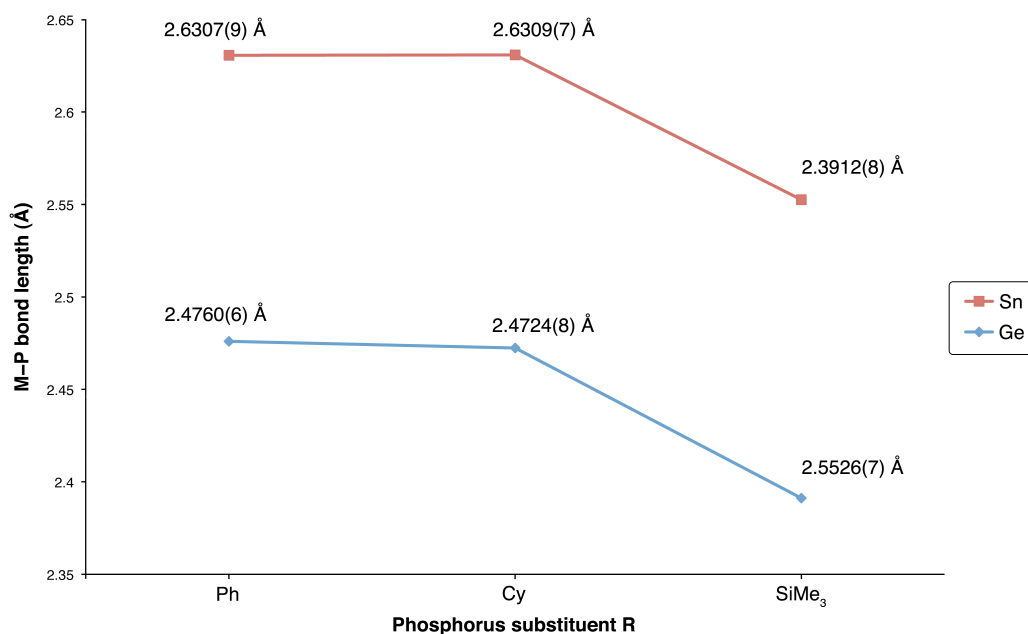
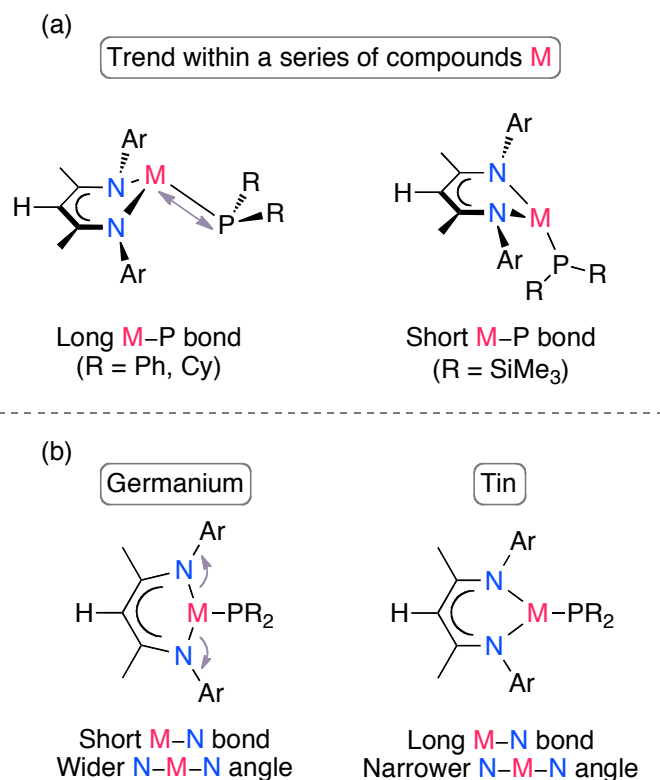


Figure 92. Factors influencing the geometry around the phosphorus atom from the *N*-aryl substituents by (a): metal-phosphorus bond and (b): bite angle of the β -diketiminato ligand



For the lead derivatives, **35**, **38** and **42**, the Pb–N bond lengths (avg. 2.337 Å) are longer than the corresponding M–N bonds in the germanium and tin derivatives, with a further reduction in the N–Pb–N angles (avg. 80.7°). This leads to an increased crowding from the *N*-aryl substituents in the lead analogues. Furthermore, there is no significant reduction in the Pb–P bond length (2.715(2) Å) in the lead(II) bis(trimethylsilyl)phosphanide **42**, compared to those in the diphenyl- (**35**, 2.720(2) Å) and dicyclohexylphosphanido analogues (**38**, 2.6945(9) Å). Hence, the *exo* conformation is predominant in the lead derivatives.

The availability of NMR active nuclei in these phosphanido complexes enabled us to obtain detailed data on these compounds. With the exception of the lead(II) bis(trimethylsilyl)phosphanide **42**, the conformations observed from their solid state structures are preserved in solution. ¹H NMR spectra show the expected signals for a structure with a pyramidal geometry around the metal centre supported by a β-diketiminato ligand. Even though the phosphorus is more than three bonds away, carbon-phosphorus J_{CP} couplings are observed in the resonances assigned to isopropyl groups. We attributed these interactions to through-space coupling between proximate nuclei in solution. Through-space carbon-tin J_{CSn} couplings are also observed in the ¹³C{¹H} NMR spectra of the tin derivatives **34**, **37** and **41**, including the tin(II) chloride **32**. These were not reported previously.^[65] The through-space J_{CP} and J_{CSn} couplings (the latter reported for the first time) are observed with *ortho*-isopropyl substituents in the *N*-aryl groups in the β-diketiminato ring, depending on the proximity between the nuclei. With present instrumentation, through-space couplings are observed from these compounds when the distance between the active nuclei is less than about 4.0 Å. This further suggests that the overall conformations obtained in the solid state are preserved in solution.

The phosphorus chemical shifts for the germanium and tin derivatives show the typical trend for the diphenyl-, dicyclohexyl- and bis(trimethylsilyl)phosphanido derivatives.^[278] To the best of our knowledge, the phosphorus-tin coupling constant in the tin(II) bis(trimethylsilyl)phosphanide **41** ($^1J_{P^{119}Sn} = 2436$ Hz) is the largest value reported to date. Crystallographic analysis and the solid state ³¹P{¹H} NMR spectrum of **41** confirm that the $^1J_{PSn}$ coupling comes from a Sn–P single bond. A simple

explanation for the large magnitude of the $^1J_{\text{PSn}}$ coupling constant is that the s-contribution within the Sn–P bond is enhanced by the change of geometry around the phosphorus, from pyramidal sp^3 to planar sp^2 . It also explains why the Sn–P single bond length in the bis(trimethylsilyl)phosphanido compound **41** is shorter than that in the other β -diketiminato(II) phosphanides **34** and **37**.

As in the tin derivatives, the lead(II) bis(trimethylsilyl)phosphanide **42** shows a large phosphorus-lead coupling constant ($^1J_{\text{PPb}} = 2874 \text{ Hz}$).^[103] However, the solid state structure shows an *exo* conformation with a pyramidal geometry at phosphorus. The solid state $^{31}\text{P}\{^1\text{H}\}$ NMR spectrum shows a phosphorus-lead coupling constant $^1J_{\text{PPb(solid)}} = 1580 \text{ Hz}$, i.e. much lower than that observed in solution. The VT- $^{31}\text{P}\{^1\text{H}\}$ NMR experiment shows two resonances in toluene- d_8 at $-90 \text{ }^\circ\text{C}$ (Figure 84, Page 184). Resonance A ($\delta_{\text{P}} -101.7 \text{ ppm}$, $^1J_{\text{PPb}} = 3478 \text{ Hz}$) is assigned to a conformation having a planar geometry at phosphorus, and resonance B ($\delta_{\text{P}} -178.5 \text{ ppm}$, $^1J_{\text{PPb}} = 1417 \text{ Hz}$) is assigned to a conformation with a pyramidal geometry at phosphorus (equation 75, Page 184). The $^1J_{\text{PPb}}$ coupling constant measured at $30 \text{ }^\circ\text{C}$ is an average of these signals in an approximate 7:3 ratio, suggesting that exchange between the two conformations is rapid on the NMR timescale at room temperature.

A series of lead(II) bis(trimethylsilyl)phosphanides **43–45** containing less sterically demanding β -diketiminato ligands were synthesised. The results show that with decreasing steric congestion from the *N*-aryl substituents, the coupling constant $^1J_{\text{PPb}}$ decreases: $[(\text{BDI}_{\text{DIPP}})\text{PbR}]$ (**42**, $^1J_{\text{PPb}} = 2874 \text{ Hz}$) $>$ $[(\text{BDI}_{\text{DMP}})\text{PbR}]$ (**43**, $^1J_{\text{PPb}} = 2317 \text{ Hz}$) $>$ $[(\text{BDI}_{\text{IPP}})\text{PbR}]$ (**44**, $^1J_{\text{PPb}} = 2061 \text{ Hz}$) ($\text{R} = \text{P}(\text{SiMe}_3)_2$). We propose that the pyramidal geometry around the phosphorus atom may be preferred in these systems in solution due to the lower steric interaction between the phosphanido ligand and the *N*-aryl substituents, resulting in a smaller coupling constant. Unfortunately, we were not able to obtain crystallographic structure or solid state NMR data for comparison with the results obtained for $[(\text{BDI}_{\text{DIPP}})\text{PbP}(\text{SiMe}_3)_2]$ (**42**).

4.4 Reactions of the β -diketiminato heavy group 14 metal phosphanides with elemental chalcogens

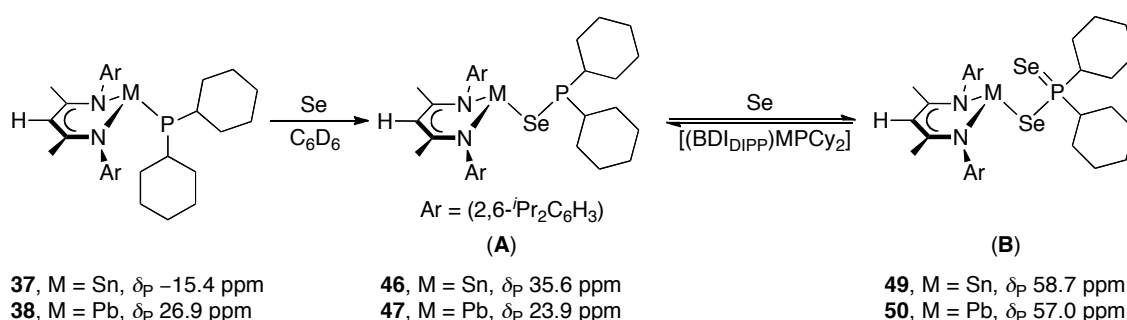
In previous work, reactions of heavy group 14 metal complexes with elemental chalcogens led either to oxidative addition of the chalcogen to the metal centre or insertion of the chalcogen between the metal centre and the substituent (Section 4.1.6, Page 118). However, as such reactions with heavy group 14 metal phosphanido complexes are rare, we examined the reactions of our β -diketiminato heavy group 14 metal phosphanides with elemental chalcogens.

4.4.1 Reactions of the β -diketiminato heavy group 14 metal dicyclohexylphosphanides **36–38** with elemental selenium

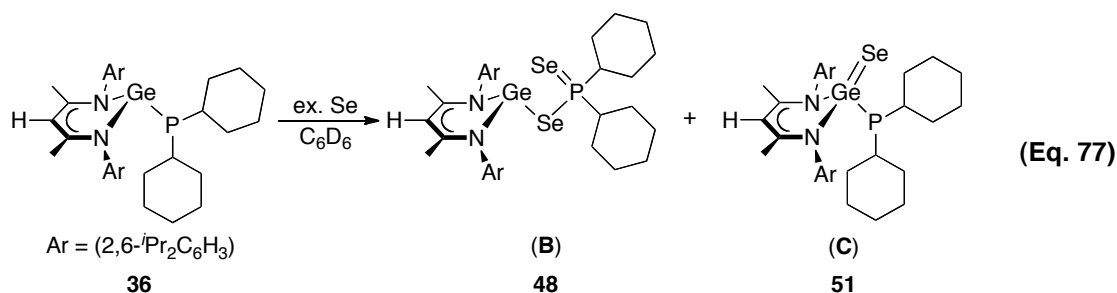
β -Diketiminato heavy group 14 metal dicyclohexylphosphanides **36–38** were used to evaluate reactions with elemental chalcogens, as they were more stable than complexes containing diphenylphosphanido or bis(trimethylsilyl)phosphanido ligands. Initial reactions on an NMR scale involved the β -diketiminatotin(II) dicyclohexylphosphanide **37** and elemental selenium in 1:1 ratio (Scheme 62). In C_6D_6 , two resonances, at δ_P 35.6 and 58.7 ppm, both with tin and selenium satellites were observed in the $^{31}P\{^1H\}$ NMR spectrum, in addition to a resonance at δ_P -15.4 ppm assigned to the tin(II) dicyclohexylphosphanide **37**. When an excess of elemental selenium was added to this mixture, the intensity of the phosphorus resonance at δ_P 35.6 ppm diminished and the intensity of the resonance at δ_P 58.7 ppm increased, relative to the resonance at δ_P 35.6 ppm. In contrast, the intensity of the phosphorus resonance at δ_P 58.7 ppm decreased upon addition of $[(BDI_{DIPP})SnPCy_2]$ (**37**) to the same mixture, relative to the resonance at δ_P 35.6 ppm. Compounds corresponding to each phosphorus resonance were successfully isolated and X-ray crystallographic analysis confirmed that the compounds are $[(BDI_{DIPP})SnSePCy_2]$ (**46**, δ_P 35.6 ppm) and $[(BDI_{DIPP})SnSeP(Se)Cy_2]$ (**49**, δ_P 58.7 ppm) (Scheme 62). These results indicate that the initial product $[(BDI_{DIPP})SnSePCy_2]$ (**46**) reacts with an excess of elemental selenium to give $[(BDI_{DIPP})SnSeP(Se)Cy_2]$ (**49**) and compound **49** reacts with $[(BDI_{DIPP})SnPCy_2]$ (**37**) to give the phosphinoselenoito complex **46**. Oxidative addition of the selenium to the metal centre of the tin derivative was not observed. The lead(II) dicyclohexylphosphanide **38** also gave the corresponding dicyclohexylphosphinoselenoito and dicyclohexylphosphinodiselenoato compounds **47**

and **50** (Scheme 62, *vide infra*). Therefore, a general reaction scheme can be established for the reaction between the β -diketiminatotin(II) and -lead(II) dicyclohexylphosphanides, **37** and **38**, and elemental selenium, which leads to the formation of the insertion product A and then to product B containing an additional P=Se bond (Scheme 62).

Scheme 62. Reactions of the β -diketiminatotin(II) and -lead(II) dicyclohexylphosphanides, **37** and **38**, with elemental selenium in C_6D_6



Although the germanium derivative [(BDI_{DIPP})GeSeP(Se)Cy₂] (**48**) was obtained when the β -diketiminatogermanium(II) dicyclohexylphosphanide **36** reacted with an excess of elemental selenium, compound C [(BDI_{DIPP})Ge(Se)PCy₂] (**51**) was obtained at the same time (equation 77) (*vide infra*). The germanium(II) dicyclohexylphosphinoselenoite [(BDI_{DIPP})GeSePCy₂] was not observed in this reaction.



4.4.2 Synthesis of β -diketiminatotin(II) and -lead(II) dicyclohexylphosphinoselenoite **46** and **47**

Isolation of the single selenium insertion product (compound A) involving tin or lead metals is difficult due to the tendency of the phosphinoselenoite complexes to react further with elemental selenium to give the phosphinodiselenoato complexes

4.4.3 X-ray crystal structures of [(BDI_{DIPP})MSePCy₂] (**46**, M = Sn and **47**, M = Pb)

Single crystals of [(BDI_{DIPP})SnSePCy₂] (**46**) were obtained from a toluene solution at -30 °C. ORTEP drawings of compound **46** are shown in Figures 93 and 94. Selected bond lengths and angles are given in Table 39, and selected crystallographic data in Table 40. Like the tin(II) dicyclohexylphosphanide **37**, the tin(II) dicyclohexylphosphinoselenoite **46** adopts an *exo* conformation, with the tin atom 1.025 Å above the mean NCCCN plane of the β-diketiminato ligand. The geometry around the tin atom is pyramidal, with the sum of bond angles around the metal centre 277.4°. The phosphorus is pyramidally coordinated, with the sum of bond angles 304.5°. Electrons are delocalised within the C₃N₂Pb unit in the β-diketiminate ring, but not on to the *N*-aryl substituents (dihedral angles: C(11)–C(6)–N(1)–Sn = 74.9(2)° and C(23)–C(18)–N(2)–Sn = -66.2(3)°). If the cyclohexyl groups are discounted, there is an approximate plane of symmetry passing through the atoms C(2), Sn, Se and P, bisecting the β-diketiminate ring. The Sn–Se bond length is 2.6059(3) Å, similar to those in Brennan's [Sn(2-SeNC₅H₄)₂]₂ (terminal Sn–Se = 2.681(2) Å), Einstein's [(^tBu₃Sn)₂Se] (2.537(2) Å) and Kato's [Ph₃SnSeCOC₇H₇] (2.5515(7) Å).^[279-281] Furthermore, the Sn–Se bond length in **46** is longer than the Sn=Se bond distance found in Parkin's [(η⁴-Me₈taa)Sn(Se)] (2.394(1) Å), Okazaki's [Tbt(Ditp)Sn(Se)] (Tbt = (C₆H₂(CH(SiMe₃)₂)₃); Ditp = (C₆H₃(C₆H₃(CHMe₂)₂)₂)) (2.375(3) Å) and Leung's [{CH(SiMe₃)C₉H₆N-8}₂Sn(Se)] (2.398(1) Å), indicating single bond character in the Sn–Se bond.^[226, 282-283] The Sn–Se–P bond angle (91.388(17)°) is similar to that in [Sn{N(P^{*i*}Pr₂Se)₂}₂-Se,Se] (avg. 95.77°).^[284] The internal C–C–C bond angles in the cyclohexyl rings do not deviate significantly from the average value (111°), indicating that there is little distortion from the cyclohexyl chair conformation.

Figure 93. ORTEP diagram of $[(\text{BDI}_{\text{DIPP}})\text{SnSePCy}_2]$ (**46**). H atoms are omitted and C atoms in the *N*-aryl groups in the β -diketiminato ring are minimised for clarity. The ellipsoid probability is shown at 30%

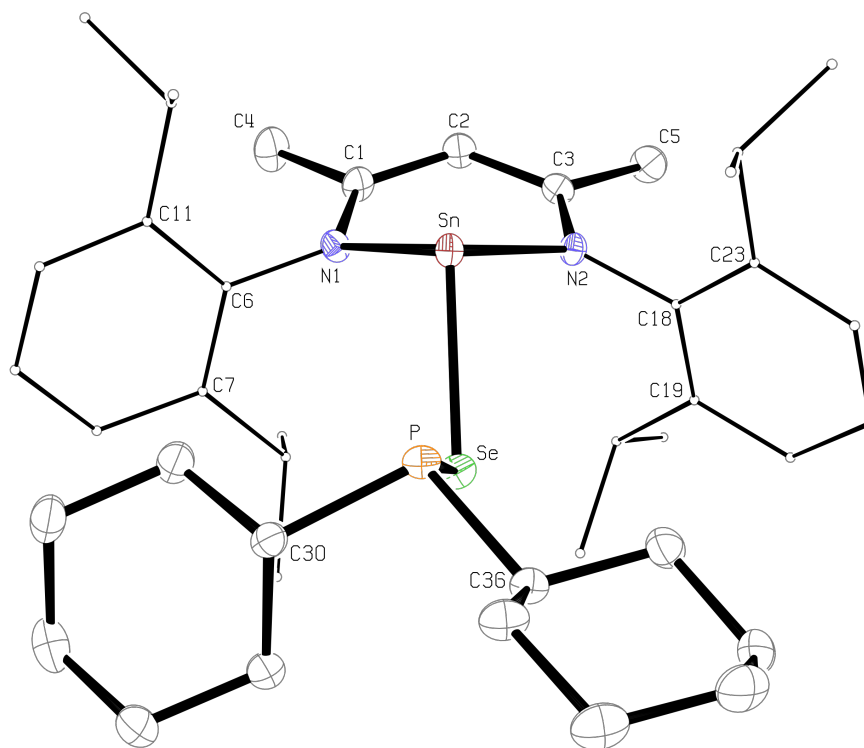


Figure 94. ORTEP diagram showing the side-on view of $[(\text{BDI}_{\text{DIPP}})\text{SnSePCy}_2]$ (**46**). H atoms are omitted, C atoms in the *N*-aryl groups in the β -diketiminato ring and the cyclohexyl groups are minimised for clarity. The ellipsoid probability is shown at 30%



Single crystals of [(BDI_{DIPP})PbSePCy₂] (**47**) were obtained by recrystallisation from an toluene solution at $-30\text{ }^{\circ}\text{C}$. ORTEP drawings of compound **47** are shown in Figures 95 and 96. Selected bond lengths and angles are given in Table 39, and selected crystallographic data in Table 40. The lead(II) dicyclohexylphosphinoselenoite **47** and the tin derivative **46** are isomorphous. Compound **47** adopts an *exo* conformation with the lead atom 1.052 Å above the mean NCCCN plane of the β -diketiminato ligand. The geometry around the lead atom is pyramidal, with the sum of bond angles around the metal centre 275.1° . The phosphorus atom is pyramidally coordinated with the sum of bond angles 305.3° . The angle between the mean NCCCN plane in the β -diketiminato ligand and the plane defined by the atoms N(1), Pb and N(2) is 35.7° , similar to that observed for the lead(II) dicyclohexylphosphanide **38** (38.7°). Delocalisation within the C₃N₂Pb unit in the β -diketiminato ring is evident, but it does not extend to the *N*-aryl substituents (dihedral angles: C(11)–C(6)–N(1)–Pb = $75.2(4)^{\circ}$ and C(23)–C(18)–N(2)–Pb = $-65.4(4)^{\circ}$). Discounting the cyclohexyl rings, there is an approximate plane of symmetry passing through the atoms C(2), Pb, Se and P, bisecting the β -diketiminato ligand. The Pb–Se bond length (2.6811(4) Å) is similar to those found in Kato's [Ph₃PbSeCOC₇H₇] (2.6365(5) Å), Jain's [Pb(SeCH₂CH₂NMe₂)] (2.727(3) Å) and Roesky's [(ArSePb)₂(μ -SeAr)] (Ar = (C₆H₂(CF₃)₃), terminal Pb–Se = 2.713(2) Å).^[281, 285-286] The P–Se bond length is 2.2543(9) Å, similar to that in the tin derivative **46** (2.2584(6) Å). As in the other complexes containing dicyclohexylphosphanido ligand reported herein, the internal C–C–C bond angles in the cyclohexyl ring do not deviate significantly from the average value (111°), indicating that there is little distortion in the cyclohexyl chair conformation.

Figure 95. ORTEP diagram of $[(\text{BDI}_{\text{DIPP}})\text{PbSePCy}_2]$ (**47**). H atoms are omitted and C atoms in the *N*-aryl groups in the β -diketiminato ring are minimised for clarity. The ellipsoid probability is shown at 30%

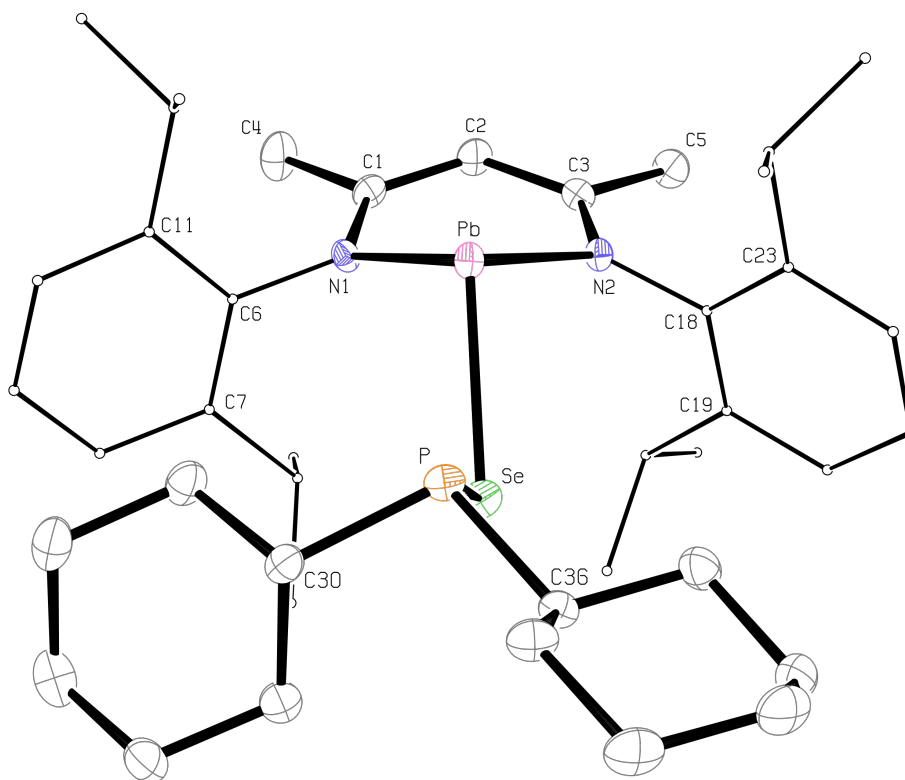


Figure 96. ORTEP diagram showing the side-on view of $[(\text{BDI}_{\text{DIPP}})\text{PbSePCy}_2]$ (**47**). H atoms are omitted and C atoms in the *N*-aryl groups in the β -diketiminato ring and the cyclohexyl groups are minimised for clarity. The ellipsoid probability is shown at 30%

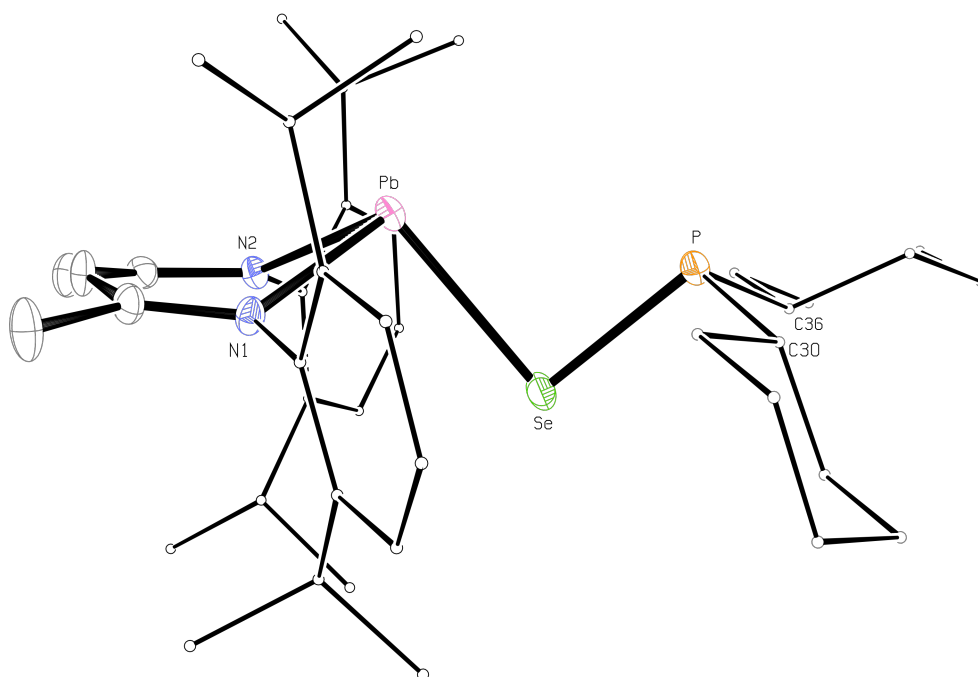


Table 39. Selected bond lengths (Å) and angles (deg) for [(BDI_{DIPP})MSePCy₂] (Cy = cyclohexyl; **46**, M = Sn and **47**, M = Pb)

	[(BDI _{DIPP})SnSePCy ₂] 46 , M = Sn	[(BDI _{DIPP})PbSePCy ₂] 47 , M = Pb
<i>Bond lengths (Å)</i>		
M–N(1)	2.2192(19)	2.326(3)
M–N(2)	2.2097(18)	2.321(3)
N(1)–C(1)	1.327(3)	1.325(4)
N(2)–C(3)	1.330(3)	1.319(4)
C(1)–C(2)	1.404(3)	1.403(5)
C(2)–C(3)	1.408(3)	1.404(5)
M–Se	2.6059(3)	2.6811(4)
P–Se	2.2584(6)	2.2543(9)
P–C(30)	1.873(2)	1.873(4)
P–C(36)	1.867(2)	1.868(4)
M–NCCCN _{plane}	1.025	1.052
<i>Bond angles (deg)</i>		
N(1)–M–N(2)	82.68(7)	79.97(9)
N(1)–M–Se	99.31(5)	99.34(7)
N(2)–M–Se	95.36(5)	95.76(7)
M–N(1)–C(1)	120.33(15)	120.8(2)
M–N(2)–C(3)	121.39(15)	122.1(2)
N(1)–C(1)–C(2)	123.8(2)	124.7(3)
N(2)–C(3)–C(2)	123.3(2)	124.7(3)
C(1)–C(2)–C(3)	128.3(2)	128.9(3)
M–Se–P	91.388(17)	88.59(3)
Se–P–C(30)	102.29(8)	102.50(12)
Se–P–C(36)	100.61(8)	100.77(11)
C(30)–P–C(36)	101.61(11)	102.07(16)
Avg. internal angles of Cy	111	111
NCCCN _{plane} –NMN _{plane}	37.4	35.7
Σ bond angle around M	277.4	275.1
DOP of M (%) ^a	92	94
Σ bond angle around P	304.5	305.3
DOP of P (%) ^a	62	61
<i>Dihedral angles (deg)</i>		
C(11)–C(6)–N(1)–M	74.9(2)	75.2(4)
C(23)–C(18)–N(2)–M	–66.2(3)	–65.4(4)

^a Degree of pyramidalisation (DOP, %) = [(360 – Σ_{bond angle}) / 0.9]^[115] When a DOP is 100%, it is equivalent to a sum of bond angles of 270°, whereas a DOP of 0% indicates a planar geometry at the central atom

Table 40. Selected crystallographic data for [(BDI_{DIPP})MSePCy₂] (Cy = cyclohexyl; **46**, M = Sn and **47**, M = Pb)

	[(BDI _{DIPP})SnSePCy ₂] (46)	[(BDI _{DIPP})PbSePCy ₂] (47)
chemical formula	C ₄₁ H ₆₃ N ₂ PSeSn	C ₄₁ H ₆₃ N ₂ PPbSe
molecular mass	812.55	901.05
temperature (K)	173(2)	173(2)
wavelength (Å)	0.71073	0.71073
crystal system	triclinic	triclinic
space group	<i>P</i> $\bar{1}$ (No. 2)	<i>P</i> $\bar{1}$ (No. 2)
<i>a</i> (Å)	12.1426(2)	12.1375(2)
<i>b</i> (Å)	12.5330(3)	12.5352(3)
<i>c</i> (Å)	14.2375(3)	14.2900(3)
α (deg)	91.844(1)	92.391(1)
β (deg)	97.593(1)	97.371(1)
γ (deg)	108.807(1)	108.474(1)
<i>V</i> (Å ³)	2026.58(7)	2037.23(7)
<i>Z</i>	2	2
ρ_{calcd} (Mg m ⁻³)	1.33	1.47
θ range (deg)	3.43–27.11	3.43–27.11
abs coeff (mm ⁻¹)	1.60	5.10
measd/indep reflns/ <i>R</i> (int)	37 018/8928/0.051	37 354/8987/0.058
reflns with $I > 2\sigma(I)$	7625	7806
data/restraints/param	8928/0/417	8987/0/417
goodness of fit on F^2	1.032	0.973
final <i>R</i> indices [$I > 2\sigma(I)$]	<i>R</i> 1 = 0.030, <i>wR</i> 2 = 0.064	<i>R</i> 1 = 0.030, <i>wR</i> 2 = 0.063
<i>R</i> indices (all data)	<i>R</i> 1 = 0.040, <i>wR</i> 2 = 0.068	<i>R</i> 1 = 0.040, <i>wR</i> 2 = 0.066
largest diff peak and hole (e Å ⁻³)	0.42 and –0.62	0.66 and –1.00

4.4.4 NMR spectra of [(BDI_{DIPP})MSePCy₂] (**46**, M = Sn and **47**, M = Pb)

Selected multinuclear NMR spectroscopic data for **46–47** are given in Table 41.

Table 41. Selected multinuclear NMR spectroscopic data (C₆D₆, 30 °C) for [(BDI_{DIPP})MSePCy₂] (Cy = cyclohexyl; **46**, M = Sn and **47**, M = Pb)

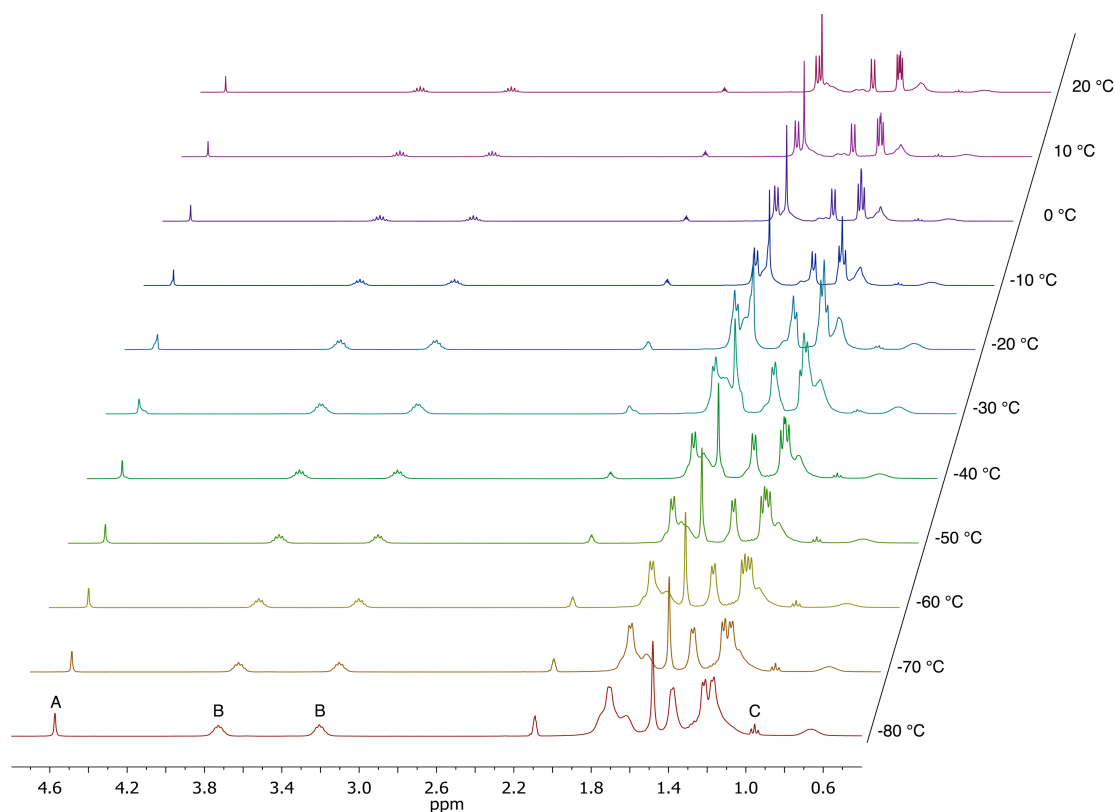
	[(BDI _{DIPP})SnSePCy ₂] (46)	[(BDI _{DIPP})PbSePCy ₂] (47)
	δ (ppm), J (Hz)	δ (ppm), J (Hz)
¹H		
γ -H	4.70 (s)	4.60 (s)
CHMe ₂	3.71 (septet), ³ J _{HH} = 6.8	3.74 (septet), ³ J _{HH} = 6.4
	3.24 (septet), ³ J _{HH} = 6.8	3.13 (septet), ³ J _{HH} = 6.4
¹³C{¹H}		
Cy-CH	35.4 ¹ J _{CP} = 27	35.3 ¹ J _{CP} = 27
CHMe ₂	29.7 (s), 29.0 (s)	30.6 (s), 30.1 (s)
CHMe ₂	27.3, 25.5, 25.2, 25.1 (s)	25.2, 24.9, 24.0, 23.8 (s)
³¹P{¹H}		
	35.6 (s) ¹ J _{PSe} = 178 ² J _{P¹¹⁹Sn} = 960 ² J _{P¹¹⁷Sn} = 916	23.9 (s) ¹ J _{PSe} = 192 ² J _{P²⁰⁷Pb} = 1469
⁷⁷Se		
	-70 (d) ¹ J _{SeP} = 179	-24 (d) ¹ J _{SeP} = 192
Other		
	δ (¹¹⁹ Sn) = 60 (d) ² J _{P¹¹⁹SnP} = 959	δ (²⁰⁷ Pb) = 2596 (d) ² J _{P²⁰⁷PbP} = 1477

4.4.4.1 The β -diketiminatotin(II) dicyclohexylphosphinoselenoite **46**

The ¹H NMR spectrum of **46** shows two septets centred at δ _H 3.71 and 3.24 ppm (³J_{HH} = 6.8 Hz) assigned to the tertiary protons in the isopropyl groups (CHMe₂). However, unlike the dicyclohexylphosphanido complexes discussed previously, no through-space proton-phosphorus coupling (J_{HP}) is observed. This is possibly due to a greater distance between the isopropyl groups and the phosphorus atom. A series of multiplets (δ _H ~ 1.2–1.8 ppm) is assigned to the cyclohexyl CH₂ protons. VT-¹H NMR spectra are

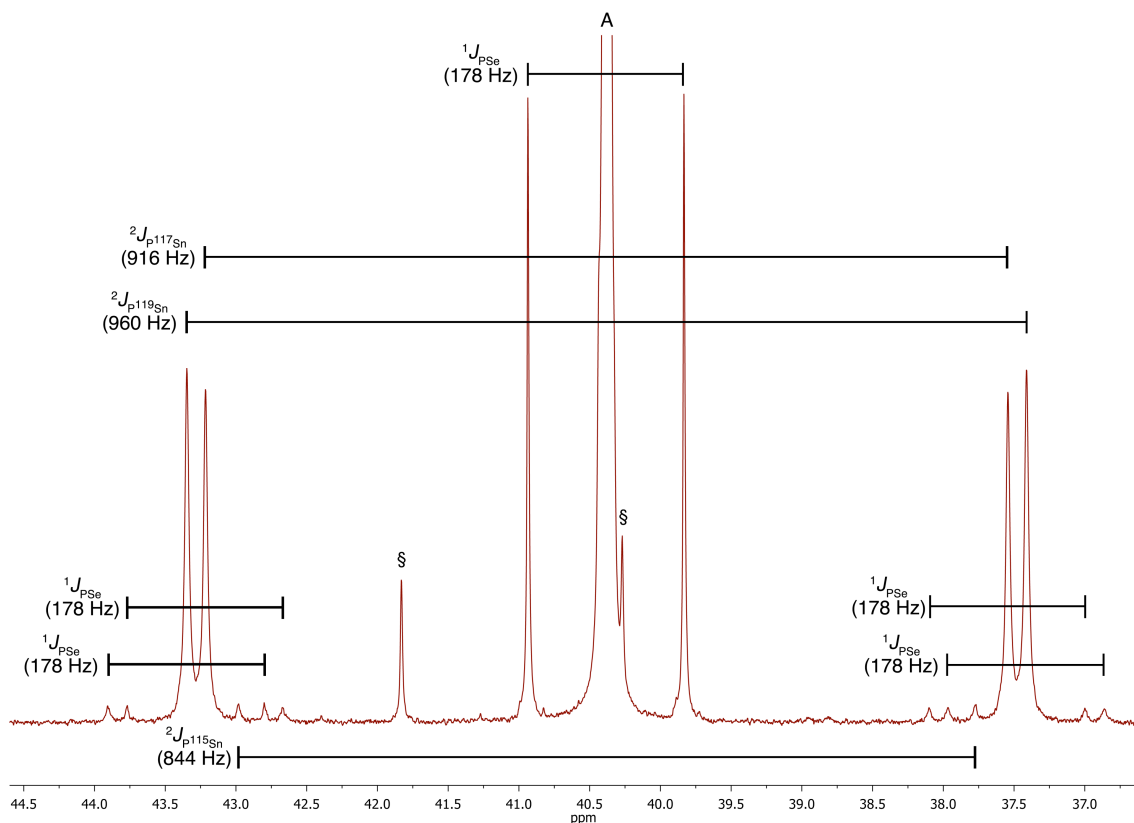
shown in Figure 97. However, the CH_2 resonances remain unresolved within the temperature range 30 to -80 °C.

Figure 97. VT- 1H NMR spectra (400MHz, toluene- d_8) of $[(BDI_{DIIP})SnSePCy_2]$ (**46**) where A = γ -H; B = $CHMe_2$ and C = Cy-CH



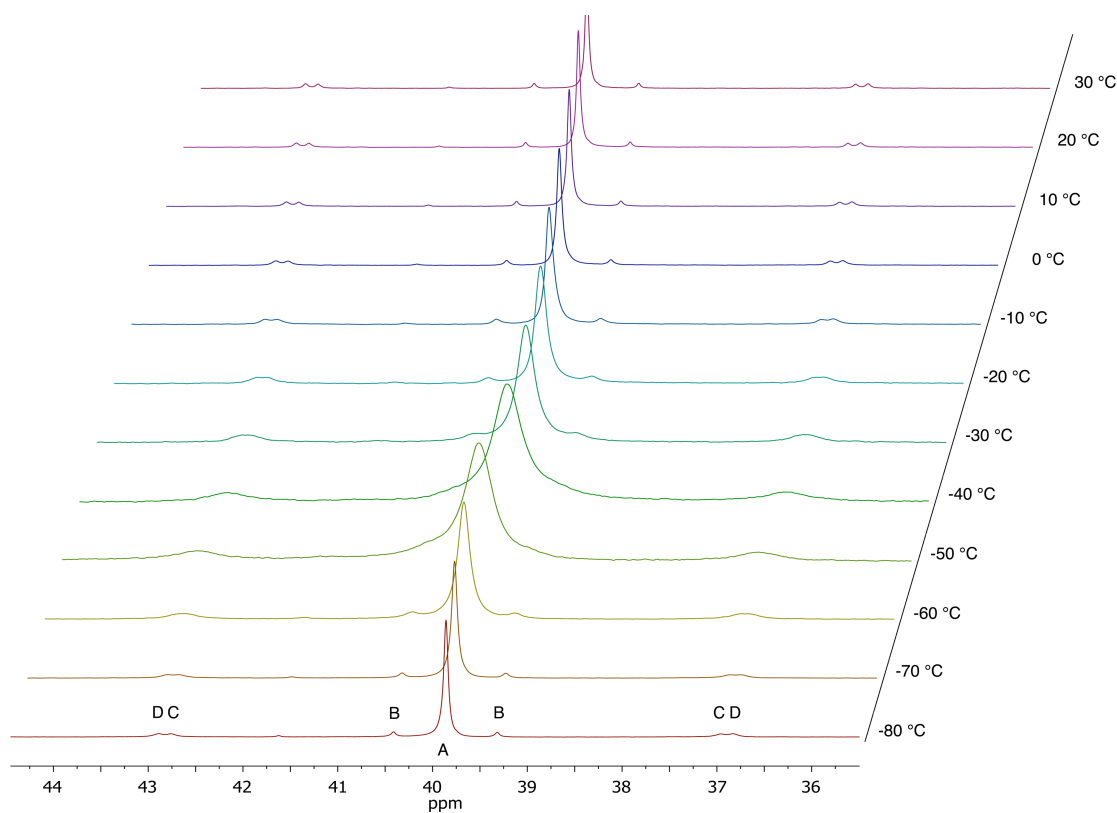
The $^{31}P\{^1H\}$ NMR spectrum of the tin(II) dicyclohexylphosphinoselenoite **46** shows a single resonance at δ_P 35.6 ppm with selenium and tin satellites ($^1J_{PSe} = 178$ Hz, $^2J_{P^{119}Sn} = 960$ Hz and $^2J_{P^{117}Sn} = 916$ Hz). This phosphorus resonance is downfield from the parent tin(II) dicyclohexylphosphanide **37** (δ_P -15.4 ppm). The phosphorus-tin and phosphorus-selenium couplings are confirmed by the ^{119}Sn (δ_{Sn} 60 ppm, $^2J_{^{119}SnP} = 959$ Hz) and the ^{77}Se NMR spectra (δ_{Se} -70 ppm, $^1J_{SeP} = 179$ Hz). A $^{31}P\{^1H\}$ NMR spectrum recorded from a concentrated sample of the tin(II) dicyclohexylphosphinoselenoite **46** in toluene- d_8 with an extended acquisition time revealed additional satellites (Figure 98). The coupling constant $^2J_{P^{115}Sn}$ is 844 Hz. Selenium satellites ($^1J_{PSe} = 178$ Hz) are found alongside the tin satellites.

Figure 98. $^{31}\text{P}\{^1\text{H}\}$ NMR spectrum (162 MHz, toluene- d_8) of $[(\text{BDI}_{\text{DIPP}})\text{SnSePCy}_2]$ (**46**) with an extended acquisition time. The enhanced satellites are indicated in the diagram, and where A = phosphorus resonance. Impurities are designated by §



The VT- $^{31}\text{P}\{^1\text{H}\}$ NMR spectra of **46** are shown in Figure 99. At 30 °C, the $^{31}\text{P}\{^1\text{H}\}$ NMR spectrum shows a single resonance at δ_{P} 40.3 ppm in toluene- d_8 , with selenium and tin satellites ($^1J_{\text{PSe}} = 178$ Hz, $^2J_{\text{P}^{119}\text{Sn}} = 960$ Hz and $^2J_{\text{P}^{117}\text{Sn}} = 917$ Hz). The spectrum recorded at -80 °C shows a single resonance at δ_{P} 39.9 ppm, with selenium and tin satellites ($^1J_{\text{PSe}} = 176$ Hz, $^2J_{\text{P}^{119}\text{Sn}} = 980$ Hz and $^2J_{\text{P}^{117}\text{Sn}} = 940$ Hz). The resonance remains as a single signal, with no significant change in the phosphorus-tin coupling constant ($\Delta^2J_{\text{P}^{119}\text{Sn}} = 20$ Hz), suggesting that there is little change in the geometry around the phosphorus atom as the temperature is lowered.

Figure 99. VT- $^{31}\text{P}\{^1\text{H}\}$ NMR spectra (162 MHz, toluene- d_6) of $[(\text{BDI}_{\text{DIPP}})\text{SnSePCy}_2]$ (**46**) where A = phosphorus resonance; B = ^{77}Se ; C = ^{117}Sn ; and D = ^{119}Sn satellites



The spectroscopic evidence on the tin(II) dicyclohexylphosphanide **37** suggests that the overall conformation observed from the solid state is preserved in solution. To examine whether this is the case for the tin(II) dicyclohexylphosphinoselenoite **46**, multinuclear solid state NMR spectra were recorded. The solid state $^{31}\text{P}\{^1\text{H}\}$ NMR spectrum of **46** shows a single resonance at $\delta_{\text{P(solid)}}$ 31.9 ppm, with selenium and tin satellites ($^1J_{\text{PSe(solid)}} = 190$ Hz and $^2J_{\text{PSn(solid)}} = 897$ Hz). Both phosphorus-selenium and phosphorus-tin coupling constants are similar to those observed in solution ($^1J_{\text{PSe(solution)}} = 178$ Hz; $^2J_{\text{P}^{119}\text{Sn(solution)}} = 960$ Hz) (Table 41, Page 205).

The solid state ^{77}Se NMR spectrum of **46** shows a doublet centred at $\delta_{\text{Se(solid)}}$ -71.3 ppm, with selenium-phosphorus coupling $^1J_{\text{SeP(solid)}} = 184$ Hz, matching that observed from the solid state $^{31}\text{P}\{^1\text{H}\}$ NMR spectrum. Tin satellites were also found around the selenium signal, with selenium-tin coupling constant $^1J_{\text{SeSn(solid)}} = 1160$ Hz. The evidence from the solid state NMR spectra suggest that the conformation of the tin(II) dicyclohexylphosphinoselenoite **46** observed in the solid state is preserved in solution.

4.4.4.2 The β -diketiminatolead(II) dicyclohexylphosphinoselenoite **47**

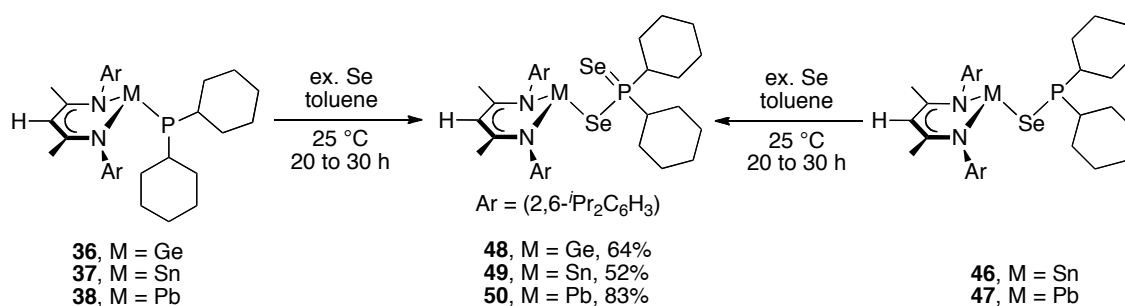
As in the tin derivative **46**, no through-space proton-phosphorus coupling is observed in the septets at δ_{H} 3.74 and 3.13 ppm, assigned to the tertiary protons in the isopropyl groups (CHMe_2) in the ^1H NMR spectrum of the lead(II) dicyclohexylphosphinoselenoite **47**. The $^{13}\text{C}\{^1\text{H}\}$ NMR spectrum does not show through-space carbon-phosphorus coupling between the carbon atoms in the isopropyl groups and the phosphorus atom.

The $^{31}\text{P}\{^1\text{H}\}$ NMR spectrum shows a single resonance at δ_{P} 23.9 ppm with selenium and lead satellites ($^1J_{\text{PSe}} = 192$ Hz and $^2J_{\text{PPb}} = 1469$ Hz). The phosphorus resonance is similar to that observed in the parent lead(II) dicyclohexylphosphanide **38** (δ_{P} 26.9 ppm). The ^{77}Se NMR spectrum shows a doublet centred at δ_{Se} -24 ppm with selenium-phosphorus coupling $^1J_{\text{SeP}} = 192$ Hz. A doublet centred at δ_{Pb} 2596 ppm with lead-phosphorus coupling $^2J_{\text{PbP}} = 1477$ Hz is shown in the ^{207}Pb NMR spectrum of **47**.

4.4.5 Synthesis of β -diketiminato heavy group 14 metal dicyclohexylphosphinodiselenoates **48–50**

Treatment of the β -diketiminato heavy group 14 metal dicyclohexylphosphanides **36–38** with an excess of elemental selenium in toluene with rapid stirring at room temperature give the corresponding heavy group 14 metal dicyclohexylphosphinodiselenoato complexes $[(\text{BDI}_{\text{DIPP}})\text{GeSeP}(\text{Se})\text{Cy}_2]$ (**48**), $[(\text{BDI}_{\text{DIPP}})\text{SnSeP}(\text{Se})\text{Cy}_2]$ (**49**) and $[(\text{BDI}_{\text{DIPP}})\text{PbSeP}(\text{Se})\text{Cy}_2]$ (**50**) in 64, 52 and 83% yields, respectively (Scheme 63). Alternatively, the tin(II) and lead(II) derivatives **49** and **50** can be synthesised *via* treatment of the corresponding dicyclohexylphosphinoselenoito complexes, **46** and **47**, with an excess of elemental selenium at room temperature. However, the latter route is not efficient as it is previously established that the dicyclohexylphosphinoselenoito complexes are difficult to isolate (Section 4.4.2, Page 197).

Scheme 63. Synthesis of $[(BDI_{DIPP})MSeP(Se)Cy_2]$ (Cy = cyclohexyl; **48**, M = Ge; **49**, M = Sn; and **50**, M = Pb)



Complexes **48–50** are sensitive to air, moisture and light. Metallic precipitates are formed when they are allowed to stand in toluene under ambient light for 24 hours at room temperature. However, they can be stored as solids at $-30\text{ }^{\circ}\text{C}$ for several weeks without decomposition. Elemental analyses of the tin(II) and lead(II) derivatives **49** and **50** are in good agreement with the calculated values. The germanium analogue **48** could not be obtained pure, hence the elemental analysis on the compound was not satisfactory.

4.4.6 X-ray crystal structures of $[(BDI_{DIPP})MSeP(Se)Cy_2]$ (**48**, M = Ge; **49**, M = Sn; and **50**, M = Pb)

Orange crystals of $[(BDI_{DIPP})GeSeP(Se)Cy_2]$ (**48**) were obtained from toluene at $-30\text{ }^{\circ}\text{C}$. ORTEP drawings of the germanium(II) dicyclohexylphosphinodiselenoate **48** are shown in Figures 100 and 101. Selected bond lengths and angles are given in Table 42, and selected crystallographic data in Table 43. The germanium compound **48** adopts an *exo* conformation with the germanium atom 0.987 \AA above the mean NCCCN plane in the β -diketiminato ligand. The geometry around the germanium atom is pyramidal, with the sum of bond angles 277.8° . The electrons are delocalised within the C_3N_2Ge unit in the β -diketiminato ligand, but not on to the *N*-aryl substituents (dihedral angles: $C(11)-C(6)-N(1)-Ge = 74.9(3)^{\circ}$ and $C(23)-C(18)-N(2)-Ge = -74.9(3)^{\circ}$). Apart from the cyclohexyl rings, there is an approximate plane of symmetry passing through the atoms C(2), Ge, Se(1), P, and Se(2). The phosphorus atom is coordinated to two selenium atoms and two carbon atoms from the cyclohexyl groups in a distorted tetrahedral geometry. The Ge–Se(1) bond length is $2.4613(4)\text{ \AA}$. It may be compared with those values in Liu's $[Ph_3GeSeP(Se)(OEt)_2]$ ($2.405(9)\text{ \AA}$) and Kato's

[Ph₃GeSeC(O)(*p*-Tol)] (2.3760(4) Å).^[245, 281] The P–Se(1) bond length is 2.2208(7) Å and the P–Se(2) bond (2.1114(7) Å) is shorter. The P–Se(2) bond distance is similar to the P=Se bond length in Liu's [Ph₃GeSeP(Se)(OEt)₂] (2.0775(17) Å) and Krauss' [Pb{SeP(Se)Ph₂}₂] (2.147(1) Å), and is indicative of a selenium-phosphorus double bond.^[245, 287] The distance between the Ge and Se(2) atoms is 3.711 Å, which is significantly longer than the Ge–Se(1) bond (2.4613(4) Å). The bond angles Ge–Se(1)–P (100.77(2)°) and Se(1)–P–Se(2) (117.92(3)°) are significantly wider than Ge–Se(2)–P (70.64°) and Se(1)–Ge–Se(2) (70.67°). This evidence suggests that the ligand (SeP(Se)Cy₂) is coordinated to the germanium atom in η^1 -fashion. These findings differ from those for related compounds containing ligands with the SeP(Se) fragment which are coordinated in η^2 -fashion, for example in Woolin's [Pb{SeP(Se)Ph(OEt)}₂] (avg. Pb–Se–P = 91.38°, avg. Se–P–Se = 111.29° and avg. Se–Pb–Se = 73.42°) and Krauss' [Pb{SeP(Se)Ph₂}₂] (avg. Pb–Se–P = 84.62°, avg. Se–P–Se = 112.91° and avg. Se–Pb–Se = 74.1°).^[247, 287]

Figure 100. ORTEP diagram of $[(\text{BDI}_{\text{DIPP}})\text{GeSeP}(\text{Se})\text{Cy}_2]$ (**48**). H atoms are omitted and C atoms in the *N*-aryl groups in the β -diketiminato ring are minimised for clarity. The ellipsoid probability is shown at 30%

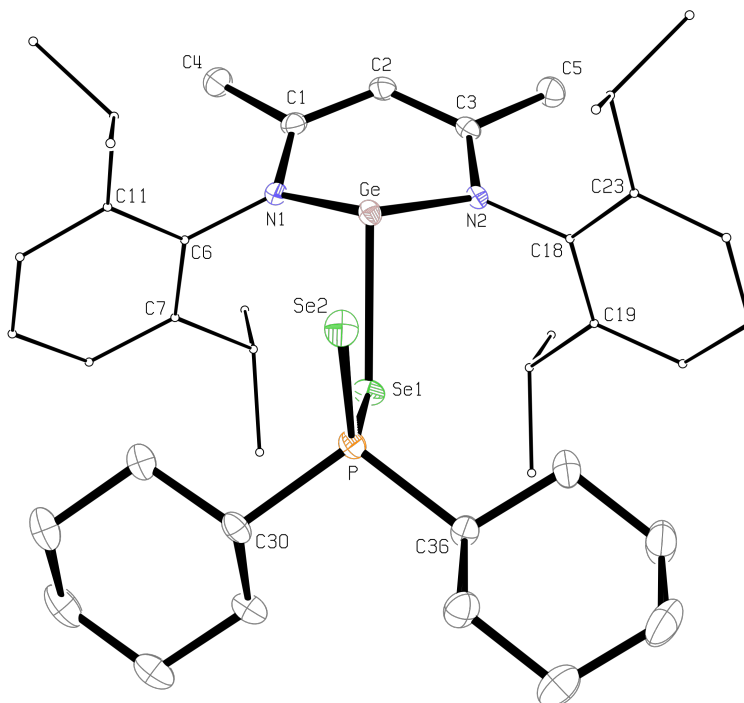
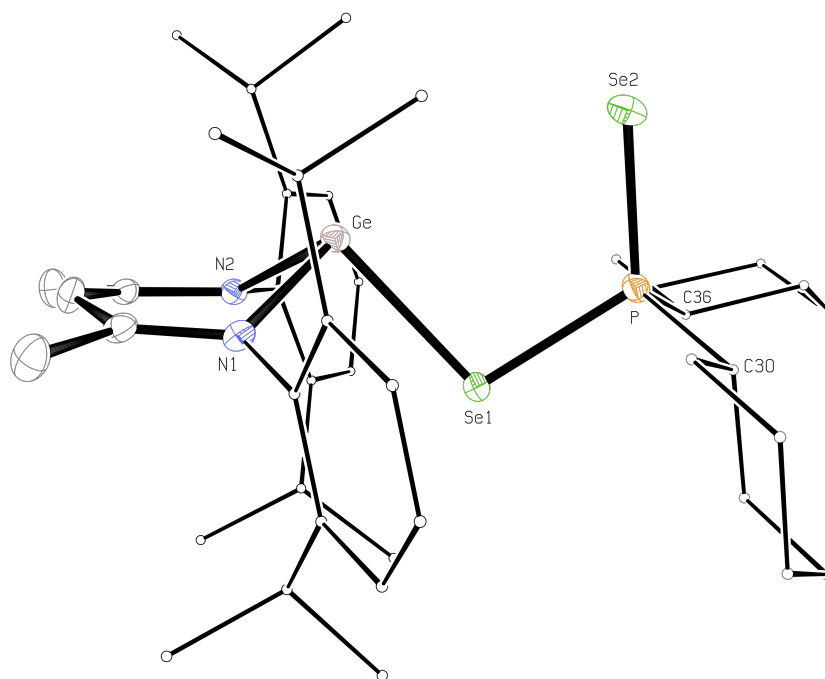


Figure 101. ORTEP diagram showing the side-on view of $[(\text{BDI}_{\text{DIPP}})\text{GeSeP}(\text{Se})\text{Cy}_2]$ (**48**). H atoms are omitted and C atoms in the *N*-aryl groups in the β -diketiminato ring and the cyclohexyl groups are minimised for clarity. The ellipsoid probability is shown at 30%



Yellow crystals of [(BDI_{DIPP})SnSeP(Se)Cy₂] (**49**) were obtained from toluene at $-30\text{ }^{\circ}\text{C}$. ORTEP drawings are shown in Figures 102 and 103. Selected bond lengths and angles are given in Table 42, and selected crystallographic data in Table 43. The tin compound **49** adopts an *exo* conformation, with the tin atom 1.089 Å above the mean NCCCN plane of the β -diketiminato ligand. The geometry around the tin atom is pyramidal with the sum of bond angles 271.3° . The electrons are delocalised within the C₃N₂Sn unit, but not on to the *N*-aryl substituents (dihedral angles: C(11)–C(6)–N(1)–Sn = $74.3(4)^{\circ}$ and C(23)–C(18)–N(2)–Sn = $-70.1(4)^{\circ}$). Discounting the cyclohexyl rings, there is an approximate plane of symmetry passing through the atoms C(2), Sn, Se(1), P, and Se(2). The phosphorus atom has a distorted tetrahedral configuration, with bond angles at phosphorus ranging from $104.39(13)^{\circ}$ to $116.62(5)^{\circ}$. The Sn–Se(1) bond length is 2.6549(5) Å, similar to that observed in the tin(II) dicyclohexylphosphinoselenoite **46** (2.6059(3) Å). As in the germanium derivative **48**, the P–Se(2) bond length (2.1197(11) Å) in **49** is shorter than the P–Se(1) bond distance (2.2194(11) Å). These P–Se bond lengths are similar to those observed in the germanium derivative **48**. The distance (3.508 Å) between the Sn and Se(2) atom is significantly longer than the typical Sn–Se bond length (2.55–2.60 Å), indicating that there is no formal bond.^[282] The bond angles Sn–Se(1)–P ($95.14(3)^{\circ}$) and Se(1)–P–Se(2) ($116.62(5)^{\circ}$) are significantly wider than Sn–Se(2)–P (75.32°) and Se(1)–Sn–Se(2) (72.12°), suggesting that the ligand (SeP(Se)Cy₂) is coordinated to the tin centre in η^1 -fashion. The internal C–C–C bond angles in the cyclohexyl group do not deviate significantly from the average value (111°), indicating that there is little distortion in the chair conformation in the cyclohexyl groups.

Figure 102. ORTEP diagram of $[(\text{BDI}_{\text{DIPP}})\text{SnSeP}(\text{Se})\text{Cy}_2]$ (**49**). H atoms are omitted and C atoms in the *N*-aryl groups in the β -diketiminato ring are minimised for clarity. The ellipsoid probability is shown at 30%

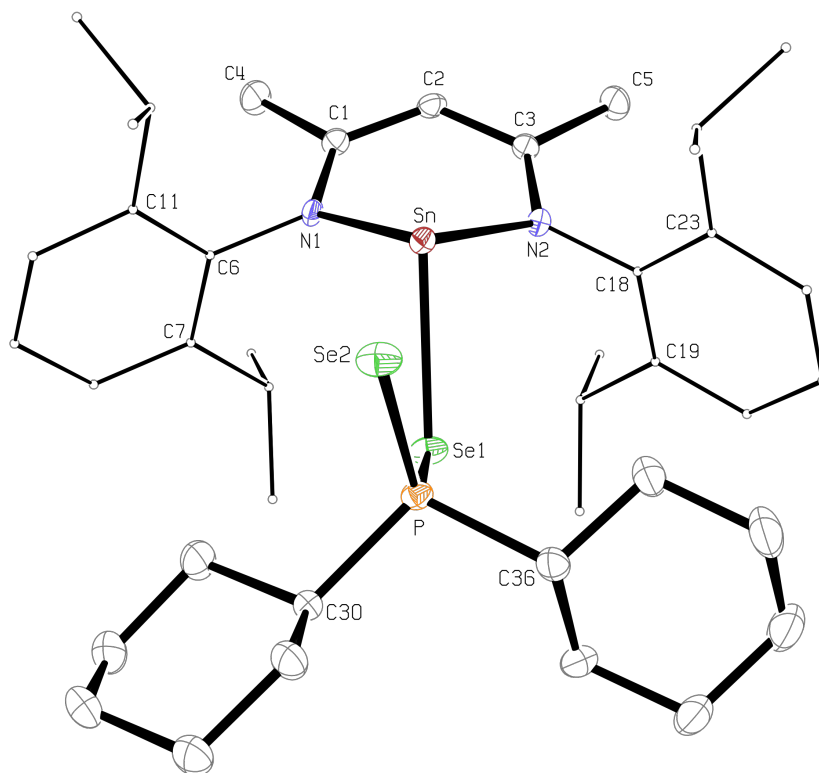
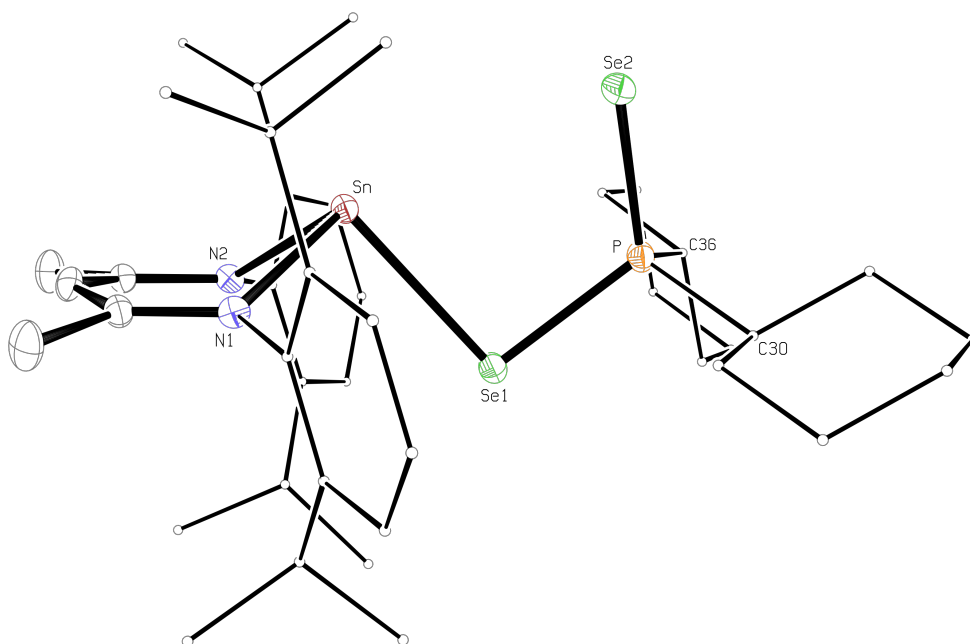


Figure 103. ORTEP diagram showing the side-on view of $[(\text{BDI}_{\text{DIPP}})\text{SnSeP}(\text{Se})\text{Cy}_2]$ (**49**). H atoms are omitted and C atoms in the *N*-aryl groups in the β -diketiminato ring and the cyclohexyl groups are minimised for clarity. The ellipsoid probability is shown at 30%



Single crystals of [(BDI_{DIPP})PbSeP(Se)Cy₂] (**50**) were obtained from toluene at $-30\text{ }^{\circ}\text{C}$. ORTEP drawings of compound **50** are shown in Figures 104 and 105. Selected bond lengths and angles are given in Table 42, and selected crystallographic data in Table 43. The lead(II) dicyclohexylphosphinodiselenoate **50** adopts an *exo* conformation, with the lead atom 1.146 Å above the mean NCCCN plane of the β-diketiminato ligand. The geometry around the lead atom is pyramidal with the sum of bond angles 268.1° . The electrons are delocalised within the C₃N₂Pb unit in the β-diketiminato ligand, but not on to the *N*-aryl substituents (dihedral angles: C(11)–C(6)–N(1)–Pb = $69.8(3)^{\circ}$ and C(23)–C(18)–N(2)–Pb = $-74.7(4)^{\circ}$). Discounting the cyclohexyl groups, there is an approximate plane of symmetry passing through the atoms C(2), Pb, Se(1), P and Se(2). The Pb–Se(1) bond length is 2.7417(4) Å, which is slightly longer than that in the lead(II) dicyclohexylphosphinoselenoite **47** (2.6811(4) Å). As in the germanium and tin analogues, **48** and **49**, the P–Se(1) bond length (2.2094(10) Å) is longer than the P–Se(2) bond distance (2.1287(11) Å). The P–Se(2) bond distance in **50** is similar to the previously identified P=Se double bond in the germanium and tin derivatives **48** and **49** (2.1114(7) Å and 2.1197(11) Å, respectively), and also to the P=Se bond in Liu's [Ph₃PbSeP(Se)(OEt₂)₂] (2.071(3) Å).^[245] The distance (3.396 Å) between the Pb and Se(2) atom in **50** is significantly longer than the Pb–Se(1) bond length (2.7417(4) Å), as well as that in [(BDI_{DIPP})PbSePCy₂] (**47**, Pb–Se = 2.6811(4) Å), suggesting the absence of a formal bond. The bond angles Pb–Se(1)–P ($92.79(3)^{\circ}$) and Se(1)–P–Se(2) ($115.97(5)^{\circ}$) are wider than the angles Pb–Se(2)–P (77.72°) and Se(1)–Pb–Se(2) (72.77°), suggesting that the ligand (SeP(Se)Cy₂) is coordinated to the lead atom in η¹-fashion. The internal C–C–C bond angles in the cyclohexyl ring do not deviate significantly from the average value (111°), indicating that there is little distortion to the chair conformation in the cyclohexyl rings.

Figure 104. ORTEP diagram of $[(\text{BDI}_{\text{DIPP}})\text{PbSeP}(\text{Se})\text{Cy}_2]$ (**50**). H atoms are omitted and C atoms in the *N*-aryl groups in the β -diketiminato ring are minimised for clarity. The ellipsoid probability is shown at 30%

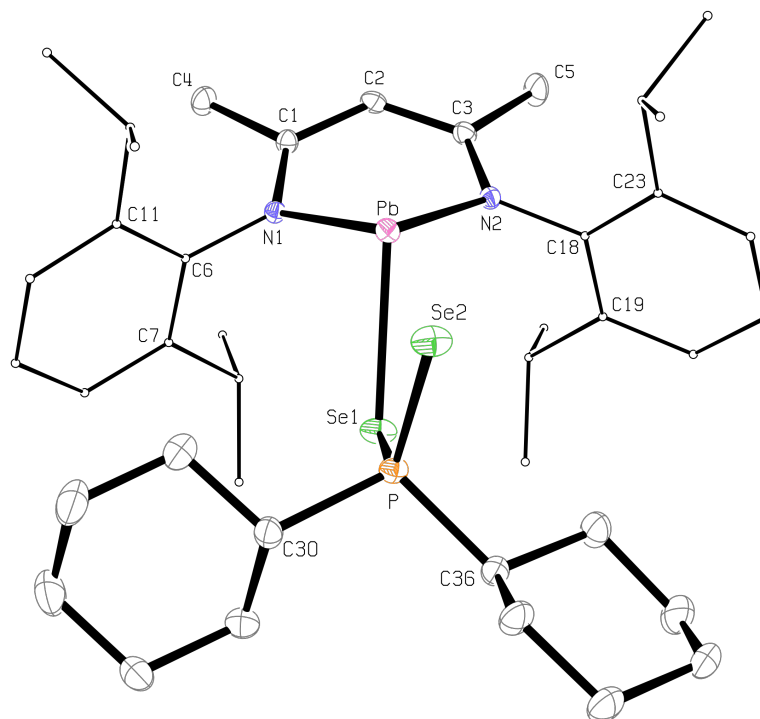


Figure 105. ORTEP diagram showing the side-on view of $[(\text{BDI}_{\text{DIPP}})\text{PbSeP}(\text{Se})\text{Cy}_2]$ (**50**). H atoms are omitted, C atoms in the *N*-aryl groups in the β -diketiminato ring and the cyclohexyl groups are minimised for clarity. The ellipsoid probability is shown at 30%

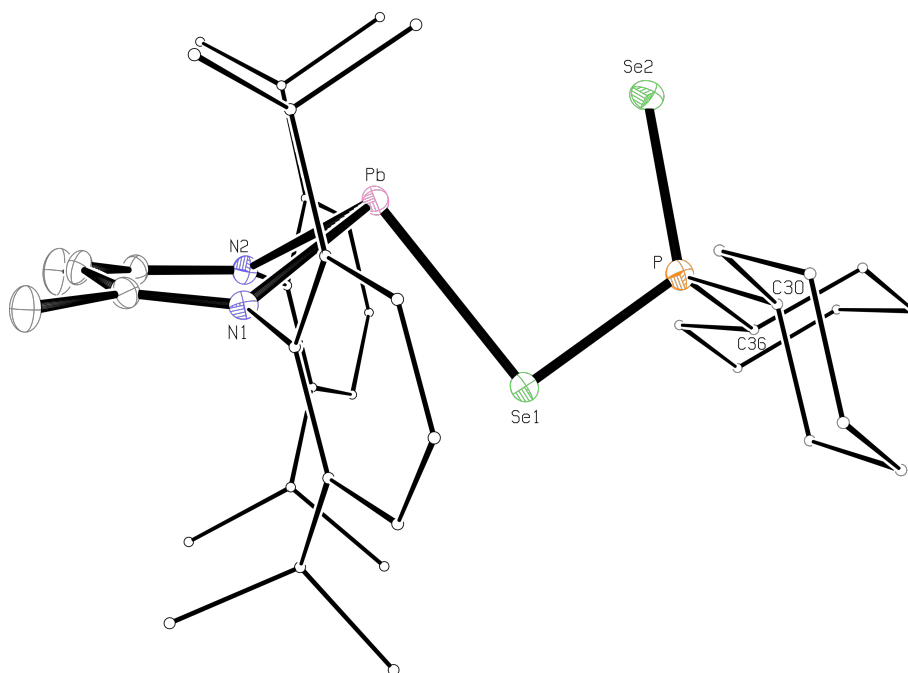


Table 42. Selected bond lengths (Å) and angles (deg) for [LMSeP(Se)Cy₂] (L = (BDI)_{DIPP}); Cy = cyclohexyl; **48**, M = Ge; **49**, M = Sn; and **50**, M = Pb)

	[LGeSeP(Se)Cy ₂] 48 , M = Ge	[LSnSeP(Se)Cy ₂] 49 , M = Sn	[LPbSeP(Se)Cy ₂] 50 , M = Pb
<i>Bond lengths (Å)</i>			
M–N(1)	2.020(2)	2.239(3)	2.346(3)
M–N(2)	2.0320(19)	2.225(3)	2.356(3)
N(1)–C(1)	1.336(3)	1.320(5)	1.319(4)
N(2)–C(3)	1.328(3)	1.328(5)	1.328(5)
C(1)–C(2)	1.396(4)	1.398(6)	1.409(5)
C(2)–C(3)	1.396(4)	1.410(6)	1.404(5)
M–Se(1)	2.4613(4)	2.6549(5)	2.7417(4)
P–Se(1)	2.2208(7)	2.2194(11)	2.2094(10)
P–Se(2)	2.1114(7)	2.1197(11)	2.1287(11)
P–C(30)	1.849(3)	1.843(4)	1.845(4)
P–C(36)	1.837(3)	1.846(4)	1.841(4)
M–Se(2)	3.711	3.508	3.396
M–NCCCN _{Plane}	0.987	1.089	1.146
<i>Bond angles (deg)</i>			
N(1)–M–N(2)	88.72(8)	82.89(11)	80.13(10)
N(1)–M–Se(1)	94.84(6)	96.83(8)	90.05(7)
N(2)–M–Se(1)	94.20(6)	91.53(8)	97.93(7)
N(1)–C(1)–C(2)	122.6(2)	125.0(4)	125.0(3)
N(2)–C(3)–C(2)	122.8(2)	123.9(4)	124.9(3)
C(1)–C(2)–C(3)	127.2(2)	128.5(4)	129.7(4)
M–Se(1)–P	100.77(2)	95.14(3)	92.79(3)
C(30)–P–C(36)	106.83(12)	107.23(18)	107.50(18)
Se(1)–P–Se(2)	117.92(3)	116.62(5)	115.97(5)
C(30)–P–Se(2)	112.52(9)	111.17(14)	110.95(14)
C(36)–P–Se(2)	113.29(10)	111.29(15)	110.82(13)
M–Se(2)–P	70.64	75.32	77.72
Se(1)–M–Se(2)	70.67	72.12	72.77
Avg. int. angles of Cy	111	111	111
NCCCN _{plane} –NMN _{plane}	42.1	40.0	39.0
Σ bond angle around M	277.8	271.3	268.1
DOP of M (%) ^a	91	99	102
<i>Dihedral angles (deg)</i>			
C(11)–C(6)–N(1)–M	74.9(3)	74.3(4)	69.8(3)
C(23)–C(18)–N(2)–M	–74.9(3)	–70.1(4)	–74.7(4)

^a Degree of pyramidalisation (DOP, %) = [(360 – Σ_{bond angle}) / 0.9]^[115] When a DOP is 100%, it is equivalent to a sum of bond angles of 270°, whereas a DOP of 0% indicates a planar geometry at the central atom

Table 43. Selected crystallographic data for [LMSeP(Se)Cy₂] (L = (BDI_{DIPP}); Cy = cyclohexyl; **48**, M = Ge; **49**, M = Sn; and **50**, M = Pb)

	[LGeSeP(Se)Cy ₂] (48)	[LSnSeP(Se)Cy ₂] (49)	[LPbSeP(Se)Cy ₂] (50)
chemical formula	C ₄₁ H ₆₃ GeN ₂ PSe ₂ , C ₇ H ₈	C ₄₁ H ₆₃ N ₂ PSe ₂ Sn, C ₇ H ₈	C ₄₁ H ₆₃ N ₂ PPbSe ₂ , C ₇ H ₈
molecular mass	937.55	983.65	1072.15
temperature (K)	173(2)	173(2)	173(2)
wavelength (Å)	0.71073	0.71073	0.71073
crystal system	monoclinic	orthorhombic	orthorhombic
space group	<i>P</i> 2 ₁ / <i>c</i> (No. 14)	<i>P</i> 2 ₁ 2 ₁ 2 ₁ (No. 19)	<i>P</i> 2 ₁ 2 ₁ 2 ₁ (No. 19)
<i>a</i> (Å)	13.1356(3)	10.3830(1)	10.3409(1)
<i>b</i> (Å)	18.3304(3)	15.4846(2)	15.5230(2)
<i>c</i> (Å)	20.4944(5)	29.7411(4)	29.7674(3)
<i>α</i> (deg)	90	90	90
<i>β</i> (deg)	103.174(1)	90	90
<i>γ</i> (deg)	90	90	90
<i>V</i> (Å ³)	4804.79(18)	4781.67(10)	4778.32(9)
<i>Z</i>	4	4	4
ρ_{calcd} (Mg m ⁻³)	1.30	1.37	1.49
θ range (deg)	3.49–27.06	3.56–27.10	3.56–27.11
abs coeff (mm ⁻¹)	2.218	2.12	5.12
measd/indepent reflins/ <i>R</i> (int)	32616/10466/0.049	78235/10512/0.079	67740/10498/0.066
data/restraints/param	10466/0/489	10512/0/454	10498/0/489
goodness of fit on <i>F</i> ²	0.997	1.022	1.031
final <i>R</i> indices [<i>I</i> > 2 σ (<i>I</i>)]	<i>R</i> 1 = 0.037, <i>wR</i> 2 = 0.076	<i>R</i> 1 = 0.037, <i>wR</i> 2 = 0.074	<i>R</i> 1 = 0.026, <i>wR</i> 2 = 0.049
<i>R</i> indices (all data)	<i>R</i> 1 = 0.058, <i>wR</i> 2 = 0.083	<i>R</i> 1 = 0.050, <i>wR</i> 2 = 0.0780	<i>R</i> 1 = 0.031, <i>wR</i> 2 = 0.051
largest diff peak and hole (e Å ⁻³)	0.66 and -0.49	1.174 and -0.473	0.65 and -0.43

4.4.7 NMR spectra of [(BDI_{DIPP})MSeP(Se)Cy₂] (**48**, M = Ge; **49**, M = Sn; and **50**, M = Pb)

Selected multinuclear NMR spectroscopic data for **48–50** are given in Table 44.

Table 44. Selected multinuclear NMR spectroscopic data (30 °C) for [LMSeP(Se)Cy₂] (L = (BDI_{DIPP}); Cy = cyclohexyl; **48**, M = Ge; **49**, M = Sn; and **50**, M = Pb)

	[LGeSeP(Se)Cy ₂] (48)	[LSnSeP(Se)Cy ₂] (49)	[LPbSeP(Se)Cy ₂] (50)
	δ (ppm), J (Hz) ^a	δ (ppm), J (Hz) ^b	δ (ppm), J (Hz) ^a
¹H			
γ -H	4.68 (s)	4.66 (s)	4.58 (s)
CHMe ₂	3.50 (septet) ³ J _{HH} = 6.8	3.49 (br) 3.18 (br)	3.36 (septet) ³ J _{HH} = 6.8
	3.31 (septet) ³ J _{HH} = 6.8		
Cy-CH	1.03 (br)	0.87 (t) ² J _{HP} = 6.8 Hz	1.02 (br)
¹³C			
Cy-CH	43.1 (d) ¹ J _{CP} = 38	42.5 (d) ¹ J _{CP} = 36	43.7 (d) ¹ J _{CP} = 34
CHMe ₂	29.8, 27.1 (s)	29.2, 25.2 (s)	29.1, 26.9 (s)
CHMe ₂	26.6, 25.7, 24.9, 23.6 (s)	23.6, 22.8 (s)	26.6, 26.1, 25.6, 24.3 (s)
³¹P{¹H}			
	63.7 (s) ¹ J _{PSe} = 551 ^c	58.7 (s) ¹ J _{PSe} = 539 ² J _{P¹¹⁹Sn} = 246 ² J _{P¹¹⁷Sn} = 236	57.0 (s) ¹ J _{PSe} = 521 ² J _{PPb} = 218
⁷⁷Se			
	-18 (d) ¹ J _{SeP} = 198 ^c	-73 (d) ^a ¹ J _{SeP} = 540 ¹ J _{SeSn} = 307	-47 (d) ¹ J _{SeP} = 544
Other			
	-	$\delta(^{119}\text{Sn}) = -88$ (d) ^a ² J _{P¹¹⁹SnP} = 247	$\delta(^{207}\text{Pb}) = 1909$ (d) ² J _{PbP} = 217

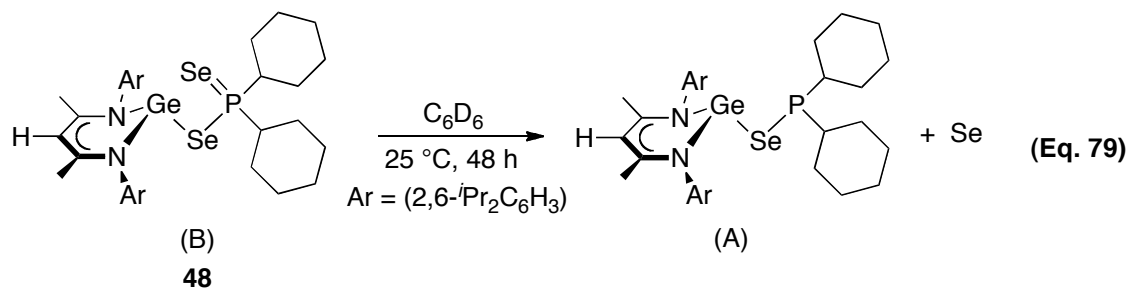
^a in C₆D₆, ^b in toluene-*d*₆ unless specified, ^c see Section 4.4.7.1, Page 219

4.4.7.1 The β -diketiminatogermanium(II) dicyclohexylphosphinodiselenoate **48**

The ¹H NMR spectrum of **48** shows two septets centred at δ_{H} 3.50 and 3.31 ppm, with through-bond proton-proton coupling (³J_{HH} = 6.8 Hz) assigned to the tertiary protons in the isopropyl groups (CHMe₂). However, unlike the parent dicyclohexylphosphanido complexes **36–38**, through-space proton-phosphorus coupling is not observed in the CHMe₃ resonance. We attribute this to the longer distance between the phosphorus and

protons in the isopropyl groups. A broad signal at δ_{H} 1.03 ppm is assigned to the tertiary CH protons in the cyclohexyl groups. The $^2J_{\text{HP}}$ coupling is not observed due to overlap of the multiplets assigned to the CH_2 protons in the cyclohexyl groups. The $^{13}\text{C}\{^1\text{H}\}$ NMR spectrum shows a doublet centred at δ_{C} 43.1 ppm ($^1J_{\text{CP}} = 38$ Hz). This is assigned to the tertiary CH carbon in the cyclohexyl groups. No through-space isopropyl carbon-phosphorus coupling is observed.

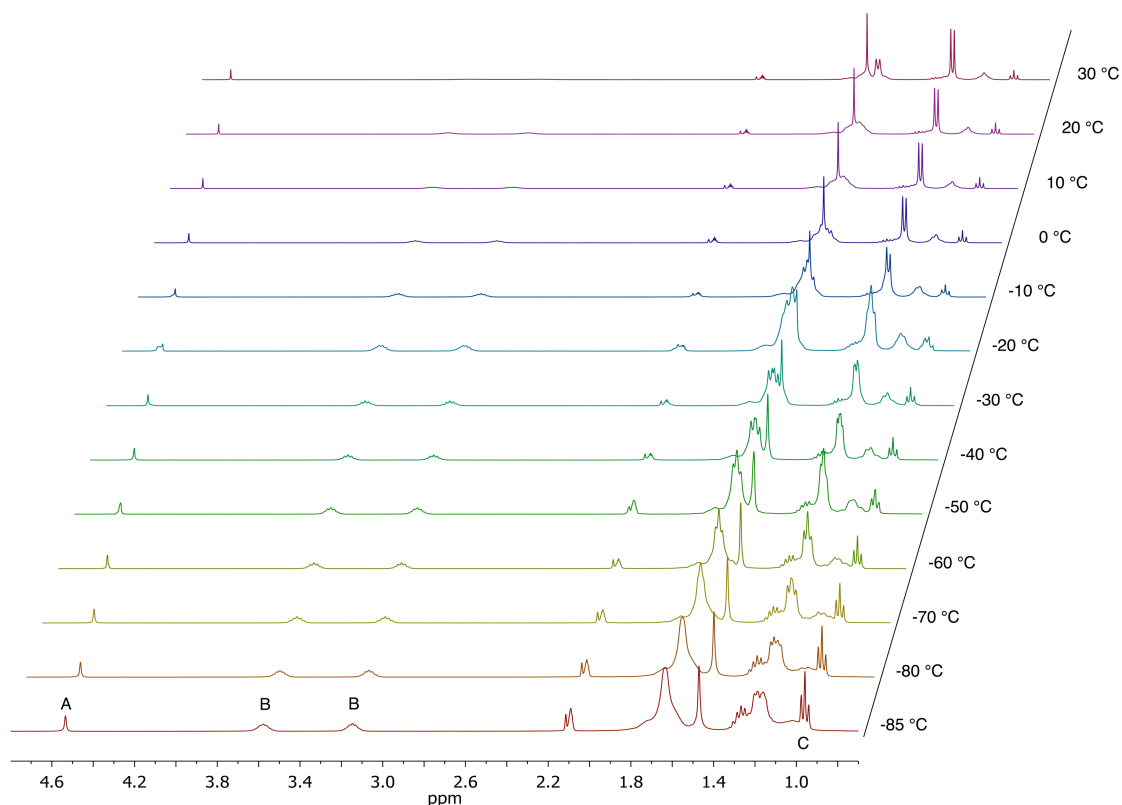
The $^{31}\text{P}\{^1\text{H}\}$ NMR spectrum of **48** shows a single resonance at δ_{P} 63.7 ppm ($^1J_{\text{PSe}} = 551$ Hz), downfield from that observed in the germanium(II) dicyclohexylphosphanide **36** ($\delta_{\text{P}} -14.1$ ppm). The ^{77}Se NMR spectrum of **48** shows a doublet centred at $\delta_{\text{Se}} -18$ ppm. However, the selenium-phosphorus coupling constant ($^1J_{\text{SeP}} = 198$ Hz) observed from the ^{77}Se NMR spectrum is not in agreement with that observed from the $^{31}\text{P}\{^1\text{H}\}$ NMR spectrum. The magnitude of the $^1J_{\text{SeP}}$ coupling constant found in the ^{77}Se NMR spectrum is similar to those in the phosphinoselenoito complexes $[(\text{BDI}_{\text{DIPP}})\text{SnSePCy}_2]$ (**46**, $^1J_{\text{SeP}} = 178$ Hz) and $[(\text{BDI}_{\text{DIPP}})\text{PbSePCy}_2]$ (**47**, $^1J_{\text{SeP}} = 192$ Hz). Several attempts to locate a second resonance associated with the selenium in the P=Se fragment were not successful. It should be noted that the ^{77}Se NMR spectrum was recorded two days after the $^{31}\text{P}\{^1\text{H}\}$ NMR spectrum was taken. Over the course of the period, the mixture was not stirred and metallic precipitates were found in the NMR tube containing the sample in C_6D_6 . Hence, based on the similarity of $^1J_{\text{SeP}}$ coupling constants to those in compounds **46** and **47**, we propose that the sample had decomposed to form the phosphinoselenoito complex A $[(\text{BDI}_{\text{DIPP}})\text{GeSePCy}_2]$ (Equation 79). The compound A in equation 79 appears to be different from its isomer $[(\text{BDI}_{\text{DIPP}})\text{Ge}(\text{Se})\text{PCy}_2]$ (**51**, $\delta_{\text{Se}} -91$ ppm in CDCl_3 , $^2J_{\text{SeP}} = 12$ Hz, Page 231). These results were obtained at the end of the project, so there was not time to obtain further evidence to substantiate this proposal.



4.4.7.2 The β -diketiminatotin(II) dicyclohexylphosphinodiselenoate **49**

The ^1H NMR spectrum of **49** shows a triplet at δ_{H} 0.87 ppm, with $^2J_{\text{HP}} = 6.8$ Hz, assigned to the tertiary CH protons in the cyclohexyl groups. A series of multiplets in the range δ_{H} 0.96–1.27 ppm is assigned to the CH_2 protons in the cyclohexyl groups. Two broad signals at δ_{H} 3.49 and 3.18 ppm in toluene- d_8 , are assigned to the tertiary protons in the isopropyl groups (CHMe_2). A VT- ^1H NMR experiment (Figure 106) showed at -85 °C, two distinctive signals at δ_{H} 3.53 and 3.12 ppm ($\Delta\delta_{\text{H}}$ 164 Hz) in toluene- d_8 were assigned to the tertiary protons in the isopropyl groups (CHMe_2). However, the coalescence temperature was not reached due to decomposition of the tin(II) dicyclohexylphosphinodiselenoate **49**.

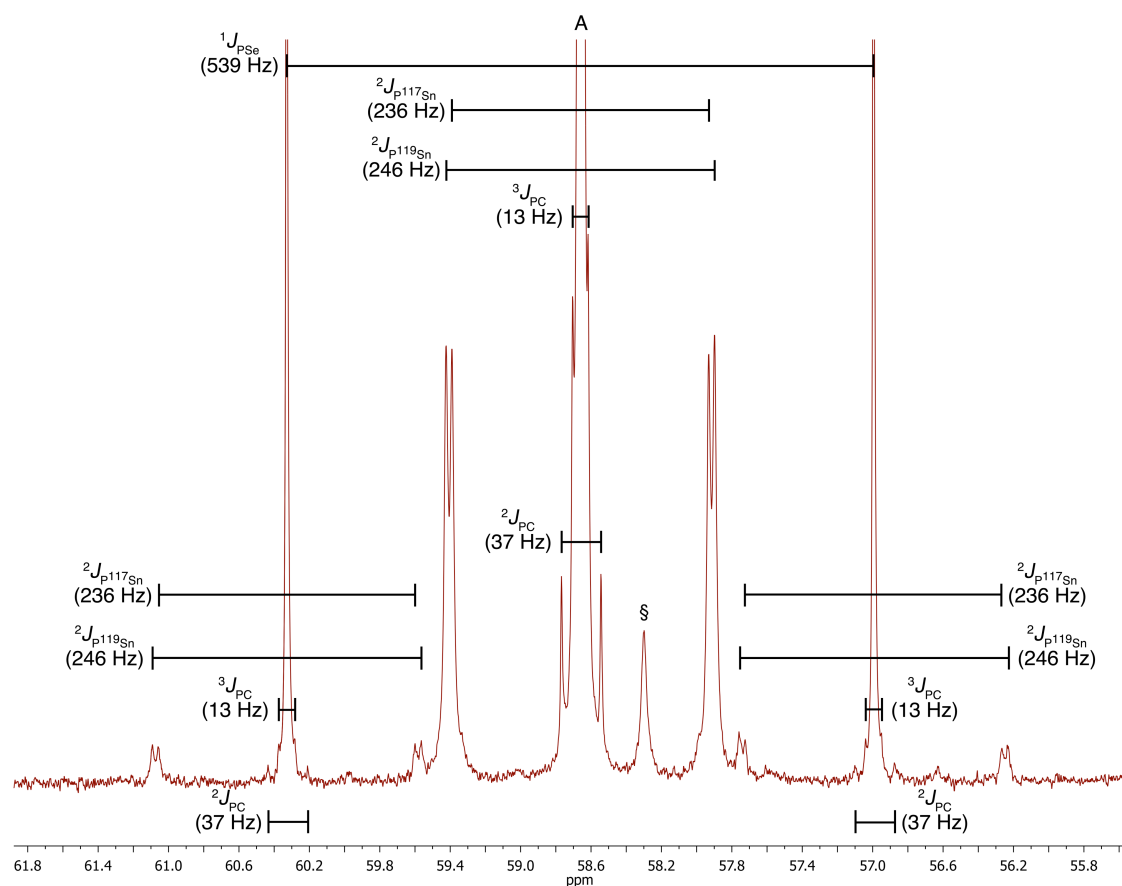
Figure 106. VT- ^1H NMR spectra (400 MHz, toluene- d_8) of $[(\text{BDI}_{\text{DIPP}})\text{SnSeP}(\text{Se})\text{Cy}_2]$ (**49**), where A = $\gamma\text{-H}$; B = CHMe_2 ; C = Cy-CH



In the $^{13}\text{C}\{^1\text{H}\}$ NMR spectrum, a doublet centred at δ_{C} 42.5 ppm, with through-bond carbon-phosphorus coupling $^1J_{\text{CP}} = 36$ Hz, is assigned to the tertiary CH carbon in the cyclohexyl groups. However, there is no through-space carbon-phosphorus coupling observed in any of the resonances assigned to the isopropyl groups. The $^{31}\text{P}\{^1\text{H}\}$ NMR

spectrum shows a single resonance at δ_P 58.7 ppm, with tin and selenium satellites (${}^2J_{P^{119}Sn} = 246$ Hz, ${}^2J_{P^{117}Sn} = 236$ Hz and ${}^1J_{PSe} = 539$ Hz). The phosphorus-tin coupling constants ${}^2J_{PSn}$ in **49** is significantly smaller than those observed in the tin(II) dicyclohexylphosphinoselenoite **46** (${}^2J_{P^{119}Sn} = 960$ Hz and ${}^2J_{P^{117}Sn} = 916$ Hz). A ${}^{31}P\{^1H\}$ NMR spectrum of a concentrated sample of the tin(II) dicyclohexylphosphinodiselenoate **49** in toluene- d_8 with an extended acquisition time revealed additional satellites (Figure 107). Tin satellites (${}^2J_{P^{119}Sn} = 246$ Hz and ${}^2J_{P^{117}Sn} = 236$ Hz) are found around the selenium satellites. The phosphorus-carbon couplings (${}^2J_{CP} = 37$ Hz and ${}^3J_{CP} = 13$ Hz) are also found from the spectrum.

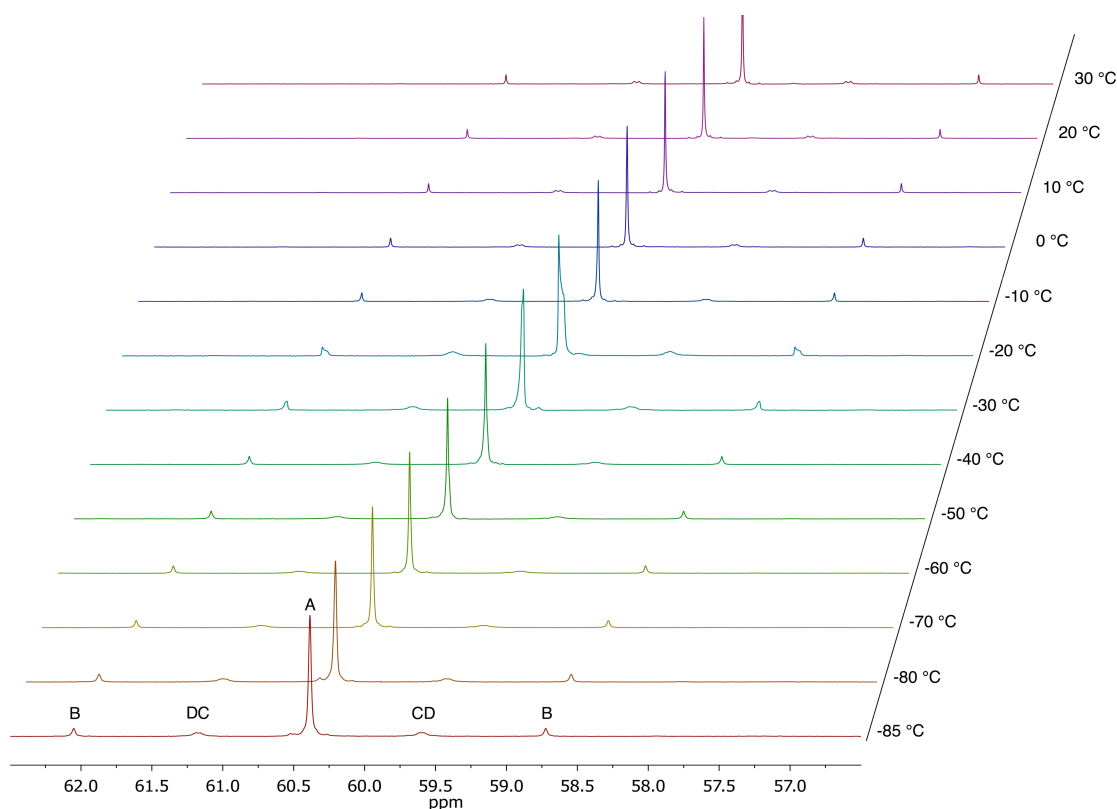
Figure 107. ${}^{31}P\{^1H\}$ NMR spectrum (162 MHz, toluene- d_8) of $[(BDI_{DIPP})SnSeP(Se)Cy_2]$ (**49**) with an extended acquisition time. The enhanced satellites are indicated in the diagram and where A = phosphorus resonance. Impurities are designated by §



A VT- ${}^{31}P\{^1H\}$ NMR experiment on **49** shows the phosphorus signal remains as a single resonance, with no significant change in the chemical shift ($\Delta\delta_P$ 1 ppm) and the coupling constants ($\Delta^1J_{PSe} = 1$ Hz, $\Delta^2J_{PSn} = 2$ Hz) within the temperature range (30 to

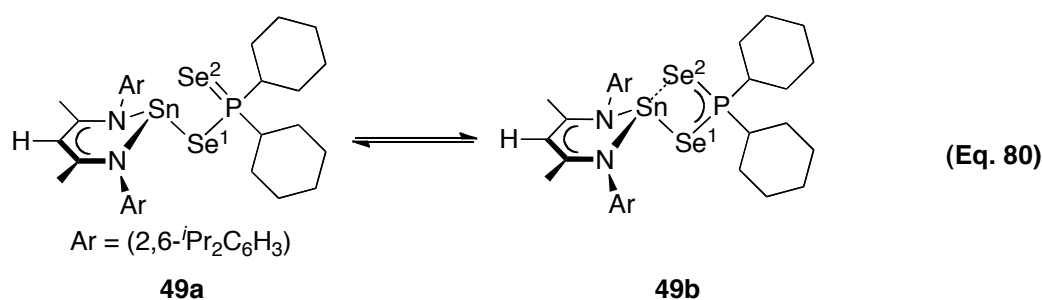
–85 °C) (Figure 108). This result suggests that there is no significant change in the environment around the phosphorus atom on cooling. The shape of the phosphorus resonance at –20 °C is ascribed to an unidentified shimming problem in the NMR instrument at this temperature. A similar problem was noted previously in the VT ^1H -NMR experiment of $[(\text{BDI}_{\text{DMP}})\text{PbCl}]$ (**24**) (Figure 17, Page 74).

Figure 108. VT- $^{31}\text{P}\{^1\text{H}\}$ NMR spectra (162 MHz, toluene- d_8) of $[(\text{BDI}_{\text{DIPP}})\text{SnSeP}(\text{Se})\text{Cy}_2]$ (**49**) where A = phosphorus resonance; B = ^{77}Se ; C = ^{117}Sn ; and D = ^{119}Sn satellites



The ^{77}Se NMR spectrum of **49** in C_6D_6 at 30 °C shows a doublet centred at $\delta_{\text{Se}} -73$ ppm, with selenium-phosphorus coupling $^1J_{\text{SeP}} = 540$ Hz. The data are similar to those in Woollins' $[\text{Sn}\{\text{PSe}_2(\text{OMe})\text{Ph}\}_2]$ ($\delta_{\text{Se}} -88$ ppm, $^1J_{\text{SeP}} = 576$ Hz).^[247] A pair of tin satellites is obtained alongside each signal ($^1J_{\text{SeSn}} = 307$ Hz). At –10 °C, the ^{77}Se NMR spectrum in toluene- d_8 shows a doublet centred at $\delta_{\text{Se}} -84$ ppm with selenium-phosphorus coupling $^1J_{\text{SeP}} = 537$ Hz. However, these results do not agree with the findings from the solid state structure, which shows the phosphinodiselenoato ligand is coordinated to the metal centre in η^1 -fashion. If such geometry persists in solution, two independent resonances, assigned individually to the selenium in the P=Se and P–Se fragments, with different selenium-phosphorus ($^1J_{\text{SeP}}$) coupling constants for each signal

are expected. Such signals are found in Liu's compounds, for example $[\text{Ph}_3\text{SnSeP}(\text{Se})(\text{OEt})_2]$ (P=Se: δ_{Se} 13.2 ppm, $^1J_{\text{SeP}} = 864$ Hz; P–Se: δ_{Se} 58.3 ppm, $^1J_{\text{SeP}} = 544$ Hz) and $[\text{Ph}_3\text{SnSeP}(\text{Se})(\text{O}^i\text{Bu})_2]$ (P=Se: δ_{Se} 19.3 ppm, $^1J_{\text{SeP}} = 867$ Hz; P–Se: δ_{Se} 62.9 ppm, $^1J_{\text{SeP}} = 515$ Hz).^[245] This contrasts with the tin(II) dicyclohexylphosphinodiselenoate **49**, which shows only one signal in the ^{77}Se NMR spectrum. We propose that the dicyclohexylphosphinodiselenoato ligand may be coordinated to the metal centre in η^2 -fashion in solution, with the electrons delocalised within the SnSe_2P unit (**49b**, equation 80).



Selected multinuclear solid state NMR spectroscopic data for **49** are given in Table 45.

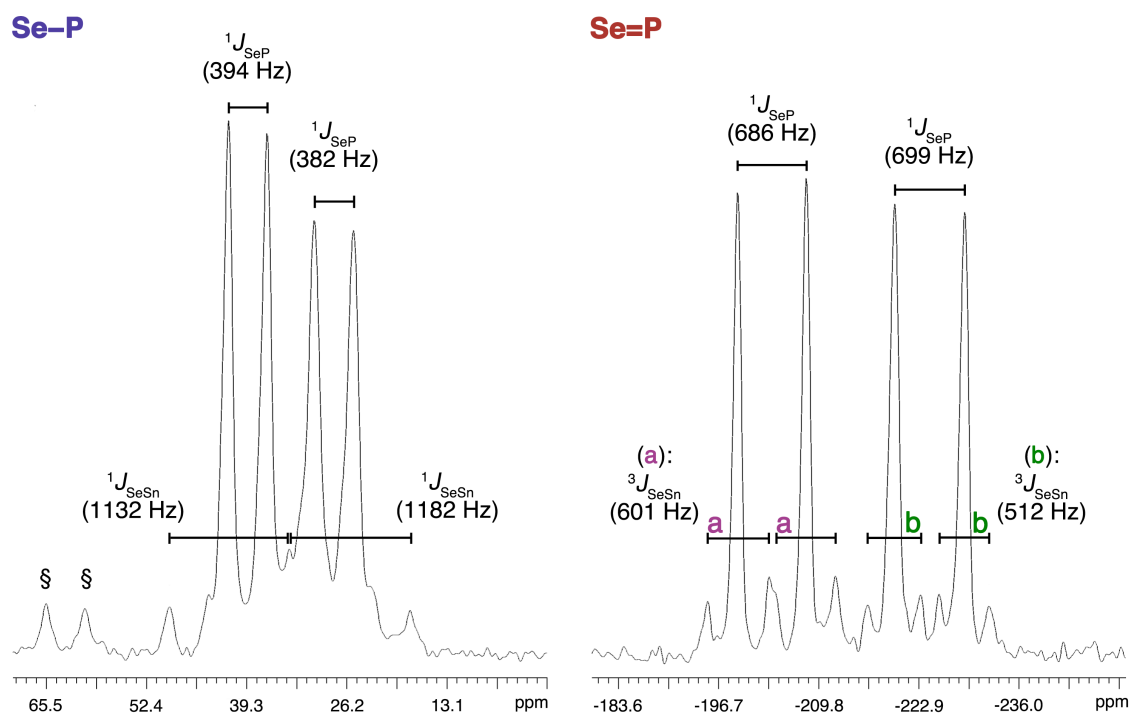
Table 45. Selected multinuclear solid state NMR spectroscopic data for $[(\text{BDI}_{\text{DIPP}})\text{SnSeP}(\text{Se})\text{Cy}_2]$ (**49**)

δ (ppm), J (Hz)	
$^{31}\text{P}\{^1\text{H}\}$	60.5, $^2J_{\text{PSn}} = 275$; $^1J_{\text{PSe}} = 684$ (P=Se); $^1J_{\text{PSe}} = 385$ (P–Se)
	58.7, $^2J_{\text{PSn}} = 232$; $^1J_{\text{PSe}} = 693$ (P=Se); $^1J_{\text{PSe}} = 385$ (P–Se)
^{77}Se	39, $^1J_{\text{SeP}} = 394$ (P–Se) $^1J_{\text{SeSn}} = 1132$
	28, $^1J_{\text{SeP}} = 382$ (P–Se) $^1J_{\text{SeSn}} = 1182$
	-204, $^1J_{\text{SeP}} = 686$ (P=Se) $^3J_{\text{SeSn}} = 601$
	-224, $^1J_{\text{SeP}} = 699$ (P=Se) $^3J_{\text{SeSn}} = 512$

The solid state $^{31}\text{P}\{^1\text{H}\}$ NMR spectrum of **49** shows two resonances at $\delta_{\text{P(solid)}}$ 58.7 and 60.5 ppm. Each signal contains a set of tin satellites and two sets of selenium satellites, as expected for η^1 -coordination of the phosphinodiselenoato ligand to the tin centre in **49a** (equation 80, Page 224). The resonance at $\delta_{\text{P(solid)}}$ 58.7 ppm shows phosphorus-tin coupling $^2J_{\text{PSn(solid)}} = 232$ Hz. Two phosphorus-selenium couplings, $^1J_{\text{PSe(solid)}} = 693$ Hz and $^1J_{\text{PSe(solid)}} = 385$ Hz, are also found, corresponding to the P=Se and P–Se fragments, respectively. Likewise, the resonance at $\delta_{\text{P(solid)}}$ 60.5 ppm shows phosphorus-tin coupling ($^2J_{\text{PSn(solid)}} = 275$ Hz) and two phosphorus-selenium couplings (P=Se: $^1J_{\text{PSe(solid)}} = 684$ Hz; P–Se: $^1J_{\text{PSe(solid)}} = 385$ Hz). In each case, the larger phosphorus-selenium ($^1J_{\text{PSe(solid)}}$) coupling constant is assigned to the P=Se fragment. These results are consistent to the findings from the X-ray crystallography, which shows the phosphinodiselenoato ligand is coordinated to the tin centre in η^1 -fashion.

The solid state ^{77}Se NMR spectrum of **49** shows two groups of signals, each with individual phosphorus couplings and tin satellites (Figure 109). There are two doublets centred at $\delta_{\text{Se(solid)}}$ 28 and 39 ppm in the high frequency region, with selenium-phosphorus couplings, $^1J_{\text{SeP(solid)}} = 382$ and 394 Hz, respectively, and tin satellites ($^1J_{\text{SeSn(solid)}} = 1182$ and 1132 Hz, respectively). We assign these signals to the selenium in the P–Se fragment. In the low frequency region, there are two doublets centred at $\delta_{\text{Se(solid)}}$ –204 and –224 ppm, with selenium-phosphorus couplings $^1J_{\text{SeP(solid)}} = 686$ and 699 Hz, respectively, and tin satellites ($^3J_{\text{SeSn(solid)}} = 601$ and 512 Hz, respectively). These signals are assigned to the selenium in the P=Se fragment. The selenium-phosphorus coupling constants obtained from the ^{77}Se NMR spectrum match those from the solid state $^{31}\text{P}\{^1\text{H}\}$ NMR spectrum (Table 45).

Figure 109. Solid state ^{77}Se NMR spectrum (79 MHz) of $[(\text{BDI}_{\text{DIPP}})\text{SnSeP}(\text{Se})\text{Cy}_2]$ (**49**). Impurities are designated by §



The reason for the doubling of the phosphorus and selenium signals in the solid state NMR spectra is not clear. In space group $P2_12_12_1$ (No. 19) with $Z = 4$, there is only one molecule in the asymmetric unit. It is possible that there were two polymorphs in the crystalline sample used for the NMR experiment, but only one was selected for X-ray crystallographic analysis. The ratio of the intensities of the signals is approximately 1:1, but we cannot be sure whether there is significant different from this ratio.

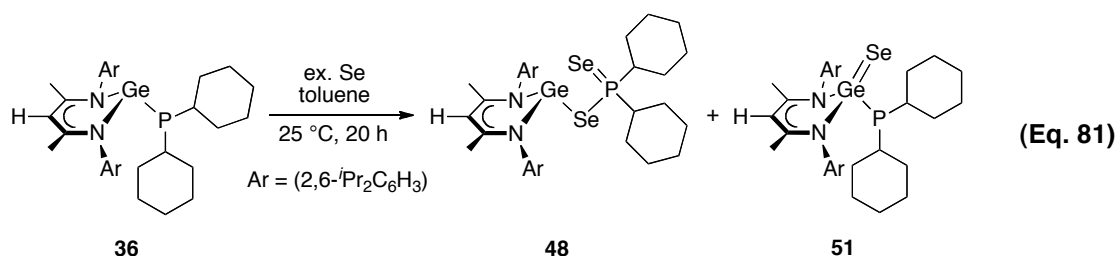
4.4.7.3 The β -diketiminatolead(II) dicyclohexylphosphinodiselenoate **50**

The ^1H NMR spectrum of **50** shows a septet at δ_{H} 3.36 ppm, with an integration of four protons, assigned to the tertiary proton in the isopropyl groups (CHMe_2). As in the other phosphinodiselenoato analogues **48** and **49**, there is no through-space proton-phosphorus coupling observed in the CHMe_2 resonance. A broad signal at δ_{H} 1.02 ppm is assigned to the tertiary CH proton in the cyclohexyl groups. In the $^{13}\text{C}\{^1\text{H}\}$ NMR spectrum, a doublet centred at δ_{C} 43.7 ppm with carbon-phosphorus coupling $^1J_{\text{CP}} = 34$ Hz is assigned to the tertiary CH carbon in the cyclohexyl group. No through-space carbon-phosphorus coupling involving isopropyl groups is observed.

A single resonance at δ_{P} 57.0 ppm, with selenium and lead satellites ($^1J_{\text{PSe}} = 521$ Hz and $^2J_{\text{PPb}} = 218$ Hz) is found in the $^{31}\text{P}\{^1\text{H}\}$ NMR spectrum. The phosphorus-selenium coupling constant ($^1J_{\text{PSe}}$) in the lead(II) dicyclohexylphosphinodiselenoate **50** is larger than that in the lead(II) dicyclohexylphosphinoselenoite **47** ($^1J_{\text{PSe}} = 192$ Hz), and the phosphorus-lead coupling constant is smaller ($^2J_{\text{PPb}} = 1469$ Hz in **47**). The ^{207}Pb NMR spectrum of the lead(II) dicyclohexylphosphinodiselenoate **50** shows a doublet centred at δ_{Pb} 1909 ppm, with lead-phosphorus coupling $^2J_{\text{PbP}} = 217$ Hz. A doublet centred at δ_{Se} -47 ppm, with selenium-phosphorus coupling $^1J_{\text{SeP}} = 544$ Hz, is shown in the ^{77}Se NMR spectrum. This result is consistent with those observed in the tin derivative **49**, for which only one selenium signal is observed in the ^{77}Se NMR spectrum in solution. Hence, we propose that the phosphinodiselenoato ligand may coordinate to the lead centre in η^2 -fashion in solution.

4.4.8 Synthesis of β -diketiminatogermanium(IV) selenide (**51**)

The germanium(IV) selenide **51** was obtained as yellow crystals as a side-product from the reaction between the germanium(II) dicyclohexylphosphanide **36** with an excess of elemental selenium (equation 81). The X-ray crystallographic analysis of the single crystals confirms the presence of Ge=Se bond. Previous products from oxidative addition of chalcogen to the heavy group 14 metal centres have been reported, for example, Roesky's $[(\text{BDI}_{\text{DIPP}})\text{Ge}(\text{Se})\text{OH}]$ and Parkin's $[(\text{Me}_4\text{taa})\text{Ge}(\text{Se})]$ ($(\text{Me}_4\text{taa})^{2-}$ = tetramethyldibenzotetraaza[14]annulene dianion).^[225, 231] However, oxidative addition of the chalcogen to the tin or lead centre in the dicyclohexylphosphanides **37** and **38** has not been observed.



4.4.9 X-ray crystal structure of [(BDI_{DIPP})Ge(Se)PCy₂] (**51**)

Yellow crystals of [(BDI_{DIPP})Ge(Se)PCy₂] (**51**) were obtained from toluene at $-30\text{ }^{\circ}\text{C}$. ORTEP drawings are shown in Figures 110 and 111. Selected bond lengths and angles are given in Table 46, and selected crystallographic data in Table 47. The geometry around the germanium atom is a distorted tetrahedral. The electrons are delocalised within the C₃N₂Ge unit in the β -diketiminato ligand, but not on to the *N*-aryl substituents (dihedral angles: C(11)–C(6)–N(1)–Ge = $88.8(4)^{\circ}$ and C(23)–C(18)–N(1)–Ge = $-84.9(4)^{\circ}$). If the cyclohexyl groups are ignored, there is an approximate plane of symmetry passing through the atoms C(2), Ge, Se and P. The mean Ge–N bond length in **51** is shorter than that in the germanium(II) dicyclohexylphosphanide **36** by about 0.08 Å. Similarly, the Ge–N bond lengths in Barrau's [(BDI_{Ph})Ge(Se)Cl] were about 0.08 Å shorter than that in [(BDI_{Ph})GeCl], which the authors attributed to a change of coordination environment around the germanium atom, from a tricoordinated germanium(II) chloride to a tetracoordinated germanium(IV) chloride.^[232] An increase in coordination number, however, normally leads to an increase in bond lengths, so it is more likely that the decrease of Ge–N bond lengths reflects the increase in germanium oxidation state. A shorter Ge–P bond distance (2.3714(11) Å) is found in the germanium(IV) selenide **51** than that in the germanium(II) dicyclohexylphosphanide **36** ($\Delta\text{Ge–P} = 0.101\text{ Å}$). The decrease in bond distance with oxidation of the germanium is also found in Roesky's [(BDI_{DIPP})Ge(Se)Me] and [(BDI_{DIPP})Ge(Se)Cl].^[228-229] The Ge=Se bond length in **51** is 2.2216(5) Å, which is shorter than the calculated Ge–Se single bond distance (2.39 Å).^[225] Furthermore, the Ge=Se bond distance is in good agreement with those in Roesky's [(BDI_{DIPP})Ge(Se)OH] (Ge–Se = 2.206(1) Å) and Okazkai's [(Tbt)(Tip)Ge(Se)] (Tbt = (2,4,6-(CH(SiMe₃)₂)₃C₆H₂); Tip = (2,4,6-(CH(CH₃)₂)₃C₆H₂), Ge–Se = 2.180(2) Å).^[231, 288] The geometry around the phosphorus atom is pyramidal, with the sum of bond angles 302.2° .

Figure 110. ORTEP diagram of $[(BDI_{DIPP})Ge(Se)PCy_2]$ (**51**). H atoms are omitted and C atoms in the *N*-aryl groups in the β -diketiminato ring are minimised for clarity. The ellipsoid probability is shown at 30%

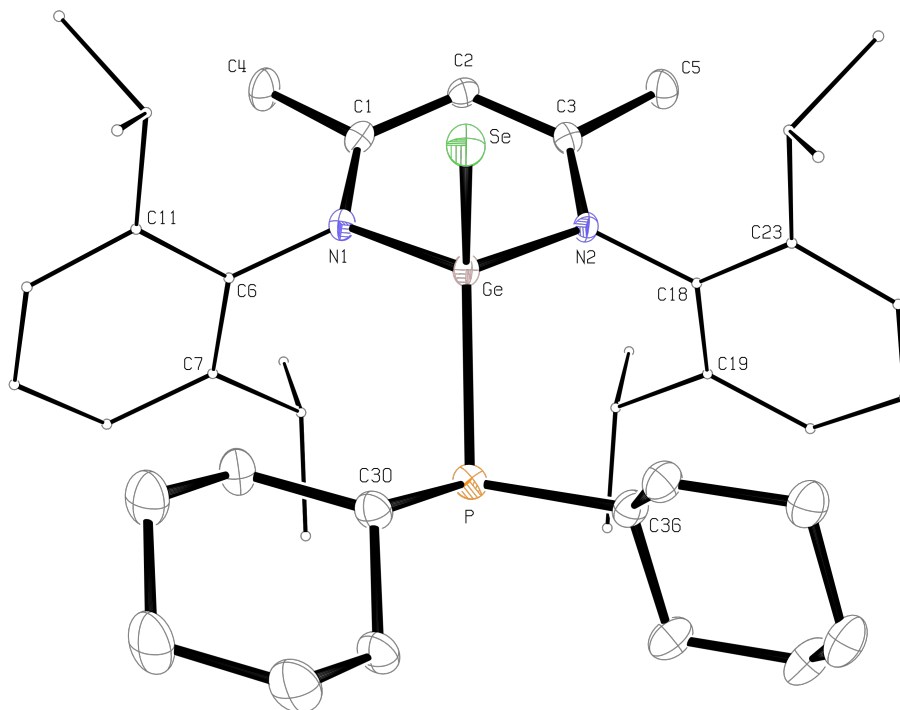


Figure 111. ORTEP diagram showing the side-on view of $[(BDI_{DIPP})Ge(Se)PCy_2]$ (**51**). H atoms are omitted and C atoms in the *N*-aryl groups in the β -diketiminato ring and the cyclohexyl groups are minimised for clarity. The ellipsoid probability is shown at 30%

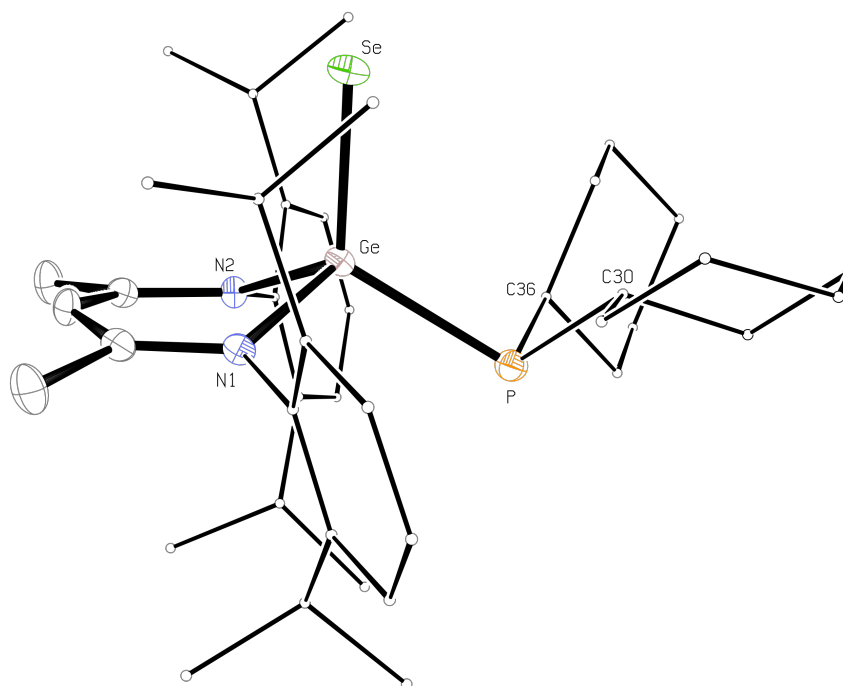


Table 46. Selected bond lengths (Å) and angles (deg) for [(BDI_{DIPP})Ge(Se)PCy₂] (**51**)

<i>Bond lengths (Å)</i>			
Ge–N(1)	1.975(3)	C(1)–C(4)	1.506(5)
Ge–N(2)	1.965(3)	C(3)–C(5)	1.506(5)
N(1)–C(1)	1.337(5)	Ge–Se	2.2216(5)
N(2)–C(3)	1.339(5)	Ge–P	2.3714(11)
C(1)–C(2)	1.385(5)	P–C(30)	1.880(4)
C(3)–C(2)	1.391(5)	P–C(36)	1.896(4)
Ge–NCCCN _{plane}	0.757		
<i>Bond angles (deg)</i>			
N(1)–Ge–N(2)	92.37(13)	N(1)–Ge–Se	110.22(9)
Ge–N(1)–C(1)	119.6(2)	N(2)–Ge–Se	112.38(9)
Ge–N(2)–C(3)	119.3(2)	N(1)–Ge–P	110.25(10)
N(1)–C(1)–C(2)	123.6(3)	N(2)–Ge–P	108.12(9)
N(2)–C(3)–C(2)	123.7(3)	Se–Ge–P	120.02(3)
C(1)–C(2)–C(3)	127.0(4)	Ge–P–C(30)	100.42(14)
N(1)–C(1)–C(4)	120.0(3)	Ge–P–C(36)	100.58(14)
N(2)–C(3)–C(5)	119.8(3)	C(30)–P–C(36)	101.15(19)
NCCCN _{plane} –NGeN _{plane}	33.1	Σ bond angles around P	302.2
Avg. int. angles of Cy	111	DOP of P (%) ^a	64
<i>Dihedral angles (deg)</i>			
C(11)–C(6)–N(1)–Ge	88.8(4)	C(23)–C(18)–N(2)–Ge	–84.9(4)

^a Degree of pyramidalisation (DOP, %) = [(360 – Σ_{bond angle}) / 0.9]^[115] When a DOP is 100%, it is equivalent to a sum of bond angles of 270°, whereas a DOP of 0% indicates a planar geometry at the central atom

Table 47. Selected crystallographic data for [(BDI_{DIPP})Ge(Se)PCy₂] (**51**)

[(BDI _{DIPP})Ge(Se)PCy ₂] (51)	
chemical formula	2(C ₄₁ H ₆₃ GeN ₂ PSe), 3(C ₇ H ₈)
molecular mass	1809.3
temperature (K)	173(2)
wavelength (Å)	0.71073
crystal system	triclinic
space group	$P\bar{1}$ (No. 2)
<i>a</i> (Å)	10.0820(1)
<i>b</i> (Å)	21.7333(4)
<i>c</i> (Å)	21.9730(4)
<i>α</i> (deg)	90.274(1)
<i>β</i> (deg)	93.478(1)
<i>γ</i> (deg)	92.394(1)
<i>V</i> (Å ³)	4801.42(13)
<i>Z</i>	4
ρ_{calcd} (Mg m ⁻³)	1.25
θ range (deg)	3.40–26.77
abs coeff (mm ⁻¹)	1.464
measd/indep reflns/ <i>R</i> (int)	71 113/20 256/0.065
data/restraints/param	20 256/141/872
goodness of fit on F^2	0.985
final <i>R</i> indices [<i>I</i> > 2 σ (<i>I</i>)]	<i>R</i> 1 = 0.056, <i>wR</i> 2 = 0.141
<i>R</i> indices (all data)	<i>R</i> 1 = 0.080, <i>wR</i> 2 = 0.154
largest diff peak and hole (e Å ⁻³)	1.80 and -0.79

4.4.10 NMR spectra of [(BDI_{DIPP})Ge(Se)PCy₂] (**51**)

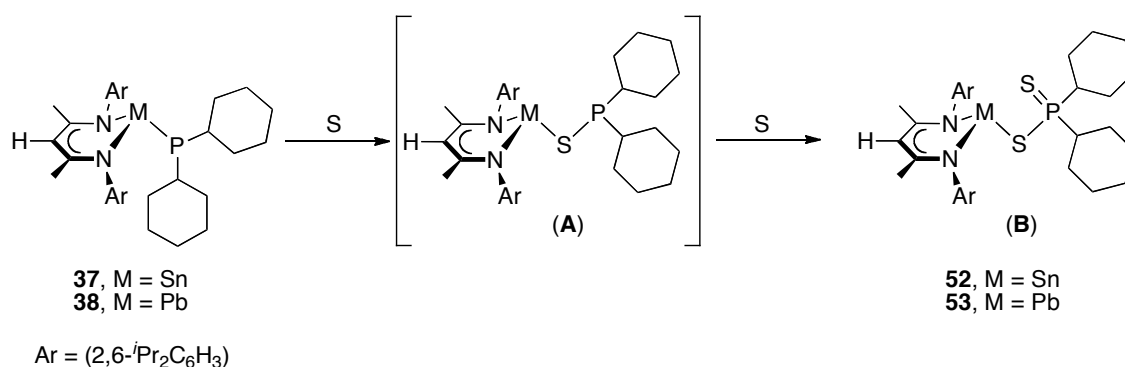
Multinuclear NMR spectra of the germanium(IV) selenide **51** were recorded in CDCl₃. The ¹H NMR spectrum shows two septets at δ_{H} 4.01 and 3.53 ppm, assigned to the tertiary protons in the isopropyl groups (CHMe₂). No through-space proton-phosphorus coupling is observed in the CHMe₂ resonances. The doublet in the ¹³C{¹H} NMR spectrum centred at δ_{C} 34.5 ppm (¹*J*_{CP} = 16 Hz) is assigned to the tertiary carbon CH in the cyclohexyl groups. However, unlike the parent germanium(II) dicyclohexylphosphanide **36**, compound **51** shows no through-space carbon-phosphorus coupling in the isopropyl signals, perhaps a consequence of the wider N–Ge–N (92.37(13)° in **51** and 88.05(8)° in **36**) and N–Ge–P bond angles (N(1)–Ge–P: 110.25(10)° in **51** and 102.52(6)° in **36**. N(2)–Ge–P: 108.12(9)° in **51** and 101.35(7)° in

36). The $^{31}\text{P}\{^1\text{H}\}$ NMR spectrum of the germanium(IV) selenide **51** shows a single resonance at δ_{P} 0.7 ppm. A doublet centred at δ_{Se} -91 ppm, with selenium-phosphorus coupling ($^2J_{\text{SeP}} = 12$ Hz) is found in the ^{77}Se NMR spectrum. This selenium may be compared with those in Roesky's $[(\text{BDI}_{\text{DIPP}})\text{Ge}(\text{Se})\text{OH}]$ (δ_{Se} -440 ppm in C_6D_6) and $[(\text{BDI}_{\text{DIPP}})\text{Ge}(\text{Se})^n\text{Bu}]$ (δ_{Se} -297 ppm in toluene- d_8).^[229, 231]

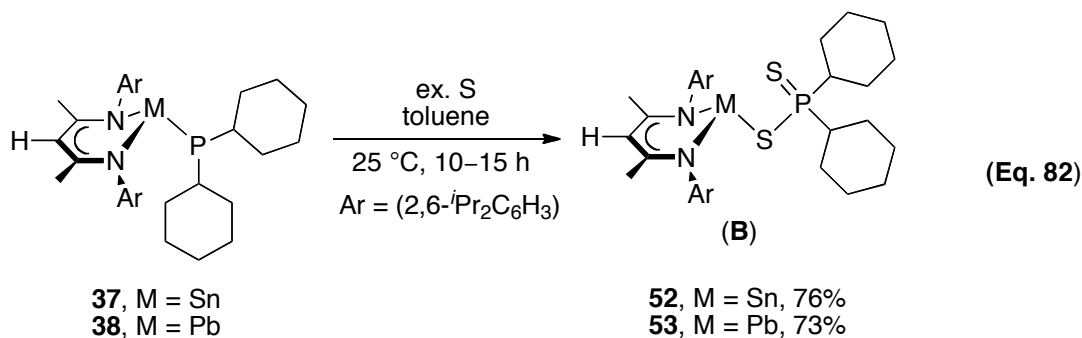
4.4.11 Synthesis of β -diketiminato heavy group 14 metal dicyclohexylphosphinodithioates **52–53**

Preliminary reactions of the β -diketiminatotin(II) or -lead(II) dicyclohexylphosphanides, **37** or **38**, with elemental sulfur in a 1:1 ratio did not give the expected phosphinothioato complexes $[(\text{BDI}_{\text{DIPP}})\text{MSPCy}_2]$ (**A**, $\text{M} = \text{Sn}$ or Pb) (Scheme 64). However, there were significant amounts of the dicyclohexylphosphinodithioates $[(\text{BDI}_{\text{DIPP}})\text{MSP}(\text{S})\text{Cy}_2]$ (**52**, $\text{M} = \text{Sn}$; **53**, $\text{M} = \text{Pb}$) together with unchanged heavy group 14 metal dicyclohexylphosphanido complexes, **37** or **38**. This preliminary result suggests that the reaction of the intermediate **A** with sulfur may be faster than the reaction of the starting dicyclohexylphosphanido complexes **37** and **38**.

Scheme 64. Preliminary reactions between the tin(II) or lead(II) dicyclohexylphosphanides, **37** or **38**, and elemental sulfur



Treatment of the β -diketiminatotin(II) or -lead(II) dicyclohexylphosphanides **37** or **38**, with an excess of elemental sulfur in toluene at room temperature give the phosphinodithioato complexes $[(\text{BDI}_{\text{DIPP}})\text{MSP}(\text{S})\text{Cy}_2]$ (**52**, $\text{M} = \text{Sn}$; and **53**, $\text{M} = \text{Pb}$) in good yields (76 and 73%, respectively) (equation 82).



The dicyclohexylphosphinodithioato complexes **52** and **53** are soluble in common organic aprotic solvents, such as toluene and pentane. They are sensitive to air, moisture and light. Metallic precipitates are found when the compounds are allowed to stand in toluene under ambient light at room temperature for 24 hours. However, the complexes can be stored as solids at $-30\text{ }^\circ\text{C}$ without decomposition for several weeks.

4.4.12 X-ray crystal structures of [(BDI_{DIPP})MSP(S)Cy₂] (**52**, M = Sn; and **53**, M = Pb)

Single crystals of [(BDI_{DIPP})SnSP(S)Cy₂] (**52**) were obtained by recrystallisation from toluene at $-30\text{ }^\circ\text{C}$. ORTEP drawings of the tin compound **52** are shown in Figures 112 and 113. Selected bond lengths and angles are given in Table 48, and selected crystallographic data in Table 49. The compound adopts an *exo* conformation, with the tin atom 1.160 Å above the mean NCCCN plane of the β-diketiminato ligand. The ligands are coordinated with a pyramidal geometry around the tin atom, with the sum of bond angles 265.2° . Delocalisation within the C₃N₂Sn unit in the β-diketiminato ring is evident, but it does not extend on to the *N*-aryl substituents (dihedral angles: C(11)–C(6)–N(1)–Sn = $74.7(2)^\circ$ and C(23)–C(18)–N(2)–Sn = $-72.0(2)^\circ$). If the cyclohexyl rings are discounted, there is an approximate plane of symmetry passing through the atoms C(2), Sn, S(1), P and S(2), bisecting the β-diketiminato ring. The four-coordinated phosphorus atom has a tetrahedral geometry, in which individual angles are ranging from $102.98(7)^\circ$ to $116.72(3)^\circ$. The Sn–S(1) bond length is 2.5107(6) Å, similar to those in Varga's [Ph₃SnSP(S)Ph₂] (Sn–S(1) = 2.452(1) Å) and Zuckerman's [Ph₃SnSP(S)(OEt)₂] (Sn–S(1) = 2.4582(9) Å).^[289-290] The P–S(2) bond distance in the tin(II) dicyclohexylphosphinodithioate **52** is 1.9655(8) Å, similar to those P=S bond length found in Varga's and Zuchkerman's structures (1.945(1) and

1.931(1) Å, respectively), suggesting the presence of a phosphorus-sulfur double bond.^[289-290] In **52**, the Sn–S(2) distance is 3.497 Å and the S(1)–Sn–S(2) angle is 67.36°. The Sn···S(2) distance is less than the sum of the van der Waals radii of tin and sulfur (4.0 Å), suggesting that there may be a weak interaction between the two atoms.^[291] Evidence for this Sn···S(2) weak interaction can also be found in the literature, for example in Casas' [SnMe₂(S₂PPh₂)₂] (Sn···S(2) = 3.325 Å, S(1)–Sn–S(2) = 68.30°) and Fild's [Me₂Sn{S₂P(*p*-C₆H₄OMe)(OMe)}₂] (Sn···S(2) = 3.1090 Å, S(1)–Sn–S(2) = 71.50°).^[244, 292] The internal C–C–C bond angles in the cyclohexyl rings are close to the average value (111°), indicating that there is little distortion of the chair conformation in the cyclohexyl rings.

Figure 112. ORTEP diagram of $[(BDI_{DIPP})SnSP(S)Cy_2]$ (**52**). H atoms are omitted and C atoms in the *N*-aryl groups in the β -diketiminato ring are minimised for clarity. The ellipsoid probability is shown at 30%

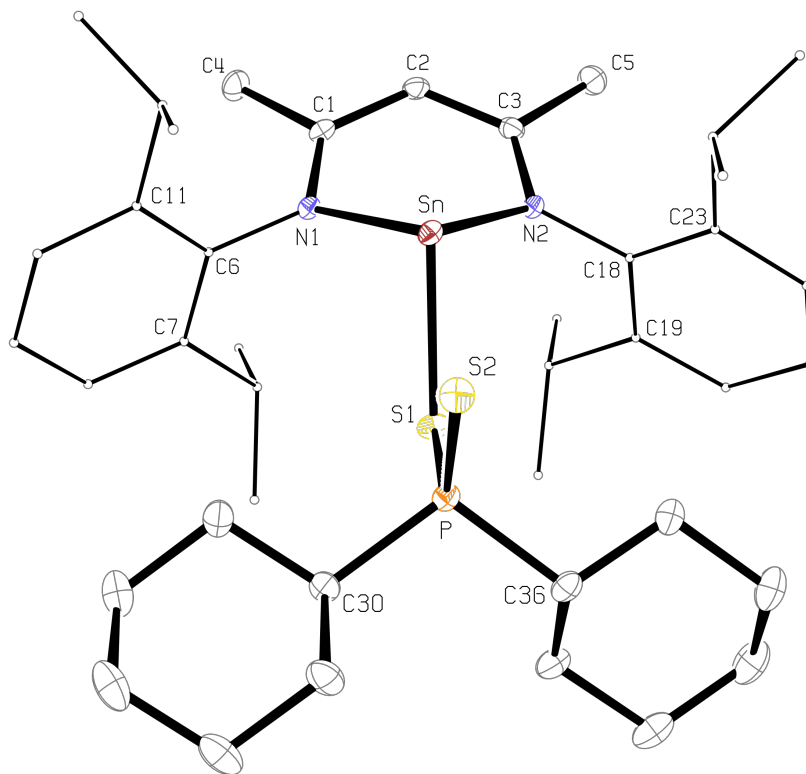
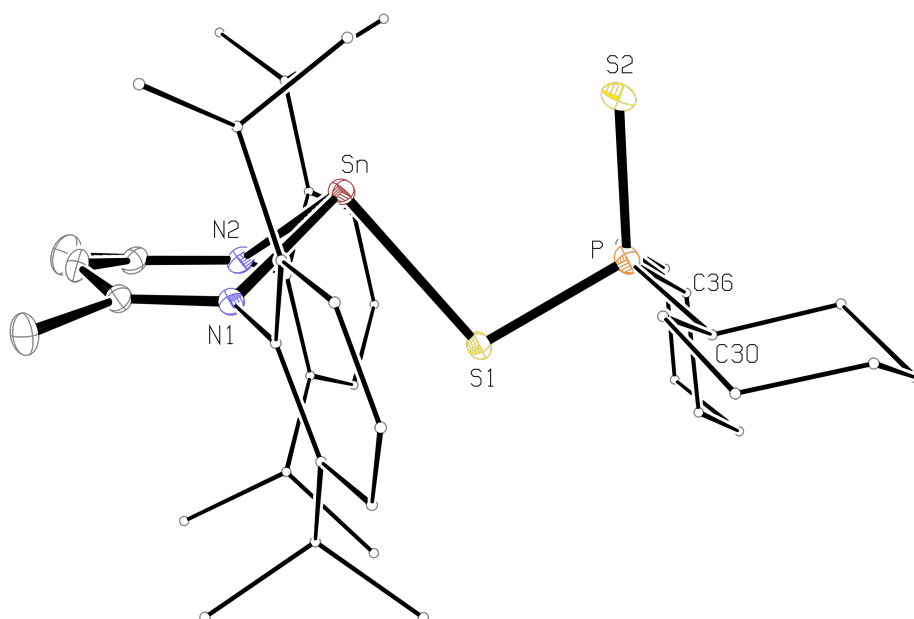


Figure 113. ORTEP diagram showing the side-on view of $[(BDI_{DIPP})SnSP(S)Cy_2]$ (**52**). H atoms are omitted, and C atoms in the *N*-aryl groups in the β -diketiminato ring and the cyclohexyl groups are minimised for clarity. The ellipsoid probability is shown at 30%



Single crystals of [(BDI_{DIPP})PbSP(S)Cy₂] (**53**) were obtained from toluene at $-30\text{ }^{\circ}\text{C}$. ORTEP drawings are shown in Figures 114 and 115. Selected bond lengths and angles are given in Table 48, and selected crystallographic data in Table 49. Compound **53** adopts an *exo* conformation, with the lead atom 1.144 Å above the mean NCCCN plane of the β -diketiminato ligand. The sum of bond angles at the pyramidal lead is 267.4° . Delocalisation within the C₃N₂Pb unit in the β -diketimate ring is evident, but it does not extend to the *N*-aryl substituents (dihedral angles: C(11)–C(6)–N(1)–Pb = $74.5(5)^{\circ}$ and C(23)–C(18)–N(2)–Pb = $-71.5(5)^{\circ}$). If the cyclohexyl rings are discounted, there is an approximate plane of symmetry passing through the atoms C(2), Pb, S(1), P and S(2), bisecting the β -diketimate ring. The four-coordinated phosphorus atom adopts a distorted tetrahedral geometry. The Pb–S(1) and P–S(1) bond distances are 2.6370(13) and 2.0528(17) Å, respectively, similar to those observed in Edelmann's [Ph₃PbSP(S)(CH₃)₂] (Pb–S(1) = 2.708(4) Å; P–S(1) = 2.043(5) Å) and Harrison's [Ph₃PbSP(S)(OEt)₂] (Pb–S(1) = 2.554(6) Å; P–S(1) = 2.035(7) Å).^[293-294] The P–S(2) bond distance (1.9755(18) Å) is similar to the typical P=S double bond lengths (1.95 Å), suggesting the presence of a phosphorus-sulfur double bond.^[237] The distance between the Pb and S(2) atoms (3.276 Å) is within the sum of van der Waals radii (3.82 Å), suggesting that there may be a weak interaction.^[291] However, the Pb–S(1)–P bond angle ($95.28(6)^{\circ}$) is significantly wider than the Pb–S(2)–P angle (79.00°). These may be compared with values in complexes containing bidentate phosphinodithioato ligands, such as Woollins' [Pb{SP(S)OEt(C₆H₄OMe)}₂] (Pb–S(1)–P = 91.08° and Pb–S(2)–P = 83.19°) and Haiduc's [Pb{SP(S)Ph₂}₂] (Pb–S(1)–P = 86.26° and Pb–S(2)–P = 85.97°).^[295-296] These results suggest that the phosphinodithioato ligand in compound **53** is coordinated to the metal centre in η^1 -fashion. The internal C–C–C bond angles in the cyclohexyl rings are close to the average value (111°), indicating that there is little distortion in the chair conformation in the cyclohexyl rings.

Figure 114. ORTEP diagram of $[(BDI_{DIPP})PbSP(S)Cy_2]$ (**53**). H atoms are omitted and C atoms in the *N*-aryl groups in the β -diketiminato ring are minimised for clarity. The ellipsoid probability is shown at 30%

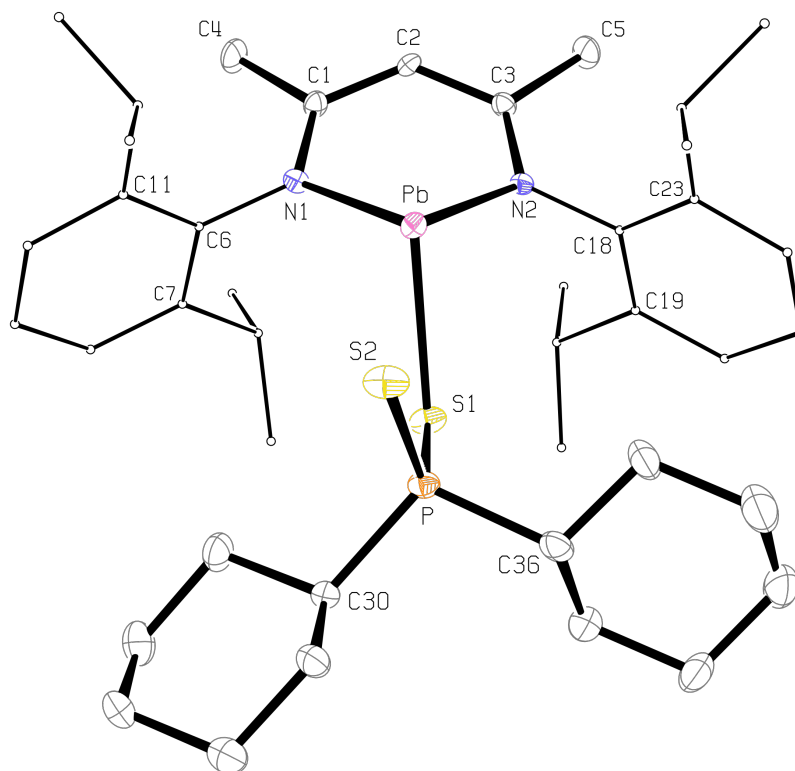


Figure 115. ORTEP diagram showing the side-on view of $[(BDI_{DIPP})PbSP(S)Cy_2]$ (**53**). H atoms are omitted, and C atoms in the *N*-aryl groups in the β -diketiminato ring and the cyclohexyl groups are minimised for clarity. The ellipsoid probability is shown at 30%

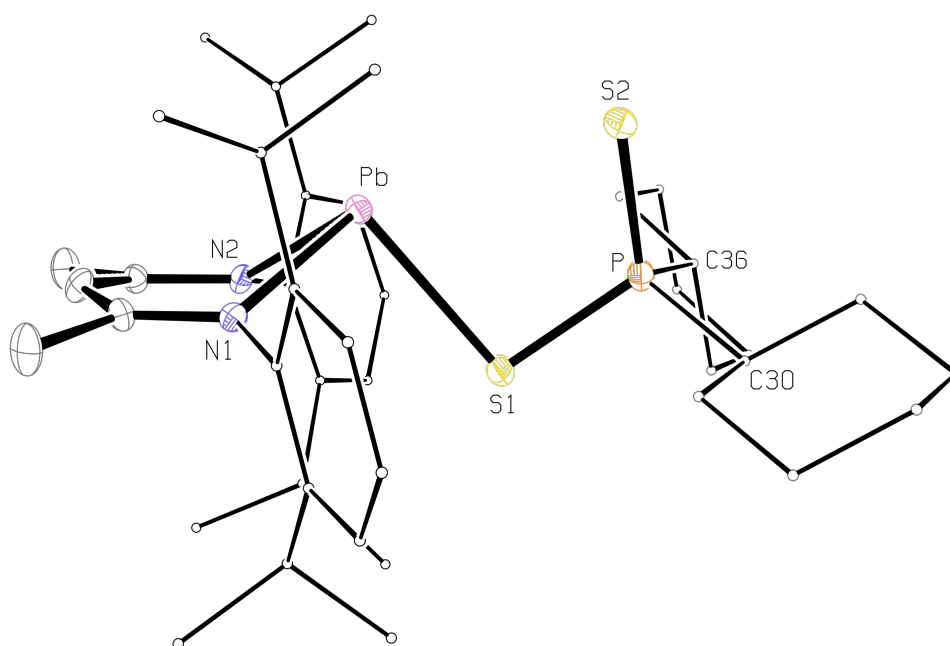


Table 48. Selected bond lengths (Å) and angles (deg) for [(BDI_{DIPP})MSP(S)Cy₂] (Cy = cyclohexyl; **52**, M = Sn; and **53**, M = Pb)

	[(BDI _{DIPP})SnSP(S)Cy ₂] 52 , M = Sn	[(BDI _{DIPP})PbSP(S)Cy ₂] 53 , M = Pb
<i>Bond lengths (Å)</i>		
M–N(1)	2.2215(16)	2.355(4)
M–N(2)	2.2107(17)	2.340(4)
N(1)–C(1)	1.328(3)	1.325(6)
N(2)–C(3)	1.330(3)	1.319(6)
C(1)–C(2)	1.408(3)	1.406(7)
C(2)–C(3)	1.397(3)	1.418(7)
M–S(1)	2.5107(6)	2.6370(13)
P–S(1)	2.0641(7)	2.0528(17)
P–S(2)	1.9655(8)	1.9755(18)
P–C(30)	1.833(2)	1.848(5)
P–C(36)	1.841(2)	1.832(6)
M–S(2)	3.497	3.276
M–NCCCN _{Plane}	1.160	1.144
<i>Bond angles (deg)</i>		
N(1)–M–N(2)	83.23(6)	80.07(14)
N(1)–M–S(1)	91.90(5)	96.92(10)
N(2)–M–S(1)	90.08(5)	90.36(10)
N(1)–C(1)–C(2)	123.44(19)	125.1(5)
N(2)–C(3)–C(2)	123.95(19)	123.7(4)
C(1)–C(2)–C(3)	128.64(19)	130.0(5)
M–S(1)–P	100.91(3)	95.28(6)
C(30)–P–C(36)	107.20(11)	107.1(2)
S(1)–P–S(2)	116.72(3)	115.43(8)
C(30)–P–S(2)	112.83(8)	110.89(17)
C(36)–P–S(2)	112.30(8)	110.70(18)
M–S(2)–P	74.98	79.00
S(1)–M–S(2)	67.36	69.37
Avg. int. angles of Cy	111	111
NCCCN _{plane} –NMN _{plane}	43.7	39.0
Σ bond angle around M ^a	265.2	267.4
DOP of M (%)	105	103
<i>Dihedral angles (deg)</i>		
C(11)–C(6)–N(1)–M	74.7(2)	74.5(5)
C(23)–C(18)–N(2)–M	–72.0(2)	–71.5(5)

^a Degree of pyramidalisation (DOP, %) = [(360 – Σ_{bond angle}) / 0.9] ^[115] When a DOP is 100%, it is equivalent to a sum of bond angles of 270°, whereas a DOP of 0% indicates a planar geometry at the central atom

Table 49. Selected crystallographic data for [(BDI_{DIPP})MSP(S)Cy₂] (Cy = cyclohexyl; **52**, M = Sn; and **53**, M = Pb)

	[(BDI _{DIPP})SnSP(S)Cy ₂] (52)	[(BDI _{DIPP})PbSP(S)Cy ₂] (53)
chemical formula	C ₄₁ H ₆₃ N ₂ PS ₂ Sn, C ₇ H ₈	C ₄₁ H ₆₃ N ₂ PPbS, C ₇ H ₈
molecular mass	889.85	978.35
temperature (K)	173(2)	173(2)
wavelength (Å)	0.71073	0.71073
crystal system	monoclinic	orthorhombic
space group	<i>P</i> 2 ₁ / <i>c</i> (No. 14)	<i>P</i> 2 ₁ 2 ₁ 2 ₁ (No. 19)
<i>a</i> (Å)	13.1888(2)	10.1944(1)
<i>b</i> (Å)	18.2309(2)	15.4698(2)
<i>c</i> (Å)	20.4088(3)	29.9406(4)
<i>α</i> (deg)	90	90
<i>β</i> (deg)	103.817(1)	90
<i>γ</i> (deg)	90	90
<i>V</i> (Å ³)	4765.17(11)	4721.79(10)
<i>Z</i>	4	4
ρ_{calcd} (Mg m ⁻³)	1.24	1.38
θ range (deg)	3.51–27.10	3.58–26.73
abs coeff (mm ⁻¹)	0.69	3.73
measd/indep reflns/ <i>R</i> (int)	74 584/10 472/0.062	74 892/10 004/0.095
reflns with <i>I</i> > 2 σ (<i>I</i>)	8789	8799
data/restraints/param	10 472/0/489	10 004/0/439
goodness of fit on <i>F</i> ²	1.018	1.087
final <i>R</i> indices [<i>I</i> > 2 σ (<i>I</i>)]	<i>R</i> 1 = 0.032, <i>wR</i> 2 = 0.071	<i>R</i> 1 = 0.035, <i>wR</i> 2 = 0.066
<i>R</i> indices (all data)	<i>R</i> 1 = 0.045, <i>wR</i> 2 = 0.076	<i>R</i> 1 = 0.047, <i>wR</i> 2 = 0.069
largest diff peak and hole (e Å ⁻³)	0.47 and –0.68	0.93 and –0.71

4.4.13 NMR spectra of [(BDI_{DIPP})MSP(S)Cy₂] (**52**, M = Sn; and **53**, M = Pb)

Selected multinuclear NMR spectroscopic data for **52–53** are given in Table 50.

Table 50. Selected multinuclear NMR spectroscopic data (C₆D₆, 30 °C) for [(BDI_{DIPP})MSP(S)Cy₂] (Cy = cyclohexyl; **52**, M = Sn; and **53**, M = Pb)

	[(BDI _{DIPP})SnSP(S)Cy ₂] (52)	[(BDI _{DIPP})PbSP(S)Cy ₂] (53)
	δ (ppm), J (Hz)	δ (ppm), J (Hz)
¹H		
γ -H	4.66 (s)	4.55 (s)
CHMe ₂	3.61 (septet) ³ J _{HH} = 6.8	3.35 (septet) ³ J _{HH} = 6.8
	3.21 (septet) ³ J _{HH} = 6.8	
Cy-CH	1.60 (br)	1.60 (br)
¹³C{¹H}		
Cy-CH	43.1 (d) ¹ J _{CP} = 50	43.8 (d) ¹ J _{CP} = 49
CHMe ₂	29.6, 29.5 (s)	29.1 (s)
CHMe ₂	25.7, 24.9 (s)	26.1 (s)
³¹P{¹H}		
	82.2 (s) ² J _{P¹¹⁹Sn} = 180 ² J _{P¹¹⁷Sn} = 173	84.6 (s) ² J _{PPb} = 189
Other		
	$\delta(^{119}\text{Sn}) = -175$ (d) ² J _{P¹¹⁹SnP} = 160	$\delta(^{207}\text{Pb}) = 1554$ (d) ² J _{PbP} = 159

4.4.13.1 The β -diketiminatotin(II) dicyclohexylphosphinodithioate **52**

The ¹H NMR spectrum of **52** shows two septets at δ_{H} 3.61 and 3.21 ppm (³J_{HH} = 6.8 Hz), assigned to the tertiary protons in the isopropyl groups (CHMe₂). No through-space proton-phosphorus coupling is observed. The ¹³C{¹H} NMR spectrum shows a doublet centred at δ_{C} 43.1 ppm, with through-bond carbon-phosphorus coupling ¹J_{CP} = 50 Hz, assigned to the tertiary CH carbons in the cyclohexyl groups. There is no through-space carbon-phosphorus coupling in any of the resonances assigned to the isopropyl groups, in contrast to the situation in the tin(II) dicyclohexylphosphanide **37**.

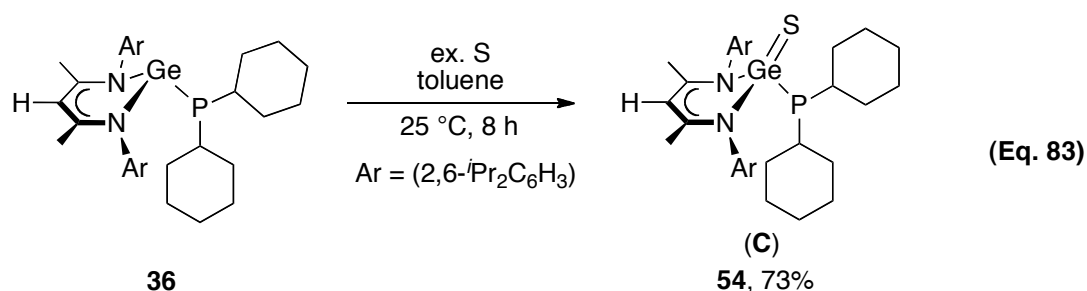
The $^{31}\text{P}\{^1\text{H}\}$ NMR spectrum of **52** shows a single resonance at δ_{P} 82.2 ppm, with tin satellites ($^2J_{\text{P}^{119}\text{Sn}} = 180$ Hz and $^2J_{\text{P}^{117}\text{Sn}} = 173$ Hz). The phosphorus resonance may be compared with those in Fild's $[\text{Me}_2\text{Sn}\{\text{S}_2\text{P}(p\text{-MeOC}_6\text{H}_4)(\text{OEt})\}_2]$ (δ_{P} 95.6 ppm) and Casas' $[\text{Me}_2\text{Sn}\{\text{S}_2\text{P}(\text{OC}_6\text{H}_4\text{Me-}o)_2\}_2]$ (δ_{P} 90.8 ppm).^[244, 248] The ^{119}Sn NMR spectrum shows a doublet centred at δ_{Sn} -175 ppm with tin-phosphorus coupling $^2J_{^{119}\text{SnP}} = 160$ Hz, upfield from that in the tin(II) dicyclohexylphosphinodiselenoate **49** (δ_{Sn} -88 ppm, $^2J_{^{119}\text{SnP}} = 247$ Hz).

4.4.13.2 The β -diketiminatolead(II) dicyclohexylphosphinodithioate **53**

The ^1H NMR spectrum of **53** shows a septet at δ_{H} 3.35 ppm ($^3J_{\text{HH}} = 6.8$ Hz), with an integration of four protons, assigned to the tertiary protons in the isopropyl groups (CHMe_2). The $^{13}\text{C}\{^1\text{H}\}$ NMR spectrum shows a doublet centred at δ_{C} 43.8 ppm, with carbon-phosphorus coupling $^1J_{\text{CP}} = 49$ Hz, assigned to the tertiary CH carbon in the cyclohexyl group. Like the tin derivative **52**, there is no through-space carbon-phosphorus coupling in any of the signals assigned to the isopropyl groups. The $^{31}\text{P}\{^1\text{H}\}$ NMR spectrum of the lead(II) dicyclohexylphosphinodithioate **53** shows a single resonance at δ_{P} 84.6 ppm, with lead satellites ($^2J_{\text{P}^{207}\text{Pb}} = 189$ Hz), slightly downfield from Haiduc's $[\text{Pb}(\text{SP}(\text{S})\text{Ph}_2)_2]$ (δ_{P} 60.1 ppm).^[296] The ^{207}Pb NMR spectrum of **53** shows a doublet centred at δ_{Pb} 1554 ppm, with lead-phosphorus coupling $^2J_{\text{PbP}} = 159$ Hz. The lead signal in **53** is significantly upfield from those in the lead(II) dicyclohexylphosphanide **38** (δ_{Pb} 3981 ppm) and the lead(II) dicyclohexylphosphinodiselenoate **50** (δ_{Pb} 1909 ppm).

4.4.14 Synthesis of β -diketiminatogermanium(IV) sulfide **54**

In contrast to the tin and lead derivatives, treatment of the germanium(II) dicyclohexylphosphanide **36** with an excess of elemental sulfur in toluene at room temperature gives the germanium(IV) sulfide $[(\text{BDI}_{\text{DIPP}})\text{Ge}(\text{S})\text{PCy}_2]$ (**54**) in 73 % yield (equation 83). X-ray crystallography confirms the atom connectivity. The germanium(IV) sulfide **54** is sensitive to air and moisture, but it can be stored as solids at -30 °C for several weeks without decomposition.



4.4.15 X-ray crystal structure of $[(\text{BDI}_{\text{DIPP}})\text{Ge}(\text{S})\text{PCy}_2]$ (**54**)

Single crystals of $[(\text{BDI}_{\text{DIPP}})\text{Ge}(\text{S})\text{PCy}_2]$ (**54**) were obtained from THF at $-30\text{ }^\circ\text{C}$. ORTEP drawings of the germanium(IV) sulfide **54** are shown in Figures 116 and 117. Selected bond lengths and angles are given in Table 51, and selected crystallographic data in Table 52. The germanium centre adopts a distorted tetrahedral geometry. There is delocalisation within the $\text{C}_3\text{N}_2\text{Pb}$ unit in the β -diketiminate ring, but it does not extend to the *N*-aryl substituents (dihedral angles: $\text{C}(11)\text{-C}(6)\text{-N}(1)\text{-Ge} = 83.7(3)^\circ$ and $\text{C}(23)\text{-C}(18)\text{-N}(2)\text{-Ge} = -85.6(3)^\circ$). Discounting the cyclohexyl rings, there is an approximate plane of symmetry passing through the atoms C(2), Ge, S and P, and bisecting the β -diketiminate ring. As with the germanium(IV) selenide **51**, the Ge–N and Ge–P bonds in the germanium(IV) sulfide **54** are shorter than those in the germanium(II) dicyclohexylphosphanide **36** precursor (avg. $\Delta\text{Ge-N} = 0.09\text{ \AA}$ and $\Delta\text{Ge-P} = 0.14\text{ \AA}$). The Ge–P bond length ($2.3322(8)\text{ \AA}$) in **54** is similar to that in the selenium analogue **51** ($2.3714(11)\text{ \AA}$). The Ge–S bond distance ($2.0954(8)\text{ \AA}$) is in good agreement with the typical Ge=S bond length (2.06 \AA), as well as with those in Roesky's $[(\text{BDI}_{\text{DIPP}})\text{Ge}(\text{S})\text{SH}]$ ($2.0641(4)\text{ \AA}$) and $[(\text{BDI}_{\text{DIPP}})\text{Ge}(\text{S})\text{OH}]$ ($2.077(1)\text{ \AA}$).^[74, 225, 230] The ligands are coordinated with a distorted pyramidal geometry around the phosphorus atom, with the sum of bond angles 313.4° . The internal C–C–C bond angles in the cyclohexyl ring do not deviate significantly from the average value (111°), indicating that there is little distortion in the cyclohexyl chair conformation.

Figure 116. ORTEP diagram of $[(\text{BDI}_{\text{DIPP}})\text{Ge}(\text{S})\text{PCy}_2]$ (**54**). H atoms are omitted and C atoms in the *N*-aryl groups in the β -diketiminato ring are minimised for clarity. The ellipsoid probability is shown at 30%

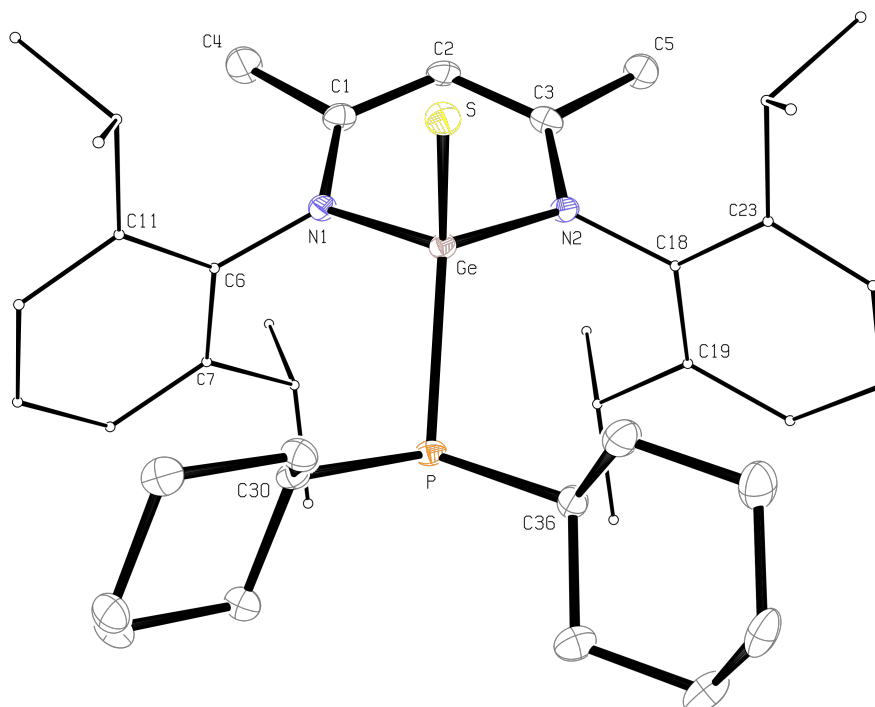


Figure 117. ORTEP diagram showing the side-on view of $[(\text{BDI}_{\text{DIPP}})\text{Ge}(\text{S})\text{PCy}_2]$ (**54**). H atoms are omitted and C atoms in the *N*-aryl groups in the β -diketiminato ring and the cyclohexyl groups are minimised for clarity. The ellipsoid probability is shown at 30%

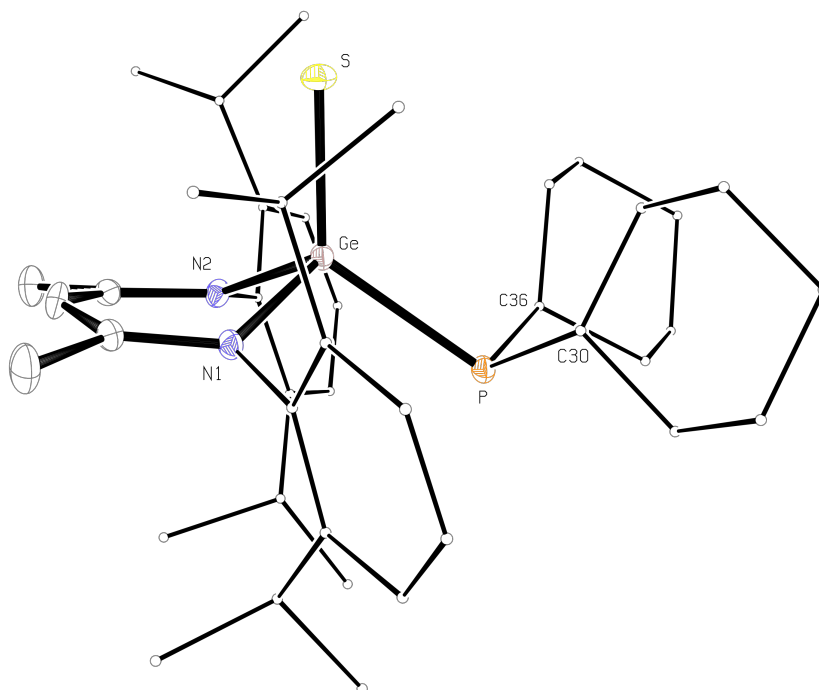


Table 51. Selected bond lengths (Å) and angles (deg) for [(BDI_{DIPP})Ge(S)PCy₂] (**54**)

<i>Bond lengths (Å)</i>			
Ge–N(1)	1.956(2)	C(1)–C(4)	1.506(4)
Ge–N(2)	1.958(2)	C(3)–C(5)	1.511(4)
N(1)–C(1)	1.343(4)	Ge–S	2.0954(8)
N(2)–C(3)	1.346(4)	Ge–P	2.3322(8)
C(1)–C(2)	1.384(4)	P–C(30)	1.883(3)
C(3)–C(2)	1.387(4)	P–C(36)	1.870(3)
Ge–NCCCN _{plane}	0.831		
<i>Bond angles (deg)</i>			
N(1)–Ge–N(2)	93.14(10)	N(1)–Ge–S	110.28(7)
Ge–N(1)–C(1)	117.70(19)	N(2)–Ge–S	110.50(7)
Ge–N(2)–C(3)	117.00(19)	N(1)–Ge–P	103.26(7)
N(1)–C(1)–C(2)	122.9(3)	N(2)–Ge–P	107.79(7)
N(2)–C(3)–C(2)	124.0(3)	S–Ge–P	126.56(3)
C(1)–C(2)–C(3)	127.3(3)	Ge–P–C(30)	100.14(9)
N(1)–C(1)–C(4)	120.0(3)	Ge–P–C(36)	103.46(10)
N(2)–C(3)–C(5)	119.8(3)	C(30)–P–C(36)	109.83(13)
NCCCN _{plane} –NGeN _{plane}	37.5	Σ bond angles around P	313.4
Avg. int. angles of Cy	111	DOP of P (%) ^a	52
<i>Dihedral angles (deg)</i>			
C(11)–C(6)–N(1)–Ge	83.7(3)	C(23)–C(18)–N(2)–Ge	–85.6(3)

^a Degree of pyramidalisation (DOP, %) = [(360 – Σ_{bond angle}) / 0.9]^[115] When a DOP is 100%, it is equivalent to a sum of bond angles of 270°, whereas a DOP of 0% indicates a planar geometry at the central atom

Table 52. Selected crystallographic data for [(BDI_{DIPP})Ge(S)PCy₂] (**54**)

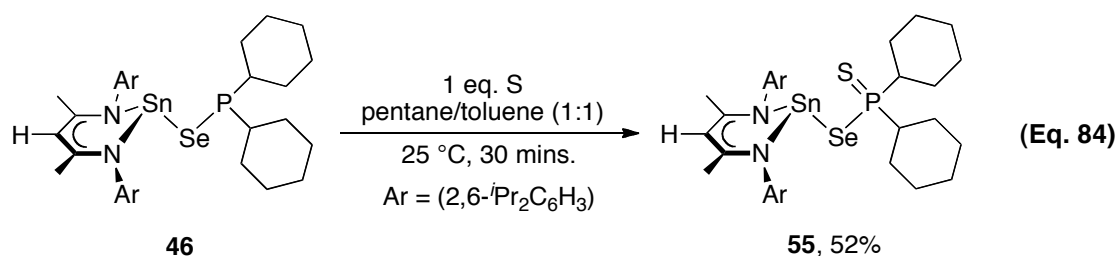
[(BDI _{DIPP})Ge(S)PCy ₂] (54)	
chemical formula	C ₄₅ H ₇₁ GeN ₂ OPS, C ₄ H ₈ O
molecular mass	791.66
temperature (K)	173(2)
wavelength (Å)	0.71073
crystal system	monoclinic
space group	<i>P</i> 2 ₁ / <i>c</i> (No. 14)
<i>a</i> (Å)	17.5377(4)
<i>b</i> (Å)	10.1519(1)
<i>c</i> (Å)	26.9248(6)
<i>α</i> (deg)	90
<i>β</i> (deg)	116.156(1)
<i>γ</i> (deg)	90
<i>V</i> (Å ³)	4302.83(14)
<i>Z</i>	4
ρ_{calcd} (Mg m ⁻³)	1.22
θ range (deg)	3.49–26.72
abs coeff (mm ⁻¹)	0.833
measd/indep reflns/ <i>R</i> (int)	45 679/9105/0.110
reflns with <i>I</i> > 2 σ (<i>I</i>)	6246
data/restraints/param	9105/6/499
goodness of fit on <i>F</i> ²	1.022
final <i>R</i> indices [<i>I</i> > 2 σ (<i>I</i>)]	<i>R</i> 1 = 0.054, <i>wR</i> 2 = 0.092
<i>R</i> indices (all data)	<i>R</i> 1 = 0.097, <i>wR</i> 2 = 0.103
largest diff peak and hole (e Å ⁻³)	0.52 and -0.50

4.4.16 NMR spectra of [(BDI_{DIPP})Ge(S)PCy₂] (**54**)

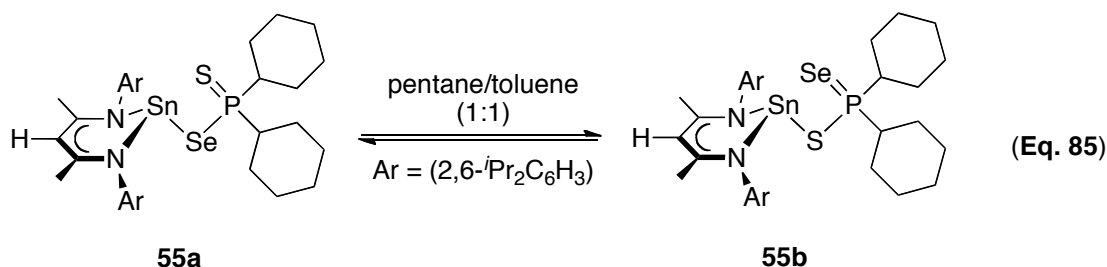
The ¹H NMR spectrum shows two septets at δ_{H} 3.86 and 3.22 ppm with through-bond proton-proton coupling $^3J_{\text{HH}} = 6.5$ Hz, assigned to the tertiary protons in the isopropyl groups (CHMe₂). In contrast to the germanium(II) dicyclohexylphosphanide **36**, there is no through-space proton-phosphorus coupling in any of the proton resonances assigned to the isopropyl groups. The ¹³C{¹H} NMR spectrum of **54** shows a doublet centred at δ_{C} 42.9 ppm, with carbon-phosphorus coupling $^1J_{\text{CP}} = 42$ Hz, assigned to the tertiary CH carbon in the cyclohexyl groups. There is no through-space carbon-phosphorus coupling observed in any of the signals assigned to the isopropyl groups. The ³¹P{¹H} NMR spectrum shows a singlet at δ_{P} -3.3 ppm.

4.4.17 Synthesis of $[(BDI_{DIPP})SnSeP(S)Cy_2]$ (**55**)

Since the reactions of the tin(II) dicyclohexylphosphanide **37** with elemental selenium or sulfur seemed to proceed *via* the same reaction pathway, we thought it would be interesting to synthesise a tin(II) dicyclohexylphosphinodichalcogenoato complex containing both selenium and sulfur. To the best of our knowledge, there are only two examples in the literature: $[Cu_3\{PhP(Se)S^tBu\}\{PhSe_2P-PSePh\}(PPh_3)_2]_2$ reported by Rothenberger and $[Ag(SSeP^iPr_2)]_4$ reported by O'Brien.^[297-298] Treatment of the tin(II) dicyclohexylphosphinoselenoite **46** with elemental sulfur in a 1:1 ratio in a pentane/toluene (1:1) solution gave the tin(II) dicyclohexylphosphinoselenothioato compound $[(BDI_{DIPP})SnSeP(S)Cy_2]$ (**55**) in 52% yield (equation 84).



Single crystals of $[(BDI_{DIPP})SnSeP(S)Cy_2]$ (**55**) were obtained by recrystallisation from pentane/toluene (1:1) at -30 °C. Connectivity was confirmed for all but the chalcogen atoms. Unfortunately, we were unable to resolve the chalcogen atoms by X-ray crystallography despite several attempts. This suggests that there is an exchange between coordination of selenium and sulfur in solution and disorder in the crystal (equation 85).



The tin(II) dicyclohexylphosphinoselenothioate **55** is sensitive to air and moisture. Metallic precipitates are found after 24 hours when a toluene solution of the compound

is allowed to stand at room temperature. This compound was characterised by multinuclear NMR spectroscopy, and selected data are given in Table 53.

Table 53. Selected multinuclear NMR spectroscopic data for [(BDI_{DIPP})SnSeP(S)Cy₂] (**55**) in C₆D₆ at 30 °C

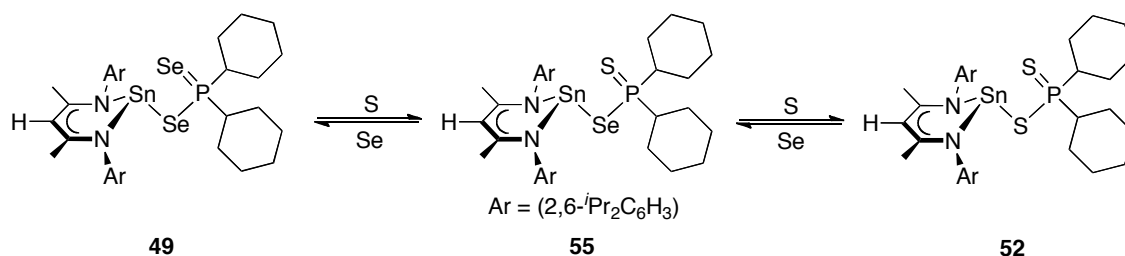
	δ (ppm), (J (Hz))
¹H	
γ -H	4.66 (s)
CHMe ₂	3.58 (br); 3.18 (br)
Cy-CH	1.58 (br)
¹³C{¹H}	
Cy-CH	43.2 (d) (¹ J _{CP} = 43)
CHMe ₂	29.6, 29.5 (s)
CHMe ₂	25.6, 24.9, 23.9, 23.8 (s)
³¹P{¹H}	
	72.3 (s) (¹ J _{PSe} = 490, ² J _{P¹¹⁹Sn} = 209, ² J _{P¹¹⁷Sn} = 200)
⁷⁷Se	
	-42 (d) (¹ J _{SeP} = 490)
¹¹⁹Sn/¹¹⁷Sn	
	$\delta(^{119}\text{Sn}) = -119$ (d) (² J ¹¹⁹ _{SnP} = 209)
	$\delta(^{117}\text{Sn}) = -119$ (d) (² J ¹¹⁷ _{SnP} = 205)

The ¹H NMR spectrum of **55** shows two broad signals at δ_{H} 3.58 and 3.18 ppm, assigned to the tertiary protons in the isopropyl groups (CHMe₂). The ¹³C{¹H} NMR spectrum shows a doublet centred at δ_{C} 43.2 ppm, with carbon-phosphorus coupling ¹J_{CP} = 43 Hz, assigned to the tertiary CH carbons in the cyclohexyl groups. As with the phosphinodiselenoato and -dithioato analogues, **49** and **52** respectively, there is no through-space carbon-phosphorus coupling in any of the signals assigned to the isopropyl groups.

The ³¹P{¹H} NMR spectrum of the tin(II) dicyclohexylphosphinoselenothioate **55** shows a major resonance at δ_{P} 72.3 ppm, with tin and selenium satellites (¹J_{PSe} = 490 Hz, ²J_{P¹¹⁹Sn} = 209 Hz and ²J_{P¹¹⁷Sn} = 200 Hz). However, there are two minor resonances, at δ_{P} 82.2 ppm and 58.8 ppm, which can be assigned, respectively, to the dithio compound **52** and the diseleno derivative **49**. Loss of chalcogen from the phosphorus(V) derivatives, as tentatively suggested by the NMR results (equation 79,

Page 220) may account for the presence of these compounds in the mixture (Scheme 65).

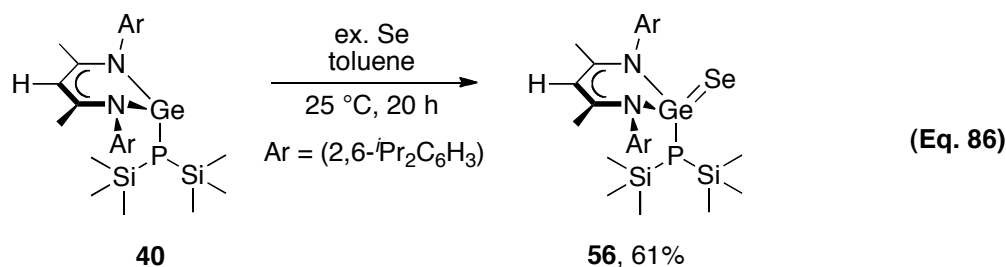
Scheme 65. Proposed interchangeable structures of $[(\text{BDI}_{\text{DIPP}})\text{SnSeP}(\text{S})\text{Cy}_2]$ (**55**) in solution



Both ^{119}Sn and ^{77}Se NMR spectra of the tin(II) dicyclohexylphosphinoselenothioate **55** confirm the findings from the $^{31}\text{P}\{^1\text{H}\}$ NMR spectrum. A major doublet centred at $\delta^{119}\text{Sn} -119$ ppm, with tin-phosphorus coupling $^2J^{119}\text{SnP} = 209$ Hz, is assigned to **55**. Two minor doublets centred at $\delta^{119}\text{Sn} -88$ ppm ($^2J^{119}\text{SnP} = 226$ Hz) and at $\delta^{119}\text{Sn} -175$ ppm ($^2J^{119}\text{SnP} = 181$ Hz) are assigned to the tin(II) dicyclohexylphosphinodiselenoate **49** and the tin(II) dicyclohexylphosphinodithioate **52**, respectively. The ^{77}Se NMR spectrum shows a major doublet centred at $\delta_{\text{Se}} -42$ ppm ($^1J_{\text{SeP}} = 490$ Hz), assigned to the tin(II) dicyclohexylphosphinoselenothioate **55**. A minor doublet centred at $\delta_{\text{Se}} -73$ ppm, with selenium-phosphorus coupling $^1J_{\text{SeP}} = 536$ Hz is assigned to the tin(II) dicyclohexylphosphinodiselenoate **49**.

4.4.18 Reactions of the β -diketiminato heavy group 14 metal bis(trimethylsilyl)phosphanides with elemental selenium

Treatment of the germanium(II) bis(trimethylsilyl)phosphanide **40** with an excess of elemental selenium gives the germanium(IV) selenide $[(\text{BDI}_{\text{DIPP}})\text{Ge}(\text{Se})\text{P}(\text{SiMe}_3)_2]$ (**56**) in 61% yield (equation 86). X-ray crystallography confirmed the connectivity of this compound. This complex is sensitive to air and moisture. Metallic precipitates are found when a toluene solution of **56** is allowed to stand at room temperature for 24 hours. However, the compound can be stored as solids at -30 °C without decomposition. It is soluble in common organic aprotic solvents. Elemental analyses are in good agreement with the calculated values.



4.4.19 X-ray crystal structure of [(BDI_{DIPP})Ge(Se)P(SiMe₃)₂] (**56**)

Yellow crystals of [(BDI_{DIPP})Ge(Se)P(SiMe₃)₂] (**56**) were obtained from an *n*-hexane solution at -30 °C. ORTEP drawings of compound **56** are shown in Figures 118 and 119. Selected bond lengths and angles are given in Table 54, and selected crystallographic data in Table 55. The ligands are coordinated in a distorted tetrahedral geometry around the germanium atom, with bond angles ranging from $94.88(8)$ – $116.22(5)^\circ$. Delocalisation within the C₃N₂Pb unit in the β-diketiminato ligand is evident, but it does not extend to the *N*-aryl substituents (dihedral angles: C(11)–C(6)–N(1)–Ge = $99.0(2)^\circ$ and C(23)–C(18)–N(2)–Ge = $-81.2(2)^\circ$). If the bis(trimethylsilyl)phosphanido ligand is discounted, there is an approximate plane of symmetry passing through the atoms C(2), Ge, and Se, bisecting the β-diketiminato ring. Due to the change in oxidation state at the germanium centre, the Ge–N ($1.9174(18)$ and $1.9923(18)$ Å) and Ge–P bond lengths ($2.2976(7)$ Å) in **56** are shorter than those in the germanium(II) bis(trimethylsilyl)phosphanide **40** (Ge–N = $2.006(2)$ and $2.046(2)$ Å; Ge–P = $2.3912(8)$ Å).^[134] The Ge=Se bond distance is $2.2163(3)$ Å, similar to the typical Ge=Se bond length (2.19 Å) in the literature and that in [(BDI_{DIPP})Ge(Se)PCy₂] (**51**, Ge=Se = $2.2216(5)$ Å).^[225] The phosphorus atom adopts a distorted planar geometry, with the Ge–P–Si(1) bond angle ($122.49(3)^\circ$) wider than the Ge–P–Si(2) bond angle ($106.77(3)^\circ$).

Figure 118. ORTEP diagram of $[(BDI_{DIPP})Ge(Se)P(SiMe_3)_2]$ (**56**). H atoms are omitted and C atoms in the *N*-aryl groups in the β -diketiminato ring are minimised for clarity. The ellipsoid probability is shown at 30%

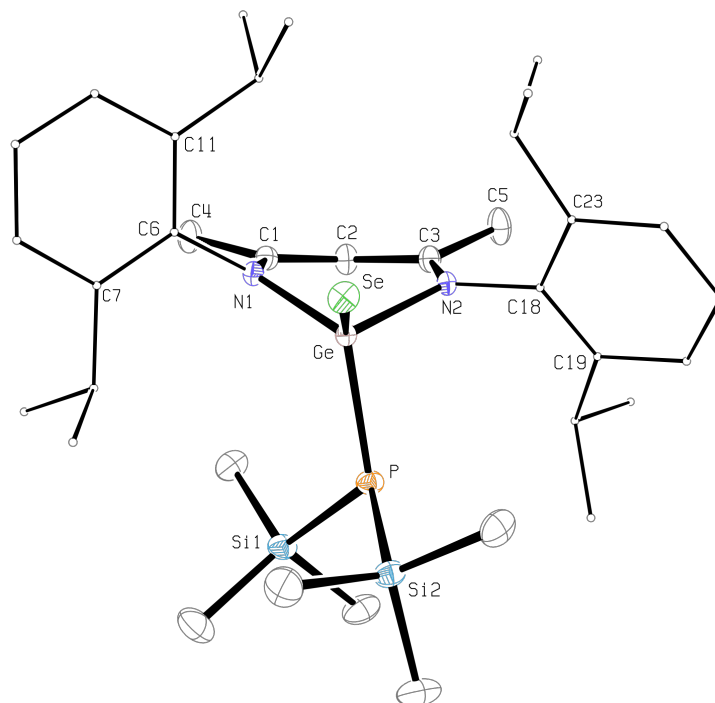


Figure 119. ORTEP diagram showing the side-on view of $[(BDI_{DIPP})Ge(Se)P(SiMe_3)_2]$ (**56**). H atoms are omitted and C atoms in the *N*-aryl groups in the β -diketiminato ring are minimised for clarity. The ellipsoid probability is shown at 30%

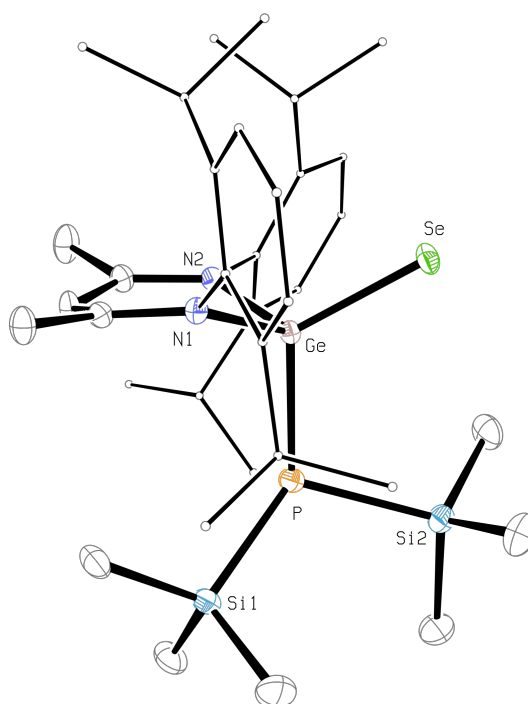


Table 54. Selected bond lengths (Å) and angles (deg) for [(BDI_{DIPP})Ge(Se)P(SiMe₃)₂] (**56**)

<i>Bond lengths (Å)</i>			
Ge–N(1)	1.9174(18)	C(1)–C(4)	1.508(3)
Ge–N(2)	1.9923(18)	C(3)–C(5)	1.502(3)
N(1)–C(1)	1.356(3)	Ge–Se	2.2163(3)
N(2)–C(3)	1.321(3)	Ge–P	2.2976(7)
C(1)–C(2)	1.370(3)	P–Si(1)	2.2415(9)
C(3)–C(2)	1.415(3)	P–Si(2)	2.2525(9)
Ge–NCCCN _{plane}	0.637		
<i>Bond angles (deg)</i>			
N(1)–Ge–N(2)	94.88(8)	N(1)–Ge–Se	111.91(6)
Ge–N(1)–C(1)	120.26(15)	N(2)–Ge–Se	116.22(5)
Ge–N(2)–C(3)	119.60(15)	N(1)–Ge–P	114.97(6)
N(1)–C(1)–C(2)	123.0(2)	N(2)–Ge–P	95.83(6)
N(2)–C(3)–C(2)	123.8(2)	Se–Ge–P	119.388(19)
C(1)–C(2)–C(3)	127.5(2)	Ge–P–Si(1)	122.49(3)
N(1)–C(1)–C(4)	118.5(2)	Ge–P–Si(2)	106.77(3)
C(2)–C(3)–C(5)	121.2(2)	Si(1)–P–Si(2)	111.65(4)
Σ bond angle around P	340.9	NCCCN _{plane} –NGeN _{plane}	28.1
DOP of P (%) ^a	21		
<i>Dihedral angles (deg)</i>			
C(11)–C(6)–N(1)–Ge	99.0(2)	C(23)–C(18)–N(2)–Ge	–81.2(2)

^a Degree of pyramidalisation (DOP, %) = [(360 – Σ_{bond angle}) / 0.9]^[115] When a DOP is 100%, it is equivalent to a sum of bond angles of 270°, whereas a DOP of 0% indicates a planar geometry at the central atom

Table 55. Selected crystallographic data for [(BDI_{DIPP})Ge(Se)P(SiMe₃)₂] (**56**)

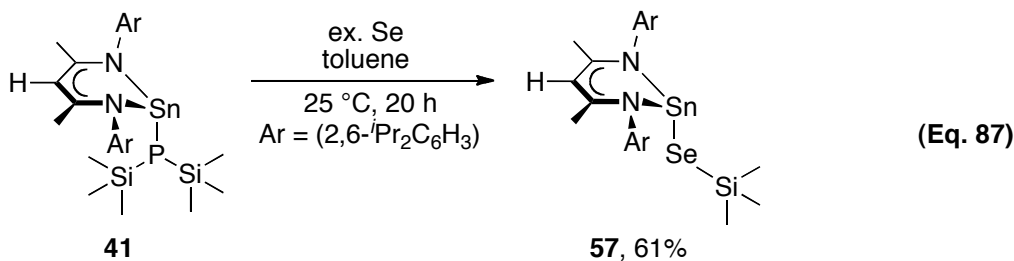
[(BDI _{DIPP})Ge(Se)P(SiMe ₃) ₂] (56)	
chemical formula	C ₃₅ H ₅₉ GeN ₂ PSeSi ₂
molecular mass	746.54
temperature (K)	173(2)
wavelength (Å)	0.71073
crystal system	monoclinic
space group	<i>P</i> 2 ₁ / <i>c</i> (No. 14)
<i>a</i> (Å)	13.5873(2)
<i>b</i> (Å)	18.7351(4)
<i>c</i> (Å)	17.6743(3)
<i>α</i> (deg)	90
<i>β</i> (deg)	117.597(1)
<i>γ</i> (deg)	90
<i>V</i> (Å ³)	3987.28(12)
<i>Z</i>	4
ρ_{calcd} (Mg m ⁻³)	1.24
θ range (deg)	3.51–26.75
abs coeff (mm ⁻¹)	1.806
measd/indep reflns/ <i>R</i> (int)	56 005/8452/0.076
data/restraints/param	8452/0/381
goodness of fit on <i>F</i> ²	0.969
final <i>R</i> indices [<i>I</i> > 2 σ (<i>I</i>)]	<i>R</i> 1 = 0.034, <i>wR</i> 2 = 0.068
<i>R</i> indices (all data)	<i>R</i> 1 = 0.054, <i>wR</i> 2 = 0.074
largest diff peak and hole (e Å ⁻³)	1.00 and -0.34

4.4.20 NMR spectra of [(BDI_{DIPP})Ge(Se)P(SiMe₃)₂] (**56**)

The ¹H NMR spectrum shows a septet centred at δ_{H} 3.60 ppm (${}^3J_{\text{HH}} = 6.8$ Hz), with an integration of four protons, assigned to the tertiary protons in the isopropyl groups (CHMe₂). Two doublets centred at δ_{H} 0.50 and 0.42 ppm, with proton-phosphorus coupling ${}^3J_{\text{HP}} = 6.0$ Hz, are assigned to the protons in the trimethylsilyl groups (SiMe₃). A single resonance at δ_{P} -172.6 ppm, with selenium and silicon satellites (${}^2J_{\text{PSe}} = 52$ Hz and ${}^1J_{\text{PSi}} = 26$ Hz), is found in the ${}^{31}\text{P}\{^1\text{H}\}$ NMR spectrum. This signal is downfield from that in the germanium(II) bis(trimethylsilyl)phosphanide precursor **40** (δ_{P} -192.8 ppm). The ⁷⁷Se NMR spectrum of the germanium(IV) selenide **56** shows a doublet centred at δ_{Se} -129 ppm in C₆D₆, with selenium-phosphorus coupling ${}^2J_{\text{SeP}} = 49$ Hz. These values may be compared with those in [(BDI_{DIPP})Ge(Se)PCy₂] (**51**, δ_{Se} -91 ppm in CDCl₃, ${}^2J_{\text{SeP}} = 12$ Hz).

4.4.21 Synthesis of β -diketiminatotin(II) trimethylsilylselenide (**57**)

Treatment of the β -diketiminatotin(II) bis(trimethylsilyl)phosphanide **41** in toluene at room temperature with an excess of elemental selenium gives the tin(II) trimethylsilylselenide [(BDI_{DIPP})SnSeSiMe₃] (**57**) in 61% yield (equation 87). The X-ray crystallography confirmed the connectivity of this complex. It is the first compound containing a Sn–Se–Si sequence, in a non-cyclic structure involving a low-valent tin atom, to be crystallographically characterised.^[299-301] Compound **57** is sensitive to air and moisture. Metallic precipitates are formed when a toluene solution of this complex is allowed to stand at room temperature for 24 hours. Elemental analyses are in good agreement with the calculated values.



4.4.22 X-ray crystal structure of [(BDI_{DIPP})SnSeSiMe₃] (**57**)

Single crystals of [(BDI_{DIPP})SnSeSiMe₃] (**57**) were obtained as a toluene solvate from toluene at $-30\text{ }^{\circ}\text{C}$. ORTEP drawings are shown in Figures 120 and 121. Selected bond lengths and angles are given in Table 56, and selected crystallographic data in Table 57. The tin(II) trimethylsilylselenide **57** adopts an *endo* conformation with the tin atom 0.508 \AA below the mean NCCCN plane of the β -diketiminato ligand. The sum of bond angles around the pyramidally coordinated tin atom is 274.2° . Delocalisation within the C₃N₂Sn unit in the β -diketiminato ring is evident, but it does not extend to the *N*-aryl substituents (dihedral angles: C(11)–C(6)–N(1)–Sn = $81.0(4)^{\circ}$ and C(23)–C(18)–N(2)–Sn = $-81.1(4)^{\circ}$). Discounting the methyl groups on the silicon atom, there is an approximate plane of symmetry passing through the atoms C(2), Sn, Se and Si, bisecting the β -diketiminato ring. The Sn–Se bond distance is $2.6333(5)\text{ \AA}$, similar to those in [(BDI_{DIPP})SnSePCy₂] (**46**, Sn–Se = $2.6059(3)\text{ \AA}$) and Herzog's [Me₂Sn(Se)₂Si₂Me₂(Se)₂SnMe₂] (Sn–Se = $2.5566(4)\text{ \AA}$).^[299] The trimethylsilylselenido ligand is singly bonded to the tin atom, with a Sn–Se–Si bond angle ($100.60(3)^{\circ}$), similar to those found in Corrigan's [(*N,N'*-TMEDA)Zn(SeSiMe₃)₂] ($101.05(4)$ – $105.02(4)^{\circ}$) and [(3,5-Me₂C₅H₃N)₂Co(SeSiMe₃)₂] ($101.30(3)$ – $106.17(3)^{\circ}$).^[302-303]

Figure 120. ORTEP diagram of $[(BDI_{DIPP})SnSeSiMe_3]$ (**57**). H atoms are omitted and C atoms in the *N*-aryl groups in the β -diketiminato ring are minimised for clarity. The ellipsoid probability is shown at 30%

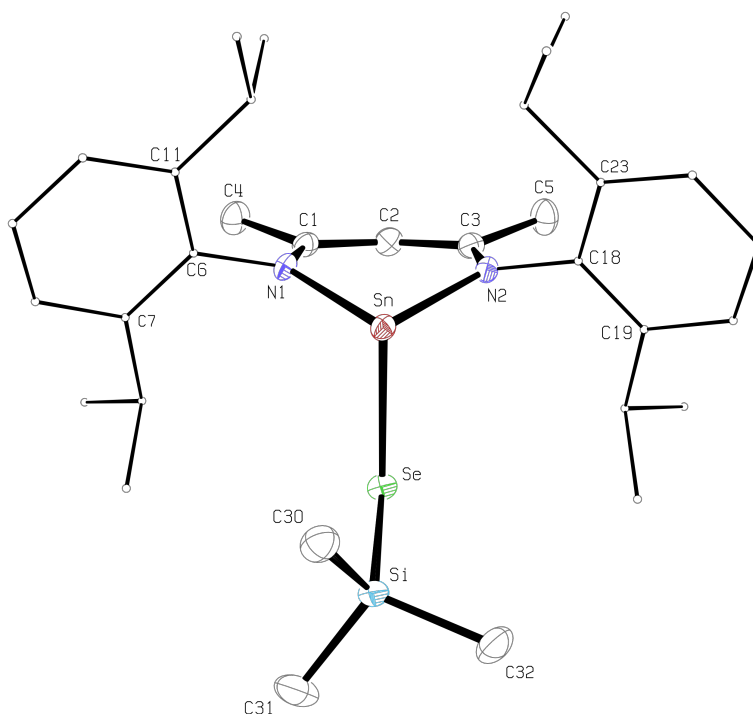


Figure 121. ORTEP diagram showing the side-on view of $[(BDI_{DIPP})SnSeSiMe_3]$ (**57**). H atoms are omitted and C atoms in the *N*-aryl groups in the β -diketiminato ring are minimised for clarity. The ellipsoid probability is shown at 30%

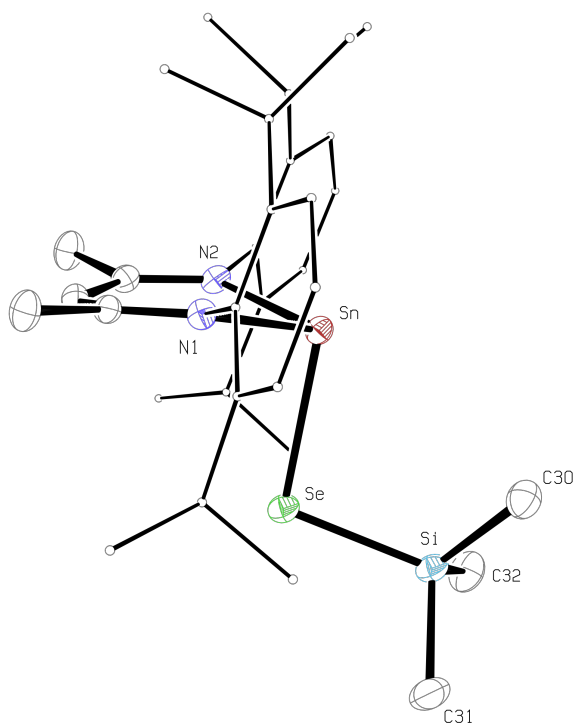


Table 56. Selected bond lengths (Å) and angles (deg) for [(BDI_{DIPP})SnSeSiMe₃] (**57**)

<i>Bond lengths (Å)</i>			
Sn–N(1)	2.207(3)	C(2)–C(3)	1.401(5)
Sn–N(2)	2.202(3)	C(1)–C(4)	1.517(5)
N(1)–C(1)	1.323(5)	C(3)–C(5)	1.511(5)
N(2)–C(3)	1.328(5)	Sn–Se	2.6333(5)
C(1)–C(2)	1.393(5)	Se–Si	2.2815(12)
Sn–NCCCN _{Plane}	0.508		
<i>Bond angles (deg)</i>			
N(1)–Sn–N(2)	85.15(11)	N(1)–C(1)–C(4)	120.0(3)
Sn–N(1)–C(1)	125.5(2)	C(2)–C(3)–C(5)	115.7(3)
Sn–N(2)–C(3)	125.8(2)	N(1)–Sn–Se	94.38(8)
N(1)–C(1)–C(2)	124.7(3)	N(2)–Sn–Se	94.65(8)
N(2)–C(3)–C(2)	124.3(3)	Sn–Se–Si	100.60(3)
C(1)–C(2)–C(3)	129.7(4)		
Σ bond angle around Sn	274.2	NCCCN _{plane} –NSnN _{plane}	17.8
DOP (%) ^a	95		
<i>Dihedral angles (deg)</i>			
C(11)–C(6)–N(1)–Sn	81.0(4)	C(23)–C(18)–N(2)–Sn	–81.1(4)

^a Degree of pyramidalisation (DOP, %) = [(360 – Σ_{bond angle}) / 0.9]^[115] When a DOP is 100%, it is equivalent to a sum of bond angles of 270°, whereas a DOP of 0% indicates a planar geometry at the central atom

Table 57. Selected crystallographic data for [(BDI_{DIPP})SnSeSiMe₃] (**57**)

[(BDI _{DIPP})SnSeSiMe ₃] (57)	
chemical formula	C ₃₂ H ₅₀ N ₂ SeSiSn, 0.5(C ₇ H ₈)
molecular mass	734.55
temperature (K)	173(2)
wavelength (Å)	0.71073
crystal system	triclinic
space group	$P\bar{1}$ (No. 2)
<i>a</i> (Å)	10.6632(13)
<i>b</i> (Å)	11.9105(13)
<i>c</i> (Å)	15.2531(18)
α (deg)	101.567(8)
β (deg)	93.519(6)
γ (deg)	105.196(7)
<i>V</i> (Å ³)	1818.2(4)
<i>Z</i>	2
ρ_{calcd} (Mg m ⁻³)	1.34
θ range (deg)	3.44–26.02
abs coeff (mm ⁻¹)	1.76
measd/indep reflns/ <i>R</i> (int)	23 354/6805/0.045
data/restraints/param	6805/7/375
goodness of fit on F^2	1.064
final <i>R</i> indices [$I > 2\sigma(I)$]	<i>R</i> 1 = 0.040, <i>wR</i> 2 = 0.088
<i>R</i> indices (all data)	<i>R</i> 1 = 0.049, <i>wR</i> 2 = 0.092
largest diff peak and hole (e Å ⁻³)	0.87 and –1.00

4.4.23 NMR spectra of [(BDI_{DIPP})SnSeSiMe₃] (**57**)

The ¹H NMR spectrum of **57** shows two septets at δ_{H} 3.90 and 3.29 ppm, with proton-proton coupling $^3J_{\text{HH}} = 6.8$ Hz, assigned to the tertiary protons in the isopropyl groups (CHMe₂). A singlet at δ_{H} 0.26 ppm is assigned to the protons in the trimethylsilyl group (SiMe₃). The ¹³C{¹H} NMR spectrum shows a single resonance at δ_{C} 6.2 ppm, assigned to the carbons in the SiMe₃ group. The absence of the phosphorus atom in the tin(II) trimethylsilylselenide **57** is confirmed by the ³¹P{¹H} NMR spectroscopy, which does not show any signal in the range tested (δ_{P} 400 to –600 ppm). The ¹¹⁹Sn NMR spectrum shows a single resonance at δ_{Sn} 87 ppm. A singlet at δ_{Se} –176 ppm is shown in the ⁷⁷Se NMR spectrum. The ²⁹Si{¹H} NMR spectrum shows a single resonance at δ_{Si} 7.4 ppm.

4.5 Conclusions

We have demonstrated that the reactions of the β -diketiminatotin(II) and -lead(II) dicyclohexylphosphanides **37** and **38** with elemental selenium in 1:1 ratio give the corresponding dicyclohexylphosphinoselenoato complexes **46** and **47**. Further reactions with elemental selenium give the dicyclohexylphosphinodiselenoato complexes **49** and **50**. The solid state structures of the latter compounds indicate that the dicyclohexylphosphinodiselenoato ligand is coordinated to the metal centre in η^1 -fashion. In contrast, the multinuclear NMR studies on these complexes suggest that in solution, the ligand is coordinated to the metal centre in η^2 -fashion.

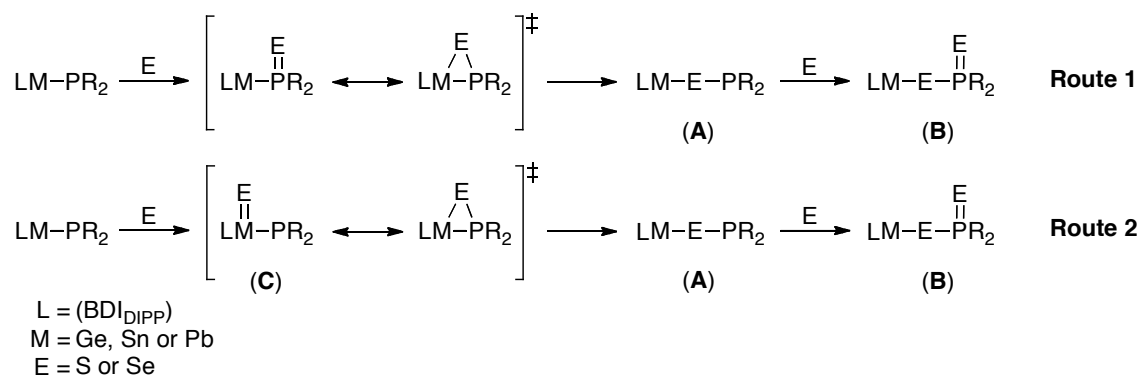
Reactions of the dicyclohexylphosphanides **37** and **38** with elemental sulfur give the corresponding dicyclohexylphosphinodithioato complexes **52** and **53**. However, isolation of the dicyclohexylphosphinothioato intermediates were not successful. The dicyclohexylphosphinodithioato complexes appear to be the preferred products from addition of elemental sulfur to the dicyclohexylphosphanido complexes.

In contrast to the reactions of the tin and lead derivatives, the reaction between the germanium(II) dicyclohexylphosphanide **36** and an excess of elemental selenium gives the germanium(IV) selenide **51**, which forms as a co-product with the germanium(II) dicyclohexylphosphinodiselenoate **48**. However, when the phosphanide **36** was treated with an excess of elemental sulfur, only the germanium(IV) sulfide **54** was isolated from the reaction. This difference is consistent with the decreasing stability of the +4 oxidation state in the series: Ge > Sn > Pb. The inert pair effect is least evident in germanium and oxidative addition to the metal centre occurs most readily.

To the best of our knowledge, the reaction pathway between the heavy group 14 metal phosphanides and elemental chalcogens has not been studied systematically. Although the heterogeneous nature of these reactions prevents detailed mechanistic studies, two reaction pathways can be envisaged from the results obtained (Scheme 66). Route 1 involves an initial oxidative addition of the chalcogen to the phosphorus, followed by an insertion of the chalcogen into the metal-phosphorus bond *via* a three-membered M–E–P transition state to give the product A. Further addition of the elemental chalcogen leads to oxidation of the phosphorus to give product B. In route 2, the initial

step involves an oxidation of the metal centre by the chalcogen to give product C. This gives the insertion product A *via* a three-membered M–E–P transition state. The remaining steps are similar to those described for the route 1. Further studies are in progress.

Scheme 66. Proposed reaction pathways for the reaction between phosphanido complex and elemental chalcogen



Preliminary studies on the reactions between the β -diketiminatogermanium(II) and –tin(II) bis(trimethylsilyl)phosphanides, **40** and **41**, and an excess of elemental selenium are described. As in the reaction of the germanium(II) dicyclohexylphosphanide **36** with elemental selenium or sulfur, the germanium(IV) selenide $[(\text{BDI}_{\text{DIPP}})\text{Ge}(\text{Se})\text{P}(\text{SiMe}_3)_2]$ (**56**) was observed as the sole product. Unlike all the previously studied compounds, however, the tin(II) bis(trimethylsilyl)phosphanide **41** reacts with elemental selenium to form the tin(II) trimethylsilylselenide **57** exclusively. This is the first heavy group 14 metal complex containing a Sn–Se–Si heteroatomic ‘heavy ether’ linkage. Due to the heterogeneous nature of this reaction, we were unable to elucidate mechanistic details and the fate of the phosphorus has not been determined.

Further work to gain more insight into the kinetics and thermodynamics of the reactions between the β -diketiminato heavy group 14 metal phosphanides and heavier chalcogens is in progress.

5. Experimental

5.1 General methods and procedures

All experiments and manipulations were carried out under dry oxygen-free nitrogen using standard Schlenk techniques or in an MBraun Unilab inert atmosphere glovebox containing purified nitrogen. Solvents were dried from the appropriate drying agent, distilled, degassed and stored over 4 Å sieves or a sodium or potassium mirror.^[304] All chemicals were purchased from Aldrich or Fisher Scientific and purified by distillation or sublimation.^[304] NMR solvents (C_6D_6 , $CDCl_3$, toluene- d_8) were purchased from Cambridge Isotope Laboratories Inc., and were degassed and stored over 4 Å sieves prior to use. Carbon dioxide was used as received (Union Carbide, 99.999%), and $^{13}CO_2$ was 99 atom %. The bis(trimethylsilyl)phosphine was received as a gift from Dr. Ian. R. Crossley (Sussex). Diphenylphosphine and dicyclohexylphosphine were purchased from Aldrich and used as received. NMR spectra were recorded on a Bruker DPX 300 MHz NMR spectrometer, or Varian 400 MHz, 500MHz and 600MHz NMR spectrometers. 1H and $^{13}C\{^1H\}$ NMR chemical shifts are measured relative to residual solvent peaks and reported relative to Me_4Si ; $^{119}Sn/^{117}Sn$, ^{207}Pb , ^{19}F , ^{29}Si , ^{31}P and ^{77}Se were externally referenced to $SnMe_4$, $PbMe_4$, $CFCl_3$, $SiMe_4$, H_3PO_4 and Me_2Se , respectively. Solid state NMR spectra were obtained from the EPSRC National Solid-state NMR Research Service at the University of Durham. C, H and N elemental analyses were obtained from London Metropolitan University. Mass spectra were measured at the Centre of Mass Spectroscopy, University of Sussex. IR spectra were recorded on a Perkin-Elmer 1500 FT-IR with a resolution of 4 cm^{-1} . UV spectra were recorded using a quartz cuvette fitted with a Young's tap on a Varian Cary 50 UV/Vis spectrometer.

The data for the X-ray structures were collected on a Nonius Kappa CCD diffractometer at 173 K, (Mo-K α radiation, $\lambda = 0.71073\text{ \AA}$) and refined using the *SHELXL-97* software package.^[305]

General procedure for small-scale reactivity study in an NMR tube. A sample of the metal complex (0.03 g) was dissolved in either C_6D_6 or toluene- d_8 (~ 0.5 mL) in an NMR tube fitted with a Young's tap. The required substrate was added to the mixture.

The reaction was monitored after 10 minutes, 1, 2 and 24 h at room temperature. The reaction was then heated to 40°C for 24 h after which a ¹H NMR spectrum was recorded again.

Lithium alkoxide or phosphanide. The alcohol or phosphine was added to *n*-hexane under an inert atmosphere. The solution was cooled to -78 °C and a molar equivalent of *n*-BuLi in *n*-hexane was added dropwise. The mixture was allowed to warm gradually to room temperature over a period of 20 h. Volatiles were evaporated from the mixture under vacuum. The residue was washed with *n*-hexane and dried *in vacuo*. The purified solid was collected and stored at -30 °C in an inert atmosphere.

5.2 Experimental procedures for Chapter 2

[CH{(CH₃)CN-2,6-ⁱPr₂C₆H₃}₂H], (BDI_{DIPP})H, (1).^[41] Acetylacetone (4.91 g, 49.0 mmol) and 2,6-diisopropylaniline (19.51 g, 110.0 mmol) were added to ethanol (200 mL). Concentrated HCl (4 mL) was added dropwise to the mixture, which was then heated under reflux for 3 days. The crude product BDI_{DIPP}·HCl was extracted with dichloromethane (100 mL) and saturated sodium carbonate (300 mL) was added. The solution was stirred for 10 minutes, and extracted with dichloromethane (3 × 100 mL). The combined organic layer was dried over magnesium sulfate. The solvent was removed under vacuum and the residue was washed with cold methanol (2 × 10 mL) and dried overnight under reduced pressure. Yield: 14.1 g, 69 %. [lit. 73 %].^[41] ¹H NMR (499.91 MHz, CDCl₃, 303 K): δ 12.45 (s, 1H, Ar-NH), 7.15 (m, 6H, Ar-H), 4.88 (s, 1H, γ-CH), 3.31 (septet, *J* = 7.0 Hz, 4H, CHMe₂), 1.66 (s, 6H, NCM_e), 1.21 (d, *J* = 7.0 Hz, 12H, CHMe₂), 1.16 (d, *J* = 7.0 Hz, 12H, CHMe₂). [lit. ¹H NMR (CDCl₃, 298 K): δ 12.12 (br, 1H), 7.12 (m, 6H), 4.84 (s, 1H), 3.10 (m, 2H), 1.72 (s, 6H), 1.22 (d, 12H), 1.12 (d, 12H)].^[41] ¹³C{¹H} NMR (125.71 MHz, CDCl₃, 303 K): δ 161.4 (NCMe), 142.7 (*ipso*-C), 141.0 (*o*-C), 125.3 (*p*-C), 123.2 (*m*-C), 93.5 (γ-CH), 28.4 (CHMe₂), 24.6 (CHMe₂), 23.4 (CHMe₂), 21.0 (NCMe). [lit. ¹³C NMR (CDCl₃, 298 K): δ 161.4, 142.6, 140.9, 125.3, 123.2, 93.4, 28.4, 24.5, 23.4, 21.0].^[41]

[CH{(CH₃)CN-2,6-ⁱPr₂C₆H₃}₂PbCl], [(BDI_{DIPP})PbCl], (2).^[62] (BDI_{DIPP})H (1) (2.56 g, 6.03 mmol) was dissolved in THF (35 mL) and a solution of *n*-BuLi in *n*-hexane (2.6 mL of 2.7 M solution, 6.03 mmol) was added. The mixture was stirred at room

temperature for 45 minutes and transferred slowly to a THF (10 mL) slurry of PbCl₂ (1.72 g, 6.03 mmol) *via* cannula. The mixture was stirred at room temperature for 20 h and the volatiles were removed under vacuum. Toluene (3 × 15 mL) was added and filtered through a pad of Celite. The solvent was removed from the filtrate under reduced pressure, and the residue was washed with pentane (3 × 15 mL). The yellow [(BDI_{DIPP})PbCl] (**2**) was collected and used without further purification. Yield: 3.14 g, 79%. [lit. 56%].^[62] ¹H NMR (499.91 MHz, C₆D₆, 303 K): δ 7.21 (dd, *J* = 7.5, 1.5 Hz, 2H, *m*-H), 7.12 (t, *J* = 7.5 Hz, 2H, *p*-H), 7.06 (dd, *J* = 7.5, 1.5 Hz, 2H, *m*-H), 4.87 (s, 1H, *γ*-CH), 3.96 (septet, *J* = 7.0 Hz, 2H, CHMe₂), 3.05 (septet, *J* = 7.0 Hz, 2H, CHMe₂), 1.68 (s, 6H, NCMe), 1.50 (d, *J* = 7.0 Hz, 6H, CHMe₂), 1.24 (d, *J* = 6.5 Hz, 6H, CHMe₂), 1.16 (d, *J* = 6.5 Hz, 6H, CHMe₂), 1.08 (d, *J* = 7.0 Hz, 6H, CHMe₂). [lit. ¹H NMR (C₆D₆, 293 K): δ 7.23 (d, *J* = 7.5 Hz, 2H), 7.18 (t, *J* = 7.5 Hz, 2H), 7.10 (d, *J* = 7.5 Hz, 2H), 4.91 (s, 1H), 3.99 (septet, *J* = 6.8 Hz, 2H), 3.08 (septet, *J* = 6.8 Hz, 2H), 1.71 (s, 6H), 1.54 (d, *J* = 6.7 Hz, 6H), 1.27 (d, *J* = 6.8 Hz, 6H), 1.19 (d, *J* = 6.9 Hz, 6H), 1.12 (d, *J* = 6.8 Hz, 6H)].^[62] ¹³C{¹H} NMR (125.71 MHz, C₆D₆, 303 K): δ 164.5 (NCMe), 146.1 (*ipso*-C), 142.9 (*o*-C), 142.9 (*o*-C), 127.4 (*p*-C), 125.8 (*m*-C), 124.1 (*m*-C), 104.7 (*γ*-CH), 29.1 (CHMe₂), 28.4 (CHMe₂), 28.1 (CHMe₂), 25.6 (CHMe₂), 25.0 (CHMe₂), 25.0 (NCMe), 24.7 (CHMe₂). [lit. ¹³C{¹H} NMR (C₆D₆, 293 K): δ 164.2, 145.7, 142.5, 127.0, 125.4, 123.7, 104.4, 28.7, 28.0, 27.7, 25.2, 24.7, 24.6 and 24.3].^[62] UV-vis (pentane), (λ_{max}, nm (ε, M⁻¹cm⁻¹)): 255.0 (9100), 370.1 (10800).

[CH{(CH₃)CN-2,6-^{*i*}Pr₂C₆H₃}₂PbO^{*i*}Pr], [(BDI_{DIPP})PbO^{*i*}Pr], (**3**).^[114] [(BDI_{DIPP})PbCl] (**2**) (0.35 g, 0.53 mmol) in toluene (15 mL) was added to a toluene (15 mL) suspension of lithium isopropoxide (0.05 g, 0.53 mmol). The mixture was stirred at room temperature for 24 h. The yellow mixture was filtered through a pad of Celite and the solvent was removed under vacuum. The crude residue was washed with cold pentane (3 mL). Yellow crystals were obtained upon standing in minimum amount of pentane at -30 °C. Yield: 0.19 g, 52%. [lit. 62%].^[114] ¹H NMR (499.91 MHz, C₆D₆, 303 K): δ 7.25 (dd, *J* = 7.5, 1.0 Hz, 2H, *m*-H), 7.13 (t, *J* = 8.0 Hz, 2H, *p*-H), 7.09 (dd, *J* = 7.5, 1.5 Hz, *m*-H), 4.93 (septet, *J* = 6.0 Hz, 1H, O-CHMe₂), 4.70 (s, 1H, *γ*-CH), 3.91 (septet, *J* = 7.0 Hz, 2H, CHMe₂), 3.16 (septet, *J* = 7.0 Hz, 2H, CHMe₂), 1.68 (s, 6H, NCMe), 1.53 (d, *J* = 7.0 Hz, 6H, CHMe₂), 1.27 (d, *J* = 6.5 Hz, 6H, CHMe₂), 1.19 (d, *J* = 7.0 Hz, 6H, CHMe₂), 1.15 (d, *J* = 6.5 Hz, 6H, CHMe₂), 1.03 (d, *J* = 6.0 Hz, 6H, O-CHMe₂). [lit.: ¹H

NMR (300 MHz, C₆D₆, 303 K): δ 7.26 (d, $J = 7.5$ Hz, 2H), 7.20 (t, $J = 7.5$ Hz, 2H), 7.09 (d, $J = 7.5$ Hz, 2H), 4.96 (septet, $J = 6.8$ Hz, 1H), 4.71 (s, 1H), 3.95 (septet, $J = 6.8$ Hz, 2H), 3.18 (septet, $J = 6.8$ Hz, 2H), 1.69 (s, 6H), 1.57 (d, $J = 6.7$ Hz, 6H), 1.29 (d, $J = 6.8$ Hz, 6H), 1.20 (d, $J = 6.9$ Hz, 6H), 1.17 (d, $J = 6.8$ Hz, 6H), 1.07 (d, $J = 5.9$ Hz, 6H)].^[114] ¹³C{¹H} NMR (125.72 MHz, C₆D₆, 303 K): δ 164.2 (NCMe), 145.5 (*ipso*-C), 143.6 (*o*-C), 142.5 (*o*-C), 126.7 (*p*-C), 125.1 (*m*-C), 124.2 (*m*-C), 100.5 (γ -CH), 66.3 (O-CHMe₂), 30.9 (O-CHMe₂), 28.6 (CHMe₂), 28.4 (CHMe₂), 26.6 (NCMe), 26.2, 25.2, 24.9, 24.6 (CHMe₂). [lit. ¹³C{¹H} NMR (100.46 MHz, C₆D₆, 303 K): δ 163.9, 145.1, 143.3, 126.4, 124.8, 123.9, 100.2, 66.0, 30.6, 28.2, 26.3, 25.7, 24.9, 24.6].^[114] ²⁰⁷Pb NMR (83.58 MHz, C₆D₆, 303 K): δ 1500. IR (Nujol, ν/cm^{-1}): 1555 (s), 1514 (s), 1171 (s), 1119 (s), 1016 (s), 966 (s). IR (CCl₄, ν/cm^{-1}): 3060 (s), 1463 (s), 1437 (s), 1396 (s), 1321 (s).

[CH{(CH₃)CN-2,6-ⁱPr₂C₆H₃}₂PbO'Bu], [(BDI_{DIPP})PbO'Bu], (4).^[114] [(BDI_{DIPP})PbCl] (**2**) (0.91 g, 1.38 mmol) in toluene (10 mL) was added to a stirred toluene (15 mL) suspension of potassium *tert*-butoxide (0.15 g, 1.38 mmol) at room temperature and the mixture was stirred for 20 h. It was filtered through a pad of Celite and the volatiles were removed under vacuum to leave an orange solid. The crude product was washed with pentane and recrystallised from toluene at -30 °C, to give yellow photo-sensitive crystals. Yield: 0.72 g, 75%. [lit. 75%].^[114] ¹H NMR (399.50MHz, C₆D₆, 303K): δ 7.27 (dd, $J = 7.6, 1.6$ Hz, 2H, *m*-H), 7.12 (t, $J = 7.6$ Hz, 2H, *p*-H), 7.06 (dd, $J = 7.6, 1.6$ Hz, 2H, *m*-H), 4.58 (s, 1H, γ -CH), 3.84 (septet, $J = 7.2$ Hz, 2H, CHMe₂), 3.14 (septet, $J = 6.8$ Hz, 2H, CHMe₂), 1.68 (s, 6H, NCMe), 1.66 (d, $J = 6.8$ Hz, 6H, CHMe₂), 1.26 (d, $J = 7.2$ Hz, 6H, CHMe₂), 1.21 (d, $J = 7.2$ Hz, 6H, CHMe₂), 1.16 (d, $J = 6.8$ Hz, 6H, CHMe₂), 0.89 (s, 9H, C(CH₃)₃). [lit. ¹H NMR (300MHz, C₆D₆, 293K): δ 7.26 (dd, $J = 7.5, 1.6$ Hz, 2H), 7.10 (t, $J = 7.5$ Hz, 2H), 7.04 (dd, $J = 7.5, 1.6$ Hz, 2H), 4.57 (s, 1H), 3.83 (septet, $J = 6.8$ Hz, 2H), 3.12 (septet, $J = 6.8$ Hz, 2H), 1.65 (s, 6H), 1.63 (d, $J = 6.8$ Hz, 6H), 1.25 (d, $J = 6.9$ Hz, 6H), 1.19 (d, $J = 6.9$ Hz, 6H), 1.14 (d, $J = 6.8$ Hz, 6H), 0.88 (s, 9H)].^[114] ¹³C{¹H} NMR (75.47 MHz, C₆D₆, 293K)*: δ 164.0 (NCMe), 145.1 (*ipso*-C), 142.8 (*o*-C), 141.5 (*o*-C), 126.0 (*p*-C), 123.7 (*m*-C), 123.6 (*m*-C), 98.0 (γ -CH), 69.1 (O-CMe₃), 36.7 (O-C(CH₃)₃), 28.4 (CHMe₂), 28.0 (CHMe₂), 26.1 (NCMe), 25.2, 24.8, 24.6, 23.9 (CHMe₂). (* These results were used in our publication.^[114]) ²⁰⁷Pb

NMR (83.83 MHz, C₆D₆, 303 K): δ 1713. IR (CCl₄, ν/cm^{-1}): 3059 (s), 2962 (s), 2868 (s), 1436 (s), 1396 (s), 1321 (s), 1183 (s), 1101 (br).

[CH{(CH₃)CN-2,6-ⁱPr₂C₆H₃}₂PbOC(CH₃)₂CHCH₂],

[(BDI_{DIPP})PbO(CH₃)₂CH=CH₂], (5). [(BDI_{DIPP})PbCl] (2) (0.40 g, 0.61 mmol) in toluene (15 mL) was added to a suspension of sodium 2-methyl-3-buten-2-oxide (0.07 g, 0.61 mmol) in toluene (5 mL). The mixture was stirred for 20 h at room temperature. The yellow suspension was filtered through a pad of Celite. Volatiles were removed *in vacuo* and the residue was washed with cold pentane (3 × 5 mL). Yellow crystals of compound **5** were obtained upon standing in a minimum amount of toluene at -30 °C. Yield: 0.37 g, 87%. ¹H NMR (399.50 MHz, C₆D₆, 303 K): δ 7.28 (d, J = 7.6 Hz, 2H, *m*-H), 7.15 (t, J = 7.6 Hz, 2H, *p*-H), 7.06 (d, J = 7.6 Hz, 2H, *m*-H), 5.70 (dd, J = 17.2, 10.4 Hz, 1H, CHCH₂), 4.59 (dd, J = 10.4 and 1.2 Hz, 1H, CHCH₂), 4.58 (s, 1H, γ -CH), 4.53 (dd, J = 10.4, 1.2 Hz, 2H, CHCH₂), 3.87 (septet, J = 6.8, 2H, CHMe₂), 3.12 (septet, J = 6.8 Hz, 2H, CHMe₂), 1.68 (s, 6H, NMe), 1.64 (d, J = 6.8 Hz, 6H, CHMe₂), 1.26 (d, J = 6.8 Hz, 6H, CHMe₂), 1.19 (d, J = 6.8 Hz, 6H, CHMe₂), 1.15 (d, J = 6.8 Hz, 6H, CHMe₂), 0.95 (s, 6H, OC(CH₃)₂). ¹³C{¹H} NMR (100.46 MHz, C₆D₆, 303 K): δ 164.3 (NMe), 153.6 (*ipso*-C), 145.5 (*o*-C), 143.6 (*o*-C), 142.1 (*p*-C), 126.5 (CHCH₂), 124.9 (*m*-C), 124.2 (*m*-C), 109.5 (CHCH₂), 98.5 (γ -CH), 71.4 (OC(CH₃)₂CH), 35.5 (OC(CH₃)₂CH), 28.9 (NMe), 28.5 (CHMe₂), 26.8 (CHMe₂), 25.6, 25.3, 25.1, 24.3 (CHMe₂). ²⁰⁷Pb NMR (83.83 MHz, C₆D₆, 303 K): δ 1685. IR (Nujol, ν/cm^{-1}): 1557 (s), 1517 (s), 1318 (s), 1169 (s), 1097 (s), 1018 (s). Anal. Calcd. for C₃₄H₅₀N₂OPb (709.97): C, 57.52; H, 7.10; N, 3.95%. Found: C, 57.40; H, 7.16; N, 3.81%.

Attempted syntheses of β -diketiminatolead(II) alkoxides 6–8. [(BDI_{DIPP})PbCl] (2) (0.60 mmol) in toluene was added to a suspension of the appropriate sodium alkoxide salt (0.60 mmol) in toluene (5 mL). The mixture was stirred at room temperature for 20 h. The suspension was filtered through a pad of Celite and the volatiles were removed under vacuum. The crude solid was characterised by ¹H NMR spectroscopy, which showed intractable mixture of products, including the β -diketimine **1**.

Reaction of the β -diketiminatolead(II) alkoxide, 4 or 5, with 2,4-di-tert-butylphenol. 2,4-di-tert-butylphenol (8.86 mg, 0.04 mmol) was added to [(BDI_{DIPP})PbOR] (3, R = ⁱPr or 4, R = ^tBu) (0.04 mmol) in C₆D₆ (~ 0.5 mL) in an NMR tube fitted with a Young's tap.

The mixture was kept at room temperature and the reaction was monitored by ^1H NMR spectroscopy after 10 minutes, 1, 2 and 24 h. The major product observed from the reaction after 2 h was $[(\text{BDI}_{\text{DIPP}})\text{PbOAr}]$ ($\text{Ar} = 2,4\text{-}^t\text{Bu}_2\text{C}_6\text{H}_3$) (**9**).^[117] ^1H NMR (399.50 MHz, C_6D_6 , 303 K): δ 7.64 (d, $J = 16.4$ Hz, 1H, $m\text{-H-}2,4\text{-}^t\text{Bu-Ar}$), 7.09 (s, 6H, Ar-H), 6.53 (d, $J = 8.0$ Hz, 1H, $o\text{-H-}2,4\text{-}^t\text{Bu-Ar}$), 4.96 (s, 1H, $\gamma\text{-CH}$), 3.71 (septet, $J = 6.8$ Hz, 2H, CHMe_2), 3.14 (septet, $J = 6.8$ Hz, 2H, CHMe_2), 1.70 (s, 9H, $o\text{-CMe}_3$), 1.67 (s, 6H, NCMe), 1.39 (s, 9H, $p\text{-CMe}_3$), 1.20 (d, $J = 6.8$ Hz, 6H, CHMe_2), 1.15 (d, $J = 6.8$ Hz, 6H, CHMe_2), 1.12 (d, $J = 3.2$ Hz, 6H, CHMe_2), 1.02 (d, $J = 6.0$ Hz, 6H, CHMe_2). [lit. ^1H NMR (300 MHz, C_6D_6 , 303K): δ 7.69 (d, $J = 2.5$ Hz, 1H), 7.09 (br-s, 6H), 6.55 (d, $J = 8.2$ Hz, 1H), 4.95 (s, 1H), 3.72 (septet, $J = 6.9$ Hz, 2H), 3.14 (septet, $J = 6.9$ Hz, 2H), 1.72 (s, 9H), 1.66 (s, 6H), 1.41 (s, 9H), 1.21 (d, $J = 6.9$ Hz, 6H), 1.13 (d, $J = 4.9$ Hz, 6H), 1.11 (d, $J = 4.9$ Hz, 6H), 1.01 (d, $J = 6.7$ Hz, 6H)].^[117]

Reaction of the β -diketiminatolead(II) alkoxide, 3 or 4, with fluorene. Similarly, fluorene (7.13 mg, 0.04 mmol) was added to $[(\text{BDI}_{\text{DIPP}})\text{PbOR}]$ (**3**, $\text{R} = ^i\text{Pr}$; or **4**, $\text{R} = ^t\text{Bu}$) (0.04 mmol) in C_6D_6 (~ 0.5 mL). The mixture was kept at room temperature and the reaction was monitored by ^1H NMR spectroscopy after 10 minutes, 1, 2 and 24 h. The mixture was then heated to 40°C for 3 days. No reaction was observed.

$[\text{CH}\{(\text{CH}_3)\text{CN-}2,6\text{-}^i\text{Pr}_2\text{C}_6\text{H}_3\}_2\text{PbC}_2\text{C}_6\text{H}_5]$, $[(\text{BDI}_{\text{DIPP}})\text{PbCCPh}]$, (**10**).^[70] Lead(II) alkoxide (**3** or **4**) (0.04 mmol) and phenylacetylene (0.04 mmol) were dissolved in C_6D_6 (~ 0.5 mL) in an NMR tube fitted with a Young's tap. The reaction was monitored by ^1H NMR spectroscopy over a period of 24 h. The major product obtained from the reaction after 1 h was $[(\text{BDI}_{\text{DIPP}})\text{PbCCPh}]$ (**10**). ^1H NMR (399.50 MHz, C_6D_6 , 303 K): δ 7.60 (d, $J = 7.6$ Hz, 2H, Ar-H), 7.04–7.18 (m, 8H, Ar-H), 6.90–6.91 (m, 1H, Ar-H), 4.88 (s, 1H, $\gamma\text{-CH}$), 4.09 (septet, $J = 6.4$ Hz, 2H, CHMe_2), 3.30 (septet, $J = 7.19$ Hz, 2H, CHMe_2), 1.72 (s, 6H, NCMe), 1.47 (d, $J = 6.8$ Hz, 6H, CHMe_2), 1.31 (d, $J = 6.8$ Hz, 6H, CHMe_2), 1.21 (d, $J = 7.2$ Hz, 6H, CHMe_2), 1.15 (d, $J = 6.4$ Hz, 6H, CHMe_2). [lit. ^1H NMR (500 MHz, C_6D_6): δ 7.59 (d, 2H), 7.05 (t, 2H), 7.03–7.17 (m, 6H), 6.96 (tt, 1H), 4.87 (s, 1H), 4.08 (septet, 2H), 3.32 (septet, 2H), 1.71 (s, 6H), 1.47 (d, 6H), 1.30 (d, 6H), 1.22 (d, 6H), 1.16 (d, 6H)].^[70]

$[\text{CH}\{(\text{CH}_3)\text{CN-}2,6\text{-}^i\text{Pr}_2\text{C}_6\text{H}_3\}_2\text{PbI}]$, $[(\text{BDI}_{\text{DIPP}})\text{PbI}]$, (**11**).^[62] Methyl iodide (0.20 g, 1.38 mmol) was added to a stirred toluene (15 mL) solution of $[(\text{BDI}_{\text{DIPP}})\text{PbO}^t\text{Bu}]$ (**4**)

(0.40 g, 0.57 mmol). The mixture was stirred for 7 days at 40 °C. The suspension was filtered through a pad of Celite and the volatiles were removed under vacuum. The crude residue was washed with pentane (3 × 5 mL) to leave [(BDI_{DIPP})PbI] (**11**) as yellow solid. Yield: 0.18 g, 41%. ¹H NMR (300.13 MHz, C₆D₆, 293 K): δ 7.03–7.18 (m, 6H, Ar-*H*), 4.94 (s, 1H, γ-*CH*), 3.99 (septet, *J* = 6.0 Hz, 2H, *CHMe*₂), 3.05 (septet, *J* = 6.0 Hz, 2H, *CHMe*₂), 1.64 (s, 6H, *NMe*), 1.48 (d, *J* = 6.0 Hz, 6H, *CHMe*₂), 1.26 (d, *J* = 9.0 Hz, 6H, *CHMe*₂), 1.18 (d, *J* = 9.0 Hz, 6H, *CHMe*₂), 1.05 (d, *J* = 6.0 Hz, 6H, *CHMe*₂). [lit. ¹H NMR (C₆D₆, 293 K): δ 7.11 (d, *J* = 7.5 Hz, 2H), 7.09 (t, *J* = 7.5 Hz, 2H), 7.06 (d, *J* = 7.5 Hz, 2H), 4.93 (s, 1H), 4.00 (septet, *J* = 6.8 Hz, 2H), 3.07 (septet, *J* = 6.8 Hz, 2H), 1.70 (s, 6H), 1.53 (d, *J* = 6.5 Hz, 6H), 1.28 (d, *J* = 6.8 Hz, 6H), 1.21 (d, *J* = 6.9 Hz, 6H), 1.10 (d, *J* = 6.7 Hz, 6H)].^[62]

Reactions of the β-diketiminatolead(II) tert-butoxide 4 with benzyl bromide or chloride.

The benzyl halide (0.04 mmol) was added to [(BDI_{DIPP})PbO^{*t*}Bu] (**4**) (0.03 g, 0.04 mmol) in C₆D₆ (~ 0.5 mL) in an NMR tube fitted with a Young's tap. The mixture was monitored by ¹H NMR spectroscopy. The mixture was kept at room temperature for the first 24 h, then held at 60 °C. A complex mixture of products was observed after 8 days.

[C₆H₅CH=C{(CH₃)CN-2,6-^{*i*}Pr₂C₆H₃}₂], (**13**). Benzaldehyde (0.03 g, 0.29 mmol) was added to [(BDI_{DIPP})PbO^{*t*}Bu] (**4**) (0.20 g, 0.29 mmol) in toluene (10 mL). The mixture was stirred at room temperature for 50 h, after which the suspension was filtered through a pad of Celite. Volatiles were removed *in vacuo* and the crude solid residue was washed with pentane (3 × 10 mL). Single Crystals of **13** were obtained by recrystallisation from THF at –30 °C. Yield: 0.09 g, 60%. ¹H NMR (300.13 MHz, CDCl₃, 303 K): δ 7.41 (br, 5H, C=CH-Ar-*H*), 7.08–7.15 (m, 3H, Ar-*H*), 7.01 (s, 1H, C=CH-Ar), 2.83 (septet, *J* = 6.9 Hz, 2H, *CHMe*₂), 2.67 (septet, *J* = 6.9 Hz, 2H, *CHMe*₂), 2.04 (s, 3H, *NMe*), 2.00 (s, 3H, *NMe*), 1.14 (d, *J* = 6.9 Hz, 6H, *CHMe*₂), 1.13 (d, *J* = 6.6 Hz, 6H, *CHMe*₂), 0.95 (d, *J* = 6.6 Hz, 6H, *CHMe*₂), 0.82 (d, *J* = 6.6 Hz, 6H, *CHMe*₂). ¹³C{¹H} NMR (75.47 MHz, C₆D₆, 303 K): δ 168.1 (*NMe*), 167.5 (C=CH), 147.3 (C=CH-*ipso*-C), 146.8 (*ipso*-C), 146.6 (C=CH-*o*-C), 137.8 (C=CH-*o*-C), 137.4 (*o*-C), 136.6 (*o*-C), 135.6 (C=CH-*p*-C), 129.3 (*p*-C), 129.0 (C=CH-*m*-C), 124.6 (C=CH-*m*-C), 123.9 (*m*-C), 123.7 (*m*-C), 28.7 (C=CH-Ar), 28.0 (*CHMe*₂), 25.1 (*CHMe*₂), 24.3, 24.0, 23.9, 23.7 (*CHMe*₂), 18.0 (*NMe*).

Reactions of the β -diketiminatolead(II) *tert*-butoxide **4** with monodentate or bidentate ligands. The substrate (0.04 mmol) was added to the lead(II) *tert*-butoxide **4** (0.04 mmol) in C₆D₆ (~ 0.5 mL) in an NMR tube fitted with a Young's tap. The ¹H NMR spectrum of the mixture was unchanged after 24 h at room temperature.

[CH{(CH₃)CN-2,6-ⁱPr₂C₆H₃}₂PbOCO₂ⁱPr], [(BDI_{DIPP})PbOCO₂ⁱPr], (14).^[114]
 [(BDI_{DIPP})PbOⁱPr] (**3**) (0.20 g, 0.29 mmol) was dissolved in toluene (10 mL) in a Schlenk flask. The gas was evacuated from the flask and an excess of CO₂ (0.03 g, 0.59 mmol) was added. After stirring at room temperature for 24 h, the mixture was filtered *via* cannula. The residue was concentrated and stored at -30 °C to give yellow crystals of [(BDI_{DIPP})PbOCO₂ⁱPr] (**14**). Yield: 0.09 g, 43%. ¹H NMR (399.50 MHz, toluene-*d*₈, 303 K): δ 7.09 (s, 6H, Ar-*H*), 4.82 (septet, *J* = 6.4 Hz, 1H, OCHMe₂), 4.78 (s, 1H, γ -CH), 3.33 (br, 4H, CHMe₂), 1.65 (s, 6H, NCMe), 1.26 (br, CHMe₂), 1.23 (d, *J* = 6.4 Hz, 9H, CHMe₂). [lit. ¹H NMR (C₆D₆, 303 K): δ 7.19 (s, 6H), 4.97 (septet, *J* = 6.3 Hz, 1H), 4.86 (s, 1H), 3.39–3.32 (br, 4H), 3.02 (septet, *J* = 6.9 Hz, 2H), 1.69 (s, 6H), 1.30 (d, *J* = 6.3 Hz, 12H), 1.20 (d, *J* = 6.3 Hz, 12H), 1.24 (d, *J* = 6.8 Hz, 6H)].^[114] ¹³C{¹H} NMR (125.72 MHz, toluene-*d*₈, 303 K): δ 164.0 (NCMe), 160.9 (OC(=O)OⁱPr), 142.7 (*ipso*-C), 137.5 (*o*-C), 129.2 (*o*-C), 128.2 (*p*-C), 126.9 (*m*-C), 124.4 (*m*-C), 103.5 (γ -CH), 68.6 (OC(CH₃)₂), 34.5 (OC(CH₃)₂), 28.2 (CHMe₂), 25.93 (CHMe₂), 24.6 (NCMe), 24.5, 22.8, 22.6, 14.2 (CHMe₂). [lit. ¹³C NMR (125.72 MHz, toluene-*d*₈, 303 K): δ 164.1, 160.9, 142.8, 129.2, 128.3, 127.0, 125.4, 124.5, 103.6, 68.7, 34.6, 28.3, 26.0, 24.7, 24.5, 22.8, 22.7, 14.3].^[114]

[CH{(CH₃)CN-2,6-ⁱPr₂C₆H₃}₂PbOCO₂ⁱBu], [(BDI_{DIPP})PbOCO₂ⁱBu], (15).^[114]
 [(BDI_{DIPP})PbOⁱBu] (**4**) (50.0 mg, 0.07 mmol) was dissolved in toluene-*d*₈ (~ 0.5 mL) in an NMR tube fitted with a Young's tap. The gas inside the NMR tube was evacuated. Carbon dioxide (4.70 mg, 0.11 mmol) was then added. A yellow solution was obtained. The mixture was kept at room temperature for 24 h and monitored by ¹H NMR spectroscopy. ¹H NMR (399.50 MHz, toluene-*d*₈, 303 K): δ 7.09 (s, 6H, Ar*H*), 4.78 (s, 1H, γ -CH), 3.32 (br, 4H, CHMe₂), 1.64 (s, 6H, NCMe), 1.48 (s, 9H, C(CH₃)₃), 1.27 (br, 12H, CHMe₂), 1.14 (d, *J* = 6.8 Hz, 12H, CHMe₂). ¹H NMR (399.50 MHz, toluene-*d*₈, 203 K)*: δ 7.15 (s, 2H, Ar*H*), 7.07 (d, *J* = 4 Hz, 2H, Ar*H*), 6.95 (d, *J* = 8 Hz, 2H, Ar*H*), 4.79 (s, 1H, γ -CH), 3.64 (m, 2H, CHMe₂), 2.94 (m, 2H, CHMe₂), 1.62 (s, 6H, NCMe),

1.58 (b, $J = 4$ Hz, 6H, CHMe_2), 1.50 (d, $J = 4$ Hz, 6H, CHMe_2), 1.17 (d, $J = 4$ Hz, 6H, CHMe_2), 1.08 (s, 9H, $\text{OC}(\text{CH}_3)_3$). $^{13}\text{C}\{^1\text{H}\}$ NMR (100.46 MHz, toluene- d_8 , 203 K)*: δ 163.5 (NCMe), 160.3 (OCO), 144.2 (*ipso*-C), 142.3 (*o*-C), 141.6 (*o*-C), 103.5 (γ -CH), 76.6 (OCHMe_2), 28.5 ($\text{OC}(\text{CH}_3)_2$), 28.1 (NCMe), 27.6 27.4, 26.8, 26.5 (CHMe_2), 25.0, 24.7, 24.3, 24.1 (CHMe_2). ^{207}Pb NMR (83.72 MHz, toluene- d_8 303K)*: δ 817. (* These results were used in our publication.^[114]) IR (CCl_4 , ν/cm^{-1}): 2336 (s, $\text{OC}(\text{=O})\text{O}$), 1731 (s, $\text{C}=\text{O}$). [lit. IR (CCl_4 , ν/cm^{-1}): 3060 (s), 2965 (s), 2928 (s), 2869 (s), 1699 (s), 1463 (s), 1438 (s), 1389 (b), 1366 (b), 1172 (b), 1102 (s)].^[114]

$^{13}\text{CO}_2$ exchange with $[(\text{BDI}_{\text{DIPP}})\text{PbOCO}_2^i\text{Pr}]$ (**14**) and $[(\text{BDI}_{\text{DIPP}})\text{PbOCO}_2^t\text{Bu}]$ (**15**). The lead(II) alkoxide (0.021 mmol) was added to toluene- d_8 (~ 0.5 mL) in an NMR tube fitted with a Young's tap. The mixture was frozen with liquid N_2 . The gas was evacuated from the tube and then filled with carbon dioxide (0.021 mmol). The mixture was allowed to warm up slowly and held at room temperature for 30 minutes. The formation of the corresponding carbonate $[(\text{BDI}_{\text{DIPP}})\text{PbOCO}_2\text{R}]$ (**14**, $\text{R} = ^i\text{Pr}$; or **15**, $\text{R} = ^t\text{Bu}$) was verified by ^1H NMR spectroscopy. The mixture was frozen in liquid N_2 . The gaseous atmosphere was evacuated under high vacuum and $^{13}\text{CO}_2$ (0.021 mmol) was added. The formation of $[(\text{BDI}_{\text{DIPP}})\text{PbO}^{13}\text{CO}_2\text{R}]$ (**16**, $\text{R} = ^i\text{Pr}$; **17**, $\text{R} = ^t\text{Bu}$) was verified by ^1H and $^{13}\text{C}\{^1\text{H}\}$ NMR spectroscopy.

Reaction of $[(\text{BDI}_{\text{DIPP}})\text{PbOCO}_2^t\text{Bu}]$ (**15**) with $[(\text{BDI}_{\text{DIPP}})\text{PbO}^i\text{Pr}]$ (**3**). $[(\text{BDI}_{\text{DIPP}})\text{PbOCO}_2^t\text{Bu}]$ (**15**) (0.04 mmol) in C_6D_6 (~ 0.5 mL) was generated *in situ* in a NMR tube fitted with a Young's tab according to the procedure above. $[(\text{BDI}_{\text{DIPP}})\text{PbO}^i\text{Pr}]$ (**3**) (0.04 mmol) was added to the mixture. ^1H NMR spectra were recorded after 10 minutes, 1, 2, and 24 h at room temperature. The mixture was then heated up to 40 °C for 24 h, after which a ^1H NMR spectrum was again recorded.

Reaction of $[(\text{BDI}_{\text{DIPP}})\text{PbOCO}_2^i\text{Pr}]$ (**14**) with phenyl isocyanate. CO_2 (0.12 mmol) was added to $[(\text{BDI}_{\text{DIPP}})\text{PbO}^i\text{Pr}]$ (**3**) (0.03 g, 0.04 mmol) in C_6D_6 (~ 0.5 mL) in an NMR tube fitted with a Young's tap. The mixture was held at room temperature for 1 h. The ^1H NMR spectrum was recorded to verify the formation of $[(\text{BDI}_{\text{DIPP}})\text{PbOCO}_2^i\text{Pr}]$ (**14**). Phenyl isocyanate (5.23 mg, 0.04 mmol) was added to the mixture. The reaction was monitored by ^1H NMR spectroscopy. $[(\text{BDI}_{\text{DIPP}})\text{PbN}(\text{Ph})\text{CO}_2^i\text{Pr}]$ (**18**) was formed almost exclusively after 2 h at room temperature. ^1H NMR (399.50 MHz, C_6D_6 , 303 K):

δ 7.65 (br, 1H, Ar-*H*), 6.82–7.36 (m, 11H, Ar-*H*), 5.01 (s, 1H, γ -*H*), 3.15 (br, 4H, CHMe₂), 1.65 (s, 6H, NCM_e), 1.04–1.27 (m, 20H, CHMe₂). [lit. ¹H NMR (500 MHz, toluene-*d*₈, 303 K): δ 7.59 (br, 2H), 7.27 (t, *J* = 15 Hz, 2H), 6.85 (t, *J* = 15 Hz, 1H), 5.03 (s, 1H), 4.91 (br, 1H), 3.13 (br, 4H), 1.67(s, 6H), 1.28 (d, *J* = 5 Hz, 1H), 1.25 (d, *J* = 5 Hz, 1H), 1.15 (br-d, *J* = 10 Hz, 2H), 0.98 (br, 6H), 0.88 (d, *J* = 10 Hz, 2H), 0.87 (d, *J* = 5 Hz, 2H)].^[114]

Reaction of the lead(II) alkoxides 3 or 4 with carbon disulfide. Carbon disulfide (3.04 mg, 0.04 mmol) was added to a C₆D₆ solution (~ 0.5 mL) of the lead(II) alkoxide (0.04 mmol) in an NMR tube fitted with a Young's tap. The mixture was held at room temperature and monitored by ¹H NMR spectroscopy. An intractable mixture was observed after 24 h.

Reaction of the lead(II) tert-butoxide 4 with N,N'-diisopropylcarbodiimide. N,N'-diisopropylcarbodiimide (5.42 mg, 0.04 mmol) was added to a C₆D₆ solution (~ 0.5 mL) of lead(II) tert-butoxide 4 (0.03 g, 0.04 mmol) in an NMR tube fitted with a Young's tap. The mixture was monitored by ¹H NMR spectroscopy. No reaction was observed after 5 days at 50 °C.

Reaction of the lead(II) tert-butoxide 4 with phenyl isocyanate. Phenyl isocyanate (5.11 mg, 0.03 mmol) was added to a C₆D₆ solution (~ 0.5 mL) of lead(II) tert-butoxide 4 (0.03 g, 0.04 mmol) in an NMR tube fitted with a Young's tap. The mixture was held at room temperature and was monitored by ¹H NMR spectroscopy. An intractable mixture was observed after 24 h.

5.3 Experimental procedures for Chapter 3

[CH{(CH₃)CN-C₆H₅}₂H], (BDI_{Ph})H, (19).^[155] Concentrated HCl (8.3 mL) was added dropwise to a mixture of acetylacetone (10.0 g, 100 mmol) and aniline (18.6 g, 200 mmol) in a round-bottomed flask at 0 °C with rapid stirring. Precipitation was observed after 24 h. The solid was filtered off and was washed with cold petroleum spirit (bp. 40–60 °C) (3 × 10 mL). Dichloromethane (~ 20 mL) and saturated sodium carbonate solution (~ 200 mL) were added to the crude solid. The aqueous layer was extracted with dichloromethane (3 × 20 mL). The combined organic layer was dried over

magnesium sulfate and volatiles were removed under vacuum. The residue was washed with cold methanol and dried under reduced pressure overnight. Yield: 19.50 g, 78%. [lit.: 92%].^[155] ¹H NMR (399.50 MHz, CDCl₃, 303 K): δ 12.69 (s, 1H, NH), 7.28 (t, J = 8.0 Hz, 4H, *m*-H), 7.04 (t, J = 7.6 Hz, 2H, *p*-H), 6.95 (d, J = 8.0 Hz, 4H, *o*-H), 4.87 (s, 1H, γ -CH), 2.00 (s, 6H, NCM*e*). [lit.: ¹H NMR (300 MHz, CDCl₃): δ 12.61 (s, 1H), 7.48–6.63 (m, 10H), 4.81 (s, 1H), 1.94 (s, 6H)].^[155] ¹³C{¹H} NMR (100.46 MHz, CDCl₃, 303 K): δ 159.7 (NCMe), 146.0 (*ipso*-C), 130.0 (*o*-C), 123.4 (*p*-C), 122.8 (*m*-C), 97.6 (γ -CH), 21.0 (NCMe). [lit.: ¹³C{¹H} NMR (300 MHz, CDCl₃): δ 156.0, 146.5, 129.4, 123.8, 123.2, 98.1, 21.4].^[155] EI-MS: m/z (%): 250, 235, 159, 118, 77, 51.

[CH{(CH₃)CN-4-ⁱPrC₆H₄}₂H], (BDI_{IPP})H, (20). Concentrated HCl (5.1 mL) was added dropwise to a mixture of 4-isopropylaniline (13.5 g, 100 mmol) and acetylacetone (5.00 g, 50 mmol) at 0 °C. The mixture was stirred and allowed to warm gradually to room temperature. A yellow precipitate was observed after 24 h. The mixture was filtered and washed with cold petroleum ether. The residue was dissolved in dichloromethane (15 mL) and saturated sodium carbonate solution (250 mL). The aqueous layer was extracted with dichloromethane (3 × 30 mL) and the combined organic layer was dried with magnesium sulfate. The volatiles were removed under vacuum to leave a brown oil. Yield: 8.54 g, 51%. ¹H NMR (399.50 MHz, CDCl₃, 303 K): δ 12.70 (s, 1H, NH), 7.16 (d, J = 8.0 Hz, 4H, *o*-H), 6.88 (d, J = 7.6 Hz, 4H, *m*-H), 4.84 (s, 1H, γ -CH), 2.87 (septet, J = 6.4 Hz, 2H, CHMe₂), 1.99 (s, 6H, NCMe), 1.24 (d, J = 6.8 Hz, 12H, CHMe₂). ¹³C{¹H} NMR (100.46 MHz, CDCl₃, 303 K): δ 159.7 (NCMe), 144.0 (*ipso*-C), 143.6 (*p*-C), 126.8 (*o*-C), 122.9 (*m*-C), 97.1 (γ -CH), 33.7 (CHMe₂), 24.3 (CHMe₂), 21.0 (NCMe).

[CH{(CH₃)CN-2,6-Me₂C₆H₃}₂H], (BDI_{DMP})H, (21).^[156] Concentrated HCl (4.2 mL) was added dropwise to a stirred mixture of 2,6-dimethylaniline (12.1 g, 100 mmol) and acetylacetone (5.00 g, 50 mmol) at 0 °C. The stirred mixture was allowed to warm gradually to room temperature over a period of 24 h. The precipitate was filtered off and washed with cold petroleum ether (3 × 20 mL). The washed solid was dissolved in dichloromethane (~ 20 mL) and saturated sodium carbonate (~ 200 mL). The aqueous layer was extracted with dichloromethane (3 × 30 mL) and the combined organic layer was dried over magnesium sulfate. After removal of solvent under vacuum, the brown

oil residue was treated with methanol to give a white precipitate, which was filtered off and crystallised from a mixture of methanol/dichloromethane (1:1) at $-30\text{ }^{\circ}\text{C}$. Yield: 6.43 g, 42%. [lit. 53 %].^[156] ^1H NMR (399.50 MHz, CDCl_3 , 303 K): δ 12.20 (s, 1H, NH), 7.04 (d, $J = 7.6$ Hz, 4H, *m*-H), 6.95 (d, $J = 7.2$ Hz, 2H, *p*-H), 4.89 (s, 1H, γ -CH), 2.17 (s, 12H, *o*-CH₃), 1.70 (s, 6H, NCM*e*). [lit. ^1H NMR (300 MHz, CDCl_3): δ 12.20 (br, 1H), 7.00 (s, 6H), 4.88 (s, 1H), 2.59 (s, 12H), 1.69 (s, 6H)].^[156] $^{13}\text{C}\{^1\text{H}\}$ NMR (100.46 MHz, CDCl_3 , 303 K): δ 161.0 (NCMe), 144.0 (*ipso*-C), 132.3 (*o*-C), 128.0 (*p*-C), 124.5 (*m*-C), 93.6 (γ -CH), 20.5 (*o*-CH₃), 18.5 (NCMe). [lit. $^{13}\text{C}\{^1\text{H}\}$ NMR (100 MHz, CDCl_3): δ 160.81, 143.76, 132.15, 127.77 124.28, 93.40, 20.35, 18.40].^[156]

[CH{(CH₃)CN-C₆H₅}₂PbCl], [(BDI_{Ph})PbCl], (22). (BDI_{Ph})H (19) (1.95 g, 7.75 mmol) was dissolved in THF (30 mL) and *n*-BuLi in *n*-hexane (3.2 mL of 2.7 M solution, 7.75 mmol) was added dropwise. The mixture was stirred for 30 minutes at room temperature, then transferred slowly to a THF (10 mL) slurry of PbCl₂ (2.16 g, 7.75 mmol) *via* cannula. The mixture was stirred at room temperature for a further 24 h. Volatiles were removed under vacuum and the residue was extracted with dichloromethane (3 \times 40 mL). The solvent was removed from the extract *in vacuo* and the crude solid was washed with pentane (5 \times 10 mL). Yellow crystals of [(BDI_{Ph})PbCl] (22) were obtained by recrystallisation from dichloromethane at $-30\text{ }^{\circ}\text{C}$. Yield: 1.83 g, 46%. ^1H NMR (499.91 MHz, C₆D₆, 303 K): δ 7.10 (m, 7H, Ar-*H*), 6.93 (m, 2H, Ar-*H*), 4.74 (s, 1H, γ -CH), 1.72 (s, 6H, NCM*e*). $^{13}\text{C}\{^1\text{H}\}$ NMR (125.72 MHz, C₆D₆, 303 K): δ 163.8 (NCMe), 148.5 (*ipso*-C), 130.1 (*o*-C), 128.7 (*o*-C), 128.5 (*p*-C), 128.3 (*m*-C), 126.0 (*m*-C), 100.5 (γ -CH), 24.6 (NCMe). ^{207}Pb NMR (83.83 MHz, C₆D₆, 303 K): δ 1228. IR (Nujol, ν/cm^{-1}): 1530 (s), 1262 (s), 1166 (s), 1018 (s), 912 (s). Anal. Calcd. for C₁₇H₁₇N₂PbCl (491.98): C, 42.64; H, 3.98; N, 5.53%. Found: C, 41.54; H, 3.56; N, 5.38%.

[CH{(CH₃)CN-4-^{*i*}PrC₆H₄}₂PbCl], [(BDI_{IPP})PbCl], (23). (BDI_{IPP})H (20) (2.15 g, 6.43 mmol) was dissolved in THF (20 mL) and *n*-BuLi in *n*-hexane (2.73 mL of 2.37 M solution, 6.43 mmol) was added dropwise. The mixture was stirred at room temperature for 30 minutes then transferred slowly *via* cannula to a THF (10 mL) slurry of PbCl₂ (1.79 g, 6.43 mmol). The mixture was then stirred at room temperature for 24 h, and volatiles were removed *in vacuo*. The residue was extracted with dichloromethane (3 \times

20 mL). The solvent was removed and the solid was washed with pentane (3×10 mL). Yellow crystals of $[(\text{BDI}_{\text{IPP}})\text{PbCl}]$ (**23**) were obtained by crystallisation from a minimum amount of dichloromethane at -30 °C. Yield: 2.01 g, 57%. ^1H NMR (399.50 MHz, C_6D_6 , 303 K): δ 7.08–7.19 (m, 4H, Ar-*H*), 7.03 (d, $J = 8.8$ Hz, 4H, Ar-*H*), 4.77 (s, 1H, γ -CH), 2.68 (septet, 2H, $J = 7.2$ Hz, 2H, CHMe₂), 1.77 (s, 6H, NCMe), 1.11 (d, $J = 6.8$ Hz, 12H, CHMe₂). $^{13}\text{C}\{^1\text{H}\}$ NMR (100.46 MHz, C_6D_6 , 303 K): δ 164.0 (NCMe), 146.5 (*ipso*-C), 146.2 (*o*-C), 125.7 (*m*-C), 105.4 (γ -CH), 34.3 (CHMe₂), 24.6 (CHMe₂), 24.5 (NCMe). ^{207}Pb NMR (83.83 MHz, C_6D_6 , 303 K): δ 1220. IR (Nujol, v/cm^{-1}): 1559 (s), 1496 (s), 1378 (s), 1194 (s), 1053 (s), 856 (s). Anal. Calcd. for $\text{C}_{23}\text{H}_{29}\text{ClN}_2\text{Pb}$ (576.14): C, 47.95; H, 5.07; N, 4.86%. Found: C, 47.83; H, 4.97; N, 4.79%.

$[(\text{CH}\{(\text{CH}_3)\text{CN}-2,6\text{-Me}_2\text{C}_6\text{H}_3\}_2\text{PbCl}]$, $[(\text{BDI}_{\text{DMP}})\text{PbCl}]$, (**24**). $(\text{BDI}_{\text{DMP}})\text{H}$ (**21**) (1.87 g, 6.13 mmol) was dissolved in THF and *n*-BuLi in *n*-hexane (2.6 mL of 2.37 M solution, 6.13 mmol) was added dropwise. The mixture was stirred at room temperature for 30 minutes, then transferred slowly *via* cannula to a THF (10 mL) slurry of PbCl_2 (1.70 g, 6.13 mmol). The mixture was stirred at room temperature for 24 h. Volatile material was removed under vacuum and the residue was extracted with toluene (3×20 mL). The solvent was removed *in vacuo* and the crude solid was washed with cold pentane (3×10 mL). Light yellow crystals of $[(\text{BDI}_{\text{DMP}})\text{PbCl}]$ (**24**) were obtained by recrystallisation from a minimum amount of toluene at -30 °C. Yield: 2.19 g, 65%. ^1H NMR (499.91 MHz, C_6D_6 , 303 K): δ 6.97 (d, $J = 7.5$ Hz, 4H, *m*-H), 6.91 (t, $J = 7.5$ Hz, 2H, *p*-H), 4.83 (s, 1H, γ -CH), 2.31 (br, 12H, *o*-CH₃), 1.58 (s, 6H, NCMe). $^{13}\text{C}\{^1\text{H}\}$ NMR (125.72 MHz, C_6D_6 , 303 K): δ 163.9 (NCMe), 146.3 (*ipso*-C), 129.7 (*o*-C), 128.9 (*p*-C), 126.3 (*m*-C), 103.7 (γ -CH), 24.2 (*o*-CH₃), 21.8 (*o*-CH₃), 19.7 (NCMe). ^{207}Pb NMR (83.83 MHz, C_6D_6 , 303 K): δ 1388. IR (Nujol, v/cm^{-1}): 1551 (s), 1522 (s), 1178.7 (s), 1093 (s), 1019 (s). Anal. Calcd. for $\text{C}_{21}\text{H}_{25}\text{N}_2\text{ClPb}$ (548.09): C, 46.02; H, 4.60; N, 5.11%. Found: C, 46.18; H, 4.49; N, 4.91%.

$[(\text{CH}\{(\text{CH}_3)\text{CN}-\text{C}_6\text{H}_5\}_2\text{Pb}]$, $[(\text{BDI}_{\text{Ph}})_2\text{Pb}]$, (**25**). A solution of $[(\text{BDI}_{\text{Ph}})\text{PbCl}]$ (**22**) (0.20 g, 0.41 mmol) in toluene (10 mL) was added to a potassium- or sodium alkoxide (0.41 mmol). The mixture was stirred at room temperature for 24 h. The suspension was filtered through a pad of Celite and volatile material was removed from the filtrate under vacuum. The residue was washed with cold pentane (5 mL) and dissolved in a

minimum amount of toluene. Yellow crystals of $[(\text{BDI}_{\text{Ph}})_2\text{Pb}]$ (**25**) were obtained at -30 °C. Yield: 0.14 g, 48%.

*Alternative synthesis of $[(\text{BDI}_{\text{Ph}})_2\text{Pb}]$ (**25**).* A suspension of $(\text{BDI}_{\text{Ph}})\text{Li}$ (**27**) (0.31 g, 1.17 mmol) in toluene was added to PbCl_2 (0.16 g, 0.58 mmol). The mixture was stirred at room temperature for 24 h. Purification of the mixture was as above. Yield: 0.34 g, 81%.

^1H NMR (399.50 MHz, C_6D_6 , 303 K): δ 7.09 (t, $J = 14.0$ Hz, 8H, *o*-H), 6.92 (t, $J = 14.8$ Hz, 4H, *p*-H), 6.52 (d, $J = 7.2$ Hz, 8H, *m*-H), 4.85 (s, 2H, γ -CH), 1.85 (s, 12H, NCM e). $^{13}\text{C}\{^1\text{H}\}$ NMR (100.46 MHz, C_6D_6 , 303 K): δ 162.2 (NCM e), 151.3 (*ipso*-C), 128.2 (*o*-C), 126.4 (*m*-C), 124.1 (*p*-C), 100.7 (γ -CH), 24.8 (NCM e). ^{207}Pb NMR (83.83 MHz, C_6D_6 , 303 K): δ 454. Anal. Calcd. for $\text{C}_{34}\text{H}_{34}\text{N}_4\text{Pb}$ (705.86): C, 57.87; H, 4.82; N, 7.94%. Found: C, 57.92; H, 4.94; N, 7.89%.

$[(\text{CH}\{(\text{CH}_3)\text{CN}-4\text{-}^i\text{PrC}_6\text{H}_4\}_2)\text{Pb}]$, $[(\text{BDI}_{\text{IPP}})_2\text{Pb}]$, (**26**). $[(\text{BDI}_{\text{IPP}})\text{PbCl}]$ (**23**) (0.14 g, 0.25 mmol) was dissolved in toluene (10 mL) and added to potassium or sodium alkoxide (0.25 mmol). After the mixture was stirred at room temperature for 24 h, the suspension was filtered through a pad of Celite. The volatiles were removed from the filtrate *in vacuo* and the residue was washed with pentane. Yellow crystals of $[(\text{BDI}_{\text{IPP}})_2\text{Pb}]$ (**26**) were obtained by recrystallisation from a minimum amount of toluene at -30 °C. Yield: 0.15 g, 71%. ^1H NMR (399.50 MHz, C_6D_6 , 303 K): δ 7.05 (d, $J = 8.4$ Hz, 8H, *o*-C), 6.53 (d, $J = 8.4$ Hz, 8H, *m*-H), 4.90 (s, 2H, γ -CH), 2.76 (septet, $J = 6.8$ Hz, 4H, CHM e_2), 1.92 (s, 12H, NCM e), 1.19 (d, $J = 6.8$ Hz, 24H, CHM e_2). $^{13}\text{C}\{^1\text{H}\}$ NMR (100.46 MHz, C_6D_6 , 303 K): δ 162.2 (NCM e), 149.3 (*ipso*-C), 144.3 (*o*-C), 126.8 (*p*-C), 126.4 (*m*-C), 103.4 (γ -CH), 34.4 (CHM e_2), 24.9 (CHM e_2), 24.8 (NCM e). ^{207}Pb NMR (83.83 MHz, C_6D_6 , 303 K): δ 476.

$[\text{CH}\{(\text{CH}_3)\text{CN}-\text{C}_6\text{H}_5\}_2\text{Li}]$, $(\text{BDI}_{\text{Ph}})\text{Li}$, (**27**). $(\text{BDI}_{\text{Ph}})\text{H}$ (**19**) (2.00 g, 8.00 mmol) was dissolved in toluene (20 mL) and cooled to -78 °C. *n*-BuLi in *n*-hexane (3.4 mL of 2.37 M solution, 8.00 mmol) was added to the solution. The mixture was stirred and allowed to warm gradually to room temperature over a period of 2 h. Volatiles were removed *in vacuo* and the residue was washed with *n*-hexane (3×5 mL). The white solid was used without further purification.

[CH{(CH₃)CN-2,6-Me₂C₆H₃}₂PbO'Bu], [(BDI_{DMP})PbO'Bu], (28). [(BDI_{DMP})PbCl] (**24**) (0.25 g, 0.46 mmol) in toluene (20 mL) was added to a suspension of potassium *tert*-butoxide (0.05 g, 0.46 mmol) in toluene (5 mL). The mixture was stirred at room temperature for 24 h. The suspension was filtered through a pad of Celite and volatile material from the filtrate was removed under vacuum. The residue was washed with pentane and crystallised from a minimum amount of toluene at -30 °C. Yellow crystals of [(BDI_{DMP})PbCl] (**28**) were obtained at -30 °C. Yield: 0.19 g, 72%. ¹H NMR (499.91 MHz, C₆D₆, 303 K): δ 7.10 (dd, *J* = 2.0, 7.0 Hz, 2H, *p*-H), 6.94–6.99 (m, 4H, *m*-H), 4.70 (s, 1H, *γ*-CH), 2.67 (s, 6H, *o*-CH₃), 2.16 (s, 6H, *o*-CH₃), 1.64 (s, 6H, NCM*e*), 1.05 (s, 9H, OC(*Me*)₃). ¹³C {¹H} NMR (125.72 MHz, C₆D₆, 303 K): δ 163.2 (NC*Me*), 146.6 (*ipso*-C), 136.1 (*o*-C), 131.1 (*o*-C), 129.7 (*p*-C), 128.8 (*m*-C), 125.7 (*m*-C), 99.4 (*γ*-CH), 69.7 (OC(*Me*)₃), 36.8 (OC(*Me*)₃), 23.9 (NC*Me*), 20.5 (*o*-CH₃), 19.2 (*o*-CH₃). ²⁰⁷Pb NMR (83.83 MHz, C₆D₆, 303 K): δ 1513. Anal. Calcd. for C₂₅H₃₄N₂OPb (585.73): C, 51.24; H, 5.85; N, 4.78%. Found: C, 51.17; H, 5.77; N, 4.76%.

[CH{(CH₃)CN-2,6-Me₂C₆H₃}₂PbOSO₂CF₃], [(BDI_{DMP})PbOTf], (29). [(BDI_{DMP})PbCl] (**24**) (0.20 g, 0.37 mmol) in toluene (10 mL) was added to a suspension of AgOTf (0.09 g, 0.37 mmol) in toluene (5 mL). The mixture was stirred at room temperature for 24 h and the yellow precipitate was filtered off and washed with cold pentane (3 × 3 mL). The yellow residue was crystallised from a minimum amount of THF and stored at -30 °C. Light yellow crystals of [(BDI_{DMP})PbOTf] (**29**) were obtained. Yield: 0.15 g, 61%. ¹H NMR (399.50 MHz, CDCl₃, 303K): δ 7.15 (br, 2H, Ar-*H*), 7.13 (br, 2H, Ar-*H*), 7.06–7.07 (br, 2H, Ar-*H*), 5.14 (s, 1H, *γ*-*H*), 2.26 (s, 12H, *o*-CH₃), 1.84 (s, 6H, NCM*e*). ¹³C NMR (100.46 MHz, CDCl₃, 303K): δ 165.2 (NC*Me*), 143.8 (*ipso*-C), 133.1 (*o*-C), 129.4 (*o*-C), 127.0 (*p*-C), 128.5 (*m*-C), 128.0 (*m*-C), 124.5 (CF₃), 107.0 (*γ*-C), 24.8 (*o*-CH₃), 18.7 (NC*Me*). ¹⁹F NMR (150.62 MHz, CDCl₃, 303K): δ -78.0. ²⁰⁷Pb NMR (83.83 MHz, CDCl₃, 303K): δ 1154.

Preliminary reaction of [(BDI_{Ph})₂Pb] (25) with potassium tert-butoxide. [(BDI_{Ph})₂Pb] (**25**) (0.30 g, 0.43 mmol) in toluene (10 mL) was added to a suspension of potassium *tert*-butoxide (0.05 g, 0.43 mmol) in toluene (5 mL). The mixture was stirred at room temperature for 20 h. The mixture was filtered through a pad of Celite and the volatiles were removed under vacuum. The residue was washed with cold pentane and dried

under reduced pressure. A light yellow solid was observed. ^1H NMR (399.50 MHz, C_6D_6 , 303 K): δ 7.16 (s, 6H, Ar-*H*), 4.71 (s, 1H, γ -CH), 1.78 (s, 6H, NCM*e*), 1.34 (s, 9H, OC(CH₃)₃).

Preliminary reaction of [(BDI_{Ph})₂Pb] (25) with methyl trifluoromethanesulfonate. Methyl trifluoromethanesulfonate (0.07 g, 0.43 mmol) was added to [(BDI_{Ph})₂Pb] (**25**) (0.03 g, 0.04 mmol) in C_6D_6 (~ 0.5 mL) was added to an NMR tube fitted with a Young's tap. The reaction was monitored by ^1H NMR spectroscopy. An intractable mixture was observed after 24 h at room temperature.

Preliminary reaction of [(BDI_{IPP})₂Pb] (26) with methyl iodide. [(BDI_{IPP})₂Pb] (**26**) (0.03 g, 0.38 mmol) and methyl iodide (0.05 g, 23.7 μL , 0.38 mmol) in C_6D_6 (~ 0.5 mL) was added to an NMR tube fitted with a Young's tap. The reaction was monitored by ^1H NMR spectroscopy over a period of 48 h. Light yellow needle-like crystals of [(BDI_{IPP})PbI] (**30**) were formed *in situ* after 7 d at room temperature. ^1H NMR (399.50 MHz, C_6D_6 , 303K): δ 7.11 (d, $J = 8.0$ Hz, 4H, Ar-*H*), 4.85 (s, 1H, γ -CH), 2.70 (septet, $J = 6.8$ Hz, 2H, CHMe₂), 1.74 (s, 6H, NCM*e*), 1.11 (d, $J = 6.8$ Hz, 12H, CHMe₂).

5.4 Experimental procedures for Chapter 4

[CH{(CH₃)CN-2,6-^{*i*}Pr₂C₆H₃}₂GeCl], [(BDI_{DIPP})GeCl], (**31**).^[65] (BDI_{DIPP})H (**1**) (2.52 g, 6.07 mmol) was dissolved in THF (30 mL). A solution of *n*-BuLi in *n*-hexane (2.6 mL of 2.37 M solution, 6.07 mmol) was added dropwise to the solution. The mixture was stirred at room temperature for 45 minutes and added slowly to a THF (10 mL) slurry of GeCl₂·dioxane (1.41 g, 6.07 mmol). The mixture was stirred at room temperature for 20 h, after which it was filtered through a pad of Celite. The volatiles were removed *in vacuo* from the filtrate. The solid residue was washed with cold pentane (3 × 10 mL). The light yellow solid, [(BDI_{DIPP})GeCl] (**31**), was used without further purification. Yield: 2.35 g, 73%. [lit.: 63%.]^[65] ^1H NMR (399.50 MHz, C_6D_6 , 303 K): δ 7.19 (dd, $J = 7.6, 2.0$ Hz, 2H, *m*-H), 7.15 (t, $J = 7.6$ Hz, 2H, *p*-H), 7.06 (dd, $J = 7.6, 2.0$ Hz, 2H, *m*-H), 5.15 (s, 1H, γ -CH), 3.93 (septet, $J = 6.8$ Hz, 2H, CHMe₂), 3.17 (septet $J = 6.8$ Hz, 2H, CHMe₂), 1.61 (s, 6H, NCM*e*), 1.49 (d, $J = 6.4$ Hz, 6H, CHMe₂), 1.23 (d, $J = 5.2$ Hz, 6H, CHMe₂), 1.21 (d, $J = 5.2$ Hz, 6H, CHMe₂), 1.03 (d, $J = 6.8$ Hz, 6H, CHMe₂). [lit.: ^1H NMR (200.1 MHz, C_6D_6 , 293 K): δ 7.00–7.10 (m, 6H), 5.14 (s,

1H), 3.80–4.00 (septet, 2H), 3.05–3.20 (septet, 2H), 1.60 (s, 6H), 1.46 (d, 6H), 1.20 (d, 6H), 1.19 (d, 6H), 1.01 (d, 6H)].^[65] ¹³C{¹H} NMR (100.46 MHz, C₆D₆, 303 K): δ 165.4 (NCMe), 147.7 (*ipso*-C), 144.0 (*o*-C), 140.2 (*o*-C), 128.5 (*p*-H), 126.0 (*o*-C), 124.5 (*o*-C), 101.1 (*γ*-CH), 29.9 (CHMe₂), 28.7 (CHMe₂), 28.2 (NCMe), 25.1, 24.9, 24.5 and 23.8 (CHMe₂). UV-vis (pentane), λ_{max}, nm (ε, M⁻¹cm⁻¹): 364.9 (46700).

[CH{(CH₃)CN-2,6-ⁱPr₂C₆H₃}₂SnCl], [(BDI_{DIPP})SnCl], (32).^[65] *n*-BuLi in *n*-hexane (2.04 mL of 2.37 M solution, 4.83 mmol) was added dropwise to (BDI_{DIPP})H (1) (2.00 g, 4.83 mmol) in THF (35 mL). The mixture was stirred for approximately 45 minutes at room temperature. The resulting solution of lithium β-diketiminate was quickly added to a THF (10 mL) slurry of SnCl₂ (0.92 g, 4.83 mmol). The mixture was stirred at room temperature for 20 h. The mixture was filtered *via* a cannula and the volatiles were removed under vacuum from the filtrate. The crude solid was washed with pentane (3 × 10 mL) to give [(BDI_{DIPP})SnCl] (32) as a pale yellow solid. Yield: 1.79 g, 56%. [lit. 73%].^[65] ¹H NMR (399.50 MHz, C₆D₆, 303 K): δ 7.18 (dd, *J* = 8.0, 2.0 Hz, 2H, *m*-H), 7.14 (t, *J* = 7.6 Hz, 2H, *p*-H), 7.06 (dd, *J* = 7.6, 2.0 Hz, 2H, *m*-H), 5.08 (s, 1H, *γ*-CH), 3.96 (septet, *J* = 6.8 Hz, 2H, CHMe₂), 3.13 (septet, *J* = 6.8 Hz, 2H, CHMe₂), 1.64 (s, 6H, NCMe), 1.45 (d, *J* = 6.4 Hz, 6H, CHMe₂), 1.23 (d, *J* = 6.8 Hz, 6H, CHMe₂), 1.20 (d, *J* = 6.8 Hz, 6H, CHMe₂), 1.07 (d, *J* = 6.8 Hz, 6H, CHMe₂). [lit. ¹H NMR (200.1 MHz, C₆D₆, 298 K): δ 7.06 (m, 6H), 5.05 (s, 1H), 3.85–3.98 (septet, 2H), 3.00–3.20 (septet, 2H), 1.61 (s, 6H), 1.42 (d, 6H), 1.19 (d, 6H), 1.16 (d, 6H), 1.03 (d, 6H)].^[65] ¹³C{¹H} NMR (100.46 MHz, C₆D₆, 303 K): δ 166.1 (NCMe), 146.6 (*ipso*-C), 143.3 (*o*-C), 141.8 (*o*-C), 127.9 (*p*-C), 125.8 (*m*-C), 124.4 (*m*-C), 101.2 (*γ*-CH), 29.6 (*J*_{C_{Sn}} = 20 Hz, CHMe₂), 28.4 (CHMe₂), 28.3 (CHMe₂), 25.2 (*J*_{C_{Sn}} = 13 Hz, CHMe₂), 25.0, 24.4 (CHMe₂), 24.3 (CHMe₂). UV-vis (pentane), λ_{max}, nm (ε, M⁻¹cm⁻¹): 366.9 (19600).

[CH{(CH₃)CN-2,6-ⁱPr₂C₆H₃}₂GeP(C₆H₅)₂], [(BDI_{DIPP})GePPh₂], (33).^[258] A toluene (15 mL) solution of [(BDI_{DIPP})GeCl] (31) (0.25 g, 0.48 mmol) was added to solid LiPPh₂ (0.09 g, 0.48 mmol). The mixture was stirred at room temperature for 30 h. The deep purple solution was filtered through a pad of Celite. The solvent was evaporated under vacuum from the filtrate. The deep purple solid was crystallised from a minimum amount of *n*-hexane at –30 °C. Indigo coloured crystals of [(BDI_{DIPP})GePPh₂] (33) were obtained. Yield: 0.27 g, 83%. [lit. 71%].^[258] ¹H NMR (399.50 MHz, C₆D₆, 303 K): δ

6.96–7.03 (m, 8H, *P-Ph*), 6.85 (dd, $J = 9.2, 1.6$ Hz, 2H, *m-H*), 6.82 (d, $J = 6.4$ Hz, 2H, *p-H*), 6.79 (dd, $J_{\text{HH}} = 7.2$ Hz, $J_{\text{HP}} = 0.8$ Hz, 2H, *m-H*), 4.75 (s, 1H, $\gamma\text{-CH}$), 4.15 (d-septet, $J_{\text{HH}} = 6.8, J_{\text{HP}} = 0.8$ Hz, 2H, CHMe_2), 3.24 (septet, $J = 6.8$ Hz, 2H, CHMe_2), 1.70 (d, $J = 6.8$ Hz, 6H, CHMe_2), 1.45 (s, 6H, NCMe), 1.21 (d, $J = 6.8$ Hz, 6H, CHMe_2), 1.08 (d, $J = 6.8$ Hz, 6H, CHMe_2), 0.99 (d, $J = 6.8$ Hz, 6H, CHMe_2). [lit. ^1H NMR (500.13 MHz, C_6D_6): δ 6.75–7.02 (*m*), 4.73 (s, 1H), 4.14 (s, 1H), 4.14 (m, 2H), 3.23 (septet, $J = 7.0$ Hz, 2H), 1.69 (d, $J = 7.0$ Hz, 6H), 1.44 (s, 6H), 1.20 (d, $J = 7.0$ Hz, 6H), 1.07 (d, $J = 7.0$ Hz, 6H), 0.98 (d, $J = 7.0$ Hz, 6H)].^[258] $^{13}\text{C}\{^1\text{H}\}$ NMR (100.46 MHz, C_6D_6 , 303 K): δ 167.4 (NCMe), 145.7 (*o-C*), 143.9 (*o-C*), 142.0 (*ipso-C*), 141.6 (*P-*ipso-C**), 141.3 (*P-Ph*), 136.2 (*p-C*), 136.0 (*P-Ph*), 128.2 (*m-C*), 127.7 (*P-Ph*), 126.4 (*P-Ph*), 125.6 (*m-C*), 124.9 (*P-Ph*), 97.7 ($\gamma\text{-CH}$), 29.7 (d, $J_{\text{CP}} = 9$ Hz, CHMe_2), 29.1 (CHMe_2), 25.9, 25.6, 25.2 (CHMe_2), 24.8 (d, $J_{\text{CP}} = 9$ Hz, CHMe_2), 23.3 (NCMe). [lit. $^{13}\text{C}\{^1\text{H}\}$ NMR (126 MHz, C_6D_6): δ 166.42, 144.98, 143.16, 141.25, 140.75 (d, $J_{\text{CP}} = 27.9$ Hz), 135.38 (d, $J_{\text{CP}} = 16.9$ Hz), 134.50 (d, $J_{\text{CP}} = 13.0$ Hz), 134.40 (d, $J_{\text{CP}} = 12.8$ Hz), 127.00, 125.70, 124.92, 124.22, 96.97, 29.00, 28.93, 28.40, 25.18, 24.90, 24.46, 24.07, 23.99, 22.58].^[258] $^{31}\text{P}\{^1\text{H}\}$ NMR (161.72 MHz, C_6D_6 , 303 K): δ -36.0. [lit. ^{31}P NMR (202 MHz, C_6D_6): δ -14.91].^[258] IR (Nujol, ν/cm^{-1}): 1557 (s), 1515 (s), 1320 (s), 1257 (s), 1177 (s), 1020 (s), 793 (s), 738 (s). [lit. IR (Nujol, ν/cm^{-1}): 2668.8, 1555.19, 1513.4, 1319.14, 1257.2, 1174.6, 1096.81, 1058.43, 1017.62, 965.87, 933.92, 853.24, 792.56, 758.11, 736.9, 694.79, 519.4, 498.68, 475.86, 445.02].^[258] UV-vis (pentane), λ_{max} , nm (ϵ , $\text{M}^{-1}\text{cm}^{-1}$): 259.1 (15200), 342.0 (12600). EI-MS: m/z (%) 676 (22, $[\text{M}+1]$), 471, 418 (10, $[\text{M}-\text{GePPh}_2]$). Anal. Calcd. for $\text{C}_{41}\text{H}_{51}\text{GeN}_2\text{P}$ (675.47): C, 72.90; H, 7.61; N, 4.15%. Found: C, 73.02; H, 7.62; N, 4.03%. [lit. Anal. Calcd. for $\text{C}_{41}\text{H}_{51}\text{GeN}_2\text{P}$ (675.47): C, 72.90; H, 7.61; N, 4.15%. Found: C, 71.81; H, 7.56; N, 4.19%].^[258]

$[\text{CH}\{(\text{CH}_3)\text{CN-2,6-}^i\text{Pr}_2\text{C}_6\text{H}_3\}_2\text{SnP}(\text{C}_6\text{H}_5)_2]$, $[(\text{BDI}_{\text{DIPP}})\text{SnPPh}_2]$, (34**).** $[(\text{BDI}_{\text{DIPP}})\text{SnCl}]$ (**32**) (0.30 g, 0.52 mmol) in toluene (15 mL) was added to solid LiPPh_2 (0.10 g, 0.52 mmol). The mixture was stirred at room temperature for 18 h. The purple solution was filtered through a pad of Celite and the volatiles were removed under vacuum from the filtrate. The red-purple solid residue was washed with cold *n*-hexane (5 mL), and dissolved in a minimum amount of *n*-hexane, then cooled to -30 °C to give red-purple crystals of $[(\text{BDI}_{\text{DIPP}})\text{SnPPh}_2]$ (**34**). Yield: 0.28 g, 75%. M.p.: 95–110 °C (decomp.). ^1H NMR (399.50 MHz, C_6D_6 , 303 K): δ 7.13 (dd, $J = 7.6, 1.2$ Hz, 2H, *m-H*), 7.06 (t, $J =$

7.6 Hz, 2H, *p*-H), 6.93 (dd, $J = 7.6, 1.2$ Hz, 2H, *m*-H), 6.72–6.86 (m, 10H, *P-Ph*), 4.71 (s, 1H, γ -CH), 4.08 (d-septet, $J_{\text{HH}} = 6.8, J_{\text{HP}} = 1.2$ Hz, 2H, CHMe₂), 3.16 (septet, $J = 6.8$ Hz, 2H, CHMe₂), 1.67 (d, $J = 7.2$, 6H, CHMe₂), 1.52 (s, 6H, NCMe), 1.23 (d, $J = 7.2$ Hz, 6H, CHMe₂), 1.11 (d, $J = 6.8$, 6H, CHMe₂), 0.96 (d, $J = 6.8$ Hz, 6H, CHMe₂). ¹³C{¹H} NMR (100.46 MHz, C₆D₆, 303 K): δ 167.9 (NCMe), 144.8 (*ipso*-C₆H₃), 143.9 (*o*-C₆H₃), 143.2 (*o*-C₆H₃), 141.5 (d, $J_{\text{PC}} = 32$ Hz, C₆H₅), 135.1 (d, $J_{\text{PC}} = 15$ Hz, C₆H₅), 128.4 (d, $J_{\text{PC}} = 6$ Hz, C₆H₅), 127.0 (*o*- / *m*-C₆H₃), 125.8 (C₆H₅), 125.2, 124.9 (*o*- / *m*-C₆H₃), 97.6 (γ -CH), 29.5 (d, $J_{\text{CP}} = 6$ Hz, CHMe₂), 28.8 ($J_{\text{CSn}} = 36$ Hz, CHMe₂), 26.6 ($J_{\text{CSn}} = 43$ Hz, CHMe₂), 25.6, 25.0 (CHMe₂), 24.7 (d, $J_{\text{CP}} = 9$ Hz, CHMe₂), 23.8 (NCMe). ³¹P{¹H} NMR (161.72 MHz, C₆D₆, 303 K): δ -30.8 ($J_{\text{P}^{10}\text{Sn}} = 978$ Hz, $J_{\text{P}^{117}\text{Sn}} = 937$ Hz). ¹¹⁹Sn NMR (148.96 MHz, C₆D₆, 303 K): δ 126 (d, $J_{\text{SnP}} = 966$ Hz). IR (Nujol, ν/cm^{-1}): 1578 (s), 1555 (s), 1516 (b), 1318 (s), 1266 (s), 1174 (s), 1099 (s), 1019 (s), 935 (s). UV-vis (pentane) λ_{max} , nm ($\epsilon, \text{M}^{-1}\text{cm}^{-1}$): 283.9 (14900), 354.0 (13700). Anal. Calcd. for C₄₁H₅₁N₂PSn (721.54): C, 68.25; H, 7.12; N, 3.88%. Found: C, 68.37; H, 7.05; N, 3.79%.

[CH{(CH₃)CN-2,6-ⁱPr₂C₆H₃}₂PbP(C₆H₅)₂], [(BDI_{DIPP})PbPPh₂], (35). A toluene (15 mL) solution of [(BDI_{DIPP})PbCl] (**2**) (0.25 g, 0.38 mmol) was added to solid LiPPh₂ (0.07 g, 0.38 mmol). The mixture was stirred at room temperature for 10 h. The deep-red mixture was filtered through a pad of Celite and the volatiles were removed under vacuum from the filtrate. The red solid residue was dissolved in a minimum amount of *n*-hexane and cooled to -30 °C to give needle-like red crystals of [(BDI_{DIPP})PbPPh₂] (**35**). Yield: 0.19 g, 61%. M.p.: 265–266 °C (decomp.). ¹H NMR (399.50 MHz, C₆D₆, 303 K): δ 7.21 (d, $J = 7.6$ Hz, 2H, *m*-H), 7.05 (t, $J = 7.6$ Hz, 2H, *p*-H), 6.96 (d, $J = 7.6$ Hz, 2H, *m*-H), 6.86 (t, $J = 7.2$ Hz, 4H, *P-o*-H), 6.75 (t, $J = 7.2$ Hz, 2H, *P-p*-H), 6.53 (t, $J = 6.8$ Hz, 4H, *P-m*-H), 4.59 (s, 1H, γ -CH), 4.04 (septet, $J = 6.8$ Hz, 2H, CHMe₂), 3.06 (septet, $J = 6.8$ Hz, 2H, CHMe₂), 1.69 (d, $J = 6.8$ Hz, 6H, CHMe₂), 1.64 (s, 6H, NCMe), 1.29 (d, $J = 6.8$, 6H, CHMe₂), 1.13 (d, $J = 6.8$ Hz, 6H, CHMe₂), 0.86 (d, $J = 6.8$ Hz, 6H, CHMe₂). ¹³C{¹H} NMR (100.46 MHz, C₆D₆, 303 K): δ 166.3 (NCMe), 144.9 (*ipso*-C₆H₃), 143.9 (*o*-C₆H₃), 143.4 (*o*-C₆H₃), 142.8 (d, $J_{\text{CP}} = 38$ Hz, C₆H₅), 135.7 (d, $J_{\text{CP}} = 16$ Hz, C₆H₅), 126.5 (*o*- / *m*-C₆H₃), 126.4 (C₆H₅), 124.8, 124.6 (*o*- / *m*-C₆H₃), 98.9 (γ -CH), 29.4 (d, $J_{\text{CP}} = 5$ Hz, CHMe₂), 28.3 ($J_{\text{CPb}} = 37$ Hz, CHMe₂), 26.9 (CHMe₂), 25.5 (d, $J_{\text{CP}} = 4$ Hz, CHMe₂), 25.4, 25.0 (CHMe₂), 24.3 (NCMe). ³¹P{¹H} NMR (161.72 MHz, C₆D₆,

303 K): δ 7.3 ($J_{\text{PbPb}} = 1130$ Hz). ^{207}Pb NMR (83.83 MHz, C_6D_6 , 303 K): δ 3011 (d, $J_{\text{PbP}} = 1138$ Hz). IR (Nujol, ν/cm^{-1}): 1552 (s), 1513 (s), 1317 (s), 1173 (s), 1018 (s), 934 (s), 793 (s). UV-vis (pentane), λ_{max} , nm (ϵ , $\text{M}^{-1}\text{cm}^{-1}$): 259.1 (18600), 312.0 (17700). Anal. Calcd. for $\text{C}_{41}\text{H}_{51}\text{N}_2\text{PPb}$ (810.03): C, 60.79; H, 6.35; N, 3.46%. Found: C, 60.92; H, 6.51; N, 3.38%.

[CH{(CH₃)CN-2,6-ⁱPr₂C₆H₃}₂GeP(C₆H₁₁)₂], [(BDI_{DIPP})GePCy₂], (36).
[(BDI_{DIPP})GeCl] (31) (0.31 g, 0.59 mmol) in diethyl ether (15 mL) was added to a suspension of LiPCy₂ (0.12 g, 0.59 mmol) in diethyl ether (5 mL). The mixture was stirred rapidly at room temperature for 40 h, after which the mixture was filtered through a pad of Celite. The volatiles were removed under vacuum from the filtrate, to leave a purple crude solid, which recrystallised from a minimum amount of *n*-hexane at -30 °C to give purple crystals of [(BDI_{DIPP})GePCy₂] (**36**). Yield: 0.38 g, 92%. M.p.: 199–200 °C (decomp.). ^1H NMR (399.50 MHz, C_6D_6 , 303 K): δ 7.17 (d, $J = 6.0$ Hz, 2H, *m*-H), 7.11 (t, $J = 7.6$ Hz, 2H, *p*-H), 7.04 (d, $J = 7.2$ Hz, 2H, *m*-H), 4.73 (s, 1H, γ -CH), 4.08 (d-septet, $J_{\text{HH}} = 6.8$, $J_{\text{HP}} = 2.8$ Hz, 2H, CHMe₂), 3.44 (septet, $J = 6.8$ Hz, 2H CHMe₂), 1.88 (br, 4H, Cy-CH₂), 1.68 (d, $J = 6.8$ Hz, 6H, CHMe₂), 1.57 (br, 6H, Cy-CH₂), 1.53 (s, 6H, NCMe), 1.37 (d, $J = 6.8$ Hz, 6H, CHMe₂), 1.30 (br, 4H, Cy-CH₂), 1.20 (d, $J = 6.8$ Hz, 6H, CHMe₂), 1.12 (d, $J = 6.8$ Hz, 6H, CHMe₂), 0.94 (br, 7H, Cy-CH₂), 0.47 (br t, $J_{\text{HP}} = 12.8$ Hz, 2H, Cy-CH). $^{13}\text{C}\{^1\text{H}\}$ NMR (100.46 MHz, C_6D_6 , 303 K): δ 167.5 (NCMe), 146.2 (*ipso*-C), 144.8 (*o*-C), 142.1 (*o*-C), 127.5 (*p*-C), 125.5 (*m*-C), 125.0 (*m*-C), 96.6 (γ -CH), 36.1 (Cy-CH₂), 35.5 (d, $J_{\text{CP}} = 29$ Hz, Cy-CH), 29.5 (d, $J_{\text{CP}} = 10$ Hz, CHMe₂), 29.2 (CHMe₂), 29.1, 28.8, 27.2 (Cy-CH₂), 26.3, 25.6, 25.5 (CHMe₂), 24.9 (d, $J_{\text{CP}} = 11$ Hz, CHMe₂), 23.4 (NCMe). $^{31}\text{P}\{^1\text{H}\}$ NMR (161.72 MHz, C_6D_6 , 303 K): δ -14.1. IR (Nujol, ν/cm^{-1}): 1557 (s), 1519 (s), 1320 (s), 1171 (s), 1019 (s), 794 (s). UV-vis (pentane) λ_{max} , nm (ϵ , $\text{M}^{-1}\text{cm}^{-1}$): 280.9 (17100), 352.0 (8870). EI-MS: m/z (%) 688 (18, M^+), 492 (100, $[\text{M}-\text{PCy}_2]^+$), 419 (10, $[\text{M}-\text{GePCy}_2]^+$). Anal. Calcd. for $\text{C}_{41}\text{H}_{63}\text{GeN}_2\text{P}$ (687.57): C, 71.62; H, 9.24; N, 4.07%. Found: C, 71.71; H, 9.21; N, 3.88%.

[CH{(CH₃)CN-2,6-ⁱPr₂C₆H₃}₂SnP(C₆H₁₁)₂], [(BDI_{DIPP})SnPCy₂], (37).
[(BDI_{DIPP})SnCl] (32) (0.38 g, 0.66 mmol) was added to a toluene suspension (15 mL) of LiPCy₂ (0.14 g, 0.66 mmol). The mixture was stirred at room temperature for 24 h, then

filtered through a pad of Celite, and the volatiles were removed under vacuum from the filtrate. The deep purple solid residue was washed with cold toluene (3 mL) and was recrystallised from a minimum amount of toluene at $-30\text{ }^{\circ}\text{C}$. Yield: 0.42 g, 87%. M.p.: $205\text{--}207\text{ }^{\circ}\text{C}$ (decomp.). ^1H NMR (399.50 MHz, C_6D_6 , 303 K): δ 7.17 (dd, $J = 7.6, 1.6$ Hz, 2H, *m*-H), 7.08 (t, $J = 7.6$ Hz, 2H, *p*-H), 7.02 (dd, $J = 7.6, 1.6$ Hz, 2H, *m*-H), 4.72 (s, 1H, γ -CH), 3.99 (d-septet, $J_{\text{HH}} = 6.8, J_{\text{HP}} = 1.6$ Hz, 2H, CHMe₂), 3.32 (septet, $J = 6.8$ Hz, 2H, CHMe₂), 1.67 (d, $J = 6.8$ Hz, 6H, CHMe₂), 1.59 (s, 6H, NCMe), 1.54 (br, 6H, Cy-CH₂), 1.31 (d, $J = 6.8$ Hz, 6H, CHMe₂), 1.21 (d, $J = 6.8$ Hz, 6H, CHMe₂), 1.15 (d, $J = 6.8$ Hz, 6H, CHMe₂), 1.00 (br, 9H, Cy-CH & Cy-CH₂). $^{13}\text{C}\{^1\text{H}\}$ NMR (100.46 MHz, C_6D_6 , 303 K): δ 168.3 (NCMe), 144.7 (*ipso*-C), 144.4 (*o*-C), 143.5 (*o*-C), 127.0 (*m*-C), 125.2 (*p*-C), 125.1 (*m*-C), 97.0 (γ -CH), 36.3 (Cy-CH₂), 33.1 (d, $^1J_{\text{CP}} = 28$ Hz, Cy-CH), 29.4 (d, $J_{\text{CP}} = 7$ Hz, CHMe₂), 28.8 (br, Cy-CH₂), 28.4 (CHMe₂), 26.9 (Cy-CH₂), 26.7, 25.7, 25.3 (CHMe₂), 25.1 (d, $J_{\text{CP}} = 10$ Hz, CHMe₂), 23.9 (NCMe). $^{31}\text{P}\{^1\text{H}\}$ NMR (161.72 MHz, C_6D_6 , 303 K): δ -15.4 ($J_{\text{PSn}} = 953$ Hz). ^{119}Sn NMR (148.96 MHz, C_6D_6 , 303 K): δ 358 (d, $J_{\text{PSn}} = 964$ Hz). IR (Nujol, ν/cm^{-1}): 1553 (s), 1518 (s), 1319 (s), 1174 (s), 1019 (s), 764 (s), 751 (s), 516 (s). UV-vis (pentane) λ_{max} , nm (ϵ , $\text{M}^{-1}\text{cm}^{-1}$): 284.0 (19400), 365.0 (10900). Anal. Calcd. for $\text{C}_{41}\text{H}_{63}\text{N}_2\text{PSn}$ (733.64): C, 67.12; H, 8.66; N, 3.82%. Found: C, 67.03; H, 8.60; N, 3.75%.

[CH{(CH₃)CN-2,6-ⁱPr₂C₆H₃}₂PbP(C₆H₁₁)₂], [(BDI_{DIPP})PbPCy₂], (38).

[(BDI_{DIPP})PbCl] (2) (0.50 g, 0.79 mmol) in toluene (20 mL) was added to a toluene (10 mL) suspension of LiPCy₂ (0.16 g, 0.79 mmol). The mixture was stirred at room temperature for 24 h. The deep red mixture was filtered through a pad of Celite and the volatiles were removed from the filtrate under vacuum. The deep red solid residue was crystallised from a minimum amount of toluene at $-30\text{ }^{\circ}\text{C}$. Yield: 0.59 g, 95%. M.p.: $154\text{--}155\text{ }^{\circ}\text{C}$ (decomp.). ^1H NMR (399.50 MHz, C_6D_6 , 303 K): δ 7.21 (dd, $J = 7.6, 1.6$ Hz, 2H, *m*-H), 7.05 (t, $J = 7.6$ Hz, 2H, *p*-H), 7.02 (dd, $J = 7.6, 1.6$ Hz, 2H, *m*-H), 4.61 (s, 1H, γ -CH), 3.95 (d-septet, $J_{\text{HH}} = 6.8, J_{\text{HP}} = 0.8$ Hz, 2H, CHMe₂), 3.25 (septet, $J = 6.8$ Hz, 2H, CHMe₂), 1.73 (s, 6H, NCMe), 1.68 (d, $J = 6.8$ Hz, 6H, CHMe₂), 1.62 (br, 6H, Cy-CH, Cy-CH₂), 1.26 (d, $J = 7.2$ Hz, 6H, CHMe₂), 1.23 (d, $J = 6.8$ Hz, 6H, CHMe₂), 1.18 (d, $J = 6.8$ Hz, 6H, CHMe₂), 1.00 (br, 6H, Cy-CH₂). $^{13}\text{C}\{^1\text{H}\}$ NMR (100.46 MHz, C_6D_6 , 303 K): δ 166.8 (NCMe), 145.1 (*ipso*-C), 144.4 (*o*-C), 143.5 (*o*-C), 126.4 (*p*-C), 124.9 (*m*-C), 124.6 (*m*-C), 98.1 (γ -CH), 39.3 (br, Cy-CH₂), 34.4 (d, $^1J_{\text{CP}} = 34$ Hz, Cy-

CH), 29.2 (d, $J_{CP} = 6$ Hz, $CHMe_2$), 28.7 (br, Cy- CH_2), 28.3 ($CHMe_2$), 26.9 ($CHMe_2$), 26.8 (Cy- CH_2), 25.8 (d, $J_{CP} = 11$ Hz, $CHMe_2$), 25.5, 25.3 ($CHMe_2$), 24.1 (NCMe). $^{31}P\{^1H\}$ NMR (161.72 MHz, C_6D_6 , 303 K): δ 26.9 ($J_{PPb} = 1103$ Hz). ^{207}Pb NMR (83.83 MHz, C_6D_6 , 303 K): δ 3981 (d, $J_{PbP} = 1074$ Hz). IR (Nujol, ν/cm^{-1}): 1556 (s), 1515 (s), 1319 (s), 1172 (s), 935 (s), 789 (s). UV-vis (pentane) λ_{max} , nm (ϵ , $M^{-1}cm^{-1}$): 280.9 (17100), 352.0 (8870). Anal. Calcd. for $C_{41}H_{63}N_2PPb$ (822.13): C, 59.90; H, 7.72; N, 3.41%. Found: C, 60.01; H, 7.59; N, 3.29%.

[CH{(CH₃)CN-2,6-ⁱPr₂C₆H₃}₂GeP(Si(CH₃)₃)₂], [(BDI_{DIPP})GeP(SiMe₃)₂], (40).^[134] [(BDI_{DIPP})GeCl] (31) (0.30 g, 0.57 mmol) in diethyl ether (15 mL) was added slowly to a diethyl ether (5 mL) solution of [LiP(SiMe₃)₂] (0.11 g, 0.57 mmol). The mixture was stirred at room temperature for 20 h. The deep orange mixture was filtered through a pad of Celite. The volatiles were removed from the filtrate *in vacuo*, leaving an orange solid that was crystallised from *n*-hexane at -30 °C to give bright yellow crystals of [(BDI_{DIPP})GeP(SiMe₃)₂] (40). Yield: 0.28 g, 73 %. [lit. 91%].^[134] 1H NMR (499.91 MHz, C_6D_6 , 303 K): δ 7.22 (dd, $J = 8.0, 1.5$ Hz, 2H, *m*-H), 7.16 (t, $J = 8.0$ Hz, 2H, *p*-H), 7.09 (dd, $J = 7.5, 1.5$ Hz, 2H, *m*-H), 5.06 (s, 1H, γ -CH), 3.90 (d-septet, $J_{HH} = 6.5, J_{HP} = 1.5$ Hz, 2H, $CHMe_2$), 3.40 (septet, $J = 6.5$ Hz, 2H, $CHMe_2$), 1.59 (s, 6H, NCMe), 1.53 (d, $J = 6.5$ Hz, 6H, $CHMe_2$), 1.30 (d, $J = 7.0$ Hz, 6H, $CHMe_2$), 1.29 (d, $J = 7.0$ Hz, 6H, $CHMe_2$), 1.08 (d, $J = 6.5$ Hz, 6H, $CHMe_2$), 0.44 (d, $J_{HP} = 5.0$ Hz, 6H, SiMe₃). [lit.: 1H NMR (200.13 MHz, C_6D_6 , 298 K): δ 7.05–7.24 (m, br, 6H), 5.04 (s, 1H), 3.89 (d-septet, $J_{HH} = 6.8$ Hz, $J_{PH} = 1.7$ Hz, 2H), 3.39 (septet, $J = 6.8$ Hz, 2H), 1.58 (s, 6H), 1.52 (d, $J = 6.8$ Hz, 6H), 1.29 (d, $J = 6.8$ Hz, 6H), 1.27 (d, $J = 6.8$ Hz, 6H), 1.07 (d, $J = 6.8$ Hz, 6H), 0.43 (d, $J_{PH} = 4.6$ Hz, 18H)].^[134] $^{13}C\{^1H\}$ NMR (125.71 MHz, C_6D_6 , 303 K): δ 166.7 (NCMe), 147.7 (*ipso*-C), 144.7 (*o*-C), 141.7 (*o*-C), 128.0 (*p*-C), 125.9 (*m*-C), 124.8 (*m*-C), 101.9 (γ -CH), 29.7 (d, $J_{CP} = 5$ Hz, $CHMe_2$), 29.5 ($CHMe_2$), 28.6 (d, $J_{CP} = 5$ Hz, $CHMe_2$), 25.6, 25.3, 25.1 ($CHMe_2$), 24.5 (NCMe), 6.0 (d, $J_{CP} = 10$ Hz, SiMe₃). [lit.: $^{13}C\{^1H\}$ NMR (50.32 MHz, C_6D_6 , 298 K): δ 166.3, 124.4, 125.5, 141.2, 144.3, 147.2, 101.4, 29.4, 28.2 (d, $J_{CP} = 5$ Hz), 24.7, 24.9, 25.2, 29.3, 24.1, 5.5 (d, $J_{CP} = 10$ Hz)].^[134] $^{31}P\{^1H\}$ NMR (161.72 MHz, C_6D_6 , 303 K): δ -192.8 ($J_{PSi} = 16$ Hz). [lit.: $^{31}P\{^1H\}$ NMR (161.97 MHz, C_6D_6 , 303 K): δ -192.7].^[134] $^{29}Si\{^1H\}$ NMR (79.37 MHz, toluene-*d*₈, 303K): δ 1.8 (d, $J_{SiP} = 17$ Hz). [lit.: $^{29}Si\{^1H\}$ NMR (79.49 MHz, C_6D_6 , 298

K): δ 2.0 (d, $J_{\text{SiP}} = 17.1$ Hz).^[134] UV-vis (pentane) λ_{max} , nm (ϵ , $\text{M}^{-1}\text{cm}^{-1}$): 259.0 (16500), 311.0 (4800), 370.9 (7700).

[CH{(CH₃)CN-2,6-ⁱPr₂C₆H₃}₂SnP(Si(CH₃)₃)₂], [(BDI_{DIPP})SnP(SiMe₃)₂], (41).
 [(BDI_{DIPP})SnCl] (32) (0.44 g, 0.76 mmol) in toluene (20 mL) was added directly to solid [LiP(SiMe₃)₂] (0.14 g, 0.76 mmol). The mixture was stirred at room temperature for 24 h, then filtered through a pad of Celite. Volatiles were removed from the filtrate under vacuum to give a yellow solid that was recrystallised from pentane at -30°C to give yellow crystals of [(BDI_{DIPP})SnP(SiMe₃)₂] (41). Yield: 0.50 g, 93%. M.p.: 192–194 $^\circ\text{C}$ (decomp.). ¹H NMR (399.50 MHz, C₆D₆, 303 K): δ 7.22 (dd, $J = 7.7$, 1.6 Hz, 2H, *m*-H), 7.16 (t, $J = 7.6$ Hz, 2H, *p*-H), 7.09 (dd, $J = 7.6$, 1.6 Hz, 2H, *m*-H), 4.95 (s, 1H, γ -CH), 3.98 (d-septet, $J_{\text{HH}} = 6.8$, $J_{\text{HP}} = 1.6$ Hz, 2H, CHMe₂), 3.38 (septet, $J = 6.8$ Hz, 2H, CHMe₂), 1.61 (s, 6H, NCMe), 1.48 (d, $J = 6.8$ Hz, 6H, CHMe₂), 1.32 (d, $J = 6.8$ Hz, 6H, CHMe₂), 1.28 (d, $J_{\text{HP}} = 7.2$ Hz, 6H, CHMe₂), 1.12 (d, $J = 6.8$ Hz, 6H, CHMe₂), 0.46 (d, $J = 4.4$ Hz, 18H, SiMe₃). ¹³C {¹H} NMR (100.46 MHz, C₆D₆, 303 K): δ 167.4 (NCMe), 146.7 (*ipso*-C), 143.9 (*o*-C), 143.0 (*o*-C), 127.5 (*p*-C), 125.8 (*m*-C), 124.6 (*m*-C), 101.5 (γ -CH), 29.9 (d, $J_{\text{CP}} = 4$ Hz, CHMe₂), 29.6 ($J_{\text{CSn}} = 21$ Hz, CHMe₂), 28.2 (d, $J_{\text{CP}} = 5$ Hz, CHMe₂), 25.5, 25.4, 25.0 (CHMe₂), 24.9 (NCMe), 6.4 (d, $J_{\text{CP}} = 11$, $J_{\text{CSi}} = 39$, $J_{\text{CSn}} = 60$ Hz, SiMe₃). ³¹P {¹H} NMR (161.72 MHz, C₆D₆, 303 K): δ -183.5 ($J_{\text{PSi}} = 16$ Hz, $J_{\text{P}^{119}\text{Sn}} = 2436$ Hz, $J_{\text{P}^{117}\text{Sn}} = 2327$ Hz). ²⁹Si {¹H} NMR (79.37 MHz, C₆D₆, 303 K): δ 4.0 (d, $J_{\text{SiP}} = 18$ Hz). ¹¹⁹Sn NMR (148.96 MHz, C₆D₆, 303 K): δ 39 (d, $J^{119}\text{SnP} = 2421$ Hz). IR (Nujol, ν/cm^{-1}): 1551 (s), 1521 (s), 1314 (s), 1239 (s), 1168 (s), 1020 (s), 935 (s), 831 (b), 795 (s), 757 (s), 628 (s). UV-vis (pentane) λ_{max} , nm (ϵ , $\text{M}^{-1}\text{cm}^{-1}$): 231.0 (34500), 373.1 (13000). MS m/z (EI): 713, 537, 403, 202, 160, 73, 46. Anal. Calcd. for C₃₅H₅₉N₂PSi₂Sn (713.71): C, 58.90; H, 8.33; N, 3.93%. Found: C, 58.94; H, 8.28; N, 3.88%.

[CH{(CH₃)CN-2,6-ⁱPr₂C₆H₃}₂PbP(Si(CH₃)₃)₂], [(BDI_{DIPP})PbP(SiMe₃)₂], (42).^[103]
 [(BDI_{DIPP})PbCl] (2) (0.24 g, 0.37 mmol) in toluene (20 mL) was added directly to solid [LiP(SiMe₃)₂] (0.07 g, 0.37 mmol). The mixture was stirred at room temperature for 4 h, then filtered through a pad of Celite. The volatiles were evaporated from the filtrate under vacuum, and the orange solid residue was dissolved in a minimum amount of *n*-hexane for crystallisation at -30°C . Yield: 0.27 g, 91%. [lit. 79%].^[103] ¹H NMR (499.91 MHz, C₆D₆, 303 K): δ 7.22 (dd, $J = 7.5$, 2.0 Hz, 2H, *m*-H), 7.12 (t, $J = 7.5$ Hz, 2H, *p*-

H), 7.09 (dd, $J = 7.5, 2.0$ Hz, 2H, *m*-H), 4.75 (s, 1H, γ -CH), 3.92 (d-septet, $J_{\text{HH}} = 6.5$, $J_{\text{HP}} = 1.0$ Hz, 2H, CHMe₂), 3.29 (septet, $J = 6.5$ Hz, 2H, CHMe₂), 1.64 (s, 6H, NCMe), 1.52 (d, $J = 6.5$ Hz, 6H, CHMe₂), 1.31 (d, $J = 7.0$ Hz, 6H, CHMe₂), 1.26 (d, $J = 6.5$ Hz, 6H, CHMe₂), 1.16 (d, $J = 7.0$ Hz, 6H, CHMe₂), 0.30 (d, $J = 4.0$ Hz, 18H, SiMe₃). [lit. ¹H NMR (200.13 MHz, C₆D₆, 298 K): δ 6.98–7.18 (m, 6H), 4.70 (s, 1H), 3.86 (septet, $J = 6.8$ Hz, 2H), 3.23 (septet, $J = 6.9$ Hz, 2H), 1.58 (s, 6H), 1.47 (d, $J = 6.7$ Hz, 6H), 1.25 (d, $J = 6.9$ Hz, 6H), 1.20, (d, $J = 6.9$ Hz, 6H), 1.10 (d, $J = 6.8$ Hz, 6H), 0.25 (d, $J = 4.2$ Hz, 18H)].^[103] ¹³C{¹H} NMR (100.46 MHz, C₆D₆, 303 K): δ 166.2 (NCMe), 145.5 (*ipso*-C), 144.7 (*o*-C), 143.6 (*o*-C), 127.0 (*m*-H), 125.6 (*m*-H), 124.4 (*p*-H), 103.0 (γ -CH), 29.0 (CHMe₂), 28.4 (d, $J_{\text{CP}} = 6$ Hz, CHMe₂), 28.2 (d, $J_{\text{CP}} = 5$ Hz, CHMe₂), 26.1, 25.2, 25.1 (CHMe₂), 25.0 (NCMe), 7.5 (d, $J_{\text{CP}} = 10$ Hz, SiMe₃). [lit. ¹³C NMR (50.32 MHz, C₆D₆, 298 K): δ 165.3, 144.6, 143.9, 142.8, 126.2, 124.8, 123.6, 102.2, 28.2, 27.7, 27.6, 27.5, 27.4, 25.2, 24.3, 24.2, 6.6 (d, $J = 10$ Hz)].^[103] ³¹P{¹H} NMR (161.72 MHz, C₆D₆, 303 K): δ -116.0 ($J_{\text{PPb}} = 2874$ Hz) [lit. ³¹P{¹H} NMR (79.49 MHz, C₆D₆, 298 K): δ -117 ($J_{\text{PPb}} = 2852$ Hz)].^[103] ²⁹Si{¹H} NMR (79.37 MHz, C₆D₆, 303 K): δ 7.2 (d, $J_{\text{SiP}} = 36$ Hz). [lit. ²⁹Si{¹H} NMR (79.49 MHz, C₆D₆, 298 K): δ 7.4 (d, $J_{\text{PSi}} = 36$ Hz)].^[103] UV-vis (pentane) λ_{max} , nm (ϵ , M⁻¹cm⁻¹): 382.0 (7900).

[CH{(CH₃)CN-2,6-Me₂C₆H₃}₂PbP(Si(CH₃)₃)₂], [(BDI_{DMP})PbP(SiMe₃)₂], (43).
 [(BDI_{DMP})PbCl] (**24**) (0.20 g 0.36 mmol) in toluene (10 mL) was added to a toluene (5 mL) slurry of [LiP(SiMe₃)₂] (0.07 g, 0.36 mmol). The mixture was stirred at room temperature for 3 h and filtered through a pad of Celite. The filtrate was concentrated and stored at -30 °C. Deep red solids of [(BDI_{DMP})PbP(SiMe₃)₂] (**43**) were obtained. Yield: 0.21 g, 82%. ¹H NMR (599.69 MHz, C₆D₆, 298 K): δ 7.00 (d, $J = 4.8$ Hz, 2H, *m*-H), 6.95 (d, $J = 6.6$ Hz, 2H, *p*-H), 6.90 (d, $J = 7.2$ Hz, 2H, *m*-H), 4.78 (s, 1H, γ -CH), 2.60 (s, 6H, NCMe), 2.21 (s, 6H, *o*-CH₃), 1.61 (s, 6H, *o*-CH₃), 0.36 (d, $J_{\text{HP}} = 3.6$ Hz, 18H, SiMe₃). ³¹P{¹H} NMR (242.72 MHz, C₆D₆, 298 K): δ -123.6 ($J_{\text{PSi}} = 44$, $J_{\text{PPb}} = 2317$ Hz).

[CH{(CH₃)CN-4-ⁱPrC₆H₄}₂PbP(Si(CH₃)₃)₂], [(BDI_{IPP})PbP(SiMe₃)₂], (44). A cold suspension of [(BDI_{IPP})PbCl] (**23**) (0.20 g, 0.35 mmol) in toluene (5 mL) was added rapidly to solid [LiP(SiMe₃)₂] (0.06 g, 0.35 mmol) and stirred vigorously for 45 minutes. The mixture was filtered quickly through a pad of Celite. The filtrate was

concentrated and kept at $-30\text{ }^{\circ}\text{C}$. Deep red solids of $[(\text{BDI}_{\text{IPP}})\text{PbP}(\text{SiMe}_3)_2]$ (**44**) were obtained. Yield: 0.16 g, 66%. ^1H NMR (399.50 MHz, C_6D_6 , 303 K): δ 7.15–7.16 (m, 4H, *m*-H), 7.06 (d, $J = 9.0$ Hz, 4H, *o*-H), 4.80 (s, 1H, γ -CH), 2.66 (septet, $J = 6.6$ Hz, 2H, CHMe₂), 1.90 (s, 6H, NCMe), 1.09 (d, $J = 6.6$ Hz, 12H, CHMe₂), 0.51 (d, $J_{\text{HP}} = 3.6$ Hz, 18H, SiMe₃). $^{31}\text{P}\{^1\text{H}\}$ NMR (242.72 MHz, C_6D_6 , 303 K): δ -139.9 ($J_{\text{PSi}} = 44$ Hz, $J_{\text{PPb}} = 2061$ Hz).

$[\text{CH}\{(\text{CH}_3)\text{CNC}_6\text{H}_5\}_2\text{PbP}(\text{Si}(\text{CH}_3)_3)_2]$, $[(\text{BDI}_{\text{Ph}})\text{PbP}(\text{SiMe}_3)_2]$, (**45**). A suspension of $[(\text{BDI}_{\text{Ph}})\text{PbCl}]$ (**22**) (0.13 g, 0.26 mmol) in toluene (10 mL) was added slowly to solid $[\text{LiP}(\text{SiMe}_3)_2]$ (0.05 g, 0.26 mmol). The mixture was stirred vigorously for 40 minutes and was filtered rapidly through a pad of Celite. The filtrate was concentrated and stored at $-30\text{ }^{\circ}\text{C}$. Deep red solids of $[(\text{BDI}_{\text{Ph}})\text{PbP}(\text{SiMe}_3)_2]$ (**45**) were obtained. Yield: 0.10 g, 59%. ^1H NMR (399.50 MHz, toluene-*d*₈, 303 K): δ 7.10 (br, 8H, Ar-*H*), 6.89 (br, 2H, Ar-*H*), 4.75 (s, 1H, γ -CH), 1.84 (s, 6H, NCMe), 0.44 (d, $J_{\text{HP}} = 4.0$ Hz, 18H, SiMe₃). $^{13}\text{C}\{^1\text{H}\}$ NMR (100.46 MHz, toluene-*d*₈, 303 K): δ 164.3 (NCMe), 148.9 (*ipso*-C), 137.4 (*o*-C), 129.4 (*o*-C), 125.3 (*m*-C), 125.1 (*m*-C), 124.9 (*p*-C), 104.4 (γ -CH), 23.7 (NCMe), 6.9 (d, $J_{\text{CP}} = 10$ Hz, SiMe₃). $^{31}\text{P}\{^1\text{H}\}$ NMR (161.72 MHz, toluene-*d*₈, 303 K): δ -137.3 ($J_{\text{PSi}} = 44$ Hz, $J_{\text{PPb}} = 2060$ Hz). $^{29}\text{Si}\{^1\text{H}\}$ NMR (79.37 MHz, toluene-*d*₈, 303 K): δ 5.1 (d, $J_{\text{SiP}} = 44$ Hz). ^{207}Pb NMR (83.83 MHz, toluene-*d*₈, 303 K): δ 2905 (d, $J_{\text{PbP}} = 2051$ Hz).

*Reaction of $[(\text{BDI}_{\text{DIPP}})\text{SnPCy}_2]$ (**37**) with elemental selenium in an NMR tube.* $[(\text{BDI}_{\text{DIPP}})\text{SnPCy}_2]$ (**37**) (0.03 g, 0.04 mmol) was added to elemental selenium (3.23 mg, 0.04 mmol) in C_6D_6 (~ 0.5 mL). The reaction was monitored by $^{31}\text{P}\{^1\text{H}\}$ NMR spectroscopy. After 12 h, the spectrum showed two resonances at δ_{P} 35.6 and 58.7 ppm, assigned to $[(\text{BDI}_{\text{DIPP}})\text{SnSePCy}_2]$ (**46**) and $[(\text{BDI}_{\text{DIPP}})\text{SnSeP}(\text{Se})\text{Cy}_2]$ (**49**), respectively, in addition to the resonance at δ_{P} -15.4 ppm, assigned to $[(\text{BDI}_{\text{DIPP}})\text{SnPCy}_2]$ (**37**). Additional elemental selenium (4.85 mg, 0.06 mmol) was added. A spectrum recorded after a further 12 h showed the relative intensity of the resonance at δ_{P} 35.6 ppm for **46** diminished, and the relative intensity of the resonance at δ_{P} 58.7 ppm for **49** increases. Additional $[(\text{BDI}_{\text{DIPP}})\text{SnPCy}_2]$ (**37**) (0.03 g, 0.04 mmol) was added to the mixture. A spectrum was recorded after 12 h, showing the relative intensity of the resonance at δ_{P} 58.7 ppm for **49** decreased, and the relative intensity of the resonance at δ_{P} 35.6 ppm

increased. An additional resonance at $\delta_P -15.4$ ppm, assigned to $[(BDI_{DIPP})SnPCy_2]$ (**37**) was also obtained.

*Reaction of $[(BDI_{DIPP})GePCy_2]$ (**36**) with elemental selenium in an NMR tube.* $[(BDI_{DIPP})GePCy_2]$ (**36**) (0.03 g, 0.04 mmol) was added to elemental selenium (17.2 mg, 0.20 mmol) in C_6D_6 (~ 0.5 mL). The reaction was monitored by $^{31}P\{^1H\}$ NMR spectroscopy. A spectrum recorded after 20 h showed three resonances at δ_P 63.7, 0.67 and -14.1 ppm, assigned to $[(BDI_{DIPP})GeSeP(Se)Cy_2]$ (**48**), $[(BDI_{DIPP})Ge(Se)PCy_2]$ (**51**) and $[(BDI_{DIPP})GePCy_2]$ (**36**), respectively.

$[CH\{(CH_3)CN-2,6-^iPr_2C_6H_3\}_2SnSeP(C_6H_{11})_2]$, $[(BDI_{DIPP})SnSePCy_2]$, (46**).** $[(BDI_{DIPP})SnPCy_2]$ (**37**) (0.22 g, 0.30 mmol) in toluene (10mL) was added to elemental selenium (0.02 g, 0.30 mmol). The mixture was stirred slowly at room temperature for 20 h, and monitored by NMR spectroscopy. It was filtered through a pad of Celite and the volatiles were removed from the filtrate. The residue was washed with cold pentane (3×5 mL) and the solid was dissolved in a minimum amount of toluene for recrystallisation. Yellow crystals of $[(BDI_{DIPP})SnSePCy_2]$ (**46**) were obtained at -30 °C. Yield: 0.12 g, 48%. M.p.: 182–184 °C. 1H NMR (399.50 MHz, C_6D_6 , 303 K): δ 7.19 (d, $J = 7.3$ Hz, 2H, *m*-H), 7.12 (t, $J = 7.6$ Hz, 2H, *p*-H), 7.05 (d, $J = 7.6$ Hz, 2H, *m*-H), 4.70 (s, 1H, γ -CH), 3.71 (septet, $J = 6.8$ Hz, 2H, CHMe₂), 3.24 (septet, $J = 6.8$ Hz, 2H, CHMe₂), 1.66 (d, $J = 6.8$ Hz, 6H, CHMe₂), 1.59 (s, 6H, NCMe), 1.46 (br, 2H, Cy-CH₂), 1.36 (d, $J = 6.8$ Hz, 6H, CHMe₂), 1.21 (d, $J = 6.8$ Hz, 6H, CHMe₂), 1.18 (d, $J = 6.8$ Hz, 6H, CHMe₂), 1.10 (br, 6H, Cy-CH₂), 0.84 (br, 2H, Cy-CH₂). $^{13}C\{^1H\}$ NMR (100.46 MHz, C_6D_6 , 303 K): δ 166.8 (NCMe), 144.4 (*ipso*-C), 144.2 (*o*-C), 144.2 (*o*-C), 126.9 (*p*-C), 124.8 (*m*-C), 124.7 (*m*-C), 97.0 (γ -CH), 35.4 (d, $J_{CP} = 27$ Hz, Cy-CH), 33.4, 31.9, 30.7, 30.5, 29.9 (Cy-CH₂), 29.7, 29.0 (CHMe₂), 28.3, 28.1, 28.0, 27.9, 27.8, 27.7 (Cy-CH₂), 27.3, 25.5, 25.2, 25.1 (CHMe₂), 23.9 (NCMe). $^{31}P\{^1H\}$ NMR (161.72 MHz, C_6D_6 , 303 K): δ 35.6 ($J_{PSe} = 178$ Hz, $J_{P^{119}Sn} = 960$ Hz, $J_{P^{117}Sn} = 916$ Hz). ^{77}Se NMR (76.19 MHz, C_6D_6 , 303K): δ -70 (d, $J_{SeP} = 179$ Hz). ^{119}Sn NMR (148.96 MHz, C_6D_6 , 303 K): δ 60 (d, $J^{119}SnP = 959$ Hz). IR (Nujol, ν/cm^{-1}): 1551 (s), 1515 (s), 1316 (s), 1262 (s), 1173 (s), 1014 (s), 792 (s). UV-vis (pentane), λ_{max} , nm, (ϵ , $M^{-1}cm^{-1}$): 366.1 (4180), 439.1 (3180). EI-MS (m/z): 812, 538, 417, 374, 202, 157, 115, 87, 59, 41. Anal. Calcd.

for $C_{41}H_{63}N_2PSeSn$ (812.60): C, 60.60; H, 7.81; N, 3.44%. Found: C, 60.65; H, 7.93; N, 3.42%.

[CH{(CH₃)CN-2,6-ⁱPr₂C₆H₃}₂PbSeP(C₆H₁₁)₂], [(BDI_{DIPP})PbSePCy₂], (47).
 [(BDI_{DIPP})PbPCy₂] (**38**) (0.15 g, 0.19 mmol) in toluene (10 mL) was added to elemental selenium (0.01 g, 0.15 mmol) suspended in toluene (5 mL). The mixture was stirred slowly at room temperature for 10 h, then filtered through a pad of Celite. Volatiles were removed under vacuum from the filtrate and the residue was washed with cold pentane (3 × 5 mL). The crude solid was dissolved in a minimum amount of toluene for recrystallisation. Orange crystals of [(BDI_{DIPP})PbSePCy₂] (**47**) were obtained at -30 °C. Yield: 0.08 g, 47%. ¹H NMR (399.50 MHz, C₆D₆, 303K): δ 7.22 (br, 2H, Ar-*H*), 7.05 (br, 4H, Ar-*H*), 4.60 (s, 1H, γ-*CH*), 3.74 (septet, *J* = 6.4 Hz, 2H, *CHMe*₂), 3.13 (septet, *J* = 6.4 Hz, 2H, *CHMe*₂), 1.66 (s, 6H, *NMe*), 1.61 (br, 8H, Cy-*CH*₂), 1.44 (br, 2H, Cy-*CH*₂), 1.26 (d, *J* = 8.0 Hz, 12H, *CHMe*₂), 1.18 (d, *J* = 6.8 Hz, 12H, *CHMe*₂), 1.10 (br, 6H, Cy-*CH*₂), 0.85 (br, 2H, Cy-*CH*₂). ¹³C{¹H} NMR (100.46 MHz, C₆D₆, 303K): δ 165.1 (*NMe*), 144.1 (*ipso-C*), 143.1 (*o-C*), 142.9 (*o-C*), 124.7 (*p-C*), 124.1 (*m-C*), 123.9 (*m-C*), 98.9 (γ-*CH*), 35.3 (d, *J* = 27 Hz, Cy-*CH*), 30.6, 30.1 (*CHMe*₂), 29.0, 28.0, 27.9, 27.8, 27.2, 25.4 (Cy-*CH*₂), 25.2, 24.9, 24.0, 23.8 (*CHMe*₂), 21.1 (*NMe*). ³¹P{¹H} NMR (161.72 MHz, C₆D₆, 303 K): δ 23.9 (*J*_{PSe} = 192 Hz, *J*_{Ppb} = 1469 Hz). ⁷⁷Se NMR (76.19 MHz, C₆D₆, 303K): δ -24 (d, *J*_{SeP} = 192 Hz). ²⁰⁷Pb NMR (83.83 MHz, C₆D₆, 303K): δ 2596 (d, *J*_{PbP} = 1477 Hz).

[CH{(CH₃)CN-2,6-ⁱPr₂C₆H₃}₂GeSeP(=Se)(C₆H₁₁)₂], [(BDI_{DIPP})GeSeP(Se)Cy₂], (48).
 [(BDI_{DIPP})GePCy₂] (**36**) (0.19 g, 0.27 mmol) in toluene (10 mL) was added to an excess of elemental selenium (0.09 g, 1.10 mmol) suspended in toluene (5mL). The mixture was stirred rapidly at room temperature for 20 h, then filtered through a pad of Celite. Volatiles were removed from filtrate under vacuum. The yellow solid residue was washed with cold pentane (3 × 3 mL). Single crystals of [(BDI_{DIPP})GeSeP(Se)Cy₂] (**48**) were found along with crystals of [(BDI_{DIPP})Ge(Se)PCy₂] (**51**) and separated from a concentrated toluene solution at -30 °C. Yield: 0.15 g, 64%. ¹H NMR (399.50 MHz, C₆D₆, 303K): δ 7.12 (br, 6H, Ar-*H*), 4.68 (s, 1H, γ-*CH*), 3.50 (septet, *J* = 6.8 Hz, 2H, *CHMe*₂), 3.31 (septet, *J* = 6.8, 2H, *CHMe*₂), 1.74 (br, 2H, Cy-*CH*₂), 1.67 (d, *J* = 6.4 Hz, 8H, *CHMe*₂ and Cy-*CH*₂), 1.59 (d, *J* = 6.4 Hz, 8H, *CHMe*₂ and Cy-*CH*₂), 1.53 (s, 12H,

NCMe, Cy-CH₂), 1.16 (d, $J = 6.4$ Hz, 6H, CHMe₂), 1.13 (d, $J = 6.8$ Hz, 6H, CHMe₂), 1.03 (br, 6H, Cy-CH₂, Cy-CH). ¹³C{¹H} NMR (100.46 MHz, C₆D₆, 303K): δ 166.2 (NCMe), 146.3 (*ipso*-C), 144.2 (*o*-C), 140.6 (*o*-C), 127.4 (*p*-C), 125.4 (*m*-C), 124.3 (*m*-C), 96.5 (γ -CH), 43.1 (d, $J_{CP} = 38$ Hz, Cy-CH), 29.8, 27.1 (CHMe₂), 26.9, 26.7 (Cy-CH₂), 26.6, 25.7, 24.9, 23.6 (CHMe₂), 21.8 (NCMe). ³¹P{¹H} NMR (161.72 MHz, C₆D₆, 303K): δ 63.7 ($J_{PSe} = 551$ Hz). ⁷⁷Se NMR (76.19 MHz, C₆D₆, 303K): δ -18 (d, $J_{SeP} = 198$ Hz).

[CH{(CH₃)CN-2,6-ⁱPr₂C₆H₃}₂SnSeP(=Se)(C₆H₁₁)₂], [(BDI_{DIPP})SnSeP(Se)Cy₂], (49). [(BDI_{DIPP})SnPCy₂] (37) (0.20 g, 0.28 mmol) in toluene (10 mL) was added to a stirred suspension of an excess of elemental selenium (0.11 g, 1.39 mmol) in toluene (5 mL). The mixture was stirred vigorously at room temperature for 30 h. The dark orange mixture was filtered through a pad of Celite and the solvent was removed from the filtrate under vacuum. The solid residue was washed with cold pentane and recrystallised from a minimum amount of toluene at -30 °C, to give orange crystals of [(BDI_{DIPP})SnSeP(Se)Cy₂] (49). Yield: 0.13 g, 52%.

Alternative synthesis of [(BDI_{DIPP})SnSeP(Se)Cy₂] (49). [(BDI_{DIPP})SnSePCy₂] (46) (0.10 g, 0.12 mmol) in toluene (5 mL) was added to a stirred suspension of elemental selenium (0.05 g, 0.62 mmol) in toluene (5 mL). The mixture was stirred vigorously at room temperature for 30 h. The work-up procedure is identical to those stated above. Yield: 0.06 g, 58%.

M.p.: 203–205 °C. ¹H NMR (399.50 MHz, toluene-*d*₈, 303 K): δ 7.09 (s, 6H, Ar-H), 4.66 (γ -CH), 3.49 (br, 2H, CHMe₂), 3.18 (br, 2H, CHMe₂), 1.58 (s, 6H, NCMe), 1.53 (d, $J = 6.8$ Hz, 12H, CHMe₂), 1.17 (d, $J = 6.8$ Hz, 12H, CHMe₂), 1.27–0.96 (m, Cy-CH₂), 0.87 (t, $J_{HP} = 6.8$ Hz, 2H, Cy-CH). ¹³C{¹H} NMR (100.46 MHz, toluene-*d*₈, 303 K): δ 166.5 (NCMe), 143.7 (*ipso*-C), 142.1 (*o*-C), 137.4 (*o*-C), 129.3 (*p*-C), 126.4 (*m*-C), 124.4 (*m*-C), 96.3 (γ -CH), 42.5 (d, $J_{CP} = 36$ Hz, Cy-CH), 34.5 (Cy-CH₂), 29.2 (CHMe₂), 26.6, 26.5, 26.3, 26.2 (Cy-CH₂), 25.2 (CHMe₂), 23.6, 22.8 (CHMe₂), 14.2 (NCMe). ³¹P{¹H} NMR (161.72 MHz, toluene-*d*₈, 303 K): δ 58.7 ($J_{PSe} = 539$ Hz, $J_{P^{119}Sn} = 246$ Hz, $J_{P^{117}Sn} = 236$ Hz). ⁷⁷Se NMR (76.19 MHz, C₆D₆, 303 K): δ -73 ($J_{SeP} = 540$ Hz, $J_{SeSn} = 307$ Hz). ¹¹⁹Sn NMR (148.96 MHz, C₆D₆, 303 K): δ -88 (d, $J_{^{119}SnP} = 247$ Hz). IR (Nujol, ν/cm^{-1}): 1539 (s), 1316 (s), 1174 (s), 790 (s). UV-vis (pentane), λ_{max} , nm, (ϵ , M⁻¹cm⁻¹): 438.0 (2660). EI-MS (m/z): 892, 538, 391, 278, 201, 160, 83, 41.

Anal. Calcd. for $C_{41}H_{63}PN_2Se_2Sn$ (891.56): C, 55.23; H, 7.12; N, 3.14%. Found: C, 55.28; H, 7.16; N, 3.16%.

[CH{(CH₃)CN-2,6-ⁱPr₂C₆H₃}₂PbSeP(=Se)(C₆H₁₁)₂], [(BDI_{DIPP})PbSeP(Se)Cy₂], (50). [(BDI_{DIPP})PbPCy₂] (**38**) (0.26 g, 0.31 mmol) in toluene (10 mL) was added to an excess of elemental selenium (0.12 g, 1.57 mmol) suspended in toluene (5 mL). The mixture was stirred at room temperature for 20 h. The mixture was filtered through a pad of Celite. Volatiles were removed from the filtrate under vacuum and the residue was washed with *n*-hexane (3 × 5 mL). Orange crystals of [(BDI_{DIPP})PbSeP(Se)Cy₂] (**50**) were obtained by recrystallisation from toluene at -30 °C. Yield: 0.25 g, 83%.

Alternative synthesis of [(BDI_{DIPP})PbSeP(Se)Cy₂] (50). [(BDI_{DIPP})PbSePCy₂] (**47**) (0.10 g, 0.11 mmol) in toluene (5 mL) was added to a stirred suspension of elemental selenium (0.04 g, 0.55 mmol) in toluene (5 mL). The mixture was stirred vigorously at room temperature for 20 h. The work-up procedure is identical to those stated above. Yield: 0.08 g, 69%.

¹H NMR (399.50 MHz, C₆D₆, 303 K): δ 7.18 (s, 2H, *p*-H), 7.01–7.14 (m, 4H, Ar-*H*), 4.58 (s, 1H, γ-CH), 3.36 (septet, *J* = 6.8 Hz, 4H, CHMe₂), 1.72 (br, 6H, Cy-CH₂), 1.65 (s, 6H, NCM_e), 1.57 (d, *J* = 6.8 Hz, 12H, CHMe₂), 1.47 (br, 2H, Cy-CH₂), 1.34 (br, 4H, Cy-CH₂), 1.22 (d, *J* = 6.8 Hz, CHMe₂, Cy-CH₂), 1.02 (br, 6H, Cy-CH₂, Cy-CH). ¹³C{¹H} NMR (100.46 MHz, C₆D₆, 303 K): δ 165.0 (NCMe), 144.9 (*ipso*-C), 143.5 (*o*-C), 129.7 (*o*-C), 128.9 (*p*-C), 126.3 (*m*-C), 124.4 (*m*-C), 98.3 (γ-CH), 43.7 (d, *J*_{CP} = 34 Hz, Cy-CH), 29.1, 26.9 (CHMe₂), 26.7, (Cy-CH₂), 26.6, 26.1, 25.6, 24.3 (CHMe₂), 21.8 (NCMe). ³¹P{¹H} NMR (161.72 MHz, C₆D₆, 303 K): δ 57.0 (*J*_{PSe} = 521 Hz, *J*_{PPb} = 218 Hz). ⁷⁷Se NMR (76.19 MHz, C₆D₆, 303 K): δ -47 (d, *J*_{SeP} = 544 Hz). ²⁰⁷Pb NMR (83.83 MHz, C₆D₆, 303 K): δ 1909 (d, *J*_{PbP} = 217 Hz). IR (Nujol, ν/cm⁻¹): 1548 (s), 1315 (s), 1170 (s), 1097 (s), 1014 (s), 934 (s). Anal. Calcd. for $C_{41}H_{63}N_2PPbSe_2$ (980.05): C, 50.25; H, 6.48; N, 2.86%. Found: C, 50.29; H, 6.62; N, 2.72%.

[CH{(CH₃)CN-2,6-ⁱPr₂C₆H₃}₂Ge(Se)P(C₆H₁₁)₂], [(BDI_{DIPP})Ge(Se)PCy₂], (51). Compound **51** was co-crystallised from the synthesis of [(BDI_{DIPP})GeSeP(Se)Cy₂] (**48**) (see Page 286). ¹H NMR (399.50 MHz, CDCl₃, 303K): δ 7.32 (d, *J* = 4.8 Hz, 3H, Ar-*H*), 7.19 (br, 3H, Ar-*H*), 5.45 (s, 1H, γ-CH), 4.01 (septet, *J* = 6.4 Hz, 2H, CHMe₂), 3.53 (septet, *J* = 6.8 Hz, 2H, CHMe₂), 2.24 (br, 3H, Cy-CH₂), 1.91 (s, 6H, NCM_e), 1.45 (d, *J*

= 7.2 Hz, 6H, CHMe₂), 1.43 (d, *J* = 6.8 Hz, 6H, CHMe₂), 1.26–1.35 (br, 6H, Cy-CH₂), 1.21 (d, *J* = 6.8 Hz, 6H, CHMe₂), 1.10–1.14 (br, 3H, Cy-CH₂), 1.06 (d, *J* = 6.8 Hz, 6H, CHMe₂), 0.66–0.87 (br, 14H, Cy-CH₂). ¹³C{¹H} NMR (100,46 MHz, CDCl₃, 303K): δ 167.3 (NCMe), 148.1 (*ipso*-C), 144.6 (*o*-C), 139.4 (*o*-C), 128.6 (*p*-C), 126.4 (*m*-C), 124.2 (*m*-C), 98.9 (γ-CH), 34.5 (d, *J*_{CP} = 16 Hz, Cy-CH), 34.3 (CHMe₂), 32.0 (CHMe₂), 29.7 (CHMe₂), 29.1, 27.9, 27.7, 27.4, 26.5 (Cy-CH₂), 25.5, 25.2, 24.4 (CHMe₂), 21.7 (NCMe). ³¹P{¹H} NMR (161.72 MHz, CDCl₃, 303K): δ 0.7. ⁷⁷Se NMR (76.19 MHz, CDCl₃, 303K): δ -91 (d, *J*_{SeP} = 12 Hz).

[CH{(CH₃)CN-2,6-ⁱPr₂C₆H₃}₂SnSP(S)(C₆H₁₁)₂], [(BDI_{DIPP})SnSP(S)Cy₂], (52).
 [(BDI_{DIPP})SnPCy₂] (37) (0.26 g, 0.35 mmol) in toluene (10 mL) was added to an excess of elemental sulfur (0.06 g, 1.76 mmol) suspended in toluene (5 mL). The mixture was stirred vigorously for 15 h at room temperature, then filtered through a pad of Celite. Volatiles were removed from the filtrate *in vacuo* and the residue was washed with pentane (3 × 5 mL). Yellow crystals of [(BDI_{DIPP})SnSP(S)Cy₂] (52) were obtained by recrystallisation from a minimum amount of toluene at -30 °C. Yield: 0.21 g, 76%. ¹H NMR (399.50 MHz, C₆D₆, 303 K): δ 7.20 (d, *J* = 7.6 Hz, 2H, *m*-H), 7.12–7.14 (m, 2H, *p*-H), 7.04 (d, *J* = 8.8 Hz, 2H, *m*-H), 4.66 (s, 1H, γ-CH), 3.61 (septet, *J* = 6.8 Hz, 2H, CHMe₂), 3.21 (septet, *J* = 6.8 Hz, 2H, CHMe₂), 1.60 (br, 16H, NCMe, Cy-CH, CHMe₂), 1.54 (d, *J* = 6.4 Hz, 6H, CHMe₂), 1.21 (d, *J* = 7.6 Hz, 13H, CHMe₂, Cy-CH₂). ¹³C{¹H} NMR (100.46 MHz, C₆D₆, 303 K): δ 166.6 (NCMe), 144.4 (*ipso*-C), 144.3 (*o*-C), 141.9 (*o*-C), 129.7 (*m*-C), 128.9 (*m*-C), 126.8 (*m*-C), 126.0 (*p*-C), 125.1 (*p*-C), 124.5 (*m*-C), 96.5 (γ-CH), 43.1 (d, *J*_{CP} = 50 Hz, Cy-CH), 29.6, 29.5 (CHMe₂), 27.2, 27.0, 26.7 (Cy-CH₂), 25.7 (CHMe₂), 25.6 (Cy-CH₂), 24.9 (CHMe₂), 23.9 (NCMe). ³¹P{¹H} NMR (161.72 MHz, C₆D₆, 303 K): δ 82.2 (*J*_{P¹¹⁹Sn} = 180 Hz, *J*_{P¹¹⁷Sn} = 173 Hz). ¹¹⁹Sn NMR (148.96 MHz, C₆D₆, 303 K): δ -175 (d, *J*_{119SnP} = 160 Hz).

[CH{(CH₃)CN-2,6-ⁱPr₂C₆H₃}₂PbSP(S)(C₆H₁₁)₂], [(BDI_{DIPP})PbSP(S)Cy₂], (53).
 [(BDI_{DIPP})PbPCy₂] (38) (0.20 g, 0.24 mmol) in toluene (15 mL) was added to an excess of elemental sulfur (0.04 g, 1.22 mmol) suspended in toluene (5 mL). The mixture was stirred at room temperature for 10 h. The orange suspension was filtered through a pad of Celite and the volatiles were removed from filtrate *in vacuo*. The residue was washed with cold *n*-hexane (3 × 5 mL). Yellow crystals of [(BDI_{DIPP})PbSP(S)Cy₂] (53) were

obtained by recrystallisation from a minimum amount of toluene at $-30\text{ }^{\circ}\text{C}$. Yield: 0.16 g, 73%. ^1H NMR (399.50 MHz, C_6D_6 , 303 K): δ 7.17 (d, $J = 7.2$ Hz, 2H, *m*-H), 7.12 (t, $J = 7.6$ Hz, 2H, *p*-H), 7.01–7.08 (m, 2H, *m*-H), 4.55 (s, 1H, γ -CH), 3.35 (septet, $J = 6.8$ Hz, 4H, CHMe_2), 1.66 (s, 6H, NCMe), 1.60 (br, 8H, Cy-CH, Cy- CH_2), 1.54 (d, $J = 6.8$ Hz, CHMe_2), 1.22 (d, $J = 6.8$ Hz, 12H, CHMe_2), 1.03 (br, 6H, Cy- CH_2). $^{13}\text{C}\{^1\text{H}\}$ NMR (100.46 MHz, C_6D_6 , 303 K): δ 164.7 (NCMe), 144.1 (*ipso*-C), 143.6 (*o*-C), 129.7 (*o*-C), 126.3 (*p*-C), 126.0 (*m*-C), 124.5 (*m*-C), 98.2 (γ -CH), 43.8 (d, $J_{\text{CP}} = 49$ Hz, Cy-CH), 29.1 (CHMe_2), 27.1, 26.9, 26.7, 26.7 (Cy- CH_2), 26.1 (CHMe_2), 25.6 (Cy- CH_2), 24.2 (NCMe). $^{31}\text{P}\{^1\text{H}\}$ NMR (161.72 MHz, C_6D_6 , 303 K): δ 84.6 ($J_{\text{PPb}} = 189$ Hz). ^{207}Pb NMR (83.83 MHz, C_6D_6 , 303 K): δ 1554 (d, $J_{\text{PbP}} = 159$ Hz).

$[\text{CH}\{(\text{CH}_3)\text{CN-2,6-}^i\text{Pr}_2\text{C}_6\text{H}_3\}_2\text{Ge(S)P}(\text{C}_6\text{H}_{11})_2]$, **$[(\text{BDI}_{\text{DIPP}})\text{Ge(S)PCy}_2]$, (54).**

$[(\text{BDI}_{\text{DIPP}})\text{GePCy}_2]$ (36) (0.19 g, 0.36 mmol) in toluene (15 mL) was added to an excess of elemental sulfur (0.04 g, 1.82 mmol) suspended in toluene (5 mL). The mixture was stirred vigorously at room temperature for 8 h. The yellow suspension was filtered through a pad of Celite and the volatiles were removed from the filtrate under vacuum. Yellow crystals of $[(\text{BDI}_{\text{DIPP}})\text{Ge(S)PCy}_2]$ (54) were obtained by recrystallisation of the residue from the minimum amount of tetrahydrofuran at $-30\text{ }^{\circ}\text{C}$. Yield: 0.15 g, 73%. ^1H NMR (499.91 MHz, C_6D_6 , 303 K): δ 7.13 (s, 6H, Ar-*H*), 4.72 (s, 1H, γ -CH), 3.86 (septet, $J = 6.5$ Hz, 2H, CHMe_2), 3.22 (septet, $J = 6.5$ Hz, 2H, CHMe_2), 2.84 (br, 2H, Cy- CH_2), 1.73 (d, $J = 6.5$ Hz, 6H, CHMe_2), 1.62 (d, $J = 6.5$ Hz, 6H, CHMe_2), 1.48 (m, 16H, NCMe , Cy- CH_2), 1.14 (d, $J = 6.5$ Hz, 6H, CHMe_2), 0.95 (d, $J = 7.0$ Hz, CHMe_2). $^{13}\text{C}\{^1\text{H}\}$ NMR (125.72 MHz, C_6D_6 , 303 K): δ 169.4 (NCMe), 147.5 (*ipso*-C), 145.8 (*o*-C), 137.3 (*o*-C), 129.5 (*p*-C), 126.6 (*m*-C), 125.0 (*m*-C), 98.2 (γ -CH), 42.9 (d, $J_{\text{CP}} = 42$ Hz, Cy-CH), 30.8, 29.3 (CHMe_2), 28.2 (CHMe_2), 27.2, 26.3, 26.3, 26.2 (Cy- CH_2), 25.8, 25.7, 24.6 (CHMe_2), 24.3 (NCMe). $^{31}\text{P}\{^1\text{H}\}$ NMR (161.72 MHz, C_6D_6 , 303K): δ -3.3.

$[\text{CH}\{(\text{CH}_3)\text{CN-2,6-}^i\text{Pr}_2\text{C}_6\text{H}_3\}_2\text{SnSeP(S)}(\text{C}_6\text{H}_{11})_2]$, **$[(\text{BDI}_{\text{DIPP}})\text{SnSeP(S)Cy}_2]$, (55).**

$[(\text{BDI}_{\text{DIPP}})\text{SnSePCy}_2]$ (46) (0.11 g, 0.13 mmol) in a 1:1 pentane/toluene (10 mL) solution and was added to elemental sulfur (4.0 mg, 0.13 mmol) in toluene (2 mL). After vigorous stirring for 30 minutes at room temperature, the mixture was filtered through a pad of Celite. The filtrate was concentrated and stored at $-30\text{ }^{\circ}\text{C}$. Bright yellow crystals of $[(\text{BDI}_{\text{DIPP}})\text{SnSeP(S)Cy}_2]$ (55) were obtained. Yield: 0.06 g, 52%. ^1H

NMR (399.50 MHz, C₆D₆, 303 K): δ 7.03–7.16 (m, 6H, Ar-*H*), 4.66 (s, 1H, γ -CH), 3.58 (br, 2H, CHMe₂), 3.18 (br, 2H, CHMe₂), 2.12 (s, 3H, NCM*e*), 1.58 (br, 10H, CHMe₂, Cy-CH, Cy-CH₂), 1.18 (d, $J = 6.4$ Hz, 10H, CHMe₂, Cy-CH₂), 1.02 (d, $J = 8.0$ Hz, 9H, CHMe₂, Cy-CH₂). ¹³C{¹H} NMR (100.46 MHz, C₆D₆, 303 K): δ 166.8 (NCMe), 142.3 (*ipso*-C), 129.7 (*o*-C), 128.9 (*o*-C), 126.8 (*p*-C), 126.0 (*m*-C), 125.1 (*m*-C), 96.7 (γ -CH), 43.2 (d, $J_{CP} = 43$ Hz, Cy-CH), 29.6, 29.5 (CHMe₂), 27.2, 27.1, 27.0, 26.9, 26.9 (Cy-CH₂), 25.6, 24.9, 23.9, 23.8 (CHMe₂), 21.8 (NCMe). ³¹P{¹H} NMR (161.72 MHz, C₆D₆, 303 K): δ 72.3 ($J_{PSe} = 490$ Hz, $J_{P^{119}Sn} = 209$ Hz and $J_{P^{117}Sn} = 200$ Hz). ⁷⁷Se NMR (76.19 MHz, C₆D₆, 303 K): δ -42 (d, $J_{SeP} = 490$ Hz). ¹¹⁹Sn NMR (148.96 MHz, C₆D₆, 303 K): δ -119 (d, $J_{119SnP} = 209$ Hz). ¹¹⁷Sn NMR (142.28 MHz, C₆D₆, 303 K): δ -119 (d, $J_{117SnP} = 205$ Hz).

[CH{(CH₃)CN-2,6-ⁱPr₂C₆H₃}₂Ge(Se)P(Si(CH₃)₃)₂], [(BDI_{DIPP})Ge(Se)P(SiMe₃)₂], (56). [(BDI_{DIPP})GeP(SiMe₃)₂] (40) (0.37 g, 0.55 mmol) in diethyl ether (15 mL) was added to an excess of elemental selenium (0.13 g, 1.64 mmol) suspended in diethyl ether (5 mL). The mixture was stirred rapidly at room temperature and filtered through a pad of Celite after 20 h. Volatiles were removed from the filtrate under vacuum. The residue was washed with *n*-hexane (3 × 5 mL). Yellow crystals of [(BDI_{DIPP})Ge(Se)P(SiMe₃)₂] (56) were obtained from a minimum amount of toluene at -30 °C. Yield: 0.25 g, 61%. ¹H NMR (399.50 MHz, C₆D₆, 303K): δ 7.18 (s, 6H, Ar-*H*), 4.90 (s, 1H, γ -CH), 3.60 (septet, $J = 6.8$ Hz, 4H, CHMe₂), 1.59 (d, $J = 6.4$ Hz, 12H, CHMe₂), 1.56 (s, 6H, NCM*e*), 1.22 (d, $J = 6.8$ Hz, 6H, CHMe₂), 1.06 (d, $J = 6.8$ Hz, 6H, CHMe₂), 0.50 (d, $J = 6.0$ Hz, 6H, SiMe₃), 0.42 (d, $J = 6.0$ Hz, 6H, SiMe₃). ³¹P{¹H} NMR (161.72 MHz, C₆D₆, 303K): δ -172.6 ($J_{PSe} = 52$ Hz, $J_{PSi} = 26$ Hz). ⁷⁷Se NMR (76.19 MHz, C₆D₆, 303K): δ -129 (d, $J_{SeP} = 49$ Hz). Anal. Calcd. for C₃₅H₅₉GeN₂PSeSi₂ (746.54): C, 56.30; H, 7.97; N, 3.75%. Found: C, 56.25; H, 7.92; N, 3.79%.

[CH{(CH₃)CN-2,6-ⁱPr₂C₆H₃}₂SnSeSi(CH₃)₃], [(BDI_{DIPP})SnSeSiMe₃], (57). [(BDI_{DIPP})SnP(SiMe₃)₂] (41) (0.19 g, 0.26 mmol) in toluene (15 mL) was added to an excess of elemental selenium (0.10 g, 1.32 mmol) suspended in toluene (5 mL). The mixture was stirred vigorously at room temperature for 20 h and the yellow suspension was filtered through a pad of Celite. Volatiles were removed from the filtrate and the

residue was washed with *n*-hexane (3 × 5 mL). Yellow crystals of [(BDI_{DIPP})SnSeSiMe₃] (**57**) were obtained by recrystallisation from toluene at -30 °C. Yield: 0.11 g, 61 %. ¹H NMR (399.50 MHz, C₆D₆, 303 K): δ 7.21 (dd, *J* = 7.6, 1.2 Hz, 2H, *m*-H), 7.13 (t, *J* = 7.6 Hz, 2H, *p*-H), 7.07 (dd, *J* = 7.6, 1.2 Hz, 2H, *m*-H), 4.79 (s, 1H, *γ*-CH), 3.90 (septet, *J* = 6.8 Hz, 2H, CHMe₂), 3.29 (septet, *J* = 6.8 Hz, 2H, CHMe₂), 1.61 (s, 6H, NCMe), 1.60 (d, *J* = 6.4 Hz, 6H, CHMe₂), 1.34 (d, *J* = 7.2 Hz, 6H, CHMe₂), 1.23 (d, *J* = 6.8 Hz, 6H, CHMe₂), 1.14 (d, *J* = 6.8 Hz, 6H, CHMe₂), 0.26 (s, 9H, SiMe₃). ¹³C{¹H} NMR (100.46 MHz, C₆D₆, 303 K): δ 167.2 (NCMe), 145.7 (*ipso*-C), 143.7 (*o*-C), 142.2 (*o*-C), 127.4 (*p*-C), 125.3 (*m*-C), 124.7 (*m*-C), 98.5 (*γ*-CH), 29.3, 29.0 (CHMe₂), 27.0, 26.2, 25.2, 25.1 (CHMe₂), 24.4 (NCMe), 6.2 (SiMe₃). ¹¹⁹Sn NMR (148.96 MHz, C₆D₆, 303 K): δ 87. ⁷⁷Se NMR (76.19 MHz, C₆D₆, 303 K): δ -176. ²⁹Si{¹H} NMR (79.37 MHz, C₆D₆, 303 K): δ 7.4. IR (Nujol, *v*/cm⁻¹): 1524 (s), 1314 (s), 1170 (s), 1021 (s), 936 (s). Anal. Calcd. for C₃₂H₅₀N₂SeSiSn (688.51): C, 55.82; H, 7.32; N, 4.07%. Found: C, 55.91; H, 7.32; N, 3.94%.

6. References

1. Claudio, E. S.; Godwin, H. A.; Magyar, J. S. *Progress in Inorganic Chemistry, Vol 51* **2003**, 51, 1.
2. Settle, D. M.; Patterson, C. C. *Science* **1980**, 207, 1167.
3. Hong, S. M.; Candelone, J. P.; Patterson, C. C.; Boutron, C. F. *Science* **1994**, 265, 1841.
4. Shreir, L. L.; Jarman, R. A.; Burstein, G. T., *Corrosion - Corrosion Control*. 3rd. ed.; Butterworth-Heinemann: Oxford, U.K., 1994; Vol. 2.
5. Nriagu, J. O. *Sci. Total Environ.* **1990**, 92, 13.
6. Hawkes, N. J. *Power Sources* **1997**, 67, 213.
7. Wallace, G. J. *2008 Minerals Yearbook - Lead*; U.S. Geological Survey Publications U.S.A., 2010.
8. Mielke, H. W.; Reagan, P. L. *Environ. Health Perspect.* **1998**, 106, 217.
9. Olson, K. W.; Skogerboe, R. K. *Environ. Sci. Technol.* **1975**, 9, 227.
10. Lagerwer, Jv; Specht, A. W. *Environ. Sci. Technol.* **1970**, 4, 583.
11. De Vleeschouwer, F.; Gerard, L.; Goormaghtigh, C.; Mattielli, N.; Le Roux, G.; Fagel, N. *Sci. Total Environ.* **2007**, 377, 282.
12. Jarup, L. *Br. Med. Bull.* **2003**, 68, 167.
13. Manahan, S. E., *Toxicological Chemistry and Biochemistry*. 3rd. ed.; CRC Press: U.S.A., 2003.
14. Bellinger, D. C.; Stiles, K. M.; Needleman, H. L. *Pediatrics* **1992**, 90, 855.
15. Shannon, M. W.; Best, D.; Binns, H. J.; Kim, J. J.; Mazur, L. J.; Weil, W. B.; Johnson, C. L.; Reynolds, D. W.; Roberts, J. R.; Blackburn, E.; Johnson, R. H.; Linet, M.; Rogan, W. J.; Spire, P.; Comm Environ, H. *Pediatrics* **2005**, 116, 1036.
16. Needleman, H. *Annu. Rev. Med.* **2004**, 55, 209.
17. Bolger, P. M.; Yess, N. J.; Gunderson, E. L.; Troxell, T. C.; Carrington, C. D. *Food Addit. Contam.* **1996**, 13, 53.
18. Goyer, R. A. *Environ. Health Perspect.* **1993**, 100, 177.

19. Graber, L. K.; Asher, D.; Anandaraja, N.; Bopp, R. F.; Merrill, K.; Cullen, M. R.; Luboga, S.; Trasande, L. *Environ. Health Perspect.* **2010**, *118*, 884.
20. He, K. M.; Wang, S. Q.; Zhang, J. L. *Sci. Total Environ.* **2009**, *407*, 3986.
21. Chen, H. Y.; Li, A. J.; Finlow, D. E. *J. Power Sources* **2009**, *191*, 22.
22. Parr, J. *Polyhedron* **1997**, *16*, 551.
23. Paver, M. A.; Russell, C. A.; Wright, D. S. *Angew. Chem.-Int. Edit. Engl.* **1995**, *34*, 1545.
24. Gade, L. H. *Eur. J. Inorg. Chem.* **2002**, 1257.
25. Leung, W. P.; So, C. W.; Wu, Y. S.; Li, H. W.; Mak, T. C. W. *Eur. J. Inorg. Chem.* **2005**, 513.
26. Stasch, A.; Forsyth, C. M.; Jones, C.; Junk, P. C. *New J. Chem.* **2008**, *32*, 829.
27. Jones, C. J. *Chem. Soc. Rev.* **1998**, *27*, 289.
28. Costamagna, J.; Ferraudi, G.; Matsuhiro, B.; Campos-Vallette, M.; Canales, J.; Villagran, M.; Vargas, J.; Aguirre, M. J. *Coord. Chem. Rev.* **2000**, *196*, 125.
29. Schmidtchen, F. P.; Berger, M. *Chem. Rev.* **1997**, *97*, 1609.
30. Cissell, J. A.; Vaid, T. P.; Yap, G. P. A. *J. Am. Chem. Soc.* **2007**, *129*, 7841.
31. Kroenke, W. J.; Kenney, M. E. *Inorg. Chem.* **1964**, *3*, 251.
32. Ukei, K. *Acta Crystallogr. Sect. B: Struct. Sci.* **1973**, *B 29*, 2290.
33. Park, I. H.; Park, K. M.; Lee, S. S. *Dalton. Trans.* **2010**, *39*, 9696.
34. Agustin, D.; Rima, G.; Gornitzka, H.; Barrau, J. J. *J. Organomet. Chem.* **1999**, *592*, 1.
35. Barker, J.; Kilner, M. *Coord. Chem. Rev.* **1994**, *133*, 219.
36. Nimitsiriwat, N.; Gibson, V. C.; Marshall, E. L.; White, A. J. P.; Dale, S. H.; Elsegood, M. R. J. *Dalton. Trans.* **2007**, 4464.
37. Dias, H. V. R.; Jin, W. C. *J. Am. Chem. Soc.* **1996**, *118*, 9123.
38. Coles, M. P.; Swenson, D. C.; Jordan, R. F.; Young, V. G. *Organometallics* **1997**, *16*, 5183.

39. Dias, H. V. R.; Jin, W. C.; Ratcliff, R. E. *Inorg. Chem.* **1995**, *34*, 6100.
40. Dove, A. P.; Gibson, V. C.; Marshall, E. L.; Rzepa, H. S.; White, A. J. P.; Williams, D. J. *J. Am. Chem. Soc.* **2006**, *128*, 9834.
41. Feldman, J.; McLain, S. J.; Parthasarathy, A.; Marshall, W. J.; Calabrese, J. C.; Arthur, S. D. *Organometallics* **1997**, *16*, 1514.
42. Burford, N.; D'Eon, M.; Ragogna, P. J.; McDonald, R.; Ferguson, M. J. *Inorg. Chem.* **2004**, *43*, 734.
43. Budzelaar, P. H. M.; van Oort, A. B.; Orpen, A. G. *Eur. J. Inorg. Chem.* **1998**, 1485.
44. Hamaki, H.; Takeda, N.; Yamasaki, T.; Sasamori, T.; Tokitoh, N. *J. Organomet. Chem.* **2007**, *692*, 44.
45. Bradley, A. Z.; Thorn, D. L.; Glover, G. V. *J. Org. Chem.* **2008**, *73*, 8673.
46. Ayala, C. N.; Chisholm, M. H.; Gallucci, J. C.; Krempner, C. *Dalton. Trans.* **2009**, 9237.
47. Smith, J. M.; Sadique, A. R.; Cundari, T. R.; Rodgers, K. R.; Lukat-Rodgers, G.; Lachicotte, R. J.; Flaschenriem, C. J.; Vela, J.; Holland, P. L. *J. Am. Chem. Soc.* **2006**, *128*, 756.
48. Bourget-Merle, L.; Lappert, M. F.; Severn, J. R. *Chem. Rev.* **2002**, *102*, 3031.
49. Green, S. P.; Jones, C.; Stasch, A. *Science* **2007**, *318*, 1754.
50. Bonyhady, S. J.; Green, S. P.; Jones, C.; Nembenna, S.; Stasch, A. *Angew. Chem. Int. Ed.* **2009**, *48*, 2973.
51. Monillas, W. H.; Yap, G. P. A.; MacAdams, L. A.; Theopold, K. H. *J. Am. Chem. Soc.* **2007**, *129*, 8090.
52. Drouin, F.; Oguadinma, P. O.; Whitehorne, T. J. J.; Prud'homme, R. E.; Schaper, F. *Organometallics* **2010**, *29*, 2139.
53. Cheng, M.; Attygalle, A. B.; Lobkovsky, E. B.; Coates, G. W. *J. Am. Chem. Soc.* **1999**, *121*, 11583.
54. Vidovic, D.; Moore, J. A.; Jones, J. N.; Cowley, A. H. *J. Am. Chem. Soc.* **2005**, *127*, 4566.
55. Vidovic, D.; Lu, Z.; Reeske, G.; Moore, J. A.; Cowley, A. H. *Chem. Commun.* **2006**, 3501.

56. Lu, Z.; Findlater, M.; Cowley, A. H. *Chem. Commun.* **2008**, 184.
57. Bambirra, S.; Perazzolo, F.; Boot, S. J.; Sciarone, T. J. J.; Meetsma, A.; Hessen, B. *Organometallics* **2008**, *27*, 704.
58. Pyykko, P. *Chem. Rev.* **1988**, *88*, 563.
59. Patai, S., *The chemistry of organic germanium, tin and lead compounds*. John Wiley & Sons, Ltd.: West Sussex, England, 1995; Vol. 1.
60. Kaupp, M.; Schleyer, P. V. *J. Am. Chem. Soc.* **1993**, *115*, 1061.
61. Shimoni-Livny, L.; Glusker, J. P.; Bock, C. W. *Inorg. Chem.* **1998**, *37*, 1853.
62. Chen, M.; Fulton, J. R.; Hitchcock, P. B.; Johnstone, N. C.; Lappert, M. F.; Protchenko, A. V. *Dalton. Trans.* **2007**, 2770.
63. Cox, H.; Stace, A. J. *J. Am. Chem. Soc.* **2004**, *126*, 3939.
64. Soudi, A. A.; Marandi, F.; Ramazani, A.; Ahmadi, E.; Morsali, A. *Comptes Rendus Chimie* **2005**, *8*, 157.
65. Ding, Y. Q.; Roesky, H. W.; Noltemeyer, M.; Schmidt, H. G.; Power, P. P. *Organometallics* **2001**, *20*, 1190.
66. Ding, Y. Q.; Hao, H. J.; Roesky, H. W.; Noltemeyer, M.; Schmidt, H. G. *Organometallics* **2001**, *20*, 4806.
67. Jana, A.; Roesky, H. W.; Schulzke, C.; Doring, A.; Back, T.; Pal, A.; Herbst-Irmer, R. *Inorg. Chem.* **2009**, *48*, 193.
68. Ayers, A. E.; Klapotke, T. M.; Dias, H. V. R. *Inorg. Chem.* **2001**, *40*, 1000.
69. Doyle, D. J.; Hitchcock, P. B.; Lappert, M. F.; Li, G. *J. Organomet. Chem.* **2009**, *694*, 2611.
70. Jana, A.; Sarish, S. P.; Roesky, H. W.; Schulzke, C.; Döring, A.; John, M. *Organometallics* **2009**, *28*, 2563.
71. Pineda, L. W.; Jancik, V.; Starke, K.; Oswald, R. B.; Roesky, H. W. *Angew. Chem. Int. Ed.* **2006**, *45*, 2602.
72. Jana, A.; Roesky, H. W.; Schulzke, C.; Doring, A. *Angew. Chem. Int. Ed.* **2009**, *48*, 1106.
73. Jana, A.; Roesky, H. W.; Schulzke, C. *Inorg. Chem.* **2009**, *48*, 9543.

74. Jana, A.; Ghoshal, D.; Roesky, H. W.; Objartel, I.; Schwab, G.; Stalke, D. *J. Am. Chem. Soc.* **2009**, *131*, 1288.
75. Jana, A.; Sen, S. S.; Roesky, H. W.; Schulzke, C.; Dutta, S.; Pati, S. K. *Angew. Chem. Int. Ed.* **2009**, *48*, 4246.
76. Ciesiolka, J.; Michalowski, D.; Wrzesinski, J.; Krajewski, J.; Krzyzosiak, W. J. *J. Mol. Biol.* **1998**, *275*, 211.
77. Brown, R. S.; Dewan, J. C.; Klug, A. *Biochemistry* **1985**, *24*, 4785.
78. Brown, R. S.; Hingerty, B. E.; Dewan, J. C.; Klug, A. *Nature* **1983**, *303*, 543.
79. Winterme, W.; Zachau, H. G. *Biochim. Biophys. Acta* **1973**, *299*, 82.
80. Farkas, W. R. *Biochim. Biophys. Acta* **1968**, *155*, 401.
81. Dahm, S. C.; Derrick, W. B.; Uhlenbeck, O. C. *Biochemistry* **1993**, *32*, 13040.
82. Cech, T. R.; Bass, B. L. *Annu. Rev. Biochem* **1986**, *55*, 599.
83. Ciesiolka, J.; Hardt, W. D.; Schlegl, J.; Erdmann, V. A.; Hartmann, R. K. *Eur. J. Biochem.* **1994**, *219*, 49.
84. Cuesta, L.; Hevia, E.; Morales, D.; Perez, J.; Riera, L.; Miguel, D. *Organometallics* **2006**, *25*, 1717.
85. Bergman, R. G. *Polyhedron* **1995**, *14*, 3227.
86. Fulton, J. R.; Holland, A. W.; Fox, D. J.; Bergman, R. G. *Acc. Chem. Res.* **2002**, *35*, 44.
87. Woerpel, K. A.; Bergman, R. G. *J. Am. Chem. Soc.* **1993**, *115*, 7888.
88. Glueck, D. S.; Winslow, L. J. N.; Bergman, R. G. *Organometallics* **1991**, *10*, 1462.
89. Brombacher, H.; Vahrenkamp, H. *Inorg. Chem.* **2004**, *43*, 6042.
90. Rombach, M.; Brombacher, H.; Vahrenkamp, H. *Eur. J. Inorg. Chem.* **2002**, *2002*, 153.
91. Gerbino, D. C.; Hevia, E.; Morales, D.; Clemente, M. E. N.; Perez, J.; Riera, L.; Riera, V.; Miguel, D. *Chem. Commun.* **2003**, 328.
92. Yeguas, V.; Campomanes, P.; Lopez, R. *Dalton. Trans.* **2010**, *39*, 874.
93. Suh, S.; Hoffman, D. M. *Inorg. Chem.* **1996**, *35*, 6164.

94. Fjeldberg, T.; Hitchcock, P. B.; Lappert, M. F.; Smith, S. J.; Thorne, A. J. *J. Chem. Soc., Chem. Commun.* **1985**, 939.
95. Veith, M.; Mathur, C.; Huch, V. *Organometallics* **1996**, *15*, 2858.
96. Veith, M.; Mathur, C.; Mathur, S.; Huch, V. *Organometallics* **1997**, *16*, 1292.
97. Jutzi, P.; Keitemeyer, S.; Neumann, B.; Stammler, H.-G. *Organometallics* **1999**, *18*, 4778.
98. Chisholm, M. H.; Gallucci, J.; Phomphrai, K. *Inorg. Chem.* **2002**, *41*, 2785.
99. Fan, H. J.; Adhikari, D.; Saleh, A. A.; Clark, R. L.; Zuno-Cruz, F. J.; Cabrera, G. S.; Huffman, J. C.; Pink, M.; Mindiola, D. J.; Baik, M. H. *J. Am. Chem. Soc.* **2008**, *130*, 17351.
100. Yang, Y.; Schulz, T.; John, M.; Yang, Z.; Jiménez-Pérez, V. M.; Roesky, H. W.; Gurubasavaraj, P. M.; Stalke, D.; Ye, H. *Organometallics* **2008**, *27*, 769.
101. Yang, Y.; Gurubasavaraj, P. M.; Ye, H. Q.; Zhang, Z. S.; Roesky, H. W.; Jones, P. G. *J. Organomet. Chem.* **2008**, *693*, 1455.
102. Seifert, A.; Scheid, D.; Linti, G.; Zessin, T. *Chem. Eur. J.* **2009**, *15*, 12114.
103. Yao, S.; Block, S.; Brym, M.; Driess, M. *Chem. Commun.* **2007**, 3844.
104. Jana, A.; Roesky, H. W.; Schulzke, C.; Samuel, P. P. *Organometallics* **2010**, *29*, 4837.
105. Jana, A.; Nekoueishahraki, B.; Roesky, H. W.; Schulzke, C. *Organometallics* **2009**, *28*, 3763.
106. Driess, M.; Yao, S.; Brym, M.; van Wuelen, C. *Angew. Chem. Int. Ed.* **2006**, *45*, 4349.
107. Pineda, L. W.; Jancik, V.; Roesky, H. W.; Necuali, D.; Neculai, A. M. *Angew. Chem. Int. Ed.* **2004**, *43*, 1419.
108. Jana, A.; Roesky, H. W.; Schulzke, C. *Dalton. Trans.* **2010**, *39*, 132.
109. Pineda, L. W.; Jancik, V.; Roesky, H. W.; Herbst-Irmer, R. *Inorg. Chem.* **2005**, *44*, 3537.
110. Yang, Y.; Roesky, H. W.; Jones, P. G.; So, C.-W.; Zhang, Z.; Herbst-Irmer, R.; Ye, H. *Inorg. Chem.* **2007**, *46*, 10860.
111. Jana, A.; Sarish, S. P.; Roesky, H. W.; Schulzke, C.; Samuel, P. P. *Chem. Commun.* **2010**, *46*, 707.

112. Mandal, S. K.; Roesky, H. W. *Chem. Commun.* **2010**, *46*, 6016.
113. Johnstone, N. C. Aluminium and lead complexes of nitrogen/oxygen donor ligands : Cyclic ester polymerisation and studies towards the understanding of lead induced RNA cleavage. University of Sussex, Sussex, 2009.
114. Tam, E. C. Y.; Johnstone, N. C.; Ferro, L.; Hitchcock, P. B.; Fulton, J. R. *Inorg. Chem.* **2009**, *48*, 8971.
115. Maksic, Z. B.; Kovacevic, B. *J. Chem. Soc.-Perkin Trans. 2* **1999**, 2623.
116. Bordwell, F. G. *Acc. Chem. Res.* **1988**, *21*, 456.
117. Fulton, J. R.; Hitchcock, P. B.; Johnstone, N. C.; Tam, E. C. Y. *Dalton. Trans.* **2007**, 3360.
118. Scherf, G. W. H.; Brown, R. K. *Can. J. Chem./Rev. Can. Chim.* **1960**, *38*, 697.
119. Bordwell, F. G.; McCollum, G. J. *J. Org. Chem.* **1976**, *41*, 2391.
120. Barnes, D.; Brown, G. L.; Brownhill, M.; German, I.; Herbert, C. J.; Jolleys, A.; Kennedy, A. R.; Liu, B.; McBride, K.; Mair, F. S.; Pritchard, R. G.; Sanders, A.; Warren, J. E. *Eur. J. Inorg. Chem.* **2009**, *2009*, 1219.
121. Stender, M.; Wright, R. J.; Eichler, B. E.; Prust, J.; Olmstead, M. M.; Roesky, H. W.; Power, P. P. *J. Chem. Soc., Dalton Trans.* **2001**, 3465.
122. Cordero, B.; Gomez, V.; Platero-Prats, A. E.; Reves, M.; Echeverria, J.; Cremades, E.; Barragan, F.; Alvarez, S. *Dalton. Trans.* **2008**, 2832.
123. Hirano, M.; Akita, M.; Tani, K.; Kumagai, K.; Kasuga, N. C.; Fukuoka, A.; Komiyama, S. *Organometallics* **1997**, *16*, 4206.
124. Alvarez, R.; Carmona, E.; Marin, J. M.; Poveda, M. L.; Gutierrez-Puebla, E.; Monge, A. *J. Am. Chem. Soc.* **1986**, *108*, 2286.
125. Castro-Rodriguez, I.; Nakai, H.; Zakharov, L. N.; Rheingold, A. L.; Meyer, K. *Science* **2004**, *305*, 1757.
126. Simpson, R. D.; Bergman, R. G. *Organometallics* **1992**, *11*, 4306.
127. Campora, J.; Matas, I.; Palma, P.; Alvarez, E.; Graiff, C.; Tiripicchio, A. *Organometallics* **2007**, *26*, 3840.
128. Ferro, L.; Hitchcock, P. B.; Coles, M. P.; Cox, H.; Fulton, J. R. *Inorg. Chem.* **2011**, *50*, 1879.

129. Bryndza, H. E.; Fong, L. K.; Paciello, R. A.; Tam, W.; Bercaw, J. E. *J. Am. Chem. Soc.* **1987**, *109*, 1444.
130. Olmstead, W. N.; Margolin, Z.; Bordwell, F. G. *J. Org. Chem.* **1980**, *45*, 3295.
131. Brauman, J. I.; Blair, L. K. *J. Am. Chem. Soc.* **1968**, *90*, 6561.
132. Brauman, J. I.; Blair, L. K. *J. Am. Chem. Soc.* **1970**, *92*, 5986.
133. Hevia, E.; Pérez, J.; Riera, L.; Riera, V.; del Río, I.; García-Granda, S.; Miguel, D. *Chem. Eur. J.* **2002**, *8*, 4510.
134. Yao, S.; Brym, M.; Merz, K.; Driess, M. *Organometallics* **2008**, *27*, 3601.
135. Hitchcock, P. B.; Lappert, M. F.; Protchenko, A. V. *Chem. Commun.* **2005**, 951.
136. Akkari, A.; Byrne, J. J.; Saur, I.; Rima, G.; Gornitzka, H.; Barrau, J. *J. Organomet. Chem.* **2001**, *622*, 190.
137. Saur, I.; Miqueu, K.; Rima, G.; Barrau, J.; Lemierre, V.; Chrostowska, A.; Sotiropoulos, J. M.; Pfister-Guillouzo, G. *Organometallics* **2003**, *22*, 3143.
138. Hitchcock, P. B.; Lappert, M. F.; Liu, D. S. *J. Chem. Soc., Chem. Commun.* **1994**, 1699.
139. Phillips, A. D.; Zava, O.; Scopelitti, R.; Nazarov, A. A.; Dyson, P. J. *Organometallics* **2010**, *29*, 417.
140. Annibale, V. T.; Lund, L. M.; Song, D. *Chem. Commun.* **2010**, *46*, 8261.
141. Uhl, W.; Jana, B. *Chem. Eur. J.* **2008**, *14*, 3067.
142. Davidovich, R. L.; Stavila, V.; Marinin, D. V.; Voit, E. I.; Whitmire, K. H. *Coord. Chem. Rev.* **2009**, *253*, 1316.
143. Cole, M. L.; Jones, C.; Junk, P. C.; Kloth, M.; Stasch, A. *Chem. Eur. J.* **2005**, *11*, 4482.
144. Zhang, B. S. *Acta Crystallogr. Sect. E: Struct. Rep. Online* **2009**, *65*, M1167.
145. Hitchcock, P. B.; Lappert, M. F.; Wang, Z. X. *J. Organomet. Chem.* **2006**, *691*, 2748.
146. Baba, I.; Farina, Y.; Othman, A. H.; Razak, I. A.; Fun, H. K.; Ng, S. W. *Acta Crystallogr. Sect. E: Struct. Rep. Online* **2001**, *57*, M35.

147. MacAdams, L. A.; Kim, W.-K.; Liable-Sands, L. M.; Guzei, I. A.; Rheingold, A. L.; Theopold, K. H. *Organometallics* **2002**, *21*, 952.
148. Shimokawa, C.; Yokota, S.; Tachi, Y.; Nishiwaki, N.; Ariga, M.; Itoh, S. *Inorg. Chem.* **2003**, *42*, 8395.
149. Harder, S. *Organometallics* **2002**, *21*, 3782.
150. Shannon, R. D. *Acta Crystallogr. Sect. A: Found. Crystallogr.* **1976**, *32*, 751.
151. Gibson, V. C.; Segal, J. A.; White, A. J. P.; Williams, D. J. *J. Am. Chem. Soc.* **2000**, *122*, 7120.
152. Harder, S. *Angew. Chem. Int. Ed.* **2004**, *43*, 2714.
153. Parks, J. E.; Holm, R. H. *Inorg. Chem.* **1968**, *7*, 1408.
154. Tian, X.; Goddard, R.; Porschke, K. R. *Organometallics* **2006**, *25*, 5854.
155. Tang, L. M.; Duan, Y. Q.; Li, X. F.; Li, Y. S. *J. Organomet. Chem.* **2006**, *691*, 2023.
156. Cheng, M.; Moore, D. R.; Reczek, J. J.; Chamberlain, B. M.; Lobkovsky, E. B.; Coates, G. W. *J. Am. Chem. Soc.* **2001**, *123*, 8738.
157. Bonyhady, S. J.; Jones, C.; Nembenna, S.; Stasch, A.; Edwards, A. J.; McIntyre, G. J. *Chem. Eur. J.* **2010**, *16*, 938.
158. Breitmaier, E., *Structure Elucidation by NMR in Organic Chemistry: A Practical Guide*. John Wiley & Sons, Ltd.: West Sussex, England, 2002.
159. For further information, please contact Dr. Iain J. Day. Email: i.j.day@sussex.ac.uk.
160. Al-Juaid, S. S.; Avent, A. G.; Eaborn, C.; Hill, M. S.; Hitchcock, P. B.; Patel, D. J.; Smith, J. D. *Organometallics* **2001**, *20*, 1223.
161. Tiekink, E. R. T.; Zukerman-Schpector, J. *Aust. J. Chem.* **2010**, *63*, 535.
162. Frank, W.; Wittmer, F.-G. *Chem. Ber.* **1997**, *130*, 1731.
163. Peedikakkal, A. M. P.; Vittal, J. J. *Cryst. Growth Des.* **2011**, *11*, 4697.
164. Goel, S. C.; Chiang, M. Y.; Buhro, W. E. *Inorg. Chem.* **1990**, *29*, 4640.
165. Schulz, S.; Eisenmann, T.; Blaser, D.; Boese, R. *Z. Anorg. Allg. Chem.* **2009**, *635*, 995.

166. Hadzovic, A.; Song, D. T. *Inorg. Chem.* **2008**, *47*, 12010.
167. Biyikal, M.; Lohnwitz, K.; Meyer, N.; Dochnahl, M.; Roesky, P. W.; Blechert, S. *Eur. J. Inorg. Chem.* **2010**, 1070.
168. Nishio, M. *Crystengcomm* **2004**, *6*, 130.
169. Filippou, A. C.; Weidemann, N.; Schnakenburg, G.; Rohde, H.; Philippopoulos, A. I. *Angew. Chem. Int. Ed.* **2004**, *43*, 6512.
170. Harris, L. A. M.; Coles, M. P.; Fulton, J. R. *Inorg. Chim. Acta* **2011**, *369*, 97.
171. Rao, C. N. R.; Deepak, F. L.; Gundiah, G.; Govindaraj, A. *Prog. Solid State Chem.* **2003**, *31*, 5.
172. Qian, C.; Kim, F.; Ma, L.; Tsui, F.; Yang, P. D.; Liu, J. *J. Am. Chem. Soc.* **2004**, *126*, 1195.
173. Phillips, D. C.; Sawhill, S. J.; Self, R.; Bussell, M. E. *J. Catal.* **2002**, *207*, 266.
174. Wang, X. Q.; Clark, P.; Oyama, S. T. *J. Catal.* **2002**, *208*, 321.
175. Oyama, S. T. *J. Catal.* **2003**, *216*, 343.
176. Burford, N.; Ragona, P. J.; Robertson, K. N.; Cameron, T. S.; Hardman, N. J.; Power, P. P. *J. Am. Chem. Soc.* **2002**, *124*, 382.
177. Crimmin, M. R.; Barrett, A. G. M.; Hill, M. S.; Hitchcock, P. B.; Procopiu, P. A. *Organometallics* **2007**, *26*, 2953.
178. Maassarani, F.; Davidson, M. F.; Wehmanooeyvaar, I. C. M.; Grove, D. M.; Vankoten, M. A.; Smeets, W. J. J.; Spek, A. L.; Vankoten, G. *Inorg. Chim. Acta* **1995**, *235*, 327.
179. Carrano, C. J.; Cowley, A. H.; Giolando, D. M.; Jones, R. A.; Nunn, C. M.; Power, J. M. *Inorg. Chem.* **1988**, *27*, 2709.
180. Arif, A. M.; Benac, B. L.; Cowley, A. H.; Geerts, R.; Jones, R. A.; Kidd, K. B.; Power, J. M.; Schwab, S. T. *J. Chem. Soc., Chem. Commun.* **1986**, 1543.
181. Tardif, O.; Nishiura, M.; Hou, Z. M. *Tetrahedron* **2003**, *59*, 10525.
182. Bredeau, S.; Altenhoff, G.; Kunz, K.; Doring, S.; Grimme, S.; Kehr, G.; Erker, G. *Organometallics* **2004**, *23*, 1836.
183. Ishiyama, T.; Miyoshi, K.; Nakazawa, H. *J. Mol. Catal. A: Chem.* **2004**, *221*, 41.
184. Planas, J. G.; Gladysz, J. A. *Inorg. Chem.* **2002**, *41*, 6947.

185. Littke, A. F.; Fu, G. C. *Angew. Chem. Int. Ed.* **1998**, *37*, 3387.
186. Scriban, C.; Wicht, D. K.; Glueck, D. S.; Zakharov, L. N.; Golen, J. A.; Rheingold, A. L. *Organometallics* **2006**, *25*, 3370.
187. Buhro, W. E.; Zwick, B. D.; Georgiou, S.; Hutchinson, J. P.; Gladysz, J. A. *J. Am. Chem. Soc.* **1988**, *110*, 2427.
188. Weber, L.; Uthmann, S.; Stammler, H. G.; Neumann, B.; Schoeller, W. W.; Boese, R.; Blaser, D. *Eur. J. Inorg. Chem.* **1999**, 2369.
189. Clegg, W.; Izod, K.; Liddle, S. T. *J. Organomet. Chem.* **2000**, *613*, 128.
190. Weber, L.; Meine, G.; Boese, R.; Augart, N. *Organometallics* **1987**, *6*, 2484.
191. Rogers, J. R.; Wagner, T. P. S.; Marynick, D. S. *Inorg. Chem.* **1994**, *33*, 3104.
192. Levin, C. C. *J. Am. Chem. Soc.* **1975**, *97*, 5649.
193. Bouhadir, G.; Bourissou, D. *Chem. Soc. Rev.* **2004**, *33*, 210.
194. Driess, M.; Merz, K.; Monse, C. Z. *Anorg. Allg. Chem.* **2000**, *626*, 2264.
195. Fischer, R. C.; Power, P. P. *Chem. Rev.* **2010**, *110*, 3877.
196. Power, P. P. *Chem. Rev.* **1999**, *99*, 3463.
197. Lide, D. R., *CRC handbook of chemistry and physics*. 85th. ed.; CRC Press: New York, 2004.
198. Eaborn, C.; Smith, J. D. *J. Chem. Soc., Dalton Trans.* **2001**, 1541.
199. Brook, M. A., *Silicon in organic, organometallic, and polymer chemistry*. John Wiley and Sons: New York, 2000.
200. Pitt, C. G. *J. Organomet. Chem.* **1973**, *61*, 49.
201. Baker, R. T.; Whitney, J. F.; Wreford, S. S. *Organometallics* **1983**, *2*, 1049.
202. Baker, R. T.; Krusic, P. J.; Tulip, T. H.; Calabrese, J. C.; Wreford, S. S. *J. Am. Chem. Soc.* **1983**, *105*, 6763.
203. Melenkivitz, R.; Mindiola, D. J.; Hillhouse, G. L. *J. Am. Chem. Soc.* **2002**, *124*, 3846.
204. Couret, C.; Escudié, J.; Satge, J.; Raharinirina, A.; Andriamizaka, J. D. *J. Am. Chem. Soc.* **1985**, *107*, 8280.

205. Ranaivonjatovo, H.; Escudié, J.; Couret, C.; Satge, J. *J. Chem. Soc., Chem. Commun.* **1992**, 1047.
206. Johnson, B. P.; Almstatter, S.; Dielmann, F.; Bodensteiner, M.; Scheer, M. *Z. Anorg. Allg. Chem.* **2010**, 636, 1275.
207. Gerstein, B. C., Nuclear Magnetic Resonance (NMR). In *Encyclopedia of Physical Science and Technology (Third Edition)*, Editor-in-Chief: Robert, A. M., Ed. Academic Press: New York, 2003; pp 701.
208. Drager, M.; Escudle, J.; Couret, C.; Ranaivonjatovo, H.; Satge, J. *Organometallics* **1988**, 7, 1010.
209. Ranaivonjatovo, H.; Escudié, J.; Couret, C.; Satge, J.; Drager, M. *New J. Chem.* **1989**, 13, 389.
210. Lee, V. Y.; Kawai, M.; Sekiguchi, A.; Ranaivonjatovo, H.; Escudié, J. *Organometallics* **2009**, 28, 4262.
211. Driess, M.; Janoschek, R.; Pritzkow, H.; Rell, S.; Winkler, U. *Angew. Chem.-Int. Edit. Engl.* **1995**, 34, 1614.
212. Izod, K.; Stewart, J.; Clark, E. R.; McFarlane, W.; Allen, B.; Clegg, W.; Harrington, R. W. *Organometallics* **2009**, 28, 3327.
213. Izod, K.; McFarlane, W.; Allen, B.; Clegg, W.; Harrington, R. W. *Organometallics* **2005**, 24, 2157.
214. Arif, A. M.; Cowley, A. H.; Jones, R. A.; Power, J. M. *J. Chem. Soc., Chem. Commun.* **1986**, 1446.
215. Noda, D.; Aoki, T.; Nakanishi, Y.; Hatanaka, Y. *Vacuum* **2000**, 59, 701.
216. Panda, A.; Mughesh, G.; Singh, H. B.; Butcher, R. J. *Organometallics* **1999**, 18, 1986.
217. Wirth, T. *Tetrahedron* **1999**, 55, 1.
218. Mughesh, G.; Singh, H. B. *Acc. Chem. Res.* **2002**, 35, 226.
219. Braverman, S.; Cherkinsky, M.; Jana, R.; Kalendar, Y.; Sprecher, M. *J. Phys. Org. Chem.* **2010**, 23, 1114.
220. Kawashima, T. *Coord. Chem. Rev.* **2003**, 244, 137.
221. Kuhn, N.; Al-Sheikh, A.; Steimann, M.; Strobele, M. *Z. Anorg. Allg. Chem.* **2003**, 629, 1541.

222. Steiner, G.; Kopacka, H.; Ongania, K. H.; Wurst, K.; Preishuber-Pflugl, P.; Bildstein, B. *Eur. J. Inorg. Chem.* **2005**, 1325.
223. Briere, J. F.; Takada, H.; Metzner, P. *Phosphorus, Sulfur Silicon Relat. Elem.* **2005**, 180, 965.
224. Okazaki, R.; Tokitoh, N. *Acc. Chem. Res.* **2000**, 33, 625.
225. Kuchta, M. C.; Parkin, G. *J. Chem. Soc., Chem. Commun.* **1994**, 1351.
226. Kuchta, M. C.; Parkin, G. *J. Am. Chem. Soc.* **1994**, 116, 8372.
227. Ding, Y. Q.; Ma, Q. J.; Uson, I.; Roesky, H. W.; Noltemeyer, M.; Schmidt, H. G. *J. Am. Chem. Soc.* **2002**, 124, 8542.
228. Ding, Y. Q.; Ma, Q. J.; Roesky, H. W.; Herbst-Irmer, R.; Uson, I.; Noltemeyer, M.; Schmidt, H. G. *Organometallics* **2002**, 21, 5216.
229. Ding, Y. Q.; Ma, Q. J.; Roesky, H. W.; Uson, I.; Noltemeyer, M.; Schmidt, H. G. *Dalton. Trans.* **2003**, 1094.
230. Pineda, L. W.; Jancik, V.; Roesky, H. W.; Herbst-Irmer, R. *Angew. Chem. Int. Ed.* **2004**, 43, 5534.
231. Pineda, L. W.; Jancik, V.; Oswald, R. B.; Roesky, H. W. *Organometallics* **2006**, 25, 2384.
232. Saur, I.; Rima, G.; Gornitzka, H.; Miqueu, K.; Barrau, J. *Organometallics* **2003**, 22, 1106.
233. Walther, B. *Coord. Chem. Rev.* **1984**, 60, 67.
234. Gallo, V.; Latronico, M.; Mastroilli, P.; Nobile, C. F.; Ciccarella, G.; Englert, U. *Eur. J. Inorg. Chem.* **2006**, 2634.
235. Mansfield, N. E.; Coles, M. P.; Hitchcock, P. B. *Phosphorus, Sulfur Silicon Relat. Elem.* **2008**, 183, 2685.
236. Gelmini, L.; Stephan, D. W. *Organometallics* **1987**, 6, 1515.
237. Gelmini, L.; Stephan, D. W. *Can. J. Chem./Rev. Can. Chim.* **1988**, 66, 2647.
238. Challet, S.; Kubicki, K. M.; Leblanc, J. C.; Moise, C.; Nuber, B. *J. Organomet. Chem.* **1994**, 483, 47.
239. Silvestru, C.; Haiduc, I.; Klima, S.; Thewalt, U.; Gielen, M.; Zuckerman, J. J. *J. Organomet. Chem.* **1987**, 327, 181.

240. Jain, V. K. *Coord. Chem. Rev.* **1994**, *135*, 809.
241. Haiduc, I.; Sowerby, D. B.; Lu, S. F. *Polyhedron* **1995**, *14*, 3389.
242. Haiduc, I. *Coord. Chem. Rev.* **1997**, *158*, 325.
243. García, P. G. Y.; Cruz-Almanza, R.; Toscano, R. A.; Cea-Olivares, R. J. *Organomet. Chem.* **2000**, *598*, 160.
244. Fild, M.; Kruger, O.; Silaghi-Dumitrescu, I.; Thone, C.; Weinkauff, A. *Phosphorus, Sulfur Silicon Relat. Elem.* **2007**, *182*, 2283.
245. Liu, C. W.; Lobana, T. S.; Xiao, J. L.; Liu, H. Y.; Liaw, B. J.; Hung, C. M.; Lin, Z. Y. *Organometallics* **2005**, *24*, 4072.
246. Davies, R. P.; Francis, C. V.; Jurd, A. P. S.; Martinelli, M. G.; White, A. J. P.; Williams, D. J. *Inorg. Chem.* **2004**, *43*, 4802.
247. Gray, I. P.; Slawin, A. M. Z.; Woollins, J. D. *Dalton. Trans.* **2005**, 2188.
248. Drake, J. E.; Gurnani, C.; Hursthouse, M. B.; Light, M. E.; Nirwan, M.; Ratnani, R. *Appl. Organomet. Chem.* **2007**, *21*, 539.
249. Silvestru, C.; Toscano, R. A.; Cardenas, J.; Ceaolivares, R.; Silvestru, A.; Haiduc, I. *Polyhedron* **1995**, *14*, 2231.
250. Andrianarison, M.; Couret, C.; Declercq, J. P.; Dubourg, A.; Escudié, J.; Ranaivonjatovo, H.; Satge, J. *Organometallics* **1988**, *7*, 1545.
251. Davies, R. P.; Martinelli, M. G. *Inorg. Chem.* **2002**, *41*, 348.
252. Mallory, F. B. *J. Am. Chem. Soc.* **1973**, *95*, 7747.
253. Mallory, F. B.; Mallory, C. W.; Ricker, W. M. *J. Org. Chem.* **1985**, *50*, 457.
254. Bifulco, G.; Mangoni, A. *Magn. Reson. Chem.* **2008**, *46*, 199.
255. Mallory, F. B.; Luzik, E. D.; Mallory, C. W.; Carroll, P. J. *J. Org. Chem.* **1992**, *57*, 366.
256. Hierso, J.-C.; Fihri, A.; Ivanov, V. V.; Hanquet, B.; Pirio, N.; Donnadiou, B.; Rebière, B.; Amardeil, R.; Meunier, P. *J. Am. Chem. Soc.* **2004**, *126*, 11077.
257. Wei, Z.; Yang, J.-H.; Vreshch, V. D.; Zabula, A. V.; Filatov, A. S.; Dikarev, E. V. *Inorg. Chem.* **2011**, *50*, 7295.
258. Yang, Y.; Zhao, N.; Wu, Y.; Zhu, H.; Roesky, H. W. *Inorg. Chem.* **2012**, *51*, 2425.

259. Druckenbrodt, C.; du Mont, W. W.; Ruthe, F. *Z. Anorg. Allg. Chem.* **1998**, *624*, 590.
260. Izod, K.; Stewart, J.; Clark, E. R.; Clegg, W.; Harrington, R. W. *Inorg. Chem.* **2010**, *49*, 4698.
261. Wang, Z. X.; Li, Y. X. *Organometallics* **2002**, *21*, 4641.
262. Cowley, A. H.; Giolando, D. M.; Jones, R. A.; Nunn, C. M.; Power, J. M. *Polyhedron* **1988**, *7*, 1909.
263. Fedotova, Y. V.; Kornev, A. N.; Sushev, V. V.; Kursky, Y. A.; Mushtina, T. G.; Makarenko, N. P.; Fukin, G. K.; Abakumov, G. A.; Zakharov, L. N.; Rheingold, A. L. *J. Organomet. Chem.* **2004**, *689*, 3060.
264. Reddy, N. D.; Jana, A.; Roesky, H. W.; Samuel, P. P.; Schulzke, C. *Dalton Trans.* **2010**, *39*, 234.
265. Balch, A. L.; Oram, D. E. *Inorg. Chem.* **1987**, *26*, 1906.
266. Allan, R. E.; Beswick, M. A.; Cromhout, N. L.; Paver, M. A.; Raithby, P. R.; Steiner, A.; Trevithick, M.; Wright, D. S. *Chem. Commun.* **1996**, 1501.
267. Brym, M.; Francis, M. D.; Jin, G. X.; Jones, C.; Mills, D. P.; Stasch, A. *Organometallics* **2006**, *25*, 4799.
268. Mansfield, N. E.; Grundy, J.; Coles, M. P.; Hitchcock, P. B. *Polyhedron* **2010**, *29*, 2481.
269. Davis, M. F.; Clarke, M.; Levason, W.; Reid, G.; Webster, M. *Eur. J. Inorg. Chem.* **2006**, 2773.
270. Gregor, L. C.; Chen, C. H.; Fafard, C. M.; Fan, L.; Guo, C. Y.; Foxman, B. M.; Gusev, D. G.; Ozerov, O. V. *Dalton Trans.* **2010**, *39*, 3195.
271. Westerhausen, M.; Hausen, H. D.; Schwarz, W. *Z. Anorg. Allg. Chem.* **1995**, *621*, 877.
272. Westerhausen, M.; Pfitzner, A. *J. Organomet. Chem.* **1995**, *487*, 187.
273. Westerhausen, M.; Digeser, M. H.; Wieneke, B.; Noth, H.; Knizek, J. *Eur. J. Inorg. Chem.* **1998**, 517.
274. Westerhausen, M.; Enzelberger, M. M.; Schwarz, W. *J. Organomet. Chem.* **1995**, *491*, 83.
275. Venanzi, T. J. *J. Chem. Educ.* **1982**, *59*, 144.

276. Murso, A.; Straka, M.; Kaupp, M.; Bertermann, R.; Stalke, D. *Organometallics* **2005**, *24*, 3576.
277. Goel, S. C.; Chiang, M. Y.; Rauscher, D. J.; Buhro, W. E. *J. Am. Chem. Soc.* **1993**, *115*, 160.
278. Sasaki, S.; Sutoh, K.; Murakami, F.; Yoshifuji, M. *J. Am. Chem. Soc.* **2002**, *124*, 14830.
279. Cheng, Y. F.; Emge, T. J.; Brennan, J. G. *Inorg. Chem.* **1996**, *35*, 342.
280. Batchelor, R. J.; Einstein, F. W. B.; Jones, C. H. W.; Sharma, R. D. *Inorg. Chem.* **1988**, *27*, 4636.
281. Tani, K.; Yamada, R.; Kanda, T.; Suzuki, M.; Kato, S.; Murai, T. *Organometallics* **2002**, *21*, 1487.
282. Saito, M.; Tokitoh, N.; Okazaki, R. *J. Am. Chem. Soc.* **1997**, *119*, 11124.
283. Leung, W. P.; Kwok, W. H.; Law, L. T. C.; Zhou, Z. Y.; Mak, T. C. W. *Chem. Commun.* **1996**, 505.
284. Cea-Olivares, R.; Moya-Cabrera, M.; Garcia-Montalvo, V.; Castro-Blanco, R.; Toscano, R. A.; Hernandez-Ortega, S. *Dalton. Trans.* **2005**, 1017.
285. Kedarnath, G.; Kumbhare, L. B.; Dey, S.; Wadawale, A. P.; Jain, V. K.; Dey, G. K. *Polyhedron* **2009**, *28*, 2749.
286. Labahn, D.; Bohnen, F. M.; Herbstirmer, R.; Pohl, E.; Stalke, D.; Roesky, H. W. *Z. Anorg. Allg. Chem.* **1994**, *620*, 41.
287. Evans, C. M.; Evans, M. E.; Krauss, T. D. *J. Am. Chem. Soc.* **2010**, *132*, 10973.
288. Matsumoto, T.; Tokitoh, N.; Okazaki, R. *Angew. Chem.-Int. Edit. Engl.* **1994**, *33*, 2316.
289. Varga, R. A.; Silvestru, C. *Main Group Met. Chem.* **2007**, *30*, 199.
290. Molloy, K. C.; Hossain, M. B.; Vanderhelm, D.; Zuckerman, J. J.; Haiduc, I. *Inorg. Chem.* **1979**, *18*, 3507.
291. Bondi, A. *J. Phys. Chem.* **1964**, *68*, 441.
292. Casas, J. S.; Castineiras, A.; Rodriguez-Arguelles, M. C.; Sanchez, A.; Sordo, J.; Vazquez-Lopez, A.; Vazquez-Lopez, E. M. *J. Chem. Soc., Dalton Trans.* **2000**, 4056.
293. Edelmann, F. T.; Haiduc, I.; Silvestru, C.; Schmidt, H. G.; Noltemeyer, M. *Polyhedron* **1998**, *17*, 2043.

294. Begley, M. G.; Gaffney, C.; Harrison, P. G.; Steel, A. J. *Organomet. Chem.* **1985**, *289*, 281.
295. Gray, I. P.; Slawin, A. M. Z.; Woollins, J. D. *Dalton. Trans.* **2004**, 2477.
296. Ebert, K. H.; Breunig, H. J.; Silvestru, C.; Stefan, I.; Haiduc, I. *Inorg. Chem.* **1994**, *33*, 1695.
297. Shi, W. F.; Shafaei-Fallah, M.; Rothenberger, A. *Dalton. Trans.* **2007**, 4255.
298. Panneerselvam, A.; Nguyen, C. Q.; Malik, M. A.; O'Brien, P.; Raftery, J. J. *Mater. Chem.* **2009**, *19*, 419.
299. Herzog, U.; Böhme, U.; Brendler, E.; Rheinwald, G. *J. Organomet. Chem.* **2001**, *630*, 139.
300. Herzog, U.; Rheinwald, G. *Organometallics* **2001**, *20*, 5369.
301. Seligson, A. L.; Arnold, J. *J. Am. Chem. Soc.* **1993**, *115*, 8214.
302. DeGroot, M. W.; Taylor, N. J.; Corrigan, J. F. *J. Am. Chem. Soc.* **2003**, *125*, 864.
303. Khadka, C. B.; Macdonald, D. G.; Lan, Y. H.; Powell, A. K.; Fenske, D.; Corrigan, J. F. *Inorg. Chem.* **2010**, *49*, 7289.
304. Armarego, W. L. F.; Chai, C. L. L., *Purification of laboratory chemicals*. 5th ed.; Butterworth-Heinemann: Amsterdam ; Boston, 2003.
305. Sheldrick, G. M., *SHELXL-97, Program for the Refinement of Crystal Structures*. University of Göttingen: Göttingen, Germany, 1997.

Appendix 1: Publications

Fulton, J. R.; Hitchcock, P. B.; Johnstone, N. C.; Tam, E. C. Y. The synthesis of monomeric terminal lead aryloxides: dependence on reagents and conditions. *Dalton Trans.* **2007**, 3360–3362

Tam, E. C. Y.; Johnstone, N. C.; Ferro, L.; Hitchcock, P. B.; Fulton, J. R. Carbon dioxide activation by ‘non-nucleophilic’ lead alkoxide. *Inorg. Chem.*, **2009**, *48*, 8971–8976

Tam, E. C. Y.; Maynard, N. A.; Apperley, D. C.; Smith, J. D.; Coles, M. P.; Fulton, J. R. Group 14 metal terminal phosphides: correlating structure with $|J_{MP}|$. *Inorg. Chem.* **2012**, *51*, 9403–9415

The synthesis of monomeric terminal lead aryloxides: dependence on reagents and conditions†‡

J. Robin Fulton,* Peter B. Hitchcock, Nick C. Johnstone and Eric C. Y. Tam

Received 25th May 2007, Accepted 14th June 2007

First published as an Advance Article on the web 26th June 2007

DOI: 10.1039/b707984b

The successful synthesis of terminal lead aryloxides is shown to be dependent upon reaction conditions, including choice of solvent and alkali metal aryloxide precursor.

There is a large literature base detailing the coordination chemistry of lead(II) and trying to address its bonding properties, with an emphasis on how divalent lead might interact with biological molecules.^{1,2} In addition, there has been considerable interest in the lead(II) lone pair with regards to both its stability and its purported stereochemical activity.^{3–6} However, the chemistry of the ligands bonded to lead, especially in mimicking the reactivity of transition metal counterparts, has been widely ignored. This is partially due to the instability of lead complexes and their tendency to form insoluble precipitates which are difficult to characterize and use in further transformations. For instance, only a handful of terminal lead alkoxide and aryloxides have been reported to date,^{7–10} and only one of these is monometallic.⁷ This is in sharp contrast with the vast array of transition metal counterparts.^{11–13}

We have recently reported the synthesis of a series of β -diketiminato lead(II) halide complexes in which we employed the bulky β -diketiminato anion, $[\{N(2,6\text{-}i\text{-Pr}_2\text{C}_6\text{H}_3)C(\text{Me})\}_2\text{CH}]$, (BDI) to support monomeric, 3-coordinate lead centres.¹⁴ These ligands have been previously utilised to stabilise low-coordinate transition metal complexes as the isopropyl groups on the ligand aryl group limit the number of coordinated ligands around the metal center.^{15–17} Both the BDI–lead chloride and bromide complexes are relatively thermally and photolytically stable and the $[(\text{BDI})\text{PbCl}]$ (**1**) can be generated in sufficient quantities for use as a starting reagent for the development of the chemistry of low-coordinate lead.

To minimize the risk of forming aggregates in solution, our initial focus was on generating bulky lead-aryloxide complexes. Synthesis of a lead-aryloxide containing the 2,6-di-*tert*-butyl-4-methylphenoxide (BHT) group was attempted by treatment of chloride **1** with LiBHT in THF. An insoluble white precipitate was formed, however, the major species remaining in solution was neutral BDI-H. Interestingly, when a solution of chloride **1** was added to a suspension of unsolvated LiBHT in toluene or benzene, the mixture became homogeneous, and formation of a yellow crystalline solid was observed upon standing for 30 min. The

¹H NMR spectrum of the reaction mixture after five min revealed new resonances corresponding to 1 : 1 mixture of lead-bound β -diketiminato ligand and BHT. However, no precipitate other than the slow forming yellow crystalline solid was observed, even upon addition of pentane or other non-polar solvents. Confused as to the identity of this new complex, an X-ray diffraction study was performed on the crystalline solid, which has crystallized about an inversion centre.¹⁸ The molecular structure revealed that a lead-aryloxide complex had not formed, but instead heterotetrametallic adduct, $[\{(\text{BDI})\text{PbCl}\}\{\text{LiO}(2,6\text{-di-}^t\text{Bu-4-MeC}_6\text{H}_2)\}]_2$ (**2**) had been generated in which a lithium-aryloxide $[\text{Li}(\text{OAr})]_2$ dimer is coordinated by two $[(\text{BDI})\text{PbCl}]$ moieties *via* a chloride–lithium interaction (Fig. 1, Scheme 1). A pyramidal geometry is observed around the lead metal centre, with the sum of the bond angles around the metal centre equal to 272.3°, or a degree of pyramidalization (DP) of 98%.^{14,19} This is similar to the parent chloride complex **1** (DP = 103%); however, as would be expected by such a complex, both the Pb–Cl and Pb–N bond distances are elongated by 0.073 Å and 0.035 Å, respectively.¹⁴ The Li_2O_2 dimer is a common binding motif for bulky lithium-aryloxide complexes, with the THF adduct of LiBHT crystallographically characterized.²⁰

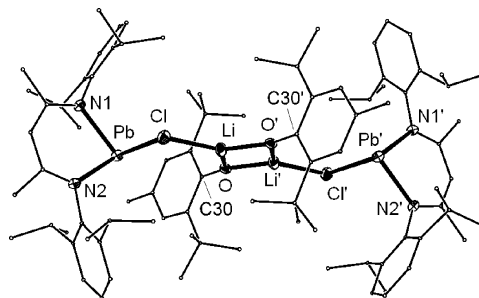


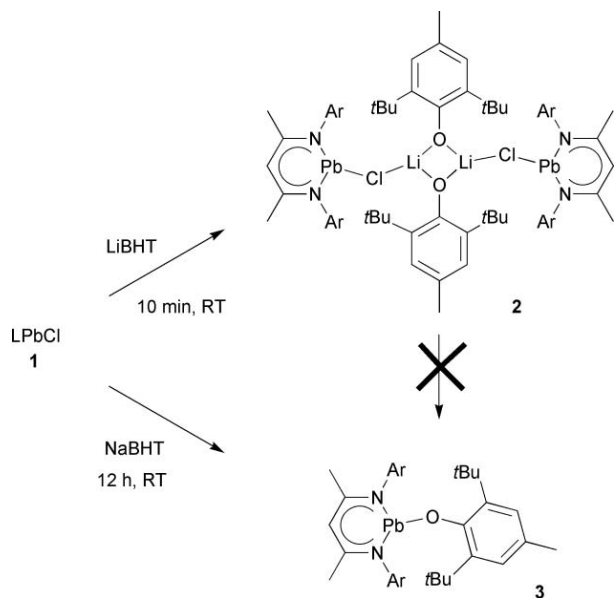
Fig. 1 ORTEP diagram of compound **2** with H atoms omitted and C atoms minimized for clarity. Ellipsoid probably shown at 30%. Atoms with a prime (') in the atoms labels are at equivalent position ($-x, -y, -z$). Selected bond lengths (Å) and angles (°): Pb–N(1), 2.315(3); Pb–N(2), 2.315(3); Pb–Cl, 2.6381(10); Li–O', 1.849(7); Li–O, 1.885(7); Li–Cl, 2.358(7); O–C(30), 1.337(4); O'–Li, 1.849(7); N(1)–Pb–N(2), 82.86(11); N(1)–Pb–Cl, 94.14(3); N(2)–Pb–Cl, 94.33(8); O'–Li–O, 96.8(3); O'–Li–Cl, 140.1(4); O–Li–Cl, 123.2(3); Li–Cl–Pb, 102.19(17); C(30)–O–Li, 145.3(3); C(30)–O–Li, 131.0(3); Li'–O–Li, 83.2(3).

Heterotetrametallic complex **2** is both light and temperature sensitive and will decompose to a black insoluble precipitate over the course of a day at ambient temperatures. We were unable to force complex **2** to eliminate lithium chloride by heating, sonicating, or addition of N,N,N',N' -tetramethylethylenediamine or AgOTf, the latter of which resulted in the immediate

Department of Chemistry, University of Sussex, Brighton, UK BN1 9QJ. E-mail: j.r.fulton@sussex.ac.uk; Fax: +44 (0)1273 677196; Tel: +44 (0)1273 873170

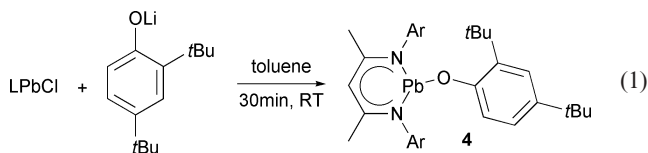
† CCDC reference numbers 641614–648823. For crystallographic data in CIF or other electronic format see DOI: 10.1039/b707984b

‡ Electronic supplementary information (ESI) available: Fig. S1. Temperature dependent NMR spectra of **3** showing the change in resonances corresponding to the (2,6-di-*t*Bu-4-MeC₆H₃) protons ($T_c = 278$ K) and the N-(2,6-di-*i*PrC₆H₃) protons ($T_c = 248$ K). See DOI: 10.1039/b707984b



Scheme 1 Reactivity of **1** with Li- and NaBHT (BHT = 2,6-di-*tert*-butyl-4-methylphenoxide).

decomposition of the complex. The inability to convert **2** to our desired lead aryloxy was initially attributed to the bulky aryl substituent, that is, we postulated the desired lead-BHT complex (**3**) would be destabilized by interaction between the *tert*-butyl groups on the aryloxy and the isopropyl groups on the β -diketiminato ligand. We reasoned that decreasing the steric bulk around the aryloxy ligand would make the synthesis of a lead-aryloxy viable, indeed, treatment of complex **1** with lithio-2,4-di-*tert*-butylphenoxide resulted in the formation of the lead aryloxy **4** after 30 min at room temperature (eqn (1)). This compound is stable indefinitely in the solid state, but will slowly decompose in solution. The X-ray crystal structure (Fig 2) revealed that the angles between the ligands around the metal centre to be even more acute than the chloride **1** (sum of the bond angles = 254.6°, DP = 118%). The Pb–N bond lengths are similar to other BDI–Pb complexes and the Pb–O bond length of 2.182(4) Å is slightly shorter than Van Zandt's lead aryloxy dimer [Pb(OAr')₂] (Ar' = 2,6-Ph₂C₆H₃) of 2.229–2.257 Å.⁹



The viability of a [(BDI)Pb(BHT)] complex **3** appeared feasible from the structural data of **4**. The 2-*tert*-butyl group on the aryloxy ligand of **4** lies directly below the BDI-plane, leaving a void in front of the Pb–O bond that is potentially large enough to accommodate another tertiary butyl group. Space filling models of the postulated BHT complex **3** revealed that this species, although sterically crowded, is potentially viable. Lithium-chloride adducts of transition metals are not unusual, and, in a few notable examples, lithium chloride adducts have been isolated as apparent intermediates in salt metathesis reactions in which the lithium ion is bound to both the leaving group, such as an amido or alkoxide functional group, as well as the transition-metal

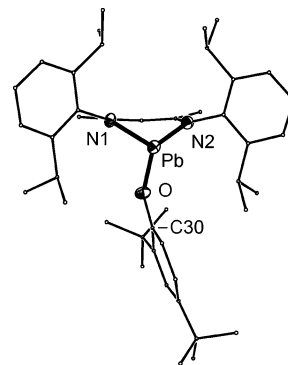


Fig. 2 ORTEP diagram of compound **4** with H atoms omitted and C atoms minimized for clarity. Ellipsoid probably shown at 30%. Selected bond lengths (Å) and angles (°): Pb–N(1), 2.270(5); Pb–N(2), 2.288(5); Pb–O, 2.182(4); O–C(30), 1.345(8); N(1)–Pb–N(2), 82.34(19); N(1)–Pb–O, 83.32(18); N(2)–Pb–O, 88.97(18); Pb–O–C(30), 127.3(4).

bound chloride.^{21–24} As there are significantly fewer examples of sodium-chloride adducts of transition metals potentially due to the weaker Na–Cl bond,²⁵ the BHT-aryloxy reagent was changed to NaBHT. This route was indeed successful as treatment of a toluene solution of chloride **1** with NaBHT resulted in clean formation of the aryloxy **3** after stirring overnight (Scheme 1). This complex is stable in the solid state but, similar to aryloxy **4**, slowly decomposes in solution.

The X-ray crystal structure of **3** revealed slightly longer Pb–O (2.212(2) Å) and Pb–N bond lengths compared to **4** (Fig 3); however, the geometry around both the metal centre as well as the aryloxy ligand are considerably distorted as compared to complex **4**. For instance, in the latter, the bond angles around the lead metal centre ranged from 82–89°. In contrast, one of the N–Pb–O bond angles of the BHT complex **3** is significantly more obtuse (103.00(7)°), leading to a larger sum of bond angles (273.4°) and a 96.2% DP. In addition, the *ipso* carbon atom of the BHT ligand lies 0.198 Å out of the plane generated by the other ring carbons (note, in the solid state structure of **4**, this distance is only 0.073 Å). The solid-state structure also revealed the BHT aryloxy ligand to be canted towards one of the 2,6-isopropyl aryl rings of the BHT ligand. Although factors governing all of these distortions are unclear, some can be

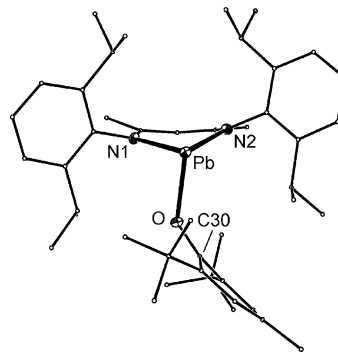


Fig. 3 ORTEP diagram of compound **3** with H atoms omitted and C atoms minimized for clarity. Ellipsoid probably shown at 30%. Selected bond lengths (Å) and angles (°): Pb–N(1), 2.309(2); Pb–N(2), 2.302(2); Pb–O, 2.212(2); O–C(30), 1.352(3); N(1)–Pb–N(2), 83.06(8); N(1)–Pb–O, 87.32(7); N(2)–Pb–O, 103.00(7); C(30)–O–Pb, 125.91(16).

attributed to solid-state packing forces. The canting of the BHT ligand was not observed in the solution phase as only two different environments were detected for the isopropyl groups, even at $-78\text{ }^{\circ}\text{C}$. However, broadening of the resonances corresponding to the BHT ligand was observed at room temperature, indicative of hindered rotation around the Pb–O bond ($\Delta G^{\ddagger} = 13\text{ kcal mol}^{-1}$), similar to that observed in the [(BDI)Pb–N(SiMe₃)₂] system.¹⁴ In addition, broadening of the *N*-aryl resonances was observed at RT, indicating a hindered rotation of the *N*_{aryl}-C bond ($\Delta G^{\ddagger} = 16\text{ kcal mol}^{-1}$). This restricted rotation has not been observed in other BDI–Pb systems and may be a function of the bulky aryloxy substituent.¹⁴

In conclusion, we have developed a reliable synthetic route towards the synthesis of rare terminal lead aryloxy complexes *via* salt metathesis from lead chloride complex **1**. We have isolated a lithium-lead heterotetrametallic complex, which initially appeared to be an intermediate in the salt metathesis pathway. However, as we were unable to force this complex to lose LiCl and form the desired BHT-aryloxy **3** and instead generated **3** from an alternative pathway, the validity of the complex as an actual intermediate in the salt metathesis pathway is in question. Reasons behind the solvent effect on the reaction outcome as well as factors governing the relative stability of the heterotetrametallic complex **2** compared to the lead-aryloxy complexes **3** and **4**, including DFT investigations, are currently in progress.

Acknowledgements

J. R. F. gratefully acknowledges the Leverhulme Trust and University of Sussex start-up funds for financial support.

Notes and references

- 1 H. Sigel, C. P. Da Costa and R. B. Martin, *Coord. Chem. Rev.*, 2001, **219**, 436–461.
- 2 J. Parr, *Polyhedron*, 1997, **16**, 551–566.

- 3 G. Akibo-Betts, P. E. Barran, L. Puskar, B. Duncombe, H. Cox and A. J. Stace, *J. Am. Chem. Soc.*, 2002, **124**, 9257–9264.
- 4 H. Cox and A. J. Stace, *J. Am. Chem. Soc.*, 2004, **126**, 3939–3947.
- 5 D. Esteben-Gomez, C. Platas-Iglesias, T. Enriquez-Perez, F. Avecilla, A. de Blas and T. Rodriguez-Blas, *Inorg. Chem.*, 2006, **45**, 5407–5416.
- 6 L. Shimoni-Livny, J. P. Glusker and C. W. Bock, *Inorg. Chem.*, 1998, **37**, 1853–1857.
- 7 P. Naumov, S. Cakir, I. Bulut, E. Bicer, O. Cakir, G. Jovanovski, A. R. Ibrahim, A. Usman, H.-K. Funs, S. Chantrapromma and S. W. Ng, *Main Group Met. Chem.*, 2002, **25**, 175.
- 8 M. A. Pierce-Butler, *Acta Crystallogr., Sect. C: Cryst. Struct. Commun.*, 1984, **40**, 1364–1367.
- 9 W. Van Zandt, J. C. Huffman and J. L. Stewart, *Main Group Met. Chem.*, 1998, **21**, 237–240.
- 10 S. Suh and D. M. Hoffman, *Inorg. Chem.*, 1996, **35**, 6164–6169.
- 11 H. E. Bryndza and W. Tam, *Chem. Rev.*, 1988, **88**, 1163–1188.
- 12 J. R. Fulton, A. W. Holland, D. J. Fox and R. G. Bergman, *Acc. Chem. Res.*, 2002, **35**, 44–56.
- 13 R. C. Mehrotra and A. Singh, *Prog. Inorg. Chem.*, 1997, **46**, 239–473.
- 14 M. Chen, J. R. Fulton, P. B. Hitchcock, N. C. Johnstone, M. F. Lappert and A. V. Protchenko, *Dalton Trans.*, 2007, 2770–2778.
- 15 L. Bourget-Merle, M. F. Lappert and J. R. Severn, *Chem. Rev.*, 2002, **102**, 3031–3065.
- 16 J. M. Smith, A. R. Sadique, T. R. Cundari, K. R. Rodgers, G. Lukat-Rodgers, R. J. Lachicotte, C. J. Flaschenriem, J. Vela and P. L. Holland, *J. Am. Chem. Soc.*, 2006, **128**, 756–769.
- 17 D. J. E. Spencer, N. W. Aboelella, A. M. Reynolds, P. L. Holland and W. B. Tolman, *J. Am. Chem. Soc.*, 2002, **124**, 2108–2109.
- 18 The crystal structure of **3** has been determined three times as C₆D₆, toluene and pentane solvates.
- 19 Z. B. Maksic and B. Kovacevic, *J. Chem. Soc., Perkin Trans. 2*, 1999, 2623–2629.
- 20 W. Clegg, E. Lamb, S. T. Liddle, R. Snaith and A. E. H. Wheatley, *J. Organomet. Chem.*, 1999, **573**, 305–312.
- 21 N. A. Eckert, J. M. Smith, R. J. Lachicotte and P. L. Holland, *Inorg. Chem.*, 2004, **43**, 3306–3321.
- 22 K. J. Weese, R. A. Bartlett, B. D. Murray, M. M. Olmstead and P. P. Power, *Inorg. Chem.*, 1987, **26**, 2409–2413.
- 23 J. Vela, S. Vaddadi, S. Kingsley, C. J. Flaschenriem, R. J. Lachicotte, T. R. Cundari and P. L. Holland, *Angew. Chem., Int. Ed.*, 2006, **45**, 1607–1611.
- 24 J. Hvoslef, H. Hope, B. D. Murray and P. P. Power, *J. Chem. Soc., Chem. Commun.*, 1983, 1438–1439.
- 25 D. J. Darensbourg, J. C. Yoder, G. E. Struck, M. W. Holtcamp, J. D. Draper and J. H. Reibenspies, *Inorg. Chim. Acta*, 1998, **274**, 115–121.

Carbon Dioxide Activation by “Non-nucleophilic” Lead Alkoxides

Eric C. Y. Tam, Nick C. Johnstone, Lorenzo Ferro, Peter B. Hitchcock, and J. Robin Fulton*

Department of Chemistry, University of Sussex, Falmer, Brighton BN1 9QJ, U.K.

Received January 21, 2009

A series of terminal lead alkoxides have been synthesized utilizing the bulky β -diketiminato ligand $[\{N(2,6\text{-}i\text{Pr}_2\text{C}_6\text{H}_3)\text{-C}(\text{Me})_2\text{CH}\}]^-$ (BDI). The nucleophilicities of these alkoxides have been examined, and unexpected trends were observed. For instance, (BDI)PbOR reacts with methyl iodide only under forcing conditions yet reacts readily, but reversibly, with carbon dioxide. The degree of reversibility is strongly dependent upon minor changes in the R group. For instance, when R = isopropyl, the reversibility is only observed when the resulting alkyl carbonate is treated with other heterocumulenes; however, when R = *tert*-butyl, the reversibility is apparent upon any application of reduced pressure to the corresponding alkyl carbonate. The differences in the reversibility of carbon dioxide insertion are attributed to the ground-state energy differences of lead alkoxides. The mechanism of carbon dioxide insertion is discussed.

Introduction

In contrast to the well-documented reactivity of transition-metal alkoxides,^{1–3} the chemistry of lead alkoxides has largely been ignored outside of gas-phase and theoretical studies.^{4–6} Divalent lead has an aqueous acidity of 7.2, much smaller than that predicted based upon electrostatic parameters.⁷ This acidity has been attributed to a more covalent Pb–O bond, in contrast to the highly polarized transition metal–oxygen bonds. In addition, lead’s aqueous acidity has been used to justify its enhanced ability to cleave RNA. At biologically relevant pHs, there will be a sufficient amount of divalent lead hydroxide present to act as a base, deprotonating the 2'-hydroxyl proton of the RNA backbone, and a nucleophile in the cleavage of the resultant cyclic phosphate intermediate.^{8,9} This implies that the Pb–O bond has some degree of polarity to be able to act as both a base and a nucleophile. However, no complementary chemical studies have been performed to back this hypothesis. As such, we set out to investigate the nature of the Pb–O bond in order to

understand the degree of polarization of the bond. Herein, the results of such studies are reported, and our findings suggest that, although nucleophilic behavior with methyl iodide is not observed, lead alkoxides readily insert carbon dioxide into the Pb–O bond.

We have recently synthesized a series of monomeric divalent lead halides utilizing the bulky β -diketiminato anion $[\{N(2,6\text{-}i\text{Pr}_2\text{C}_6\text{H}_3)\text{C}(\text{Me})_2\text{CH}\}]^-$ (BDI) to stabilize the resulting three-coordinate lead complexes.¹⁰ The chloride complex (BDI)PbCl (**1**) was used to synthesize monomeric lead aryloxy complexes in good yield.¹¹ Because metal aryloxy complexes are generally not as reactive as their alkoxide counterparts, for our reactivity studies, we turned our attention toward the synthesis of monomeric, terminal lead alkoxide complexes.

Results and Discussion

The treatment of a toluene solution of chloride **1** with KO^tPr or KO^tBu affords lead alkoxides (BDI)PbO^tPr (**2**) and (BDI)PbO^tBu (**3**), respectively (eq 1). Although these lead alkoxide complexes form a stable solid, they will slowly decompose in solution at ambient temperatures. The X-ray crystal structures were determined for both **2** and **3**, showing the expected pyramidal geometry of the ligands around the lead center (Figure 1).^{10,11} Selected bond lengths and angles for alkoxides **2** and **3** are listed in Table 1, and data collection parameters are given in Table 2. Both alkyl groups of complexes **2** and **3** lie away from the BDI–Pb core; this is

*To whom correspondence should be addressed. E-mail: j.r.fulton@sussex.ac.uk.

(1) Bryndza, H. E.; Fong, L. K.; Paciello, R. A.; Tam, W.; Bercaw, J. E. *J. Am. Chem. Soc.* **1987**, *109*, 1444.

(2) Bryndza, H. E.; Tam, W. *Chem. Rev.* **1988**, *88*, 1163.

(3) Fulton, J. R.; Holland, A. W.; Fox, D. J.; Bergman, R. G. *Acc. Chem. Res.* **2002**, *35*, 44.

(4) Akibo-Betts, G.; Barran, P. E.; Puskar, L.; Duncombe, B.; Cox, H.; Stace, A. J. *J. Am. Chem. Soc.* **2002**, *124*, 9257.

(5) Cox, H.; Stace, A. J. *J. Am. Chem. Soc.* **2004**, *126*, 3939.

(6) Stace, A. J. *J. Phys. Chem. A* **2002**, *106*, 7993.

(7) Burgess, J. *Metal Ions in Solution*; Ellis Horwood Ltd.: Chichester, U.K., 1978.

(8) Barciszewska, M. Z.; Szymanski, M.; Wyszko, E.; Pas, J.; Rychlewski, L.; Barciszewski, J. *Mutat. Res.* **2005**, *589*, 103.

(9) Winter, D.; Polacek, N.; Halama, E.; Streicher, B.; Barta, A. *Nucleic Acids Res.* **1997**, *25*, 1817.

(10) Chen, M.; Fulton, J. R.; Hitchcock, P. B.; Johnstone, N. C.; Lappert, M. F.; Protchenko, A. V. *Dalton Trans.* **2007**, 2770.

(11) Fulton, J. R.; Hitchcock, P. B.; Johnstone, N. C.; Tam, E. C. Y. *Dalton Trans.* **2007**, 3360.

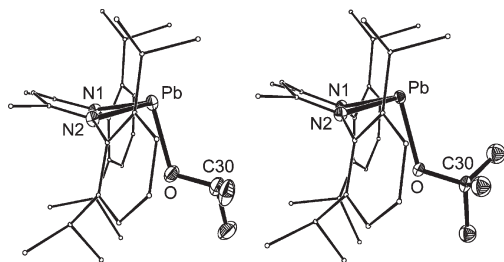


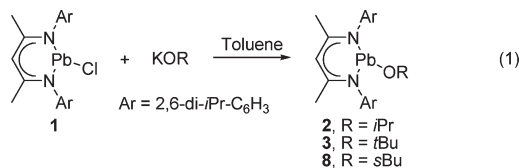
Figure 1. ORTEP diagram of lead isopropoxide **2** (left) and lead *tert*-butoxide **3** (right), with H atoms omitted and BDI C atoms minimized for clarity. The ellipsoid probability is shown at 30%.

Table 1. Selected Bond Lengths and Angles for Compounds **2** and **3**

	LPbO ^{<i>i</i>} Pr (2)	LPbO ^{<i>t</i>} Bu (3)
Pb–O	2.135(3)	2.126(3)
Pb–N1	2.307(3)	2.317(3)
Pb–N2	2.311(3)	2.299(3)
O–C30	1.413(5)	1.415(4)
N1–Pb–N2	80.56(9)	81.04(10)
N1–Pb–O	94.94(10)	92.74(10)
N2–Pb–O	93.49(10)	92.26(10)
Pb–O–C30	118.0(2)	121.4(2)
sum of the angles around Pb	268.99	266.04
DOP ^{<i>a</i>} (%)	101	104

^{*a*} Degree of pyramidalization (DOP) = $[360 - (\text{sum of the angles})] / 0.9$.²⁰

in contrast to the isostructural tin system, in which the alkyl group lies below the plane consisting of N1–Pb–N2.¹²



Two different types of lead alkoxide reactivities were investigated: basicity and nucleophilicity. The treatment of alkoxides **2** or **3** with 2,4-di-*tert*-butylphenol results in alcohol exchange reactions to form the known (BDI)Pb–OAr (Ar = 2,4-*t*Bu₂C₆H₃) complex **4** with elimination of the corresponding aliphatic alcohols. This reactivity is similar to that observed in late-transition-metal alkoxide systems. However, the presence of free alcohol results in decomposition of aryloxide **4** to an insoluble white precipitate and protonated BDI. Potentially because of their higher p*K*_a, carboxylic acids are not reactive toward **2** and **3**; the treatment of isopropoxide **2** with fluorene did not yield the fluorenyl anion, and the addition of 1,4-cyclohexadiene did not result in dimerization to an equilibrium mixture of 1,4- and 1,2-cyclohexadiene.

Both lead alkoxides **2** and **3** display seemingly contradictory reactivities toward electrophiles. For instance, neither reacts with benzyl bromide. When methyl iodide was added to either **2** or **3**, the formation of lead iodide was only observed after 2 days at 60 °C.¹⁰ In sharp contrast, both alkoxides react readily with CO₂ (eq 2). The treatment of isopropoxide **2** with 1 equiv of CO₂ results in the clean and quantitative conversion to lead alkyl carbonate **5** after 30 min at room temperature. The IR spectrum shows a stretch at 1695 cm⁻¹ (CCl₄), indicative of a carbonate carbonyl functionality; this is further supported by a

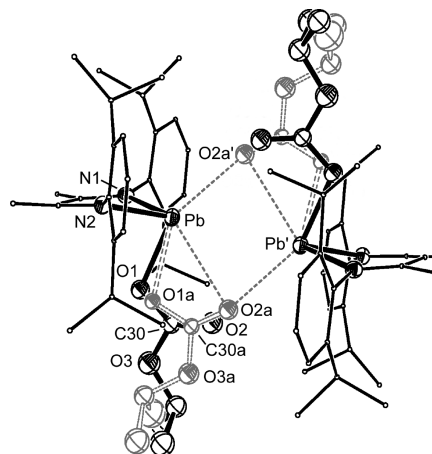
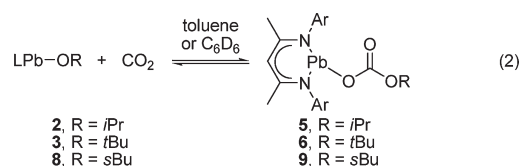


Figure 2. ORTEP diagram of lead carbonate **5** showing both components of the unit cell (major = black; minor = gray). H atoms are omitted and BDI C atoms minimized for clarity. Atoms with a prime are at equivalent positions ($-x, -y, -z$).

¹³C NMR spectral resonance at 160.9 ppm. Crystals suitable for an X-ray diffraction study were grown at –30 °C in toluene. Two different binding modes for lead carbonate were observed in the solid state (Figure 2; see Table 3 for selected bond lengths and angles). In the major component, the carbonate is bound in an η^1 fashion and there is weak, long-distance interaction between O2 and Pb'. In the minor component, the carbonate is bound in an η^2 fashion and there is a shorter distance between O2a and Pb', indicative of a stronger interaction between the two lead carbonate molecules.



Because insertion of CO₂ into transition-metal alkoxides can be reversible,¹³ we investigated whether the same was true for carbonate **5**. Although the formation of isopropoxide **2** is not observed when **5** is subjected to reduced pressure, the addition of ¹³CO₂ to the carbonate does result in ¹³C incorporation into **5**.

Lead *tert*-butoxide **3** also reacts readily with CO₂ to form lead carbonate **6** (IR: 1699 cm⁻¹, CCl₄). In contrast to the isopropoxide system, the reaction is markedly reversible: the application of reduced pressure results in the almost quantitative formation of alkoxide **3**, thwarting attempts to characterize **6** in the solid state.

Pronounced differences in the reactivity of isopropoxide **2** and *tert*-butoxide **3** were observed upon treatment with phenyl isocyanate. With the former, insertion into the Pb–O bond to generate lead carbamate **7** is observed after 1 day at room temperature (eq 3). X-ray crystallography confirmed the presence of a Pb–N carbamate bond (Figure 3), with the *N*-phenyl group lying perpendicular to and below the plane consisting of N1–Pb–N2. Selected bond lengths and angles are listed in Table 4. In contrast, with *tert*-butoxide **3**, an

(12) Dove, A. P.; Gibson, V. C.; Marshall, E. L.; Rzepa, H. S.; White, A. J. P.; Williams, D. J. *J. Am. Chem. Soc.* **2006**, *128*, 9834.

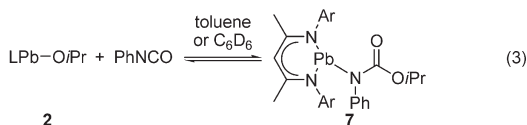
(13) For example, see: Tsuda, T.; Saegusa, T. *Inorg. Chem.* **1972**, *11*, 2561. Simpson, R. D.; Bergman, R. G. *Organometallics* **1992**, *11*, 4306. Mandal, S. K.; Ho, D. M.; Orchin, M. *Organometallics* **1993**, *12*, 1714.

Table 2. Crystallographic Data for Compounds 2, 3, 5, and 7

	LPbO ^t Pr (2)	LPbO ^t Bu (3)	LPbOCO ₂ ^t Pr (5) ^a	LPb[N(Ph)C(O)O ^t Pr (7) ^b
chemical formula	C ₃₂ H ₄₈ N ₂ O ₂ Pb	C ₃₃ H ₅₀ N ₂ O ₂ Pb	C ₃₃ H ₄₈ N ₂ O ₃ Pb·0.5(C ₇ H ₈)	C ₄₄ H ₆₅ N ₃ O ₂ Pb
fw	683.91	697.94	773.99	875.18
temperature (K)	172(2)	173(2)	173(2)	173(2)
wavelength (Å)	0.710 73	0.710 70	0.710 73	0.710 73
cryst size (mm ³)	0.20 × 0.20 × 0.15	0.25 × 0.20 × 0.10	0.15 × 0.10 × 0.05	0.15 × 0.15 × 0.1
cryst syst	triclinic	monoclinic	triclinic	triclinic
space group	<i>P</i> $\bar{1}$ (No. 2)	<i>P</i> 2 ₁ / <i>n</i> (No. 14)	<i>P</i> $\bar{1}$ (No. 2)	<i>P</i> $\bar{1}$ (No. 2)
<i>a</i> (Å)	8.6979(2)	13.3743(1)	11.9673(4)	11.5616(3)
<i>b</i> (Å)	12.1195(3)	16.8363(2)	13.2339(5)	11.6261(3)
<i>c</i> (Å)	15.1146(3)	15.2434(2)	13.5828(3)	18.2619(4)
α (deg)	92.885(1)	90	99.649(2)	102.146(1)
β (deg)	98.639(1)	108.168(1)	106.996(2)	95.723(2)
γ (deg)	97.444(1)	90	113.105(1)	112.814(1)
<i>V</i> (Å ³)	1559.71(6)	3261.29(6)	1792.09(10)	2166.78(9)
<i>Z</i>	2	4	2	2
<i>p</i> _c (Mg m ⁻³)	1.46	1.42	1.43	1.34
abs coeff (mm ⁻¹)	5.43	5.20	4.74	3.93
θ range for data collection (deg)	3.40–26.02	3.43–25.82	3.47–26.02	3.44–26.01
measd/indep reflns/ <i>R</i> (int)	23 519/6112/0.044	41 847/6251/0.061	26 307/7017/0.066	23 224/8472/ 0.054
reflns with <i>I</i> > 2 σ (<i>I</i>)	5783	5497	5851	7159
data/restraints/param	6112/0/337	6251/30/334	7017/34/380	8472/7/438
GOF on <i>F</i> ²	0.826	1.051	0.962	1.027
final <i>R</i> indices [<i>I</i> > 2 σ (<i>I</i>)]	<i>R</i> 1 = 0.023, <i>wR</i> 2 = 0.059	<i>R</i> 1 = 0.027, <i>wR</i> 2 = 0.064	<i>R</i> 1 = 0.047, <i>wR</i> 2 = 0.107	<i>R</i> 1 = 0.041, <i>wR</i> 2 = 0.083
<i>R</i> indices (all data)	<i>R</i> 1 = 0.026, <i>wR</i> 2 = 0.061	<i>R</i> 1 = 0.033, <i>wR</i> 2 = 0.067	<i>R</i> 1 = 0.0631, <i>wR</i> 2 = 0.11571	<i>R</i> 1 = 0.057, <i>wR</i> 2 = 0.090
largst diff peak and hole (e Å ⁻³)	0.78 and -1.37	1.37 and -1.40 (near Pb)	2.45 and -0.72 (close to Pb)	0.96 and 1.40

^aThe OC(O)O^tPr group is disordered unequally over two arrangements with only some of the atoms resolved. The positions for the major component could be located, and for the minor component, approximate starting positions were estimated. The two orientations were then restrained to have similar geometry by use of the *same* instruction. This refinement converged successfully. There is a molecule of toluene solvate disordered about an inversion center for which the H atoms were omitted. All disordered atoms were left isotropic. ^bThe poorly defined pentane solvate was included with isotropic C atoms and restrained geometry.

intractable reaction mixture is found. Even though the reaction between isopropoxide **2** and CO₂ is much faster than the reaction between **2** and phenyl isocyanate, there is a thermodynamic preference for the latter; the treatment of alkyl carbonate **5** with phenyl isocyanate results in an exclusive conversion to carbamate **7**. Neither alkoxide reacts with dicyclohexylcarbodiimide, even at elevated temperatures. Both alkoxides **2** and **3**, and their corresponding alkyl carbonates **5** and **6**, react with CS₂ to give intractable reaction mixtures.



To further understand the differences observed in the reactivity between isopropoxide **2** and *tert*-butoxide **3**, we synthesized the *sec*-butoxide complex **8**. The treatment of *sec*-butoxide **8** with CO₂ resulted in the expected formation of the corresponding carbonate **9** (IR: 1645 cm⁻¹, CCl₄). The degree of reversibility of this reaction is intermediate between the isopropoxide and *tert*-butoxide systems. For instance, when a vacuum is applied for 10 min to an NMR-scale solution of *tert*-butoxide carbonate **6**, almost complete reversion to alkoxide **3** is observed; however, when a similar procedure is repeated for a solution of *sec*-butoxide carbonate **9**, only 20% reversion to alkoxide **8** is observed. Unfortunately, as in the *tert*-butoxide case, this reversibility has prevented solid-state characterization of *sec*-butoxide carbonate **9**. Interestingly, solutions of both the isopropoxide carbonate **4** and *sec*-butoxide carbonate **9** are thermally stable to 60 °C, whereas the *tert*-butoxide carbonate **5** decomposes after standing at room temperature overnight.

The noticeable difference in reactivity with respect to deinsertion of CO₂ from carbonates **5**, **6**, and **9** can be

attributed to the ground-state energy differences of the alkoxides. The stability of transition-metal alkoxides correlates to the p*K*_a of the corresponding alcohol; that is, the higher the p*K*_a, the more stable the metal alkoxide.¹ If a similar trend is assumed for lead alkoxides, then the lead isopropoxide **2** is less stable than the lead *tert*-butoxide **3** (p*K*_a of isopropyl alcohol is 30.2, whereas the p*K*_a of *tert*-butanol is 2 p*K*_a units higher).¹⁴ The alkyl group will have a much smaller effect on the p*K*_a of the corresponding alkyl carbonates. An attempt was made to determine the rate of ¹³C exchange with each of the carbonates using ¹³C NMR spectroscopy. Although exchange was observed, we were unable to obtain reproducible rate data. As such, we investigated the relative ground-state differences between the reactants and products using the B3LYP density functional theory and LanL2DZ pseudopotentials (and basis set) implemented in *Gaussian 03*.¹⁵ The ΔH° value for the insertion of CO₂ into lead isopropoxide **2** was slightly greater than the analogous reaction for both the lead *sec*-butoxide **8** and

(14) Olmstead, W. M.; Margolin, Z.; Bordwell, F. G. *J. Org. Chem.* **1980**, *45*, 3295.

(15) Frisch, M. J.; Trucks, G. W.; Schlegel, H. B.; Scuseria, G. E.; Robb, M. A.; Cheeseman, J. R.; Montgomery, J. A., Jr.; Vreven, T.; Kudin, K. N.; Burant, J. C.; Millam, J. M.; Iyengar, S. S.; Tomasi, J.; Barone, V.; Mennucci, B.; Cossi, M.; Scalmani, G.; Rega, N.; Petersson, G. A.; Nakatsuji, H.; Hada, M.; Ehara, M.; Toyota, K.; Fukuda, R.; Hasegawa, J.; Ishida, M.; Nakajima, T.; Honda, Y.; Kitao, O.; Nakai, H.; Klene, M.; Li, X.; Knox, J. E.; Hratchian, H. P.; Cross, J. B.; Adamo, C.; Jaramillo, J.; Gomperts, R.; Stratmann, R. E.; Yazyev, O.; Austin, A. J.; Cammi, R.; Pomelli, C.; Ochterski, J. W.; Ayala, P. Y.; Morokuma, K.; Voth, G. A.; Salvador, P.; Dannenberg, J. J.; Zakrzewski, V. G.; Dapprich, S.; Daniels, A. D.; Strain, M. C.; Farkas, O.; Malick, D. K.; Rabuck, A. D.; Raghavachari, K.; Foresman, J. B.; Ortiz, J. V.; Cui, Q.; Baboul, A. G.; Clifford, S.; Cioslowski, J.; Stefanov, B. B.; Liu, G.; Liashenko, A.; Piskorz, P.; Komaromi, I.; Martin, R. L.; Fox, D. J.; Keith, T.; Al-Laham, M. A.; Peng, C. Y.; Nanayakkara, A.; Challacombe, M.; Pople, J. A. *Gaussian 03*, revision C.02; Gaussian Inc.: Wallingford, CT, **2004**.

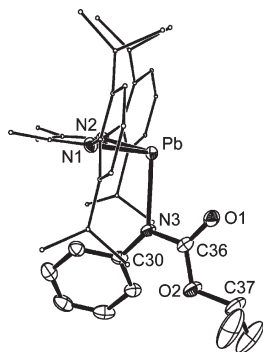


Figure 3. ORTEP diagram of lead carbamate **7** with H atoms omitted and BDI C atoms minimized for clarity. The ellipsoid probability is shown at 30%.

Table 3. Selected Bond Lengths and Angles for Compound **5**

Pb–O1	2.217(10)	N1–Pb–N2	83.23(18)
Pb–N1	2.292(5)	N1–Pb–O1	83.5(3)
Pb–N2	2.291(5)	N2–Pb–O1	82.2(3)
Pb–O1A	2.399(13)	N1–Pb–O1A	91.7(3)
Pb–O2A'	2.777(13)	N2–Pb–O1A	90.2(3)
Pb...Pb'	3.7842(5)	O1–Pb–O2A'	145.7(4)
O1–C30	1.309(16)	N1–Pb–O2A'	130.5(3)
O2–C30	1.188(17)	N2–Pb–O2A'	96.3(3)
O3–C30	1.372(14)	O1A–Pb–O2A'	137.8(4)
O3–C31	1.451(15)	Pb–O1–C30	113.5(8)
O1A–C30A	1.314(18)	O1–C30–O2	127.9(12)
O2A–C30A	1.18(2)	O1–C30–O3	107.9(12)
O3A–C30A	1.355(15)	O2–C30–O3	124.1(13)
O3A–C31A	1.453(16)	Pb–O1A–C30A	106.2(9)
		Pb'–O2A–C30A	148.4(11)
sum of the angles around Pb	266.04	O1A–C30–O2A	125.1(13)
DOP ^a (%)	104	O1A–C30–O3A	114.9(16)
		O2A–C30–O3A	119.8(16)

^a Degree of pyramidalization (DOP) = [360 – (sum of the angles)/0.9].²⁰

Table 4. Selected Bond Lengths and Angles for Compound **7**

Pb–N1	2.335(4)	N1–Pb–N2	82.47(14)
Pb–N2	2.321(4)	N1–Pb–N3	95.94(14)
Pb–N3	2.340(4)	N2–Pb–N3	96.84(14)
N3–C30	1.420(6)	Pb–N3–C30	132.5(3)
N3–C36	1.340(6)	Pb–N3–C36	103.2(3)
C36–O1	1.236(6)	N3–C36–O1	121.8(5)
C36–O2	1.348(6)	N3–C36–O2	116.4(5)
O2–C37	1.466(7)	O1–C36–O2	121.7(5)
		C36–O2–C37	116.9(4)
		sum of the angles around Pb	275.25
		DOP ^a	94%

^a Degree of pyramidalization (DOP) = [360 – (sum of the angles)/0.9].²⁰

tert-butoxide **3** cases (–9.4 kcal mol^{–1} vs –8.9 and –8.4 kcal mol^{–1}, respectively). Although these are gas-phase calculations, it is reassuring that the trends observed are similar to our experimental results.

The slow to nonexistent reactivity of our lead alkoxides with aliphatic electrophiles is in sharp contrast to the reactivity observed with transition-metal alkoxides. The most striking difference is with Vahrenkamp's pyrazolborate–zinc methoxide complex (Tp^{Ph,Me}Zn-OMe),¹⁶ which reacts readily with methyl iodide to generate the corresponding dimethyl

ether and pyrazolborate–zinc iodide complex, yet only reacts with CO₂ under forced conditions and not at all with phenyl isocyanate. This implies that the lead alkoxides lack nucleophilic characteristics. Space-filling models of alkoxide **2** reveal that the O atom lies inside a pocket surrounded by the BDI isopropyl groups and the alkyl group on the O atom. Thus, we cannot conclusively state that our lead alkoxides are non-nucleophilic because of potential steric arguments. However, we can conclude that a nucleophilic O atom is *not available* for reactivity.

The mechanism of CO₂ insertion into transition-metal alkoxides is generally thought to proceed via a concerted process in which the new carbon–oxygen and metal–carbonate bonds form at the same time as the cleavage of the metal–alkoxide bond.¹⁷ The symmetry of this transition state must vary depending upon the nucleophilicity of the O atom and the propensity for CO₂ to bind to the metal center. In our examples, the lack of an available nucleophilic O atom implies that coordination of CO₂ to the metal center is key, and it must be this coordination that induces the alkoxide to react with CO₂. This can occur either by changing the steric environment around the alkoxide or by shifting the electron density such that the alkoxide ligand becomes more nucleophilic and CO₂ becomes more electrophilic. However, we have been unable to observe the binding of additional ligands to the metal center, nor can we gain evidence for binding using computational analysis. The addition of extraneous ligands such as CH₃CN, THF, TMEDA, and N-heterocyclic carbenes as well as softer ligands such as trimethyl- and triphenylphosphine did not result in either measurable inhibition of CO₂ insertion or strong evidence of coordination. Indeed, crystals of the alkoxides **2**, **3**, or **8** grown in a 50:50 mixture of CH₃CN and hexane did not result in coordinated CH₃CN in the solid state.

The differing reactivity between our lead alkoxides and transition-metal alkoxides is intriguing both from a fundamental viewpoint and from implications in the mechanism of lead-mediated RNA cleavage, and we are testing whether our apparent non-nucleophilic behavior can be reproduced with less sterically hindered lead alkoxides. In addition, we are currently investigating the mechanism of CO₂ insertion using kinetic studies on the slower isostructural tin system.¹²

Experimental Section

All manipulations were carried out in an atmosphere of dry nitrogen or argon using standard Schlenk techniques or in an inert-atmosphere glovebox. Solvents were dried from the appropriate drying agent, distilled, degassed, and stored over 4 Å sieves. (BDI)PbCl (**1**) was prepared according to the literature.¹⁰ Potassium alkoxide salts were prepared by the slow addition of the relevant alcohol (dried and distilled) to a suspension of potassium hydride. Phenyl isocyanate and carbon disulfide were freshly dried and distilled before use. Carbon dioxide was used as received (Union Carbide, 99.999%), and ¹³CO₂ was 99 atom %. The ¹H and ¹³C NMR spectra were recorded on a Bruker DPX 300 MHz spectrometer, a Varian 400 MHz spectrometer, or a Varian 500 MHz spectrometer. The ¹H and ¹³C NMR spectroscopy chemical shifts are given relative to residual solvent peaks,

(17) For a few examples, see ref 15 as well as the following: Chisholm, M. H.; Cotton, F. A.; Extine, M. W.; Reichert, W. W. *J. Am. Chem. Soc.* **1978**, *100*, 1727. Darensbourg, D. J.; Sanchez, K. M.; Rheingold, A. L. *J. Am. Chem. Soc.* **1987**, *109*, 290. Campora, J.; Matas, I.; Palma, P.; Alvarez, E.; Graiff, C.; Tiripicchio, A. *Organometallics* **2007**, *26*, 3840.

(16) Brombacher, H.; Vahrenkamp, H. *Inorg. Chem.* **2004**, *43*, 6042.

and the ^{207}Pb elements were externally referenced to PbMe_4 . The data for the X-ray structures were collected at 173 K on a Nonius Kappa CCD diffractometer, $k(\text{Mo K}\alpha) = 0.710\ 73\ \text{\AA}$ and refined using the *SHELXL-97* software package.¹⁸

[CH₂{(CH₃)₂CN-2,6-ⁱPr₂C₆H₃}₂PbOⁱPr] (2). 1 (1.08 g, 1.64 mmol) was added to a stirred suspension of KOⁱPr (0.127 g, 1.64 mmol) in 10 mL of toluene at room temperature. The reaction vessel was wrapped in foil, and the mixture was stirred overnight. The mixture was filtered through a pad of Celite, and the solvent was removed in a vacuum. The resulting brown oil was dissolved in a minimum of pentane and **2** crystallized upon standing at $-30\ ^\circ\text{C}$ overnight (0.686 g, 62%). ^1H NMR (C_6D_6 , 293 K): δ 7.26 (d, 2H, $J = 7.5$ Hz, *m*-H), 7.20 (t, 2H, $J = 7.5$ Hz, *p*-H), 7.09 (d, 2H, $J = 7.5$ Hz, *m*-H), 4.96 (septet, 1H, $J = 6.8$ Hz, *CHMe*₂), 4.71 (s, 1H, middle CH), 3.95 (septet, 2H, $J = 6.8$ Hz, *CHMe*₂), 3.18 (septet, 2H, $J = 6.8$ Hz, *CHMe*₂), 1.69 (s, 6H, *NMe*), 1.57 (d, 6H, $J = 6.7$ Hz, *CHMe*₂), 1.29 (d, 6H, $J = 6.8$ Hz, *CHMe*₂), 1.20 (d, 6H, $J = 6.9$ Hz, *CHMe*₂), 1.17 (d, 6H, $J = 6.8$ Hz, *CHMe*₂), 1.07 (d, 6H, $J = 5.9$ Hz, *CHMe*₂). $^{13}\text{C}\{^1\text{H}\}$ NMR (C_6D_6 , 293 K): δ 163.9 (*NMe*), 145.1 and 143.3 (*ipso*- and *o*-C of Ar), 126.4, 124.8, and 123.9 (*m*- and *p*-CH of Ar), 100.2 (middle CH), 66.0 (*OCHMe*₂), 30.6 (*NMe*), 28.2 (*OCHMe*₂), 26.3, 25.7, 24.9, and 24.6 (*CHMe*₂). IR (Nujol, ν/cm^{-1}): 1553 (s), 1512 (s), 1317 (s), 1265 (s), 1172 (s), 1117 (s), 1012 (s), 960 (s), 790 (s), 752 (s), 722 (s). Anal. Calcd for $\text{C}_{32}\text{H}_{48}\text{ON}_2\text{Pb}$: C, 56.20; H, 7.07; N, 4.10. Found: C, 56.30; H, 7.17; N, 4.13.

[CH₂{(CH₃)₂CN-2,6-ⁱPr₂C₆H₃}₂PbOⁱBu] (3). 1 (0.908 g, 1.38 mmol) was added to a stirred suspension of KOⁱBu (0.154 g, 1.38 mmol) in toluene (15 mL) at room temperature, and the mixture was stirred overnight. The reaction mixture was filtered through Celite. The solvent was removed under vacuum, producing an orange solid as the crude product. The crude product was washed with pentane and recrystallized from toluene overnight, yielding yellow light-sensitive crystals of **3** (0.720 g, 75%). ^1H NMR (300 MHz, C_6D_6 , 293 K): δ 7.26 (dd, 2H, $J = 7.5$ Hz, *ArH*), 7.10 (d, 2H, $J = 7.5$ Hz, *ArH*), 7.04 (dd, 2H, $J = 7.5$ Hz, *ArH*), 4.57 (s, 1H, middle CH), 3.83 (septet, 2H, $J = 6.8$ Hz, *CHMe*₂), 3.12 (septet, 2H, $J = 6.8$ Hz, *CHMe*₂), 1.65 (s, 6H, *CCH*₃), 1.63 (d, 6H, $J = 6.8$ Hz, *C(CH*₃)₂), 1.25 (d, 6H, $J = 6.9$ Hz, *C(CH*₃)₂), 1.19 (d, 6H, $J = 6.9$ Hz, *C(CH*₃)₂), 1.14 (d, 6H, $J = 6.8$ Hz, *C(CH*₃)₂), 0.88 (s, 9H, *C(CH*₃)₃). $^{13}\text{C}\{^1\text{H}\}$ NMR (300 MHz, C_6D_6 , 293 K): 164.0 (*NMe*), 145.1 (*ipso*-C), 142.8 (*o*-C), 141.5 (*o*-C), 126.0 (*p*-C), 123.7 (*m*-C), 123.6 (*m*-C), 98.0 (middle CH), 69.1 (*OCMe*₃), 36.7 (*OC(CH*₃)₃), 28.4 (*CHMe*₂), 28.0 (*CHMe*₂), 26.1 (*NCCH*₃), 25.2 (*C(CH*₃)₂), 24.8 (*C(CH*₃)₂), 24.6 (*C(CH*₃)₂), 23.9 (*C(CH*₃)₂). IR (Nujol, ν/cm^{-1}): 1556 (s), 1511 (s), 1318 (s), 1262 (s), 1227 (s), 1015 (s), 941 (s), 838 (s), 791 (s), 751 (s). Anal. Calcd for $\text{C}_{33}\text{H}_{50}\text{N}_2\text{OPb}$: C, 56.79; H, 7.22; N, 4.01. Found: C, 56.70; H, 7.15; N, 3.97.

[CH₂{(CH₃)₂CN-2,6-ⁱPr₂C₆H₃}₂Pb(CO₂OⁱPr)] (5). 2 was dissolved in toluene (2 mL) and loaded into an ampule wrapped in aluminum foil. The reaction vessel was connected to a Schlenk line and a cylinder of high-purity CO₂. The vessel was submerged in a dry ice/acetone bath, and after three pump/refill cycles, CO₂ was introduced at a pressure of 1.5 bar. Thawing followed by removal of the solvent gave **5** as a yellow solid in quantitative yield. ^1H NMR (C_6D_6 , 300 K): δ 7.19 (s, 6H, *ArH*), 4.97 (septet, 1H, $J = 6.3$ Hz, *OCHMe*₂), 4.86 (s, 1H, middle CH), 3.39–3.32 (br multiplet, 4H), 3.02 (septet, 2H, $J = 6.9$ Hz, *CHMe*₂), 1.69 (s, 6H, *NMe*), 1.30 (d, 12H, $J = 6.3$ Hz, *CHMe*₂), 1.20 (d, 12H, $J = 6.3$ Hz, *CHMe*₂), 1.24 (d, 6H, $J = 6.8$ Hz, *OCHMe*₂). $^{13}\text{C}\{^1\text{H}\}$ NMR (500 MHz, toluene-*d*₈, 303 K): δ 164.1 (*NMe*), 160.9 (*OC=O*), 142.8 (*ipso*-C), 129.2 (*o*-C), 128.3 (*o*-C), 127.0 (*p*-C), 125.4 (*m*-C), 124.5 (*m*-C), 103.6 (middle CH), 68.7 (*OC(CH*₃)₂), 34.6 (*OC(CH*₃)₂), 28.3 (*CHMe*₂), 26.0

(*CHMe*₂), 24.7 (*NCCH*₃), 24.5 (*CH(CH*₃)₂), 22.8 (*CH(CH*₃)₂), 22.7 (*CH(CH*₃)₂), 14.3 (*CH(CH*₃)₂). ^{207}Pb NMR (400 MHz, toluene-*d*₈, 303 K): δ 808.7. IR (Nujol, ν/cm^{-1}): 3056 (s), 1611 (s), 1583 (s), 1551 (s), 1519 (s), 1317 (s), 1294 (s), 1171 (s), 1108 (s), 1055 (s), 1020 (s). IR (CCl_4 , ν/cm^{-1}): 3060 (s), 2963 (s), 2928 (s), 2871 (s), 2335 (br), 1699 (s), 1463 (s), 1438 (s), 1387 (br), 1319 (s), 1292 (s), 1173 (s), 1115 (s). Anal. Calcd for $\text{C}_{33}\text{H}_{48}\text{N}_2\text{O}_3\text{Pb}$: C, 54.45; H, 6.65; N, 3.85. Found: C, 54.49; H, 6.71; N, 3.75.

[CH₂{(CH₃)₂CN-2,6-ⁱPr₂C₆H₃}₂Pb(CO₂OⁱBu)] (6). 3 (0.050 g, 0.072 mmol) was dissolved in toluene-*d*₈ in an NMR tube sealed with a Young's tap. The gas inside the NMR tube was evacuated. CO₂ (0.0047 mg, 0.109 mmol) was then added. A yellow solution mixture was observed, and the reaction mixture was kept at room temperature for 24 h and was monitored by ^1H NMR spectroscopy. ^1H NMR (400 MHz, toluene-*d*₈, 203 K): δ 7.15 (s, 2H, *ArH*), 7.07 (d, 2H, $J = 4$ Hz, *ArH*), 6.95 (d, 2H, $J = 8$ Hz, *ArH*), 4.79 (s, 1H, middle CH), 3.64 (m, 2H, *CHMe*₂), 2.94 (m, 2H, *CHMe*₂), 1.62 (s, 6H, *CCH*₃), 1.58 (br, 6H, $J = 4$ Hz, *C(CH*₃)₂), 1.50 (d, 6H, $J = 4$ Hz, *C(CH*₃)₂), 1.17 (d, 6H, $J = 4$ Hz, *C(CH*₃)₂), 1.08 (s, 9H, *C(CH*₃)₃). $^{13}\text{C}\{^1\text{H}\}$ NMR (400 MHz, toluene-*d*₈, 203 K): δ 163.5 (*NMe*), 160.3 (*OC*), 144.2 (*ipso*-C), 142.3 (*o*-C), 141.6 (*o*-C), 103.5 (middle CH), 76.6 (*OCHMe*₂), 28.5 (*OCH(CH*₃)₂), 28.1 (*NCCH*₃), 27.6 (*CHMe*₂), 27.4 (*CHMe*₂), 26.8 (*CHMe*₂), 26.5 (*CHMe*₂), 25.0 (*C(CH*₃)₂), 24.7 (*C(CH*₃)₂), 24.3 (*C(CH*₃)₂), 24.1 (*C(CH*₃)₂). ^{207}Pb NMR (400 MHz, toluene-*d*₈, 303 K): δ 817.4. IR (CCl_4 , ν/cm^{-1}): 3060 (s), 2965 (s), 2928 (s), 2869 (s), 1699 (s), 1463 (s), 1438 (s), 1389 (b), 1366 (b), 1172 (s), 1102 (s).

[CH₂{(CH₃)₂CN-2,6-ⁱPr₂C₆H₃}₂Pb(N(Ph)CO)OⁱPr] (7). 19 Phenyl isocyanate (0.032 mL, 0.294 mmol) was added to a solution of **2** (0.196 g, 0.287 mmol) in toluene (3 mL). The reaction vessel was wrapped in foil and stirred at room temperature for 3 h. The volatiles were removed, and the resulting orange residue was dissolved in a minimum of pentane. **7** crystallized upon standing at $-30\ ^\circ\text{C}$ overnight (0.100 g, 44%). ^1H NMR (500 MHz, toluene-*d*₈, 303 K): δ 7.59 (br, 2H, *ArH*), 7.27 (t, 2H, $J = 15$ Hz, *ArH*), 6.85 (t, 1H, $J = 15$ Hz, *ArH*), 5.03 (s, 1H, middle CH), 4.91 (br, 1H, *OCHMe*₂), 3.13 (br, 4H, *CHMe*₂), 1.67 (s, 6H, *CCH*₃), 1.28 (d, 1H, $J = 5$ Hz, *C(CH*₃)₂), 1.25 (d, 1H, $J = 5$ Hz, *C(CH*₃)₂), 1.15 (2H, br d, $J = 10$ Hz, *C(CH*₃)₂), 0.98 (6H, br, *C(CH*₃)₂), 0.88 (d, 2H, $J = 10$ Hz, *C(CH*₃)₂), 0.87 (d, 2H, $J = 5$ Hz, *OC(CH*₃)₂). $^{13}\text{C}\{^1\text{H}\}$ NMR (500 MHz, toluene-*d*₈, 303 K): δ 165.0, 143.3, 129.2, 128.3, 127.9, 126.8, 126.0, 121.7, 103.2, 67.2, 34.6, 28.2, 25.5, 25.2, 24.6, 22.8, 22.4, 14.3. $^{13}\text{C}\{^1\text{H}\}$ NMR (400 MHz, toluene-*d*₈, 198 K): δ 164.7, 164.0, 163.7, 161.4, 158.9, 147.7, 146.6, 144.6, 144.1, 142.9, 142.4, 141.7, 141.4, 129.7, 127.3, 126.5, 126.0, 125.4, 68.0, 67.1, 66.8, 66.4, 65.8, 65.3, 34.5, 27.2, 26.7, 25.8, 25.0, 24.9, 24.4, 24.3, 24.2, 23.1, 22.3, 22.2, 21.9, 14.6. IR (Nujol, ν/cm^{-1}): 1745 (s), 1688 (s), 1578 (s), 1546 (s), 1515 (s), 1483 (s), 1315 (s), 1231 (s), 1168 (s), 1109 (s), 1054 (s), 1035 (s), 1021 (s). Anal. Calcd for $\text{C}_{39}\text{H}_{53}\text{N}_3\text{O}_2\text{Pb}$: C, 58.31; H, 6.66; N, 5.23. Found: C, 58.39; H, 6.54; N, 5.24.

[CH₂{(CH₃)₂CN-2,6-ⁱPr₂C₆H₃}₂PbO^sBu]. A suspension of KO^sBu (0.085 g, 757 mmol) in 3 mL of toluene was added dropwise to a stirred solution of **1** (0.500 g, 757 mmol) in toluene (10 mL) at room temperature. The reaction mixture was stirred overnight. The deep-yellow solution was filtered through Celite, and the solvent was removed under vacuum. The resulting yellow solid was dissolved in the minimum amount of pentane (~7 mL) and stored at $-30\ ^\circ\text{C}$ overnight, yielding yellow crystals of (BDI)PbOsBu (0.441 g, 83%). ^1H NMR (toluene-*d*₈, 303 K): δ 7.17 (d, 2H, $J = 7.5$ Hz, *m*-H), 7.03 (t, 2H, $J = 16.9$ Hz, *p*-H),

(18) Sheldrick, G. M. *SHELXL-97, Program for the Refinement of Crystal Structures*; University of Göttingen: Göttingen, Germany, 1997.

(19) The solution-phase chemistry of this compound is complex and is undergoing further studies to understand the variable-temperature NMR spectroscopic behavior.

(20) Maksic, Z. B.; Kovacevic, B. *J. Chem. Soc., Perkin Trans. 2* 1999, 2623.

7.02 (d, 2H, $J = 18.4$ Hz, *m-H*), 4.60 (s, 1H, middle *CH*), 4.56 (m, 1H, $\text{OCH}(\text{CH}_3)\text{CH}_2\text{CH}_3$), 3.79 (hept, 1H, $J = 6.9$ Hz, CHMe_2), 3.77 (hept, 1H, $J = 7.1$ Hz, CHMe_2), 3.10 (septet, 2H, $J = 6.8$ Hz, CHMe_2), 1.64 (s, 3H, *NMe*), 1.63 (s, 3H, *NMe*), 1.47 (dd, 6H, $J_1 = 6.5$ Hz, $J_2 = 4.8$ Hz, CHMe_2), 1.21 (dd, 6H, $J_1 = 6.8$ Hz, $J_2 = 1.7$ Hz, CHMe_2), 1.15 (d, 6H, $J = 6.8$ Hz, CHMe_2), 1.12 (d, 6H, $J = 6.8$ Hz, CHMe_2), 0.78 (d, 3H, $J = 6.0$ Hz, $\text{OCH}(\text{CH}_3)\text{CH}_2\text{CH}_3$). $^{13}\text{C}\{^1\text{H}\}$ NMR (C_6D_6 , 303 K): δ 163.4 (*NMe*), 144.7 (*ipso-C*), 142.8 and 141.6 (*o-C*), 125.8 (*p-C*), 123.4 and 123.3 (*m-C*), 99.1 (middle *CH*), 70.8 ($\text{OC}(\text{CH}_3)\text{CH}_2\text{CH}_3$), 36.3 ($\text{OC}(\text{CH}_3)\text{CH}_2\text{CH}_3$), 27.9 (*NMe*), 27.8 and 27.7 (CHMe_2), 26.0, 25.0, 24.2, and 23.7 (CHMe_2), 24.4 ($\text{OC}(\text{CH}_3)\text{CH}_2\text{CH}_3$), 10.5 ($\text{OC}(\text{CH}_3)\text{CH}_2\text{CH}_3$). ^{207}Pb NMR (400 MHz, C_6D_6): δ 1542.8. IR (Nujol, ν/cm^{-1}): 3057, 1556 (s), 1516 (s), 1437 (s), 1251, 1171, 1100 (s), 1023 (s), 986, 961, 936, 917, 840, 791 (s), 750. IR (CCl_4 , ν/cm^{-1}): 3059 (w), 2962, 2927, 2989, 2291 (w), 2004 (w), 1857 (w), 1550 (s), 1463, 1437, 1359, 1320, 1252 (s), 1217 (s), 1172. Anal. Calcd for $\text{C}_{33}\text{H}_{48}\text{N}_2\text{O}_3\text{Pb}$: C, 56.79; H, 7.22; N, 4.01. Found: C, 56.66; H, 7.08; N, 3.89.

$[\text{CH}\{(\text{CH}_3)_2\text{CN-2,6-}^i\text{Pr}_2\text{C}_6\text{H}_3\}_2\text{Pb}(\text{CO}_2)\text{O}^i\text{Pr}]$ (**9**). **8** (101 mg, 0.145 mmol) was dissolved in toluene (8 mL) in a sealable ampule. The gas was evacuated, and CO_2 was added (0.220 mmol). The reaction mixture was cooled to -80 °C to give a yellow powder. ^1H NMR (C_6D_6 , 303 K): δ 7.09 (s, br, 6H, *ArH*), 4.78 (s, 1H, middle *CH*), 4.71 (sext, 1H, $J = 6.21$ Hz, $\text{OCH}(\text{CH}_3)\text{CH}_2\text{CH}_3$), 3.30 (br, 4H, CHMe_2), 1.67 (m, 1H, $\text{OCH}(\text{CH}_3)\text{CH}_2\text{CH}_3$), 1.62 (s, 6H, *NMe*), 1.48 (m, 1H, $\text{OCH}(\text{CH}_3)\text{CH}_2\text{CH}_3$), 1.26 (d, 12H, $J_1 = 6.2$ Hz, CHMe_2), 1.18 (d,

3H, $J = 6.9$ Hz, $\text{OCH}(\text{CH}_3)\text{CH}_2\text{CH}_3$), 1.11 (d, 12H, CHMe_2), 0.90 (t, 3H, $J = 7.4$ Hz, $\text{OCH}(\text{CH}_3)\text{CH}_2\text{CH}_3$). $^{13}\text{C}\{^1\text{H}\}$ NMR (C_6D_6 , 303 K): δ 163.7 (*NMe*), 160.7 (OCO_2), 142.4 (*ipso-C*), 127.7 and 127.5 (*o-C*), 126.5 (*p-C*), 124.4 and 124.0 (*m-C*), 103.2 (middle *CH*), 73.2 ($\text{OC}(\text{CH}_3)\text{CH}_2\text{CH}_3$), 29.3 ($\text{OC}(\text{CH}_3)\text{CH}_2\text{CH}_3$), 27.8 (*NMe*), 24.2 (CHMe_2), 24.1 (CHMe_2), 19.7 ($\text{OC}(\text{CH}_3)\text{CH}_2\text{CH}_3$), 9.8 ($\text{OC}(\text{CH}_3)\text{CH}_2\text{CH}_3$). ^{207}Pb NMR (400 MHz, C_6D_6): δ 810.3. IR (Nujol, ν/cm^{-1}): 3027, 2336 (w), 1940 (w), 1855 (w), 1800 (w), 1604, 1549 (s), 1260 (s), 1081 (s, br), 804 (s), 694 (s). IR (CCl_4 , ν/cm^{-1}): 3723, 2693, 3621, 3590, 3063 (w), 2963, 2928, 2870, 2337 (s), 2005 (w), 1857 (w), 1645, 1550 (s), 1459, 1437, 1383, 1364, 1319, 1254 (s), 1217 (s), 1174. Note: traces of **8** were found in isolated solid-state samples of **9** (even crystallized samples), preventing acceptable elemental analysis.

Computational Details. All calculations were performed using the *Gaussian 03*, revision C.02, suite of programs using the B3LYP density functional theory and LanL2DZ pseudopotentials (and basis set).¹⁵

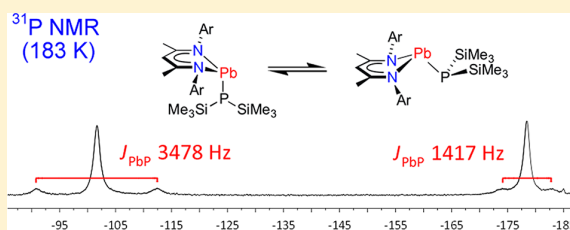
Acknowledgment. The authors are grateful for financial support from the EPSRC (Grant EP/E032575/1 to L.F.) and the University of Sussex.

Supporting Information Available: ORTEP diagram, crystallographic data, and selected bond lengths and angles for complex **8** and crystallographic data in CIF format for complexes **2**, **3**, **5**, **7**, and **8**. This material is available free of charge via the Internet at <http://pubs.acs.org>.

Group 14 Metal Terminal Phosphides: Correlating Structure with $|J_{MP}|$ Eric C. Y. Tam,[†] Nicola A. Maynard,[†] David C. Apperley,[‡] J. David Smith,[†] Martyn P. Coles,^{*,†,§} and J. Robin Fulton^{*,†,§}[†]Department of Chemistry, University of Sussex, Falmer, Brighton, U.K.[‡]Department of Chemistry, University of Durham, South Road, Durham, U.K.

Supporting Information

ABSTRACT: A series of heavier group 14 element, terminal phosphide complexes, $M(\text{BDI})(\text{PR}_2)$ ($M = \text{Ge}, \text{Sn}, \text{Pb}$; $\text{BDI} = \text{CH}\{(\text{CH}_3)_2\text{CN}-2,6\text{-iPr}_2\text{C}_6\text{H}_3\}_2$; $\text{R} = \text{Ph}, \text{Cy}, \text{SiMe}_3$) have been synthesized. Two different conformations (*endo* and *exo*) are observed in the solid-state; the complexes with an *endo* conformation have a planar coordination geometry at phosphorus ($M = \text{Ge}, \text{Sn}$; $\text{R} = \text{SiMe}_3$) whereas the complexes possessing an *exo* conformation have a pyramidal geometry at phosphorus. Solution-state NMR studies reveal through-space scalar coupling between the tin and the isopropyl groups on the *N*-aryl moiety of the BDI ligand, with *endo* and *exo* exhibiting different J_{SnC} values. The magnitudes of the tin–phosphorus and lead–phosphorus coupling constants, $|J_{\text{SnP}}|$ and $|J_{\text{PbP}}|$, differ significantly depending upon the hybridization of the phosphorus atom. For $\text{Sn}(\text{BDI})(\text{P}\{\text{SiMe}_3\}_2)$, $|J_{\text{SnP}}|$ is the largest reported in the literature, surpassing values attributed to compounds with tin–phosphorus multiple-bonds. Low temperature NMR studies of $\text{Pb}(\text{BDI})(\text{P}\{\text{SiMe}_3\}_2)$ show two species with vastly different $|J_{\text{PbP}}|$ values, interpreted as belonging to the *endo* and *exo* conformations, with sp^2 - and sp^3 -hybridized phosphorus, respectively.



INTRODUCTION

$M(\text{BDI})\text{X}$ complexes of the heavier group 14 elements, ($M = \text{Ge}, \text{Sn}, \text{Pb}$; $\text{BDI} = \text{CH}\{(\text{CH}_3)_2\text{CN}-2,6\text{-iPr}_2\text{C}_6\text{H}_3\}_2$; $\text{X} =$ monoanionic, terminal ligand) were initially synthesized over 10 years ago.¹ In the past 5 years, many studies have focused on the synthesis and structural characterization of new examples,² while others have explored the chemistry of the terminal ligands.³ Although the geometry of the central atom, M , in these three-coordinate complexes is pyramidal, two different conformations are observed in the solid-state (Figure 1).⁴ In

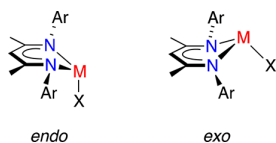


Figure 1. *Endo* and *exo* conformations of $M(\text{BDI})\text{X}$ ($\text{Ar} = 2,6\text{-iPr}_2\text{-C}_6\text{H}_3$).

the *endo* conformation, M and X are on the same side of the NCCC plane of the BDI ligand with an approximately perpendicular $M\text{--}X$ bond, and in the *exo* conformation M and X generally lie on opposite sides of the NCCC plane, and the terminal ligand points away from the $M(\text{BDI})$ core. To a first approximation these conformations can be attributed to interactions of the terminal ligand, X , and the *N*-aryl groups of the BDI ligand. Smaller X -groups or those able to adopt a planar geometry can find room between the two *N*-aryl groups in an *endo* conformation whereas larger ligands force the

molecule into the *exo* conformation to avoid steric conflict. Currently these observations are restricted to the solid-state and no spectroscopic markers differentiating these two conformations have been noted in solution.

Terminal phosphide complexes, $M(\text{BDI})(\text{PR}_2)$, have recently been reported. Roesky and Zhu have synthesized $\text{Ge}(\text{BDI})(\text{PPh}_2)$,⁵ which is *exo* in the solid-state with a pyramidal geometry at phosphorus. Driess has made the germanium^{2d} and lead^{2g} *bis*(trimethylsilyl) phosphide derivatives, $M(\text{BDI})(\text{P}\{\text{SiMe}_3\}_2)$. Although crystal structure data for the latter two compounds show the germanium complex to be *endo* with a planar geometry at the phosphorus atom, and the lead homologue to be *exo* with a pyramidal phosphorus environment, no explanation for these differences has been presented. We show in this contribution that the shorter $\text{Ge}\text{--}\text{P}$ bond (2.3912(8) Å) compared with $\text{Pb}\text{--}\text{P}$ bond (2.715(2) Å) is not sufficient to account for this dichotomy.

To understand the preference for the group 14 phosphides to adopt either the *endo* or *exo* conformation, we have expanded this series of compounds. In particular we have targeted the previously unknown tin derivatives as intermediate between the germanium and the lead species, and taken advantage of additional spectroscopic information available from ^{119}Sn NMR experiments. Our spectroscopic studies have revealed previously unreported through-space scalar coupling between Sn and the isopropyl groups on the BDI *N*-aryl group, allowing us

Received: June 7, 2012

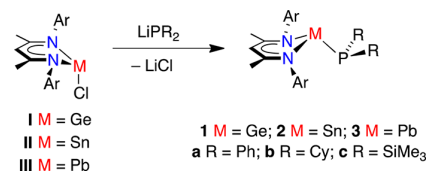
Published: August 17, 2012

to look at the solution-phase conformations of these compounds. In addition, an exceptionally large coupling constant is observed in the tin *bis*(trimethylsilyl) phosphide derivative, prompting us to re-examine the lead homologue.

RESULTS AND DISCUSSION

Synthesis. The group 14 chlorides $M(\text{BDI})\text{Cl}$ (**I** $M = \text{Ge}$,¹ **II** $M = \text{Sn}$,¹ **III** $M = \text{Pb}^{2e}$) were synthesized according to literature procedures. Reaction of **I–III** with 1 equiv of LiPR_2 ($R = \text{Ph}$, Cy , SiMe_3) afforded the heteroleptic compounds $M(\text{BDI})(\text{PR}_2)$ (**1** $M = \text{Ge}$, **2** $M = \text{Sn}$, **3** $M = \text{Pb}$; **a** $R = \text{Ph}$, **b** $R = \text{Cy}$, **c** $R = \text{SiMe}_3$) (Scheme 1). This strategy has previously

Scheme 1



been used to synthesize $\text{Ge}(\text{BDI})(\text{PPh}_2)$ **1a**⁵ and $\text{Ge}(\text{BDI})(\text{P}\{\text{SiMe}_3\}_2)$ **1c**,^{2d} the lead analogue **3c** was made from the aryloxide $\text{Pb}(\text{BDI})(\text{OAr}^\dagger)$ ($\text{Ar}^\dagger = 2,6\text{-tBu}_2\text{C}_6\text{H}_3$).^{2g} We found that **3c** may be synthesized in excellent yield (91%) by treatment of **III** with $\text{LiP}\{\text{SiMe}_3\}_2$. All compounds were isolated as solids that are stable at room temperature and could be handled under an inert atmosphere with no other precautions. In contrast solutions of **1–3**, in particular the lead derivatives, must be handled in the dark, as insoluble metallic precipitates were formed under ambient light conditions. Purification was achieved by crystallization, affording analytically pure products in good to excellent yields. In general, yields for the diphenylphosphides (**1a**, **2a**, and **3a**) were lower than those for other derivatives, and the compounds decomposed at lower temperatures. The frequent formation of tetraphenyldiphosphine, detected by $^{31}\text{P}\{^1\text{H}\}$ NMR ($\delta_{\text{P}} -14.8$)⁶ and crystal structure determination (see Supporting Information), suggests that the group 14 elements may mediate single-electron decomposition processes in the $M\text{-PPh}_2$ unit.

Crystallographic Analysis. Single crystal X-ray diffraction data have been obtained for all new phosphide compounds. Selected interatomic distances (Å) and angles (deg) are collected in Tables 1 (**1b**), 2 (**2a**, **2b**, **2c**), and 3 (**3a**, **3b**); these data are presented alongside those for **1a** and **1c** (Table 1) and **3c** (Table 3) for comparison. Crystal structure and refinement data are collected in Tables 6 (**1b**, **2a**, **2b**, **2c**) and 7 (**3a**, **3b**).

The germanium compound **1b** crystallizes as the monomeric, three-coordinate species, with a terminal- PCy_2 phosphide fragment (Figure 2). An *exo*-conformation is adopted in the solid-state, with the germanium 0.963(6) Å out of the plane defined by the NCCCN backbone of the BDI ligand. The coordination at germanium is pyramidal, with a degree of pyramidalization (DP),⁷ of 80%. This latter measurement is a useful tool when comparing three-coordinate species; a DP of 100% is equivalent to a sum of angles of 270°, where as a DP of 0% is indicative of a planar geometry at the central atom (eq 1). The large DP at the germanium atom **1b** suggests that its lone-pair possesses marked *s*-character. The phosphorus atom also has a pyramidal coordination geometry (DP = 69%). The Ge–P bond length of 2.4724(8) Å is similar to that of **1a**

Table 1. Selected Bond Lengths (Å) and Angles (deg) for $\text{Ge}(\text{BDI})(\text{PCy}_2)$ **1b** Presented with Those for $\text{Ge}(\text{BDI})(\text{PPh}_2)$ (**1a**)⁵ and $\text{Ge}(\text{BDI})(\text{P}\{\text{SiMe}_3\}_2)$ (**1c**)^{2d} for Comparison

	1a ^a	1b	1c ^d
Ge–P	2.4746(11)	2.4724(8)	2.3912(8)
Ge–N1	2.003(3)	2.049(2)	2.006(2)
Ge–N2	2.029(3)	2.048(2)	2.046(2)
P–C30	1.846(3)	1.900(3)	
P–C36	1.844(4)	1.889(3)	
P–Si1			2.219(1)
P–Si2			2.227(1)
N1–Ge–N2	88.20(11)	88.05(8)	90.20(9)
N1–Ge–P	99.24(8)	102.52(6)	103.46(7)
N2–Ge–P	99.29(8)	101.35(7)	94.93(6)
C30–P–C36	99.14(16)	102.25(13)	
Ge–P–C30	100.25(10)	98.12(10)	
Ge–P–C36	100.69(12)	97.97(9)	
Si1–P–Si2			110.13(5)
Ge–P–Si1			111.14(4)
Ge–P–Si2			133.93(4)
DP(%) at Ge	82	76	79
DP(%) at P	67	69	5
θ^b	+39.4(1)	+39.9(1)	–22.1

^aDifferent numbering scheme used; corresponding bond length/angle listed. ^bFold angle between the planes defined by N1,C1,C2,C3,N2 atoms (plane 1) and N1,Ge,N2 atoms (plane 2). Positive values indicate *exo*-conformer.

Table 2. Selected Bond Lengths (Å) and Angles (deg) for $\text{Sn}(\text{BDI})(\text{PPh}_2)$ **2a**, $\text{Sn}(\text{BDI})(\text{PCy}_2)$ **2b**, and $\text{Sn}(\text{BDI})(\text{P}\{\text{SiMe}_3\}_2)$ **2c**

	2a ^a	2b	2c
Sn–P	2.6612(12), 2.6417(12)	2.6309(7)	2.5526(7)
Sn–N(1)	2.211(3), 2.205(4)	2.233(2)	2.217(2)
Sn–N(2)	2.220(3), 2.224(4)	2.227(2)	2.2210(19)
P–C(30)	1.839(5), 1.844(5)	1.881(3)	
P–C(36)	1.836(5), 1.844(5)	1.892(3)	
P–Si(1)			2.2166(10)
P–Si(2)			2.2215(11)
N1–Sn–N2	83.76(13), 83.96(13)	83.23(8)	85.17(7)
N1–Sn–P	95.78(9), 96.11(10)	102.60(6)	101.77(5)
N2–Sn–P	104.53(10), 102.83(10)	99.95(6)	95.55(5)
C30–P–C36	102.5(2), 100.6(2)	103.30(12)	
Sn–P–C30	91.21(15), 94.49(14)	95.33(9)	
Sn–P–C36	102.07(15), 99.91(14)	96.18(8)	
Si1–P–Si2			111.32(4)
Sn–P–Si1			111.29(4)
Sn–P–Si2			136.45(4)
DP(%) Sn	84, 86	83	86
DP(%) P	71, 72	72	1
θ^b	+39.5(2), +39.8(2)	+39.0(1)	–20.9

^aTwo independent molecules in the unit cell; second value corresponds to equivalent bond in second molecule. ^bFold angle between the planes defined by N1,C1,C2,C3,N2 atoms (plane 1) and N1,Sn,N2 atoms (plane 2). Positive values indicate *exo*-conformer.

(2.4746(11) Å),⁵ but long compared with other terminal $\text{Ge}(\text{II})\text{-PR}_2$ distances ($R = \text{aryl}$ or alkyl ; range 2.3938(13) to 2.4151(13) Å).⁸ The Ge–P bonds in **1a** and **1b** are also longer

Table 3. Selected Bond Lengths (Å) and Angles (deg) for Pb(BDI)(PPh₂) 3a and Pb(BDI)(PCy₂) 3b, Presented with Those for Pb(BDI)(P{SiMe₃})₂ (3c)^{2g} for Comparison

	3a	3b	3c ^a
Pb–P	2.720(2)	2.6945(9)	2.715(2)
Pb–N(1)	2.324(6)	2.342(3)	2.359(6)
Pb–N(2)	2.347(6)	2.326(3)	2.325(6)
P–C(30)	1.845(8)	1.880(3)	
P–C(36)	1.818(9)	1.887(3)	
P–Si(1)			2.260(3)
P–Si(2)			2.248(3)
N1–Pb–N2	80.2(2)	80.79(9)	81.2(2)
N1–Pb–P	98.21(15)	102.03(7)	97.32(15)
N2–Pb–P	105.98(15)	99.25(7)	103.18(16)
C30–P–C36	101.3(4)	103.79(15)	
Pb–P–C30	87.3(2)	93.57(11)	
Pb–P–C36	101.1(3)	95.17(11)	
Si1–P–Si2			99.45(11)
Pb–P–Si1			96.00(9)
Pb–P–Si2			110.25(10)
DP(%) at Pb	84	87	87
DP(%) at P	78	75	60
θ ^b	+34.3(3)	+38.7(1)	+43.9

^aDifferent numbering scheme used; corresponding bond length/angle listed. ^bFold angle between the planes defined by N1,C1,C2,C3,N2 atoms (plane 1) and N1,Pb,N2 atoms (plane 2). Positive values indicate *exo*-conformer.

Table 4. Selected Spectroscopic Data for M(BDI)X (M = Ge, Sn, Pb; X = Cl, N{SiMe₃})₂, PPh₂, PCy₂, P{SiMe₃})₂ in C₆D₆^a

	Cl	N{SiMe ₃ }) ₂	PPh ₂	PCy ₂	P{SiMe ₃ }) ₂	
Ge	³¹ P		−36.0 ^b	−14.1	−192.7 ^{2d}	
	²⁹ Si				2.0 ^{2d}	
	J _{Psi}				17 ^{2d}	
Sn	³¹ P		−30.7	−15.4	−183.5	
	²⁹ Si	0.61/−4.7 ²⁵			4.0	
	¹¹⁹ Sn	−224 ¹	−134 ²⁵	125	358	39
	J _{Psi}				17	
	J _{SnP}		978	964	2427	
Pb	³¹ P		7.3	26.9	−116.6 ^{2g}	
	²⁹ Si	−2.4/−3.1 ^{2g}			7.4 ^{2g}	
	²⁰⁷ Pb	1413 ²⁶	1824 ^{2g}	3011	3981	−1737 ^{2g}
	J _{Psi}					36 ^{2g}
	J _{PbP}		1129	1084	2852 ^{2g}	

^aChemical shift/ppm; coupling constants/Hz. ^bReference 5 reports the ³¹P NMR chemical shift for Ge(BDI)(PPh₂) (1a) as δ −14.9 ppm.

than those in terminal silyl-substituted phosphides (2.291(4) to 2.426(7) Å),^{2d,9} including 1c (2.3912(8) Å).

$$DP(\%) = [360 - \sum_{i=1}^3 \alpha_i] / 0.9 \quad (1)$$

In contrast to the *exo*-conformation in 1a⁵ and 1b, Ge(BDI)(P{SiMe₃})₂ (1c) is *endo*.^{2d} The germanium atom shows a similar degree of pyramidalization (DP = 79%) but it is 0.55 Å below the diketimate plane (θ = −22.1°). In contrast with the three coordinate, Ge(II) terminal phosphide Ge(2,6-{trip}₂C₆H₃)(P{SiMe₃})₂ (trip = 2,4,6-*i*Pr₃C₆H₂),⁹ which has a DP at phosphorus of 37%, and most tris(silyl-substituted)

phosphines, where the DP ranges from 34 to 54%,¹⁰ the phosphorus atom in 1c has an almost planar geometry (DP = 5%). The only other structurally characterized example of a planar geometry at the phosphorus atom is that in P{Si(*i*Pr)₃}.¹¹ Although transition metal phosphide complexes can possess a phosphorus atom with a planar coordination geometry because of donation of the lone pair into an empty d orbital,¹² this is not the case with group 14 derivatives. Our observations suggest that the planarity of the geometry at phosphorus in 1c derives from the steric influence of the BDI ligand rather than from electronic effects associated with the silyl-groups.

The molecular structures of tin compounds 2a–2c (Figure 3) closely resemble those of their germanium analogues; each is monomeric with terminal phosphido groups. For compounds 2a and 2b, the tin atom is located 1.063(5)/1.067(6) Å and 1.067(3) Å above the NCCCN plane, respectively, corresponding to *exo*- conformations. In contrast, the conformation of 2c is *endo*, with the tin 0.595(3) Å below the plane. The DP at tin (range 83 to 86%) does not vary significantly between conformations and does not depend on the phosphorus substituent.

The Sn–P distances in 2a and 2b (2.6612(12)/2.6417(12) Å and 2.6309(7) Å, respectively) are similar to those in other terminal Sn(II) phosphides with alkyl or aryl substituents, although examples are limited to the ate complex [Li(THF){Sn(P(*t*Bu)₂)(μ-P(*t*Bu)₂)₂}] (Sn–P = 2.684(4) Å),¹³ and the amino-stabilized diphosphastannylenes, Sn[P(CH{SiMe₃})₂-(C₆H₄-2-CH₂NMe₂)₂],¹⁴ and Sn[P(CH{SiMe₃})₂-(C₆H₄-2-NMe₂)₂],^{8b} (range Sn–P = 2.5995(10) to 2.6439(9) Å). The Sn–P bond in the silyl-derivative 2c (2.5526(7) Å) is similar to those in other Sn(II) phosphides containing the -P{SiR₃})₂ group, that is, heterometallic Ba/Sn¹⁵ and Ca/Sn¹⁶ systems (Sn–P range 2.597(3)–2.615(2) Å), the diphosphanylstannylenes, Sn(P{Si(*t*Bu)(trip)F₂})₂ (Sn–P = 2.567(1) Å),¹⁷ and Sn(2,6-{trip}₂C₆H₃)(P{SiMe₃})₂ (Sn–P = 2.527(1) Å).⁹

As in the germanium series, the geometry of the phosphorus atom is different in 2c (DP = 1%), from that in both 2a (DP = 71/72%) and 2b (DP = 72%), and the compounds described above,^{8b,13,14} (DP ranges from 25 to 47%) and is specific to the BDI-ligand system. The planar geometry is distorted, with the Sn–P–Si₂ angle (136.45(4)°) significantly greater than the remaining angles (Figure 3b), presumably to relieve crowding by the aryl substituents.

As for 3c,^{2g} compounds 3a and 3b are monomers with terminal phosphido groups (Figure 4) and the pyramidally coordinated lead atoms (DP: 3a, 84%; 3b, 87%; 3c, 87%) above the ligand plane (3a, 1.02(1) Å; 3b, 1.127(4) Å; 3c, 1.25 Å). The conformations are therefore *exo* for all members of the series, and in each case the geometry at phosphorus is pyramidal (DP: 3a, 78%; 3b, 75%; 3c, 60%).

The Pb–P distances in 3a (2.720(2) Å) and 3b (2.6945(9) Å) are shorter than the terminal Pb–P bond lengths in [Li(THF){Pb(P(*t*Bu)₂)(μ-P(*t*Bu)₂)₂}] (Pb–P = 2.766(7) Å)¹³ and [Pb(P(*t*Bu)₂)(μ-P(*t*Bu)₂)₂]₂ (Pb–P = 2.781(4) Å).¹⁸ In contrast to the germanium and tin compounds, where the M–P distances for the silyl-substituted derivatives are about 3.5% shorter than the M–PR₂ distances, the Pb–P distance in 3c (2.715(2) Å),^{2g} is similar to the average of those in 3a and 3b.

Spectroscopic Analysis. In general, spectra obtained from solutions of *endo*- and *exo*- isomers of M(BDI)X show that the methyl groups within each *iso*-propyl group are inequivalent; that is, there are two apparent septets and four doublets in the

Table 5. Selected Spectroscopic Data for Previously Reported Compounds That Contain Tin–Phosphorus Multiple Bond Character, and Related Species^a

compound	³¹ P	¹¹⁹ Sn	J _{SnP}	solvent
2c	−183.5	39	2427	C ₆ D ₆
R ₂ Sn=P(mes*) ^{27a}	204.7	658	2295	C ₆ D ₆
(Ar [‡]) ₂ Sn=P(mes*) ^{27b}	170.7	500	2208	not reported
(Ar) ₂ Sn(F)–P(Li)(mes)·W(CO) ₅ ^{27c}	−121.0	35	2099	CDCl ₃
Li[(Ar [‡]) ₂ Sn=P(Ar [‡])] ⁹	229.7	<i>b</i>	2004	C ₆ D ₆
Sn(P{Si [†] Pr ₃ }{Si(Ar [‡]) ₂ F}) ₂ ¹⁷	−102.5	1551	1682	not reported
Sn(P{Si [†] Pr ₃ }{Si(Ar [‡])(^t Bu)F}) ₂ ¹⁷	−121.3	<i>b</i>	1628	not reported
[Sn(μ-P{Ar [‡] })] ₂ ^{27d}	255.6	967	1464	C ₆ D ₆
Sn(P{SiPh ₃ }) ₂ ^{27e}	−175.4	<i>b</i>	1323	C ₆ D ₆
[Sn(P{SiMe ₃ }) ₂ (μ-P{SiMe ₃ }) ₂] ^{27f}	−231.8 ^c		1117 ^c 1012 ^d	C ₆ D ₆
	−236.4 ^d		1224 ^e 1298 ^f	
	−281.4 ^e −295.3 ^f			
Sn(P{Ph}{Ar [‡] }) ₂ ^{27g}	0.1	1101	891	C ₆ D ₆

^aChemical shift/ppm; coupling constants/Hz; Ar[‡] = 2,4,6-*i*-Pr₃C₆H₃; Ar[§] = 2,6-(Ar[‡])₂C₆H₃; Ar[¶] = 2,6-(Ar)₂C₆H₃; Ar^γ = 2,6-(mes)₂C₆H₃. ^b¹¹⁹Sn chemical shift not reported. ^c*trans*-terminal. ^d*cis*-terminal. ^e*cis*-bridging. ^f*trans*-bridging.

Table 6. Crystal Structure and Refinement Data for Ge(BDI)(PCy₂) **1b**, Sn(BDI)(PPh₂) **2a**, Sn(BDI)(PCy₂) **2b**, and Sn(BDI)(P{SiMe₃})₂ **2c**

	1b	2a	2b	2c
formula	C ₄₁ H ₆₃ GeN ₂ P	C ₄₁ H ₅₁ N ₂ PSn·0.5(C ₇ H ₈)	C ₄₁ H ₆₃ N ₂ PSn	C ₃₅ H ₅₉ N ₂ PSi ₂ Sn
formula weight	687.49	767.57	733.59	713.68
temperature (K)	173(2)	173(2)	173(2)	173(2)
wavelength (Å)	0.71073	0.71073	0.71073	0.71073
crystal size (mm)	0.21 × 0.09 × 0.06	0.16 × 0.10 × 0.08	0.17 × 0.11 × 0.07	0.18 × 0.10 × 0.06
crystal system	monoclinic	triclinic	monoclinic	monoclinic
space group	P2 ₁ /c (No.14)	P $\bar{1}$ (No.2)	P2 ₁ /c (No.14)	P2 ₁ /c (No.14)
<i>a</i> (Å)	10.0941(2)	12.6382(3)	9.9722(1)	12.1569(2)
<i>b</i> (Å)	23.5171(5)	17.6553(4)	23.7044(4)	15.7065(2)
<i>c</i> (Å)	17.2689(3)	19.5975(4)	17.4243(3)	23.4050(4)
α (deg)	90	69.422(1)	90	90
β (deg)	110.600(1)	84.810(1)	109.003(1)	119.547(1)
γ (deg)	90	74.862(1)	90	90
<i>V</i> (Å ³)	3837.24(13)	3951.75(15)	3894.37(10)	3887.82(10)
<i>Z</i>	4	4	4	4
<i>D_c</i> (Mg m ^{−3})	1.19	1.29	1.25	1.22
absorption coefficient (mm ^{−1})	0.87	0.72	0.73	0.78
θ range for data collection (deg)	3.47 to 26.73	3.40 to 27.09	3.44 to 27.11	3.48 to 27.10
reflections collected	48350	66909	57848	60531
independent reflections	8127 [R _{int} = 0.079]	17382 [R _{int} = 0.089]	8576 [R _{int} = 0.077]	8547 [R _{int} = 0.076]
reflections [<i>I</i> > 2 σ (<i>I</i>)	6180	11616	6730	6661
data/restraints/parameters	8127/0/408	17382/1/828	8576/0/408	8547/0/372
goodness-of-fit on <i>F</i> ²	0.990	1.030	1.023	0.991
final <i>R</i> indices [<i>I</i> > 2 σ (<i>I</i>)	<i>R</i> 1 = 0.046 <i>wR</i> 2 = 0.108	<i>R</i> 1 = 0.055 <i>wR</i> 2 = 0.123	<i>R</i> 1 = 0.037 <i>wR</i> 2 = 0.072	<i>R</i> 1 = 0.034 <i>wR</i> 2 = 0.070
<i>R</i> indices (all data)	<i>R</i> 1 = 0.070 <i>wR</i> 2 = 0.119	<i>R</i> 1 = 0.099 <i>wR</i> 2 = 0.139	<i>R</i> 1 = 0.058 <i>wR</i> 2 = 0.079	<i>R</i> 1 = 0.056 <i>wR</i> 2 = 0.078
largest diff. peak/hole (e Å ^{−3})	0.79 and −0.44	1.81 and −0.82	0.48 and −0.83	0.45 and −0.69

¹H NMR spectra. Correspondingly there are two resonances attributed to the CHMe₂ carbons and four assigned to the CHMe₂ carbons in the ¹³C{¹H} NMR spectra. Analysis of the ¹³C{¹H} NMR spectrum of chloride **II** revealed previously unreported coupling between *iso*-propyl-methine (⁴J_{SnC}) and -methyl (⁵J_{SnC}) resonances and tin, present as unresolved ¹¹⁷Sn and ¹¹⁹Sn satellites (Figure S). Given the 4- and 5-bond separation between these atoms (for which through-bond coupling is likely to be weak) and the variation in J_{SnC} from resonance to resonance, we assign this to through-space scalar

coupling (note: we have denoted the number of bonds between relevant nuclei as superscript *n*, i.e., ^{*n*}J; however, this is used as a nomenclature tool and not an indication that the observed coupling is a through-bond phenomenon).¹⁹ This through-space scalar coupling has previously been restricted to examples of coupling between NMR active nuclei, one of which is effectively 100% naturally abundant (i.e., ¹H, ¹⁹F, ³¹P); a recent observation of {¹⁹F–^{117/119}Sn} and {¹⁹F–²⁰⁷Pb} coupling is most pertinent to this work.²⁰ Our results are the first to demonstrate that this phenomenon may be observed with

Table 7. Crystal Structure and Refinement Data for Pb(BDI)(PPh₂) 3a and Pb(BDI)(PCy₂) 3b

	3a	3b
formula	C ₄₁ H ₅₁ N ₂ PPb	C ₄₁ H ₆₃ N ₂ PPb
formula weight	810.01	822.09
temperature (K)	173(2)	173(2)
wavelength (Å)	0.71073	0.71073
crystal size (mm)	0.15 × 0.07 × 0.03	0.22 × 0.11 × 0.04
Crystal system	orthorhombic	monoclinic
space group	<i>I</i> 2 <i>cb</i> (No.45)	<i>P</i> 2 ₁ / <i>c</i> (No.14)
<i>a</i> (Å)	15.9697(5)	9.9586(2)
<i>b</i> (Å)	18.3168(6)	23.7678(4)
<i>c</i> (Å)	25.8355(6)	17.4757(2)
β (deg)	90	108.531(1)
<i>V</i> (Å ³)	7557.2(4)	3921.93(11)
<i>Z</i>	8	4
<i>D</i> _c (Mg m ⁻³)	1.42	1.39
absorption coefficient (mm ⁻¹)	4.54	4.37
θ range for data collection (deg)	3.43 to 27.09	3.43 to 27.09
reflections collected	24237	57828
independent reflections	8198 [<i>R</i> _{int} = 0.081]	8624 [<i>R</i> _{int} = 0.068]
reflections [<i>I</i> > 2 σ (<i>I</i>)]	5814	6904
data/restraints/parameters	8198/1/408	8624/0/408
goodness-of-fit on <i>F</i> ²	0.986	1.031
final <i>R</i> indices [<i>I</i> > 2 σ (<i>I</i>)]	<i>R</i> 1 = 0.047 <i>wR</i> 2 = 0.085	<i>R</i> 1 = 0.029 <i>wR</i> 2 = 0.054
<i>R</i> indices (all data)	<i>R</i> 1 = 0.086 <i>wR</i> 2 = 0.096	<i>R</i> 1 = 0.047 <i>wR</i> 2 = 0.058
largest diff. peak/hole (e Å ⁻³)	0.68 and -1.40	0.99 and -0.97

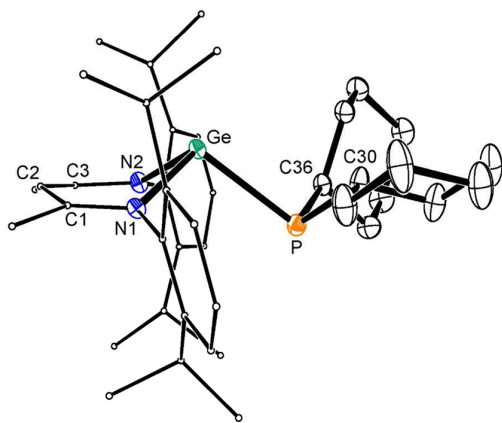


Figure 2. Molecular structure of Ge(BDI)(PCy₂) (**1b**) (H atoms omitted and BDI aryl groups C atoms minimized). Ellipsoid probability at 30%.

relatively insensitive but ubiquitous carbon-13 nuclei and to suggest that it may find general application for the study of species in solution.

Through-space scalar coupling implies that the nuclei come into close proximity in solution. The molecular structure of Sn(BDI)Cl is *endo*,¹ where for orthorhombic polymorph **II'** (see Supporting Information) the metal is displaced 0.801(3)/0.760(3) Å below the ligand plane ($\theta = -29.5(1)/-27.9(1)^\circ$). In the solid-state the range of Sn...C distances to the *iso*-propyl groups does not distinguish between those “adjacent” and “opposite” the chloride (Figure 5). For species with these precise conformations in solution, the coupling of the tin with

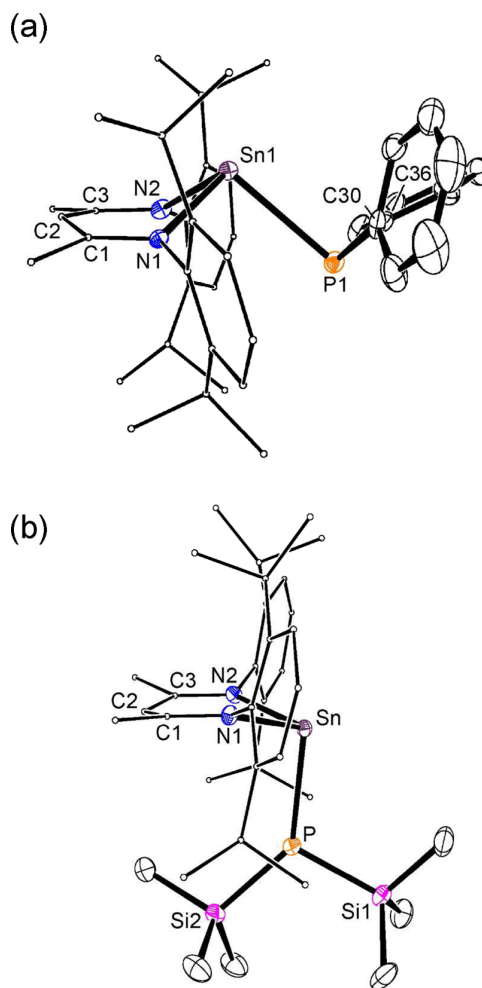


Figure 3. Molecular structure of (a) one of the independent molecules of Sn(BDI)(PPh₂) (**2a**) and (b) Sn(BDI)(P{SiMe₃}₂) (**2c**) (toluene solvate (**2a**) and H atoms omitted, and BDI aryl groups C atoms minimized). Ellipsoid probability 30%.

both *iso*-propyl groups should be similar. This is in contrast with the observed data where, within the resolution of the instrument, ^{4/5}*J*_{SnC} is only observed for one *iso*-propyl group (Figure 5a, a(b)₂). As such, although we are confident that the *endo* and *exo* conformations of M(BDI)X are maintained in solution (*vide infra*), their precise geometries are not static.

The NMR spectra for **1–3** conform to the same general pattern, consistent with a pyramidal coordination at the central atom in solution. The *iso*-propyl resonances in the ¹H and ¹³C{¹H} NMR spectra show ^{6/7}*J*_{PH} and ^{5/6}*J*_{PC} coupling, respectively, which we also attribute to through-space scalar coupling between proximate nuclei. For example in **2a**, the low field septet in the ¹H NMR spectrum shows an additional coupling of 1.2 Hz (Supporting Information, Figure S7). The ³¹P–¹H HMBC experiment shows correlation between phosphorus and this septet (⁶*J*_{PH}) and between phosphorus and two CHMe₂ doublets (⁷*J*_{PH}) (Supporting Information, Figure S8).

In the ¹³C{¹H} NMR spectrum of **2a**, one of the methine- and one of the methyl-carbon resonances of the *iso*-propyl groups appears as a doublet with ⁵*J*_{PC} of 6 Hz and ⁶*J*_{PC} 8 Hz,

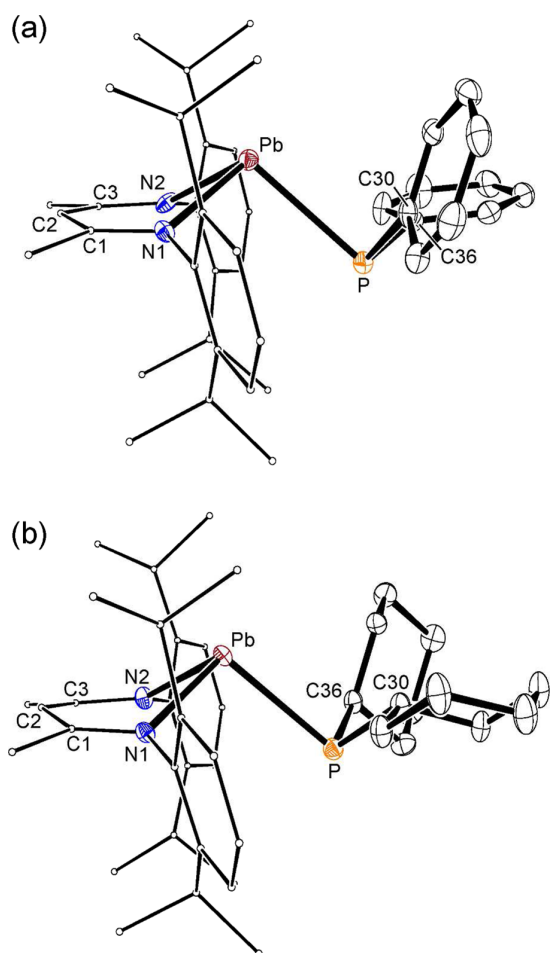


Figure 4. Molecular structures of (a) $\text{Pb}(\text{BDI})(\text{PPh}_2)$ (**3a**) and (b) $\text{Pb}(\text{BDI})(\text{PCy}_2)$ (**3b**) (H atoms omitted and BDI aryl groups C atoms minimized). Ellipsoid probability 30%.

respectively (Figure 6). There are also couplings to tin as described for **II** above. The coupling constants $^4/5J_{\text{SnC}}$ and $^5/6J_{\text{PC}}$ are observed from different resonances, suggesting that the tin and phosphorus atoms interact with different isopropyl groups. This correlates with the solid-state structure in which the opposite *iso*-propyl substituent is closest to the tin and the adjacent *iso*-propyl is closest to the phosphorus (Figure 6). The spectra of **2b** show similar couplings.

The tin atom in the *endo* isomer **2c** is approximately the same distance from the opposite and adjacent *iso*-propyl groups (Figure 7). However, only the adjacent substituents are close enough to interact with the phosphorus atom, suggesting that for both **II** and **2c**, it is the opposite *iso*-propyl groups that exhibit $\text{Sn}\cdots\text{C}$ coupling. For the methine resonance, there is an approximate difference of 15 Hz in $^4J_{\text{SnC}}$ between the *exo*-**2a** (36 Hz) and the *endo*-**2c** (21 Hz)/**II** (20 Hz). The tin amides $\text{Sn}(\text{BDI})(\text{N}^i\text{Pr}_2)$ (*exo*) and $\text{Sn}(\text{BDI})(\text{NHAr})$ (*endo*) show a similar difference with couplings of 35 and 19 Hz, respectively.⁴ We feel confident, therefore, that the magnitude of this coupling may be used to determine whether an *exo*- or *endo*-conformation predominates in solution for compounds of general formula $\text{Sn}(\text{BDI})\text{X}$.

The $^{13}\text{C}\{^1\text{H}\}$ NMR spectra of lead chloride $\text{Pb}(\text{BDI})\text{Cl}$ (**III**) and the phosphides **3a**, **3b**, and **3c** were examined to determine

whether the corresponding through-space scalar coupling to ^{207}Pb nuclei was observable. Unfortunately, overlapping carbon resonances and the inherently lower receptivity of the lead atom relative to tin, prevented assignment of coupling in most cases. However, in *exo* compound $\text{Pb}(\text{BDI})(\text{PPh}_2)$ (**3a**), satellites due to $^{207}\text{Pb}\cdots^{13}\text{C}$ coupling between the “opposite” methine resonance and the lead was noted, with $^4J_{\text{PbC}} = 37$ Hz (Supporting Information, Figure S9). Although $|J_{\text{PbC}}|$ for this interaction is similar to the values obtained for the *exo*-tin compounds, without further data we can not definitively say whether a similar trend in the magnitude of the through-space coupling is in operation for lead.

The ^{31}P NMR chemical shifts of **1–3** (Table 4) follow the expected pattern for a series of substituted compounds X-PR_2 , with $\delta_{\text{p}}(\text{X-PCy}_2)$ (**b**) $>$ $\delta_{\text{p}}(\text{X-PPh}_2)$ (**a**) \gg $\delta_{\text{p}}(\text{X-P}\{\text{SiMe}_3\}_2)$ (**c**). Recent studies of sterically crowded triarylphosphines show an upfield shift as the substituents become more bulky, for example, in CDCl_3 : δ_{p} (ppm): PPh_3 -6 ; $\text{P}(\text{mes})_3$ -36 ; $\text{P}(\text{Ar})_3$ -50 ; $\text{P}(\text{trip})_3$ -53 ($\text{mes} = 2,4,6\text{-Me}_3\text{C}_6\text{H}_2$, $\text{Ar} = 2,6\text{-iPr}_2\text{-C}_6\text{H}_3$), and the coordination at phosphorus becomes more planar (DP: PPh_3 57%;²¹ $\text{P}(\text{mes})_3$ 34%;²² $\text{P}(\text{Ar})_3$ 27%;²³ $\text{P}(\text{trip})_3$ 28%²⁴). Thus, a low frequency resonance is observed when the phosphorus is bound to silyl groups and as the atom adopts a more planar geometry.

The ^{119}Sn NMR chemical shifts for **2a–2c** appear at higher frequency than those from the chloride¹ and *bis*(trimethylsilyl)-amide²⁵ (Table 4), with **2b** $>$ **2a** $>$ **2c**. In contrast, while the ^{207}Pb chemical shifts for the diphenyl and dicyclohexyl compounds are at higher frequency than those of $\text{Pb}(\text{BDI})\text{-chloride}$ ²⁶ and *bis*(trimethylsilyl)amide,²⁸ the *bis*(trimethylsilyl)phosphide **3c** is very strongly shielded and appears at $\delta_{\text{pb}} -1737$ ppm,²⁸ corresponding to a $\Delta\delta_{\text{pb}}$ of 5718 ppm compared with **3b**.

The $^1J_{\text{MPl}}$ for **2** and **3** indicates that bonding within the $\text{M-P}\{\text{SiMe}_3\}_2$ group differs considerably from that in the alkyl and aryl substituted phosphides. Previous work concluded that the large $^1J_{\text{PbP}}$ in **3c** arose from a high 3s contribution from phosphorus in an intrinsically polarized $\text{Pb}(\delta^-)\text{-P}(\delta^+)$ σ -bond.²⁸ The couplings in **3a** (1129 Hz) and **3b** (1084 Hz) are considerably lower and similar to that reported for the terminal $\text{Pb-P}(\text{tBu})_2$ group in the homoleptic dimer, $[\text{Pb}(\text{P}(\text{tBu})_2)_2](\mu\text{-P}(\text{tBu})_2)_2$ (1100 Hz).¹⁸

The coupling constant $^1J_{\text{SnP}}$ in **2c**, 2427 Hz, is exceptionally large (cf. **2a** 978 Hz, **2b** 964 Hz). The solid-state ^{31}P NMR spectrum (Supporting Information, Figure S10), with $^1J_{\text{SnP}}$ 2508 Hz, is in excellent agreement with the solution spectrum indicating the molecular species in solution and in the solid-state are similar. Previously large couplings have been considered indicative of compounds containing tin–phosphorus double bonds (Table 5).^{9,17,27} For example, $\text{R}_2\text{Sn}=\text{P}(\text{mes}^*)$ ($\text{R} = \text{CH}\{\text{SiMe}_3\}_2$, $\text{mes}^* = 2,4,6\text{-tBu}_3\text{C}_6\text{H}_2$) was reported as the first stable stannaphosphene (J_{SnP} 2295 Hz).^{27a} As far as we are aware, however, there have been no examples of structurally characterized compounds having tin–phosphorus multiple bonds,²⁸ and therefore, given that the coupling constant in **2c** which contains a Sn-P single bond exceeds all those previously reported, we urge caution when parameter is cited as evidence for multiple bonding.

$^1J_{\text{PbS}}$ for **1c**^{2d} and **2c** (both 17 Hz) from the $^{31}\text{P}\{^1\text{H}\}$ NMR spectra are toward the low end of the range observed for triorganosilylphosphines (7 to 50 Hz).²⁹ The small coupling constant (9.0 and 9.4 Hz for two diastereoisomers) observed in $\text{P}(\text{Si}(\text{iPr})_3)_3$ was previously attributed to high ionic character in

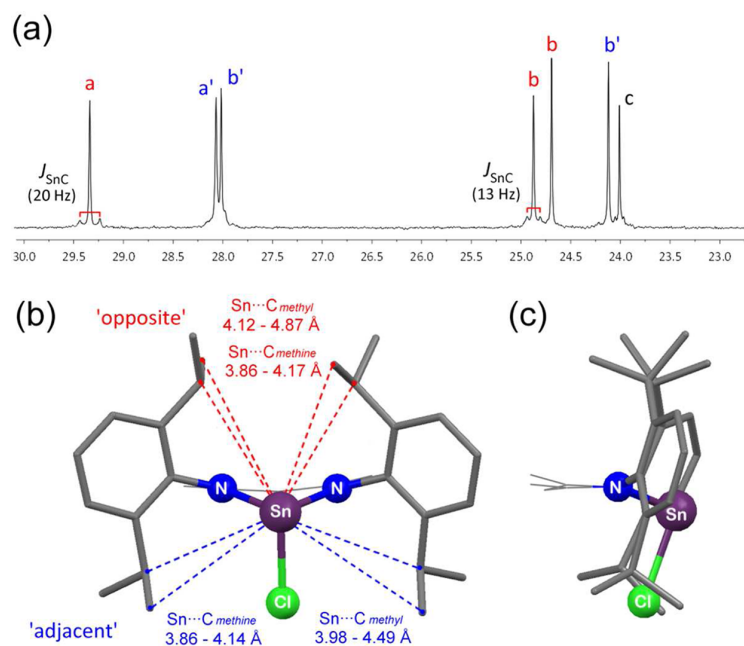


Figure 5. (a) $^{13}\text{C}\{^1\text{H}\}$ NMR spectra of $\text{Sn}(\text{BDI})\text{Cl}$ (**II**) in C_6D_6 showing J_{SnC} : **a** and **a'** CHMe_2 , **b** and **b'** CHMe_2 , **c** NCMe (where $\text{a}(\text{b})_2$ and $\text{a}'(\text{b}')_2$ indicate resonances from different pairs of iso-propyl groups); Schematic views of the relative position of the iso-propyl substituents with respect to the tin atom, with range of distances taken from crystal structure data, (b) facing the metallacycle; (c) side-view.

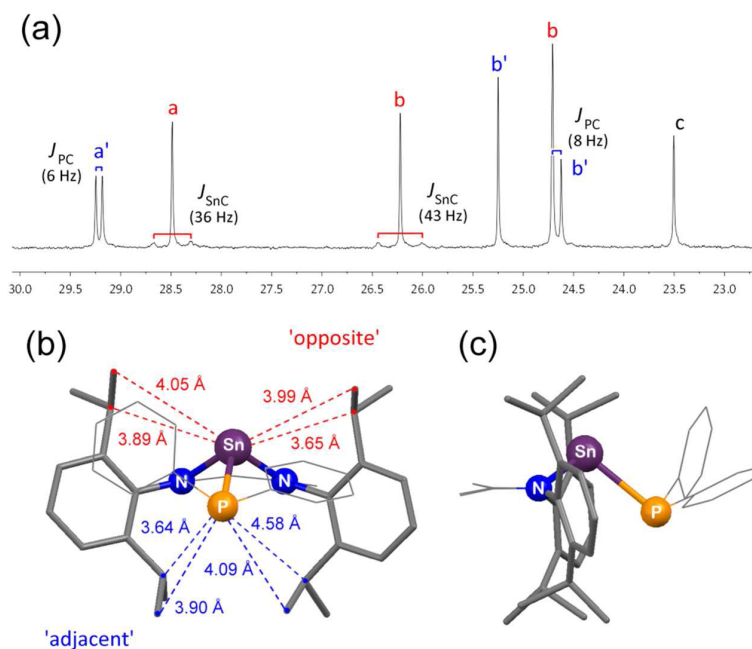


Figure 6. (a) $^{13}\text{C}\{^1\text{H}\}$ NMR spectra of $\text{Sn}(\text{BDI})(\text{PPh}_2)$ (**2a**) in C_6D_6 showing J_{SnC} and J_{PC} : **a** and **a'** CHMe_2 , **b** and **b'** CHMe_2 , **c** NCMe (where $\text{a}(\text{b})_2$ and $\text{a}'(\text{b}')_2$ indicate resonances from different pairs of iso-propyl groups); Schematic views of the relative position of the iso-propyl substituents with respect to the tin atom, taken from X-ray diffraction data: (b) facing the metallacycle; (c) side-view.

the Si–P bonds.¹¹ The coupling constant in the lead complex **3c** is 36 Hz.^{2g}

As a first approximation, 1J coupling constants involving phosphorus are dependent on the s-orbital contribution in the bonds and variations in the valence angle at phosphorus,³⁰ although account must also be taken of the ionicity within the bond and a possible change in the sign of J .¹¹ According to a

simple valence bond description, one would therefore expect that compounds with an sp^3 phosphorus would show a lower $^1J_{\text{MP}}$ coupling than those with a sp^2 phosphorus atom with planar geometry. This fits the data for the tin compounds **2** if the solid-state structures are maintained in solution. However, the exceptionally large $|^1J_{\text{PbP}}|$ in **3c**, which is known to have a solid-state structure with a pyramidal geometry at the

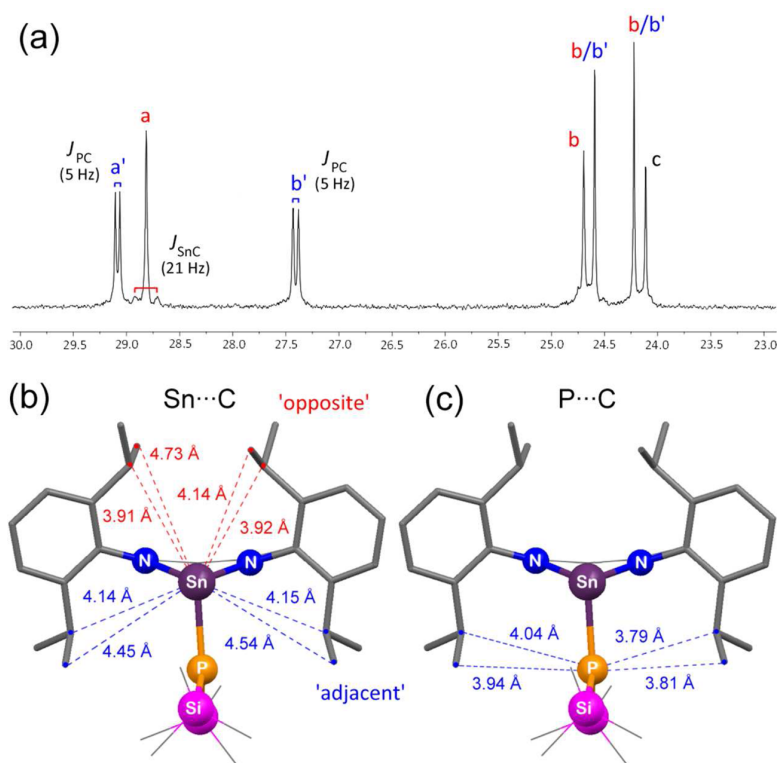


Figure 7. (a) $^{13}\text{C}\{^1\text{H}\}$ NMR spectra of $\text{Sn}(\text{BDI})(\text{P}\{\text{SiMe}_3\}_2)$ (**2c**) in C_6D_6 showing J_{SnC} and J_{PC} : a and a' CHMe_2 , b and b' CHMe_2 , c NCMe (where a(b) $_2$ and a'(b') $_2$ indicate resonances from different pairs of iso-propyl groups); Schematic views of the relative position of the iso-propyl substituents with respect to the tin atom, taken from X-ray diffraction data; (b) showing $\text{Sn}\cdots\text{C}$ distances; (c) showing $\text{P}\cdots\text{C}$ distances.

phosphorus atom, prompted us to examine the solution-state structures of the bis(trimethylsilyl) phosphido compounds in more detail.

The ^1H NMR spectra of **1c** and **2c**, recorded over the temperature range $+30$ to -80 $^\circ\text{C}$, show that the SiMe_3 doublets observed at room temperature separate into two resonances of equal intensity as the temperature is lowered (**2c**, Supporting Information, Figure S11). The energy associated with this process is 11.2 kcal mol^{-1} (**1c**) and 10.5 kcal mol^{-1} (**2c**). The low temperature $^{31}\text{P}\{^1\text{H}\}$ spectra of each compound retain a single resonance, and in the case of tin, there is no significant increase in the $^1J_{\text{SnP}}$, suggesting that the $\text{M}-\text{P}$ bond does not change significantly in this temperature range.

The separation of the SiMe_3 resonances in the ^1H NMR spectra at low temperature is reflected in silicon NMR experiments. At room temperature the $^{29}\text{Si}\{^1\text{H}\}$ NMR of **1c**^{2d} and **2c** are doublets with $^1J_{\text{PSi}} = 17$ Hz (Figure 8). As the temperature is lowered, two silicon resonances are observed, each of which shows coupling to phosphorus (not fully resolved for tin compound **2c**). These two silicon resonances reflect the different proton environments observed in the low temperature ^1H NMR spectra, confirmed through $^1\text{H}-^{29}\text{Si}$ HMBC experiments (Supporting Information, Figure S12). In each case there is a large disparity in the magnitude of the coupling to phosphorus, most evidently in the two low temperature resonances in **1c** where the difference in coupling constant (ΔJ_{PSi}) is 33 Hz (Figure 8). We propose that the large ΔJ_{PSi} is related to the variation in the bond angles about the planar coordination at phosphorus noted in the solid-state structures of **1c** and **2c** (Figure 3b). This is also supported by solid-state

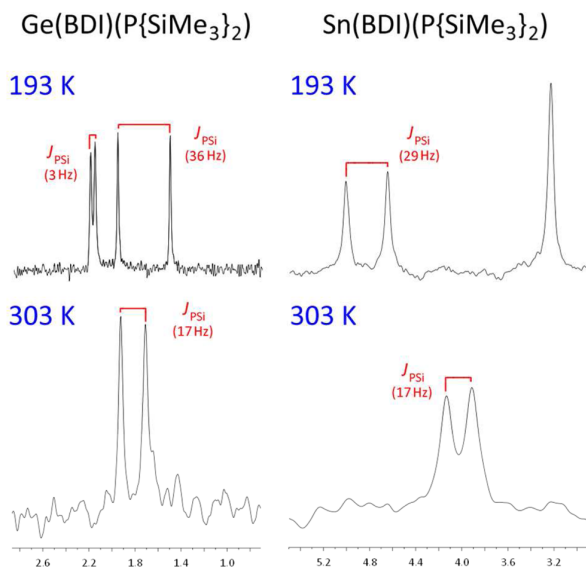


Figure 8. Solution-phase $^{29}\text{Si}\{^1\text{H}\}$ NMR spectra in toluene- d_8 for $\text{Ge}(\text{BDI})(\text{P}\{\text{SiMe}_3\}_2)$ (**1c**) and $\text{Sn}(\text{BDI})(\text{P}\{\text{SiMe}_3\}_2)$ (**2c**), recorded at 303 and 193 K.

$^{29}\text{Si}\{^1\text{H}\}$ NMR experiments (Figure 9a) that show two resonances for **2c**, with coupling resolved in one signal.

Variable temperature and solid-state NMR data have been obtained for $\text{Pb}(\text{BDI})(\text{P}\{\text{SiMe}_3\}_2)$. In contrast to the spectra of the tin compound, the solid-state $^{31}\text{P}\{^1\text{H}\}$ NMR spectrum of

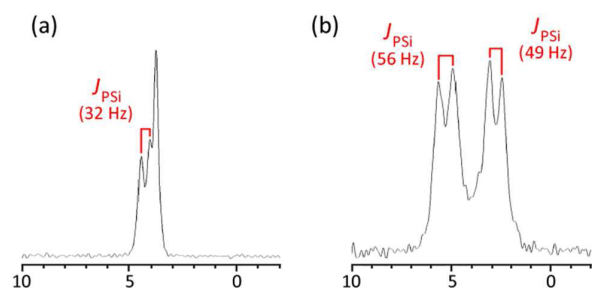


Figure 9. Solid-state $^{29}\text{Si}\{^1\text{H}\}$ NMR spectrum (a) $\text{Sn}(\text{BDI})(\text{P}(\text{SiMe}_3)_2)$ (**2c**); (b) $\text{Pb}(\text{BDI})(\text{P}(\text{SiMe}_3)_2)$ (**3c**) showing $^1J_{\text{PSi}}$ coupling.

3c differs from that acquired in solution. The chemical shift $\delta_{\text{P}}(\text{solid})$ (ppm) is -173.5 (c.f. $\delta_{\text{P}}(\text{solution})$ (ppm) -116.6), but the coupling is significantly lower ($^1J_{\text{PbP}}(\text{solid})$ 1580 Hz), close to that predicted for phosphorus with a pyramidal geometry (vide supra). The solid-state ^{29}Si NMR spectrum (Figure 9b) shows two signals reflecting the different crystallographic environments for the two silicon atoms (torsion angle: $\text{Si}1-\text{P}1-\text{Pb}1-\text{N}1 = -97.4^\circ$, $\text{Si}2-\text{P}1-\text{Pb}1-\text{N}2 = 77.6^\circ$, Supporting Information, Figure S13). Each resonance shows a resolved one-bond coupling to phosphorus with similar $^1J_{\text{PSi}}$ (confirmed with decoupling experiments), indicating a similar magnetic environment for each SiMe_3 group consistent with the X-ray data.

Low temperature solution-state NMR spectra showed a broadening of the resonances for the SiMe_3 protons in the ^1H spectra although separation was not achieved at the low temperature limit. However, of major significance and in contrast to all other systems investigated, the $^{31}\text{P}\{^1\text{H}\}$ NMR spectra separated into two distinct resonances **A** and **B** at low temperature (Figure 10). The higher field resonance **B** is identified with that shown in the solid-state spectrum ($\delta_{\text{P}}(\text{solid})$ (ppm): -173.5 , J_{PbP} 1580 Hz; $\delta_{\text{P}}(\text{B})$ (ppm): -178.5 , J_{PbP} 1417

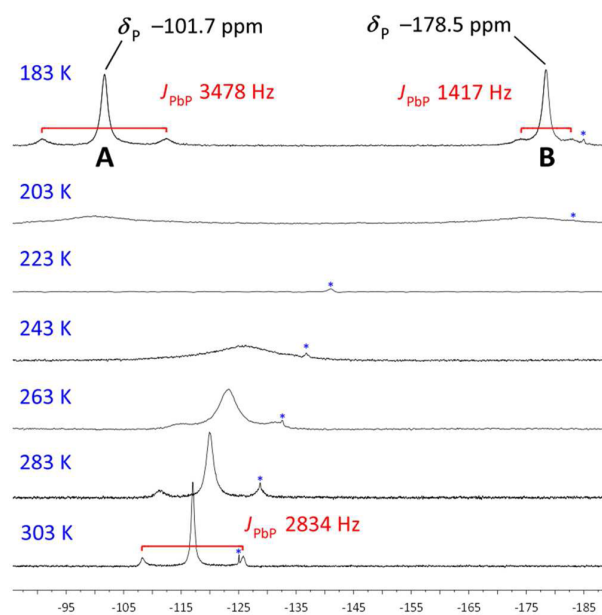
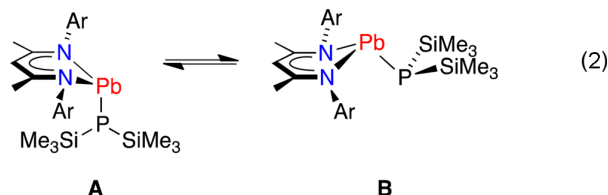


Figure 10. Variable temperature $^{31}\text{P}\{^1\text{H}\}$ NMR spectra in toluene- d_6 of $\text{Pb}(\text{BDI})(\text{P}(\text{SiMe}_3)_2)$ (**3c**) (* unidentified impurity).

Hz) which we assign to the structure in which the coordination geometry at phosphorus is pyramidal. Resonance **A**, however, shows a much larger one-bond coupling between the lead and phosphorus bonds, as predicted for a planar sp^2 -phosphorus coordination geometry ($\delta_{\text{P}(\text{A})}$ (ppm): -101.7 , J_{PbP} 3478 Hz).

These data lead us to conclude that the previously reported spectroscopic data for **3c** actually corresponds to an equilibrium mixture of two species (eq 2), one of which has a pyramidal



geometry at phosphorus (*exo* conformation, **B**) and the other having a planar geometry at phosphorus (*endo* conformation, **A**). It is important to note that in the tin and lead compounds **2c** and **3c** the one-bond coupling between the metal and phosphorus, for a planar coordination environment at phosphorus, vastly exceeds previously reported data.

CONCLUSIONS

The planar coordination at phosphorus in the bis-(trimethylsilyl) substituted phosphides **1c** and **2c** is unique to the BDI-system and has not been recorded previously in germanium and tin compounds. Terminal phosphides of heavier group 14 elements in sterically nonrestraining ligand systems have phosphorus atoms with pyramidal geometries, suggesting that this is most stable. It is tempting to assume that the different geometries noted in this study are a consequence of the shorter M–P bond lengths in the silyl-substituted phosphides (ave. **1a** and **1b** $2.4742(7)$ Å, **1c** $2.3912(8)$ Å; ave. **2a** and **2b** $2.6446(11)$ Å, **2c** $2.5526(7)$ Å). This contraction brings the phosphorus substituents into steric conflict with the N-aryl groups of the BDI ligand, forcing a planar arrangement to be more energetically favorable. This is a reasonable argument within the series of compounds containing a common central atom (Figure 11a). However, if considered in isolation, this parameter does not explain why compounds **1a**

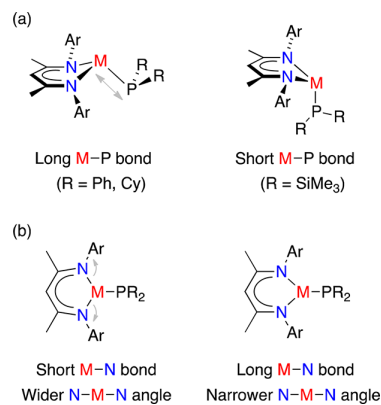


Figure 11. Factors that contribute to whether the phosphorus substituents are strongly influenced by proximity to the aryl groups of the BDI ligand (a) metal–phosphorus bond length; (b) bite angle of the ligand.

and **1b** have pyramidal coordination at phosphorus when the Ge–P bonds are shorter than the Sn–P bond in **2c**. One must also consider the reduced Ge–N bond lengths in **1a**, **1b**, and **1c** (ave. 2.061(2) Å, compared with those in the tin compounds ave. 2.220(3) Å). This causes the mouth of the ligand to be wider for germanium species (ave. N–Ge–N 88.80(8)°) than for tin (ave. N–Sn–N 84.03(1)°), reducing the influence of the aryl substituents in **1a** and **1b** (Figure 11b).

The Pb–N bond lengths in **3a**, **3b**, and **3c** are longer than those of the lighter homologues (ave. 2.337(5) Å) with a further reduction in N–M–N angle (ave. 80.7(2)°), in agreement with the arguments presented above. In this instance, however, there is no significant reduction in the Pb–P bond length for the *bis*(trimethylsilyl) derivative so that, in the solid-state at least, the *exo* form predominates in all cases.

We have invoked through-space scalar coupling to explain the remarkable four to five bond coupling observed between Sn and C, five to six bond coupling observed between P and C as well as the six to seven bond coupling observed between P and H. Both ${}^{6/7}J_{\text{PH}}$ as well as ${}^{5/6}J_{\text{PC}}$ have been observed by others,³¹ and through-space scalar coupling has been used to explain some of these long-range couplings.^{31d} Our results are the first to report this phenomenon between relatively insensitive nuclei using standard one-dimensional ${}^{13}\text{C}$ and ${}^{119}\text{Sn}$ NMR spectroscopic techniques, although it is not unimaginable that this coupling has been previously overlooked. This scalar coupling is probably due to some as yet undetermined molecular orbital overlap between relevant nuclei. The analogous ${}^4J_{\text{PbC}}$ coupling was observed in **3a**, although we were unable to definitively observe coupling in **3b** and **3c**. This lack of coupling could partially be due to the smaller relative receptivity of ${}^{207}\text{Pb}$ nuclei relative to ${}^{119}\text{Sn}$ nuclei (2.01×10^{-3} and 4.53×10^{-3} , respectively, relative to the ${}^1\text{H}$ nuclei).³²

The $|J_{\text{SnP}}|$ value for **2c** (2427 Hz) is the largest tin–phosphorus coupling reported to date, surpassing even those of compounds containing tin–phosphorus multiple bonds. The agreement between the solution- and solid-state NMR spectra confirm that this coupling comes from a Sn–P single bond, significantly widening the range of such $|J_{\text{SnP}}|$ values. A simple interpretation of this data is that the larger coupling in **2c** is due to the increased s-component to the Sn–P bond caused by a rehybridization of the phosphorus from sp^3 (pyramidal geometry) to sp^2 (planar geometry). This change in hybridization would result in greater s character in the bonding orbital on the phosphorus, thus further explaining the shorter Sn–P (and by analogy, Ge–P) bonds of the silyl substituted phosphide ligands. Computational studies to help understand these results are ongoing.

A similarly large coupling (2852 Hz) was previously noted for $|J_{\text{PbP}}|$ in **3c**, following the same general trend as that noted for the tin series. However, this result seems to be inconsistent with the pyramidal coordination at phosphorus observed in the crystal structure and the solid-state ${}^{31}\text{P}$ NMR data, for which a much lower value of $|J_{\text{PbP}}|$ was recorded (1580 Hz). Low temperature, solution-state ${}^{31}\text{P}$ NMR spectra of **3c** showed that the spectral data at 30 °C are an average of two signals **A** and **B**, which we assign to species in which the coordination at phosphorus is planar (**A**) and pyramidal (**B**). This once again increases the range of *J* values for Pb–P single bonds and the value previously reported as “unprecedentedly large” underestimates the upper limit by over 600 Hz.

We conclude that these J_{SnP} and J_{PbP} coupling data will be important in future work that investigates multiple bonding

between these elements. While we have concentrated on the steric arguments in this contribution, possible underlying electronic effects are also under investigation, and we will report the results from these studies in due course.

EXPERIMENTAL SECTION

General Procedures. All manipulations were carried out under an inert atmosphere of dry nitrogen using standard Schlenk techniques or in an inert-atmosphere glovebox. Solvents were dried from the appropriate drying agent, distilled, degassed, and stored over 4 Å molecular sieves. ${}^1\text{H}$ and ${}^{13}\text{C}$ NMR spectra were recorded on Varian 400 and 500 MHz spectrometers. The solution-phase ${}^{29}\text{Si}$, ${}^{31}\text{P}$, ${}^{119}\text{Sn}$ and ${}^{207}\text{Pb}$ NMR spectra were recorded on a Varian 400 MHz spectrometer that was equipped with a $\text{X}\{^1\text{H}\}$ broadband-observe probe. All spectra were recorded in C_6D_6 at 300 K, unless stated otherwise. The ${}^1\text{H}$ and ${}^{13}\text{C}$ NMR chemical shifts are given relative to residual solvent peaks, the ${}^{29}\text{Si}$ signals were externally referenced to SiMe_4 , the ${}^{31}\text{P}$ signals were externally referenced to $\text{H}_3\text{PO}_4(\text{aq})$, the ${}^{119}\text{Sn}$ signals were externally referenced to SnMe_4 , and the ${}^{207}\text{Pb}$ signals were externally referenced to PbMe_4 . All assignments were confirmed by two-dimensional spectroscopy. Coupling constants *J* are quoted in hertz (Hz); coupling involving tin is quoted for the ${}^{119}\text{Sn}$ isotope. Solid-state NMR data were recorded on a Varian VNMRs spectrometer operating at 79.45 MHz (${}^{29}\text{Si}$), 149.17 MHz (${}^{119}\text{Sn}$), and 161.87 MHz (${}^{31}\text{P}$). Spectral referencing is with respect to neat SiMe_4 , 85% H_3PO_4 (by setting the signal from Brushite to 1 ppm) and $\text{Sn}(\text{CH}_3)_4$ (by setting the signal from $\text{Sn}(\text{C}_6\text{H}_{12})_4$ to –97.4 ppm). The samples were packed under nitrogen or helium; the spinning gas was nitrogen. The data for the X-ray structures were collected at 173 K on a Nonius Kappa CCD diffractometer [λ (Mo, $K\alpha$) 0.71073 Å] and refined using the SHELXL-97 software package.³³ $\text{Ge}(\text{BDI})\text{Cl}$ (**I**),¹ $\text{Sn}(\text{BDI})\text{Cl}$ (**II**),¹ $\text{Pb}(\text{BDI})\text{Cl}$ (**III**),^{2c} $\text{Ge}(\text{BDI})(\text{PPh}_2)$ (**1a**),⁵ and $\text{Ge}(\text{BDI})(\text{P}(\text{SiMe}_3)_2)$ (**1c**)^{2d} were made according to published procedures.

Synthesis of LiPR_2 . The required primary phosphine (HPR_2 , R = Cy, Ph, SiMe_3) was added to an *n*-hexane solution under inert atmosphere. The solution mixture was cooled to –78 °C and an equimolecular amount of *n*-BuLi was added dropwise to the solution. The reaction was allowed to warm gradually to room temperature over a period of 20 h. Volatiles were evaporated under vacuum. The crude solid was washed with *n*-hexane and dried in vacuo. The purified solid was collected and stored at –35 °C under an inert atmosphere.

$[\text{CH}\{(\text{CH}_3)\text{CN}-2,6\text{-}i\text{-Pr}_2\text{C}_6\text{H}_3\}_2\text{GeP}(\text{C}_6\text{H}_{11})_2]$ (1b**).** $\text{Ge}(\text{BDI})\text{Cl}$ (0.311 g, 0.59 mmol) was dissolved in diethyl ether (~15 mL) and added to LiPCy_2 (0.121 g, 0.59 mmol). The reaction mixture was stirred at room temperature for 40 h, after which the solution was filtered through a pad of Celite. The solvent was removed under vacuum, and the resulting crude purple solid was dissolved in a minimum amount of hexane, affording **1a** as purple crystals. Yield 0.375 g (92%). M.pt.: 199–200 °C (decomp.). Anal. Calcd. for $\text{C}_{41}\text{H}_{63}\text{GeN}_2\text{P}$ (687.54): C, 71.62; H, 9.24; N, 4.07. Found: C, 71.62; H, 9.21; N, 3.88. ${}^1\text{H}$ NMR: δ 7.17 (d, *J* = 7.6, 2H, ArH), 7.11 (t, *J* = 7.6, 2H, ArH), 7.04 (d, *J* = 7.6, 2H, ArH), 4.74 (s, 1H, CH_7), 4.08 (d sept, *J* = 6.8 and 2.4, 2H, CHMe_2), 3.44 (sept, *J* = 6.8, 2H, CHMe_2), 1.87 (Cy*), 1.67 (d, *J* = 6.8, 6H, CHMe_2), 1.57 (Cy*), 1.53 (s, 6H, NCMe), 1.37 (d, *J* = 6.8, 6H, CHMe_2), 1.30 (Cy*), 1.20, 1.12 (d, *J* = 6.8, 6H, CHMe_2), 1.06–0.87 (Cy*) 0.47 (br t, 2H, J_{HP} = 12.8 Hz, Cy-CH). * accurate integration of cyclohexyl proton resonances not possible because of overlap with other signals. ${}^{13}\text{C}\{^1\text{H}\}$ NMR: δ 167.2 (NCMe), 145.9, 144.5, 141.8 (*i*- and *o*- C_6H_3), 127.1, 125.1, 124.7 (*m*- and *p*- C_6H_3), 96.3 (γ -CH), 35.9 (br, Cy- CH_2), 35.2 (d, J_{PC} = 29, Cy-CH), 29.2 (d, J_{PC} = 9, CHMe_2), 28.9 (CHMe_2), 28.8 (d, J_{PC} = 7, Cy- CH_2), 26.8 (Cy- CH_2), 26.0, 25.3, 25.1 (CHMe_2), 24.6 (d, J_{PC} = 11, CHMe_2), 23.1 (NCMe). ${}^{31}\text{P}\{^1\text{H}\}$ NMR: δ –14.1. IR (Nujol, ν/cm^{-1}): 1556.6 (s), 1519.4 (s), 1319.5 (s), 1170.8 (s), 1019.0 (s), 793.7 (s). UV–vis (pentane), (λ_{max} nm, (ϵ , $\text{M}^{-1}\text{cm}^{-1}$): 280.9 (17118), 352.0 (8874). EI-MS: *m/z* (%) 688 (18, M^+), 492 (100, $[\text{M-PCy}_2]^+$), 419 (10, $[\text{M-GePCy}_2]^+$).

[CH((CH₃)CN-2,6-*i*-Pr₂C₆H₃)₂SnP(C₆H₅)₂] (2a). Compound 2a was made according to the general procedure outlined for **1b** using Sn(BDI)Cl (0.300 g, 0.52 mmol) and LiPPh₂ (0.101 g, 0.52 mmol). The product was isolated as red-purple crystals from toluene. Yield 0.283 g (75%). M.pt.: 95–110 °C (decomp.). Anal. Calcd. for C₄₁H₅₁N₂PSn (721.54): C, 68.25; H, 7.12; N, 3.88. Found: C, 68.06; H, 7.19; N, 3.95. ¹H NMR: δ 7.14 (dd, *J* = 7.6, 1.6, 2H, ArH), 7.06 (t, *J* = 7.6, 2H, ArH), 6.93 (dd, *J* = 7.6, 1.6, 2H, ArH), 6.84–6.72 (m, 10H, PPh₂), 4.71 (s, 1H, CH₇), 4.08 (d sept, *J* = 6.8, 1.2, 2H, CHMe₂), 3.16 (sept, *J* = 6.8, 2H, CHMe₂), 1.67 (d, *J* = 6.8, 6H, CHMe₂), 1.52 (s, 6H, NCMe), 1.23, 1.12, 0.96 (d, 6H, *J* = 6.8, CHMe₂). ¹³C{¹H} NMR: δ 167.6 (NCMe), 144.2, 143.5, 142.9 (*i*- and *o*-C₆H₃), 141.5 (d, *J*_{PC} = 32, C₆H₅), 135.1 (d, *J*_{PC} = 15, C₆H₅), 128.4 (d, *J*_{PC} = 6, C₆H₅), 127.0 (*o*-/*m* C₆H₃), 125.8 (C₆H₅), 125.2, 124.9 (*o*-/*m*-C₆H₃), 97.3 (*γ*-CH), 29.2 (d, *J*_{PC} = 6, CHMe₂), 28.5 (*J*_{SnC} = 36, CHMe₂), 26.2 (*J*_{SnC} = 43, CHMe₂), 25.3, 24.7 (CHMe₂), 24.7 (d, *J*_{PC} = 8, CHMe₂), 23.5 (NCMe). ³¹P{¹H} NMR: δ -30.7 (*J*_{SnP} = 978). ¹¹⁹Sn{¹H} NMR: δ 125 (d, *J*_{SnP} = 978). IR (Nujol, ν/cm⁻¹): 1578.2 (s), 1555.3 (s), 1515.8 (b), 1317.9 (s), 1265.3 (s), 1174.3 (s), 1099.4 (s), 1018.7 (s), 935.1 (s). UV-vis (pentane), (λ_{max} nm, (ε, M⁻¹ cm⁻¹): 283.9 (14960), 354.0 (13706).

[CH((CH₃)CN-2,6-*i*-Pr₂C₆H₃)₂SnP(C₆H₁₁)₂] (2b). Compound 2b was made according to the general procedure outlined for **1b** using Sn(BDI)Cl (0.380 g, 0.66 mmol) and a suspension of LiPCy₂ (0.135 g, 0.66 mmol) in toluene. The product was isolated as purple crystals from toluene at -30 °C. Yield 0.423 g (87%). M.pt.: 205–207 °C (decomp.). Anal. Calcd. for C₄₁H₆₃N₂PSn (733.64): C, 67.12; H, 8.66; N, 3.82. Found: C, 67.03; H, 8.60; N, 3.75. ¹H NMR: δ 7.17 (dd, 2H, *J* = 7.7, 1.4, ArH), 7.08 (t, 2H, *J* = 7.7, ArH), 7.02 (dd, 2H, *J* = 7.7, 1.4, ArH), 4.72 (s, 1H, CH₇), 3.99 (d sept, 2H, *J* = 6.8, 1.6, CHMe₂), 3.32 (sept, 2H, *J* = 6.8, CHMe₂), 1.67 (d, 6H, *J* = 6.8, CHMe₂), 1.59 (s, 6H, NCMe), 1.54 (br, 6H, Cy^β), 1.31, 1.21, 1.15 (d, 6H, *J* = 6.8, CHMe₂), 1.00 (br, 8H, Cy^α). ‡ resonances for the remaining protons of the cyclohexyl substituents appear as an ill-defined broad feature spanning the region 0.6 and 2.1 ppm. ¹³C{¹H} NMR: δ 167.9 (NCMe), 144.4, 144.1, 143.2 (*i*- and *o*-C₆H₃), 126.6, 124.9, 124.8 (*m*- and *p*-C₆H₃), 96.6 (*γ*-CH), 36.0 (br, Cy-CH₂), 32.8 (d, *J*_{PC} = 29, Cy-CH), 29.0 (d, *J*_{PC} = 7, CHMe₂), 28.5 (br, Cy-CH₂), 28.4 (CHMe₂), 26.6 (Cy-CH₂), 26.3, 25.3, 25.0 (CHMe₂), 24.8 (d, *J*_{PC} = 10, CHMe₂), 23.6 (NCMe). ³¹P{¹H} NMR: δ -15.4 (*J*_{SnP} = 953[§]) § coupling to ¹¹⁷Sn and ¹¹⁹Sn not resolved, therefore average coupling observed. ¹¹⁹Sn{¹H} NMR: δ 358 (d, *J*_{SnP} = 964). IR (Nujol, ν/cm⁻¹): 1552.6 (s), 1517.6 (s), 1318.9 (s), 1173.8 (s), 1019.1 (s), 763.9 (s), 751.1 (s), 515.8 (s). UV-vis (pentane), λ_{max} nm (ε, M⁻¹ cm⁻¹): 284.0 (19409), 365.0 (10939).

[CH((CH₃)CN-2,6-*i*-Pr₂C₆H₃)₂SnP(Si(CH₃)₃)₂] (2c). Compound 2c was made according to the general procedure outlined for **1b** using Sn(BDI)Cl (0.436 g, 0.76 mmol) and a suspension of LiP(SiMe₃)₂ (0.140 g, 0.76 mmol) in toluene. The product was isolated as yellow crystals from pentane at -30 °C. Yield 0.503 g (93%). M.p.: 192–194 °C (decomp.). Anal. Calcd. for C₃₅H₅₉N₂PSi₂Sn (713.71): C, 58.90; H, 8.33; N, 3.93. Found: C, 58.94; H, 8.28; N, 3.88. ¹H NMR: δ 7.22 (dd, *J* = 7.7, 1.6, 2H, ArH), 7.16 (t, *J* = 7.6, 2H, ArH), 7.09 (dd, *J* = 7.6, 1.6, 2H, ArH), 4.95 (s, 1H, CH₇), 3.97 (d sept, *J* = 6.8, 1.6, 2H, CHMe₂), 3.38 (sept, *J* = 6.8, 2H, CHMe₂), 1.61 (s, 6H, NCMe), 1.48, 1.32, 1.28, 1.12 (d, *J* = 6.8, 6H, CHMe₂), 0.46 (d, *J*_{SnH} = 124, *J*_{PH} = 4.4, *J*_{SiH} = 11.2, 18H, SiMe₃). ¹³C{¹H} NMR: δ 167.1 (NCMe), 146.3, 143.6, 142.7 (*i*- and *o*-C₆H₃), 127.2, 125.5, 124.3 (*m*- and *p*-C₆H₃), 101.2 (*γ*-CH), 29.5 (d, *J*_{PC} = 5, CHMe₂), 29.3 (*J*_{SnC} = 21, CHMe₂), 27.8 (d, *J*_{PC} = 5, CHMe₂), 25.1, 25.0, 24.7 (CHMe₂), 24.5 (NCMe), 6.0 (d, *J*_{PC} = 10, *J*_{SnC} = 60, SiMe₃). ³¹P{¹H} NMR: δ -183.5 (s, *J*_{PSi} = 17, *J*_{SnP} = 2427). ¹¹⁹Sn{¹H} NMR: δ 39 (d, *J*_{SnP} = 2427). ²⁹Si{¹H} NMR: δ 4.0 (d, *J*_{PSi} = 17). IR (Nujol, ν/cm⁻¹): 1551.4 (s), 1521.0 (s), 1314.4 (s), 1239.1 (s), 1167.6 (s), 1020.4 (s), 935.2 (s), 831.3 (b), 794.8 (s), 757.2 (s), 628.1 (s). UV-vis (pentane), λ_{max} nm (ε, M⁻¹ cm⁻¹): 231.0 (34501), 373.1 (13015). MS *m/z* (EI): 713, 537, 403, 202, 160, 73, 46.

[CH((CH₃)CN-2,6-*i*-Pr₂C₆H₃)₂PbP(C₆H₅)₂] (3a). Compound 3a was made according to the general procedure outlined for **1b** using Pb(BDI)Cl (0.250 g, 0.38 mmol) and LiPPh₂ (0.073 g, 0.38 mmol). The product was isolated as red crystals from hexane. Yield 0.189 g (61%). M.pt.: 265–266 °C (decomp.). Anal. Calcd. for C₄₁H₅₁N₂PbPb

(810.03): C, 60.79; H, 6.35; N, 3.46. Found: C, 60.92; H, 6.51; N, 3.38. ¹H NMR: δ 7.21 (d, *J* = 7.6, 2H, ArH), 7.05 (t, *J* = 7.6, 2H, ArH), 6.96 (d, *J* = 7.6, 2H, ArH), 6.86 (t, *J* = 7.3, 4H, C₆H₅), 6.75 (t, *J* = 7.3, 2H, C₆H₅), 6.53 (t, *J* = 7.3, 4H, C₆H₅), 4.59 (s, 1H, CH₇), 4.04 (sept, *J* = 6.8, 2H, CHMe₂), 3.06 (sept, *J* = 6.8, 2H, CHMe₂), 1.69 (d, *J* = 6.8, 6H, CHMe₂), 1.64 (s, 6H, NCMe), 1.29, 1.13, 0.86 (d, 6H, *J* = 6.8, CHMe₂). ¹³C{¹H} NMR: δ 166.0 (NCMe), 144.6, 143.6, 143.1 (*i*- and *o*-C₆H₃), 142.3 (d, *J*_{PC} = 38, C₆H₅), 135.7 (d, *J*_{PC} = 16, C₆H₅), *, 126.5 (*o*-/*m* C₆H₃), 126.4 (C₆H₅), 124.8, 124.6 (*o*-/*m*-C₆H₃), 98.6 (*γ*-CH), 29.0 (d, *J*_{PC} = 5, CHMe₂), 28.0 (*J*_{PbC} = 37, CHMe₂), 26.5 (CHMe₂), 25.1 (d, *J*_{PC} = 9, CHMe₂), 25.1, 24.7 (CHMe₂), 23.9 (NCMe) * remaining C₆H₅ resonance obscured by solvent. ³¹P{¹H} NMR: δ 7.3 (*J*_{PbP} = 1129). ²⁰⁷Pb{¹H} NMR: 3011 (d, *J*_{PbP} = 1129). IR (Nujol, ν/cm⁻¹): 1551.7 (s), 1512.8 (s), 1317.4 (s), 1172.7 (s), 1017.6 (s), 933.5 (s), 793.2 (s). UV-vis (pentane), (λ_{max} nm, (ε, M⁻¹ cm⁻¹): 259.1 (18623), 312.0 (17694).

[CH((CH₃)CN-2,6-*i*-Pr₂C₆H₃)₂PbP(C₆H₁₁)₂] (3b). Compound 3b was made according to the general procedure outlined for **1b** using Pb(BDI)Cl (0.500 g, 0.79 mmol) and a suspension of LiPCy₂ (0.155 g, 0.79 mmol) in toluene. The product was isolated as deep red crystals from toluene and -30 °C. Yield 0.59 g (95%). M.pt.: 154–155 °C (decomp.). Anal. Calcd. for C₄₁H₆₃N₂PbPb (822.13): C, 59.90; H, 7.72; N, 3.41. Found: C, 60.01; H, 7.59; N, 3.29. ¹H NMR: δ 7.21 (dd, *J* = 7.4, 1.6, 2H, ArH), 7.05 (t, *J* = 7.4, 2H, ArH), 7.02 (dd, *J* = 7.4, 1.6, 2H, ArH), 4.61 (s, 1H, CH₇), 3.95 (d sept, *J* = 6.8, 0.8, 2H, CHMe₂), 3.25 (sept, *J* = 6.8, 2H, CHMe₂), 1.73 (s, 6H, NCMe), 1.69 (d, *J* = 6.8, 6H, CHMe₂), 1.63 (br, 6H, Cy-CH and Cy^β), 1.25, 1.24, 1.18 (d, 6H, *J* = 6.8, CHMe₂), 1.01 (br, 8H, Cy^α) ‡ resonances for the remaining protons of the cyclohexyl substituents appear as an ill-defined broad feature spanning the region 0.5 and 1.9 ppm. ¹³C{¹H} NMR: δ 166.5 (NCMe), 144.8, 144.0, 143.1 (*i*- and *o*-C₆H₃), 126.0, 124.6, 124.3 (*m*- and *p*-C₆H₃), 97.8 (*γ*-CH), 39.0 (br, Cy-CH₂), 34.0 (d, *J*_{PC} = 34, Cy-CH), 28.8 (d, *J*_{PC} = 5, CHMe₂), 28.7 (br, Cy-CH₂), 27.9 (CHMe₂), 26.6 (CHMe₂), 26.5 (Cy-CH₂), 25.5 (d, *J*_{PC} = 10, CHMe₂), 25.1, 25.0 (CHMe₂), 23.8 (NCMe). ³¹P{¹H} NMR: δ 26.9 (*J*_{PbP} = 1084). ²⁰⁷Pb{¹H} NMR: δ 3981 (d, *J*_{PbP} = 1084). IR (Nujol, ν/cm⁻¹): 1555.7 (s), 1514.57 (s), 1318.71 (s), 1172.0 (s), 934.7 (s), 788.5 (s). UV-vis (pentane), (λ_{max} nm, (ε, M⁻¹ cm⁻¹): 280.9 (17118), 352.0 (8874).

[CH((CH₃)CN-2,6-*i*-Pr₂C₆H₃)₂PbP(Si(CH₃)₃)₂] (3c). Pb(BDI)Cl (0.24 g, 0.369 mmol) was dissolved in toluene (20 mL) and added directly to LiP(TMS)₂ (0.07 g, 0.369 mmol). The reaction mixture was stirred at room temperature for 4 h. The red solution was filtered through a pad of Celite. The volatiles were evaporated under vacuum, and the solid was dissolved *n*-hexane for recrystallization at -35 °C (0.27 g, 91%). ¹H NMR (499.91 MHz, C₆D₆, 303 K): δ 7.22 (dd, *J* = 7.5, 2.0, 2H, *m*-H), 7.12 (t, *J* = 7.5, 2H, *p*-H), 7.09 (dd, *J* = 7.5, 2.0, 2H, *m*-H), 4.75 (s, 1H, *γ*-CH), 3.92 (d sept, *J* = 7.0, 1.0, 2H, CHMe₂), 3.29 (sept, *J* = 6.5, 2H, CHMe₂), 1.64 (s, 6H, NCMe), 1.52 (d, *J* = 6.5, 6H, CHMe₂), 1.31 (d, *J* = 7.0, 6H, CHMe₂), 1.26 (d, *J* = 6.5, 6H, CHMe₂), 1.16 (d, *J* = 7.0, 6H, CHMe₂), 0.30 (d, *J* = 4.0, 18H, SiMe₃). ¹³C{¹H} NMR (100.46 MHz, C₆D₆, 303 K): δ 166.2 (NCMe), 145.5 (*ipso*-C), 144.7 (*o*-C), 143.6 (*o*-C), 127.0 (*m*-H), 125.6 (*m*-H), 124.4 (*p*-H), 103.0 (*γ*-CH), 29.0 (CHMe₂), 28.4 (d, *J*_{PC} = 6.3, CHMe₂), 28.2 (d, *J*_{PC} = 5.0, CHMe₂), 26.1 (CHMe₂), 25.1 (CHMe₂), 25.1 (CHMe₂), 25.0 (NCMe), 7.5 (d, *J*_{SiC} = 9.8, SiMe₃). ³¹P{¹H} NMR (161.72 MHz, C₆D₆, 303 K): δ -116.6 (*J*_{PbP} = 2874). ²⁹Si{¹H} NMR (79.37 MHz, C₆D₆, 303 K): δ 7.2 (d, *J*_{PSi} = 36). UV-vis (pentane) λ_{max} nm (ε, M⁻¹ cm⁻¹): 382.0 (7900).

■ ASSOCIATED CONTENT

● Supporting Information

Thermal ellipsoid plots of **1b**, **2a–2c**, **3a–3b**; selected solution- and solid-state NMR data; crystal structure data for polymorphic Sn(BDI)Cl (**II'**) and Ph₂P-PPh₂. This material is available free of charge via the Internet at <http://pubs.acs.org>.

AUTHOR INFORMATION

Corresponding Author

*Fax: +64 (0)4 463 5237. Phone: +64 (0)4 463 9799. E-mail: martyncoles@vuw.ac.nz (M.P.C.); j.robin.fulton@vuw.ac.nz (J.R.F.).

Present Address

[§]School of Chemical and Physical Sciences, P.O. Box 600, Victoria University of Wellington, Wellington, New Zealand.

Author Contributions

The manuscript was written through contributions of all authors. All authors have given approval to the final version of the manuscript.

Notes

The authors declare no competing financial interest.

ACKNOWLEDGMENTS

We wish to thank Dr. Ian Crossley for the kind donation of $\text{HP}\{\text{SiMe}_3\}_2$ and Dr. Iain Day for helpful and stimulating discussion during the preparation of this manuscript. We acknowledge Dr. Lorenzo Ferro for X-ray data of $\text{Sn}(\text{BDI})\text{Cl}$ (**II'**) and Lisa Harris for the X-ray data of $\text{Ph}_2\text{P}-\text{PPh}_2$. We thank the University of Sussex for financial support.

REFERENCES

- (1) Ding, Y.; Roesky, H. W.; Noltemeyer, M.; Schmidt, H.-G.; Power, P. P. *Organometallics* **2001**, *20*, 1190–1194.
- (2) (a) Taylor, M. J.; Saunders, A. J.; Coles, M. P.; Fulton, J. R. *Organometallics* **2011**, *30*, 1334–1339. (b) Jana, A.; Sarish, S. P.; Roesky, H. W.; Schulzke, C.; Samuel, P. P. *Chem. Commun.* **2010**, *46*, 707–709. (c) Jana, A.; Nekoueiashahraki, B.; Roesky, H. W.; Schulzke, C. *Organometallics* **2009**, *28*, 3763–3766. (d) Yao, S.; Brym, M.; Merz, K.; Driess, M. *Organometallics* **2008**, *27*, 3601–3607. (e) Chen, M.; Fulton, J. R.; Hitchcock, P. B.; Johnstone, N. C.; Lappert, M. F.; Protchenko, A. V. *Dalton Trans.* **2007**, 2770–2778. (f) Fulton, J. R.; Hitchcock, P. B.; Johnstone, N. C.; Tam, E. C. Y. *Dalton Trans.* **2007**, 3360–3362. (g) Yao, S.; Block, S.; Brym, M.; Driess, M. *Chem. Commun.* **2007**, 3844–3846. (h) Pineda, L. W.; Jancik, V.; Starke, K.; Oswald, R. B.; Roesky, H. W. *Angew. Chem., Int. Ed.* **2006**, *45*, 2602–2605.
- (3) (a) Ferro, L.; Hitchcock, P. B.; Coles, M. P.; Fulton, J. R. *Inorg. Chem.* **2012**, *51*, 1544–1551. (b) Ferro, L.; Hitchcock, P. B.; Coles, M. P.; Cox, H.; Fulton, J. R. *Inorg. Chem.* **2011**, *50*, 1879–1888. (c) Jana, A.; Objartel, I.; Roesky, H. W.; Stalke, D. *Dalton Trans.* **2010**, *39*, 4647–4650. (d) Jana, A.; Roesky, H. W.; Schulzke, C. *Dalton Trans.* **2010**, *39*, 132–138. (e) Jana, A.; Tavcar, G.; Roesky, H. W.; John, M. *Dalton Trans.* **2010**, *39*, 9487–9489. (f) Jana, A.; Roesky, H. W.; Schulzke, C.; Samuel, P. P. *Organometallics* **2010**, *29*, 4837–4841. (g) Tam, E. C. Y.; Johnstone, N. C.; Ferro, L.; Hitchcock, P. B.; Fulton, J. R. *Inorg. Chem.* **2009**, *48*, 8971–8976. (h) Jana, A.; Roesky, H. W.; Schulzke, C. *Inorg. Chem.* **2009**, *48*, 9543–9548. (i) Jana, A.; Objartel, I.; Roesky, H. W.; Stalke, D. *Inorg. Chem.* **2009**, *48*, 7645–7649. (j) Jana, A.; Objartel, I.; Roesky, H. W.; Stalke, D. *Inorg. Chem.* **2009**, *48*, 798–800. (k) Dove, A. P.; Gibson, V. C.; Marshall, E. L.; Rzepa, H. S.; White, A. J. P.; Williams, D. J. *J. Am. Chem. Soc.* **2006**, *128*, 9834–9843.
- (4) Harris, L. A.-M.; Coles, M. P.; Fulton, J. R. *Inorg. Chim. Acta* **2011**, *369*, 97–102.
- (5) Yang, Y.; Zhao, N.; Zhu, H.; Roesky, H. W. *Inorg. Chem.* **2012**, *51*, 2425–2431.
- (6) Appel, R.; Milker, R. *Chem. Ber.* **1975**, *108*, 1783–1790.
- (7) Maksić, Z. B.; Kovačević, B. *J. Chem. Soc., Perkin Trans. 2* **1999**, 2623–2629.
- (8) (a) Izod, K.; Stewart, J.; Clark, E. R.; Clegg, W.; Harrington, R. W. *Inorg. Chem.* **2010**, *49*, 4698–4707. (b) Izod, K.; Stewart, J.; Clegg, W.; Harrington, R. W. *Organometallics* **2010**, *29*, 108–116. (c) Izod, K.; McFarlane, W.; Allen, B.; Clegg, W.; Harrington, R. W. *Organometallics* **2005**, *24*, 2157–2167. (d) Druckenbrodt, C.; du Mont, W.-W.; Ruthe, F.; Jones, P. G. *Z. Anorg. Allg. Chem.* **1998**, *624*, 590–594.
- (9) Johnson, B. P.; Almstätter, S.; Dielmann, F.; Bodensteiner, M.; Scheer, M. Z. *Anorg. Allg. Chem.* **2010**, *636*, 1275–1285.
- (10) (a) Dzambasky, A.; Baumgartner, J.; Hassler, K. *J. Organomet. Chem.* **2009**, *694*, 757–762. (b) Cappello, V.; Baumgartner, J.; Dransfield, A.; Hassler, K. *Eur. J. Inorg. Chem.* **2006**, 4589–4599. (c) Nieger, M.; Niecke, E.; Dany, S. Z. *Kristallogr.–New Cryst. Struct.* **1997**, *212*, 249–250. (d) Westerhausen, M.; Lang, G.; Schwarz, W. *Chem. Ber.* **1996**, *129*, 1035–1040. (e) Bruckmann, J.; Krüger, C. *Acta Crystallogr.* **1995**, *C51*, 1152–1155. (f) Petrie, M. A.; Power, P. P. *J. Chem. Soc., Dalton Trans.* **1993**, 1737–1745.
- (11) Driess, M.; Merz, K.; Monsé, C. Z. *Anorg. Allg. Chem.* **2000**, *626*, 2264–2268.
- (12) Weber, L.; Meine, G.; Boese, R.; Augart, N. *Organometallics* **1987**, *6*, 2484–2488.
- (13) Arif, A. M.; Cowley, A. H.; Jones, R. A.; Power, J. M. *J. Chem. Soc., Chem. Commun.* **1986**, 1446–1447.
- (14) Izod, K.; Stewart, J.; Clark, E. R.; McFarlane, W.; Allen, B.; Clegg, W.; Harrington, R. W. *Organometallics* **2009**, *28*, 3327–3337.
- (15) Westerhausen, M.; Hausen, H.-D.; Schwarz, W. Z. *Anorg. Allg. Chem.* **1995**, *621*, 877–888.
- (16) Westerhausen, M.; Enzelberger, M. M.; Schwarz, W. *J. Organomet. Chem.* **1995**, *491*, 83–90.
- (17) Driess, M.; Janoschek, R.; Pritzkow, H.; Rell, S.; Winkler, U. *Angew. Chem., Int. Ed. Engl.* **1995**, *34*, 1614–1616.
- (18) Cowley, A. H.; Giolando, D. M.; Jones, R. A.; Nunn, C. M.; Power, J. M. *Polyhedron* **1988**, *7*, 1909–1910.
- (19) Mallory, F. B. *J. Am. Chem. Soc.* **1973**, *95*, 7747–7752.
- (20) Wei, Z.; Yang, J.-H.; Vreshch, V. D.; Zabula, A. V.; Filatov, A. S.; Dikarev, E. V. *Inorg. Chem.* **2011**, *50*, 7295–7300.
- (21) Daly, J. J. *J. Chem. Soc.* **1964**, 3799–3810.
- (22) Blount, J. F.; Maryanoff, C. A.; Mislaw, K. *Tetrahedron Lett.* **1975**, *16*, 913–916.
- (23) Boeré, R. T.; Bond, A. M.; Cronin, S.; Duffy, N. W.; Hazendonk, P.; Masuda, J. D.; Pollard, K.; Roemmele, T. L.; Tran, P.; Zhang, Y. *New J. Chem.* **2008**, *32*, 214–231.
- (24) Sasaki, S.; Sutoh, K.; Murakami, F.; Yoshifujii, M. *J. Am. Chem. Soc.* **2002**, *124*, 14830–14831.
- (25) Jana, A.; Roesky, H. W.; Schulzke, C.; Döring, A.; Beck, T.; Pal, A.; Herbst-Irmer, R. *Inorg. Chem.* **2009**, *48*, 193–197.
- (26) Jana, A.; Sarish, S. P.; Roesky, H. W.; Schulzke, C.; Döring, A.; John, M. *Organometallics* **2009**, *28*, 2563–2567.
- (27) (a) Couret, C.; Escudie, J.; Satge, J.; Raharinirina, A.; Andriamizaka, J. D. *J. Am. Chem. Soc.* **1985**, *107*, 8280–8281. (b) Ranaivonjatovo, H.; Escudie, J.; Couret, C.; Satge, J. *J. Chem. Soc., Chem. Commun.* **1992**, 1047–1048. (c) Rodi, A. K.; Ranaivonjatovo, H.; Escudie, J.; Kerbal, A. *Phosphorus, Sulfur Silicon Relat. Elem.* **1997**, *126*, 157–169. (d) Merrill, W. A.; Wright, R. J.; Stanciu, C. S.; Olmstead, M. M.; Fettingner, J. C.; Power, P. P. *Inorg. Chem.* **2010**, *49*, 7097–7105. (e) Matchett, M. A.; Chiang, M. Y.; Buhro, W. E. *Inorg. Chem.* **1994**, *33*, 1109–1114. (f) Goel, S. C.; Chiang, M. Y.; Rauscher, D. J.; Buhro, W. E. *J. Am. Chem. Soc.* **1993**, *115*, 160–169. (g) Rivard, E.; Sutton, A. D.; Fettingner, J. C.; Power, P. P. *Inorg. Chim. Acta* **2007**, *360*, 1278–1286.
- (28) Fischer, R. C.; Power, P. P. *Chem. Rev.* **2010**, *110*, 3877–3923.
- (29) Verkade, J. G.; Mosbo, Z. A. *³¹P NMR Spectroscopy in Stereochemical Analysis*; VCH: Weinheim, Germany, 1987.
- (30) Pople, J. A.; Santry, D. P. *Mol. Phys.* **1964**, *8*, 1–18.
- (31) (a) Gholivand, K.; Ghadimi, S.; Naderimanes, H.; Forouzanfar, A. *Magn. Reson. Chem.* **2001**, *39*, 684–688. (b) Griffin, C. E.; Gordon, M. J. *Am. Chem. Soc.* **1967**, *89*, 4427–4431. (c) Malon, M.; Koshino, H. *Magn. Reson. Chem.* **2007**, *45*, 770–776. (d) Hierso, J.-C.; Armspach, D.; Matt, D. C. R. *Chim.* **2009**, *12*, 1002–1013.
- (32) Harris, R. K.; Becker, E. D.; de Menezes, S. M. C.; Goodfellow, R.; Granger, P.; Int, C. *Magn. Reson. Chem.* **2002**, *40*, 489–505.

(33) Sheldrick, G. M. *SHELXL-97, Program for the Refinement of Crystal Structures*; University of Göttingen: Göttingen, Germany, 1997.

Appendix 2. X-ray crystal structure of [(BDI_{DIPP})SnⁿBu] (**39**)

Single crystals of [(BDI_{DIPP})SnⁿBu] (**39**) were obtained adventitiously from a C₆D₆ solution at room temperature. ORTEP drawings of the *n*-butyl(β-diketiminato)tin(II) **39** are shown in Figures A1 and A2. Selected bond lengths and angles are given in Table A1, and selected crystallographic data in Table A2. Compound **39** adopts an *exo* conformation, with the metal centre 1.060 Å above the mean NCCCN plane of the β-diketiminato ligand. The geometry around the tin atom is pyramidal, with the sum of bond angles 279.7°. Delocalisation within the C₃N₂Sn unit is evident, but it does not extend to the *N*-aryl substituents (dihedral angles: C(11)–C(6)–N(1)–Sn = 71.2(4)° and C(23)–C(18)–N(2)–Sn = –78.7(4)°). If the alkyl substituent is discounted, there is an approximate plane of symmetry passing through the atoms C(2) and Sn, bisecting the β-diketiminato ring. The Sn–C(30) bond length is 2.189(11) Å and the Sn–C(30)–C(31) bond angle is 102.6(7)°. The Sn–C(30) bond distance (2.189(11) Å) may be compared to that in Roesky's [(BDI_{DIPP})SnMe] (Sn–C = 2.253(2) Å).^[1]

Figure A1. ORTEP diagram of [(BDI_{DIPP})SnⁿBu] (**39**). H atoms are omitted and C atoms in the *N*-aryl groups in the β-diketiminato ring are minimised for clarity. The ellipsoid probability is shown at 30%

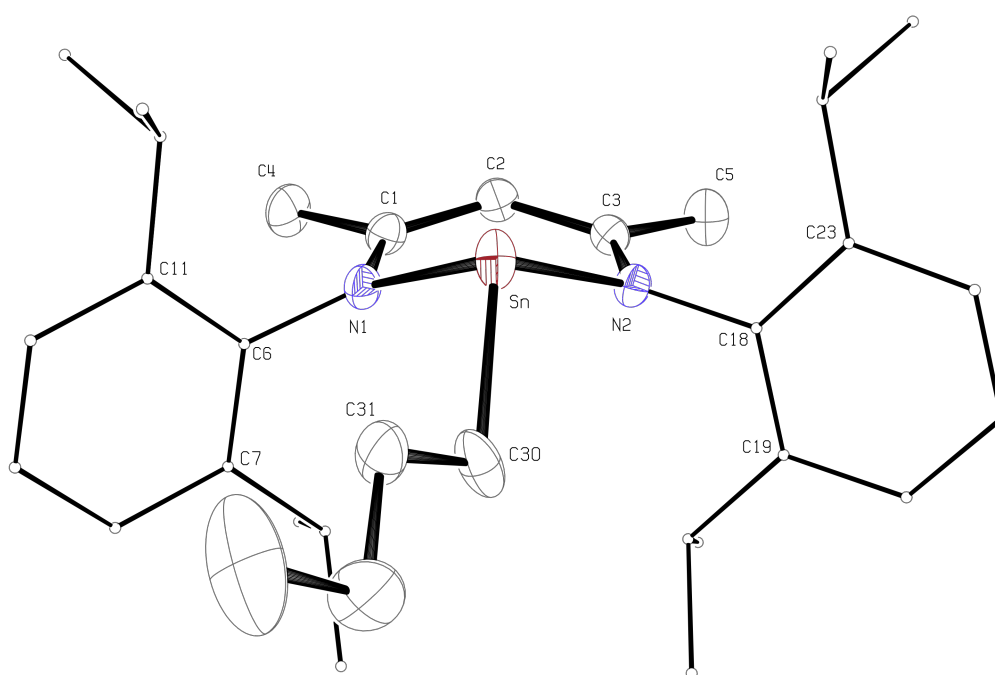


Figure A2. ORTEP diagram showing the side-on view of [(BDI_{DIPP})SnⁿBu] (**39**). H atoms are omitted and C atoms in the *N*-aryl groups in the β-diketiminato ring are minimised for clarity. The ellipsoid probability is shown at 30%

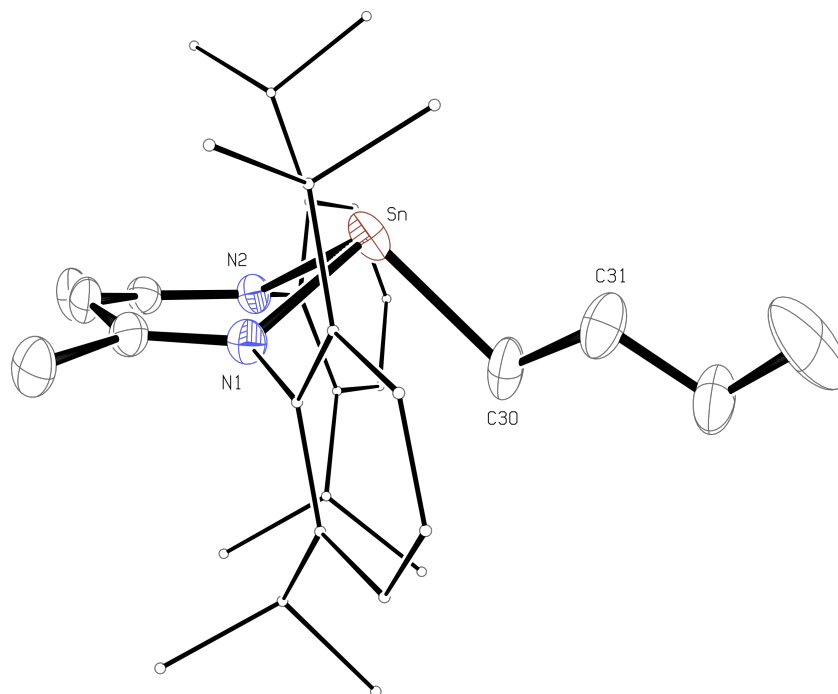


Table A1. Selected bond lengths (Å) and angles (deg) for [(BDI_{DIPP})SnⁿBu] (**39**)

<i>Bond lengths (Å)</i>			
Sn–N(1)	2.209(3)	C(1)–C(2)	1.387(5)
Sn–N(2)	2.216(2)	C(2)–C(3)	1.415(5)
N(1)–C(1)	1.331(4)	Sn–C(30)	2.189(11)
N(2)–C(3)	1.317(4)	C(30)–C(31)	1.536(12)
Sn–NCCCN _{Plane}	1.060		
<i>Bond angles (deg)</i>			
N(1)–Sn–N(2)	82.72(9)	N(2)–C(3)–C(2)	123.8(3)
N(1)–Sn–C(30)	95.6(11)	C(1)–C(2)–C(3)	128.2(3)
N(2)–Sn–C(30)	101.3(4)	Sn–C(30)–C(31)	102.6(7)
N(1)–C(1)–C(2)	123.6(3)		
Σ bond angle around Sn	279.7	NCCCN _{plane} –NSnN _{plane}	39.0
DOP (%) ^a	89		
<i>Dihedral angles (deg)</i>			
C(11)–C(6)–N(1)–Sn	71.2(4)	C(23)–C(18)–N(2)–Sn	–78.7(4)

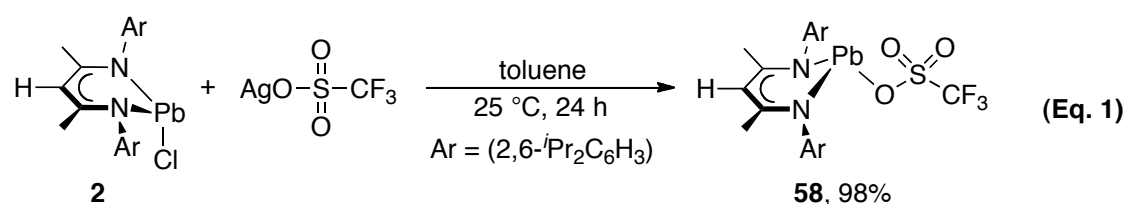
^a Degree of pyramidalisation (DOP, %) = [(360 – Σ_{bond angle}) / 0.9]^[2] When a DOP is 100%, it is equivalent to a sum of bond angles of 270°, whereas a DOP of 0% indicates a planar geometry at the central atom

Table A2. Selected crystallographic data for [(BDI_{DIPP})SnⁿBu] (**39**)

[(BDI _{DIPP})Sn ⁿ Bu] (39)	
chemical formula	C ₃₃ H ₅₀ N ₂ Sn
molecular mass	593.46
temperature (K)	173(2)
wavelength (Å)	0.71073
crystal system	orthorhombic
space group	<i>Fdd2</i> (No. 43)
<i>a</i> (Å)	23.1850(4)
<i>b</i> (Å)	63.1825(9)
<i>c</i> (Å)	8.9095(1)
<i>α</i> (deg)	90
<i>β</i> (deg)	90
<i>γ</i> (deg)	90
<i>V</i> (Å ³)	13051.4(3)
<i>Z</i>	16
ρ_{calcd} (Mg m ⁻³)	1.21
θ range (deg)	3.50–27.49
abs coeff (mm ⁻¹)	0.80
measd/indep reflns/ <i>R</i> (int)	39 667/7387/0.061
reflns with $I > 2\sigma(I)$	6472
data/restraints/param	7387/17/364
goodness of fit on F^2	1.056
final <i>R</i> indices [$I > 2\sigma(I)$]	<i>R</i> 1 = 0.038, <i>wR</i> 2 = 0.078
<i>R</i> indices (all data)	<i>R</i> 1 = 0.049, <i>wR</i> 2 = 0.083
largest diff peak and hole (e Å ⁻³)	0.48 and -0.61

Appendix 3. Synthesis of β -diketiminatolead(II) triflate **58**

Treatment of the lead(II) chloride **2** with silver triflate in toluene at room temperature give the β -diketiminatolead(II) triflate **58** in near quantitative yield (98%) (equation 1). Unfortunately, Roesky *et al.* reported this compound before the submission of this thesis.^[3] The multinuclear NMR spectra of this compound are in good agreement with those reported in literature.



Single crystals of [(BDI_{DIPP})PbOTf] (**58**) were obtained from toluene at -30 °C. ORTEP drawings are shown in Figures A3 and A4. Selected bond lengths and angles are given in Table A3, and selected crystallographic data in Table A4. The polymeric structure of the lead(II) triflate **58** consists of four crystallographically independent monomeric units. It differs from the germanium and tin analogues, which are monomeric in the solid state.^[4-5] The triflate anion acts as a bridge between the two lead atoms. The bond length of Pb(1)–O(1) (2.591(6) Å) is shorter than the Pb(2)–O(2) (2.613(5) Å). These lead-oxygen bonds are longer than the sum of covalent radii of lead and oxygen (2.12 Å), but within the sum of van der Waals radii (3.44 Å).^[6-7] Recently our group reported a series of β -diketiminato heavy group 14 cation complexes, but found no significant intermolecular contacts in the crystalline lattice.^[8] The contacts in **58** reflect a strong electrostatic interaction between the lead centre and triflate ligand. The average intermolecular O–Pb–O' bond angle is 167.5° , indicating that the four monomeric units are not connected in a linear fashion. The crystallographic parameters of this compound are similar to those reported in Roesky's publication.^[3]

Figure A3. ORTEP diagram of $[(\text{BDI}_{\text{DIPP}})\text{PbOTf}]$ (**58**). H atoms are omitted and C atoms in the *N*-aryl group in the β -diketiminato ring are minimised for clarity. The ellipsoid probability is shown at 30%

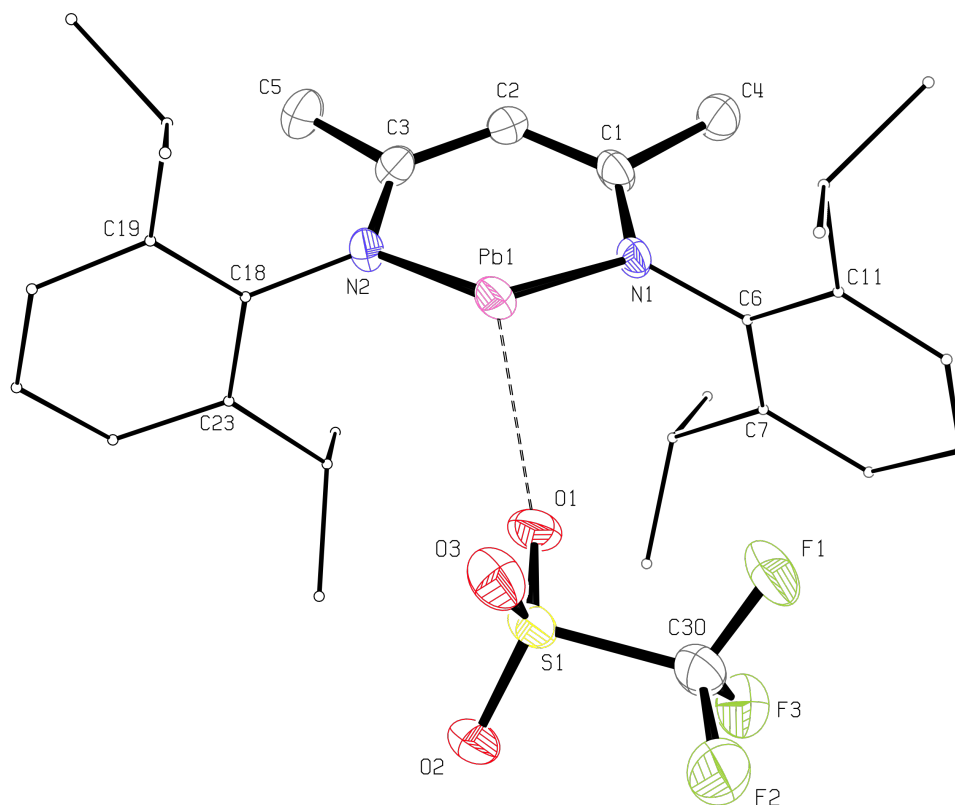


Figure A4. ORTEP diagram of $[(\text{BDI}_{\text{DIPP}})\text{PbOTf}]$ (**58**) showing the polymeric chain. H atoms are omitted and C atoms in the *N*-aryl group in the β -diketiminato ring are minimised for clarity. The ellipsoid probability is shown at 30%

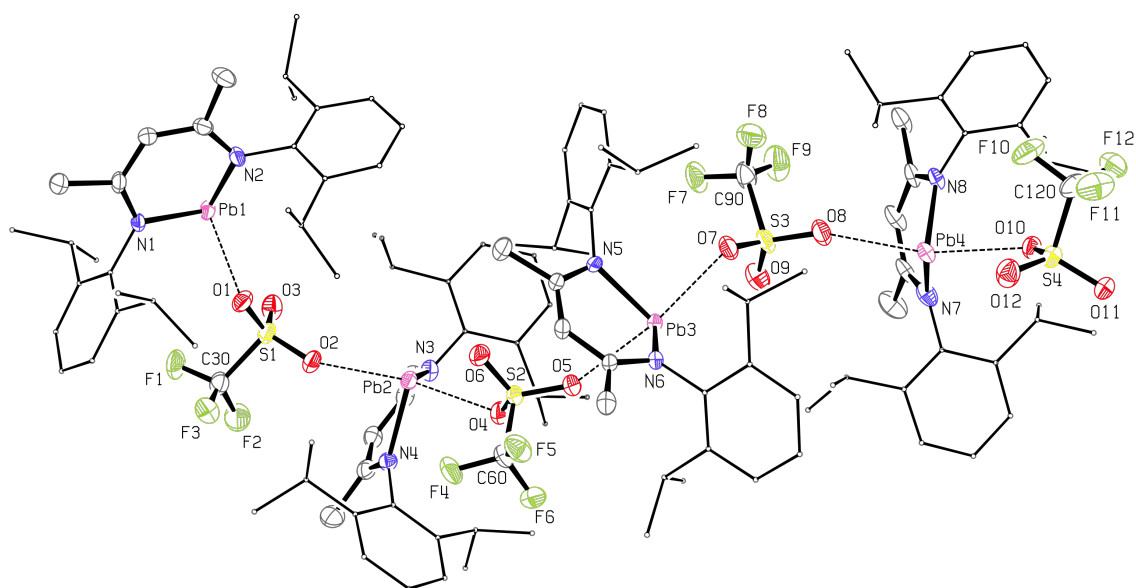


Table A3. Selected bond lengths (Å) and angles (deg) for [(BDI_{DIPP})PbOTf] (**58**)

<i>Bond lengths (Å)^a</i>			
Pb(1)–N(1)	2.263(6)	Pb(1)–O(1)	2.591(6)
Pb(1)–N(2)	2.280(7)	Pb(2)–O(2)	2.613(5)
N(1)–C(1)	1.320(10)	S(1)–O(1)	1.452(6)
N(2)–C(3)	1.335(11)	S(1)–O(2)	1.449(6)
C(1)–C(2)	1.393(11)	S(1)–O(3)	1.430(7)
C(3)–C(2)	1.393(11)	C(30)–F(1)	1.311(11)
C(1)–C(4)	1.525(11)	C(30)–F(2)	1.320(11)
C(3)–C(5)	1.519(12)	C(30)–F(3)	1.337(12)
Pb–NCCCN _{plane}	0.919		
<i>Bond angles (deg)^a</i>			
N(1)–Pb(1)–N(2)	82.2(2)	N(4)–Pb(2)–O(2)	82.7(2)
Pb(1)–N(1)–C(1)	120.9(5)	O(2)–Pb(2)–O(4)	168.0(2)
Pb(1)–N(2)–C(3)	121.0(5)	Pb(1)–O(1)–S(1)	117.9(3)
N(1)–C(1)–C(2)	125.3(7)	O(1)–S(1)–O(3)	114.7(4)
N(2)–C(3)–C(2)	124.7(8)	O(1)–S(1)–O(2)	112.6(4)
C(1)–C(2)–C(3)	129.4(8)	O(1)–S(1)–C(30)	103.2(4)
N(1)–Pb(1)–O(1)	87.2(2)	S(1)–C(30)–F(1)	111.6(7)
N(2)–Pb(1)–O(1)	101.4(2)	F(1)–C(30)–F(2)	109.1(9)
N(3)–Pb(2)–O(2)	88.7(2)		
Σ bond angle around Pb	270.8	NCCCN _{plane} –NPbN _{plane}	32.2
DOP of Pb (%) ^b	99		
<i>Dihedral angles (deg)^a</i>			
C(11)–C(6)–N(1)–Pb(1)	–70.9(9)	C(19)–C(18)–N(2)–Pb(1)	84.0(1)

^a Only one of the crystallographically independent molecule is documented; ^b Degree of pyramidalisation (DOP, %) = $[(360 - \sum_{\text{bond angle}}) / 0.9]^{[2]}$ When a DOP is 100%, it is equivalent to a sum of bond angles of 270°, whereas a DOP of 0% indicates a planar geometry at the central atom

Table A4. Selected crystallographic data for [(BDI_{DIPP})PbOTf] (**58**)

[(BDI _{DIPP})PbOTf] (58)	
chemical formula	C ₃₀ H ₄₁ F ₃ N ₂ O ₃ PbS, 7/8(C ₇ H ₈)
molecular mass	854.52
temperature (K)	173(2)
wavelength (Å)	0.71073
crystal system	Triclinic
space group	<i>P</i> $\bar{1}$ (No. 2)
<i>a</i> (Å)	12.9485(2)
<i>b</i> (Å)	24.6426(4)
<i>c</i> (Å)	25.1412(4)
α (deg)	106.740(1)
β (deg)	100.768(1)
γ (deg)	92.445(1)
<i>V</i> (Å ³)	7507.1(2)
<i>Z</i>	8
ρ_{calcd} (Mg m ⁻³)	1.51
θ range (deg)	3.42–26.03
abs coeff (mm ⁻¹)	4.60
measd/indep reflns/ <i>R</i> (int)	76 006/29 301/0.057
data/restraints/param	29 301/0/1581
goodness of fit on <i>F</i> ²	1.048
final <i>R</i> indices [<i>I</i> > 2 σ (<i>I</i>)]	<i>R</i> 1 = 0.056, <i>wR</i> 2 = 0.107
<i>R</i> indices (all data)	<i>R</i> 1 = 0.099, <i>wR</i> 2 = 0.123
largest diff peak and hole (e Å ⁻³)	2.31 and -2.11

Experimental procedure for [(BDI_{DIPP})PbOTf] (**58**)

[CH{(CH₃)CN-2,6-^{*i*}Pr₂C₆H₃}₂PbOSO₂CF₃], (BDI_{DIPP})PbOTf, (**58**).^[3]
 [(BDI_{DIPP})PbCl] (**2**) (0.40 g, 0.61 mmol) in toluene (15 mL) was added slowly to silver trifluoromethanesulfonate (0.16 g, 0.61 mmol) suspended in toluene (5 mL). The mixture was stirred at room temperature for 24 h. The yellow suspension was filtered through a pad of Celite and the volatiles were removed from the filtrate under vacuum. The crude yellow solid residue was washed with cold pentene (3 × 5 mL). Yellow crystals of [(BDI_{DIPP})PbOTf] (**58**) were obtained from toluene at -30 °C. Yield: 0.46 g, 98%. [lit. 90%].^[3] ¹H NMR (300.13 MHz, C₆D₆, 303 K): δ 6.99–7.15 (m, 6H, Ar-*H*), 4.88 (s, 1H, γ -*CH*), 3.27 (septet, *J* = 6.9 Hz, 4H, *CHMe*₂), 1.59 (s, 6H, *NMe*), 1.27 (d,

$J = 6.9$ Hz, 12H, CHMe_2), 1.19 (d, $J = 6.9$ Hz, 12H, CHMe_2). [lit. ^1H NMR (500 MHz, C_6D_6): δ 6.99–7.12 (m, 6H), 4.88 (s, 1H), 3.26 (septet, 4H), 1.60 (s, 6H), 1.26 (d, 12H), 1.19 (d, 12H)].^[3] $^{13}\text{C}\{^1\text{H}\}$ NMR (100.46 MHz, C_6D_6 , 303 K): δ 165.9 (NCMe), 144.6 (*ipso*-C), 141.31 (*o*-C), 129.7 (*o*-C), 128.9 (*p*-C), 128.1 (*m*-C), 125.0 (*m*-C), 109.9 (γ -CH), 28.2 (CHMe_2), 26.6 (CHMe_2), 25.0 (CHMe_2), 24.8 (CHMe_2). [lit. $^{13}\text{C}\{^1\text{H}\}$ NMR (125.75 MHz, C_6D_6): δ 165.5, 144.3, 140.9, 127.7, 124.7, 109.6, 28.6, 27.8, 26.2, 24.6].^[3]

Appendix 4. Calculations of the free energy of activation from variable-temperature NMR spectroscopic studies

The rate constant (k_c) at coalescence temperature (T_c) for uncoupled signals can be approximated by:^[9-10]

$$k_c = \frac{\pi(\Delta\delta)}{\sqrt{2}} \quad (\text{i})$$

where:

$\Delta\delta$ = difference in chemical shift (in Hz) at the slow exchange limit

For coupled signals:

$$k_c = \pi \sqrt{\frac{(\Delta\delta)^2 + 6(J_{AB})^2}{2}} \quad (\text{ii})$$

Where:

J_{AB} = coupling constant of the signal

Using the Eyring equation, the free energy of activation (ΔG^\ddagger) can be calculated:

$$k_c = \frac{kT_c}{h} e^{(-\Delta G^\ddagger/RT_c)} \quad (\text{iii})$$

where:

k = Boltzmann constant ($1.381 \times 10^{-23} \text{ J K}^{-1}$)

h = Planck constant ($6.626 \times 10^{-34} \text{ J s}$)

R = gas constant ($8.314 \text{ J mol}^{-1} \text{ K}^{-1}$)

T_c = coalescence temperature (K)

By substituting fundamental constants, equation (iii) can be converted into equation (iv) for the calculation of the free energy of activation (ΔG^\ddagger):^[9-10]

$$\Delta G^\ddagger = (1.914 \times 10^{-2})(T_c)[10.319 + \log_{10}(T_c/k_c)] \quad (\text{iv})$$

Chapter 3. Free energy of activation for exchange of N-aryl substituents in the β -diketiminato ligand in [(BDI_{DMP})PbCl] (24) (Figure 17, Page 74)

The coalescence temperature (T_c) is found at -10 °C (263 K). The lowest exchange limit is found at -80 °C and the two proton resonances assigned to the *ortho*-methyl groups are separated by $\Delta\delta_H$ 296 Hz. Hence, the rate constant (k_c) for this exchange at the coalescence temperature (263 K) can be obtained using equation (i):

$$k_c = \frac{\pi(296)}{\sqrt{2}}$$

$$k_c = 657.5 \text{ s}^{-1}$$

Using equation (iv), the free activation energy in [(BDI_{DMP})PbCl] (24) is:

$$\Delta G^\ddagger = (1.914 \times 10^{-2})(263)[10.319 + \log_{10}(263/657.5)]$$

$$\Delta G^\ddagger = 49.9 \text{ kJ mol}^{-1}$$

Thus, for [(BDI_{DMP})PbCl] (24), the free energy of activation (ΔG^\ddagger) associated with the restricted rotation about the *N*-aryl substituents in the β -diketiminato ligand is estimated to be 49.9 kJ mol⁻¹.

Chapter 4. Free energy of activation for exchange of SiMe₃ groups from the ¹H NMR spectra in [(BDI_{DMP})GeP(SiMe₃)₂] (40) (Figure 70, Page 171)

The coalescence temperature (T_c) is found at -30 °C (243 K). The lowest exchange limit is found at -80 °C and the two proton resonances assigned to the trimethylsilyl groups are separated by $\Delta\delta_H$ 76 Hz. Hence, the rate constant (k_c) for this exchange at the coalescence temperature (243 K) can be obtained using equation (i):

$$k_c = \frac{\pi(76)}{\sqrt{2}}$$

$$k_c = 168.6 \text{ s}^{-1}$$

Using equation (iv), the free energy of activation for exchange of the SiMe₃ groups in [(BDI_{DIPP})GeP(SiMe₃)₂] (**40**) is:

$$\Delta G^{\ddagger} = (1.914 \times 10^{-2})(243)[10.319 + \log_{10}(243/168.6)]$$

$$\Delta G^{\ddagger} = 48.7 \text{ kJ mol}^{-1}$$

Thus, for [(BDI_{DIPP})GeP(SiMe₃)₂] (**40**), the free energy of activation (ΔG^{\ddagger}) associated with exchange of the SiMe₃ groups is estimated to be 48.7 kJ mol⁻¹.

*Chapter 4. Free energy of activation for exchange of SiMe₃ groups from the ²⁹Si{¹H} NMR spectra in [(BDI_{DIPP})GeP(SiMe₃)₂] (**40**) (Figure 72, Page 173)*

The coalescence temperature (T_c) is estimated to be at -60 °C (213 K). The lowest exchange limit is found at -80 °C and the two silicon resonances assigned to the trimethylsilyl groups are separated by $\Delta\delta_{\text{Si}}$ 40 Hz with $^1J_{\text{SiP}} = 36$ Hz. Hence, the rate constant (k_c) for this exchange at the coalescence temperature (213 K) can be obtained using equation (ii):

$$k_c = \pi \sqrt{\frac{(40)^2 + 6(36)^2}{2}}$$

$$k_c = 214.8 \text{ s}^{-1}$$

Using equation (iv), the free energy of activation of the change in bond angles around the phosphorus in [(BDI_{DIPP})GeP(SiMe₃)₂] (**40**):

$$\Delta G^{\ddagger} = (1.914 \times 10^{-2})(213)[10.319 + \log_{10}(213/214.8)]$$

$$\Delta G^{\ddagger} = 42.1 \text{ kJ mol}^{-1}$$

Thus, for [(BDI_{DIPP})GeP(SiMe₃)₂] (**40**), the free energy of activation (ΔG^{\ddagger}) associated with the exchange of SiMe₃ groups around the phosphorus is estimated to be 42.1 kJ mol⁻¹.

Chapter 4. Free energy of activation for exchange of SiMe₃ groups from the ¹H NMR spectra in [(BDI_{DIPP})SnP(SiMe₃)₂] (41) (Figure 73, Page 174)

The coalescence temperature (T_c) is found at -50 °C (223 K). The lowest exchange limit is found at -80 °C and the two proton resonances assigned to the trimethylsilyl groups are separated by $\Delta\delta_H$ 60 Hz. Hence, the rate constant (k_c) for this exchange at the coalescence temperature (223 K) can be obtained using equation (i):

$$k_c = \frac{\pi(60)}{\sqrt{2}}$$

$$k_c = 133.1 \text{ s}^{-1}$$

Using equation (iv), the free energy of activation for exchange of the SiMe₃ groups in [(BDI_{DIPP})SnP(SiMe₃)₂] (41) is:

$$\Delta G^\ddagger = (1.914 \times 10^{-2})(223)[10.319 + \log_{10}(223/133.1)]$$

$$\Delta G^\ddagger = 45.0 \text{ kJ mol}^{-1}$$

Thus, for [(BDI_{DIPP})SnP(SiMe₃)₂] (41), the free energy of activation (ΔG^\ddagger) associated with exchange of the SiMe₃ groups is estimated to be 45.0 kJ mol⁻¹.

Chapter 4. Free energy of activation for exchange of SiMe₃ groups from the ²⁹Si{¹H} NMR spectra in [(BDI_{DIPP})SnP(SiMe₃)₂] (41) (Figure 78, Page 178)

The coalescence temperature (T_c) is estimated to be at -50 °C (223 K). The lowest exchange limit is found at -80 °C and the two silicon resonances assigned to the trimethylsilyl groups are separated by $\Delta\delta_{Si}$ 127 Hz with $^1J_{SiP} = 29$ Hz. Hence, the rate constant (k_c) for this exchange at the coalescence temperature (223 K) can be obtained using equation (ii):

$$k_c = \pi \sqrt{\frac{(127)^2 + 6(29)^2}{2}}$$

$$k_c = 323.2 \text{ s}^{-1}$$

Using equation (iv), the free energy of activation for exchange of the SiMe₃ groups in [(BDI_{DIPP})SnP(SiMe₃)₂] (**41**):

$$\Delta G^{\ddagger} = (1.914 \times 10^{-2})(223)[10.319 + \log_{10}(223/323.2)]$$

$$\Delta G^{\ddagger} = 43.4 \text{ kJ mol}^{-1}$$

Thus, for [(BDI_{DIPP})SnP(SiMe₃)₂] (**41**), the free energy of activation (ΔG^{\ddagger}) associated with exchange of the SiMe₃ groups is estimated to be 43.4 kJ mol⁻¹.

*Chapter 4. Free energy of activation for exchange of SiMe₃ groups from the ³¹P{¹H} NMR spectra in [(BDI_{DIPP})PbP(SiMe₃)₂] (**42**) (Figure 84, Page 184)*

The coalescence temperature (T_c) is found at -50 °C (223 K). The lowest exchange limit is found at -90 °C and the two phosphorus resonances are separated by $\Delta\delta_P$ 12420 Hz. Hence, the rate constant (k_c) for this exchange at the coalescence temperature (223 K) can be obtained using equation (i):

$$k_c = \frac{\pi(12420)}{\sqrt{2}}$$

$$k_c = 27590.3 \text{ s}^{-1}$$

Using equation (iv), the free energy of activation for exchange of the SiMe₃ groups in [(BDI_{DIPP})PbP(SiMe₃)₂] (**42**) is:

$$\Delta G^{\ddagger} = (1.914 \times 10^{-2})(223)[10.319 + \log_{10}(223/27590.3)]$$

$$\Delta G^{\ddagger} = 35.1 \text{ kJ mol}^{-1}$$

Thus, for [(BDI_{DIPP})PbP(SiMe₃)₂] (**42**), the free energy of activation (ΔG^{\ddagger}) associated with exchange of the SiMe₃ groups is estimated to be 35.3 kJ mol⁻¹.

Appendix 5. X-ray crystallographic data

Index

[(BDI _{DIPP})PbOC(CH ₃) ₂ CH=CH ₂] (5).....	347
[PhCH=C{C(CH ₃)N(2,6- <i>i</i> -Pr ₂ C ₆ H ₃) ₂ }] (13)	351
[(BDI _{Ph})PbCl] (22)	356
(BDI _{DMP})PbCl] (24).....	360
[(BDI _{Ph}) ₂ Pb] (25)	364
[(BDI _{DIPP}) ₂ Pb] (26)	371
[(BDI _{DMP})PbO ^{<i>t</i>} Bu] (28)	378
[(BDI _{DMP})PbOTf] (29)	385
[(BDI _{DIPP})PbI] (30).....	390
[(BDI _{DIPP})GePPh ₂] (33).....	394
[(BDI _{DIPP})SnPPh ₂] (34)	400
[(BDI _{DIPP})PbPPh ₂] (35).....	406
[(BDI _{DIPP})GePCy ₂] (36).....	412
[(BDI _{DIPP})SnPCy ₂] (37)	418
[(BDI _{DIPP})PbPCy ₂] (38).....	424
[(BDI _{DIPP})Sn ^{<i>n</i>} Bu] (39)	430
[(BDI _{DIPP})SnP(SiMe ₃) ₂] (41).....	436
[(BDI _{DIPP})SnSePCy ₂] (46).....	442
[(BDI _{DIPP})PbSePCy ₂] (47).....	448
[(BDI _{DIPP})GeSeP(Se)Cy ₂] (48)	454
[(BDI _{DIPP})SnSeP(Se)Cy ₂] (49).....	461
[(BDI _{DIPP})PbSeP(Se)Cy ₂] (50).....	468
[(BDI _{DIPP})Ge(Se)PCy ₂] (51).....	475
[(BDI _{DIPP})SnSP(S)Cy ₂] (52).....	486
[(BDI _{DIPP})PbSP(S)Cy ₂] (53).....	493
[(BDI _{DIPP})Ge(S)PCy ₂] (54).....	500
[(BDI _{DIPP})Ge(Se)P(SiMe ₃) ₂] (56)	507
[(BDI _{DIPP})SnSeSiMe ₃] (57)	513
[(BDI _{DIPP})PbOTf] (58).....	519

Table A5. Crystal data and structure refinement for [(BDI_{DIPP})PbOC(CH₃)₂CH=CH₂] (5)

Identification code	sep209	
Empirical formula	C ₃₄ H ₅₀ N ₂ O Pb	
Formula weight	709.95	
Temperature	173(2) K	
Wavelength	0.71073 Å	
Crystal system	Orthorhombic	
Space group	P n m a	
Unit cell dimensions	a = 16.7481(2) Å	a = 90°.
	b = 21.1755(3) Å	b = 90°.
	c = 9.3249(1) Å	g = 90°.
Volume	3307.07(7) Å ³	
Z	4	
Density (calculated)	1.43 Mg/m ³	
Absorption coefficient	5.13 mm ⁻¹	
F(000)	1432	
Crystal size	0.20 x 0.13 x 0.09 mm ³	
Theta range for data collection	3.41 to 27.47°.	
Index ranges	-21 ≤ h ≤ 21, -27 ≤ k ≤ 27, -12 ≤ l ≤ 12	
Reflections collected	48777	
Independent reflections	3866 [R(int) = 0.052]	
Reflections with I > 2σ(I)	3608	
Completeness to theta = 27.47°	99.5 %	
Absorption correction	Semi-empirical from equivalents	
Tmax. and Tmin.	0.5899 and 0.4029	
Refinement method	Full-matrix least-squares on F ²	
Data / restraints / parameters	3866 / 0 / 194	
Goodness-of-fit on F ²	0.913	
Final R indices [I > 2σ(I)]	R1 = 0.019, wR2 = 0.051	
R indices (all data)	R1 = 0.021, wR2 = 0.052	
Largest diff. peak and hole	0.65 and -1.46 e.Å ⁻³	

The alkoxy ligand is disordered across the mirror plane and was refined in one orientation with the atoms at ½ occupancy

Data collection KappaCCD , Program package WinGX , Abs correction MULTISCAN
Refinement using SHELXL-97 , Drawing using ORTEP-3 for Windows

Table A6. Atomic coordinates ($\times 10^4$) and equivalent isotropic displacement parameters ($\text{\AA}^2 \times 10^3$) for $[(\text{BDI}_{\text{DIPP}})\text{PbOC}(\text{CH}_3)_2\text{CH}=\text{CH}_2]$ (**5**). $U(\text{eq})$ is defined as one third of the trace of the orthogonalized U^{ij} tensor

	x	y	z	$U(\text{eq})$
Pb	1084(1)	2500	2357(1)	18(1)
O	2304(1)	2500	1637(2)	25(1)
N	689(1)	3204(1)	594(2)	18(1)
C(1)	98(1)	3102(1)	-317(2)	19(1)
C(2)	-206(2)	2500	-656(3)	20(1)
C(3)	-298(1)	3655(1)	-1058(3)	30(1)
C(4)	1049(1)	3816(1)	729(2)	22(1)
C(5)	759(1)	4247(1)	1739(3)	26(1)
C(6)	1169(2)	4820(1)	1901(3)	37(1)
C(7)	1828(2)	4956(1)	1088(3)	43(1)
C(8)	2107(2)	4529(1)	92(3)	38(1)
C(9)	1732(1)	3945(1)	-100(2)	27(1)
C(10)	29(2)	4113(1)	2661(2)	31(1)
C(11)	-613(2)	4626(2)	2475(3)	45(1)
C(12)	255(2)	4045(1)	4245(3)	47(1)
C(13)	2050(2)	3466(1)	-1162(3)	37(1)
C(14)	2958(2)	3488(2)	-1323(4)	56(1)
C(15)	1653(3)	3533(2)	-2631(3)	60(1)
C(16)	2882(2)	2500	2729(4)	39(1)
C(17)	3711(2)	2500	1989(5)	48(1)
C(18)	2779(6)	1792(4)	3505(12)	44(2)
C(19)	2878(6)	2964(4)	3795(10)	37(2)
C(20)	2568(4)	3528(3)	3575(7)	41(2)

Table A7. Bond lengths [Å] and angles [deg] for [(BDI_{DIPP})PbOC(CH₃)₂CH=CH₂] (5)

Pb-O	2.150(2)
Pb-N	2.3151(16)
O-C(16)	1.404(4)
N-C(1)	1.322(3)
N-C(4)	1.436(3)
C(1)-C(2)	1.408(2)
C(1)-C(3)	1.514(3)
C(4)-C(5)	1.399(3)
C(4)-C(9)	1.408(3)
C(5)-C(6)	1.401(3)
C(5)-C(10)	1.522(3)
C(6)-C(7)	1.369(4)
C(7)-C(8)	1.379(4)
C(8)-C(9)	1.397(3)
C(9)-C(13)	1.513(3)
C(10)-C(12)	1.531(3)
C(10)-C(11)	1.538(4)
C(13)-C(14)	1.529(4)
C(13)-C(15)	1.529(4)
C(16)-C(19)	1.398(10)
C(16)-C(17)	1.551(6)
C(16)-C(18)	1.673(10)
C(19)-C(20)	1.318(9)
O-Pb-N	92.87(6)
N'-Pb-N	80.13(8)
C(16)-O-Pb	115.4(2)
C(1)-N-C(4)	121.23(17)
C(1)-N-Pb	124.39(13)
C(4)-N-Pb	113.53(12)
N-C(1)-C(2)	124.28(19)
N-C(1)-C(3)	119.64(18)
C(2)-C(1)-C(3)	116.08(19)
C(1)-C(2)-C(1)	129.6(3)
C(5)-C(4)-C(9)	121.7(2)
C(5)-C(4)-N	120.16(19)

C(9)-C(4)-N	117.94(19)
C(4)-C(5)-C(6)	117.8(2)
C(4)-C(5)-C(10)	122.6(2)
C(6)-C(5)-C(10)	119.6(2)
C(7)-C(6)-C(5)	121.2(3)
C(6)-C(7)-C(8)	120.4(2)
C(7)-C(8)-C(9)	121.0(2)
C(8)-C(9)-C(4)	117.8(2)
C(8)-C(9)-C(13)	121.3(2)
C(4)-C(9)-C(13)	121.0(2)
C(5)-C(10)-C(12)	111.3(2)
C(5)-C(10)-C(11)	111.5(2)
C(12)-C(10)-C(11)	110.4(2)
C(9)-C(13)-C(14)	113.2(2)
C(9)-C(13)-C(15)	111.8(3)
C(14)-C(13)-C(15)	110.0(3)
C(19)-C(16)-O	120.8(4)
C(19)-C(16)-C(17)	108.7(5)
O-C(16)-C(17)	107.1(3)
C(19)-C(16)-C(18)	108.7(5)
O-C(16)-C(18)	104.0(4)
C(17)-C(16)-C(18)	106.5(4)
C(20)-C(19)-C(16)	121.9(7)

Symmetry transformations used to generate equivalent atoms:

$x, -y+1/2, z$

Table A8. Crystal data and structure refinement for [PhCH=C{C(CH₃)N(2,6-*i*-Pr₂C₆H₃)}₂] (**13**)

Identification code	may207	
Empirical formula	C ₃₆ H ₄₆ N ₂	
Formula weight	506.75	
Temperature	173(2) K	
Wavelength	0.71073 Å	
Crystal system	Monoclinic	
Space group	P2 ₁ /c (No.14)	
Unit cell dimensions	a = 13.2095(3) Å	a = 90°.
	b = 8.8710(2) Å	b = 91.691(1)°.
	c = 26.1615(5) Å	g = 90°.
Volume	3064.31(11) Å ³	
Z	4	
Density (calculated)	1.10 Mg/m ³	
Absorption coefficient	0.06 mm ⁻¹	
F(000)	1104	
Crystal size	0.40 x 0.40 x 0.35 mm ³	
Theta range for data collection	3.42 to 26.02°.	
Index ranges	-16 ≤ h ≤ 15, -10 ≤ k ≤ 10, -32 ≤ l ≤ 25	
Reflections collected	20035	
Independent reflections	5950 [R(int) = 0.048]	
Reflections with I > 2σ(I)	4443	
Completeness to theta = 26.02°	98.6 %	
Refinement method	Full-matrix least-squares on F ²	
Data / restraints / parameters	5950 / 0 / 353	
Goodness-of-fit on F ²	1.008	
Final R indices [I > 2σ(I)]	R1 = 0.051, wR2 = 0.120	
R indices (all data)	R1 = 0.074, wR2 = 0.134	
Largest diff. peak and hole	0.19 and -0.23 e.Å ⁻³	

Data collection KappaCCD , Program package WinGX , Abs correction not applied ,
 Refinement using SHELXL-97 , Drawing using ORTEP-3 for Windows

Table A9. Atomic coordinates ($\times 10^4$) and equivalent isotropic displacement parameters ($\text{\AA}^2 \times 10^3$) for $[\text{PhCH}=\text{C}\{\text{C}(\text{CH}_3)\text{N}(2,6\text{-}i\text{-Pr}_2\text{C}_6\text{H}_3)\}_2]$ (**13**). $U(\text{eq})$ is defined as one third of the trace of the orthogonalized U^{ij} tensor

	x	y	z	U(eq)
N(1)	2530(1)	4117(1)	3447(1)	26(1)
N(2)	2877(1)	5290(1)	4665(1)	26(1)
C(1)	3178(1)	3176(2)	3633(1)	26(1)
C(2)	3287(1)	3075(2)	4199(1)	25(1)
C(3)	2565(1)	4017(2)	4500(1)	25(1)
C(4)	3817(1)	2148(2)	3316(1)	34(1)
C(5)	1538(1)	3346(2)	4580(1)	39(1)
C(6)	2342(1)	4235(2)	2907(1)	27(1)
C(7)	1665(1)	3228(2)	2661(1)	29(1)
C(8)	1461(1)	3411(2)	2141(1)	35(1)
C(9)	1902(1)	4563(2)	1868(1)	40(1)
C(10)	2556(1)	5555(2)	2115(1)	38(1)
C(11)	2790(1)	5416(2)	2637(1)	31(1)
C(12)	1154(1)	1984(2)	2958(1)	33(1)
C(13)	223(1)	2592(2)	3226(1)	49(1)
C(14)	859(2)	616(2)	2634(1)	47(1)
C(15)	3544(1)	6475(2)	2896(1)	37(1)
C(16)	4624(1)	5908(2)	2829(1)	51(1)
C(17)	3458(2)	8094(2)	2703(1)	56(1)
C(18)	2218(1)	6261(2)	4940(1)	26(1)
C(19)	2209(1)	6197(2)	5475(1)	30(1)
C(20)	1613(1)	7238(2)	5730(1)	38(1)
C(21)	1047(1)	8308(2)	5469(1)	40(1)
C(22)	1075(1)	8369(2)	4942(1)	37(1)
C(23)	1661(1)	7363(2)	4668(1)	29(1)
C(24)	2845(1)	5069(2)	5779(1)	35(1)
C(25)	3703(2)	5865(3)	6068(1)	72(1)
C(26)	2230(2)	4131(3)	6134(1)	89(1)
C(27)	1695(1)	7479(2)	4089(1)	36(1)
C(28)	678(2)	7114(3)	3832(1)	64(1)
C(29)	2071(2)	9020(2)	3926(1)	57(1)
C(30)	3958(1)	2147(2)	4427(1)	31(1)
C(31)	4104(1)	1874(2)	4985(1)	31(1)
C(32)	3514(1)	820(2)	5232(1)	42(1)
C(33)	3682(2)	501(2)	5745(1)	50(1)
C(34)	4440(2)	1239(2)	6020(1)	51(1)
C(35)	5039(2)	2269(3)	5776(1)	52(1)
C(36)	4877(1)	2587(2)	5263(1)	44(1)

Table A10. Bond lengths [Å] and angles [deg] for [PhCH=C{C(CH₃)N(2,6-*i*-Pr₂C₆H₃)₂}] (**13**)

N(1)-C(1)	1.281(2)
N(1)-C(6)	1.431(2)
N(2)-C(3)	1.273(2)
N(2)-C(18)	1.433(2)
C(1)-C(2)	1.486(2)
C(1)-C(4)	1.507(2)
C(2)-C(30)	1.337(2)
C(2)-C(3)	1.508(2)
C(3)-C(5)	1.501(2)
C(6)-C(11)	1.405(2)
C(6)-C(7)	1.407(2)
C(7)-C(8)	1.387(2)
C(7)-C(12)	1.521(2)
C(8)-C(9)	1.384(2)
C(9)-C(10)	1.381(2)
C(10)-C(11)	1.395(2)
C(11)-C(15)	1.515(2)
C(12)-C(14)	1.525(2)
C(12)-C(13)	1.530(2)
C(15)-C(17)	1.526(3)
C(15)-C(16)	1.528(3)
C(18)-C(19)	1.402(2)
C(18)-C(23)	1.405(2)
C(19)-C(20)	1.396(2)
C(19)-C(24)	1.516(2)
C(20)-C(21)	1.378(2)
C(21)-C(22)	1.381(2)
C(22)-C(23)	1.394(2)
C(23)-C(27)	1.520(2)
C(24)-C(26)	1.504(3)
C(24)-C(25)	1.518(3)
C(27)-C(28)	1.518(3)
C(27)-C(29)	1.520(3)
C(30)-C(31)	1.487(2)
C(31)-C(36)	1.388(2)
C(31)-C(32)	1.389(2)

C(32)-C(33)	1.384(2)
C(33)-C(34)	1.380(3)
C(34)-C(35)	1.377(3)
C(35)-C(36)	1.382(3)
C(1)-N(1)-C(6)	121.12(12)
C(3)-N(2)-C(18)	120.49(13)
N(1)-C(1)-C(2)	117.47(13)
N(1)-C(1)-C(4)	124.38(13)
C(2)-C(1)-C(4)	118.13(13)
C(30)-C(2)-C(1)	121.66(13)
C(30)-C(2)-C(3)	121.97(13)
C(1)-C(2)-C(3)	116.31(12)
N(2)-C(3)-C(5)	126.13(14)
N(2)-C(3)-C(2)	117.74(13)
C(5)-C(3)-C(2)	116.13(13)
C(11)-C(6)-C(7)	120.89(14)
C(11)-C(6)-N(1)	119.26(13)
C(7)-C(6)-N(1)	119.74(13)
C(8)-C(7)-C(6)	118.55(14)
C(8)-C(7)-C(12)	120.68(14)
C(6)-C(7)-C(12)	120.76(13)
C(9)-C(8)-C(7)	121.25(16)
C(10)-C(9)-C(8)	119.77(15)
C(9)-C(10)-C(11)	121.22(15)
C(10)-C(11)-C(6)	118.33(15)
C(10)-C(11)-C(15)	120.41(14)
C(6)-C(11)-C(15)	121.21(14)
C(7)-C(12)-C(14)	113.70(13)
C(7)-C(12)-C(13)	110.70(14)
C(14)-C(12)-C(13)	109.88(15)
C(11)-C(15)-C(17)	113.21(15)
C(11)-C(15)-C(16)	110.42(14)
C(17)-C(15)-C(16)	109.43(16)
C(19)-C(18)-C(23)	120.95(13)
C(19)-C(18)-N(2)	119.99(13)
C(23)-C(18)-N(2)	118.77(13)
C(20)-C(19)-C(18)	118.23(14)

C(20)-C(19)-C(24)	119.75(14)
C(18)-C(19)-C(24)	122.00(13)
C(21)-C(20)-C(19)	121.54(15)
C(20)-C(21)-C(22)	119.52(15)
C(21)-C(22)-C(23)	121.33(15)
C(22)-C(23)-C(18)	118.40(14)
C(22)-C(23)-C(27)	120.16(14)
C(18)-C(23)-C(27)	121.43(13)
C(26)-C(24)-C(19)	112.88(15)
C(26)-C(24)-C(25)	111.0(2)
C(19)-C(24)-C(25)	110.41(15)
C(28)-C(27)-C(29)	111.13(16)
C(28)-C(27)-C(23)	112.03(15)
C(29)-C(27)-C(23)	111.05(14)
C(2)-C(30)-C(31)	127.10(14)
C(36)-C(31)-C(32)	118.50(15)
C(36)-C(31)-C(30)	120.80(15)
C(32)-C(31)-C(30)	120.55(15)
C(33)-C(32)-C(31)	120.90(17)
C(34)-C(33)-C(32)	120.00(19)
C(35)-C(34)-C(33)	119.47(17)
C(34)-C(35)-C(36)	120.73(18)
C(35)-C(36)-C(31)	120.38(18)

Table A11. Crystal data and structure refinement for [(BDI_{Ph})PbCl] (**22**)

Identification code	may1110	
Empirical formula	C ₁₇ H ₁₇ Cl N ₂ Pb, 0.5 (C ₇ H ₈)	
Formula weight	538.03	
Temperature	173(2) K	
Wavelength	0.71073 Å	
Crystal system	Monoclinic	
Space group	C 2/c (No.15)	
Unit cell dimensions	a = 23.4501(5) Å	a = 90°.
	b = 10.0070(2) Å	b = 106.434(1)°.
	c = 16.7676(4) Å	g = 90°.
Volume	3774.02(14) Å ³	
Z	8	
Density (calculated)	1.89 Mg/m ³	
Absorption coefficient	9.09 mm ⁻¹	
F(000)	2056	
Crystal size	0.20 x 0.04 x 0.04 mm ³	
Theta range for data collection	3.40 to 27.10°.	
Index ranges	-30 ≤ h ≤ 30, -12 ≤ k ≤ 12, -21 ≤ l ≤ 21	
Reflections collected	29205	
Independent reflections	4164 [R(int) = 0.061]	
Reflections with I > 2σ(I)	3591	
Completeness to theta = 27.10°	99.8 %	
Tmax. and Tmin.	0.5152 and 0.3975	
Refinement method	Full-matrix least-squares on F ²	
Data / restraints / parameters	4164 / 0 / 206	
Goodness-of-fit on F ²	1.009	
Final R indices [I > 2σ(I)]	R1 = 0.027, wR2 = 0.056	
R indices (all data)	R1 = 0.037, wR2 = 0.059	
Largest diff. peak and hole	1.95 and -0.94 e.Å ⁻³ (near disordered solvent)	

The toluene solvate has unresolved disorder

Data collection KappaCCD , Program package WinGX , Abs correction MULTISCAN

Refinement using SHELXL-97 , Drawing using ORTEP-3 for Windows

Table A12. Atomic coordinates ($\times 10^4$) and equivalent isotropic displacement parameters ($\text{\AA}^2 \times 10^3$) for [(BDI_{Ph})PbCl] (**22**). U(eq) is defined as one third of the trace of the orthogonalized U^{ij} tensor

	x	y	z	U(eq)
Pb	2544(1)	6927(1)	2393(1)	22(1)
Cl	2156(1)	9190(1)	3083(1)	29(1)
N(1)	1613(2)	6034(4)	2083(2)	22(1)
N(2)	2667(2)	5961(4)	3666(2)	22(1)
C(1)	1398(2)	5267(4)	2576(3)	22(1)
C(2)	1712(2)	4870(4)	3381(3)	26(1)
C(3)	2287(2)	5151(4)	3885(3)	22(1)
C(4)	762(2)	4770(5)	2277(3)	32(1)
C(5)	2461(2)	4470(5)	4722(3)	31(1)
C(6)	1295(2)	6295(4)	1239(3)	22(1)
C(7)	1230(2)	7612(5)	967(3)	27(1)
C(8)	946(2)	7907(5)	141(3)	30(1)
C(9)	722(2)	6902(5)	-413(3)	32(1)
C(10)	793(2)	5579(5)	-147(3)	32(1)
C(11)	1086(2)	5273(5)	668(3)	28(1)
C(12)	3235(2)	6282(4)	4207(3)	23(1)
C(13)	3313(2)	6859(4)	4991(3)	27(1)
C(14)	3877(2)	7208(5)	5481(3)	30(1)
C(15)	4369(2)	6993(5)	5198(3)	32(1)
C(16)	4298(2)	6459(5)	4416(3)	29(1)
C(17)	3733(2)	6098(4)	3921(3)	24(1)
C(1S)	0	7461(7)	2500	28(1)
C(2S)	0	8801(9)	2500	48(2)
C(3S)	536(2)	9442(5)	2674(3)	39(1)
C(4S)	526(2)	10817(5)	2685(3)	37(1)
C(5S)	0	11498(8)	2500	37(2)

Table A13. Bond lengths [Å] and angles [deg] for [(BDI_{Ph})PbCl] (**22**)

Pb-N(1)	2.279(3)
Pb-N(2)	2.285(4)
Pb-Cl	2.8081(11)
Pb-Cl'	2.9928(11)
N(1)-C(1)	1.328(5)
N(1)-C(6)	1.425(5)
N(2)-C(3)	1.332(5)
N(2)-C(12)	1.419(5)
C(1)-C(2)	1.399(6)
C(1)-C(4)	1.516(6)
C(2)-C(3)	1.402(6)
C(3)-C(5)	1.509(6)
C(6)-C(7)	1.389(6)
C(6)-C(11)	1.392(6)
C(7)-C(8)	1.388(6)
C(8)-C(9)	1.370(7)
C(9)-C(10)	1.392(7)
C(10)-C(11)	1.379(7)
C(12)-C(17)	1.396(6)
C(12)-C(13)	1.399(6)
C(13)-C(14)	1.389(7)
C(14)-C(15)	1.383(7)
C(15)-C(16)	1.381(7)
C(16)-C(17)	1.397(6)
N(1)-Pb-N(2)	84.68(12)
N(1)-Pb-Cl	90.52(9)
N(2)-Pb-Cl	85.78(9)
N(1)-Pb-Cl'	82.10(9)
N(2)-Pb-Cl'	83.40(9)
Cl-Pb-Cl'	167.42(2)
Pb-Cl-Pb''	120.00(4)
C(1)-N(1)-C(6)	122.7(4)
C(1)-N(1)-Pb	126.4(3)
C(6)-N(1)-Pb	110.7(3)
C(3)-N(2)-C(12)	122.8(4)

C(3)-N(2)-Pb	126.7(3)
C(12)-N(2)-Pb	110.5(3)
N(1)-C(1)-C(2)	125.1(4)
N(1)-C(1)-C(4)	119.7(4)
C(2)-C(1)-C(4)	115.2(4)
C(1)-C(2)-C(3)	132.7(4)
N(2)-C(3)-C(2)	124.1(4)
N(2)-C(3)-C(5)	120.3(4)
C(2)-C(3)-C(5)	115.6(4)
C(7)-C(6)-C(11)	119.1(4)
C(7)-C(6)-N(1)	118.6(4)
C(11)-C(6)-N(1)	122.1(4)
C(8)-C(7)-C(6)	120.5(4)
C(9)-C(8)-C(7)	120.3(4)
C(8)-C(9)-C(10)	119.5(4)
C(11)-C(10)-C(9)	120.7(4)
C(10)-C(11)-C(6)	119.9(4)
C(17)-C(12)-C(13)	118.5(4)
C(17)-C(12)-N(2)	118.4(4)
C(13)-C(12)-N(2)	123.0(4)
C(14)-C(13)-C(12)	120.6(4)
C(15)-C(14)-C(13)	120.3(4)
C(16)-C(15)-C(14)	119.8(4)
C(15)-C(16)-C(17)	120.3(4)
C(12)-C(17)-C(16)	120.4(4)

Symmetry transformations used to generate equivalent atoms:

' $-x+1/2, y-1/2, -z+1/2$ " $-x+1/2, y+1/2, -z+1/2$

Table A14. Crystal data and structure refinement for [(BDI_{DMP})PbCl] (**24**)

Identification code	jul611	
Empirical formula	2(C ₂₁ H ₂₅ Cl N ₂ Pb), C ₇ H ₈	
Formula weight	1188.28	
Temperature	173(2) K	
Wavelength	0.71073 Å	
Crystal system	Triclinic	
Space group	P $\bar{1}$ (No.2)	
Unit cell dimensions	a = 8.3126(3) Å	a = 112.537(2)°.
	b = 12.5001(4) Å	b = 94.850(2)°.
	c = 12.9418(4) Å	g = 104.513(1)°.
Volume	1177.65(7) Å ³	
Z	1	
Density (calculated)	1.68 Mg/m ³	
Absorption coefficient	7.289 mm ⁻¹	
F(000)	578	
Crystal size	0.15 x 0.07 x 0.05 mm ³	
Theta range for data collection	3.40 to 26.76°.	
Index ranges	-10 ≤ h ≤ 10, -15 ≤ k ≤ 15, -16 ≤ l ≤ 16	
Reflections collected	15979	
Independent reflections	4989 [R(int) = 0.056]	
Reflections with I > 2σ(I)	4563	
Completeness to theta = 26.76°	99.2 %	
Absorption correction	Semi-empirical from equivalents	
Tmax. and Tmin.	0.5616 and 0.4731	
Refinement method	Full-matrix least-squares on F ²	
Data / restraints / parameters	4989 / 0 / 239	
Goodness-of-fit on F ²	1.038	
Final R indices [I > 2σ(I)]	R1 = 0.027, wR2 = 0.060	
R indices (all data)	R1 = 0.032, wR2 = 0.062	
Largest diff. peak and hole	1.77 and -1.03 e.Å ⁻³ (near disordered toluene)	

The toluene solvate lies on an inversion centre and was modeled as a rigid body with common thermal displacement parameters and all carbon atoms isotropic

Data collection KappaCCD , Program package WinGX , Abs correction MULTISCAN
Refinement using SHELXL-97 , Drawing using ORTEP-3 for Windows

Table A15. Atomic coordinates ($\times 10^4$) and equivalent isotropic displacement parameters ($\text{\AA}^2 \times 10^3$) for [(BDI_{DMP})PbCl] (**24**). U(eq) is defined as one third of the trace of the orthogonalized U^{ij} tensor

	x	y	z	U(eq)
Pb	5393(1)	6023(1)	9100(1)	22(1)
Cl	7623(1)	5286(1)	7992(1)	38(1)
N(1)	5535(4)	7537(3)	8499(3)	21(1)
N(2)	7301(4)	7585(3)	10671(3)	23(1)
C(1)	6471(5)	8696(4)	9017(3)	24(1)
C(2)	7660(5)	9213(4)	10052(4)	28(1)
C(3)	7992(5)	8736(4)	10834(3)	25(1)
C(4)	6213(6)	9553(4)	8499(4)	33(1)
C(5)	9180(6)	9627(5)	11969(4)	41(1)
C(6)	4336(5)	7104(4)	7449(3)	22(1)
C(7)	4890(6)	6750(4)	6400(3)	29(1)
C(8)	3684(7)	6273(4)	5402(4)	41(1)
C(9)	1988(7)	6155(5)	5426(4)	50(1)
C(10)	1474(6)	6508(5)	6451(4)	44(1)
C(11)	2626(5)	6988(4)	7489(4)	28(1)
C(12)	6741(6)	6925(5)	6370(4)	39(1)
C(13)	2047(6)	7342(5)	8608(4)	40(1)
C(14)	7560(5)	7219(3)	11575(3)	21(1)
C(15)	8889(5)	6739(4)	11685(3)	26(1)
C(16)	8996(6)	6298(4)	12515(4)	33(1)
C(17)	7858(6)	6337(4)	13235(4)	32(1)
C(18)	6568(6)	6847(4)	13137(4)	30(1)
C(19)	6388(5)	7280(4)	12308(3)	25(1)
C(20)	10187(6)	6727(5)	10939(4)	38(1)
C(21)	4966(6)	7804(4)	12195(4)	35(1)
C(1S)	3984(9)	9843(10)	4897(9)	91(2)
C(2S)	4838(11)	9246(10)	5350(10)	91(2)
C(3S)	6599(11)	9576(11)	5539(10)	91(2)
C(4S)	7506(9)	10502(10)	5276(10)	91(2)
C(5S)	6652(11)	11098(10)	4823(10)	91(2)
C(6S)	4891(11)	10769(10)	4634(10)	91(2)
C(7S)	2024(9)	9566(13)	4701(12)	91(2)

Table A16. Bond lengths [\AA] and angles [deg] for $[(\text{BDI}_{\text{DMP}})\text{PbCl}]$ (**24**)

Pb-N(1)	2.288(3)
Pb-N(2)	2.306(3)
Pb-Cl	2.5757(11)
N(1)-C(1)	1.325(5)
N(1)-C(6)	1.439(5)
N(2)-C(3)	1.334(5)
N(2)-C(14)	1.429(5)
C(1)-C(2)	1.408(6)
C(1)-C(4)	1.511(6)
C(2)-C(3)	1.397(6)
C(3)-C(5)	1.524(6)
C(6)-C(11)	1.400(6)
C(6)-C(7)	1.414(6)
C(7)-C(8)	1.385(6)
C(7)-C(12)	1.505(6)
C(8)-C(9)	1.384(8)
C(9)-C(10)	1.371(8)
C(10)-C(11)	1.399(6)
C(11)-C(13)	1.502(6)
C(14)-C(15)	1.404(6)
C(14)-C(19)	1.412(6)
C(15)-C(16)	1.388(6)
C(15)-C(20)	1.507(6)
C(16)-C(17)	1.380(6)
C(17)-C(18)	1.398(6)
C(18)-C(19)	1.388(6)
C(19)-C(21)	1.510(6)
N(1)-Pb-N(2)	82.56(12)
N(1)-Pb-Cl	93.49(8)
N(2)-Pb-Cl	96.29(9)
C(1)-N(1)-C(6)	120.3(3)
C(1)-N(1)-Pb	128.6(3)
C(6)-N(1)-Pb	111.0(2)
C(3)-N(2)-C(14)	120.5(3)
C(3)-N(2)-Pb	128.0(3)

C(14)-N(2)-Pb	111.2(2)
N(1)-C(1)-C(2)	124.7(4)
N(1)-C(1)-C(4)	118.6(4)
C(2)-C(1)-C(4)	116.6(4)
C(3)-C(2)-C(1)	130.8(4)
N(2)-C(3)-C(2)	124.7(4)
N(2)-C(3)-C(5)	118.7(4)
C(2)-C(3)-C(5)	116.5(4)
C(11)-C(6)-C(7)	121.5(4)
C(11)-C(6)-N(1)	118.9(3)
C(7)-C(6)-N(1)	119.6(4)
C(8)-C(7)-C(6)	118.0(4)
C(8)-C(7)-C(12)	121.0(4)
C(6)-C(7)-C(12)	121.0(4)
C(9)-C(8)-C(7)	121.3(5)
C(10)-C(9)-C(8)	120.0(4)
C(9)-C(10)-C(11)	121.6(5)
C(10)-C(11)-C(6)	117.7(4)
C(10)-C(11)-C(13)	121.3(4)
C(6)-C(11)-C(13)	121.0(4)
C(15)-C(14)-C(19)	120.9(4)
C(15)-C(14)-N(2)	120.6(3)
C(19)-C(14)-N(2)	118.4(3)
C(16)-C(15)-C(14)	118.3(4)
C(16)-C(15)-C(20)	120.8(4)
C(14)-C(15)-C(20)	120.9(4)
C(17)-C(16)-C(15)	121.9(4)
C(16)-C(17)-C(18)	119.2(4)
C(19)-C(18)-C(17)	121.0(4)
C(18)-C(19)-C(14)	118.6(4)
C(18)-C(19)-C(21)	120.5(4)
C(14)-C(19)-C(21)	120.9(4)

Table A17. Crystal data and structure refinement for [(BDI_{Ph})₂Pb] (25)

Identification code	nov809	
Empirical formula	C ₃₄ H ₃₄ N ₄ Pb · C ₇ H ₈	
Formula weight	798.01	
Temperature	173(2) K	
Wavelength	0.71073 Å	
Crystal system	Triclinic	
Space group	P $\bar{1}$ (No.2)	
Unit cell dimensions	a = 10.3923(2) Å	a = 104.310(1)°.
	b = 11.5345(4) Å	b = 96.037(2)°.
	c = 17.0319(5) Å	g = 113.289(2)°.
Volume	1769.24(9) Å ³	
Z	2	
Density (calculated)	1.50 Mg/m ³	
Absorption coefficient	4.80 mm ⁻¹	
F(000)	796	
Crystal size	0.20 x 0.09 x 0.06 mm ³	
Theta range for data collection	3.49 to 27.09°.	
Index ranges	-13 ≤ h ≤ 13, -14 ≤ k ≤ 14, -21 ≤ l ≤ 21	
Reflections collected	31069	
Independent reflections	7797 [R(int) = 0.0548]	
Reflections with I > 2σ(I)	7106	
Completeness to theta = 27.09°	99.8 %	
Tmax. and Tmin.	0.3773 and 0.3137	
Refinement method	Full-matrix least-squares on F ²	
Data / restraints / parameters	7797 / 0 / 420	
Goodness-of-fit on F ²	0.837	
Final R indices [I > 2σ(I)]	R1 = 0.029, wR2 = 0.069	
R indices (all data)	R1 = 0.037, wR2 = 0.073	
Largest diff. peak and hole	0.91 and -1.44 e.Å ⁻³	

Data collection KappaCCD , Program package WinGX , Abs correction MULTISCAN

Refinement using SHELXL-97 , Drawing using ORTEP-3 for Windows

Table A18. Atomic coordinates ($\times 10^4$) and equivalent isotropic displacement parameters ($\text{\AA}^2 \times 10^3$) for $[(\text{BDI}_{\text{Ph}})_2\text{Pb}]$ (**25**). $U(\text{eq})$ is defined as one third of the trace of the orthogonalized U^{ij} tensor

	x	y	z	$U(\text{eq})$
Pb	5129(1)	2441(1)	2490(1)	21(1)
N(1)	7683(3)	3389(3)	2391(2)	25(1)
N(2)	6218(3)	1335(3)	3109(2)	24(1)
N(3)	5935(3)	4168(3)	3751(2)	21(1)
N(4)	3275(3)	1680(3)	3280(2)	23(1)
C(1)	8763(4)	3680(4)	2994(3)	27(1)
C(2)	8620(4)	3099(4)	3632(3)	28(1)
C(3)	7498(4)	1909(4)	3628(2)	25(1)
C(4)	10265(4)	4659(5)	3013(3)	38(1)
C(5)	7863(5)	1234(5)	4218(3)	39(1)
C(6)	7933(4)	3799(4)	1677(3)	27(1)
C(7)	8367(5)	3103(5)	1059(3)	39(1)
C(8)	8544(6)	3449(5)	340(3)	49(1)
C(9)	8277(5)	4480(5)	234(3)	47(1)
C(10)	7837(5)	5169(5)	837(3)	41(1)
C(11)	7661(4)	4838(4)	1564(3)	32(1)
C(12)	5259(4)	-25(4)	2967(2)	24(1)
C(13)	4591(4)	-510(4)	3561(3)	32(1)
C(14)	3613(5)	-1836(4)	3354(3)	40(1)
C(15)	3264(5)	-2695(4)	2557(4)	45(1)
C(16)	3920(5)	-2219(5)	1963(3)	43(1)
C(17)	4906(4)	-896(4)	2163(3)	30(1)
C(18)	5894(4)	3972(4)	4494(2)	23(1)
C(19)	4896(4)	2837(4)	4619(2)	25(1)
C(20)	3577(4)	1866(4)	4082(2)	25(1)
C(21)	6920(4)	5059(4)	5278(3)	32(1)
C(22)	2468(4)	1047(4)	4479(3)	33(1)
C(23)	6769(4)	5447(3)	3683(2)	24(1)
C(24)	8270(4)	6116(4)	3936(3)	29(1)
C(25)	9018(4)	7314(4)	3790(3)	35(1)
C(26)	8298(5)	7861(4)	3390(3)	36(1)
C(27)	6814(5)	7215(4)	3140(3)	35(1)

C(28)	6051(4)	6014(4)	3281(3)	29(1)
C(29)	1849(4)	846(4)	2781(2)	24(1)
C(30)	799(4)	1313(4)	2798(3)	31(1)
C(31)	-558(4)	539(5)	2269(3)	37(1)
C(32)	-879(4)	-695(5)	1718(3)	37(1)
C(33)	178(5)	-1141(4)	1710(3)	38(1)
C(34)	1525(4)	-381(4)	2231(3)	31(1)
C(35)	2758(6)	2636(6)	790(4)	57(1)
C(36)	3999(5)	2961(6)	460(3)	54(1)
C(37)	4361(6)	2002(8)	71(4)	72(2)
C(38)	3541(7)	684(7)	-31(4)	67(2)
C(39)	2302(7)	341(6)	285(4)	64(2)
C(40)	1939(5)	1328(6)	682(3)	49(1)
C(41)	2416(8)	3661(8)	1257(5)	83(2)

Table A19. Bond lengths [\AA] and angles [deg] for $[(\text{BDI}_{\text{Ph}})_2\text{Pb}]$ (**25**)

Pb-N(3)	2.338(3)
Pb-N(2)	2.363(3)
Pb-N(4)	2.466(3)
Pb-N(1)	2.482(3)
N(1)-C(1)	1.310(5)
N(1)-C(6)	1.424(5)
N(2)-C(3)	1.325(5)
N(2)-C(12)	1.427(5)
N(3)-C(18)	1.341(5)
N(3)-C(23)	1.427(4)
N(4)-C(20)	1.312(5)
N(4)-C(29)	1.431(5)
C(1)-C(2)	1.403(5)
C(1)-C(4)	1.514(5)
C(2)-C(3)	1.404(5)
C(3)-C(5)	1.516(5)
C(6)-C(7)	1.387(6)
C(6)-C(11)	1.387(6)
C(7)-C(8)	1.387(6)
C(8)-C(9)	1.370(7)
C(9)-C(10)	1.370(7)
C(10)-C(11)	1.392(6)
C(12)-C(13)	1.392(5)
C(12)-C(17)	1.394(6)
C(13)-C(14)	1.387(6)
C(14)-C(15)	1.379(7)
C(15)-C(16)	1.384(7)
C(16)-C(17)	1.388(6)
C(18)-C(19)	1.396(5)
C(18)-C(21)	1.519(6)
C(19)-C(20)	1.410(5)
C(20)-C(22)	1.515(5)
C(23)-C(28)	1.397(5)
C(23)-C(24)	1.399(5)
C(24)-C(25)	1.392(5)
C(25)-C(26)	1.378(6)

C(26)-C(27)	1.382(6)
C(27)-C(28)	1.394(6)
C(29)-C(34)	1.377(6)
C(29)-C(30)	1.395(5)
C(30)-C(31)	1.392(6)
C(31)-C(32)	1.384(7)
C(32)-C(33)	1.385(6)
C(33)-C(34)	1.378(6)
C(35)-C(40)	1.360(8)
C(35)-C(36)	1.412(7)
C(35)-C(41)	1.444(9)
C(36)-C(37)	1.350(9)
C(37)-C(38)	1.372(9)
C(38)-C(39)	1.397(8)
C(39)-C(40)	1.382(8)
N(3)-Pb-N(2)	89.87(11)
N(3)-Pb-N(4)	75.40(10)
N(2)-Pb-N(4)	85.22(10)
N(3)-Pb-N(1)	85.01(10)
N(2)-Pb-N(1)	73.44(10)
N(4)-Pb-N(1)	151.05(11)
C(1)-N(1)-C(6)	120.5(3)
C(1)-N(1)-Pb	123.7(2)
C(6)-N(1)-Pb	115.1(2)
C(3)-N(2)-C(12)	121.4(3)
C(3)-N(2)-Pb	125.5(2)
C(12)-N(2)-Pb	112.5(2)
C(18)-N(3)-C(23)	121.4(3)
C(18)-N(3)-Pb	123.6(2)
C(23)-N(3)-Pb	113.6(2)
C(20)-N(4)-C(29)	121.4(3)
C(20)-N(4)-Pb	123.2(2)
C(29)-N(4)-Pb	114.8(2)
N(1)-C(1)-C(2)	123.3(3)
N(1)-C(1)-C(4)	120.1(4)
C(2)-C(1)-C(4)	116.6(4)
C(1)-C(2)-C(3)	127.4(4)

N(2)-C(3)-C(2)	123.6(3)
N(2)-C(3)-C(5)	120.4(3)
C(2)-C(3)-C(5)	115.8(4)
C(7)-C(6)-C(11)	119.3(4)
C(7)-C(6)-N(1)	119.9(4)
C(11)-C(6)-N(1)	120.7(4)
C(6)-C(7)-C(8)	120.5(4)
C(9)-C(8)-C(7)	119.9(5)
C(10)-C(9)-C(8)	120.2(4)
C(9)-C(10)-C(11)	120.6(4)
C(6)-C(11)-C(10)	119.5(4)
C(13)-C(12)-C(17)	118.5(4)
C(13)-C(12)-N(2)	124.3(4)
C(17)-C(12)-N(2)	117.1(3)
C(14)-C(13)-C(12)	120.3(4)
C(15)-C(14)-C(13)	121.1(4)
C(14)-C(15)-C(16)	118.9(4)
C(15)-C(16)-C(17)	120.6(4)
C(16)-C(17)-C(12)	120.6(4)
N(3)-C(18)-C(19)	124.3(3)
N(3)-C(18)-C(21)	120.2(3)
C(19)-C(18)-C(21)	115.4(3)
C(18)-C(19)-C(20)	128.2(4)
N(4)-C(20)-C(19)	123.2(3)
N(4)-C(20)-C(22)	120.2(4)
C(19)-C(20)-C(22)	116.6(3)
C(28)-C(23)-C(24)	118.2(3)
C(28)-C(23)-N(3)	117.8(3)
C(24)-C(23)-N(3)	123.8(3)
C(25)-C(24)-C(23)	120.5(4)
C(26)-C(25)-C(24)	120.8(4)
C(25)-C(26)-C(27)	119.4(4)
C(26)-C(27)-C(28)	120.5(4)
C(27)-C(28)-C(23)	120.7(4)
C(34)-C(29)-C(30)	119.1(4)
C(34)-C(29)-N(4)	120.6(3)
C(30)-C(29)-N(4)	120.1(3)
C(31)-C(30)-C(29)	120.1(4)

C(32)-C(31)-C(30)	120.6(4)
C(31)-C(32)-C(33)	118.5(4)
C(34)-C(33)-C(32)	121.4(4)
C(29)-C(34)-C(33)	120.4(4)
C(40)-C(35)-C(36)	117.4(6)
C(40)-C(35)-C(41)	121.5(6)
C(36)-C(35)-C(41)	121.0(6)
C(37)-C(36)-C(35)	120.6(6)
C(36)-C(37)-C(38)	121.9(6)
C(37)-C(38)-C(39)	118.3(6)
C(40)-C(39)-C(38)	119.4(6)
C(35)-C(40)-C(39)	122.3(5)

Least-squares planes (x,y,z in crystal coordinates) and deviations from them
(* indicates atom used to define plane)

$$4.8518 (0.0188) x - 4.1994 (0.0211) y + 14.0689 (0.0203) z = 1.3671 (0.0062)$$

- * -0.0243 (0.0050) C35
- * -0.0230 (0.0043) C36
- * 0.0072 (0.0044) C37
- * 0.0198 (0.0051) C38
- * 0.0080 (0.0043) C39
- * -0.0242 (0.0044) C40
- * 0.0366 (0.0040) C41
- 3.5993 (0.0022) Pb

Rms deviation of fitted atoms = 0.0225

Table A20. Crystal data and structure refinement for [(BDI_{IPP})₂Pb] (**26**)

Identification code	may1010	
Empirical formula	C ₄₆ H ₅₈ N ₄ Pb	
Formula weight	874.15	
Temperature	173(2) K	
Wavelength	0.71073 Å	
Crystal system	Triclinic	
Space group	P $\bar{1}$ (No.2)	
Unit cell dimensions	a = 10.9335(3) Å	a = 85.690(2)°.
	b = 12.1290(2) Å	b = 73.900(1)°.
	c = 16.9989(4) Å	g = 74.641(1)°.
Volume	2088.50(8) Å ³	
Z	2	
Density (calculated)	1.39 Mg/m ³	
Absorption coefficient	4.07 mm ⁻¹	
F(000)	888	
Crystal size	0.20 x 0.14 x 0.12 mm ³	
Theta range for data collection	3.42 to 26.72°.	
Index ranges	-13 ≤ h ≤ 13, -15 ≤ k ≤ 15, -21 ≤ l ≤ 21	
Reflections collected	30694	
Independent reflections	8825 [R(int) = 0.051]	
Reflections with I > 2σ(I)	8166	
Completeness to theta = 26.72°	99.7 %	
Tmax. and Tmin.	0.5902 and 0.4721	
Refinement method	Full-matrix least-squares on F ²	
Data / restraints / parameters	8825 / 0 / 464	
Goodness-of-fit on F ²	1.210	
Final R indices [I > 2σ(I)]	R1 = 0.034, wR2 = 0.079	
R indices (all data)	R1 = 0.039, wR2 = 0.080	
Largest diff. peak and hole	1.12 and -1.49 e.Å ⁻³	

Data collection KappaCCD , Program package WinGX , Abs correction MULTISCAN

Refinement using SHELXL-97 , Drawing using ORTEP-3 for Windows

Table A21. Atomic coordinates ($\times 10^4$) and equivalent isotropic displacement parameters ($\text{\AA}^2 \times 10^3$) for $[(\text{BDI}_{\text{IPP}})_2\text{Pb}]$ (**26**). $U(\text{eq})$ is defined as one third of the trace of the orthogonalized U^{ij} tensor

	x	y	z	U(eq)
Pb	1423(1)	2228(1)	2590(1)	21(1)
N(1)	353(4)	2057(3)	1611(2)	23(1)
N(2)	1900(4)	170(3)	2371(2)	23(1)
N(3)	1161(4)	4245(3)	2184(2)	24(1)
N(4)	3366(4)	2203(3)	1554(2)	23(1)
C(1)	764(5)	1287(4)	1013(3)	25(1)
C(2)	1683(5)	233(4)	1008(3)	28(1)
C(3)	2088(4)	-347(4)	1678(3)	23(1)
C(4)	143(6)	1502(5)	308(3)	41(1)
C(5)	2680(5)	-1623(4)	1603(3)	30(1)
C(6)	-842(4)	2925(4)	1672(3)	24(1)
C(7)	-909(5)	3932(4)	1213(3)	25(1)
C(8)	-2093(5)	4772(4)	1336(3)	26(1)
C(9)	-3235(5)	4639(4)	1900(3)	26(1)
C(10)	-3153(5)	3639(4)	2358(3)	32(1)
C(11)	-1975(5)	2791(4)	2243(3)	30(1)
C(12)	-4523(5)	5532(4)	1997(3)	28(1)
C(13)	-5247(6)	5824(5)	2890(4)	42(1)
C(14)	-5390(5)	5149(5)	1569(4)	38(1)
C(15)	2168(5)	-450(4)	3078(3)	24(1)
C(16)	3421(5)	-820(4)	3171(3)	33(1)
C(17)	3644(5)	-1342(5)	3890(3)	36(1)
C(18)	2610(5)	-1516(4)	4541(3)	30(1)
C(19)	1359(5)	-1130(5)	4444(3)	35(1)
C(20)	1128(5)	-601(4)	3727(3)	31(1)
C(21)	2879(6)	-2129(5)	5315(3)	38(1)
C(22)	3581(7)	-1501(5)	5712(4)	48(2)
C(23)	3643(9)	-3355(5)	5153(4)	67(2)
C(24)	1592(4)	4615(4)	1439(3)	22(1)
C(25)	2586(5)	3937(4)	824(3)	26(1)
C(26)	3496(5)	2908(4)	907(3)	24(1)
C(27)	1039(5)	5847(4)	1199(3)	31(1)

C(28)	4746(5)	2633(4)	221(3)	35(1)
C(29)	396(4)	4992(4)	2846(3)	23(1)
C(30)	909(5)	5785(4)	3109(3)	33(1)
C(31)	236(6)	6409(4)	3819(3)	38(1)
C(32)	-969(5)	6263(4)	4296(3)	33(1)
C(33)	-1486(5)	5493(4)	4018(3)	35(1)
C(34)	-830(5)	4869(4)	3302(3)	30(1)
C(35)	-1632(6)	6957(5)	5086(4)	44(1)
C(36)	-2214(7)	8191(5)	4905(4)	56(2)
C(37)	-2650(7)	6446(6)	5684(4)	52(2)
C(38)	4472(4)	1298(4)	1625(3)	23(1)
C(39)	5095(5)	1374(4)	2217(3)	34(1)
C(40)	6170(5)	507(4)	2312(3)	36(1)
C(41)	6667(5)	-449(4)	1818(3)	27(1)
C(42)	6018(5)	-527(4)	1235(3)	26(1)
C(43)	4943(5)	318(4)	1139(3)	25(1)
C(44)	7803(5)	-1421(4)	1944(3)	32(1)
C(45)	8870(6)	-1024(5)	2155(5)	58(2)
C(46)	7301(6)	-2251(5)	2590(4)	51(2)

Table A22. Bond lengths [Å] and angles [deg] for [(BDI_{IPP})₂Pb] (**26**)

Pb-N(1)	2.333(4)
Pb-N(4)	2.348(4)
Pb-N(2)	2.446(4)
Pb-N(3)	2.456(4)
N(1)-C(1)	1.333(6)
N(1)-C(6)	1.427(6)
N(2)-C(3)	1.316(6)
N(2)-C(15)	1.427(6)
N(3)-C(24)	1.312(6)
N(3)-C(29)	1.420(6)
N(4)-C(26)	1.341(6)
N(4)-C(38)	1.428(5)
C(1)-C(2)	1.400(7)
C(1)-C(4)	1.509(7)
C(2)-C(3)	1.408(7)
C(3)-C(5)	1.511(6)
C(6)-C(11)	1.386(7)
C(6)-C(7)	1.395(6)
C(7)-C(8)	1.393(6)
C(8)-C(9)	1.387(7)
C(9)-C(10)	1.388(7)
C(9)-C(12)	1.508(6)
C(10)-C(11)	1.394(7)
C(12)-C(14)	1.519(7)
C(12)-C(13)	1.523(7)
C(15)-C(16)	1.374(7)
C(15)-C(20)	1.388(7)
C(16)-C(17)	1.387(7)
C(17)-C(18)	1.394(7)
C(18)-C(19)	1.375(7)
C(18)-C(21)	1.525(7)
C(19)-C(20)	1.387(7)
C(21)-C(23)	1.504(9)
C(21)-C(22)	1.516(8)
C(24)-C(25)	1.406(6)
C(24)-C(27)	1.528(6)

C(25)-C(26)	1.400(6)
C(26)-C(28)	1.507(6)
C(29)-C(30)	1.388(7)
C(29)-C(34)	1.391(7)
C(30)-C(31)	1.387(7)
C(31)-C(32)	1.391(8)
C(32)-C(33)	1.382(7)
C(32)-C(35)	1.532(7)
C(33)-C(34)	1.391(7)
C(35)-C(36)	1.508(8)
C(35)-C(37)	1.516(9)
C(38)-C(39)	1.383(7)
C(38)-C(43)	1.395(6)
C(39)-C(40)	1.393(7)
C(40)-C(41)	1.381(7)
C(41)-C(42)	1.390(7)
C(41)-C(44)	1.521(6)
C(42)-C(43)	1.379(6)
C(44)-C(45)	1.508(8)
C(44)-C(46)	1.521(8)
N(1)-Pb-N(4)	90.33(13)
N(1)-Pb-N(2)	75.10(13)
N(4)-Pb-N(2)	87.13(13)
N(1)-Pb-N(3)	87.03(13)
N(4)-Pb-N(3)	76.71(13)
N(2)-Pb-N(3)	155.86(12)
C(1)-N(1)-C(6)	119.4(4)
C(1)-N(1)-Pb	127.2(3)
C(6)-N(1)-Pb	113.3(3)
C(3)-N(2)-C(15)	121.8(4)
C(3)-N(2)-Pb	127.0(3)
C(15)-N(2)-Pb	110.5(3)
C(24)-N(3)-C(29)	122.7(4)
C(24)-N(3)-Pb	125.3(3)
C(29)-N(3)-Pb	111.9(3)
C(26)-N(4)-C(38)	119.1(4)
C(26)-N(4)-Pb	126.4(3)

C(38)-N(4)-Pb	114.4(3)
N(1)-C(1)-C(2)	124.9(4)
N(1)-C(1)-C(4)	119.0(4)
C(2)-C(1)-C(4)	115.9(4)
C(1)-C(2)-C(3)	127.7(4)
N(2)-C(3)-C(2)	122.4(4)
N(2)-C(3)-C(5)	119.8(4)
C(2)-C(3)-C(5)	117.7(4)
C(11)-C(6)-C(7)	118.3(4)
C(11)-C(6)-N(1)	118.6(4)
C(7)-C(6)-N(1)	123.0(4)
C(8)-C(7)-C(6)	120.0(4)
C(9)-C(8)-C(7)	122.1(4)
C(8)-C(9)-C(10)	117.3(4)
C(8)-C(9)-C(12)	121.4(4)
C(10)-C(9)-C(12)	121.3(4)
C(9)-C(10)-C(11)	121.3(5)
C(6)-C(11)-C(10)	121.0(4)
C(9)-C(12)-C(14)	110.2(4)
C(9)-C(12)-C(13)	112.7(4)
C(14)-C(12)-C(13)	110.8(4)
C(16)-C(15)-C(20)	118.2(4)
C(16)-C(15)-N(2)	122.0(4)
C(20)-C(15)-N(2)	119.5(4)
C(15)-C(16)-C(17)	120.9(5)
C(16)-C(17)-C(18)	121.4(5)
C(19)-C(18)-C(17)	117.2(4)
C(19)-C(18)-C(21)	122.3(5)
C(17)-C(18)-C(21)	120.6(5)
C(18)-C(19)-C(20)	121.8(5)
C(19)-C(20)-C(15)	120.6(5)
C(23)-C(21)-C(22)	110.7(5)
C(23)-C(21)-C(18)	112.0(5)
C(22)-C(21)-C(18)	111.0(5)
N(3)-C(24)-C(25)	123.5(4)
N(3)-C(24)-C(27)	120.6(4)
C(25)-C(24)-C(27)	115.9(4)
C(26)-C(25)-C(24)	128.6(4)

N(4)-C(26)-C(25)	125.4(4)
N(4)-C(26)-C(28)	118.9(4)
C(25)-C(26)-C(28)	115.6(4)
C(30)-C(29)-C(34)	118.0(4)
C(30)-C(29)-N(3)	120.8(4)
C(34)-C(29)-N(3)	120.8(4)
C(31)-C(30)-C(29)	121.0(5)
C(30)-C(31)-C(32)	121.4(5)
C(33)-C(32)-C(31)	117.1(5)
C(33)-C(32)-C(35)	124.5(5)
C(31)-C(32)-C(35)	118.4(5)
C(32)-C(33)-C(34)	122.1(5)
C(29)-C(34)-C(33)	120.3(5)
C(36)-C(35)-C(37)	111.1(5)
C(36)-C(35)-C(32)	111.1(5)
C(37)-C(35)-C(32)	112.9(5)
C(39)-C(38)-C(43)	117.8(4)
C(39)-C(38)-N(4)	118.9(4)
C(43)-C(38)-N(4)	123.3(4)
C(38)-C(39)-C(40)	120.8(4)
C(41)-C(40)-C(39)	121.8(5)
C(40)-C(41)-C(42)	116.9(4)
C(40)-C(41)-C(44)	121.8(4)
C(42)-C(41)-C(44)	121.1(4)
C(43)-C(42)-C(41)	122.0(4)
C(42)-C(43)-C(38)	120.7(4)
C(45)-C(44)-C(41)	113.7(4)
C(45)-C(44)-C(46)	110.4(5)
C(41)-C(44)-C(46)	110.6(4)

Table A23. Crystal data and structure refinement for [(BDI_{DMP})PbO^tBu] (**28**)

Identification code	aug1011	
Empirical formula	C ₂₅ H ₃₄ N ₂ O Pb	
Formula weight	585.73	
Temperature	173(2) K	
Wavelength	0.71073 Å	
Crystal system	Triclinic	
Space group	P $\bar{1}$ (No.2)	
Unit cell dimensions	a = 12.0429(4) Å	a = 70.951(2)°.
	b = 12.2155(4) Å	b = 73.482(2)°.
	c = 18.6440(5) Å	g = 88.626(1)°.
Volume	2478.36(13) Å ³	
Z	4	
Density (calculated)	1.57 Mg/m ³	
Absorption coefficient	6.824 mm ⁻¹	
F(000)	1152	
Crystal size	0.20 x 0.18 x 0.13 mm ³	
Theta range for data collection	3.44 to 26.76°.	
Index ranges	-14 ≤ h ≤ 15, -15 ≤ k ≤ 15, -18 ≤ l ≤ 23	
Reflections collected	30981	
Independent reflections	10379 [R(int) = 0.057]	
Reflections with I > 2σ(I)	8521	
Completeness to theta = 26.76°	98.2 %	
Absorption correction	Semi-empirical from equivalents	
Tmax. and Tmin.	0.3561 and 0.2814	
Refinement method	Full-matrix least-squares on F ²	
Data / restraints / parameters	10379 / 0 / 535	
Goodness-of-fit on F ²	1.000	
Final R indices [I > 2σ(I)]	R1 = 0.030, wR2 = 0.067	
R indices (all data)	R1 = 0.042, wR2 = 0.072	
Largest diff. peak and hole	0.73 and -1.62 e.Å ⁻³	

There are two essentially equivalent molecules in the unit cell

Data collection KappaCCD , Program package WinGX , Abs correction MULTISCAN

Refinement using SHELXL-97 , Drawing using ORTEP-3 for Windows

Table A24. Atomic coordinates ($\times 10^4$) and equivalent isotropic displacement parameters ($\text{\AA}^2 \times 10^3$) for $[(\text{BDI}_{\text{DMP}})\text{PbO}^t\text{Bu}]$ (**28**). $U(\text{eq})$ is defined as one third of the trace of the orthogonalized U^{ij} tensor

	x	y	z	$U(\text{eq})$
Pb(1)	6041(1)	8031(1)	2478(1)	25(1)
Pb(2)	1241(1)	4385(1)	2536(1)	24(1)
O(1)	5098(2)	8424(2)	3522(2)	29(1)
O(2)	1203(3)	4314(3)	1408(2)	33(1)
N(1)	5854(3)	9826(3)	1611(2)	26(1)
N(2)	4334(3)	7589(3)	2251(2)	25(1)
N(3)	265(3)	2576(3)	3176(2)	25(1)
N(4)	-648(3)	4930(3)	2834(2)	24(1)
C(1)	5045(4)	10156(3)	1242(2)	26(1)
C(2)	4083(4)	9446(4)	1344(2)	28(1)
C(3)	3754(4)	8271(4)	1796(2)	28(1)
C(4)	5147(4)	11380(4)	672(3)	38(1)
C(5)	2645(4)	7794(4)	1748(3)	40(1)
C(6)	6874(4)	10588(4)	1408(3)	35(1)
C(7)	6916(5)	11290(4)	1859(3)	43(1)
C(8)	7960(6)	11952(5)	1662(4)	57(2)
C(9)	8898(5)	11908(5)	1057(4)	64(2)
C(10)	8839(5)	11201(5)	621(3)	56(2)
C(11)	7829(4)	10523(4)	787(3)	40(1)
C(12)	5865(5)	11359(4)	2511(3)	55(2)
C(13)	7771(5)	9775(5)	301(3)	52(1)
C(14)	3993(4)	6383(3)	2667(2)	26(1)
C(15)	3211(4)	6021(4)	3443(3)	31(1)
C(16)	3031(4)	4834(4)	3857(3)	41(1)
C(17)	3571(5)	4031(4)	3532(3)	46(1)
C(18)	4303(4)	4394(4)	2768(3)	43(1)
C(19)	4530(4)	5575(4)	2326(3)	33(1)
C(20)	2610(4)	6901(4)	3797(3)	41(1)
C(21)	5337(5)	5968(5)	1487(3)	47(1)
C(22)	5401(4)	7974(4)	4244(3)	34(1)
C(23)	6637(5)	8332(8)	4122(4)	94(3)
C(24)	4581(6)	8444(5)	4845(3)	64(2)

C(25)	5189(6)	6645(5)	4570(3)	63(2)
C(26)	-863(4)	2276(3)	3397(3)	30(1)
C(27)	-1726(4)	3067(4)	3337(3)	32(1)
C(28)	-1634(4)	4277(4)	3116(2)	28(1)
C(29)	-1280(5)	1007(4)	3744(3)	47(1)
C(30)	-2774(4)	4851(4)	3247(3)	46(1)
C(31)	1076(4)	1713(3)	3332(2)	27(1)
C(32)	1565(4)	1173(4)	2780(3)	34(1)
C(33)	2416(4)	412(4)	2919(3)	44(1)
C(34)	2780(5)	206(4)	3585(3)	46(1)
C(35)	2295(4)	749(4)	4129(3)	40(1)
C(36)	1417(4)	1501(4)	4020(3)	31(1)
C(37)	1174(5)	1381(4)	2044(3)	46(1)
C(38)	845(4)	2046(4)	4629(3)	40(1)
C(39)	-644(3)	6157(3)	2666(2)	25(1)
C(40)	-704(4)	6881(4)	1921(3)	30(1)
C(41)	-633(4)	8077(4)	1770(3)	41(1)
C(42)	-499(4)	8539(4)	2319(4)	50(1)
C(43)	-423(4)	7812(4)	3048(3)	45(1)
C(44)	-495(4)	6611(4)	3238(3)	34(1)
C(45)	-874(4)	6392(4)	1314(3)	41(1)
C(46)	-419(5)	5811(5)	4032(3)	49(1)
C(47)	2165(4)	4688(4)	713(3)	39(1)
C(48)	1804(6)	4396(7)	81(3)	88(3)
C(49)	3227(5)	4034(6)	847(4)	69(2)
C(50)	2475(7)	5972(5)	456(4)	81(2)

Table A25. Bond lengths [Å] and angles [deg] for [(BDI_{DMP})PbO^tBu] (**28**)

Pb(1)-O(1)	2.154(3)
Pb(1)-N(1)	2.311(3)
Pb(1)-N(2)	2.322(3)
Pb(2)-O(2)	2.146(3)
Pb(2)-N(3)	2.301(3)
Pb(2)-N(4)	2.318(3)
O(1)-C(22)	1.426(5)
O(2)-C(47)	1.419(5)
N(1)-C(1)	1.329(5)
N(1)-C(6)	1.441(5)
N(2)-C(3)	1.323(5)
N(2)-C(14)	1.429(5)
N(3)-C(26)	1.326(5)
N(3)-C(31)	1.436(5)
N(4)-C(28)	1.318(5)
N(4)-C(39)	1.428(5)
C(1)-C(2)	1.396(6)
C(1)-C(4)	1.509(6)
C(2)-C(3)	1.404(6)
C(3)-C(5)	1.506(6)
C(6)-C(7)	1.395(7)
C(6)-C(11)	1.402(7)
C(7)-C(8)	1.400(7)
C(7)-C(12)	1.508(8)
C(8)-C(9)	1.366(9)
C(9)-C(10)	1.381(9)
C(10)-C(11)	1.388(7)
C(11)-C(13)	1.497(8)
C(14)-C(19)	1.394(6)
C(14)-C(15)	1.415(6)
C(15)-C(16)	1.391(6)
C(15)-C(20)	1.506(6)
C(16)-C(17)	1.373(7)
C(17)-C(18)	1.376(7)
C(18)-C(19)	1.397(6)
C(19)-C(21)	1.512(7)
C(22)-C(23)	1.494(7)
C(22)-C(24)	1.525(7)

C(22)-C(25)	1.535(7)
C(26)-C(27)	1.405(6)
C(26)-C(29)	1.508(6)
C(27)-C(28)	1.397(6)
C(28)-C(30)	1.520(6)
C(31)-C(32)	1.387(6)
C(31)-C(36)	1.399(6)
C(32)-C(33)	1.389(6)
C(32)-C(37)	1.517(7)
C(33)-C(34)	1.377(7)
C(34)-C(35)	1.376(7)
C(35)-C(36)	1.399(6)
C(36)-C(38)	1.495(6)
C(39)-C(40)	1.402(6)
C(39)-C(44)	1.407(6)
C(40)-C(41)	1.395(6)
C(40)-C(45)	1.502(6)
C(41)-C(42)	1.367(7)
C(42)-C(43)	1.387(8)
C(43)-C(44)	1.390(6)
C(44)-C(46)	1.511(7)
C(47)-C(50)	1.505(8)
C(47)-C(48)	1.509(7)
C(47)-C(49)	1.530(8)
O(1)-Pb(1)-N(1)	94.17(11)
O(1)-Pb(1)-N(2)	91.92(11)
N(1)-Pb(1)-N(2)	81.32(11)
O(2)-Pb(2)-N(3)	91.06(12)
O(2)-Pb(2)-N(4)	92.79(11)
N(3)-Pb(2)-N(4)	80.63(11)
C(22)-O(1)-Pb(1)	121.2(2)
C(47)-O(2)-Pb(2)	123.4(3)
C(1)-N(1)-C(6)	120.2(3)
C(1)-N(1)-Pb(1)	129.4(3)
C(6)-N(1)-Pb(1)	109.9(2)
C(3)-N(2)-C(14)	122.6(3)
C(3)-N(2)-Pb(1)	128.8(3)
C(14)-N(2)-Pb(1)	108.5(2)
C(26)-N(3)-C(31)	120.6(3)

C(26)-N(3)-Pb(2)	129.5(3)
C(31)-N(3)-Pb(2)	109.9(2)
C(28)-N(4)-C(39)	120.8(3)
C(28)-N(4)-Pb(2)	129.1(3)
C(39)-N(4)-Pb(2)	110.1(2)
N(1)-C(1)-C(2)	124.5(4)
N(1)-C(1)-C(4)	119.1(4)
C(2)-C(1)-C(4)	116.3(4)
C(1)-C(2)-C(3)	131.0(4)
N(2)-C(3)-C(2)	124.9(4)
N(2)-C(3)-C(5)	119.5(4)
C(2)-C(3)-C(5)	115.6(4)
C(7)-C(6)-C(11)	122.4(4)
C(7)-C(6)-N(1)	120.0(4)
C(11)-C(6)-N(1)	117.4(4)
C(6)-C(7)-C(8)	117.1(5)
C(6)-C(7)-C(12)	121.0(4)
C(8)-C(7)-C(12)	121.9(5)
C(9)-C(8)-C(7)	121.5(6)
C(8)-C(9)-C(10)	120.3(5)
C(9)-C(10)-C(11)	120.9(6)
C(10)-C(11)-C(6)	117.7(5)
C(10)-C(11)-C(13)	120.3(5)
C(6)-C(11)-C(13)	121.9(4)
C(19)-C(14)-C(15)	121.0(4)
C(19)-C(14)-N(2)	118.6(4)
C(15)-C(14)-N(2)	120.1(4)
C(16)-C(15)-C(14)	117.3(4)
C(16)-C(15)-C(20)	122.1(4)
C(14)-C(15)-C(20)	120.5(4)
C(17)-C(16)-C(15)	122.2(5)
C(16)-C(17)-C(18)	119.8(5)
C(17)-C(18)-C(19)	120.7(5)
C(14)-C(19)-C(18)	118.9(4)
C(14)-C(19)-C(21)	120.7(4)
C(18)-C(19)-C(21)	120.4(4)
O(1)-C(22)-C(23)	110.9(4)
O(1)-C(22)-C(24)	107.1(4)
C(23)-C(22)-C(24)	110.7(5)
O(1)-C(22)-C(25)	110.1(4)

C(23)-C(22)-C(25)	110.6(5)
C(24)-C(22)-C(25)	107.3(4)
N(3)-C(26)-C(27)	124.5(4)
N(3)-C(26)-C(29)	119.3(4)
C(27)-C(26)-C(29)	116.2(4)
C(28)-C(27)-C(26)	129.8(4)
N(4)-C(28)-C(27)	125.0(4)
N(4)-C(28)-C(30)	119.1(4)
C(27)-C(28)-C(30)	115.9(4)
C(32)-C(31)-C(36)	121.4(4)
C(32)-C(31)-N(3)	120.0(4)
C(36)-C(31)-N(3)	118.4(4)
C(31)-C(32)-C(33)	118.5(4)
C(31)-C(32)-C(37)	121.4(4)
C(33)-C(32)-C(37)	120.1(4)
C(34)-C(33)-C(32)	121.1(5)
C(35)-C(34)-C(33)	120.2(5)
C(34)-C(35)-C(36)	120.5(5)
C(31)-C(36)-C(35)	118.3(4)
C(31)-C(36)-C(38)	121.0(4)
C(35)-C(36)-C(38)	120.7(4)
C(40)-C(39)-C(44)	121.7(4)
C(40)-C(39)-N(4)	119.8(4)
C(44)-C(39)-N(4)	118.4(4)
C(41)-C(40)-C(39)	117.6(4)
C(41)-C(40)-C(45)	120.9(4)
C(39)-C(40)-C(45)	121.6(4)
C(42)-C(41)-C(40)	121.8(5)
C(41)-C(42)-C(43)	119.9(4)
C(42)-C(43)-C(44)	121.2(5)
C(43)-C(44)-C(39)	117.8(4)
C(43)-C(44)-C(46)	121.6(4)
C(39)-C(44)-C(46)	120.6(4)
O(2)-C(47)-C(50)	111.7(4)
O(2)-C(47)-C(48)	106.0(4)
C(50)-C(47)-C(48)	110.3(5)
O(2)-C(47)-C(49)	110.8(4)
C(50)-C(47)-C(49)	109.0(5)
C(48)-C(47)-C(49)	108.9(5)

Table A26. Crystal data and structure refinement for [(BDI_{DMP})PbOTf] (**29**)

Identification code	jul811	
Empirical formula	C ₂₂ H ₂₅ F ₃ N ₂ O ₃ Pb S	
Formula weight	661.69	
Temperature	173(2) K	
Wavelength	0.71073 Å	
Crystal system	Monoclinic	
Space group	<i>P</i> 2 ₁ /c (No.14)	
Unit cell dimensions	a = 11.4124(2) Å	a = 90°.
	b = 11.5990(3) Å	b = 117.144(2)°.
	c = 20.5159(6) Å	g = 90°.
Volume	2416.63(10) Å ³	
Z	4	
Density (calculated)	1.82 Mg/m ³	
Absorption coefficient	7.116 mm ⁻¹	
F(000)	1280	
Crystal size	0.15 x 0.13 x 0.13 mm ³	
Theta range for data collection	3.49 to 26.72°.	
Index ranges	-14 ≤ h ≤ 12, -14 ≤ k ≤ 14, -24 ≤ l ≤ 25	
Reflections collected	25271	
Independent reflections	5100 [R(int) = 0.056]	
Reflections with I > 2σ(I)	4472	
Completeness to theta = 26.72°	99.3 %	
Absorption correction	Semi-empirical from equivalents	
Tmax. and Tmin.	0.4234 and 0.3459	
Refinement method	Full-matrix least-squares on F ²	
Data / restraints / parameters	5100 / 0 / 295	
Goodness-of-fit on F ²	1.046	
Final R indices [I > 2σ(I)]	R1 = 0.028, wR2 = 0.053	
R indices (all data)	R1 = 0.031, wR2 = 0.055	
Largest diff. peak and hole	0.54 and -1.05 e.Å ⁻³	

Forms a polymer through bridging [OTf] anions

Data collection KappaCCD , Program package WinGX , Abs correction MULTISCAN

Refinement using SHELXL-97 , Drawing using ORTEP-3 for Windows

Table A27. Atomic coordinates ($\times 10^4$) and equivalent isotropic displacement parameters ($\text{\AA}^2 \times 10^3$) for [(BDI_{DMP})PbOTf] (**29**). U(eq) is defined as one third of the trace of the orthogonalized U^{ij} tensor

	x	y	z	U(eq)
Pb	5641(1)	1118(1)	2171(1)	23(1)
S	3054(1)	-899(1)	1604(1)	30(1)
F(1)	2076(3)	-2065(2)	383(2)	73(1)
F(2)	674(3)	-1599(3)	768(2)	78(1)
F(3)	1370(2)	-352(2)	262(1)	49(1)
O(1)	4111(3)	-560(2)	1431(2)	40(1)
O(2)	3276(3)	-1971(2)	1989(2)	48(1)
O(3)	2554(3)	25(2)	1866(2)	46(1)
N(1)	5303(3)	2066(2)	1135(2)	25(1)
N(2)	7286(3)	252(2)	2009(2)	23(1)
C(1)	5634(4)	1676(3)	629(2)	30(1)
C(2)	6521(4)	780(3)	735(2)	35(1)
C(3)	7377(4)	220(3)	1386(2)	29(1)
C(4)	5066(4)	2273(4)	-106(2)	40(1)
C(5)	8513(4)	-434(4)	1372(2)	45(1)
C(6)	4657(4)	3170(3)	1041(2)	25(1)
C(7)	3311(4)	3222(3)	803(2)	30(1)
C(8)	2727(4)	4298(4)	758(2)	36(1)
C(9)	3487(5)	5291(4)	953(2)	41(1)
C(10)	4811(5)	5213(3)	1181(2)	40(1)
C(11)	5438(4)	4171(3)	1231(2)	32(1)
C(12)	2475(4)	2144(4)	577(2)	40(1)
C(13)	6893(4)	4123(4)	1463(3)	46(1)
C(14)	8311(3)	-248(3)	2660(2)	25(1)
C(15)	8227(4)	-1418(3)	2819(2)	34(1)
C(16)	9242(4)	-1872(4)	3450(2)	47(1)
C(17)	10279(4)	-1206(5)	3923(2)	53(1)
C(18)	10335(4)	-57(5)	3764(2)	46(1)
C(19)	9371(4)	438(4)	3126(2)	34(1)
C(20)	7083(5)	-2153(4)	2329(3)	54(1)
C(21)	9491(4)	1674(4)	2934(3)	49(1)
C(22)	1717(4)	-1242(3)	712(2)	39(1)

Table A28. Bond lengths [Å] and angles [deg] for [(BDI_{DMP})PbOTf] (**29**)

Pb-N(1)	2.266(3)
Pb-N(2)	2.282(3)
Pb-O(1)	2.593(3)
Pb-O(2)'	2.733(3)
S-O(3)	1.430(3)
S-O(2)	1.432(3)
S-O(1)	1.458(3)
S-C(22)	1.813(4)
F(1)-C(22)	1.337(5)
F(2)-C(22)	1.313(5)
F(3)-C(22)	1.319(4)
O(2)-Pb''	2.733(3)
N(1)-C(1)	1.335(4)
N(1)-C(6)	1.446(4)
N(2)-C(3)	1.330(4)
N(2)-C(14)	1.436(4)
C(1)-C(2)	1.397(5)
C(1)-C(4)	1.510(5)
C(2)-C(3)	1.403(5)
C(3)-C(5)	1.514(5)
C(6)-C(7)	1.385(5)
C(6)-C(11)	1.406(5)
C(7)-C(8)	1.398(5)
C(7)-C(12)	1.511(5)
C(8)-C(9)	1.387(6)
C(9)-C(10)	1.365(6)
C(10)-C(11)	1.384(5)
C(11)-C(13)	1.506(6)
C(14)-C(19)	1.398(5)
C(14)-C(15)	1.409(5)
C(15)-C(16)	1.389(5)
C(15)-C(20)	1.498(6)
C(16)-C(17)	1.374(7)
C(17)-C(18)	1.380(7)
C(18)-C(19)	1.392(5)
C(19)-C(21)	1.511(6)

N(1)-Pb-N(2)	82.88(10)
N(1)-Pb-O(1)	91.94(10)
N(2)-Pb-O(1)	87.90(9)
N(1)-Pb-O(2)'	91.86(10)
N(2)-Pb-O(2)'	106.45(10)
O(1)-Pb-O(2)'	165.50(9)
O(3)-S-O(2)	116.34(19)
O(3)-S-O(1)	113.94(18)
O(2)-S-O(1)	114.25(18)
O(3)-S-C(22)	104.30(19)
O(2)-S-C(22)	102.82(18)
O(1)-S-C(22)	102.88(18)
S-O(1)-Pb	118.10(15)
S-O(2)-Pb''	165.28(19)
C(1)-N(1)-C(6)	120.3(3)
C(1)-N(1)-Pb	125.3(2)
C(6)-N(1)-Pb	114.4(2)
C(3)-N(2)-C(14)	119.6(3)
C(3)-N(2)-Pb	125.6(2)
C(14)-N(2)-Pb	114.72(19)
N(1)-C(1)-C(2)	124.9(3)
N(1)-C(1)-C(4)	118.4(3)
C(2)-C(1)-C(4)	116.6(3)
C(1)-C(2)-C(3)	129.3(3)
N(2)-C(3)-C(2)	125.2(3)
N(2)-C(3)-C(5)	118.4(3)
C(2)-C(3)-C(5)	116.4(3)
C(7)-C(6)-C(11)	121.5(3)
C(7)-C(6)-N(1)	120.1(3)
C(11)-C(6)-N(1)	118.3(3)
C(6)-C(7)-C(8)	118.7(4)
C(6)-C(7)-C(12)	121.1(3)
C(8)-C(7)-C(12)	120.2(4)
C(9)-C(8)-C(7)	120.4(4)
C(10)-C(9)-C(8)	119.5(4)
C(9)-C(10)-C(11)	122.5(4)
C(10)-C(11)-C(6)	117.4(4)

C(10)-C(11)-C(13)	121.0(4)
C(6)-C(11)-C(13)	121.6(3)
C(19)-C(14)-C(15)	121.2(3)
C(19)-C(14)-N(2)	119.3(3)
C(15)-C(14)-N(2)	119.4(3)
C(16)-C(15)-C(14)	117.7(4)
C(16)-C(15)-C(20)	120.7(4)
C(14)-C(15)-C(20)	121.6(3)
C(17)-C(16)-C(15)	121.9(4)
C(16)-C(17)-C(18)	119.6(4)
C(17)-C(18)-C(19)	121.2(4)
C(18)-C(19)-C(14)	118.3(4)
C(18)-C(19)-C(21)	120.7(4)
C(14)-C(19)-C(21)	121.0(3)
F(2)-C(22)-F(3)	108.3(3)
F(2)-C(22)-F(1)	108.5(4)
F(3)-C(22)-F(1)	105.5(4)
F(2)-C(22)-S	111.1(3)
F(3)-C(22)-S	112.4(3)
F(1)-C(22)-S	110.8(3)

Symmetry transformations used to generate equivalent atoms:

' $-x+1, y+1/2, -z+1/2$ " $-x+1, y-1/2, -z+1/2$

Table A29. Crystal data and structure refinement for [(BDI_{IP})Pb] (**30**)

Identification code	jun110	
Empirical formula	C ₂₃ H ₂₉ I N ₂ Pb, C ₆ D ₆	
Formula weight	745.69	
Temperature	173(2) K	
Wavelength	0.71073 Å	
Crystal system	Monoclinic	
Space group	<i>C</i> 2/ <i>c</i>	
Unit cell dimensions	a = 28.2581(5) Å	a = 90°.
	b = 9.9106(2) Å	b = 90.889(1)°.
	c = 20.1416(3) Å	g = 90°.
Volume	5640.07(17) Å ³	
Z	8	
Density (calculated)	1.76 Mg/m ³	
Absorption coefficient	7.10 mm ⁻¹	
F(000)	2864	
Crystal size	0.22 x 0.06 x 0.04 mm ³	
Theta range for data collection	3.50 to 27.10°.	
Index ranges	-36 ≤ h ≤ 36, -12 ≤ k ≤ 12, -25 ≤ l ≤ 25	
Reflections collected	44103	
Independent reflections	6196 [R(int) = 0.074]	
Completeness to theta = 27.10°	99.6 %	
Tmax and Tmin	0.5927 and 0.3716	
Refinement method	Full-matrix least-squares on F ²	
Data / restraints / parameters	6196 / 78 / 328	
Goodness-of-fit on F ²	1.084	
Final R indices [I > 2σ(I)]	R1 = 0.031, wR2 = 0.056	
R indices (all data)	R1 = 0.045, wR2 = 0.059	
Largest diff. peak and hole	0.72 and -0.87 e.Å ⁻³	

There are two 1/2-molecules of benzene solvate located at special positions; one of the ⁱPr groups is disordered and was refined over two positions.

Data collection KappaCCD , Program package WinGX , Abs correction MULTISCAN
Refinement using SHELXL-97 , Drawing using ORTEP-3 for Windows

Table A30. Atomic coordinates ($\times 10^4$) and equivalent isotropic displacement parameters ($\text{\AA}^2 \times 10^3$) for [(BDI_{IPP})Pb] (**30**). U(eq) is defined as one third of the trace of the orthogonalized U^{ij} tensor

	x	y	z	U(eq)
Pb	2434(1)	9690(1)	2497(1)	31(1)
I	3121(1)	7535(1)	1832(1)	45(1)
N(1)	1778(1)	8439(4)	2243(2)	31(1)
N(2)	2444(1)	8405(3)	3432(2)	31(1)
C(1)	1627(1)	7339(4)	2548(2)	29(1)
C(2)	1807(1)	6853(4)	3156(2)	29(1)
C(3)	2175(1)	7339(4)	3574(2)	28(1)
C(4)	1250(1)	6484(5)	2218(2)	41(1)
C(5)	2265(2)	6564(5)	4202(2)	37(1)
C(6)	1558(1)	8892(4)	1638(2)	30(1)
C(7)	1790(1)	8765(4)	1043(2)	36(1)
C(8)	1586(1)	9243(4)	455(2)	35(1)
C(9)	1144(1)	9861(4)	451(2)	31(1)
C(10)	921(2)	10000(5)	1053(2)	42(1)
C(11)	1123(1)	9533(5)	1640(2)	42(1)
C(12)	900(2)	10340(5)	-186(2)	41(1)
C(13)	1238(2)	10833(6)	-707(2)	58(1)
C(14)	576(2)	9249(6)	-458(3)	82(2)
C(15)	2834(1)	8799(4)	3856(2)	35(1)
C(16)	3252(2)	8074(5)	3868(2)	45(1)
C(17)	3637(2)	8595(7)	4243(3)	59(2)
C(18)	3605(2)	9811(6)	4593(2)	56(2)
C(19)	3189(2)	10486(5)	4562(2)	55(1)
C(20)	2808(2)	10015(4)	4201(2)	42(1)
C(21)	4003(3)	10477(8)	5001(4)	38(2) ^a
C(22)	4212(4)	9509(10)	5517(5)	53(3) ^a
C(23)	4378(7)	10929(18)	4516(11)	61(5) ^a
C(21A)	4174(7)	9850(20)	4851(7)	34(5) ^b
C(22A)	4089(8)	10130(30)	5580(9)	39(5) ^b
C(23A)	4419(14)	11050(30)	4530(20)	36(8) ^b
C(1S)	59(2)	6588(5)	2829(3)	61(2)
C(2S)	125(2)	7774(6)	3158(3)	55(1)
C(3S)	63(2)	8971(5)	2829(2)	49(1)
C(4S)	388(2)	12834(5)	2917(3)	58(1)
C(5S)	449(2)	12830(5)	2246(3)	56(1)
C(6S)	63(2)	12830(5)	1822(3)	58(1)

^a = 72.3 %, ^b = 27.7 %

Table A31. Bond lengths [Å] and angles [deg] for [(BDI_{IPP})Pb] (**30**)

Pb-N(2)	2.275(3)
Pb-N(1)	2.284(3)
Pb-I	3.1928(3)
Pb-I'	3.5079(4)
N(1)-C(1)	1.324(5)
N(1)-C(6)	1.431(5)
N(2)-C(3)	1.335(5)
N(2)-C(15)	1.437(5)
C(1)-C(2)	1.404(6)
C(1)-C(4)	1.507(5)
C(2)-C(3)	1.411(5)
C(3)-C(5)	1.499(6)
C(6)-C(7)	1.382(5)
C(6)-C(11)	1.383(5)
C(7)-C(8)	1.393(6)
C(8)-C(9)	1.390(6)
C(9)-C(10)	1.382(6)
C(9)-C(12)	1.522(6)
C(10)-C(11)	1.386(6)
C(12)-C(13)	1.511(6)
C(12)-C(14)	1.515(7)
C(15)-C(16)	1.382(6)
C(15)-C(20)	1.394(6)
C(16)-C(17)	1.414(7)
C(17)-C(18)	1.399(8)
C(18)-C(19)	1.355(8)
C(18)-C(21)	1.530(8)
C(19)-C(20)	1.372(6)
C(21)-C(23)	1.520(11)
C(21)-C(22)	1.527(9)
I-Pb-I'	167.809(9)
N(2)-Pb-N(1)	83.11(11)
N(2)-Pb-I	88.47(8)
N(1)-Pb-I	92.28(8)
N(2)-Pb-I'	97.49(8)
N(1)-Pb-I'	98.97(9)
C(1)-N(1)-C(6)	121.0(3)
C(1)-N(1)-Pb	127.5(3)
C(6)-N(1)-Pb	111.1(2)

C(3)-N(2)-C(15)	121.5(3)
C(3)-N(2)-Pb	128.3(3)
C(15)-N(2)-Pb	109.8(2)
N(1)-C(1)-C(2)	124.9(4)
N(1)-C(1)-C(4)	119.3(4)
C(2)-C(1)-C(4)	115.8(4)
C(1)-C(2)-C(3)	131.0(4)
N(2)-C(3)-C(2)	124.0(4)
N(2)-C(3)-C(5)	119.7(3)
C(2)-C(3)-C(5)	116.2(4)
C(7)-C(6)-C(11)	118.6(4)
C(7)-C(6)-N(1)	120.3(3)
C(11)-C(6)-N(1)	121.0(3)
C(6)-C(7)-C(8)	120.6(4)
C(9)-C(8)-C(7)	121.1(4)
C(10)-C(9)-C(8)	117.4(4)
C(10)-C(9)-C(12)	120.1(4)
C(8)-C(9)-C(12)	122.5(4)
C(9)-C(10)-C(11)	121.9(4)
C(6)-C(11)-C(10)	120.3(4)
C(13)-C(12)-C(14)	111.4(5)
C(13)-C(12)-C(9)	113.8(4)
C(14)-C(12)-C(9)	110.3(4)
C(16)-C(15)-C(20)	119.6(4)
C(16)-C(15)-N(2)	121.0(4)
C(20)-C(15)-N(2)	119.0(4)
C(15)-C(16)-C(17)	118.0(5)
C(18)-C(17)-C(16)	121.9(5)
C(19)-C(18)-C(17)	117.7(4)
C(19)-C(18)-C(21)	116.2(6)
C(17)-C(18)-C(21)	126.1(6)
C(18)-C(19)-C(20)	122.0(5)
C(19)-C(20)-C(15)	120.7(5)
C(23)-C(21)-C(22)	110.8(11)
C(23)-C(21)-C(18)	107.3(11)
C(22)-C(21)-C(18)	111.6(6)

Symmetry transformations used to generate equivalent atoms:

' -x+1/2, y+1/2, -z+1/2

Table A32. Crystal data and structure refinement for [(BDI_{DIPP})GePPh₂] (**33**)

Identification code	jun1810	
Empirical formula	C ₄₁ H ₅₁ Ge N ₂ P	
Formula weight	675.40	
Temperature	173(2) K	
Wavelength	0.71073 Å	
Crystal system	Monoclinic	
Space group	<i>P</i> 2 ₁ /c (No.14)	
Unit cell dimensions	a = 17.2186(4) Å	a = 90°.
	b = 12.0952(3) Å	b = 99.289(1)°.
	c = 18.0061(3) Å	g = 90°.
Volume	3700.82(14) Å ³	
Z	4	
Density (calculated)	1.21 Mg/m ³	
Absorption coefficient	0.90 mm ⁻¹	
F(000)	1432	
Crystal size	0.22 x 0.13 x 0.09 mm ³	
Theta range for data collection	3.47 to 27.11°.	
Index ranges	-22 ≤ h ≤ 22, -15 ≤ k ≤ 15, -22 ≤ l ≤ 23	
Reflections collected	57250	
Independent reflections	8144 [R(int) = 0.073]	
Reflections with I > 2σ(I)	6099	
Completeness to theta = 27.11°	99.8 %	
Tmax. and Tmin.	0.9328 and 0.8387	
Refinement method	Full-matrix least-squares on F ²	
Data / restraints / parameters	8144 / 156 / 446	
Goodness-of-fit on F ²	1.027	
Final R indices [I > 2σ(I)]	R1 = 0.044, wR2 = 0.087	
R indices (all data)	R1 = 0.072, wR2 = 0.097	
Largest diff. peak and hole	0.49 and -0.38 e.Å ⁻³	

Two of the iso-propyl groups were modeled with disorder

Data collection KappaCCD , Program package WinGX , Abs correction MULTISCAN

Refinement using SHELXL-97 , Drawing using ORTEP-3 for Windows

Table A33. Atomic coordinates ($\times 10^4$) and equivalent isotropic displacement parameters ($\text{\AA}^2 \times 10^3$) for $[(\text{BDI}_{\text{DIPP}})\text{GePPh}_2]$ (**33**). $U(\text{eq})$ is defined as one third of the trace of the orthogonalized U^{ij} tensor

	x	y	z	U(eq)
Ge	2851(1)	7966(1)	2136(1)	25(1)
P	2505(1)	7915(1)	747(1)	29(1)
N(1)	2572(1)	6389(2)	2373(1)	28(1)
N(2)	1808(1)	8437(2)	2391(1)	27(1)
C(1)	2234(1)	6186(2)	2969(1)	31(1)
C(2)	1837(2)	6996(2)	3312(1)	35(1)
C(3)	1570(1)	8002(2)	3003(1)	31(1)
C(4)	2257(2)	5050(2)	3313(2)	45(1)
C(5)	967(2)	8623(3)	3371(2)	47(1)
C(6)	2951(2)	5519(2)	2024(2)	38(1)
C(7)	2519(2)	5002(2)	1374(2)	48(1)
C(8)	2905(3)	4193(3)	1033(2)	75(1)
C(9)	3658(3)	3917(3)	1298(3)	86(1)
C(10)	4079(2)	4403(3)	1927(3)	77(1)
C(11)	3721(2)	5234(2)	2320(2)	53(1)
C(12)	1673(2)	5287(2)	1080(2)	48(1) ^a
C(13)	1397(6)	5162(10)	223(3)	61(2) ^a
C(14)	1075(5)	4688(8)	1479(5)	59(2) ^a
C(12A)	1673(2)	5287(2)	1080(2)	48(1) ^b
C(13A)	1750(20)	5070(30)	239(9)	70(8) ^b
C(14A)	1280(30)	4310(30)	1410(20)	92(10) ^b
C(15)	4156(2)	5726(3)	3048(2)	67(1) ^c
C(16)	4397(9)	4728(12)	3589(8)	75(3) ^c
C(17)	4856(8)	6476(18)	2997(12)	94(5) ^c
C(15A)	4156(2)	5726(3)	3048(2)	67(1) ^d
C(16A)	4447(18)	5130(40)	3802(16)	90(9) ^d
C(17A)	4923(14)	6200(30)	2821(17)	69(6) ^d
C(18)	1379(2)	9372(2)	2035(1)	31(1)
C(19)	675(2)	9176(2)	1547(1)	39(1)
C(20)	242(2)	10107(3)	1248(2)	54(1)
C(21)	513(2)	11155(3)	1418(2)	62(1)
C(22)	1218(2)	11327(3)	1876(2)	55(1)

C(23)	1674(2)	10447(2)	2200(2)	39(1)
C(24)	370(2)	8023(3)	1344(2)	51(1)
C(25)	245(2)	7831(3)	494(2)	59(1)
C(26)	-403(2)	7764(4)	1631(2)	87(1)
C(27)	2449(2)	10672(2)	2710(2)	48(1)
C(28)	2353(2)	11254(4)	3442(2)	84(1)
C(29)	3002(3)	11329(5)	2327(2)	111(2)
C(30)	3404(2)	7290(2)	498(1)	35(1)
C(31)	3359(2)	6871(3)	-223(2)	66(1)
C(32)	4022(3)	6445(4)	-472(2)	92(1)
C(33)	4724(3)	6398(3)	-4(3)	83(1)
C(34)	4787(2)	6798(3)	714(2)	76(1)
C(35)	4128(2)	7249(3)	961(2)	55(1)
C(36)	2683(1)	9374(2)	523(1)	28(1)
C(37)	3415(2)	9806(2)	448(2)	39(1)
C(38)	3493(2)	10894(2)	225(2)	46(1)
C(39)	2846(2)	11570(2)	74(2)	47(1)
C(40)	2119(2)	11169(2)	159(2)	45(1)
C(41)	2035(2)	10080(2)	377(1)	37(1)

a 72.3%, *b* 27.7%; *c* 69.3%, *d* 30.7%

Table A34. Bond lengths [Å] and angles [deg] for [(BDI_{DIPP})GePPh₂] (**33**)

Ge-N(2)	2.0071(19)
Ge-N(1)	2.0281(19)
Ge-P	2.4760(6)
P-C(30)	1.842(3)
P-C(36)	1.847(2)
N(1)-C(1)	1.324(3)
N(1)-C(6)	1.436(3)
N(2)-C(3)	1.343(3)
N(2)-C(18)	1.443(3)
C(1)-C(2)	1.395(4)
C(1)-C(4)	1.506(3)
C(2)-C(3)	1.385(4)
C(3)-C(5)	1.517(3)
C(6)-C(11)	1.390(4)
C(6)-C(7)	1.426(4)
C(7)-C(8)	1.381(4)
C(7)-C(12)	1.508(4)
C(8)-C(9)	1.350(6)
C(9)-C(10)	1.373(6)
C(10)-C(11)	1.426(5)
C(11)-C(15)	1.522(5)
C(12)-C(14)	1.530(6)
C(12)-C(13)	1.546(6)
C(15)-C(17)	1.523(8)
C(15)-C(16)	1.563(7)
C(18)-C(19)	1.399(4)
C(18)-C(23)	1.409(4)
C(19)-C(20)	1.408(4)
C(19)-C(24)	1.513(4)
C(20)-C(21)	1.368(5)
C(21)-C(22)	1.369(5)
C(22)-C(23)	1.393(4)
C(23)-C(27)	1.518(4)
C(24)-C(25)	1.529(4)
C(24)-C(26)	1.536(5)
C(27)-C(29)	1.493(5)
C(27)-C(28)	1.525(4)
C(30)-C(31)	1.383(4)
C(30)-C(35)	1.385(4)
C(31)-C(32)	1.391(5)

C(32)-C(33)	1.359(6)
C(33)-C(34)	1.368(6)
C(34)-C(35)	1.394(4)
C(36)-C(37)	1.391(4)
C(36)-C(41)	1.395(3)
C(37)-C(38)	1.389(4)
C(38)-C(39)	1.372(4)
C(39)-C(40)	1.374(4)
C(40)-C(41)	1.389(4)
N(2)-Ge-N(1)	88.16(8)
N(2)-Ge-P	99.20(6)
N(1)-Ge-P	99.33(6)
C(30)-P-C(36)	99.38(11)
C(30)-P-Ge	100.49(9)
C(36)-P-Ge	100.11(7)
C(1)-N(1)-C(6)	120.6(2)
C(1)-N(1)-Ge	119.66(16)
C(6)-N(1)-Ge	117.20(15)
C(3)-N(2)-C(18)	117.96(19)
C(3)-N(2)-Ge	118.66(16)
C(18)-N(2)-Ge	122.26(15)
N(1)-C(1)-C(2)	122.7(2)
N(1)-C(1)-C(4)	121.1(2)
C(2)-C(1)-C(4)	116.1(2)
C(3)-C(2)-C(1)	126.4(2)
N(2)-C(3)-C(2)	123.2(2)
N(2)-C(3)-C(5)	119.0(2)
C(2)-C(3)-C(5)	117.7(2)
C(11)-C(6)-C(7)	123.1(3)
C(11)-C(6)-N(1)	119.1(3)
C(7)-C(6)-N(1)	117.8(2)
C(8)-C(7)-C(6)	116.8(3)
C(8)-C(7)-C(12)	120.8(3)
C(6)-C(7)-C(12)	122.3(2)
C(9)-C(8)-C(7)	121.4(4)
C(8)-C(9)-C(10)	122.4(4)
C(9)-C(10)-C(11)	119.9(4)
C(6)-C(11)-C(10)	116.5(3)
C(6)-C(11)-C(15)	122.7(3)
C(7)-C(12)-C(14)	114.4(4)
C(7)-C(12)-C(13)	116.9(5)

C(10)-C(11)-C(15)	120.8(3)
C(11)-C(15)-C(17)	117.7(9)
C(11)-C(15)-C(16)	106.3(7)
C(14)-C(12)-C(13)	107.5(5)
C(17)-C(15)-C(16)	111.4(10)
C(19)-C(18)-C(23)	122.4(2)
C(19)-C(18)-N(2)	118.4(2)
C(23)-C(18)-N(2)	119.2(2)
C(18)-C(19)-C(20)	117.1(3)
C(18)-C(19)-C(24)	122.7(2)
C(20)-C(19)-C(24)	120.3(3)
C(21)-C(20)-C(19)	121.0(3)
C(20)-C(21)-C(22)	120.9(3)
C(21)-C(22)-C(23)	121.4(3)
C(22)-C(23)-C(18)	117.2(3)
C(22)-C(23)-C(27)	119.8(3)
C(18)-C(23)-C(27)	123.0(2)
C(19)-C(24)-C(25)	111.6(3)
C(19)-C(24)-C(26)	113.1(3)
C(25)-C(24)-C(26)	108.4(3)
C(29)-C(27)-C(23)	112.3(3)
C(29)-C(27)-C(28)	108.6(3)
C(23)-C(27)-C(28)	113.5(3)
C(31)-C(30)-C(35)	117.4(3)
C(31)-C(30)-P	117.2(2)
C(35)-C(30)-P	125.3(2)
C(30)-C(31)-C(32)	121.0(4)
C(33)-C(32)-C(31)	120.5(4)
C(32)-C(33)-C(34)	120.0(3)
C(33)-C(34)-C(35)	119.6(4)
C(30)-C(35)-C(34)	121.5(3)
C(37)-C(36)-C(41)	117.4(2)
C(37)-C(36)-P	124.42(19)
C(41)-C(36)-P	118.08(19)
C(38)-C(37)-C(36)	121.1(3)
C(39)-C(38)-C(37)	120.5(3)
C(38)-C(39)-C(40)	119.5(3)
C(39)-C(40)-C(41)	120.2(3)
C(40)-C(41)-C(36)	121.2(3)

Table A35. Crystal data and structure refinement for [(BDI_{DIPP})SnPPh₂] (**34**)

Identification code	oct509b	
Empirical formula	C ₄₁ H ₅₁ N ₂ P Sn	
Formula weight	721.50	
Temperature	173(2) K	
Wavelength	0.71073 Å	
Crystal system	Monoclinic	
Space group	<i>P</i> 2 ₁ (No.4)	
Unit cell dimensions	a = 11.2633(2) Å	a = 90°.
	b = 12.5856(3) Å	b = 90.02°.
	c = 12.9200(3) Å	g = 90°.
Volume	1831.48(7) Å ³	
Z	2	
Density (calculated)	1.31 Mg/m ³	
Absorption coefficient	0.77 mm ⁻¹	
F(000)	752	
Crystal size	0.20 x 0.20 x 0.16 mm ³	
Theta range for data collection	3.54 to 27.11°.	
Index ranges	-14 ≤ h ≤ 14, -16 ≤ k ≤ 16, -16 ≤ l ≤ 16	
Reflections collected	29273	
Independent reflections	8017 [R(int) = 0.053]	
Reflections with I > 2σ(I)	7400	
Completeness to theta = 27.11°	99.8 %	
Absorption correction	Semi-empirical from equivalents	
Tmax. and Tmin.	0.9076 and 0.7974	
Refinement method	Full-matrix least-squares on F ²	
Data / restraints / parameters	8017 / 1 / 408	
Goodness-of-fit on F ²	1.008	
Final R indices [I > 2σ(I)]	R1 = 0.033, wR2 = 0.073	
R indices (all data)	R1 = 0.038, wR2 = 0.076	
Absolute structure parameter	-0.014(17)	
Largest diff. peak and hole	1.69 and -0.48 e.Å ⁻³	

Residual electron density believed to be from a minor component in which the positions of the Sn and P are reversed with respect to the plane of the ligand

Data collection KappaCCD , Program package WinGX , Abs correction MULTISCAN

Refinement using SHELXL-97 , Drawing using ORTEP-3 for Windows

Table A36. Atomic coordinates ($\times 10^4$) and equivalent isotropic displacement parameters ($\text{\AA}^2 \times 10^3$) for $[(\text{BDI}_{\text{DIPP}})\text{SnPPh}_2]$ (**34**). $U(\text{eq})$ is defined as one third of the trace of the orthogonalized U^{ij} tensor

	x	y	z	$U(\text{eq})$
Sn	6892(1)	3448(1)	3379(1)	20(1)
P	5903(1)	2188(1)	2002(1)	25(1)
N(1)	8460(2)	3922(2)	2438(2)	20(1)
N(2)	8155(2)	2328(2)	4117(2)	20(1)
C(1)	9503(3)	4013(3)	2906(3)	25(1)
C(2)	9775(3)	3558(4)	3871(3)	32(1)
C(3)	9230(3)	2696(3)	4363(3)	25(1)
C(4)	10503(3)	4646(4)	2419(3)	42(1)
C(5)	9929(4)	2155(3)	5217(3)	40(1)
C(6)	8318(3)	4251(3)	1376(3)	21(1)
C(7)	8789(3)	3619(3)	585(3)	26(1)
C(8)	8605(4)	3925(3)	-436(3)	34(1)
C(9)	7961(3)	4826(3)	-670(3)	34(1)
C(10)	7495(3)	5434(3)	113(3)	29(1)
C(11)	7675(3)	5184(2)	1152(3)	23(1)
C(12)	9516(4)	2620(3)	789(4)	42(1)
C(13)	10775(4)	2725(4)	356(5)	67(2)
C(14)	8899(5)	1634(3)	318(4)	52(1)
C(15)	7170(4)	5904(3)	1996(3)	33(1)
C(16)	8142(5)	6420(4)	2644(4)	52(1)
C(17)	6347(4)	6772(3)	1585(4)	45(1)
C(18)	7713(3)	1384(3)	4615(3)	21(1)
C(19)	7838(3)	404(3)	4110(3)	22(1)
C(20)	7378(3)	-498(3)	4592(3)	29(1)
C(21)	6795(3)	-434(3)	5529(3)	35(1)
C(22)	6656(4)	548(3)	5999(3)	37(1)
C(23)	7114(3)	1476(3)	5561(3)	29(1)
C(24)	8425(4)	318(3)	3063(3)	35(1)
C(25)	9704(4)	-61(7)	3167(5)	85(2)
C(26)	7763(4)	-403(4)	2325(4)	50(1)
C(27)	6897(4)	2530(3)	6108(3)	44(1)
C(28)	7331(6)	2516(4)	7231(4)	71(2)

C(29)	5573(5)	2825(4)	6053(4)	63(2)
C(30)	5261(3)	3253(3)	1202(3)	28(1)
C(31)	5502(3)	3252(3)	145(3)	34(1)
C(32)	5017(4)	4031(4)	-499(3)	45(1)
C(33)	4283(4)	4798(3)	-98(4)	47(1)
C(34)	4034(4)	4817(3)	942(4)	48(1)
C(35)	4531(4)	4043(3)	1594(3)	37(1)
C(36)	4607(3)	1779(3)	2777(3)	27(1)
C(37)	3424(3)	1966(3)	2503(3)	38(1)
C(38)	2496(3)	1575(4)	3098(4)	46(1)
C(39)	2734(4)	981(4)	3982(4)	48(1)
C(40)	3878(4)	785(4)	4260(4)	56(1)
C(41)	4803(3)	1180(4)	3666(4)	45(1)

Table A37. Bond lengths [Å] and angles [deg] for [(BDI_{DIPP})SnPPh₂] (**34**)

Sn-N(2)	2.218(3)
Sn-N(1)	2.226(3)
Sn-P	2.6307(9)
P-C(30)	1.841(3)
P-C(36)	1.843(4)
N(1)-C(1)	1.325(4)
N(1)-C(6)	1.443(4)
N(2)-C(3)	1.335(4)
N(2)-C(18)	1.439(4)
C(1)-C(2)	1.406(5)
C(1)-C(4)	1.517(5)
C(2)-C(3)	1.400(6)
C(3)-C(5)	1.516(5)
C(6)-C(7)	1.399(5)
C(6)-C(11)	1.409(4)
C(7)-C(8)	1.391(5)
C(7)-C(12)	1.523(5)
C(8)-C(9)	1.380(5)
C(9)-C(10)	1.373(5)
C(10)-C(11)	1.394(5)
C(11)-C(15)	1.527(5)
C(12)-C(13)	1.531(6)
C(12)-C(14)	1.547(6)
C(15)-C(16)	1.524(6)
C(15)-C(17)	1.528(5)
C(18)-C(23)	1.401(5)
C(18)-C(19)	1.402(5)
C(19)-C(20)	1.395(5)
C(19)-C(24)	1.510(5)
C(20)-C(21)	1.380(5)
C(21)-C(22)	1.386(6)
C(22)-C(23)	1.396(5)
C(23)-C(27)	1.523(5)
C(24)-C(26)	1.513(6)
C(24)-C(25)	1.524(7)
C(27)-C(28)	1.530(6)
C(27)-C(29)	1.539(7)
C(30)-C(35)	1.386(5)
C(30)-C(31)	1.393(5)
C(31)-C(32)	1.397(6)

C(32)-C(33)	1.372(7)
C(33)-C(34)	1.374(7)
C(34)-C(35)	1.405(5)
C(36)-C(41)	1.391(6)
C(36)-C(37)	1.399(5)
C(37)-C(38)	1.388(6)
C(38)-C(39)	1.390(7)
C(39)-C(40)	1.360(6)
C(40)-C(41)	1.386(6)
N(2)-Sn-N(1)	84.06(10)
N(2)-Sn-P	100.32(7)
N(1)-Sn-P	97.35(7)
C(30)-P-C(36)	101.38(16)
C(30)-P-Sn	96.12(11)
C(36)-P-Sn	97.82(11)
C(1)-N(1)-C(6)	120.5(3)
C(1)-N(1)-Sn	118.5(2)
C(6)-N(1)-Sn	120.58(19)
C(3)-N(2)-C(18)	119.6(3)
C(3)-N(2)-Sn	117.6(2)
C(18)-N(2)-Sn	119.66(19)
N(1)-C(1)-C(2)	124.2(3)
N(1)-C(1)-C(4)	120.9(3)
C(2)-C(1)-C(4)	114.8(3)
C(3)-C(2)-C(1)	128.5(3)
N(2)-C(3)-C(2)	124.0(3)
N(2)-C(3)-C(5)	119.3(3)
C(2)-C(3)-C(5)	116.8(3)
C(7)-C(6)-C(11)	121.3(3)
C(7)-C(6)-N(1)	119.3(3)
C(11)-C(6)-N(1)	119.4(3)
C(8)-C(7)-C(6)	118.6(3)
C(8)-C(7)-C(12)	118.2(3)
C(6)-C(7)-C(12)	123.2(3)
C(9)-C(8)-C(7)	120.9(4)
C(10)-C(9)-C(8)	119.9(3)
C(9)-C(10)-C(11)	121.9(3)
C(10)-C(11)-C(6)	117.4(3)
C(10)-C(11)-C(15)	119.9(3)
C(6)-C(11)-C(15)	122.6(3)
C(7)-C(12)-C(13)	111.3(4)

C(7)-C(12)-C(14)	110.7(4)
C(13)-C(12)-C(14)	110.0(4)
C(16)-C(15)-C(11)	112.2(3)
C(16)-C(15)-C(17)	108.8(3)
C(11)-C(15)-C(17)	113.7(3)
C(23)-C(18)-C(19)	121.8(3)
C(23)-C(18)-N(2)	119.3(3)
C(19)-C(18)-N(2)	118.9(3)
C(20)-C(19)-C(18)	118.1(3)
C(20)-C(19)-C(24)	120.3(3)
C(18)-C(19)-C(24)	121.6(3)
C(21)-C(20)-C(19)	121.4(3)
C(20)-C(21)-C(22)	119.3(3)
C(21)-C(22)-C(23)	121.8(4)
C(22)-C(23)-C(18)	117.6(3)
C(22)-C(23)-C(27)	118.8(3)
C(18)-C(23)-C(27)	123.6(3)
C(19)-C(24)-C(26)	113.1(3)
C(19)-C(24)-C(25)	111.0(4)
C(26)-C(24)-C(25)	109.5(4)
C(23)-C(27)-C(28)	112.3(4)
C(23)-C(27)-C(29)	110.1(4)
C(28)-C(27)-C(29)	110.8(4)
C(35)-C(30)-C(31)	118.4(3)
C(35)-C(30)-P	123.4(3)
C(31)-C(30)-P	118.2(3)
C(30)-C(31)-C(32)	120.4(4)
C(33)-C(32)-C(31)	120.3(4)
C(32)-C(33)-C(34)	120.3(4)
C(33)-C(34)-C(35)	119.5(4)
C(30)-C(35)-C(34)	121.0(4)
C(41)-C(36)-C(37)	116.8(3)
C(41)-C(36)-P	118.3(3)
C(37)-C(36)-P	124.8(3)
C(38)-C(37)-C(36)	121.2(4)
C(37)-C(38)-C(39)	120.0(4)
C(40)-C(39)-C(38)	119.8(4)
C(39)-C(40)-C(41)	120.0(4)
C(40)-C(41)-C(36)	122.2(4)

Table A38. Crystal data and structure refinement for [(BDI_{DIPP})PbPPh₂] (35)

Identification code	jun1710	
Empirical formula	C ₄₁ H ₅₁ N ₂ P Pb	
Formula weight	810.01	
Temperature	173(2) K	
Wavelength	0.71073 Å	
Crystal system	Orthorhombic	
Space group	<i>I</i> 2 c b (No.45)	
Unit cell dimensions	a = 15.9697(5) Å	a = 90°.
	b = 18.3168(6) Å	b = 90°.
	c = 25.8355(6) Å	g = 90°.
Volume	7557.2(4) Å ³	
Z	8	
Density (calculated)	1.42 Mg/m ³	
Absorption coefficient	4.54 mm ⁻¹	
F(000)	3264	
Crystal size	0.15 x 0.07 x 0.03 mm ³	
Theta range for data collection	3.43 to 27.09°.	
Index ranges	-20 ≤ h ≤ 20, -23 ≤ k ≤ 17, -32 ≤ l ≤ 33	
Reflections collected	24237	
Independent reflections	8198 [R(int) = 0.081]	
Reflections with I > 2σ(I)	5814	
Completeness to theta = 27.09°	99.7 %	
Tmax. and Tmin.	0.7662 and 0.6155	
Refinement method	Full-matrix least-squares on F ²	
Data / restraints / parameters	8198 / 1 / 408	
Goodness-of-fit on F ²	0.986	
Final R indices [I > 2σ(I)]	R1 = 0.047, wR2 = 0.085	
R indices (all data)	R1 = 0.086, wR2 = 0.096	
Absolute structure parameter	-0.006(8)	
Largest diff. peak and hole	0.68 and -1.40 e.Å ⁻³	

Data collection KappaCCD , Program package WinGX , Abs correction MULTISCAN

Refinement using SHELXL-97 , Drawing using ORTEP-3 for Windows

Table A39. Atomic coordinates ($\times 10^4$) and equivalent isotropic displacement parameters ($\text{\AA}^2 \times 10^3$) for $[(\text{BDI}_{\text{DIPP}})\text{PbPPh}_2]$ (**35**). $U(\text{eq})$ is defined as one third of the trace of the orthogonalized U^{ij} tensor

	x	y	z	U(eq)
Pb	8978(1)	2212(1)	4041(1)	22(1)
P	10188(1)	2022(1)	3313(1)	27(1)
N(1)	8556(4)	3380(4)	3805(2)	20(1)
N(2)	9600(4)	2890(4)	4709(2)	22(2)
C(1)	8340(5)	3861(5)	4152(3)	29(2)
C(2)	8598(5)	3868(5)	4675(3)	28(2)
C(3)	9226(4)	3447(5)	4916(3)	22(2)
C(4)	7785(6)	4502(5)	3989(3)	41(2)
C(5)	9460(5)	3706(6)	5458(3)	41(3)
C(6)	8371(5)	3499(5)	3263(3)	23(2)
C(7)	8972(9)	3830(4)	2951(2)	29(2)
C(8)	8800(6)	3940(5)	2428(3)	39(3)
C(9)	8050(7)	3721(5)	2229(3)	43(3)
C(10)	7462(5)	3389(5)	2531(3)	34(2)
C(11)	7606(5)	3267(5)	3060(3)	27(2)
C(12)	9819(5)	4072(5)	3178(3)	33(2)
C(13)	9775(6)	4865(6)	3370(4)	59(3)
C(14)	10549(5)	3995(6)	2808(4)	60(3)
C(15)	6939(5)	2881(5)	3381(3)	32(2)
C(16)	6089(6)	3292(7)	3368(4)	56(3)
C(17)	6821(7)	2108(5)	3200(3)	45(3)
C(18)	10298(5)	2542(5)	4959(3)	25(2)
C(19)	11114(5)	2780(5)	4813(3)	28(2)
C(20)	11790(6)	2447(6)	5036(4)	37(3)
C(21)	11668(6)	1872(6)	5384(3)	43(3)
C(22)	10882(6)	1627(6)	5500(3)	39(2)
C(23)	10187(5)	1966(5)	5296(3)	30(2)
C(24)	11221(5)	3369(6)	4402(3)	42(2)
C(25)	11259(7)	4111(6)	4637(4)	65(3)
C(26)	11992(7)	3235(8)	4066(4)	70(4)
C(27)	9307(5)	1685(7)	5441(3)	49(3)
C(28)	9155(8)	1735(8)	6026(3)	87(5)

C(29)	9177(8)	902(6)	5254(4)	71(4)
C(30)	9371(5)	1624(5)	2894(3)	27(2)
C(31)	8930(9)	982(4)	3007(3)	29(2)
C(32)	8317(5)	729(5)	2681(4)	39(2)
C(33)	8115(6)	1122(6)	2241(4)	45(3)
C(34)	8525(6)	1760(6)	2127(3)	44(2)
C(35)	9152(6)	2005(5)	2442(3)	35(3)
C(36)	10704(5)	1204(5)	3553(3)	29(2)
C(37)	10902(5)	610(5)	3225(3)	36(2)
C(38)	11403(8)	57(8)	3380(3)	35(2)
C(39)	11723(5)	28(6)	3867(3)	43(3)
C(40)	11549(6)	586(6)	4207(4)	49(3)
C(41)	11053(6)	1157(6)	4052(3)	42(2)

Table A40. Bond lengths [Å] and angles [deg] for [(BDI_{DIPP})PbPPh₂] (**35**)

Pb-N(1)	2.324(6)
Pb-N(2)	2.347(6)
Pb-P	2.720(2)
P-C(36)	1.818(9)
P-C(30)	1.845(8)
N(1)-C(1)	1.303(10)
N(1)-C(6)	1.446(9)
N(2)-C(3)	1.297(9)
N(2)-C(18)	1.436(10)
C(1)-C(2)	1.413(11)
C(1)-C(4)	1.530(12)
C(2)-C(3)	1.410(10)
C(3)-C(5)	1.526(10)
C(6)-C(7)	1.394(14)
C(6)-C(11)	1.395(11)
C(7)-C(8)	1.395(10)
C(7)-C(12)	1.538(16)
C(8)-C(9)	1.364(14)
C(9)-C(10)	1.363(12)
C(10)-C(11)	1.404(10)
C(11)-C(15)	1.523(11)
C(12)-C(14)	1.514(11)
C(12)-C(13)	1.537(13)
C(15)-C(17)	1.502(12)
C(15)-C(16)	1.553(12)
C(18)-C(23)	1.379(12)
C(18)-C(19)	1.425(11)
C(19)-C(20)	1.367(12)
C(19)-C(24)	1.524(13)
C(20)-C(21)	1.398(14)
C(21)-C(22)	1.367(13)
C(22)-C(23)	1.377(11)
C(23)-C(27)	1.543(12)
C(24)-C(25)	1.489(14)
C(24)-C(26)	1.526(13)
C(27)-C(29)	1.527(15)
C(27)-C(28)	1.535(11)
C(30)-C(31)	1.402(12)
C(30)-C(35)	1.403(11)
C(31)-C(32)	1.372(14)

C(32)-C(33)	1.383(13)
C(33)-C(34)	1.372(14)
C(34)-C(35)	1.367(12)
C(36)-C(41)	1.408(11)
C(36)-C(37)	1.414(11)
C(37)-C(38)	1.352(15)
C(38)-C(39)	1.357(11)
C(39)-C(40)	1.377(13)
C(40)-C(41)	1.372(13)

N(1)-Pb-N(2)	80.2(2)
N(1)-Pb-P	98.21(15)
N(2)-Pb-P	105.98(15)
C(36)-P-C(30)	101.3(4)
C(36)-P-Pb	101.1(3)
C(30)-P-Pb	87.3(2)
C(1)-N(1)-C(6)	120.7(7)
C(1)-N(1)-Pb	121.2(5)
C(6)-N(1)-Pb	116.8(5)
C(3)-N(2)-C(18)	121.4(6)
C(3)-N(2)-Pb	121.6(5)
C(18)-N(2)-Pb	115.1(5)
N(1)-C(1)-C(2)	125.9(8)
N(1)-C(1)-C(4)	118.8(7)
C(2)-C(1)-C(4)	115.2(8)
C(3)-C(2)-C(1)	128.7(8)
N(2)-C(3)-C(2)	125.2(7)
N(2)-C(3)-C(5)	120.7(7)
C(2)-C(3)-C(5)	114.1(7)
C(7)-C(6)-C(11)	121.2(7)
C(7)-C(6)-N(1)	119.0(7)
C(11)-C(6)-N(1)	119.8(7)
C(6)-C(7)-C(8)	119.2(11)
C(6)-C(7)-C(12)	120.7(6)
C(8)-C(7)-C(12)	120.0(10)
C(9)-C(8)-C(7)	119.7(10)
C(10)-C(9)-C(8)	121.5(8)
C(9)-C(10)-C(11)	120.9(8)
C(6)-C(11)-C(10)	117.5(7)
C(6)-C(11)-C(15)	123.3(7)
C(10)-C(11)-C(15)	119.2(7)
C(14)-C(12)-C(13)	109.1(8)

C(14)-C(12)-C(7)	114.2(8)
C(13)-C(12)-C(7)	110.8(7)
C(17)-C(15)-C(11)	110.9(7)
C(17)-C(15)-C(16)	109.9(8)
C(11)-C(15)-C(16)	112.0(8)
C(23)-C(18)-C(19)	121.2(8)
C(23)-C(18)-N(2)	121.6(7)
C(19)-C(18)-N(2)	117.1(7)
C(20)-C(19)-C(18)	118.3(8)
C(20)-C(19)-C(24)	121.4(7)
C(18)-C(19)-C(24)	120.2(7)
C(19)-C(20)-C(21)	119.9(8)
C(22)-C(21)-C(20)	121.0(9)
C(21)-C(22)-C(23)	120.6(9)
C(22)-C(23)-C(18)	118.9(8)
C(22)-C(23)-C(27)	119.4(8)
C(18)-C(23)-C(27)	121.7(8)
C(25)-C(24)-C(19)	111.5(8)
C(25)-C(24)-C(26)	110.2(9)
C(19)-C(24)-C(26)	111.9(9)
C(29)-C(27)-C(28)	110.2(9)
C(29)-C(27)-C(23)	111.1(8)
C(28)-C(27)-C(23)	111.3(8)
C(31)-C(30)-C(35)	117.7(8)
C(31)-C(30)-P	124.3(6)
C(35)-C(30)-P	117.9(7)
C(32)-C(31)-C(30)	120.9(7)
C(31)-C(32)-C(33)	119.7(9)
C(34)-C(33)-C(32)	120.6(9)
C(35)-C(34)-C(33)	120.0(9)
C(34)-C(35)-C(30)	121.0(9)
C(41)-C(36)-C(37)	114.4(8)
C(41)-C(36)-P	122.8(7)
C(37)-C(36)-P	122.0(6)
C(38)-C(37)-C(36)	122.0(8)
C(37)-C(38)-C(39)	121.8(11)
C(38)-C(39)-C(40)	119.1(10)
C(41)-C(40)-C(39)	119.7(8)
C(40)-C(41)-C(36)	122.9(9)

Table A41. Crystal data and structure refinement for [(BDI_{DIPP})GePCy₂] (36)

Identification code	jun1910	
Empirical formula	C ₄₁ H ₆₃ Ge N ₂ P	
Formula weight	687.49	
Temperature	173(2) K	
Wavelength	0.71073 Å	
Crystal system	Monoclinic	
Space group	<i>P</i> 2 ₁ /c (No.14)	
Unit cell dimensions	a = 10.0941(2) Å	a = 90°.
	b = 23.5171(5) Å	b = 110.600(1)°.
	c = 17.2689(3) Å	g = 90°.
Volume	3837.24(13) Å ³	
Z	4	
Density (calculated)	1.19 Mg/m ³	
Absorption coefficient	0.87 mm ⁻¹	
F(000)	1480	
Crystal size	0.21 x 0.09 x 0.06 mm ³	
Theta range for data collection	3.47 to 26.73°.	
Index ranges	-12 ≤ h ≤ 12, -29 ≤ k ≤ 29, -21 ≤ l ≤ 21	
Reflections collected	48350	
Independent reflections	8127 [R(int) = 0.079]	
Reflections with I > 2σ(I)	6180	
Completeness to theta = 26.73°	99.8 %	
Tmax. and Tmin.	0.9472 and 0.8301	
Refinement method	Full-matrix least-squares on F ²	
Data / restraints / parameters	8127 / 0 / 408	
Goodness-of-fit on F ²	0.990	
Final R indices [I > 2σ(I)]	R1 = 0.046, wR2 = 0.108	
R indices (all data)	R1 = 0.070, wR2 = 0.119	
Largest diff. peak and hole	0.79 and -0.44 e.Å ⁻³	

Data collection KappaCCD , Program package WinGX , Abs correction MULTISCAN

Refinement using SHELXL-97 , Drawing using ORTEP-3 for Windows

Table A42. Atomic coordinates ($\times 10^4$) and equivalent isotropic displacement parameters ($\text{\AA}^2 \times 10^3$) for [(BDI_{DIPP})GePCy₂] (**36**). U(eq) is defined as one third of the trace of the orthogonalized U^{ij} tensor

	x	y	z	U(eq)
Ge	7977(1)	8178(1)	2055(1)	20(1)
P	8414(1)	8309(1)	3545(1)	27(1)
N(1)	6587(2)	8823(1)	1525(1)	20(1)
N(2)	6287(2)	7633(1)	1721(1)	22(1)
C(1)	5584(3)	8725(1)	796(2)	23(1)
C(2)	5093(3)	8184(1)	507(2)	27(1)
C(3)	5284(3)	7689(1)	981(2)	25(1)
C(4)	4870(3)	9210(1)	230(2)	34(1)
C(5)	4252(3)	7211(1)	623(2)	40(1)
C(6)	6887(3)	9403(1)	1791(2)	23(1)
C(7)	6271(3)	9630(1)	2333(2)	26(1)
C(8)	6553(3)	10202(1)	2564(2)	35(1)
C(9)	7418(3)	10526(1)	2279(2)	40(1)
C(10)	8044(3)	10293(1)	1761(2)	34(1)
C(11)	7796(3)	9728(1)	1502(2)	27(1)
C(12)	5318(3)	9276(1)	2655(2)	30(1)
C(13)	3786(3)	9292(2)	2071(2)	47(1)
C(14)	5409(4)	9437(2)	3527(2)	51(1)
C(15)	8544(3)	9480(1)	953(2)	30(1)
C(16)	8266(4)	9815(2)	154(2)	44(1)
C(17)	10129(3)	9437(2)	1418(2)	45(1)
C(18)	6325(3)	7119(1)	2183(2)	25(1)
C(19)	5561(3)	7098(1)	2720(2)	34(1)
C(20)	5682(4)	6601(2)	3190(2)	45(1)
C(21)	6495(4)	6150(1)	3112(2)	47(1)
C(22)	7189(4)	6174(1)	2555(2)	42(1)
C(23)	7124(3)	6655(1)	2070(2)	31(1)
C(24)	4573(4)	7574(2)	2769(2)	45(1)
C(25)	3016(4)	7366(2)	2438(3)	82(2)
C(26)	4907(5)	7803(2)	3636(3)	62(1)
C(27)	7809(4)	6651(1)	1417(2)	38(1)
C(28)	7125(4)	6205(2)	751(2)	67(1)

C(29)	9392(4)	6551(2)	1772(2)	50(1)
C(30)	10111(4)	8739(1)	3820(2)	39(1)
C(31)	10953(4)	8742(2)	4756(2)	52(1)
C(32)	12340(4)	9092(2)	4959(2)	61(1)
C(33)	12049(5)	9675(2)	4648(3)	65(1)
C(34)	11205(5)	9688(2)	3722(3)	72(1)
C(35)	9827(4)	9339(2)	3521(2)	57(1)
C(36)	9101(3)	7572(1)	3905(2)	27(1)
C(37)	9145(4)	7452(1)	4782(2)	38(1)
C(38)	9570(4)	6839(1)	5044(2)	45(1)
C(39)	10952(4)	6675(1)	4941(2)	43(1)
C(40)	10877(4)	6779(1)	4060(2)	38(1)
C(41)	10488(3)	7396(1)	3798(2)	30(1)

Table A43. Bond lengths [Å] and angles [deg] for [(BDI_{DIPP})GePCy₂] (**36**)

Ge-N(2)	2.048(2)
Ge-N(1)	2.049(2)
Ge-P	2.4724(8)
P-C(36)	1.889(3)
P-C(30)	1.900(3)
N(1)-C(1)	1.329(3)
N(1)-C(6)	1.438(3)
N(2)-C(3)	1.328(3)
N(2)-C(18)	1.442(3)
C(1)-C(2)	1.393(4)
C(1)-C(4)	1.512(4)
C(2)-C(3)	1.397(4)
C(3)-C(5)	1.509(4)
C(6)-C(7)	1.400(4)
C(6)-C(11)	1.412(4)
C(7)-C(8)	1.403(4)
C(7)-C(12)	1.519(4)
C(8)-C(9)	1.372(5)
C(9)-C(10)	1.378(5)
C(10)-C(11)	1.397(4)
C(11)-C(15)	1.521(4)
C(12)-C(13)	1.520(4)
C(12)-C(14)	1.523(4)
C(15)-C(17)	1.520(4)
C(15)-C(16)	1.527(4)
C(18)-C(19)	1.399(4)
C(18)-C(23)	1.410(4)
C(19)-C(20)	1.404(4)
C(19)-C(24)	1.520(5)
C(20)-C(21)	1.377(5)
C(21)-C(22)	1.376(5)
C(22)-C(23)	1.396(4)
C(23)-C(27)	1.517(5)
C(24)-C(26)	1.515(5)
C(24)-C(25)	1.550(5)
C(27)-C(29)	1.516(5)
C(27)-C(28)	1.529(5)
C(30)-C(35)	1.494(5)
C(30)-C(31)	1.538(4)
C(31)-C(32)	1.553(5)

C(32)-C(33)	1.465(5)
C(33)-C(34)	1.525(5)
C(34)-C(35)	1.546(5)
C(36)-C(37)	1.526(4)
C(36)-C(41)	1.533(4)
C(37)-C(38)	1.526(4)
C(38)-C(39)	1.517(5)
C(39)-C(40)	1.516(5)
C(40)-C(41)	1.530(4)

N(2)-Ge-N(1)	88.05(8)
N(2)-Ge-P	101.35(7)
N(1)-Ge-P	102.52(6)
C(36)-P-C(30)	102.25(13)
C(36)-P-Ge	97.97(9)
C(30)-P-Ge	98.12(10)
C(1)-N(1)-C(6)	118.2(2)
C(1)-N(1)-Ge	117.92(17)
C(6)-N(1)-Ge	121.69(16)
C(3)-N(2)-C(18)	118.5(2)
C(3)-N(2)-Ge	119.10(18)
C(18)-N(2)-Ge	120.79(16)
N(1)-C(1)-C(2)	123.8(2)
N(1)-C(1)-C(4)	120.8(2)
C(2)-C(1)-C(4)	115.4(2)
C(1)-C(2)-C(3)	126.3(3)
N(2)-C(3)-C(2)	123.2(2)
N(2)-C(3)-C(5)	120.2(2)
C(2)-C(3)-C(5)	116.6(2)
C(7)-C(6)-C(11)	121.8(2)
C(7)-C(6)-N(1)	118.9(2)
C(11)-C(6)-N(1)	119.4(2)
C(6)-C(7)-C(8)	117.5(3)
C(6)-C(7)-C(12)	121.5(2)
C(8)-C(7)-C(12)	120.9(3)
C(9)-C(8)-C(7)	121.3(3)
C(8)-C(9)-C(10)	120.6(3)
C(9)-C(10)-C(11)	120.9(3)
C(10)-C(11)-C(6)	117.9(3)
C(10)-C(11)-C(15)	119.5(3)
C(6)-C(11)-C(15)	122.6(2)
C(7)-C(12)-C(13)	111.8(3)

C(7)-C(12)-C(14)	113.5(3)
C(13)-C(12)-C(14)	110.1(3)
C(17)-C(15)-C(11)	111.0(3)
C(17)-C(15)-C(16)	109.7(3)
C(11)-C(15)-C(16)	113.0(2)
C(19)-C(18)-C(23)	122.7(3)
C(19)-C(18)-N(2)	118.8(3)
C(23)-C(18)-N(2)	118.5(3)
C(18)-C(19)-C(20)	117.1(3)
C(18)-C(19)-C(24)	122.4(3)
C(20)-C(19)-C(24)	120.4(3)
C(21)-C(20)-C(19)	121.2(3)
C(22)-C(21)-C(20)	120.3(3)
C(21)-C(22)-C(23)	121.6(3)
C(22)-C(23)-C(18)	116.9(3)
C(22)-C(23)-C(27)	120.2(3)
C(18)-C(23)-C(27)	122.7(3)
C(26)-C(24)-C(19)	113.2(3)
C(26)-C(24)-C(25)	108.7(3)
C(19)-C(24)-C(25)	110.4(3)
C(29)-C(27)-C(23)	113.1(3)
C(29)-C(27)-C(28)	109.2(3)
C(23)-C(27)-C(28)	111.1(3)
C(35)-C(30)-C(31)	109.1(3)
C(35)-C(30)-P	111.7(2)
C(31)-C(30)-P	112.4(2)
C(30)-C(31)-C(32)	111.2(3)
C(33)-C(32)-C(31)	111.3(3)
C(32)-C(33)-C(34)	111.6(3)
C(33)-C(34)-C(35)	110.6(4)
C(30)-C(35)-C(34)	112.1(3)
C(37)-C(36)-C(41)	111.2(2)
C(37)-C(36)-P	112.0(2)
C(41)-C(36)-P	116.94(19)
C(36)-C(37)-C(38)	112.0(3)
C(39)-C(38)-C(37)	112.3(3)
C(40)-C(39)-C(38)	110.7(3)
C(39)-C(40)-C(41)	111.5(3)
C(40)-C(41)-C(36)	111.7(2)

Table A44. Crystal data and structure refinement for [(BDI_{DIPP})SnPCy₂] (**37**)

Identification code	dec409	
Empirical formula	C ₄₁ H ₆₃ N ₂ P Sn	
Formula weight	733.59	
Temperature	173(2) K	
Wavelength	0.71073 Å	
Crystal system	Monoclinic	
Space group	<i>P</i> 21/ <i>c</i> (No.14)	
Unit cell dimensions	a = 9.9722(1) Å	a = 90°.
	b = 23.7044(4) Å	b = 109.003(1)°.
	c = 17.4243(3) Å	g = 90°.
Volume	3894.37(10) Å ³	
Z	4	
Density (calculated)	1.25 Mg/m ³	
Absorption coefficient	0.73 mm ⁻¹	
F(000)	1552	
Crystal size	0.17 x 0.11 x 0.07 mm ³	
Theta range for data collection	3.44 to 27.11°.	
Index ranges	-12 ≤ h ≤ 12, -30 ≤ k ≤ 30, -22 ≤ l ≤ 22	
Reflections collected	57848	
Independent reflections	8576 [R(int) = 0.077]	
Reflections with I > 2σ(I)	6730	
Completeness to theta = 27.11°	99.8 %	
Absorption correction	Semi-empirical from equivalents	
Tmax. and Tmin.	0.9735 and 0.8580	
Refinement method	Full-matrix least-squares on F ²	
Data / restraints / parameters	8576 / 0 / 408	
Goodness-of-fit on F ²	1.023	
Final R indices [I > 2σ(I)]	R1 = 0.037, wR2 = 0.072	
R indices (all data)	R1 = 0.058, wR2 = 0.079	
Largest diff. peak and hole	0.48 and -0.81 e.Å ⁻³	

Data collection KappaCCD , Program package WinGX , Abs correction MULTISCAN

Refinement using SHELXL-97 , Drawing using ORTEP-3 for Windows

Table A45. Atomic coordinates ($\times 10^4$) and equivalent isotropic displacement parameters ($\text{\AA}^2 \times 10^3$) for $[(\text{BDI}_{\text{DIPP}})\text{SnPCy}_2]$ (**37**). $U(\text{eq})$ is defined as one third of the trace of the orthogonalized U^{ij} tensor

	x	y	z	$U(\text{eq})$
Sn	1843(1)	8175(1)	2868(1)	18(1)
P	1512(1)	8293(1)	1316(1)	23(1)
N(1)	3436(2)	8841(1)	3442(1)	18(1)
N(2)	3734(2)	7612(1)	3239(1)	19(1)
C(1)	4435(3)	8726(1)	4143(2)	21(1)
C(2)	4902(3)	8181(1)	4406(2)	25(1)
C(3)	4715(3)	7682(1)	3950(2)	23(1)
C(4)	5163(3)	9197(1)	4710(2)	33(1)
C(5)	5742(3)	7208(1)	4319(2)	37(1)
C(6)	3159(3)	9421(1)	3191(2)	19(1)
C(7)	3777(3)	9643(1)	2636(2)	24(1)
C(8)	3514(3)	10204(1)	2407(2)	31(1)
C(9)	2654(3)	10534(1)	2703(2)	35(1)
C(10)	2015(3)	10308(1)	3226(2)	30(1)
C(11)	2248(3)	9748(1)	3479(2)	23(1)
C(12)	4713(3)	9276(1)	2300(2)	28(1)
C(13)	6250(3)	9280(2)	2856(2)	50(1)
C(14)	4638(4)	9435(2)	1438(2)	46(1)
C(15)	1468(3)	9505(1)	4024(2)	25(1)
C(16)	1761(3)	9832(1)	4821(2)	36(1)
C(17)	-128(3)	9487(1)	3578(2)	36(1)
C(18)	3713(3)	7107(1)	2780(2)	23(1)
C(19)	4458(3)	7094(1)	2224(2)	32(1)
C(20)	4350(3)	6611(1)	1752(2)	41(1)
C(21)	3540(4)	6156(1)	1828(2)	43(1)
C(22)	2841(3)	6171(1)	2393(2)	38(1)
C(23)	2908(3)	6640(1)	2885(2)	26(1)
C(24)	5431(3)	7575(1)	2167(2)	43(1)
C(25)	6996(4)	7399(2)	2537(3)	89(2)
C(26)	5163(4)	7780(2)	1310(2)	59(1)
C(27)	2194(3)	6628(1)	3536(2)	33(1)
C(28)	2857(4)	6174(2)	4174(2)	56(1)

C(29)	604(4)	6531(2)	3187(2)	43(1)
C(30)	-174(3)	8714(1)	1072(2)	24(1)
C(31)	-982(3)	8748(1)	159(2)	32(1)
C(32)	-2318(3)	9107(1)	-21(2)	40(1)
C(33)	-1976(4)	9701(1)	327(2)	45(1)
C(34)	-1152(3)	9676(1)	1233(2)	44(1)
C(35)	178(3)	9312(1)	1403(2)	34(1)
C(36)	861(3)	7550(1)	1010(2)	23(1)
C(37)	832(3)	7412(1)	141(2)	32(1)
C(38)	435(4)	6796(1)	-78(2)	39(1)
C(39)	-966(3)	6645(1)	41(2)	36(1)
C(40)	-928(3)	6765(1)	900(2)	33(1)
C(41)	-545(3)	7386(1)	1125(2)	25(1)

Table A46. Bond lengths [Å] and angles [deg] for [(BDI_{DIPP})SnPCy₂] (**37**)

Sn-N(2)	2.227(2)
Sn-N(1)	2.233(2)
Sn-P	2.6309(7)
P-C(30)	1.881(3)
P-C(36)	1.892(3)
N(1)-C(1)	1.328(3)
N(1)-C(6)	1.442(3)
N(2)-C(3)	1.315(3)
N(2)-C(18)	1.437(3)
C(1)-C(2)	1.398(4)
C(1)-C(4)	1.512(4)
C(2)-C(3)	1.404(4)
C(3)-C(5)	1.515(4)
C(6)-C(11)	1.405(4)
C(6)-C(7)	1.407(4)
C(7)-C(8)	1.388(4)
C(7)-C(12)	1.525(4)
C(8)-C(9)	1.380(4)
C(9)-C(10)	1.379(4)
C(10)-C(11)	1.396(4)
C(11)-C(15)	1.522(4)
C(12)-C(13)	1.523(4)
C(12)-C(14)	1.526(4)
C(15)-C(17)	1.528(4)
C(15)-C(16)	1.533(4)
C(18)-C(19)	1.399(4)
C(18)-C(23)	1.414(4)
C(19)-C(20)	1.392(4)
C(19)-C(24)	1.521(4)
C(20)-C(21)	1.379(5)
C(21)-C(22)	1.381(5)
C(22)-C(23)	1.391(4)
C(23)-C(27)	1.523(4)
C(24)-C(26)	1.508(5)
C(24)-C(25)	1.538(5)
C(27)-C(29)	1.519(4)
C(27)-C(28)	1.534(4)
C(30)-C(35)	1.528(4)
C(30)-C(31)	1.533(4)
C(31)-C(32)	1.525(4)

C(32)-C(33)	1.527(4)
C(33)-C(34)	1.525(4)
C(34)-C(35)	1.528(4)
C(36)-C(41)	1.530(4)
C(36)-C(37)	1.539(4)
C(37)-C(38)	1.529(4)
C(38)-C(39)	1.521(4)
C(39)-C(40)	1.512(4)
C(40)-C(41)	1.537(4)

N(2)-Sn-N(1)	83.23(8)
N(2)-Sn-P	99.95(6)
N(1)-Sn-P	102.60(6)
C(30)-P-C(36)	103.30(12)
C(30)-P-Sn	95.33(9)
C(36)-P-Sn	96.18(8)
C(1)-N(1)-C(6)	119.2(2)
C(1)-N(1)-Sn	118.50(16)
C(6)-N(1)-Sn	120.05(15)
C(3)-N(2)-C(18)	120.1(2)
C(3)-N(2)-Sn	119.85(17)
C(18)-N(2)-Sn	118.71(16)
N(1)-C(1)-C(2)	124.1(2)
N(1)-C(1)-C(4)	120.4(2)
C(2)-C(1)-C(4)	115.5(2)
C(1)-C(2)-C(3)	128.7(2)
N(2)-C(3)-C(2)	124.0(2)
N(2)-C(3)-C(5)	120.0(2)
C(2)-C(3)-C(5)	116.0(2)
C(11)-C(6)-C(7)	121.3(2)
C(11)-C(6)-N(1)	119.9(2)
C(7)-C(6)-N(1)	118.8(2)
C(8)-C(7)-C(6)	118.1(2)
C(8)-C(7)-C(12)	121.2(2)
C(6)-C(7)-C(12)	120.7(2)
C(9)-C(8)-C(7)	121.2(3)
C(10)-C(9)-C(8)	120.3(3)
C(9)-C(10)-C(11)	120.9(3)
C(10)-C(11)-C(6)	118.1(2)
C(10)-C(11)-C(15)	119.4(2)
C(6)-C(11)-C(15)	122.4(2)
C(13)-C(12)-C(7)	111.6(2)

C(13)-C(12)-C(14)	109.9(3)
C(7)-C(12)-C(14)	113.4(2)
C(11)-C(15)-C(17)	110.7(2)
C(11)-C(15)-C(16)	112.9(2)
C(17)-C(15)-C(16)	109.6(2)
C(19)-C(18)-C(23)	121.6(3)
C(19)-C(18)-N(2)	119.3(2)
C(23)-C(18)-N(2)	119.2(2)
C(20)-C(19)-C(18)	118.1(3)
C(20)-C(19)-C(24)	120.3(3)
C(18)-C(19)-C(24)	121.5(3)
C(21)-C(20)-C(19)	121.4(3)
C(20)-C(21)-C(22)	119.8(3)
C(21)-C(22)-C(23)	121.6(3)
C(22)-C(23)-C(18)	117.5(3)
C(22)-C(23)-C(27)	120.2(3)
C(18)-C(23)-C(27)	122.2(2)
C(26)-C(24)-C(19)	113.3(3)
C(26)-C(24)-C(25)	109.4(3)
C(19)-C(24)-C(25)	110.6(3)
C(29)-C(27)-C(23)	112.6(2)
C(29)-C(27)-C(28)	109.3(3)
C(23)-C(27)-C(28)	110.9(3)
C(35)-C(30)-C(31)	108.7(2)
C(35)-C(30)-P	109.13(19)
C(31)-C(30)-P	113.09(19)
C(32)-C(31)-C(30)	111.8(2)
C(31)-C(32)-C(33)	111.5(3)
C(34)-C(33)-C(32)	110.5(3)
C(33)-C(34)-C(35)	111.4(3)
C(30)-C(35)-C(34)	111.9(2)
C(41)-C(36)-C(37)	110.5(2)
C(41)-C(36)-P	116.44(18)
C(37)-C(36)-P	111.71(19)
C(38)-C(37)-C(36)	111.7(2)
C(39)-C(38)-C(37)	111.4(2)
C(40)-C(39)-C(38)	111.3(3)
C(39)-C(40)-C(41)	110.9(2)
C(36)-C(41)-C(40)	111.9(2)

Table A47. Crystal data and structure refinement for [(BDI_{DIPP})PbPCy₂] (**38**)

Identification code	dec509	
Empirical formula	C ₄₁ H ₆₃ N ₂ P Pb	
Formula weight	822.09	
Temperature	173(2) K	
Wavelength	0.71073 Å	
Crystal system	Monoclinic	
Space group	<i>P</i> 2 ₁ / <i>c</i> (No.14)	
Unit cell dimensions	a = 9.9586(2) Å	a = 90°.
	b = 23.7678(4) Å	b = 108.531(1)°.
	c = 17.4757(2) Å	g = 90°.
Volume	3921.93(11) Å ³	
Z	4	
Density (calculated)	1.39 Mg/m ³	
Absorption coefficient	4.37 mm ⁻¹	
F(000)	1680	
Crystal size	0.22 x 0.11 x 0.04 mm ³	
Theta range for data collection	3.43 to 27.09°.	
Index ranges	-12 ≤ h ≤ 12, -30 ≤ k ≤ 30, -22 ≤ l ≤ 22	
Reflections collected	57828	
Independent reflections	8624 [R(int) = 0.068]	
Reflections with I > 2σ(I)	6904	
Completeness to theta = 27.09°	99.7 %	
Absorption correction	Semi-empirical from equivalents	
Tmax. and Tmin.	0.6490 and 0.5526	
Refinement method	Full-matrix least-squares on F ²	
Data / restraints / parameters	8624 / 0 / 408	
Goodness-of-fit on F ²	1.031	
Final R indices [I > 2σ(I)]	R1 = 0.029, wR2 = 0.054	
R indices (all data)	R1 = 0.047, wR2 = 0.058	
Largest diff. peak and hole	0.99 and -0.97 e.Å ⁻³	

Isomorphous with the tin analogue

Data collection KappaCCD , Program package WinGX , Abs correction MULTISCAN
Refinement using SHELXL-97 , Drawing using ORTEP-3 for Windows

Table A48. Atomic coordinates ($\times 10^4$) and equivalent isotropic displacement parameters ($\text{\AA}^2 \times 10^3$) for [(BDI_{DIPP})PbPCy₂] (**38**). U(eq) is defined as one third of the trace of the orthogonalized U^{ij} tensor

	x	y	z	U(eq)
Pb	1749(1)	8172(1)	2829(1)	20(1)
P	1484(1)	8295(1)	1255(1)	26(1)
N(1)	3452(3)	8854(1)	3436(2)	19(1)
N(2)	3751(3)	7602(1)	3222(2)	23(1)
C(1)	4437(3)	8728(1)	4126(2)	22(1)
C(2)	4913(4)	8181(1)	4379(2)	27(1)
C(3)	4733(4)	7679(1)	3930(2)	25(1)
C(4)	5168(4)	9190(2)	4698(2)	34(1)
C(5)	5753(4)	7209(2)	4301(2)	41(1)
C(6)	3177(3)	9429(1)	3191(2)	21(1)
C(7)	3792(3)	9649(1)	2633(2)	26(1)
C(8)	3531(4)	10208(2)	2402(2)	34(1)
C(9)	2658(4)	10540(2)	2694(2)	40(1)
C(10)	2022(4)	10313(2)	3223(2)	33(1)
C(11)	2260(4)	9755(1)	3478(2)	26(1)
C(12)	4723(4)	9284(2)	2296(2)	31(1)
C(13)	6262(4)	9284(2)	2840(3)	51(1)
C(14)	4657(5)	9439(2)	1435(2)	51(1)
C(15)	1474(4)	9514(2)	4018(2)	27(1)
C(16)	1756(4)	9834(2)	4813(2)	38(1)
C(17)	-118(4)	9492(2)	3571(2)	38(1)
C(18)	3735(4)	7098(1)	2766(2)	25(1)
C(19)	4469(4)	7092(2)	2202(2)	34(1)
C(20)	4356(5)	6613(2)	1727(3)	45(1)
C(21)	3559(5)	6159(2)	1807(3)	47(1)
C(22)	2855(4)	6167(2)	2374(2)	39(1)
C(23)	2934(4)	6633(1)	2870(2)	30(1)
C(24)	5428(4)	7578(2)	2141(3)	45(1)
C(25)	6995(6)	7415(3)	2520(4)	102(2)
C(26)	5178(6)	7778(2)	1287(3)	65(1)
C(27)	2207(4)	6619(2)	3515(2)	37(1)
C(28)	626(4)	6530(2)	3179(2)	46(1)

C(29)	2879(5)	6164(2)	4152(3)	56(1)
C(30)	-198(4)	8715(1)	1031(2)	25(1)
C(31)	-1009(4)	8758(2)	127(2)	34(1)
C(32)	-2342(4)	9116(2)	-31(2)	41(1)
C(33)	-1996(5)	9705(2)	323(2)	45(1)
C(34)	-1153(4)	9674(2)	1219(2)	46(1)
C(35)	169(4)	9308(2)	1370(2)	34(1)
C(36)	848(4)	7554(1)	963(2)	27(1)
C(37)	795(4)	7414(2)	95(2)	34(1)
C(38)	426(5)	6795(2)	-114(2)	41(1)
C(39)	-964(5)	6640(2)	24(2)	39(1)
C(40)	-908(4)	6765(2)	886(2)	36(1)
C(41)	-551(4)	7382(1)	1092(2)	27(1)

Table A49. Bond lengths [Å] and angles [deg] for [(BDI_{DIPP})PbPCy₂] (**38**)

Pb-N(2)	2.326(3)
Pb-N(1)	2.342(3)
Pb-P	2.6945(9)
P-C(30)	1.880(3)
P-C(36)	1.887(3)
N(1)-C(1)	1.325(4)
N(1)-C(6)	1.433(4)
N(2)-C(3)	1.324(4)
N(2)-C(18)	1.436(4)
C(1)-C(2)	1.407(5)
C(1)-C(4)	1.508(5)
C(2)-C(3)	1.408(5)
C(3)-C(5)	1.510(5)
C(6)-C(11)	1.406(5)
C(6)-C(7)	1.406(5)
C(7)-C(8)	1.389(5)
C(7)-C(12)	1.520(5)
C(8)-C(9)	1.384(5)
C(9)-C(10)	1.384(5)
C(10)-C(11)	1.397(5)
C(11)-C(15)	1.516(5)
C(12)-C(13)	1.526(5)
C(12)-C(14)	1.531(5)
C(15)-C(17)	1.529(5)
C(15)-C(16)	1.530(5)
C(18)-C(19)	1.401(5)
C(18)-C(23)	1.408(5)
C(19)-C(20)	1.393(5)
C(19)-C(24)	1.524(6)
C(20)-C(21)	1.372(6)
C(21)-C(22)	1.384(6)
C(22)-C(23)	1.395(5)
C(23)-C(27)	1.522(5)
C(24)-C(26)	1.510(6)
C(24)-C(25)	1.539(7)
C(27)-C(28)	1.511(6)
C(27)-C(29)	1.543(5)
C(30)-C(35)	1.529(5)
C(30)-C(31)	1.532(4)
C(31)-C(32)	1.526(5)

C(32)-C(33)	1.525(5)
C(33)-C(34)	1.526(5)
C(34)-C(35)	1.528(5)
C(36)-C(41)	1.535(5)
C(36)-C(37)	1.538(5)
C(37)-C(38)	1.532(5)
C(38)-C(39)	1.524(6)
C(39)-C(40)	1.518(5)
C(40)-C(41)	1.525(5)

N(2)-Pb-N(1)	80.79(9)
N(2)-Pb-P	99.25(7)
N(1)-Pb-P	102.03(7)
C(30)-P-C(36)	103.79(15)
C(30)-P-Pb	93.57(11)
C(36)-P-Pb	95.17(11)
C(1)-N(1)-C(6)	120.3(3)
C(1)-N(1)-Pb	118.4(2)
C(6)-N(1)-Pb	118.89(19)
C(3)-N(2)-C(18)	120.5(3)
C(3)-N(2)-Pb	120.3(2)
C(18)-N(2)-Pb	117.7(2)
N(1)-C(1)-C(2)	125.0(3)
N(1)-C(1)-C(4)	120.0(3)
C(2)-C(1)-C(4)	115.0(3)
C(1)-C(2)-C(3)	129.7(3)
N(2)-C(3)-C(2)	124.2(3)
N(2)-C(3)-C(5)	119.8(3)
C(2)-C(3)-C(5)	116.0(3)
C(11)-C(6)-C(7)	121.2(3)
C(11)-C(6)-N(1)	120.2(3)
C(7)-C(6)-N(1)	118.5(3)
C(8)-C(7)-C(6)	118.3(3)
C(8)-C(7)-C(12)	121.0(3)
C(6)-C(7)-C(12)	120.6(3)
C(9)-C(8)-C(7)	121.2(3)
C(10)-C(9)-C(8)	119.9(3)
C(9)-C(10)-C(11)	121.1(4)
C(10)-C(11)-C(6)	118.2(3)
C(10)-C(11)-C(15)	119.3(3)
C(6)-C(11)-C(15)	122.5(3)
C(7)-C(12)-C(13)	111.9(3)

C(7)-C(12)-C(14)	113.7(3)
C(13)-C(12)-C(14)	109.5(3)
C(11)-C(15)-C(17)	110.5(3)
C(11)-C(15)-C(16)	113.3(3)
C(17)-C(15)-C(16)	110.0(3)
C(19)-C(18)-C(23)	121.7(3)
C(19)-C(18)-N(2)	118.9(3)
C(23)-C(18)-N(2)	119.3(3)
C(20)-C(19)-C(18)	117.8(4)
C(20)-C(19)-C(24)	120.8(4)
C(18)-C(19)-C(24)	121.3(3)
C(21)-C(20)-C(19)	121.4(4)
C(20)-C(21)-C(22)	120.2(4)
C(21)-C(22)-C(23)	121.0(4)
C(22)-C(23)-C(18)	117.8(4)
C(22)-C(23)-C(27)	119.8(3)
C(18)-C(23)-C(27)	122.4(3)
C(26)-C(24)-C(19)	113.4(4)
C(26)-C(24)-C(25)	109.3(4)
C(19)-C(24)-C(25)	110.6(4)
C(28)-C(27)-C(23)	113.4(3)
C(28)-C(27)-C(29)	110.0(3)
C(23)-C(27)-C(29)	110.6(4)
C(35)-C(30)-C(31)	108.7(3)
C(35)-C(30)-P	108.7(2)
C(31)-C(30)-P	113.1(2)
C(32)-C(31)-C(30)	111.5(3)
C(33)-C(32)-C(31)	111.5(3)
C(32)-C(33)-C(34)	110.6(3)
C(33)-C(34)-C(35)	111.6(3)
C(34)-C(35)-C(30)	111.8(3)
C(41)-C(36)-C(37)	109.8(3)
C(41)-C(36)-P	116.8(2)
C(37)-C(36)-P	111.9(2)
C(38)-C(37)-C(36)	111.9(3)
C(39)-C(38)-C(37)	110.8(3)
C(40)-C(39)-C(38)	111.1(3)
C(39)-C(40)-C(41)	110.8(3)
C(40)-C(41)-C(36)	112.1(3)

Table A50. Crystal data and structure refinement for [(BDI_{DIPP})SnⁿBu] (**39**)

Identification code	nov409b	
Empirical formula	C ₃₃ H ₅₀ N ₂ Sn	
Formula weight	593.46	
Temperature	173(2) K	
Wavelength	0.71073 Å	
Crystal system	Orthorhombic	
Space group	<i>F d d 2</i> (No.43)	
Unit cell dimensions	a = 23.1850(4) Å	a = 90°.
	b = 63.1825(9) Å	b = 90°.
	c = 8.9095(1) Å	g = 90°.
Volume	13051.4(3) Å ³	
Z	16	
Density (calculated)	1.21 Mg/m ³	
Absorption coefficient	0.80 mm ⁻¹	
F(000)	4992	
Crystal size	0.24 x 0.08 x 0.06 mm ³	
Theta range for data collection	3.50 to 27.49°.	
Index ranges	-29 ≤ h ≤ 29, -81 ≤ k ≤ 82, -11 ≤ l ≤ 11	
Reflections collected	39667	
Independent reflections	7387 [R(int) = 0.061]	
Reflections with I > 2σ(I)	6472	
Completeness to theta = 27.49°	99.2 %	
Absorption correction	Semi-empirical from equivalents	
Tmax. and Tmin.	0.9937 and 0.8389	
Refinement method	Full-matrix least-squares on F ²	
Data / restraints / parameters	7387 / 17 / 364	
Goodness-of-fit on F ²	1.056	
Final R indices [I > 2σ(I)]	R1 = 0.038, wR2 = 0.078	
R indices (all data)	R1 = 0.049, wR2 = 0.083	
Absolute structure parameter	-0.03(2)	
Largest diff. peak and hole	0.48 and -0.61 e.Å ⁻³	

The *n*-butyl substituent was disordered over two positions

Data collection KappaCCD , Program package WinGX , Abs correction MULTISCAN
Refinement using SHELXL-97 , Drawing using ORTEP-3 for Windows

Table A51. Atomic coordinates ($\times 10^4$) and equivalent isotropic displacement parameters ($\text{\AA}^2 \times 10^3$) for [(BDI_{DIPP})SnⁿBu] (**39**). U(eq) is defined as one third of the trace of the orthogonalized U^{ij} tensor

	x	y	z	U(eq)
Sn	472(1)	436(1)	-2(1)	42(1)
N(1)	384(1)	557(1)	2312(3)	35(1)
N(2)	1386(1)	527(1)	331(3)	32(1)
C(1)	782(2)	510(1)	3337(4)	38(1)
C(2)	1346(2)	456(1)	2987(4)	39(1)
C(3)	1644(2)	488(1)	1620(4)	34(1)
C(4)	623(2)	513(1)	4981(6)	55(1)
C(5)	2289(2)	480(1)	1708(4)	52(1)
C(6)	-161(1)	649(1)	2710(4)	39(1)
C(7)	-204(2)	870(1)	2809(4)	47(1)
C(8)	-745(2)	960(1)	3059(5)	64(1)
C(9)	-1229(2)	833(1)	3230(6)	76(2)
C(10)	-1176(2)	614(1)	3144(6)	70(1)
C(11)	-645(2)	521(1)	2886(4)	51(1)
C(12)	317(2)	1012(1)	2641(5)	56(1)
C(13)	202(3)	1213(1)	1721(6)	85(2)
C(14)	558(3)	1078(1)	4184(7)	84(2)
C(15)	-618(2)	280(1)	2793(6)	65(1)
C(16)	-990(3)	192(1)	1542(7)	90(2)
C(17)	-784(3)	179(1)	4314(7)	99(2)
C(18)	1714(1)	569(1)	-1002(4)	37(1)
C(19)	1791(2)	780(1)	-1459(4)	46(1)
C(20)	2095(2)	816(1)	-2782(5)	61(1)
C(21)	2313(2)	655(1)	-3618(5)	64(1)
C(22)	2233(2)	449(1)	-3177(5)	54(1)
C(23)	1930(2)	402(1)	-1856(4)	39(1)
C(24)	1564(2)	960(1)	-528(5)	56(1)
C(25)	2014(3)	1044(1)	570(8)	102(2)
C(26)	1329(3)	1146(1)	-1460(7)	83(2)
C(27)	1850(2)	170(1)	-1410(4)	46(1)
C(28)	2426(2)	54(1)	-1281(5)	72(1)
C(29)	1452(2)	56(1)	-2527(6)	62(1)

C(30)	127(8)	719(3)	-1100(40)	59(6) ^a
C(31)	-494(4)	653(2)	-1470(12)	63(2) ^a
C(32)	-789(4)	817(2)	-2398(14)	79(3) ^a
C(33)	-1405(7)	722(4)	-2580(40)	148(11) ^a
C(30A)	240(10)	724(3)	-1240(40)	56(7) ^b
C(31A)	-326(3)	735(2)	-2138(11)	52(2) ^b
C(32A)	-847(4)	767(2)	-1139(11)	60(2) ^b
C(33A)	-1409(7)	760(3)	-2120(30)	84(7) ^b

a 53.4 %, *b* 46.6 %

Table A52. Bond lengths [Å] and angles [deg] for [(BDI_{DIPP})SnⁿBu] (**39**)

Sn-C(30)	2.189(11)
Sn-N(1)	2.209(3)
Sn-N(2)	2.216(2)
N(1)-C(1)	1.331(4)
N(1)-C(6)	1.436(4)
N(2)-C(3)	1.317(4)
N(2)-C(18)	1.435(4)
C(1)-C(2)	1.387(5)
C(1)-C(4)	1.510(6)
C(2)-C(3)	1.415(5)
C(3)-C(5)	1.499(5)
C(6)-C(11)	1.391(5)
C(6)-C(7)	1.403(5)
C(7)-C(8)	1.397(6)
C(7)-C(12)	1.515(6)
C(8)-C(9)	1.389(7)
C(9)-C(10)	1.389(8)
C(10)-C(11)	1.384(6)
C(11)-C(15)	1.527(6)
C(12)-C(13)	1.534(7)
C(12)-C(14)	1.539(7)
C(15)-C(16)	1.515(7)
C(15)-C(17)	1.546(7)
C(18)-C(23)	1.396(5)
C(18)-C(19)	1.405(5)
C(19)-C(20)	1.393(6)
C(19)-C(24)	1.502(6)
C(20)-C(21)	1.356(7)
C(21)-C(22)	1.377(7)
C(22)-C(23)	1.403(5)
C(23)-C(27)	1.529(6)
C(24)-C(25)	1.525(7)
C(24)-C(26)	1.536(6)
C(27)-C(28)	1.527(6)
C(27)-C(29)	1.535(6)
C(30)-C(31)	1.536(12)

C(31)-C(32)	1.494(10)
C(32)-C(33)	1.561(14)
C(30)-Sn-N(1)	95.6(11)
C(30)-Sn-N(2)	101.3(4)
N(1)-Sn-N(2)	82.72(9)
C(1)-N(1)-C(6)	122.0(3)
C(1)-N(1)-Sn	119.9(2)
C(6)-N(1)-Sn	116.9(2)
C(3)-N(2)-C(18)	121.1(3)
C(3)-N(2)-Sn	120.0(2)
C(18)-N(2)-Sn	116.39(18)
N(1)-C(1)-C(2)	123.6(3)
N(1)-C(1)-C(4)	119.6(3)
C(2)-C(1)-C(4)	116.8(3)
C(1)-C(2)-C(3)	128.2(3)
N(2)-C(3)-C(2)	123.8(3)
N(2)-C(3)-C(5)	120.2(3)
C(2)-C(3)-C(5)	115.9(3)
C(11)-C(6)-C(7)	121.0(3)
C(11)-C(6)-N(1)	120.2(3)
C(7)-C(6)-N(1)	118.7(3)
C(8)-C(7)-C(6)	118.7(4)
C(8)-C(7)-C(12)	119.4(4)
C(6)-C(7)-C(12)	122.0(3)
C(9)-C(8)-C(7)	120.3(4)
C(10)-C(9)-C(8)	120.1(4)
C(11)-C(10)-C(9)	120.6(5)
C(10)-C(11)-C(6)	119.3(4)
C(10)-C(11)-C(15)	117.9(4)
C(6)-C(11)-C(15)	122.7(3)
C(7)-C(12)-C(13)	113.9(4)
C(7)-C(12)-C(14)	111.1(4)
C(13)-C(12)-C(14)	108.6(4)
C(16)-C(15)-C(11)	112.4(4)
C(16)-C(15)-C(17)	110.7(4)
C(11)-C(15)-C(17)	110.8(4)
C(23)-C(18)-C(19)	121.1(3)

C(23)-C(18)-N(2)	120.0(3)
C(19)-C(18)-N(2)	118.8(3)
C(20)-C(19)-C(18)	117.7(4)
C(20)-C(19)-C(24)	121.3(4)
C(18)-C(19)-C(24)	120.9(3)
C(21)-C(20)-C(19)	122.0(4)
C(20)-C(21)-C(22)	120.2(4)
C(21)-C(22)-C(23)	120.6(4)
C(18)-C(23)-C(22)	118.3(4)
C(18)-C(23)-C(27)	122.8(3)
C(22)-C(23)-C(27)	118.8(4)
C(19)-C(24)-C(25)	112.3(4)
C(19)-C(24)-C(26)	113.8(4)
C(25)-C(24)-C(26)	108.8(4)
C(28)-C(27)-C(23)	112.0(4)
C(28)-C(27)-C(29)	110.5(4)
C(23)-C(27)-C(29)	110.6(3)
C(31)-C(30)-Sn	102.6(7)
C(32)-C(31)-C(30)	111.0(8)
C(31)-C(32)-C(33)	101.9(15)

Table A53. Crystal data and structure refinement for [(BDI_{DIPP})SnP(SiMe₃)₂] (**41**)

Identification code	mar210	
Empirical formula	C ₃₅ H ₅₉ N ₂ P Si ₂ Sn	
Formula weight	713.68	
Temperature	173(2) K	
Wavelength	0.71073 Å	
Crystal system	Monoclinic	
Space group	<i>P</i> 2 ₁ /c (No.14)	
Unit cell dimensions	a = 12.1569(2) Å	a = 90°.
	b = 15.7065(2) Å	b = 119.547(1)°.
	c = 23.4050(4) Å	g = 90°.
Volume	3887.82(10) Å ³	
Z	4	
Density (calculated)	1.22 Mg/m ³	
Absorption coefficient	0.78 mm ⁻¹	
F(000)	1504	
Crystal size	0.18 x 0.10 x 0.06 mm ³	
Theta range for data collection	3.48 to 27.10°.	
Index ranges	-15 ≤ h ≤ 15, -19 ≤ k ≤ 20, -29 ≤ l ≤ 29	
Reflections collected	60531	
Independent reflections	8547 [R(int) = 0.076]	
Completeness to theta = 27.10°	99.7 %	
Tmax. and Tmin	0.9663 and 0.8629	
Refinement method	Full-matrix least-squares on F ²	
Data / restraints / parameters	8547 / 0 / 372	
Goodness-of-fit on F ²	0.991	
Final R indices [I > 2σ(I)]	R1 = 0.034, wR2 = 0.070	
R indices (all data)	R1 = 0.056, wR2 = 0.078	
Largest diff. peak and hole	0.45 and -0.69 e.Å ⁻³	

Data collection KappaCCD , Program package WinGX , Abs correction MULTISCAN

Refinement using SHELXL-97 , Drawing using ORTEP-3 for Windows

Table A54. Atomic coordinates ($\times 10^4$) and equivalent isotropic displacement parameters ($\text{\AA}^2 \times 10^3$) for $[(\text{BDI}_{\text{DIPP}})\text{SnP}(\text{SiMe}_3)_2]$ (**41**). $U(\text{eq})$ is defined as one third of the trace of the orthogonalized U^{ij} tensor

	x	y	z	U(eq)
Sn	2275(1)	1626(1)	1538(1)	20(1)
P	3773(1)	2822(1)	1625(1)	37(1)
Si(1)	5291(1)	2342(1)	1445(1)	33(1)
Si(2)	3781(1)	4234(1)	1670(1)	34(1)
N(1)	401(2)	2206(1)	888(1)	22(1)
N(2)	1998(2)	2088(1)	2355(1)	21(1)
C(1)	-104(2)	2839(2)	1061(1)	27(1)
C(2)	338(3)	3098(2)	1709(1)	32(1)
C(3)	1209(3)	2705(2)	2300(1)	29(1)
C(4)	-1260(3)	3303(2)	546(1)	41(1)
C(5)	1176(4)	3015(2)	2905(2)	52(1)
C(6)	-271(2)	1882(2)	223(1)	26(1)
C(7)	-150(2)	2283(2)	-281(1)	32(1)
C(8)	-824(3)	1947(2)	-913(1)	47(1)
C(9)	-1574(3)	1242(2)	-1043(2)	51(1)
C(10)	-1662(3)	841(2)	-546(2)	44(1)
C(11)	-1019(2)	1144(2)	99(1)	31(1)
C(12)	687(3)	3049(2)	-171(1)	40(1)
C(13)	1759(3)	2812(3)	-307(2)	58(1)
C(14)	-64(4)	3812(3)	-596(2)	66(1)
C(15)	-1150(3)	694(2)	635(2)	37(1)
C(16)	-2060(3)	1157(2)	806(2)	51(1)
C(17)	-1570(3)	-232(2)	470(2)	60(1)
C(18)	2643(2)	1632(2)	2974(1)	24(1)
C(19)	3834(3)	1888(2)	3471(1)	33(1)
C(20)	4391(3)	1428(2)	4058(1)	43(1)
C(21)	3797(3)	740(2)	4149(2)	44(1)
C(22)	2637(3)	493(2)	3656(2)	39(1)
C(23)	2033(3)	926(2)	3059(1)	28(1)
C(24)	4547(3)	2635(2)	3397(2)	49(1)
C(25)	4784(5)	3334(3)	3908(2)	93(2)
C(26)	5791(3)	2331(3)	3449(2)	75(1)

C(27)	764(3)	615(2)	2520(2)	36(1)
C(28)	-240(3)	572(2)	2731(2)	54(1)
C(29)	943(3)	-249(2)	2282(2)	52(1)
C(30)	4928(3)	1211(2)	1165(2)	63(1)
C(31)	5450(3)	2980(3)	816(2)	58(1)
C(32)	6885(3)	2366(2)	2196(2)	53(1)
C(33)	3148(3)	4755(2)	847(2)	58(1)
C(34)	5430(3)	4619(2)	2193(2)	57(1)
C(35)	2807(4)	4601(2)	2035(2)	65(1)

Table A55. Bond lengths [Å] and angles [deg] for [(BDI_{DIPP})SnP(SiMe₃)₂] (**41**)

Sn-N(1)	2.217(2)
Sn-N(2)	2.2210(19)
Sn-P	2.5526(7)
P-Si(1)	2.2166(10)
P-Si(2)	2.2215(11)
Si(1)-C(32)	1.866(3)
Si(1)-C(31)	1.868(3)
Si(1)-C(30)	1.870(3)
Si(2)-C(34)	1.861(3)
Si(2)-C(35)	1.861(3)
Si(2)-C(33)	1.873(3)
N(1)-C(1)	1.331(3)
N(1)-C(6)	1.448(3)
N(2)-C(3)	1.324(3)
N(2)-C(18)	1.452(3)
C(1)-C(2)	1.397(4)
C(1)-C(4)	1.514(4)
C(2)-C(3)	1.404(4)
C(3)-C(5)	1.516(4)
C(6)-C(7)	1.405(4)
C(6)-C(11)	1.413(4)
C(7)-C(8)	1.394(4)
C(7)-C(12)	1.514(4)
C(8)-C(9)	1.370(5)
C(9)-C(10)	1.373(5)
C(10)-C(11)	1.397(4)
C(11)-C(15)	1.516(4)
C(12)-C(13)	1.532(4)
C(12)-C(14)	1.538(4)
C(15)-C(17)	1.528(4)
C(15)-C(16)	1.532(4)
C(18)-C(19)	1.396(4)
C(18)-C(23)	1.401(4)
C(19)-C(20)	1.397(4)
C(19)-C(24)	1.518(4)
C(20)-C(21)	1.373(4)

C(21)-C(22)	1.366(4)
C(22)-C(23)	1.393(4)
C(23)-C(27)	1.514(4)
C(24)-C(26)	1.533(5)
C(24)-C(25)	1.542(5)
C(27)-C(29)	1.522(4)
C(27)-C(28)	1.527(4)
N(1)-Sn-N(2)	85.17(7)
N(1)-Sn-P	101.77(5)
N(2)-Sn-P	95.55(5)
Si(1)-P-Si(2)	111.32(4)
Si(1)-P-Sn	111.29(4)
Si(2)-P-Sn	136.45(4)
C(32)-Si(1)-C(31)	105.55(17)
C(32)-Si(1)-C(30)	107.77(17)
C(31)-Si(1)-C(30)	109.33(18)
C(32)-Si(1)-P	112.97(12)
C(31)-Si(1)-P	112.72(11)
C(30)-Si(1)-P	108.35(11)
C(34)-Si(2)-C(35)	108.67(18)
C(34)-Si(2)-C(33)	107.35(16)
C(35)-Si(2)-C(33)	107.81(18)
C(34)-Si(2)-P	109.46(11)
C(35)-Si(2)-P	109.98(11)
C(33)-Si(2)-P	113.44(12)
C(1)-N(1)-C(6)	119.2(2)
C(1)-N(1)-Sn	124.76(17)
C(6)-N(1)-Sn	115.96(14)
C(3)-N(2)-C(18)	117.9(2)
C(3)-N(2)-Sn	124.42(16)
C(18)-N(2)-Sn	117.48(14)
N(1)-C(1)-C(2)	124.0(2)
N(1)-C(1)-C(4)	120.3(2)
C(2)-C(1)-C(4)	115.7(2)
C(1)-C(2)-C(3)	129.9(2)
N(2)-C(3)-C(2)	125.1(2)
N(2)-C(3)-C(5)	119.7(2)

C(2)-C(3)-C(5)	115.1(2)
C(7)-C(6)-C(11)	121.2(2)
C(7)-C(6)-N(1)	120.5(2)
C(11)-C(6)-N(1)	118.3(2)
C(8)-C(7)-C(6)	118.1(3)
C(8)-C(7)-C(12)	118.3(3)
C(6)-C(7)-C(12)	123.6(2)
C(9)-C(8)-C(7)	121.4(3)
C(8)-C(9)-C(10)	120.2(3)
C(9)-C(10)-C(11)	121.6(3)
C(10)-C(11)-C(6)	117.6(3)
C(10)-C(11)-C(15)	120.3(3)
C(6)-C(11)-C(15)	122.2(2)
C(7)-C(12)-C(13)	109.9(3)
C(7)-C(12)-C(14)	112.0(3)
C(13)-C(12)-C(14)	110.5(3)
C(11)-C(15)-C(17)	113.2(3)
C(11)-C(15)-C(16)	112.3(2)
C(17)-C(15)-C(16)	108.9(3)
C(19)-C(18)-C(23)	121.0(2)
C(19)-C(18)-N(2)	121.1(2)
C(23)-C(18)-N(2)	117.9(2)
C(18)-C(19)-C(20)	118.0(3)
C(18)-C(19)-C(24)	123.0(2)
C(20)-C(19)-C(24)	119.0(3)
C(21)-C(20)-C(19)	121.5(3)
C(22)-C(21)-C(20)	119.6(3)
C(21)-C(22)-C(23)	121.5(3)
C(22)-C(23)-C(18)	118.3(3)
C(22)-C(23)-C(27)	119.6(2)
C(18)-C(23)-C(27)	122.0(2)
C(19)-C(24)-C(26)	110.3(3)
C(19)-C(24)-C(25)	111.2(3)
C(26)-C(24)-C(25)	111.2(3)
C(23)-C(27)-C(29)	108.8(2)
C(23)-C(27)-C(28)	113.1(3)
C(29)-C(27)-C(28)	111.1(2)

Table A56. Crystal data and structure refinement for [(BDI_{DIPP})SnSePCy₂] (46)

Identification code	dec1009	
Empirical formula	C ₄₁ H ₆₃ N ₂ P Se Sn	
Formula weight	812.55	
Temperature	173(2) K	
Wavelength	0.71073 Å	
Crystal system	Triclinic	
Space group	P $\bar{1}$ (No.2)	
Unit cell dimensions	a = 12.1426(2) Å	a = 91.844(1)°.
	b = 12.5330(3) Å	b = 97.593(1)°.
	c = 14.2375(3) Å	g = 108.807(1)°.
Volume	2026.58(7) Å ³	
Z	2	
Density (calculated)	1.33 Mg/m ³	
Absorption coefficient	1.60 mm ⁻¹	
F(000)	844	
Crystal size	0.21 x 0.10 x 0.08 mm ³	
Theta range for data collection	3.43 to 27.11°.	
Index ranges	-15 ≤ h ≤ 15, -16 ≤ k ≤ 16, -18 ≤ l ≤ 18	
Reflections collected	37018	
Independent reflections	8928 [R(int) = 0.051]	
Reflections with I > 2σ(I)	7625	
Completeness to theta = 27.11°	99.7 %	
Absorption correction	Semi-empirical from equivalents	
Tmax. and Tmin.	0.8561 and 0.7410	
Refinement method	Full-matrix least-squares on F ²	
Data / restraints / parameters	8928 / 0 / 417	
Goodness-of-fit on F ²	1.032	
Final R indices [I > 2σ(I)]	R1 = 0.030, wR2 = 0.064	
R indices (all data)	R1 = 0.040, wR2 = 0.068	
Largest diff. peak and hole	0.42 and -0.62 e.Å ⁻³	

Data collection KappaCCD , Program package WinGX , Abs correction MULTISCAN

Refinement using SHELXL-97 , Drawing using ORTEP-3 for Windows

Table A57. Atomic coordinates ($\times 10^4$) and equivalent isotropic displacement parameters ($\text{\AA}^2 \times 10^3$) for $[(\text{BDI}_{\text{DIPP}})\text{SnSePCy}_2]$ (**46**). $U(\text{eq})$ is defined as one third of the trace of the orthogonalized U^{ij} tensor

	x	y	z	U(eq)
Sn	7380(1)	6971(1)	2050(1)	22(1)
Se	8405(1)	9014(1)	2852(1)	28(1)
P	8692(1)	9714(1)	1429(1)	24(1)
N(1)	5774(2)	6484(2)	2742(1)	24(1)
N(2)	8038(2)	6124(2)	3227(1)	22(1)
C(1)	5390(2)	5472(2)	3070(2)	29(1)
C(2)	6113(2)	4823(2)	3340(2)	30(1)
C(3)	7351(2)	5172(2)	3517(2)	26(1)
C(4)	4102(2)	4958(2)	3177(2)	43(1)
C(5)	7889(2)	4425(2)	4087(2)	37(1)
C(6)	5010(2)	7148(2)	2539(2)	26(1)
C(7)	5059(2)	8006(2)	3224(2)	29(1)
C(8)	4333(2)	8657(2)	3004(2)	35(1)
C(9)	3612(2)	8483(2)	2137(2)	36(1)
C(10)	3612(2)	7672(2)	1467(2)	32(1)
C(11)	4301(2)	6979(2)	1648(2)	27(1)
C(12)	5861(2)	8214(2)	4174(2)	35(1)
C(13)	5247(3)	7530(3)	4936(2)	64(1)
C(14)	6384(3)	9466(3)	4527(2)	50(1)
C(15)	4259(2)	6087(2)	882(2)	30(1)
C(16)	2994(3)	5327(2)	510(2)	48(1)
C(17)	4836(2)	6626(2)	44(2)	37(1)
C(18)	9286(2)	6541(2)	3569(2)	24(1)
C(19)	9688(2)	7140(2)	4462(2)	32(1)
C(20)	10899(2)	7615(3)	4745(2)	42(1)
C(21)	11681(2)	7503(3)	4166(2)	47(1)
C(22)	11275(2)	6905(2)	3294(2)	40(1)
C(23)	10069(2)	6413(2)	2963(2)	28(1)
C(24)	8860(2)	7295(3)	5132(2)	43(1)
C(25)	8985(3)	6698(3)	6042(2)	54(1)
C(26)	9062(3)	8535(3)	5397(2)	58(1)
C(27)	9672(2)	5792(2)	1985(2)	33(1)

C(28)	10119(3)	4787(3)	1897(2)	52(1)
C(29)	10045(3)	6582(3)	1206(2)	45(1)
C(30)	7769(2)	10660(2)	1333(2)	27(1)
C(31)	8090(2)	11621(2)	2112(2)	36(1)
C(32)	7283(3)	12342(3)	1959(2)	47(1)
C(33)	6000(3)	11616(3)	1897(2)	49(1)
C(34)	5676(2)	10693(2)	1099(2)	42(1)
C(35)	6467(2)	9954(2)	1234(2)	35(1)
C(36)	10205(2)	10761(2)	1739(2)	26(1)
C(37)	10494(2)	11510(2)	914(2)	34(1)
C(38)	11739(3)	12354(2)	1107(2)	44(1)
C(39)	12652(3)	11792(3)	1365(2)	47(1)
C(40)	12366(2)	11058(2)	2187(2)	41(1)
C(41)	11135(2)	10180(2)	1971(2)	36(1)

Table A58. Bond lengths [Å] and angles [deg] for [(BDI_{DIPP})SnSePCy₂] (**46**)

Sn-N(2)	2.2097(18)
Sn-N(1)	2.2192(19)
Sn-Se	2.6059(3)
Se-P	2.2584(6)
P-C(36)	1.867(2)
P-C(30)	1.873(2)
N(1)-C(1)	1.327(3)
N(1)-C(6)	1.442(3)
N(2)-C(3)	1.330(3)
N(2)-C(18)	1.444(3)
C(1)-C(2)	1.404(3)
C(1)-C(4)	1.517(3)
C(2)-C(3)	1.408(3)
C(3)-C(5)	1.506(3)
C(6)-C(11)	1.404(3)
C(6)-C(7)	1.410(3)
C(7)-C(8)	1.396(4)
C(7)-C(12)	1.520(4)
C(8)-C(9)	1.382(4)
C(9)-C(10)	1.372(4)
C(10)-C(11)	1.395(3)
C(11)-C(15)	1.520(3)
C(12)-C(13)	1.527(4)
C(12)-C(14)	1.530(4)
C(15)-C(17)	1.529(4)
C(15)-C(16)	1.535(4)
C(18)-C(19)	1.399(3)
C(18)-C(23)	1.407(3)
C(19)-C(20)	1.395(4)
C(19)-C(24)	1.525(4)
C(20)-C(21)	1.373(4)
C(21)-C(22)	1.373(4)
C(22)-C(23)	1.401(4)
C(23)-C(27)	1.513(4)
C(24)-C(26)	1.520(4)
C(24)-C(25)	1.531(4)
C(27)-C(29)	1.527(4)
C(27)-C(28)	1.531(4)
C(30)-C(31)	1.525(3)
C(30)-C(35)	1.527(3)

C(31)-C(32)	1.533(4)
C(32)-C(33)	1.519(4)
C(33)-C(34)	1.513(4)
C(34)-C(35)	1.534(4)
C(36)-C(37)	1.534(3)
C(36)-C(41)	1.537(3)
C(37)-C(38)	1.523(4)
C(38)-C(39)	1.509(4)
C(39)-C(40)	1.518(4)
C(40)-C(41)	1.528(4)
N(2)-Sn-N(1)	82.68(7)
N(2)-Sn-Se	95.36(5)
N(1)-Sn-Se	99.31(5)
P-Se-Sn	91.388(17)
C(36)-P-C(30)	101.61(11)
C(36)-P-Se	100.61(8)
C(30)-P-Se	102.29(8)
C(1)-N(1)-C(6)	121.39(19)
C(1)-N(1)-Sn	120.33(15)
C(6)-N(1)-Sn	115.38(14)
C(3)-N(2)-C(18)	120.75(18)
C(3)-N(2)-Sn	121.39(15)
C(18)-N(2)-Sn	117.16(14)
N(1)-C(1)-C(2)	123.8(2)
N(1)-C(1)-C(4)	119.9(2)
C(2)-C(1)-C(4)	116.3(2)
C(1)-C(2)-C(3)	128.3(2)
N(2)-C(3)-C(2)	123.3(2)
N(2)-C(3)-C(5)	120.0(2)
C(2)-C(3)-C(5)	116.7(2)
C(11)-C(6)-C(7)	121.8(2)
C(11)-C(6)-N(1)	119.6(2)
C(7)-C(6)-N(1)	118.5(2)
C(8)-C(7)-C(6)	117.6(2)
C(8)-C(7)-C(12)	120.8(2)
C(6)-C(7)-C(12)	121.6(2)
C(9)-C(8)-C(7)	121.2(2)
C(10)-C(9)-C(8)	120.2(2)
C(9)-C(10)-C(11)	121.5(2)
C(10)-C(11)-C(6)	117.7(2)
C(10)-C(11)-C(15)	119.2(2)

C(6)-C(11)-C(15)	123.1(2)
C(7)-C(12)-C(13)	112.1(2)
C(7)-C(12)-C(14)	113.0(2)
C(13)-C(12)-C(14)	110.1(3)
C(11)-C(15)-C(17)	111.4(2)
C(11)-C(15)-C(16)	112.0(2)
C(17)-C(15)-C(16)	108.8(2)
C(19)-C(18)-C(23)	121.7(2)
C(19)-C(18)-N(2)	119.1(2)
C(23)-C(18)-N(2)	119.0(2)
C(20)-C(19)-C(18)	118.1(2)
C(20)-C(19)-C(24)	119.0(2)
C(18)-C(19)-C(24)	122.9(2)
C(21)-C(20)-C(19)	121.2(3)
C(20)-C(21)-C(22)	120.1(3)
C(21)-C(22)-C(23)	121.7(3)
C(22)-C(23)-C(18)	117.2(2)
C(22)-C(23)-C(27)	119.4(2)
C(18)-C(23)-C(27)	123.4(2)
C(26)-C(24)-C(19)	112.1(3)
C(26)-C(24)-C(25)	109.1(2)
C(19)-C(24)-C(25)	111.4(2)
C(23)-C(27)-C(29)	111.7(2)
C(23)-C(27)-C(28)	111.9(2)
C(29)-C(27)-C(28)	110.2(2)
C(31)-C(30)-C(35)	111.1(2)
C(31)-C(30)-P	116.10(16)
C(35)-C(30)-P	109.99(16)
C(30)-C(31)-C(32)	111.6(2)
C(33)-C(32)-C(31)	110.9(2)
C(34)-C(33)-C(32)	110.2(2)
C(33)-C(34)-C(35)	111.3(2)
C(30)-C(35)-C(34)	111.6(2)
C(37)-C(36)-C(41)	110.1(2)
C(37)-C(36)-P	109.51(17)
C(41)-C(36)-P	111.86(16)
C(38)-C(37)-C(36)	112.1(2)
C(39)-C(38)-C(37)	112.4(2)
C(38)-C(39)-C(40)	111.1(2)
C(39)-C(40)-C(41)	111.7(2)
C(40)-C(41)-C(36)	110.5(2)

Table A59. Crystal data and structure refinement for [(BDI_{DIPP})PbSePCy₂] (47)

Identification code	jun1510	
Empirical formula	C ₄₁ H ₆₃ N ₂ P Pb Se	
Formula weight	901.05	
Temperature	173(2) K	
Wavelength	0.71073 Å	
Crystal system	Triclinic	
Space group	P $\bar{1}$ (No.2)	
Unit cell dimensions	a = 12.1375(2) Å	a = 92.391(1)°.
	b = 12.5352(3) Å	b = 97.371(1)°.
	c = 14.2900(3) Å	g = 108.474(1)°.
Volume	2037.23(7) Å ³	
Z	2	
Density (calculated)	1.47 Mg/m ³	
Absorption coefficient	5.10 mm ⁻¹	
F(000)	908	
Crystal size	0.16 x 0.14 x 0.05 mm ³	
Theta range for data collection	3.43 to 27.11°.	
Index ranges	-15 ≤ h ≤ 15, -16 ≤ k ≤ 16, -18 ≤ l ≤ 18	
Reflections collected	37354	
Independent reflections	8987 [R(int) = 0.058]	
Reflections with I > 2σ(I)	7806	
Completeness to theta = 27.11°	99.8 %	
Tmax. and Tmin.	0.6008 and 0.5157	
Refinement method	Full-matrix least-squares on F ²	
Data / restraints / parameters	8987 / 0 / 417	
Goodness-of-fit on F ²	0.973	
Final R indices [I > 2σ(I)]	R1 = 0.030, wR2 = 0.063	
R indices (all data)	R1 = 0.040, wR2 = 0.066	
Largest diff. peak and hole	0.66 and -1.00 e.Å ⁻³	

Data collection KappaCCD , Program package WinGX , Abs correction MULTISCAN

Refinement using SHELXL-97 , Drawing using ORTEP-3 for Windows

Table A60. Atomic coordinates ($\times 10^4$) and equivalent isotropic displacement parameters ($\text{\AA}^2 \times 10^3$) for $[(\text{BDI}_{\text{DIPP}})\text{PbSePCy}_2]$ (**47**). $U(\text{eq})$ is defined as one third of the trace of the orthogonalized U^{ij} tensor

	x	y	z	U(eq)
Pb	7420(1)	7023(1)	7006(1)	22(1)
Se	8455(1)	9105(1)	7876(1)	29(1)
P	8712(1)	9755(1)	6446(1)	26(1)
N(1)	5742(2)	6479(2)	7732(2)	23(1)
N(2)	8041(2)	6089(2)	8229(2)	21(1)
C(1)	5376(3)	5468(3)	8053(3)	28(1)
C(2)	6101(3)	4827(3)	8333(3)	31(1)
C(3)	7333(3)	5164(3)	8510(2)	26(1)
C(4)	4087(3)	4946(4)	8160(3)	45(1)
C(5)	7857(3)	4408(3)	9089(3)	35(1)
C(6)	4978(3)	7141(3)	7536(3)	26(1)
C(7)	5031(3)	8002(3)	8219(3)	29(1)
C(8)	4317(3)	8669(3)	8005(3)	36(1)
C(9)	3601(3)	8496(4)	7142(3)	38(1)
C(10)	3591(3)	7676(3)	6468(3)	33(1)
C(11)	4272(3)	6975(3)	6648(3)	25(1)
C(12)	5842(3)	8216(4)	9162(3)	36(1)
C(13)	5238(4)	7535(5)	9920(3)	65(2)
C(14)	6369(4)	9461(4)	9520(3)	50(1)
C(15)	4249(3)	6093(3)	5878(3)	29(1)
C(16)	2988(4)	5336(4)	5480(4)	51(1)
C(17)	4847(4)	6632(4)	5060(3)	39(1)
C(18)	9283(3)	6504(3)	8569(2)	24(1)
C(19)	9676(3)	7094(3)	9470(2)	31(1)
C(20)	10885(3)	7579(4)	9750(3)	41(1)
C(21)	11670(3)	7473(4)	9165(3)	46(1)
C(22)	11273(3)	6892(4)	8290(3)	39(1)
C(23)	10072(3)	6393(3)	7966(3)	28(1)
C(24)	8846(3)	7244(4)	10144(3)	41(1)
C(25)	9008(4)	6658(4)	11053(3)	49(1)
C(26)	9014(5)	8478(4)	10395(3)	55(1)
C(27)	9674(3)	5778(3)	6986(3)	31(1)

C(28)	10120(4)	4773(4)	6880(3)	53(1)
C(29)	10057(4)	6572(4)	6214(3)	43(1)
C(30)	7772(3)	10688(3)	6334(3)	28(1)
C(31)	8087(4)	11668(4)	7093(3)	38(1)
C(32)	7271(4)	12376(4)	6934(3)	45(1)
C(33)	5996(4)	11655(4)	6889(3)	50(1)
C(34)	5673(3)	10710(4)	6103(3)	44(1)
C(35)	6473(3)	9967(3)	6243(3)	36(1)
C(36)	10221(3)	10805(3)	6725(3)	26(1)
C(37)	10485(3)	11522(3)	5891(3)	34(1)
C(38)	11729(4)	12384(4)	6073(3)	43(1)
C(39)	12649(4)	11823(4)	6325(3)	46(1)
C(40)	12377(3)	11118(4)	7160(3)	40(1)
C(41)	11149(3)	10229(3)	6955(3)	37(1)

Table A61. Bond lengths [Å] and angles [deg] for [(BDI_{DIPP})PbSePCy₂] (**47**)

Pb-N(2)	2.321(3)
Pb-N(1)	2.326(3)
Pb-Se	2.6811(4)
Se-P	2.2543(9)
P-C(36)	1.868(4)
P-C(30)	1.873(4)
N(1)-C(1)	1.325(4)
N(1)-C(6)	1.438(4)
N(2)-C(3)	1.319(4)
N(2)-C(18)	1.439(4)
C(1)-C(2)	1.403(5)
C(1)-C(4)	1.523(5)
C(2)-C(3)	1.404(5)
C(3)-C(5)	1.517(5)
C(6)-C(11)	1.404(5)
C(6)-C(7)	1.405(5)
C(7)-C(8)	1.399(5)
C(7)-C(12)	1.523(5)
C(8)-C(9)	1.380(6)
C(9)-C(10)	1.375(6)
C(10)-C(11)	1.395(5)
C(11)-C(15)	1.519(5)
C(12)-C(13)	1.524(6)
C(12)-C(14)	1.525(6)
C(15)-C(17)	1.524(5)
C(15)-C(16)	1.541(5)
C(18)-C(23)	1.403(5)
C(18)-C(19)	1.404(5)
C(19)-C(20)	1.396(5)
C(19)-C(24)	1.527(5)
C(20)-C(21)	1.378(6)
C(21)-C(22)	1.368(6)
C(22)-C(23)	1.398(5)
C(23)-C(27)	1.512(5)
C(24)-C(26)	1.516(7)
C(24)-C(25)	1.541(6)
C(27)-C(28)	1.530(6)
C(27)-C(29)	1.535(5)
C(30)-C(31)	1.522(5)
C(30)-C(35)	1.535(5)

C(31)-C(32)	1.528(6)
C(32)-C(33)	1.517(6)
C(33)-C(34)	1.516(7)
C(34)-C(35)	1.547(6)
C(36)-C(37)	1.528(5)
C(36)-C(41)	1.528(5)
C(37)-C(38)	1.535(5)
C(38)-C(39)	1.512(6)
C(39)-C(40)	1.523(6)
C(40)-C(41)	1.535(5)
N(2)-Pb-N(1)	79.97(9)
N(2)-Pb-Se	95.76(7)
N(1)-Pb-Se	99.34(7)
P-Se-Pb	88.59(3)
C(36)-P-C(30)	102.07(16)
C(36)-P-Se	100.77(11)
C(30)-P-Se	102.50(12)
C(1)-N(1)-C(6)	122.2(3)
C(1)-N(1)-Pb	120.8(2)
C(6)-N(1)-Pb	114.2(2)
C(3)-N(2)-C(18)	122.4(3)
C(3)-N(2)-Pb	122.1(2)
C(18)-N(2)-Pb	114.96(19)
N(1)-C(1)-C(2)	124.7(3)
N(1)-C(1)-C(4)	119.5(3)
C(2)-C(1)-C(4)	115.7(3)
C(1)-C(2)-C(3)	128.9(3)
N(2)-C(3)-C(2)	124.7(3)
N(2)-C(3)-C(5)	119.2(3)
C(2)-C(3)-C(5)	116.1(3)
C(11)-C(6)-C(7)	121.7(3)
C(11)-C(6)-N(1)	119.7(3)
C(7)-C(6)-N(1)	118.4(3)
C(8)-C(7)-C(6)	117.8(4)
C(8)-C(7)-C(12)	120.6(4)
C(6)-C(7)-C(12)	121.6(3)
C(9)-C(8)-C(7)	120.8(4)
C(10)-C(9)-C(8)	120.6(4)
C(9)-C(10)-C(11)	121.1(4)
C(10)-C(11)-C(6)	117.9(3)
C(10)-C(11)-C(15)	119.3(3)

C(6)-C(11)-C(15)	122.8(3)
C(7)-C(12)-C(13)	111.8(3)
C(7)-C(12)-C(14)	113.5(4)
C(13)-C(12)-C(14)	110.2(4)
C(11)-C(15)-C(17)	111.7(3)
C(11)-C(15)-C(16)	112.2(3)
C(17)-C(15)-C(16)	108.6(3)
C(23)-C(18)-C(19)	121.6(3)
C(23)-C(18)-N(2)	119.3(3)
C(19)-C(18)-N(2)	118.9(3)
C(20)-C(19)-C(18)	117.9(3)
C(20)-C(19)-C(24)	118.9(4)
C(18)-C(19)-C(24)	123.2(3)
C(21)-C(20)-C(19)	121.1(4)
C(22)-C(21)-C(20)	120.3(4)
C(21)-C(22)-C(23)	121.4(4)
C(22)-C(23)-C(18)	117.7(4)
C(22)-C(23)-C(27)	119.5(3)
C(18)-C(23)-C(27)	122.7(3)
C(26)-C(24)-C(19)	112.1(4)
C(26)-C(24)-C(25)	109.9(3)
C(19)-C(24)-C(25)	110.7(3)
C(23)-C(27)-C(28)	112.1(3)
C(23)-C(27)-C(29)	111.7(3)
C(28)-C(27)-C(29)	109.5(3)
C(31)-C(30)-C(35)	111.5(3)
C(31)-C(30)-P	116.1(2)
C(35)-C(30)-P	109.7(3)
C(30)-C(31)-C(32)	111.8(3)
C(33)-C(32)-C(31)	111.2(4)
C(34)-C(33)-C(32)	109.9(4)
C(33)-C(34)-C(35)	111.6(3)
C(30)-C(35)-C(34)	110.8(3)
C(37)-C(36)-C(41)	110.5(3)
C(37)-C(36)-P	109.5(3)
C(41)-C(36)-P	111.7(3)
C(36)-C(37)-C(38)	111.8(3)
C(39)-C(38)-C(37)	111.7(4)
C(38)-C(39)-C(40)	110.7(3)
C(39)-C(40)-C(41)	111.4(4)
C(36)-C(41)-C(40)	110.0(3)

Table A62. Crystal data and structure refinement for [(BDI_{DIPP})GeSeP(Se)Cy₂] (**48**)

Identification code	jun911	
Empirical formula	C ₄₁ H ₆₃ Ge N ₂ P Se ₂ , C ₇ H ₈	
Formula weight	937.55	
Temperature	173(2) K	
Wavelength	0.71073 Å	
Crystal system	Monoclinic	
Space group	<i>P</i> 2 ₁ /c (No.14)	
Unit cell dimensions	a = 13.1356(3) Å	a = 90°.
	b = 18.3304(3) Å	b = 103.174(1)°.
	c = 20.4944(5) Å	g = 90°.
Volume	4804.79(18) Å ³	
Z	4	
Density (calculated)	1.30 Mg/m ³	
Absorption coefficient	2.218 mm ⁻¹	
F(000)	1952	
Crystal size	0.24 x 0.22 x 0.13 mm ³	
Theta range for data collection	3.49 to 27.06°.	
Index ranges	-16 ≤ h ≤ 16, -23 ≤ k ≤ 19, -26 ≤ l ≤ 26	
Reflections collected	32616	
Independent reflections	10466 [R(int) = 0.049]	
Completeness to theta = 27.06°	99.1 %	
Absorption correction	Semi-empirical from equivalents	
Max. and min. transmission	0.6643 and 0.6107	
Refinement method	Full-matrix least-squares on F ²	
Data / restraints / parameters	10466 / 0 / 489	
Goodness-of-fit on F ²	0.997	
Final R indices [I > 2σ(I)]	R1 = 0.037, wR2 = 0.076	
R indices (all data)	R1 = 0.058, wR2 = 0.083	
Largest diff. peak and hole	0.66 and -0.49 e.Å ⁻³	

Data collection KappaCCD , Program package WinGX , Abs correction MULTISCAN
 Refinement using SHELXL-97 , Drawing using ORTEP-3 for Windows

Table A63. Atomic coordinates ($\times 10^4$) and equivalent isotropic displacement parameters ($\text{\AA}^2 \times 10^3$) for $[(\text{BDI}_{\text{DIPP}})\text{GeSeP}(\text{Se})\text{Cy}_2]$ (**48**). $U(\text{eq})$ is defined as one third of the trace of the orthogonalized U^{ij} tensor

	x	y	z	$U(\text{eq})$
Se(1)	2423(1)	3279(1)	1828(1)	24(1)
Se(2)	4055(1)	2351(1)	3313(1)	30(1)
Ge	3883(1)	4081(1)	2354(1)	19(1)
P	2740(1)	2314(1)	2499(1)	21(1)
N(1)	2986(2)	4979(1)	2334(1)	20(1)
N(2)	4185(2)	4402(1)	1468(1)	18(1)
C(1)	3375(2)	5612(1)	2177(1)	24(1)
C(2)	4127(2)	5651(1)	1794(1)	26(1)
C(3)	4415(2)	5100(1)	1402(1)	21(1)
C(4)	3011(2)	6322(2)	2413(2)	37(1)
C(5)	5011(2)	5333(2)	890(1)	31(1)
C(6)	2086(2)	4966(1)	2628(1)	23(1)
C(7)	1089(2)	4912(1)	2201(1)	25(1)
C(8)	225(2)	4887(2)	2487(2)	35(1)
C(9)	346(3)	4902(2)	3173(2)	43(1)
C(10)	1327(3)	4947(2)	3585(2)	42(1)
C(11)	2221(2)	4982(2)	3328(1)	30(1)
C(12)	938(2)	4898(2)	1441(1)	31(1)
C(13)	92(2)	4358(2)	1104(2)	42(1)
C(14)	689(3)	5656(2)	1135(2)	49(1)
C(15)	3286(3)	5046(2)	3804(1)	41(1)
C(16)	3587(3)	4338(3)	4187(2)	67(1)
C(17)	3332(3)	5692(3)	4284(2)	69(1)
C(18)	4494(2)	3848(1)	1051(1)	20(1)
C(19)	3762(2)	3582(2)	490(1)	25(1)
C(20)	4075(2)	3033(2)	114(1)	35(1)
C(21)	5076(3)	2743(2)	283(2)	42(1)
C(22)	5785(2)	3007(2)	839(2)	36(1)
C(23)	5512(2)	3563(1)	1234(1)	24(1)
C(24)	2659(2)	3893(2)	281(1)	29(1)
C(25)	2595(3)	4499(2)	-233(2)	60(1)
C(26)	1839(3)	3305(2)	12(2)	46(1)

C(27)	6322(2)	3831(2)	1839(1)	25(1)
C(28)	7336(2)	4078(2)	1658(2)	41(1)
C(29)	6553(2)	3243(2)	2377(2)	37(1)
C(30)	1501(2)	2197(1)	2771(1)	25(1)
C(31)	552(2)	2122(2)	2179(2)	33(1)
C(32)	-467(2)	2057(2)	2415(2)	43(1)
C(33)	-600(2)	2683(2)	2875(2)	47(1)
C(34)	326(2)	2738(2)	3466(2)	41(1)
C(35)	1358(2)	2821(2)	3238(1)	32(1)
C(36)	2802(2)	1575(1)	1905(1)	26(1)
C(37)	2716(3)	811(2)	2190(2)	35(1)
C(38)	2714(3)	228(2)	1654(2)	47(1)
C(39)	3688(3)	290(2)	1372(2)	54(1)
C(40)	3795(3)	1049(2)	1099(2)	49(1)
C(41)	3794(2)	1634(2)	1632(2)	36(1)
C(1S)	-1012(5)	1780(3)	-77(2)	80(1)
C(2S)	-1891(6)	1581(3)	-538(2)	90(2)
C(3S)	-2706(5)	2079(6)	-738(3)	119(3)
C(4S)	-2619(6)	2752(5)	-471(4)	116(2)
C(5S)	-1755(7)	2938(4)	-10(4)	113(2)
C(6S)	-961(5)	2469(3)	171(3)	88(2)
C(7S)	-107(6)	1270(4)	145(3)	141(3)

Table A64. Bond lengths [Å] and angles [deg] for [(BDI_{DIPP})GeSeP(Se)Cy₂] (**48**)

Se(1)-P	2.2208(7)
Se(1)-Ge	2.4613(4)
Se(2)-P	2.1114(7)
Ge-N(1)	2.020(2)
Ge-N(2)	2.0320(19)
P-C(36)	1.837(3)
P-C(30)	1.849(3)
N(1)-C(1)	1.336(3)
N(1)-C(6)	1.444(3)
N(2)-C(3)	1.328(3)
N(2)-C(18)	1.445(3)
C(1)-C(2)	1.396(4)
C(1)-C(4)	1.503(4)
C(2)-C(3)	1.396(4)
C(3)-C(5)	1.508(3)
C(6)-C(7)	1.403(4)
C(6)-C(11)	1.404(4)
C(7)-C(8)	1.392(4)
C(7)-C(12)	1.524(4)
C(8)-C(9)	1.378(4)
C(9)-C(10)	1.373(5)
C(10)-C(11)	1.394(4)
C(11)-C(15)	1.517(4)
C(12)-C(14)	1.529(4)
C(12)-C(13)	1.530(4)
C(15)-C(16)	1.522(5)
C(15)-C(17)	1.532(5)
C(18)-C(23)	1.404(4)
C(18)-C(19)	1.407(4)
C(19)-C(20)	1.386(4)
C(19)-C(24)	1.523(4)
C(20)-C(21)	1.388(4)
C(21)-C(22)	1.384(4)
C(22)-C(23)	1.398(4)
C(23)-C(27)	1.520(4)
C(24)-C(25)	1.521(4)

C(24)-C(26)	1.534(4)
C(27)-C(29)	1.521(4)
C(27)-C(28)	1.531(4)
C(30)-C(35)	1.528(4)
C(30)-C(31)	1.536(4)
C(31)-C(32)	1.528(4)
C(32)-C(33)	1.520(5)
C(33)-C(34)	1.511(5)
C(34)-C(35)	1.539(4)
C(36)-C(37)	1.531(4)
C(36)-C(41)	1.534(4)
C(37)-C(38)	1.532(4)
C(38)-C(39)	1.524(5)
C(39)-C(40)	1.517(5)
C(40)-C(41)	1.532(4)
C(1S)-C(6S)	1.357(7)
C(1S)-C(2S)	1.363(7)
C(1S)-C(7S)	1.499(8)
C(2S)-C(3S)	1.396(9)
C(3S)-C(4S)	1.344(9)
C(4S)-C(5S)	1.345(9)
C(5S)-C(6S)	1.337(8)
P-Ge(1)-Ge	100.77(2)
N(1)-Ge-N(2)	88.72(8)
N(1)-Ge-Se(1)	94.84(6)
N(2)-Ge-Se(1)	94.20(6)
C(36)-P-C(30)	106.83(12)
C(36)-P-Se(2)	113.29(10)
C(30)-P-Se(2)	112.52(9)
C(36)-P-Se(1)	102.00(9)
C(30)-P-Se(1)	103.01(9)
Se(2)-P-Se(1)	117.92(3)
C(1)-N(1)-C(6)	120.7(2)
C(1)-N(1)-Ge	117.27(17)
C(6)-N(1)-Ge	120.49(16)
C(3)-N(2)-C(18)	121.1(2)
C(3)-N(2)-Ge	117.69(16)

C(18)-N(2)-Ge	117.59(15)
N(1)-C(1)-C(2)	122.6(2)
N(1)-C(1)-C(4)	120.4(2)
C(2)-C(1)-C(4)	116.9(2)
C(3)-C(2)-C(1)	127.2(2)
N(2)-C(3)-C(2)	122.8(2)
N(2)-C(3)-C(5)	120.6(2)
C(2)-C(3)-C(5)	116.6(2)
C(7)-C(6)-C(11)	121.4(2)
C(7)-C(6)-N(1)	118.5(2)
C(11)-C(6)-N(1)	120.1(2)
C(8)-C(7)-C(6)	118.3(3)
C(8)-C(7)-C(12)	120.0(3)
C(6)-C(7)-C(12)	121.7(2)
C(9)-C(8)-C(7)	120.9(3)
C(10)-C(9)-C(8)	120.2(3)
C(9)-C(10)-C(11)	121.5(3)
C(10)-C(11)-C(6)	117.7(3)
C(10)-C(11)-C(15)	119.5(3)
C(6)-C(11)-C(15)	122.8(2)
C(7)-C(12)-C(14)	111.7(2)
C(7)-C(12)-C(13)	112.7(2)
C(14)-C(12)-C(13)	109.7(2)
C(11)-C(15)-C(16)	111.0(3)
C(11)-C(15)-C(17)	111.6(3)
C(16)-C(15)-C(17)	111.2(3)
C(23)-C(18)-C(19)	121.5(2)
C(23)-C(18)-N(2)	118.9(2)
C(19)-C(18)-N(2)	119.6(2)
C(20)-C(19)-C(18)	118.1(3)
C(20)-C(19)-C(24)	119.9(2)
C(18)-C(19)-C(24)	122.0(2)
C(19)-C(20)-C(21)	121.6(3)
C(22)-C(21)-C(20)	119.6(3)
C(21)-C(22)-C(23)	121.2(3)
C(22)-C(23)-C(18)	118.1(3)
C(22)-C(23)-C(27)	119.0(2)
C(18)-C(23)-C(27)	123.0(2)

C(25)-C(24)-C(19)	111.5(2)
C(25)-C(24)-C(26)	109.9(3)
C(19)-C(24)-C(26)	112.6(2)
C(23)-C(27)-C(29)	110.4(2)
C(23)-C(27)-C(28)	112.5(2)
C(29)-C(27)-C(28)	110.1(2)
C(35)-C(30)-C(31)	111.6(2)
C(35)-C(30)-P	110.11(19)
C(31)-C(30)-P	112.53(18)
C(32)-C(31)-C(30)	111.6(2)
C(33)-C(32)-C(31)	111.7(3)
C(34)-C(33)-C(32)	111.3(3)
C(33)-C(34)-C(35)	111.5(3)
C(30)-C(35)-C(34)	111.0(2)
C(37)-C(36)-C(41)	110.3(2)
C(37)-C(36)-P	113.75(19)
C(41)-C(36)-P	111.01(19)
C(36)-C(37)-C(38)	110.6(2)
C(39)-C(38)-C(37)	110.9(3)
C(40)-C(39)-C(38)	111.4(3)
C(39)-C(40)-C(41)	111.3(3)
C(40)-C(41)-C(36)	110.4(3)

Table A65. Crystal data and structure refinement for [(BDI_{DIPP})SnSeP(Se)Cy₂] (49)

Identification code	dec709	
Empirical formula	C ₄₁ H ₆₃ N ₂ P Se ₂ Sn, C ₇ H ₈	
Formula weight	983.65	
Temperature	173(2) K	
Wavelength	0.71073 Å	
Crystal system	Orthorhombic	
Space group	<i>P</i> 2 ₁ 2 ₁ 2 ₁ (No.19)	
Unit cell dimensions	a = 10.3830(1) Å	a = 90°.
	b = 15.4846(2) Å	b = 90°.
	c = 29.7411(4) Å	g = 90°.
Volume	4781.67(10) Å ³	
Z	4	
Density (calculated)	1.37 Mg/m ³	
Absorption coefficient	2.12 mm ⁻¹	
F(000)	2024	
Crystal size	0.18 x 0.11 x 0.09 mm ³	
Theta range for data collection	3.56 to 27.10°.	
Index ranges	-13 ≤ h ≤ 13, -19 ≤ k ≤ 19, -38 ≤ l ≤ 38	
Reflections collected	78235	
Independent reflections	10512 [R(int) = 0.079]	
Reflections with I > 2σ(I)	8993	
Completeness to theta = 27.10°	99.6 %	
Absorption correction	Semi-empirical from equivalents	
Tmax. and Tmin.	0.8777 and 0.8109	
Refinement method	Full-matrix least-squares on F ²	
Data / restraints / parameters	10512 / 0 / 454	
Goodness-of-fit on F ²	1.022	
Final R indices [I > 2σ(I)]	R1 = 0.037, wR2 = 0.074	
R indices (all data)	R1 = 0.050, wR2 = 0.0780	
Absolute structure parameter	-0.001(8)	
Largest diff. peak and hole	1.174 and -0.473 e.Å ⁻³	

The toluene solvate was refined without restraints and with the carbons left isotropic

Data collection KappaCCD , Program package WinGX , Abs correction MULTISCAN
Refinement using SHELXL-97 , Drawing using ORTEP-3 for Windows

Table A66. Atomic coordinates ($\times 10^4$) and equivalent isotropic displacement parameters ($\text{\AA}^2 \times 10^3$) for $[(\text{BDI}_{\text{DIPP}})\text{SnSeP}(\text{Se})\text{Cy}_2]$ (**49**). $U(\text{eq})$ is defined as one third of the trace of the orthogonalized U^{ij} tensor

	x	y	z	$U(\text{eq})$
Sn	2520(1)	5300(1)	1389(1)	19(1)
Se(1)	3471(1)	4448(1)	689(1)	28(1)
Se(2)	-11(1)	4921(1)	633(1)	34(1)
P	1581(1)	4247(1)	357(1)	23(1)
N(1)	4012(3)	6343(2)	1406(1)	20(1)
N(2)	3880(3)	4644(2)	1856(1)	20(1)
C(1)	4544(4)	6545(3)	1795(1)	22(1)
C(2)	4605(4)	6000(3)	2169(1)	24(1)
C(3)	4393(3)	5101(3)	2188(1)	21(1)
C(4)	5171(5)	7421(3)	1860(2)	37(1)
C(5)	4779(4)	4653(3)	2622(1)	34(1)
C(6)	4109(4)	6906(2)	1020(1)	20(1)
C(7)	5116(4)	6768(2)	714(1)	25(1)
C(8)	5171(5)	7299(3)	336(2)	36(1)
C(9)	4264(5)	7937(3)	259(2)	40(1)
C(10)	3280(4)	8055(3)	563(1)	35(1)
C(11)	3171(4)	7541(3)	948(1)	26(1)
C(12)	6139(4)	6088(3)	790(2)	33(1)
C(13)	7363(6)	6497(4)	983(2)	69(2)
C(14)	6481(4)	5579(3)	370(2)	41(1)
C(15)	2066(4)	7711(3)	1271(2)	33(1)
C(16)	2138(5)	8631(4)	1469(2)	61(2)
C(17)	762(5)	7563(4)	1049(2)	50(1)
C(18)	3814(4)	3714(2)	1871(1)	20(1)
C(19)	4784(4)	3234(3)	1651(1)	24(1)
C(20)	4648(4)	2340(3)	1632(1)	27(1)
C(21)	3587(4)	1932(3)	1819(1)	28(1)
C(22)	2642(4)	2410(2)	2033(1)	26(1)
C(23)	2744(3)	3311(2)	2064(1)	20(1)
C(24)	5952(4)	3661(3)	1438(2)	31(1)
C(25)	7054(5)	3752(4)	1778(2)	58(2)
C(26)	6442(5)	3196(4)	1023(2)	47(1)

C(27)	1676(4)	3802(3)	2306(1)	26(1)
C(28)	1559(5)	3504(3)	2796(1)	35(1)
C(29)	387(4)	3685(3)	2061(2)	36(1)
C(30)	1858(4)	4559(3)	-233(1)	26(1)
C(31)	660(4)	4398(3)	-522(1)	37(1)
C(32)	889(5)	4670(3)	-1014(2)	45(1)
C(33)	1337(6)	5589(3)	-1048(2)	54(2)
C(34)	2529(6)	5747(3)	-765(2)	51(1)
C(35)	2301(5)	5505(3)	-272(1)	39(1)
C(36)	1311(4)	3069(3)	366(1)	31(1)
C(37)	2414(6)	2542(3)	151(1)	37(1)
C(38)	2136(6)	1573(3)	173(2)	50(2)
C(39)	1890(7)	1281(3)	653(2)	65(2)
C(40)	785(7)	1785(4)	858(2)	65(2)
C(41)	1039(5)	2760(3)	847(2)	43(1)
C(1S)	-557(7)	960(5)	2198(3)	80(2)
C(2S)	476(5)	512(4)	2067(2)	59(2)
C(3S)	1506(7)	379(5)	2338(2)	80(2)
C(4S)	1526(7)	733(4)	2788(2)	74(2)
C(5S)	508(8)	1136(5)	2908(3)	91(2)
C(6S)	-597(6)	1295(4)	2632(2)	56(2)
C(7S)	-1613(8)	1074(5)	1901(2)	87(2)

Table A67. Bond lengths [Å] and angles [deg] for [(BDI_{DIPP})SnSeP(Se)Cy₂] (**49**)

Sn-N(2)	2.225(3)
Sn-N(1)	2.239(3)
Sn-Se(1)	2.6549(5)
Se(1)-P	2.2194(11)
Se(2)-P	2.1197(11)
P-C(30)	1.843(4)
P-C(36)	1.846(4)
N(1)-C(1)	1.320(5)
N(1)-C(6)	1.446(5)
N(2)-C(3)	1.328(5)
N(2)-C(18)	1.443(5)
C(1)-C(2)	1.398(6)
C(1)-C(4)	1.516(6)
C(2)-C(3)	1.410(6)
C(3)-C(5)	1.517(5)
C(6)-C(11)	1.399(6)
C(6)-C(7)	1.402(5)
C(7)-C(8)	1.395(6)
C(7)-C(12)	1.512(6)
C(8)-C(9)	1.383(7)
C(9)-C(10)	1.375(6)
C(10)-C(11)	1.400(6)
C(11)-C(15)	1.519(6)
C(12)-C(14)	1.519(6)
C(12)-C(13)	1.530(7)
C(15)-C(17)	1.524(7)
C(15)-C(16)	1.544(7)
C(18)-C(23)	1.397(5)
C(18)-C(19)	1.413(5)
C(19)-C(20)	1.392(6)
C(19)-C(24)	1.519(6)
C(20)-C(21)	1.386(6)
C(21)-C(22)	1.384(6)
C(22)-C(23)	1.403(5)
C(23)-C(27)	1.524(5)
C(24)-C(26)	1.517(6)

C(24)-C(25)	1.533(7)
C(27)-C(28)	1.534(5)
C(27)-C(29)	1.534(6)
C(30)-C(31)	1.531(6)
C(30)-C(35)	1.540(6)
C(31)-C(32)	1.541(6)
C(32)-C(33)	1.500(8)
C(33)-C(34)	1.516(8)
C(34)-C(35)	1.534(6)
C(36)-C(41)	1.537(6)
C(36)-C(37)	1.544(6)
C(37)-C(38)	1.530(6)
C(38)-C(39)	1.521(8)
C(39)-C(40)	1.515(9)
C(40)-C(41)	1.532(7)
N(2)-Sn-N(1)	82.89(11)
N(2)-Sn-Se(1)	91.53(8)
N(1)-Sn-Se(1)	96.83(8)
P-Se(1)-Sn	95.14(3)
C(30)-P-C(36)	107.23(18)
C(30)-P-Se(2)	111.17(14)
C(36)-P-Se(2)	111.29(15)
C(30)-P-Se(1)	104.39(13)
C(36)-P-Se(1)	105.48(14)
Se(2)-P-Se(1)	116.62(5)
C(1)-N(1)-C(6)	121.6(3)
C(1)-N(1)-Sn	118.7(3)
C(6)-N(1)-Sn	117.8(2)
C(3)-N(2)-C(18)	121.8(3)
C(3)-N(2)-Sn	118.5(2)
C(18)-N(2)-Sn	116.4(2)
N(1)-C(1)-C(2)	125.0(4)
N(1)-C(1)-C(4)	120.2(4)
C(2)-C(1)-C(4)	114.8(4)
C(1)-C(2)-C(3)	128.5(4)
N(2)-C(3)-C(2)	123.9(4)
N(2)-C(3)-C(5)	119.7(3)

C(2)-C(3)-C(5)	116.5(4)
C(11)-C(6)-C(7)	121.9(4)
C(11)-C(6)-N(1)	119.7(3)
C(7)-C(6)-N(1)	118.4(3)
C(8)-C(7)-C(6)	117.6(4)
C(8)-C(7)-C(12)	120.2(4)
C(6)-C(7)-C(12)	122.2(4)
C(9)-C(8)-C(7)	121.7(4)
C(10)-C(9)-C(8)	119.6(4)
C(9)-C(10)-C(11)	121.4(4)
C(6)-C(11)-C(10)	117.8(4)
C(6)-C(11)-C(15)	123.5(4)
C(10)-C(11)-C(15)	118.7(4)
C(7)-C(12)-C(14)	113.7(4)
C(7)-C(12)-C(13)	110.6(4)
C(14)-C(12)-C(13)	109.1(4)
C(11)-C(15)-C(17)	111.8(4)
C(11)-C(15)-C(16)	111.4(4)
C(17)-C(15)-C(16)	110.3(4)
C(23)-C(18)-C(19)	121.5(3)
C(23)-C(18)-N(2)	119.7(3)
C(19)-C(18)-N(2)	118.5(3)
C(20)-C(19)-C(18)	118.0(4)
C(20)-C(19)-C(24)	119.8(4)
C(18)-C(19)-C(24)	122.2(3)
C(21)-C(20)-C(19)	121.2(4)
C(22)-C(21)-C(20)	120.3(4)
C(21)-C(22)-C(23)	120.6(4)
C(18)-C(23)-C(22)	118.5(4)
C(18)-C(23)-C(27)	123.4(3)
C(22)-C(23)-C(27)	118.1(3)
C(26)-C(24)-C(19)	113.6(4)
C(26)-C(24)-C(25)	109.3(4)
C(19)-C(24)-C(25)	111.2(4)
C(23)-C(27)-C(28)	110.9(3)
C(23)-C(27)-C(29)	110.6(3)
C(28)-C(27)-C(29)	110.3(4)
C(31)-C(30)-C(35)	110.8(4)

C(31)-C(30)-P	111.4(3)
C(35)-C(30)-P	111.6(3)
C(30)-C(31)-C(32)	111.3(4)
C(33)-C(32)-C(31)	111.8(4)
C(32)-C(33)-C(34)	111.6(4)
C(33)-C(34)-C(35)	111.4(5)
C(34)-C(35)-C(30)	110.5(3)
C(41)-C(36)-C(37)	111.0(4)
C(41)-C(36)-P	110.4(3)
C(37)-C(36)-P	113.8(3)
C(38)-C(37)-C(36)	111.1(4)
C(39)-C(38)-C(37)	111.3(4)
C(40)-C(39)-C(38)	110.7(5)
C(39)-C(40)-C(41)	111.6(5)
C(40)-C(41)-C(36)	111.0(4)

Table A68. Crystal data and structure refinement for [(BDI_{DIPP})PbSeP(Se)Cy₂] (50)

Identification code	apr1010	
Empirical formula	C41 H63 N2 P Pb Se2, C7 H8	
Formula weight	1072.15	
Temperature	173(2) K	
Wavelength	0.71073 Å	
Crystal system	Orthorhombic	
Space group	<i>P</i> 2 ₁ 2 ₁ 2 ₁ (No.19)	
Unit cell dimensions	a = 10.3409(1) Å	a = 90°.
	b = 15.5230(2) Å	b = 90°.
	c = 29.7674(3) Å	g = 90°.
Volume	4778.32(9) Å ³	
Z	4	
Density (calculated)	1.49 Mg/m ³	
Absorption coefficient	5.12 mm ⁻¹	
F(000)	2152	
Crystal size	0.19 x 0.08 x 0.08 mm ³	
Theta range for data collection	3.56 to 27.11°.	
Index ranges	-13 ≤ h ≤ 13, -19 ≤ k ≤ 19, -38 ≤ l ≤ 38	
Reflections collected	67740	
Independent reflections	10498 [R(int) = 0.066]	
Reflections with I > 2σ(I)	9794	
Completeness to theta = 27.11°	99.6 %	
Absorption correction	Semi-empirical from equivalents	
Tmax. and Tmin.	0.6283 and 0.4654	
Refinement method	Full-matrix least-squares on F ²	
Data / restraints / parameters	10498 / 0 / 489	
Goodness-of-fit on F ²	1.031	
Final R indices [I > 2σ(I)]	R1 = 0.026, wR2 = 0.049	
R indices (all data)	R1 = 0.031, wR2 = 0.051	
Absolute structure parameter	-0.012(4)	
Largest diff. peak and hole	0.65 and -0.43 e.Å ⁻³	

Data collection KappaCCD , Program package WinGX , Abs correction MULTISCAN

Refinement using SHELXL-97 , Drawing using ORTEP-3 for Windows

Table A69. Atomic coordinates ($\times 10^4$) and equivalent isotropic displacement parameters ($\text{\AA}^2 \times 10^3$) for $[(\text{BDI}_{\text{DIPP}})\text{PbSeP}(\text{Se})\text{Cy}_2]$ (**50**). $U(\text{eq})$ is defined as one third of the trace of the orthogonalized U^{ij} tensor

	x	y	z	$U(\text{eq})$
Pb	7587(1)	4692(1)	8631(1)	19(1)
Se(1)	6547(1)	5606(1)	9331(1)	28(1)
Se(2)	10012(1)	5077(1)	9373(1)	32(1)
P	8449(1)	5785(1)	9656(1)	21(1)
N(1)	6115(2)	5342(2)	8136(1)	17(1)
N(2)	6009(3)	3600(2)	8591(1)	17(1)
C(1)	5616(3)	4873(2)	7810(1)	19(1)
C(2)	5410(4)	3976(2)	7830(1)	22(1)
C(3)	5459(4)	3417(2)	8200(1)	21(1)
C(4)	5211(4)	5305(3)	7373(1)	28(1)
C(5)	4833(5)	2547(3)	8125(2)	34(1)
C(6)	6181(3)	6257(2)	8121(1)	19(1)
C(7)	5213(4)	6742(2)	8341(1)	22(1)
C(8)	5367(4)	7635(2)	8364(1)	25(1)
C(9)	6418(4)	8040(2)	8177(1)	28(1)
C(10)	7360(4)	7564(2)	7962(1)	24(1)
C(11)	7255(3)	6667(2)	7928(1)	19(1)
C(12)	4048(3)	6314(3)	8565(2)	29(1)
C(13)	2960(4)	6186(4)	8229(2)	54(1)
C(14)	3540(4)	6793(3)	8974(2)	41(1)
C(15)	8329(4)	6178(2)	7686(1)	22(1)
C(16)	8455(4)	6465(3)	7197(1)	32(1)
C(17)	9625(4)	6292(3)	7930(2)	34(1)
C(18)	5886(4)	3040(2)	8972(1)	21(1)
C(19)	4870(4)	3180(2)	9277(1)	26(1)
C(20)	4806(4)	2651(3)	9655(1)	32(1)
C(21)	5711(4)	2018(3)	9739(2)	37(1)
C(22)	6707(4)	1896(3)	9438(1)	34(1)
C(23)	6827(4)	2397(2)	9049(1)	24(1)
C(24)	3856(4)	3864(3)	9192(2)	34(1)
C(25)	2612(5)	3460(4)	9009(2)	71(2)
C(26)	3544(4)	4389(3)	9611(2)	40(1)

C(27)	7947(4)	2231(3)	8732(1)	32(1)
C(28)	7875(5)	1317(3)	8534(2)	63(2)
C(29)	9249(4)	2380(4)	8957(2)	48(1)
C(30)	8775(4)	6953(3)	9639(1)	28(1)
C(31)	7703(5)	7496(2)	9851(1)	35(1)
C(32)	8011(5)	8462(3)	9826(2)	48(1)
C(33)	8260(6)	8744(3)	9345(2)	63(2)
C(34)	9340(6)	8211(3)	9140(2)	61(2)
C(35)	9051(5)	7246(3)	9159(2)	43(1)
C(36)	8198(4)	5486(2)	10248(1)	26(1)
C(37)	9420(4)	5623(3)	10529(1)	34(1)
C(38)	9218(5)	5363(3)	11020(1)	44(1)
C(39)	8715(5)	4448(3)	11062(2)	47(1)
C(40)	7492(6)	4322(3)	10787(1)	48(1)
C(41)	7719(5)	4549(2)	10293(1)	36(1)
C(1S)	9341(5)	3992(4)	7217(2)	54(1)
C(2S)	9328(5)	3652(3)	7653(2)	49(1)
C(3S)	10385(6)	3788(4)	7930(2)	63(2)
C(4S)	11456(6)	4219(4)	7801(2)	60(2)
C(5S)	11457(6)	4565(3)	7359(2)	64(2)
C(6S)	10418(5)	4440(3)	7083(2)	47(1)
C(7S)	8261(6)	3872(4)	6919(2)	79(2)

Table A70. Bond lengths [Å] and angles [deg] for [(BDI_{DIPP})PbSeP(Se)Cy₂] (50)

Pb-N(1)	2.346(3)
Pb-N(2)	2.356(3)
Pb-Se(1)	2.7417(4)
Se(1)-P	2.2094(10)
Se(2)-P	2.1287(11)
P-C(36)	1.841(4)
P-C(30)	1.845(4)
N(1)-C(1)	1.319(4)
N(1)-C(6)	1.422(5)
N(2)-C(3)	1.328(5)
N(2)-C(18)	1.434(5)
C(1)-C(2)	1.409(5)
C(1)-C(4)	1.522(5)
C(2)-C(3)	1.404(5)
C(3)-C(5)	1.513(5)
C(6)-C(11)	1.403(5)
C(6)-C(7)	1.413(5)
C(7)-C(8)	1.397(5)
C(7)-C(12)	1.529(5)
C(8)-C(9)	1.373(6)
C(9)-C(10)	1.381(5)
C(10)-C(11)	1.400(5)
C(11)-C(15)	1.526(5)
C(12)-C(13)	1.519(6)
C(12)-C(14)	1.519(6)
C(15)-C(16)	1.529(5)
C(15)-C(17)	1.535(6)
C(18)-C(19)	1.406(5)
C(18)-C(23)	1.413(5)
C(19)-C(20)	1.395(5)
C(19)-C(24)	1.513(5)
C(20)-C(21)	1.379(6)
C(21)-C(22)	1.378(6)
C(22)-C(23)	1.400(5)
C(23)-C(27)	1.515(5)
C(24)-C(26)	1.524(6)

C(24)-C(25)	1.532(7)
C(27)-C(29)	1.522(6)
C(27)-C(28)	1.539(6)
C(30)-C(35)	1.527(6)
C(30)-C(31)	1.529(6)
C(31)-C(32)	1.534(6)
C(32)-C(33)	1.520(7)
C(33)-C(34)	1.516(8)
C(34)-C(35)	1.530(7)
C(36)-C(37)	1.531(5)
C(36)-C(41)	1.542(5)
C(37)-C(38)	1.532(6)
C(38)-C(39)	1.518(7)
C(39)-C(40)	1.518(7)
C(40)-C(41)	1.532(5)
N(1)-Pb-N(2)	80.13(10)
N(1)-Pb-Se(1)	90.05(7)
N(2)-Pb-Se(1)	97.93(7)
P-Se(1)-Pb	92.79(3)
C(36)-P-C(30)	107.50(18)
C(36)-P-Se(2)	110.82(13)
C(30)-P-Se(2)	110.95(14)
C(36)-P-Se(1)	105.18(13)
C(30)-P-Se(1)	105.91(14)
Se(2)-P-Se(1)	115.97(5)
C(1)-N(1)-C(6)	123.2(3)
C(1)-N(1)-Pb	118.6(2)
C(6)-N(1)-Pb	114.7(2)
C(3)-N(2)-C(18)	121.7(3)
C(3)-N(2)-Pb	119.6(2)
C(18)-N(2)-Pb	117.3(2)
N(1)-C(1)-C(2)	125.0(3)
N(1)-C(1)-C(4)	119.5(3)
C(2)-C(1)-C(4)	115.5(3)
C(3)-C(2)-C(1)	129.7(4)
N(2)-C(3)-C(2)	124.9(3)
N(2)-C(3)-C(5)	120.2(3)

C(2)-C(3)-C(5)	114.9(3)
C(11)-C(6)-C(7)	120.6(3)
C(11)-C(6)-N(1)	120.2(3)
C(7)-C(6)-N(1)	119.0(3)
C(8)-C(7)-C(6)	118.1(3)
C(8)-C(7)-C(12)	120.0(3)
C(6)-C(7)-C(12)	121.9(3)
C(9)-C(8)-C(7)	121.7(4)
C(8)-C(9)-C(10)	120.1(4)
C(9)-C(10)-C(11)	120.7(4)
C(10)-C(11)-C(6)	118.9(3)
C(10)-C(11)-C(15)	118.2(3)
C(6)-C(11)-C(15)	123.0(3)
C(13)-C(12)-C(14)	109.5(3)
C(13)-C(12)-C(7)	110.7(4)
C(14)-C(12)-C(7)	114.1(4)
C(11)-C(15)-C(16)	111.5(3)
C(11)-C(15)-C(17)	110.8(3)
C(16)-C(15)-C(17)	110.1(3)
C(19)-C(18)-C(23)	121.3(3)
C(19)-C(18)-N(2)	118.9(3)
C(23)-C(18)-N(2)	119.7(3)
C(20)-C(19)-C(18)	117.7(4)
C(20)-C(19)-C(24)	121.0(4)
C(18)-C(19)-C(24)	121.2(4)
C(21)-C(20)-C(19)	122.2(4)
C(22)-C(21)-C(20)	119.2(4)
C(21)-C(22)-C(23)	121.8(4)
C(22)-C(23)-C(18)	117.7(4)
C(22)-C(23)-C(27)	119.2(4)
C(18)-C(23)-C(27)	123.1(3)
C(19)-C(24)-C(26)	112.6(4)
C(19)-C(24)-C(25)	110.8(4)
C(26)-C(24)-C(25)	109.4(4)
C(23)-C(27)-C(29)	112.1(4)
C(23)-C(27)-C(28)	111.0(4)
C(29)-C(27)-C(28)	110.6(4)
C(35)-C(30)-C(31)	111.0(4)

C(35)-C(30)-P	110.7(3)
C(31)-C(30)-P	113.4(3)
C(30)-C(31)-C(32)	111.6(4)
C(33)-C(32)-C(31)	111.2(4)
C(34)-C(33)-C(32)	110.2(4)
C(33)-C(34)-C(35)	112.1(5)
C(30)-C(35)-C(34)	111.2(4)
C(37)-C(36)-C(41)	110.5(3)
C(37)-C(36)-P	111.8(3)
C(41)-C(36)-P	111.5(3)
C(36)-C(37)-C(38)	111.9(4)
C(39)-C(38)-C(37)	111.7(4)
C(40)-C(39)-C(38)	111.3(4)
C(39)-C(40)-C(41)	111.1(4)
C(40)-C(41)-C(36)	110.4(3)

Table A71. Crystal data and structure refinement for [(BDI_{DIPP})Ge(Se)PCy₂] (**51**)

Identification code	jun1011	
Empirical formula	C ₁₀₃ H ₁₅₀ Ge ₂ N ₄ P ₂ Se ₂	
Formula weight	1809.3	
Temperature	173(2) K	
Wavelength	0.71073 Å	
Crystal system	Triclinic	
Space group	P $\bar{1}$ (No.2)	
Unit cell dimensions	a = 10.0820(1) Å	a = 90.274(1)°.
	b = 21.7333(4) Å	b = 93.478(1)°.
	c = 21.9730(4) Å	g = 92.394(1)°.
Volume	4801.42(13) Å ³	
Z	4	
Density (calculated)	1.25 Mg/m ³	
Absorption coefficient	1.464 mm ⁻¹	
F(000)	1916	
Crystal size	0.24 x 0.18 x 0.11 mm ³	
Theta range for data collection	3.40 to 26.77°.	
Index ranges	-12 ≤ h ≤ 12, -27 ≤ k ≤ 27, -27 ≤ l ≤ 27	
Reflections collected	71113	
Independent reflections	20256 [R(int) = 0.065]	
Completeness to theta = 26.77°	99.0 %	
Absorption correction	Semi-empirical from equivalents	
Max. and min. transmission	0.7167 and 0.6347	
Refinement method	Full-matrix least-squares on F ²	
Data / restraints / parameters	20256 / 141 / 872	
Goodness-of-fit on F ²	0.985	
Final R indices [I > 2σ(I)]	R1 = 0.056, wR2 = 0.141	
R indices (all data)	R1 = 0.080, wR2 = 0.154	
Largest diff. peak and hole	1.80 and -0.79 e.Å ⁻³ (near toluene solvate)	

The toluene solvate molecules were refined with rigid C6-rings and all carbon atoms isotropic

Data collection KappaCCD , Program package WinGX , Abs correction MULTISCAN
Refinement using SHELXL-97 , Drawing using ORTEP-3 for Windows

Table A72. Atomic coordinates ($\times 10^4$) and equivalent isotropic displacement parameters ($\text{\AA}^2 \times 10^3$) for $[(\text{BDI}_{\text{DIPP}})\text{Ge}(\text{Se})\text{PCy}_2]$ (**51**). $U(\text{eq})$ is defined as one third of the trace of the orthogonalized U^{ij} tensor

	x	y	z	$U(\text{eq})$
Se(1)	940(1)	4062(1)	2395(1)	30(1)
Se(2)	-3997(1)	-249(1)	2561(1)	29(1)
Ge(1)	3022(1)	4440(1)	2512(1)	19(1)
Ge(2)	-1999(1)	-639(1)	2517(1)	18(1)
P(1)	3460(1)	5466(1)	2861(1)	25(1)
P(2)	-1518(1)	-1673(1)	2413(1)	25(1)
N(1)	4130(3)	3870(1)	2997(1)	20(1)
N(2)	4018(3)	4319(1)	1782(1)	19(1)
N(3)	-974(3)	-188(2)	1919(1)	21(1)
N(4)	-809(3)	-350(2)	3208(1)	23(1)
C(1)	4586(4)	3374(2)	2728(2)	24(1)
C(2)	4623(4)	3305(2)	2103(2)	25(1)
C(3)	4465(4)	3761(2)	1665(2)	23(1)
C(4)	5140(5)	2861(2)	3111(2)	36(1)
C(5)	4874(5)	3609(2)	1035(2)	34(1)
C(6)	4295(4)	3936(2)	3657(2)	23(1)
C(7)	5384(4)	4298(2)	3905(2)	25(1)
C(8)	5524(5)	4366(2)	4535(2)	34(1)
C(9)	4622(5)	4089(2)	4908(2)	36(1)
C(10)	3578(5)	3727(2)	4658(2)	34(1)
C(11)	3387(4)	3634(2)	4030(2)	27(1)
C(12)	6455(4)	4567(2)	3513(2)	33(1)
C(13)	7617(5)	4138(3)	3492(3)	59(2)
C(14)	6963(5)	5209(2)	3717(2)	45(1)
C(15)	2220(4)	3214(2)	3786(2)	32(1)
C(16)	2326(6)	2558(2)	4036(3)	50(1)
C(17)	880(5)	3454(3)	3951(2)	46(1)
C(18)	4110(4)	4797(2)	1327(2)	22(1)
C(19)	5234(4)	5202(2)	1367(2)	24(1)
C(20)	5303(4)	5673(2)	942(2)	31(1)
C(21)	4306(5)	5742(2)	493(2)	35(1)
C(22)	3235(4)	5328(2)	447(2)	33(1)
C(23)	3100(4)	4846(2)	863(2)	26(1)
C(24)	6387(4)	5130(2)	1839(2)	34(1)

C(25)	7006(5)	5729(3)	2097(3)	53(1)
C(26)	7467(6)	4756(3)	1577(4)	80(2)
C(27)	1916(4)	4392(2)	772(2)	29(1)
C(28)	1894(5)	4067(2)	150(2)	41(1)
C(29)	599(4)	4709(2)	829(2)	35(1)
C(30)	2093(4)	5541(2)	3398(2)	29(1)
C(31)	2025(5)	6212(2)	3611(2)	37(1)
C(32)	893(5)	6284(3)	4032(2)	48(1)
C(33)	1058(6)	5865(3)	4586(2)	55(2)
C(34)	1178(5)	5200(3)	4392(2)	45(1)
C(35)	2283(4)	5125(2)	3955(2)	34(1)
C(36)	2779(4)	5910(2)	2179(2)	28(1)
C(37)	3417(4)	6568(2)	2189(2)	36(1)
C(38)	2994(5)	6920(2)	1612(2)	42(1)
C(39)	1476(5)	6927(2)	1521(2)	42(1)
C(40)	883(5)	6275(2)	1493(2)	38(1)
C(41)	1261(4)	5924(2)	2076(2)	31(1)
C(42)	-513(4)	379(2)	2070(2)	26(1)
C(43)	-323(4)	584(2)	2674(2)	30(1)
C(44)	-335(4)	229(2)	3204(2)	28(1)
C(45)	-152(5)	832(2)	1582(2)	37(1)
C(46)	248(5)	532(2)	3784(2)	43(1)
C(47)	-909(4)	-424(2)	1304(2)	25(1)
C(48)	196(4)	-767(2)	1169(2)	29(1)
C(49)	221(5)	-1030(2)	596(2)	40(1)
C(50)	-804(5)	-953(3)	155(2)	45(1)
C(51)	-1841(5)	-594(2)	281(2)	41(1)
C(52)	-1928(4)	-315(2)	852(2)	29(1)
C(53)	1383(4)	-821(2)	1623(2)	38(1)
C(54)	2352(6)	-275(3)	1573(4)	77(2)
C(55)	2115(7)	-1407(3)	1573(4)	82(2)
C(56)	-3068(4)	103(2)	945(2)	32(1)
C(57)	-2993(5)	654(2)	507(2)	47(1)
C(58)	-4422(5)	-235(2)	846(2)	40(1)
C(59)	-646(4)	-732(2)	3751(2)	25(1)
C(60)	410(4)	-1138(2)	3789(2)	32(1)
C(61)	507(5)	-1521(2)	4296(2)	43(1)
C(62)	-407(5)	-1508(2)	4740(2)	44(1)
C(63)	-1414(5)	-1105(2)	4701(2)	37(1)
C(64)	-1559(4)	-699(2)	4211(2)	28(1)

C(65)	1457(5)	-1148(3)	3321(2)	45(1)
C(66)	2615(6)	-705(4)	3507(3)	80(2)
C(67)	1974(7)	-1796(4)	3214(3)	78(2)
C(68)	-2636(4)	-237(2)	4228(2)	34(1)
C(69)	-2412(6)	183(3)	4797(2)	49(1)
C(70)	-4020(5)	-555(3)	4225(2)	49(1)
C(71)	-2375(4)	-1884(2)	1657(2)	32(1)
C(72)	-2000(6)	-2537(3)	1483(3)	63(2)
C(73)	-2385(6)	-2664(3)	809(3)	73(2)
C(74)	-3851(5)	-2591(2)	665(2)	45(1)
C(75)	-4259(6)	-1957(3)	860(2)	54(1)
C(76)	-3852(5)	-1828(2)	1531(2)	41(1)
C(77)	-2439(4)	-2040(2)	3044(2)	30(1)
C(78)	-1948(6)	-2681(3)	3172(3)	64(2)
C(79)	-2492(6)	-2948(3)	3756(3)	60(2)
C(80)	-3962(5)	-2944(3)	3747(3)	51(1)
C(81)	-4444(6)	-2313(3)	3623(3)	77(2)
C(82)	-3931(5)	-2051(3)	3026(3)	59(2)
C(1S)	8002(3)	2682(1)	1430(1)	51(1)
C(2S)	8578(3)	3145(1)	1086(1)	59(2)
C(3S)	8264(4)	3172(2)	462(1)	60(2)
C(4S)	7373(4)	2738(2)	183(1)	59(2)
C(5S)	6797(3)	2275(2)	527(1)	59(2)
C(6S)	7112(3)	2248(1)	1151(1)	54(1)
C(7S)	8340(5)	2652(2)	2103(1)	72(2)
C(8S)	2457(4)	2087(2)	1458(2)	89(2)
C(9S)	3285(5)	1665(2)	1217(2)	87(2)
C(10S)	3914(5)	1242(2)	1596(3)	109(3)
C(11S)	3715(6)	1242(3)	2217(3)	134(4)
C(12S)	2887(6)	1664(3)	2458(2)	132(4)
C(13S)	2258(5)	2086(2)	2079(2)	62(2)
C(14S)	1793(7)	2534(3)	1062(3)	152(5)
C(15S)	6585(5)	2154(2)	4490(2)	87(2)
C(16S)	7703(5)	2231(3)	4154(3)	104(3)
C(17S)	7881(6)	1839(3)	3667(3)	140(4)
C(18S)	6940(7)	1369(3)	3516(3)	110(3)
C(19S)	5821(6)	1291(3)	3852(3)	166(5)
C(20S)	5644(5)	1683(3)	4339(3)	116(3)
C(21S)	6650(9)	2648(3)	4988(3)	179(6)

Table A73. Bond lengths [Å] and angles [deg] for [(BDI_{DIPP})Ge(Se)PCy₂] (**51**)

Se(1)-Ge(1)	2.2216(5)
Se(2)-Ge(2)	2.2258(5)
Ge(1)-N(2)	1.965(3)
Ge(1)-N(1)	1.975(3)
Ge(1)-P(1)	2.3714(11)
Ge(2)-N(4)	1.960(3)
Ge(2)-N(3)	1.962(3)
Ge(2)-P(2)	2.3325(11)
P(1)-C(30)	1.880(4)
P(1)-C(36)	1.896(4)
P(2)-C(71)	1.871(4)
P(2)-C(77)	1.878(4)
N(1)-C(1)	1.337(5)
N(1)-C(6)	1.456(5)
N(2)-C(3)	1.339(5)
N(2)-C(18)	1.450(5)
N(3)-C(42)	1.332(5)
N(3)-C(47)	1.449(5)
N(4)-C(44)	1.328(5)
N(4)-C(59)	1.463(5)
C(1)-C(2)	1.385(5)
C(1)-C(4)	1.506(5)
C(2)-C(3)	1.391(5)
C(3)-C(5)	1.506(5)
C(6)-C(7)	1.404(6)
C(6)-C(11)	1.410(5)
C(7)-C(8)	1.389(6)
C(7)-C(12)	1.522(6)
C(8)-C(9)	1.383(6)
C(9)-C(10)	1.373(7)
C(10)-C(11)	1.393(6)
C(11)-C(15)	1.527(6)
C(12)-C(14)	1.522(7)
C(12)-C(13)	1.529(7)
C(15)-C(17)	1.532(6)
C(15)-C(16)	1.537(7)

C(18)-C(19)	1.403(6)
C(18)-C(23)	1.404(5)
C(19)-C(20)	1.392(5)
C(19)-C(24)	1.524(6)
C(20)-C(21)	1.379(6)
C(21)-C(22)	1.374(7)
C(22)-C(23)	1.401(6)
C(23)-C(27)	1.519(6)
C(24)-C(25)	1.514(7)
C(24)-C(26)	1.524(7)
C(27)-C(29)	1.532(6)
C(27)-C(28)	1.534(6)
C(30)-C(35)	1.532(6)
C(30)-C(31)	1.535(6)
C(31)-C(32)	1.525(6)
C(32)-C(33)	1.528(7)
C(33)-C(34)	1.517(8)
C(34)-C(35)	1.527(6)
C(36)-C(41)	1.535(6)
C(36)-C(37)	1.544(6)
C(37)-C(38)	1.532(6)
C(38)-C(39)	1.532(7)
C(39)-C(40)	1.514(7)
C(40)-C(41)	1.531(6)
C(42)-C(43)	1.398(6)
C(42)-C(45)	1.509(6)
C(43)-C(44)	1.399(6)
C(44)-C(46)	1.507(5)
C(47)-C(48)	1.412(6)
C(47)-C(52)	1.412(6)
C(48)-C(49)	1.382(6)
C(48)-C(53)	1.519(6)
C(49)-C(50)	1.390(7)
C(50)-C(51)	1.372(7)
C(51)-C(52)	1.399(6)
C(52)-C(56)	1.517(6)
C(53)-C(55)	1.505(8)
C(53)-C(54)	1.514(8)

C(56)-C(58)	1.526(6)
C(56)-C(57)	1.542(6)
C(59)-C(60)	1.410(6)
C(59)-C(64)	1.412(6)
C(60)-C(61)	1.396(6)
C(60)-C(65)	1.518(6)
C(61)-C(62)	1.383(7)
C(62)-C(63)	1.368(7)
C(63)-C(64)	1.399(6)
C(64)-C(68)	1.512(6)
C(65)-C(66)	1.517(8)
C(65)-C(67)	1.544(8)
C(68)-C(70)	1.531(7)
C(68)-C(69)	1.544(6)
C(71)-C(76)	1.508(6)
C(71)-C(72)	1.537(7)
C(72)-C(73)	1.529(8)
C(73)-C(74)	1.507(8)
C(74)-C(75)	1.520(7)
C(75)-C(76)	1.527(6)
C(77)-C(82)	1.501(6)
C(77)-C(78)	1.520(7)
C(78)-C(79)	1.534(8)
C(79)-C(80)	1.481(8)
C(80)-C(81)	1.496(8)
C(81)-C(82)	1.541(7)
N(2)-Ge(1)-N(1)	92.37(13)
N(2)-Ge(1)-Se(1)	112.38(9)
N(1)-Ge(1)-Se(1)	110.22(9)
N(2)-Ge(1)-P(1)	108.12(9)
N(1)-Ge(1)-P(1)	110.25(10)
Se(1)-Ge(1)-P(1)	120.02(3)
N(4)-Ge(2)-N(3)	93.23(13)
N(4)-Ge(2)-Se(2)	110.90(10)
N(3)-Ge(2)-Se(2)	109.94(9)
N(4)-Ge(2)-P(2)	103.78(10)
N(3)-Ge(2)-P(2)	106.32(10)

Se(2)-Ge(2)-P(2)	127.25(3)
C(30)-P(1)-C(36)	101.15(19)
C(30)-P(1)-Ge(1)	100.42(14)
C(36)-P(1)-Ge(1)	100.58(14)
C(71)-P(2)-C(77)	110.1(2)
C(71)-P(2)-Ge(2)	102.37(15)
C(77)-P(2)-Ge(2)	102.00(14)
C(1)-N(1)-C(6)	119.5(3)
C(1)-N(1)-Ge(1)	119.6(2)
C(6)-N(1)-Ge(1)	120.3(2)
C(3)-N(2)-C(18)	119.3(3)
C(3)-N(2)-Ge(1)	119.3(2)
C(18)-N(2)-Ge(1)	120.8(2)
C(42)-N(3)-C(47)	121.1(3)
C(42)-N(3)-Ge(2)	117.4(3)
C(47)-N(3)-Ge(2)	120.8(2)
C(44)-N(4)-C(59)	121.3(3)
C(44)-N(4)-Ge(2)	118.1(3)
C(59)-N(4)-Ge(2)	119.8(2)
N(1)-C(1)-C(2)	123.6(3)
N(1)-C(1)-C(4)	120.0(3)
C(2)-C(1)-C(4)	116.3(4)
C(1)-C(2)-C(3)	127.0(4)
N(2)-C(3)-C(2)	123.7(3)
N(2)-C(3)-C(5)	119.8(3)
C(2)-C(3)-C(5)	116.5(4)
C(7)-C(6)-C(11)	121.7(4)
C(7)-C(6)-N(1)	118.2(3)
C(11)-C(6)-N(1)	120.1(3)
C(8)-C(7)-C(6)	117.9(4)
C(8)-C(7)-C(12)	119.8(4)
C(6)-C(7)-C(12)	122.2(3)
C(9)-C(8)-C(7)	121.3(4)
C(10)-C(9)-C(8)	120.0(4)
C(9)-C(10)-C(11)	121.7(4)
C(10)-C(11)-C(6)	117.4(4)
C(10)-C(11)-C(15)	118.8(4)
C(6)-C(11)-C(15)	123.8(4)

C(7)-C(12)-C(14)	113.1(4)
C(7)-C(12)-C(13)	110.9(4)
C(14)-C(12)-C(13)	110.0(4)
C(11)-C(15)-C(17)	112.0(4)
C(11)-C(15)-C(16)	111.4(4)
C(17)-C(15)-C(16)	108.0(4)
C(19)-C(18)-C(23)	121.9(3)
C(19)-C(18)-N(2)	117.8(3)
C(23)-C(18)-N(2)	120.3(3)
C(20)-C(19)-C(18)	117.8(4)
C(20)-C(19)-C(24)	119.4(4)
C(18)-C(19)-C(24)	122.7(3)
C(21)-C(20)-C(19)	121.4(4)
C(22)-C(21)-C(20)	119.9(4)
C(21)-C(22)-C(23)	121.6(4)
C(22)-C(23)-C(18)	117.3(4)
C(22)-C(23)-C(27)	118.8(4)
C(18)-C(23)-C(27)	123.9(4)
C(25)-C(24)-C(26)	109.0(4)
C(25)-C(24)-C(19)	114.7(4)
C(26)-C(24)-C(19)	110.6(4)
C(23)-C(27)-C(29)	111.5(4)
C(23)-C(27)-C(28)	111.5(4)
C(29)-C(27)-C(28)	109.2(3)
C(35)-C(30)-C(31)	109.4(4)
C(35)-C(30)-P(1)	111.9(3)
C(31)-C(30)-P(1)	110.4(3)
C(32)-C(31)-C(30)	111.0(4)
C(31)-C(32)-C(33)	110.7(4)
C(34)-C(33)-C(32)	111.2(4)
C(33)-C(34)-C(35)	112.2(4)
C(34)-C(35)-C(30)	111.2(4)
C(41)-C(36)-C(37)	110.8(3)
C(41)-C(36)-P(1)	117.3(3)
C(37)-C(36)-P(1)	109.7(3)
C(38)-C(37)-C(36)	111.1(4)
C(37)-C(38)-C(39)	111.1(4)
C(40)-C(39)-C(38)	110.2(4)

C(39)-C(40)-C(41)	111.1(4)
C(40)-C(41)-C(36)	110.5(4)
N(3)-C(42)-C(43)	122.8(4)
N(3)-C(42)-C(45)	120.4(4)
C(43)-C(42)-C(45)	116.8(4)
C(42)-C(43)-C(44)	127.8(4)
N(4)-C(44)-C(43)	122.9(4)
N(4)-C(44)-C(46)	120.3(4)
C(43)-C(44)-C(46)	116.8(4)
C(48)-C(47)-C(52)	120.9(4)
C(48)-C(47)-N(3)	118.2(3)
C(52)-C(47)-N(3)	120.8(4)
C(49)-C(48)-C(47)	118.6(4)
C(49)-C(48)-C(53)	119.6(4)
C(47)-C(48)-C(53)	121.7(4)
C(48)-C(49)-C(50)	121.3(4)
C(51)-C(50)-C(49)	119.6(4)
C(50)-C(51)-C(52)	122.0(4)
C(51)-C(52)-C(47)	117.4(4)
C(51)-C(52)-C(56)	118.7(4)
C(47)-C(52)-C(56)	123.8(4)
C(55)-C(53)-C(54)	109.3(5)
C(55)-C(53)-C(48)	114.8(5)
C(54)-C(53)-C(48)	110.6(4)
C(52)-C(56)-C(58)	112.2(4)
C(52)-C(56)-C(57)	109.9(4)
C(58)-C(56)-C(57)	109.5(4)
C(60)-C(59)-C(64)	121.9(4)
C(60)-C(59)-N(4)	118.3(4)
C(64)-C(59)-N(4)	119.8(4)
C(61)-C(60)-C(59)	117.4(4)
C(61)-C(60)-C(65)	119.9(4)
C(59)-C(60)-C(65)	122.6(4)
C(62)-C(61)-C(60)	121.2(4)
C(63)-C(62)-C(61)	120.6(4)
C(62)-C(63)-C(64)	121.3(4)
C(63)-C(64)-C(59)	117.5(4)
C(63)-C(64)-C(68)	117.7(4)

C(59)-C(64)-C(68)	124.7(4)
C(66)-C(65)-C(60)	110.3(4)
C(66)-C(65)-C(67)	109.6(5)
C(60)-C(65)-C(67)	113.2(5)
C(64)-C(68)-C(70)	111.6(4)
C(64)-C(68)-C(69)	110.8(4)
C(70)-C(68)-C(69)	109.4(4)
C(76)-C(71)-C(72)	108.8(4)
C(76)-C(71)-P(2)	122.2(3)
C(72)-C(71)-P(2)	108.6(3)
C(73)-C(72)-C(71)	110.1(5)
C(74)-C(73)-C(72)	111.5(5)
C(73)-C(74)-C(75)	110.8(4)
C(74)-C(75)-C(76)	111.3(4)
C(71)-C(76)-C(75)	111.2(4)
C(82)-C(77)-C(78)	110.0(4)
C(82)-C(77)-P(2)	120.6(3)
C(78)-C(77)-P(2)	110.2(3)
C(77)-C(78)-C(79)	111.6(5)
C(80)-C(79)-C(78)	112.3(5)
C(79)-C(80)-C(81)	111.1(5)
C(80)-C(81)-C(82)	111.6(5)
C(77)-C(82)-C(81)	110.9(4)

Table A74. Crystal data and structure refinement for [(BDI_{DIPP})SnSP(S)Cy₂] (**52**)

Identification code	may210	
Empirical formula	C ₄₁ H ₆₃ N ₂ P S ₂ Sn, C ₇ H ₈	
Formula weight	889.85	
Temperature	173(2) K	
Wavelength	0.71073 Å	
Crystal system	Monoclinic	
Space group	<i>P</i> 2 ₁ / <i>c</i> (No.14)	
Unit cell dimensions	a = 13.1888(2) Å	a = 90°.
	b = 18.2309(2) Å	b = 103.817(1)°.
	c = 20.4088(3) Å	g = 90°.
Volume	4765.17(11) Å ³	
Z	4	
Density (calculated)	1.24 Mg/m ³	
Absorption coefficient	0.69 mm ⁻¹	
F(000)	1880	
Crystal size	0.20 x 0.10 x 0.07 mm ³	
Theta range for data collection	3.51 to 27.10°.	
Index ranges	-16 ≤ h ≤ 16, -23 ≤ k ≤ 23, -26 ≤ l ≤ 26	
Reflections collected	74584	
Independent reflections	10472 [R(int) = 0.062]	
Reflections with I > 2σ(I)	8789	
Completeness to theta = 27.10°	99.7 %	
Tmax. and Tmin.	0.9636 and 0.8254	
Refinement method	Full-matrix least-squares on F ²	
Data / restraints / parameters	10472 / 0 / 489	
Goodness-of-fit on F ²	1.018	
Final R indices [I > 2σ(I)]	R1 = 0.032, wR2 = 0.071	
R indices (all data)	R1 = 0.045, wR2 = 0.076	
Largest diff. peak and hole	0.47 and -0.68 e.Å ⁻³	

Data collection KappaCCD , Program package WinGX , Abs correction MULTISCAN

Refinement using SHELXL-97 , Drawing using ORTEP-3 for Windows

Table A75. Atomic coordinates ($\times 10^4$) and equivalent isotropic displacement parameters ($\text{\AA}^2 \times 10^3$) for $[(\text{BDI}_{\text{DIPP}})\text{SnSP}(\text{S})\text{Cy}_2]$ (**52**). $U(\text{eq})$ is defined as one third of the trace of the orthogonalized U^{ij} tensor

	x	y	z	$U(\text{eq})$
Sn	4027(1)	5950(1)	2468(1)	17(1)
S(1)	2476(1)	6718(1)	1918(1)	22(1)
S(2)	3975(1)	7638(1)	3274(1)	26(1)
P	2741(1)	7647(1)	2511(1)	19(1)
N(1)	4258(1)	5586(1)	1476(1)	16(1)
N(2)	3018(1)	4968(1)	2366(1)	17(1)
C(1)	4451(2)	4879(1)	1405(1)	18(1)
C(2)	4152(2)	4322(1)	1798(1)	21(1)
C(3)	3405(2)	4349(1)	2182(1)	20(1)
C(4)	5015(2)	4622(1)	884(1)	28(1)
C(5)	3042(2)	3618(1)	2391(1)	32(1)
C(6)	4552(2)	6130(1)	1043(1)	18(1)
C(7)	3795(2)	6415(1)	495(1)	21(1)
C(8)	4098(2)	6954(1)	101(1)	31(1)
C(9)	5110(2)	7220(1)	244(1)	37(1)
C(10)	5839(2)	6945(1)	789(1)	33(1)
C(11)	5584(2)	6400(1)	1200(1)	21(1)
C(12)	2676(2)	6133(1)	326(1)	25(1)
C(13)	2532(2)	5520(2)	-196(2)	54(1)
C(14)	1879(2)	6743(2)	89(1)	42(1)
C(15)	6409(2)	6128(1)	1804(1)	24(1)
C(16)	6678(2)	6727(1)	2339(1)	34(1)
C(17)	7404(2)	5869(2)	1615(2)	40(1)
C(18)	2115(2)	4964(1)	2647(1)	20(1)
C(19)	1120(2)	5033(1)	2202(1)	23(1)
C(20)	254(2)	5053(1)	2479(1)	33(1)
C(21)	356(2)	5021(2)	3167(2)	41(1)
C(22)	1329(2)	4961(2)	3593(1)	39(1)
C(23)	2229(2)	4927(1)	3345(1)	28(1)
C(24)	991(2)	5075(1)	1444(1)	28(1)
C(25)	169(2)	5638(2)	1110(1)	40(1)
C(26)	724(3)	4327(2)	1111(1)	48(1)

C(27)	3292(2)	4856(2)	3841(1)	39(1)
C(28)	3567(3)	5557(2)	4256(2)	63(1)
C(29)	3334(3)	4183(2)	4297(2)	63(1)
C(30)	2788(2)	8376(1)	1901(1)	23(1)
C(31)	2717(2)	9146(1)	2183(1)	33(1)
C(32)	2715(3)	9722(1)	1635(2)	44(1)
C(33)	3665(3)	9645(2)	1340(2)	48(1)
C(34)	3751(3)	8876(2)	1073(2)	45(1)
C(35)	3763(2)	8301(1)	1619(1)	32(1)
C(36)	1520(2)	7768(1)	2786(1)	24(1)
C(37)	559(2)	7824(1)	2193(1)	31(1)
C(38)	-447(2)	7889(2)	2436(1)	39(1)
C(39)	-558(2)	7275(2)	2914(2)	43(1)
C(40)	386(2)	7233(2)	3505(1)	39(1)
C(41)	1397(2)	7147(1)	3269(1)	29(1)
C(1S)	-969(4)	6767(2)	4918(2)	70(1)
C(2S)	-947(4)	7449(3)	5167(2)	88(2)
C(3S)	-1728(7)	7906(3)	4977(4)	117(2)
C(4S)	-2598(6)	7726(5)	4506(4)	125(3)
C(5S)	-2668(5)	7021(5)	4236(2)	119(3)
C(6S)	-1829(5)	6540(3)	4452(2)	84(2)
C(7S)	-37(5)	6269(4)	5160(3)	144(3)

Table A76. Bond lengths [Å] and angles [deg] for [(BDI_{DIPP})SnSP(S)Cy₂] (**52**)

Sn-N(2)	2.2107(17)
Sn-N(1)	2.2215(16)
Sn-S(1)	2.5107(6)
S(1)-P	2.0641(7)
S(2)-P	1.9655(8)
P-C(30)	1.833(2)
P-C(36)	1.841(2)
N(1)-C(1)	1.328(3)
N(1)-C(6)	1.442(3)
N(2)-C(3)	1.330(3)
N(2)-C(18)	1.440(3)
C(1)-C(2)	1.408(3)
C(1)-C(4)	1.510(3)
C(2)-C(3)	1.397(3)
C(3)-C(5)	1.512(3)
C(6)-C(7)	1.409(3)
C(6)-C(11)	1.410(3)
C(7)-C(8)	1.389(3)
C(7)-C(12)	1.522(3)
C(8)-C(9)	1.384(4)
C(9)-C(10)	1.378(4)
C(10)-C(11)	1.393(3)
C(11)-C(15)	1.520(3)
C(12)-C(13)	1.523(3)
C(12)-C(14)	1.527(3)
C(15)-C(16)	1.524(3)
C(15)-C(17)	1.529(3)
C(18)-C(23)	1.399(3)
C(18)-C(19)	1.411(3)
C(19)-C(20)	1.390(3)
C(19)-C(24)	1.518(3)
C(20)-C(21)	1.380(4)
C(21)-C(22)	1.372(4)
C(22)-C(23)	1.399(3)
C(23)-C(27)	1.525(3)
C(24)-C(26)	1.527(4)

C(24)-C(25)	1.530(3)
C(27)-C(28)	1.529(5)
C(27)-C(29)	1.533(4)
C(30)-C(31)	1.529(3)
C(30)-C(35)	1.535(3)
C(31)-C(32)	1.534(3)
C(32)-C(33)	1.520(4)
C(33)-C(34)	1.519(4)
C(34)-C(35)	1.526(4)
C(36)-C(37)	1.533(3)
C(36)-C(41)	1.535(3)
C(37)-C(38)	1.529(3)
C(38)-C(39)	1.514(4)
C(39)-C(40)	1.515(4)
C(40)-C(41)	1.530(3)
N(2)-Sn-N(1)	83.23(6)
N(2)-Sn-S(1)	90.08(5)
N(1)-Sn-S(1)	91.90(5)
P-S(1)-Sn	100.91(3)
C(30)-P-C(36)	107.20(11)
C(30)-P-S(2)	112.83(8)
C(36)-P-S(2)	112.30(8)
C(30)-P-S(1)	102.98(7)
C(36)-P-S(1)	103.84(7)
S(2)-P-S(1)	116.72(3)
C(1)-N(1)-C(6)	121.00(17)
C(1)-N(1)-Sn	117.44(14)
C(6)-N(1)-Sn	117.92(12)
C(3)-N(2)-C(18)	121.17(17)
C(3)-N(2)-Sn	116.79(14)
C(18)-N(2)-Sn	120.24(13)
N(1)-C(1)-C(2)	123.44(19)
N(1)-C(1)-C(4)	121.11(19)
C(2)-C(1)-C(4)	115.46(19)
C(3)-C(2)-C(1)	128.64(19)
N(2)-C(3)-C(2)	123.95(19)
N(2)-C(3)-C(5)	119.94(19)

C(2)-C(3)-C(5)	116.10(19)
C(7)-C(6)-C(11)	121.0(2)
C(7)-C(6)-N(1)	119.71(19)
C(11)-C(6)-N(1)	119.17(19)
C(8)-C(7)-C(6)	118.2(2)
C(8)-C(7)-C(12)	120.4(2)
C(6)-C(7)-C(12)	121.46(19)
C(9)-C(8)-C(7)	121.5(2)
C(10)-C(9)-C(8)	119.7(2)
C(9)-C(10)-C(11)	121.5(2)
C(10)-C(11)-C(6)	118.1(2)
C(10)-C(11)-C(15)	119.5(2)
C(6)-C(11)-C(15)	122.40(19)
C(7)-C(12)-C(13)	111.0(2)
C(7)-C(12)-C(14)	112.5(2)
C(13)-C(12)-C(14)	110.6(2)
C(11)-C(15)-C(16)	110.33(19)
C(11)-C(15)-C(17)	112.7(2)
C(16)-C(15)-C(17)	109.6(2)
C(23)-C(18)-C(19)	121.1(2)
C(23)-C(18)-N(2)	120.5(2)
C(19)-C(18)-N(2)	118.26(19)
C(20)-C(19)-C(18)	118.0(2)
C(20)-C(19)-C(24)	120.6(2)
C(18)-C(19)-C(24)	121.4(2)
C(21)-C(20)-C(19)	121.5(2)
C(22)-C(21)-C(20)	119.8(2)
C(21)-C(22)-C(23)	121.4(2)
C(22)-C(23)-C(18)	118.2(2)
C(22)-C(23)-C(27)	119.3(2)
C(18)-C(23)-C(27)	122.6(2)
C(19)-C(24)-C(26)	111.5(2)
C(19)-C(24)-C(25)	112.6(2)
C(26)-C(24)-C(25)	109.8(2)
C(23)-C(27)-C(28)	110.8(2)
C(23)-C(27)-C(29)	111.4(2)
C(28)-C(27)-C(29)	111.3(3)
C(31)-C(30)-C(35)	110.9(2)

C(31)-C(30)-P	113.23(16)
C(35)-C(30)-P	110.95(16)
C(30)-C(31)-C(32)	110.1(2)
C(33)-C(32)-C(31)	111.5(2)
C(34)-C(33)-C(32)	111.5(2)
C(33)-C(34)-C(35)	111.1(2)
C(34)-C(35)-C(30)	110.4(2)
C(37)-C(36)-C(41)	111.26(19)
C(37)-C(36)-P	112.67(16)
C(41)-C(36)-P	110.02(16)
C(38)-C(37)-C(36)	111.5(2)
C(39)-C(38)-C(37)	112.1(2)
C(38)-C(39)-C(40)	111.3(2)
C(39)-C(40)-C(41)	111.5(2)
C(40)-C(41)-C(36)	111.1(2)

Table A77. Crystal data and structure refinement for [(BDI_{DIPP})PbSP(S)Cy₂] (**53**)

Identification code	jun1610	
Empirical formula	C ₄₁ H ₆₃ N ₂ P Pb S ₂ , C ₇ H ₈	
Formula weight	978.35	
Temperature	173(2) K	
Wavelength	0.71073 Å	
Crystal system	Orthorhombic	
Space group	<i>P</i> 2 ₁ 2 ₁ 2 ₁ (No.19)	
Unit cell dimensions	a = 10.1944(1) Å	a = 90°.
	b = 15.4698(2) Å	b = 90°.
	c = 29.9406(4) Å	g = 90°.
Volume	4721.79(10) Å ³	
Z	4	
Density (calculated)	1.38 Mg/m ³	
Absorption coefficient	3.73 mm ⁻¹	
F(000)	2008	
Crystal size	0.1 x 0.08 x 0.08 mm ³	
Theta range for data collection	3.58 to 26.73°.	
Index ranges	-12 ≤ h ≤ 12, -19 ≤ k ≤ 19, -37 ≤ l ≤ 37	
Reflections collected	74892	
Independent reflections	10004 [R(int) = 0.095]	
Reflections with I > 2σ(I)	8799	
Completeness to theta = 26.73°	99.6 %	
Tmax. and Tmin.	0.7788 and 0.6499	
Refinement method	Full-matrix least-squares on F ²	
Data / restraints / parameters	10004 / 0 / 439	
Goodness-of-fit on F ²	1.087	
Final R indices [I > 2σ(I)]	R1 = 0.035, wR2 = 0.066	
R indices (all data)	R1 = 0.047, wR2 = 0.069	
Absolute structure parameter	-0.009(4)	
Largest diff. peak and hole	0.93 and -0.71 e.Å ⁻³	

The toluene solvate was refined as a rigid body with isotropic carbon atoms

Data collection KappaCCD , Program package WinGX , Abs correction MULTISCAN

Refinement using SHELXL-97 , Drawing using ORTEP-3 for Windows

Table A78. Atomic coordinates ($\times 10^4$) and equivalent isotropic displacement parameters ($\text{\AA}^2 \times 10^3$) for $[(\text{BDI}_{\text{DIPP}})\text{PbSP}(\text{S})\text{Cy}_2]$ (**53**). $U(\text{eq})$ is defined as one third of the trace of the orthogonalized U^{ij} tensor

	x	y	z	$U(\text{eq})$
Pb	7624(1)	4700(1)	1363(1)	19(1)
S(1)	6641(1)	5568(1)	683(1)	28(1)
S(2)	9890(1)	5076(1)	612(1)	35(1)
P	8404(1)	5741(1)	364(1)	23(1)
N(1)	5996(3)	3622(2)	1391(1)	20(1)
N(2)	6125(3)	5362(3)	1846(1)	19(1)
C(1)	5428(5)	3441(3)	1778(2)	21(1)
C(2)	5362(5)	4005(3)	2146(2)	23(1)
C(3)	5576(4)	4910(3)	2169(2)	20(1)
C(4)	4762(6)	2577(4)	1846(2)	37(1)
C(5)	5165(5)	5348(4)	2599(2)	32(1)
C(6)	5872(4)	3061(3)	1013(2)	22(1)
C(7)	4845(5)	3211(3)	710(2)	26(1)
C(8)	4770(5)	2684(4)	334(2)	32(1)
C(9)	5651(6)	2051(4)	253(2)	38(2)
C(10)	6675(5)	1899(4)	553(2)	34(1)
C(11)	6804(5)	2409(3)	939(2)	26(1)
C(12)	3811(5)	3902(4)	793(2)	36(1)
C(13)	2519(6)	3491(5)	959(2)	72(2)
C(14)	3524(5)	4457(4)	380(2)	42(2)
C(15)	7926(5)	2232(3)	1256(2)	33(1)
C(16)	7860(7)	1311(4)	1441(2)	64(2)
C(17)	9245(6)	2390(5)	1037(2)	49(2)
C(18)	6187(4)	6296(3)	1860(2)	20(1)
C(19)	5237(4)	6780(3)	1628(2)	21(1)
C(20)	5374(5)	7666(4)	1613(2)	30(1)
C(21)	6413(5)	8078(4)	1812(2)	29(1)
C(22)	7348(5)	7598(3)	2037(2)	24(1)
C(23)	7249(5)	6698(3)	2064(2)	21(1)
C(24)	4076(4)	6334(3)	1392(2)	29(1)
C(25)	2946(5)	6195(4)	1711(2)	50(2)
C(26)	3596(5)	6827(4)	983(2)	43(2)

C(27)	8344(5)	6209(3)	2307(2)	24(1)
C(28)	8459(5)	6497(4)	2795(2)	36(1)
C(29)	9639(5)	6331(4)	2070(2)	34(1)
C(30)	8107(5)	5448(3)	-226(2)	26(1)
C(31)	9336(6)	5580(4)	-507(2)	36(1)
C(32)	9092(6)	5327(4)	-1000(2)	47(2)
C(33)	8591(6)	4408(4)	-1037(2)	47(2)
C(34)	7354(7)	4290(4)	-756(2)	54(2)
C(35)	7597(6)	4519(3)	-265(2)	37(1)
C(36)	8753(5)	6902(4)	378(2)	30(1)
C(37)	7643(6)	7465(3)	180(2)	39(1)
C(38)	7962(7)	8429(4)	205(2)	54(2)
C(39)	8259(9)	8707(5)	682(2)	73(2)
C(40)	9340(8)	8171(5)	881(3)	65(2)
C(41)	9065(6)	7199(4)	855(2)	44(2)
C(1S)	9303(3)	3994(3)	2772(1)	77(2)
C(2S)	9276(4)	3642(3)	2344(1)	52(2)
C(3S)	10331(5)	3765(3)	2057(1)	90(3)
C(4S)	11414(4)	4240(3)	2197(2)	72(2)
C(5S)	11441(4)	4591(3)	2625(2)	86(3)
C(6S)	10385(4)	4468(3)	2912(1)	57(2)
C(7S)	8215(4)	3861(4)	3066(2)	83(3)

Table A79. Bond lengths [Å] and angles [deg] for [(BDI_{DIPP})PbSP(S)Cy₂] (**53**)

Pb-N(2)	2.340(4)
Pb-N(1)	2.355(4)
Pb-S(1)	2.6370(13)
S(1)-P	2.0528(17)
S(2)-P	1.9755(18)
P-C(36)	1.832(6)
P-C(30)	1.848(5)
N(1)-C(1)	1.325(6)
N(1)-C(6)	1.432(6)
N(2)-C(3)	1.319(6)
N(2)-C(18)	1.447(6)
C(1)-C(2)	1.406(7)
C(1)-C(4)	1.513(7)
C(2)-C(3)	1.418(7)
C(3)-C(5)	1.514(7)
C(6)-C(11)	1.403(7)
C(6)-C(7)	1.404(7)
C(7)-C(8)	1.392(7)
C(7)-C(12)	1.522(7)
C(8)-C(9)	1.352(8)
C(9)-C(10)	1.397(8)
C(10)-C(11)	1.407(7)
C(11)-C(15)	1.510(7)
C(12)-C(14)	1.533(8)
C(12)-C(13)	1.545(8)
C(15)-C(17)	1.516(8)
C(15)-C(16)	1.532(8)
C(18)-C(23)	1.390(7)
C(18)-C(19)	1.406(7)
C(19)-C(20)	1.378(7)
C(19)-C(24)	1.542(7)
C(20)-C(21)	1.374(7)
C(21)-C(22)	1.383(7)
C(22)-C(23)	1.398(6)
C(23)-C(27)	1.532(6)
C(24)-C(25)	1.512(7)

C(24)-C(26)	1.523(8)
C(27)-C(29)	1.510(7)
C(27)-C(28)	1.531(7)
C(30)-C(31)	1.523(7)
C(30)-C(35)	1.533(6)
C(31)-C(32)	1.547(8)
C(32)-C(33)	1.514(9)
C(33)-C(34)	1.527(9)
C(34)-C(35)	1.531(7)
C(36)-C(41)	1.535(8)
C(36)-C(37)	1.547(8)
C(37)-C(38)	1.528(7)
C(38)-C(39)	1.522(9)
C(39)-C(40)	1.501(11)
C(40)-C(41)	1.533(9)
N(2)-Pb-N(1)	80.07(14)
N(2)-Pb-S(1)	90.36(10)
N(1)-Pb-S(1)	96.92(10)
P-S(1)-Pb	95.28(6)
C(36)-P-C(30)	107.1(2)
C(36)-P-S(2)	110.70(18)
C(30)-P-S(2)	110.89(17)
C(36)-P-S(1)	106.70(18)
C(30)-P-S(1)	105.56(16)
S(2)-P-S(1)	115.43(8)
C(1)-N(1)-C(6)	121.6(4)
C(1)-N(1)-Pb	119.3(3)
C(6)-N(1)-Pb	117.6(3)
C(3)-N(2)-C(18)	121.9(4)
C(3)-N(2)-Pb	119.9(3)
C(18)-N(2)-Pb	115.2(3)
N(1)-C(1)-C(2)	125.1(5)
N(1)-C(1)-C(4)	120.0(5)
C(2)-C(1)-C(4)	114.9(4)
C(1)-C(2)-C(3)	130.0(5)
N(2)-C(3)-C(2)	123.7(4)
N(2)-C(3)-C(5)	120.2(5)

C(2)-C(3)-C(5)	116.1(4)
C(11)-C(6)-C(7)	121.5(5)
C(11)-C(6)-N(1)	120.0(4)
C(7)-C(6)-N(1)	118.5(4)
C(8)-C(7)-C(6)	117.8(5)
C(8)-C(7)-C(12)	120.3(5)
C(6)-C(7)-C(12)	121.9(5)
C(9)-C(8)-C(7)	122.3(5)
C(8)-C(9)-C(10)	120.1(5)
C(9)-C(10)-C(11)	120.3(5)
C(6)-C(11)-C(10)	118.0(5)
C(6)-C(11)-C(15)	123.0(5)
C(10)-C(11)-C(15)	119.0(5)
C(7)-C(12)-C(14)	113.3(5)
C(7)-C(12)-C(13)	110.7(5)
C(14)-C(12)-C(13)	109.1(4)
C(11)-C(15)-C(17)	111.8(5)
C(11)-C(15)-C(16)	111.2(5)
C(17)-C(15)-C(16)	110.3(5)
C(23)-C(18)-C(19)	121.0(5)
C(23)-C(18)-N(2)	119.5(4)
C(19)-C(18)-N(2)	119.2(4)
C(20)-C(19)-C(18)	118.5(5)
C(20)-C(19)-C(24)	120.4(4)
C(18)-C(19)-C(24)	121.1(4)
C(21)-C(20)-C(19)	121.6(5)
C(20)-C(21)-C(22)	119.6(5)
C(21)-C(22)-C(23)	120.9(5)
C(18)-C(23)-C(22)	118.4(4)
C(18)-C(23)-C(27)	123.7(4)
C(22)-C(23)-C(27)	117.8(4)
C(25)-C(24)-C(26)	109.5(4)
C(25)-C(24)-C(19)	111.0(5)
C(26)-C(24)-C(19)	113.1(4)
C(29)-C(27)-C(28)	110.1(4)
C(29)-C(27)-C(23)	110.7(4)
C(28)-C(27)-C(23)	111.4(4)
C(31)-C(30)-C(35)	111.2(4)

C(31)-C(30)-P	111.2(3)
C(35)-C(30)-P	111.0(3)
C(30)-C(31)-C(32)	111.2(4)
C(33)-C(32)-C(31)	111.1(5)
C(32)-C(33)-C(34)	110.5(5)
C(33)-C(34)-C(35)	111.6(5)
C(34)-C(35)-C(30)	110.2(4)
C(41)-C(36)-C(37)	109.9(5)
C(41)-C(36)-P	110.8(4)
C(37)-C(36)-P	113.7(4)
C(38)-C(37)-C(36)	112.0(5)
C(39)-C(38)-C(37)	111.3(5)
C(40)-C(39)-C(38)	111.3(6)
C(39)-C(40)-C(41)	112.8(6)
C(40)-C(41)-C(36)	112.2(5)

Table A80. Crystal data and structure refinement for [(BDI_{DIPP})Ge(S)PCy₂] (**54**)

Identification code	jul911	
Empirical formula	C ₄₅ H ₇₁ Ge N ₂ O P S	
Formula weight	791.66	
Temperature	173(2) K	
Wavelength	0.71073 Å	
Crystal system	Monoclinic	
Space group	<i>P</i> 2 ₁ / <i>c</i> (No.14)	
Unit cell dimensions	a = 17.5377(4) Å	a = 90°.
	b = 10.1519(1) Å	b = 116.156(1)°.
	c = 26.9248(6) Å	g = 90°.
Volume	4302.83(14) Å ³	
Z	4	
Density (calculated)	1.22 Mg/m ³	
Absorption coefficient	0.833 mm ⁻¹	
F(000)	1704	
Crystal size	0.11 x 0.10 x 0.05 mm ³	
Theta range for data collection	3.49 to 26.72°.	
Index ranges	-22 ≤ h ≤ 22, -12 ≤ k ≤ 12, -34 ≤ l ≤ 34	
Reflections collected	45679	
Independent reflections	9105 [R(int) = 0.110]	
Reflections with I > 2σ(I)	6246	
Completeness to theta = 26.72°	99.7 %	
Absorption correction	Semi-empirical from equivalents	
Tmax. and Tmin.	1.0648 and 0.8640	
Refinement method	Full-matrix least-squares on F ²	
Data / restraints / parameters	9105 / 6 / 499	
Goodness-of-fit on F ²	1.022	
Final R indices [I > 2σ(I)]	R1 = 0.054, wR2 = 0.092	
R indices (all data)	R1 = 0.097, wR2 = 0.103	
Largest diff. peak and hole	0.52 and -0.50 e.Å ⁻³	

The methylene groups of the THF solvate are disordered over two positions.

Data collection KappaCCD , Program package WinGX , Abs correction MULTISCAN

Refinement using SHELXL-97 , Drawing using ORTEP-3 for Windows

Table A81. Atomic coordinates ($\times 10^4$) and equivalent isotropic displacement parameters ($\text{\AA}^2 \times 10^3$) for $[(\text{BDI}_{\text{DIPP}})\text{Ge}(\text{S})\text{PCy}_2]$ (**54**). $U(\text{eq})$ is defined as one third of the trace of the orthogonalized U^{ij} tensor

	x	y	z	U(eq)
Ge	8161(1)	2874(1)	1267(1)	15(1)
S	8470(1)	907(1)	1507(1)	24(1)
P	6911(1)	3641(1)	545(1)	18(1)
O	4686(2)	2493(3)	2397(1)	68(1)
N(1)	8257(1)	3938(2)	1898(1)	17(1)
N(2)	9115(1)	3766(2)	1218(1)	18(1)
C(1)	9041(2)	4199(3)	2294(1)	23(1)
C(2)	9757(2)	4150(3)	2203(1)	24(1)
C(3)	9787(2)	4072(3)	1697(1)	22(1)
C(4)	9165(2)	4599(3)	2864(1)	36(1)
C(5)	10631(2)	4393(3)	1701(1)	31(1)
C(6)	7502(2)	4247(3)	1967(1)	20(1)
C(7)	7081(2)	5444(3)	1747(1)	23(1)
C(8)	6305(2)	5675(3)	1755(1)	30(1)
C(9)	5965(2)	4775(3)	1985(1)	35(1)
C(10)	6405(2)	3643(3)	2229(1)	30(1)
C(11)	7177(2)	3356(3)	2225(1)	22(1)
C(12)	7480(2)	6510(3)	1538(1)	28(1)
C(13)	6841(2)	7327(3)	1060(2)	46(1)
C(14)	8031(3)	7425(3)	2015(2)	52(1)
C(15)	7639(2)	2099(3)	2512(1)	25(1)
C(16)	7124(2)	867(3)	2240(2)	34(1)
C(17)	7833(2)	2133(4)	3128(1)	41(1)
C(18)	9154(2)	3846(3)	690(1)	19(1)
C(19)	8807(2)	4964(3)	357(1)	24(1)
C(20)	8792(2)	4977(3)	-164(1)	32(1)
C(21)	9110(2)	3953(3)	-351(1)	35(1)
C(22)	9470(2)	2894(3)	-12(1)	30(1)
C(23)	9511(2)	2809(3)	516(1)	23(1)
C(24)	8454(2)	6124(3)	549(1)	31(1)
C(25)	7879(2)	7034(4)	78(2)	54(1)
C(26)	9168(2)	6953(3)	992(2)	45(1)

C(27)	9976(2)	1637(3)	875(1)	27(1)
C(28)	10910(2)	1612(4)	972(2)	39(1)
C(29)	9558(2)	322(3)	618(2)	36(1)
C(30)	6102(2)	2761(3)	706(1)	19(1)
C(31)	5960(2)	1283(3)	600(1)	22(1)
C(32)	5296(2)	779(3)	780(1)	28(1)
C(33)	4460(2)	1510(3)	485(1)	28(1)
C(34)	4589(2)	2991(3)	583(2)	30(1)
C(35)	5257(2)	3510(3)	413(1)	24(1)
C(36)	6936(2)	2902(3)	-84(1)	22(1)
C(37)	6109(2)	3216(3)	-604(1)	31(1)
C(38)	6195(2)	2896(3)	-1131(1)	40(1)
C(39)	6453(2)	1467(3)	-1134(1)	34(1)
C(40)	7263(2)	1143(3)	-621(1)	36(1)
C(41)	7178(2)	1457(3)	-95(1)	30(1)
C(42)	4339(12)	1680(20)	1919(10)	65(8)
C(43)	3395(11)	1978(14)	1672(6)	62(5)
C(44)	3419(12)	3441(19)	1803(8)	112(9)
C(45)	4117(11)	3413(15)	2396(5)	38(4)
C(42A)	4252(13)	1714(15)	1920(10)	54(9)
C(43A)	3455(13)	2426(18)	1528(6)	68(6)
C(44A)	3212(10)	3130(20)	1936(8)	74(6)
C(45A)	4082(14)	3610(20)	2348(10)	119(11)

Table A82. Bond lengths [Å] and angles [deg] for [(BDI_{DIPP})Ge(S)PCy₂] (**54**)

Ge-S	2.0954(8)
Ge-N(1)	1.956(2)
Ge-N(2)	1.958(2)
Ge-P	2.3322(8)
P-C(36)	1.870(3)
P-C(30)	1.883(3)
O-C(45)	1.366(17)
O-C(42)	1.42(2)
N(1)-C(1)	1.343(4)
N(1)-C(6)	1.451(4)
N(2)-C(3)	1.346(4)
N(2)-C(18)	1.454(4)
C(1)-C(2)	1.384(4)
C(1)-C(4)	1.506(4)
C(2)-C(3)	1.387(4)
C(3)-C(5)	1.511(4)
C(6)-C(11)	1.405(4)
C(6)-C(7)	1.410(4)
C(7)-C(8)	1.390(4)
C(7)-C(12)	1.525(4)
C(8)-C(9)	1.378(5)
C(9)-C(10)	1.377(4)
C(10)-C(11)	1.390(4)
C(11)-C(15)	1.526(4)
C(12)-C(13)	1.526(4)
C(12)-C(14)	1.533(4)
C(15)-C(16)	1.527(4)
C(15)-C(17)	1.540(4)
C(18)-C(23)	1.408(4)
C(18)-C(19)	1.408(4)
C(19)-C(20)	1.392(4)
C(19)-C(24)	1.520(4)
C(20)-C(21)	1.376(5)
C(21)-C(22)	1.370(4)
C(22)-C(23)	1.394(4)
C(23)-C(27)	1.524(4)

C(24)-C(25)	1.533(4)
C(24)-C(26)	1.544(5)
C(27)-C(29)	1.533(4)
C(27)-C(28)	1.540(4)
C(30)-C(31)	1.527(4)
C(30)-C(35)	1.538(4)
C(31)-C(32)	1.533(4)
C(32)-C(33)	1.517(4)
C(33)-C(34)	1.526(4)
C(34)-C(35)	1.526(4)
C(36)-C(41)	1.530(4)
C(36)-C(37)	1.541(4)
C(37)-C(38)	1.528(4)
C(38)-C(39)	1.521(5)
C(39)-C(40)	1.517(4)
C(40)-C(41)	1.523(4)
C(42)-C(43)	1.517(13)
C(43)-C(44)	1.523(15)
C(44)-C(45)	1.525(14)
N(1)-Ge-N(2)	93.14(10)
N(1)-Ge-S	110.28(7)
N(2)-Ge-S	110.50(7)
N(1)-Ge-P	103.26(7)
N(2)-Ge-P	107.79(7)
S-Ge-P	126.56(3)
C(36)-P-C(30)	109.83(13)
C(36)-P-Ge	103.46(10)
C(30)-P-Ge	100.14(9)
C(45)-O-C(42)	111.9(10)
C(1)-N(1)-C(6)	121.8(2)
C(1)-N(1)-Ge	117.70(19)
C(6)-N(1)-Ge	119.81(17)
C(3)-N(2)-C(18)	121.8(2)
C(3)-N(2)-Ge	117.00(19)
C(18)-N(2)-Ge	120.12(17)
N(1)-C(1)-C(2)	122.9(3)
N(1)-C(1)-C(4)	120.0(3)

C(2)-C(1)-C(4)	117.1(3)
C(1)-C(2)-C(3)	127.3(3)
N(2)-C(3)-C(2)	124.0(3)
N(2)-C(3)-C(5)	119.8(3)
C(2)-C(3)-C(5)	116.2(3)
C(11)-C(6)-C(7)	120.8(3)
C(11)-C(6)-N(1)	121.1(3)
C(7)-C(6)-N(1)	118.1(3)
C(8)-C(7)-C(6)	118.2(3)
C(8)-C(7)-C(12)	119.9(3)
C(6)-C(7)-C(12)	121.8(3)
C(9)-C(8)-C(7)	121.1(3)
C(10)-C(9)-C(8)	120.3(3)
C(9)-C(10)-C(11)	121.0(3)
C(10)-C(11)-C(6)	118.5(3)
C(10)-C(11)-C(15)	118.3(3)
C(6)-C(11)-C(15)	123.2(3)
C(7)-C(12)-C(13)	114.3(3)
C(7)-C(12)-C(14)	110.0(3)
C(13)-C(12)-C(14)	109.6(3)
C(11)-C(15)-C(16)	111.9(3)
C(11)-C(15)-C(17)	110.0(2)
C(16)-C(15)-C(17)	109.7(3)
C(23)-C(18)-C(19)	121.5(3)
C(23)-C(18)-N(2)	120.3(2)
C(19)-C(18)-N(2)	118.2(3)
C(20)-C(19)-C(18)	117.4(3)
C(20)-C(19)-C(24)	120.3(3)
C(18)-C(19)-C(24)	122.4(3)
C(21)-C(20)-C(19)	122.1(3)
C(22)-C(21)-C(20)	119.5(3)
C(21)-C(22)-C(23)	121.9(3)
C(22)-C(23)-C(18)	117.6(3)
C(22)-C(23)-C(27)	118.0(3)
C(18)-C(23)-C(27)	124.3(3)
C(19)-C(24)-C(25)	113.8(3)
C(19)-C(24)-C(26)	111.8(3)
C(25)-C(24)-C(26)	108.9(3)

C(23)-C(27)-C(29)	112.2(3)
C(23)-C(27)-C(28)	110.6(3)
C(29)-C(27)-C(28)	108.8(3)
C(31)-C(30)-C(35)	110.4(2)
C(31)-C(30)-P	120.1(2)
C(35)-C(30)-P	107.56(19)
C(30)-C(31)-C(32)	110.7(2)
C(33)-C(32)-C(31)	111.4(3)
C(32)-C(33)-C(34)	110.9(3)
C(35)-C(34)-C(33)	111.4(3)
C(34)-C(35)-C(30)	111.7(2)
C(41)-C(36)-C(37)	109.9(2)
C(41)-C(36)-P	121.2(2)
C(37)-C(36)-P	110.5(2)
C(38)-C(37)-C(36)	111.1(3)
C(39)-C(38)-C(37)	111.1(3)
C(40)-C(39)-C(38)	111.3(3)
C(39)-C(40)-C(41)	111.5(3)
C(40)-C(41)-C(36)	111.1(3)
O-C(42)-C(43)	103.5(12)
C(42)-C(43)-C(44)	100.2(12)
C(43)-C(44)-C(45)	98.8(12)
O-C(45)-C(44)	105.3(9)

Table A83. Crystal data and structure refinement for [(BDI_{DIPP})Ge(Se)P(SiMe₃)₂] (**56**)

Identification code	jun811	
Empirical formula	C ₃₅ H ₅₉ Ge N ₂ P Se Si ₂	
Formula weight	746.54	
Temperature	173(2) K	
Wavelength	0.71073 Å	
Crystal system	Monoclinic	
Space group	<i>P</i> 2 ₁ /c (No.14)	
Unit cell dimensions	a = 13.5873(2) Å	a = 90°.
	b = 18.7351(4) Å	b = 117.597(1)°.
	c = 17.6743(3) Å	g = 90°.
Volume	3987.28(12) Å ³	
Z	4	
Density (calculated)	1.24 Mg/m ³	
Absorption coefficient	1.806 mm ⁻¹	
F(000)	1568	
Crystal size	0.20 x 0.15 x 0.08 mm ³	
Theta range for data collection	3.51 to 26.75°.	
Index ranges	-16 ≤ h ≤ 17, -23 ≤ k ≤ 23, -22 ≤ l ≤ 22	
Reflections collected	56005	
Independent reflections	8452 [R(int) = 0.076]	
Completeness to theta = 26.75°	99.6 %	
Absorption correction	Semi-empirical from equivalents	
Max. and min. transmission	0.8407 and 0.7162	
Refinement method	Full-matrix least-squares on F ²	
Data / restraints / parameters	8452 / 0 / 381	
Goodness-of-fit on F ²	0.969	
Final R indices [I > 2σ(I)]	R1 = 0.034, wR2 = 0.068	
R indices (all data)	R1 = 0.054, wR2 = 0.074	
Largest diff. peak and hole	1.00 and -0.34 e.Å ⁻³	

Data collection KappaCCD , Program package WinGX , Abs correction MULTISCAN
 Refinement using SHELXL-97 , Drawing using ORTEP-3 for Windows

Table A84. Atomic coordinates ($\times 10^4$) and equivalent isotropic displacement parameters ($\text{\AA}^2 \times 10^3$) for $[(\text{BDI}_{\text{DIPP}})\text{Ge}(\text{Se})\text{P}(\text{SiMe}_3)_2]$ (**56**). $U(\text{eq})$ is defined as one third of the trace of the orthogonalized U^{ij} tensor

	x	y	z	$U(\text{eq})$
Se	8152(1)	7945(1)	9240(1)	28(1)
Ge	7678(1)	7948(1)	7860(1)	17(1)
P	5841(1)	7826(1)	6879(1)	25(1)
Si(1)	4994(1)	8566(1)	5765(1)	29(1)
Si(2)	4881(1)	7717(1)	7624(1)	30(1)
N(1)	8476(2)	8658(1)	7583(1)	19(1)
N(2)	8222(2)	7130(1)	7436(1)	18(1)
C(1)	8661(2)	8569(1)	6897(1)	23(1)
C(2)	8589(2)	7920(1)	6518(2)	26(1)
C(3)	8534(2)	7238(1)	6840(2)	24(1)
C(4)	8995(2)	9211(1)	6554(2)	32(1)
C(5)	8911(3)	6631(1)	6483(2)	37(1)
C(6)	9032(2)	9243(1)	8164(1)	22(1)
C(7)	8439(2)	9852(1)	8174(2)	25(1)
C(8)	9028(2)	10412(1)	8718(2)	31(1)
C(9)	10158(2)	10369(1)	9239(2)	33(1)
C(10)	10723(2)	9765(1)	9224(2)	31(1)
C(11)	10183(2)	9189(1)	8700(2)	25(1)
C(12)	7197(2)	9930(1)	7629(2)	31(1)
C(13)	6921(3)	10540(2)	6982(2)	46(1)
C(14)	6621(2)	10042(2)	8187(2)	46(1)
C(15)	10848(2)	8520(1)	8762(2)	31(1)
C(16)	11708(3)	8635(2)	8443(2)	57(1)
C(17)	11422(2)	8250(2)	9686(2)	42(1)
C(18)	8114(2)	6409(1)	7702(1)	22(1)
C(19)	7221(2)	5971(1)	7161(2)	28(1)
C(20)	7124(2)	5304(2)	7472(2)	42(1)
C(21)	7882(3)	5072(2)	8272(2)	52(1)
C(22)	8770(2)	5497(2)	8779(2)	45(1)
C(23)	8914(2)	6170(1)	8508(2)	28(1)
C(24)	6387(2)	6133(1)	6235(2)	32(1)
C(25)	5182(2)	6064(2)	6071(2)	43(1)

C(26)	6536(3)	5615(2)	5612(2)	49(1)
C(27)	9972(2)	6583(1)	9048(2)	31(1)
C(28)	10370(3)	6511(2)	10010(2)	54(1)
C(29)	10877(3)	6341(2)	8822(2)	62(1)
C(30)	5416(2)	6908(2)	8303(2)	42(1)
C(31)	3408(2)	7542(2)	6809(2)	50(1)
C(32)	4902(3)	8496(2)	8279(2)	51(1)
C(33)	5991(2)	8971(2)	5440(2)	37(1)
C(34)	4050(2)	7956(2)	4887(2)	44(1)
C(35)	4142(3)	9276(2)	5924(2)	53(1)

Table A85. Bond lengths [Å] and angles [deg] for [(BDI_{DIPP})Ge(Se)P(SiMe₃)₂] (**56**)

Se-Ge	2.2163(3)
Ge-N(1)	1.9174(18)
Ge-N(2)	1.9923(18)
Ge-P	2.2976(7)
P-Si(1)	2.2415(9)
P-Si(2)	2.2525(9)
Si(1)-C(33)	1.861(3)
Si(1)-C(35)	1.868(3)
Si(1)-C(34)	1.874(3)
Si(2)-C(32)	1.855(3)
Si(2)-C(30)	1.859(3)
Si(2)-C(31)	1.875(3)
N(1)-C(1)	1.356(3)
N(1)-C(6)	1.453(3)
N(2)-C(3)	1.321(3)
N(2)-C(18)	1.460(3)
C(1)-C(2)	1.370(3)
C(1)-C(4)	1.508(3)
C(2)-C(3)	1.415(3)
C(3)-C(5)	1.502(3)
C(6)-C(7)	1.401(3)
C(6)-C(11)	1.408(3)
C(7)-C(8)	1.397(3)
C(7)-C(12)	1.513(4)
C(8)-C(9)	1.380(4)
C(9)-C(10)	1.373(4)
C(10)-C(11)	1.391(3)
C(11)-C(15)	1.518(3)
C(12)-C(14)	1.533(4)
C(12)-C(13)	1.534(4)
C(15)-C(16)	1.530(4)
C(15)-C(17)	1.533(4)
C(18)-C(23)	1.406(3)
C(18)-C(19)	1.409(3)
C(19)-C(20)	1.394(4)
C(19)-C(24)	1.529(3)
C(20)-C(21)	1.378(4)
C(21)-C(22)	1.376(4)

C(22)-C(23)	1.394(4)
C(23)-C(27)	1.517(3)
C(24)-C(25)	1.530(4)
C(24)-C(26)	1.550(4)
C(27)-C(29)	1.528(4)
C(27)-C(28)	1.534(4)
N(1)-Ge-N(2)	94.88(8)
N(1)-Ge-Se	111.91(6)
N(2)-Ge-Se	116.22(5)
N(1)-Ge-P	114.97(6)
N(2)-Ge-P	95.83(6)
Se-Ge-P	119.388(19)
Si(1)-P-Si(2)	111.65(4)
Si(1)-P-Ge	122.49(3)
Si(2)-P-Ge	106.77(3)
C(33)-Si(1)-C(35)	110.28(15)
C(33)-Si(1)-C(34)	108.03(13)
C(35)-Si(1)-C(34)	108.96(15)
C(33)-Si(1)-P	111.88(9)
C(35)-Si(1)-P	114.19(11)
C(34)-Si(1)-P	103.06(10)
C(32)-Si(2)-C(30)	110.49(15)
C(32)-Si(2)-C(31)	108.60(16)
C(30)-Si(2)-C(31)	108.25(15)
C(32)-Si(2)-P	116.64(11)
C(30)-Si(2)-P	106.95(10)
C(31)-Si(2)-P	105.54(10)
C(1)-N(1)-C(6)	118.26(18)
C(1)-N(1)-Ge	120.26(15)
C(6)-N(1)-Ge	120.89(14)
C(3)-N(2)-C(18)	121.00(18)
C(3)-N(2)-Ge	119.60(15)
C(18)-N(2)-Ge	118.79(13)
N(1)-C(1)-C(2)	123.0(2)
N(1)-C(1)-C(4)	118.5(2)
C(2)-C(1)-C(4)	118.5(2)
C(1)-C(2)-C(3)	127.5(2)
N(2)-C(3)-C(2)	123.8(2)
N(2)-C(3)-C(5)	121.2(2)

C(2)-C(3)-C(5)	115.0(2)
C(7)-C(6)-C(11)	121.1(2)
C(7)-C(6)-N(1)	120.7(2)
C(11)-C(6)-N(1)	118.2(2)
C(8)-C(7)-C(6)	118.1(2)
C(8)-C(7)-C(12)	118.7(2)
C(6)-C(7)-C(12)	123.2(2)
C(9)-C(8)-C(7)	121.3(2)
C(10)-C(9)-C(8)	119.7(2)
C(9)-C(10)-C(11)	121.7(2)
C(10)-C(11)-C(6)	118.0(2)
C(10)-C(11)-C(15)	118.7(2)
C(6)-C(11)-C(15)	123.2(2)
C(7)-C(12)-C(14)	110.8(2)
C(7)-C(12)-C(13)	111.2(2)
C(14)-C(12)-C(13)	110.9(2)
C(11)-C(15)-C(16)	112.8(2)
C(11)-C(15)-C(17)	110.0(2)
C(16)-C(15)-C(17)	109.9(2)
C(23)-C(18)-C(19)	121.4(2)
C(23)-C(18)-N(2)	118.3(2)
C(19)-C(18)-N(2)	120.3(2)
C(20)-C(19)-C(18)	117.6(2)
C(20)-C(19)-C(24)	116.2(2)
C(18)-C(19)-C(24)	126.0(2)
C(21)-C(20)-C(19)	121.7(3)
C(22)-C(21)-C(20)	119.8(3)
C(21)-C(22)-C(23)	121.4(3)
C(22)-C(23)-C(18)	118.0(2)
C(22)-C(23)-C(27)	119.2(2)
C(18)-C(23)-C(27)	122.5(2)
C(19)-C(24)-C(25)	112.5(2)
C(19)-C(24)-C(26)	111.1(2)
C(25)-C(24)-C(26)	107.0(2)
C(23)-C(27)-C(29)	109.1(2)
C(23)-C(27)-C(28)	113.4(2)
C(29)-C(27)-C(28)	110.6(3)

Table A86. Crystal data and structure refinement for [(BDI_{DIPP})SnSeSiMe₃] (57)

Identification code	feb110	
Empirical formula	C ₃₂ H ₅₀ N ₂ Se Si Sn, 0.5(C ₇ H ₈)	
Formula weight	734.55	
Temperature	173(2) K	
Wavelength	0.71073 Å	
Crystal system	Triclinic	
Space group	P $\bar{1}$ (No.2)	
Unit cell dimensions	a = 10.6632(13) Å	a = 101.567(8)°.
	b = 11.9105(13) Å	b = 93.519(6)°.
	c = 15.2531(18) Å	g = 105.196(7)°.
Volume	1818.2(4) Å ³	
Z	2	
Density (calculated)	1.34 Mg/m ³	
Absorption coefficient	1.76 mm ⁻¹	
F(000)	758	
Crystal size	0.20 x 0.08 x 0.08 mm ³	
Theta range for data collection	3.44 to 26.02°.	
Index ranges	-13 ≤ h ≤ 13, -14 ≤ k ≤ 14, -18 ≤ l ≤ 18	
Reflections collected	23354	
Independent reflections	6805 [R(int) = 0.045]	
Completeness to theta = 26.02°	94.9 %	
Absorption correction	Semi-empirical from equivalents	
Max. and min. transmission	0.877 and 0.735	
Refinement method	Full-matrix least-squares on F ²	
Data / restraints / parameters	6805 / 7 / 375	
Goodness-of-fit on F ²	1.064	
Final R indices [I > 2σ(I)]	R1 = 0.040, wR2 = 0.088	
R indices (all data)	R1 = 0.049, wR2 = 0.092	
Largest diff. peak and hole	0.87 and -1.00 e.Å ⁻³	

Diffraction was weak; one of the ¹Pr groups is disordered; the toluene was refined as a rigid body at half occupancy with carbon atoms isotropic

Data collection KappaCCD , Program package WinGX , Abs correction MULTISCAN
Refinement using SHELXL-97 , Drawing using ORTEP-3 for Windows

Table A87. Atomic coordinates ($\times 10^4$) and equivalent isotropic displacement parameters ($\text{\AA}^2 \times 10^3$) for $[(\text{BDI}_{\text{DIPP}})\text{SnSeSiMe}_3]$ (**57**). $U(\text{eq})$ is defined as one third of the trace of the orthogonalized U^{ij} tensor

	x	y	z	U(eq)
Sn	463(1)	2290(1)	1804(1)	26(1)
Se	2908(1)	2211(1)	1801(1)	32(1)
Si	2853(1)	1197(1)	355(1)	33(1)
N(1)	985(3)	4185(2)	2517(2)	26(1)
N(2)	279(3)	1915(3)	3154(2)	27(1)
C(1)	1404(3)	4604(3)	3386(2)	27(1)
C(2)	1400(4)	3901(3)	4014(3)	31(1)
C(3)	791(4)	2683(3)	3931(2)	29(1)
C(4)	1892(4)	5941(3)	3767(3)	41(1)
C(5)	672(5)	2273(4)	4806(3)	43(1)
C(6)	815(4)	4983(3)	1947(2)	28(1)
C(7)	1869(4)	5596(3)	1562(3)	31(1)
C(8)	1623(4)	6323(3)	997(3)	37(1)
C(9)	395(5)	6433(4)	816(3)	44(1)
C(10)	-640(4)	5817(4)	1195(3)	40(1)
C(11)	-463(4)	5079(3)	1763(3)	32(1)
C(12)	3252(4)	5509(4)	1718(3)	36(1)
C(13)	3689(4)	4944(4)	840(3)	46(1)
C(14)	4229(5)	6727(4)	2135(3)	53(1)
C(15)	-1612(4)	4414(3)	2174(3)	36(1)
C(16)	-2920(5)	4149(7)	1618(4)	89(2)
C(17)	-1675(6)	5046(5)	3139(4)	71(2)
C(18)	-480(4)	710(3)	3141(2)	30(1)
C(19)	148(4)	-185(3)	3199(3)	35(1)
C(20)	-645(5)	-1346(4)	3125(3)	43(1)
C(21)	-1986(5)	-1620(4)	3013(3)	51(1)
C(22)	-2587(4)	-738(4)	2967(3)	45(1)
C(23)	-1859(4)	436(3)	3034(3)	34(1)
C(24)	1617(4)	52(4)	3333(3)	40(1)
C(25)	2089(6)	-680(4)	2554(4)	63(2)
C(26)	2085(5)	-226(5)	4221(4)	58(1)
C(27)	-2555(19)	1390(20)	3097(13)	43(6) ^a

C(28)	-3190(30)	1633(17)	3949(8)	66(4) ^a
C(29)	-3590(20)	1180(20)	2305(14)	62(5) ^a
C(27A)	-2570(20)	1410(30)	2922(17)	27(5) ^b
C(28A)	-2560(30)	2110(30)	3868(13)	59(6) ^b
C(29A)	-3900(20)	820(20)	2380(20)	49(6) ^b
C(30)	1507(5)	1303(4)	-430(3)	46(1)
C(31)	4442(5)	1857(5)	-36(3)	57(1)
C(32)	2691(5)	-407(4)	307(3)	50(1)
C(1S)	4764(8)	4184(5)	5049(5)	80(4)
C(2S)	5029(9)	5128(7)	5800(5)	78(4)
C(3S)	5424(9)	6297(5)	5697(5)	92(4)
C(4S)	5554(8)	6523(5)	4842(6)	85(4)
C(5S)	5288(8)	5579(7)	4092(5)	80(4)
C(6S)	4893(8)	4410(6)	4195(5)	56(3)
C(7S)	4299(12)	2797(6)	5190(9)	160(8)

a 58.7%, *b* 41.3%

Table A88. Bond lengths [Å] and angles [deg] for [(BDI_{DIPP})SnSeSiMe₃] (57)

Sn-N(2)	2.202(3)
Sn-N(1)	2.207(3)
Sn-Se	2.6333(5)
Se-Si	2.2815(12)
Si-C(32)	1.858(4)
Si-C(30)	1.859(5)
Si-C(31)	1.860(4)
N(1)-C(1)	1.323(5)
N(1)-C(6)	1.448(5)
N(2)-C(3)	1.328(5)
N(2)-C(18)	1.447(5)
C(1)-C(2)	1.393(5)
C(1)-C(4)	1.517(5)
C(2)-C(3)	1.401(5)
C(3)-C(5)	1.511(5)
C(6)-C(7)	1.401(5)
C(6)-C(11)	1.413(5)
C(7)-C(8)	1.397(5)
C(7)-C(12)	1.513(5)
C(8)-C(9)	1.366(6)
C(9)-C(10)	1.384(6)
C(10)-C(11)	1.390(5)
C(11)-C(15)	1.519(5)
C(12)-C(13)	1.531(6)
C(12)-C(14)	1.533(6)
C(15)-C(16)	1.510(6)
C(15)-C(17)	1.527(6)
C(18)-C(23)	1.411(5)
C(18)-C(19)	1.413(5)
C(19)-C(20)	1.398(6)
C(19)-C(24)	1.510(6)
C(20)-C(21)	1.373(6)
C(21)-C(22)	1.377(6)
C(22)-C(23)	1.390(6)
C(23)-C(27)	1.50(3)
C(24)-C(25)	1.520(6)

C(24)-C(26)	1.541(6)
C(27)-C(28)	1.513(12)
C(27)-C(29)	1.522(12)
N(2)-Sn-N(1)	85.15(11)
N(2)-Sn-Se	94.65(8)
N(1)-Sn-Se	94.38(8)
Si-Se-Sn	100.60(3)
C(32)-Si-C(30)	108.5(2)
C(32)-Si-C(31)	108.3(2)
C(30)-Si-C(31)	108.6(2)
C(32)-Si-Se	110.85(16)
C(30)-Si-Se	113.44(14)
C(31)-Si-Se	107.03(16)
C(1)-N(1)-C(6)	120.6(3)
C(1)-N(1)-Sn	125.5(2)
C(6)-N(1)-Sn	113.9(2)
C(3)-N(2)-C(18)	120.5(3)
C(3)-N(2)-Sn	125.8(2)
C(18)-N(2)-Sn	113.8(2)
N(1)-C(1)-C(2)	124.7(3)
N(1)-C(1)-C(4)	120.0(3)
C(2)-C(1)-C(4)	115.2(3)
C(1)-C(2)-C(3)	129.7(4)
N(2)-C(3)-C(2)	124.3(3)
N(2)-C(3)-C(5)	119.9(3)
C(2)-C(3)-C(5)	115.7(3)
C(7)-C(6)-C(11)	121.4(3)
C(7)-C(6)-N(1)	121.1(3)
C(11)-C(6)-N(1)	117.4(3)
C(8)-C(7)-C(6)	117.9(4)
C(8)-C(7)-C(12)	118.3(3)
C(6)-C(7)-C(12)	123.8(3)
C(9)-C(8)-C(7)	121.5(4)
C(8)-C(9)-C(10)	120.1(4)
C(9)-C(10)-C(11)	121.4(4)
C(10)-C(11)-C(6)	117.7(4)
C(10)-C(11)-C(15)	120.5(4)

C(6)-C(11)-C(15)	121.8(3)
C(7)-C(12)-C(13)	111.0(3)
C(7)-C(12)-C(14)	112.2(3)
C(13)-C(12)-C(14)	109.7(4)
C(16)-C(15)-C(11)	113.9(4)
C(16)-C(15)-C(17)	109.7(4)
C(11)-C(15)-C(17)	112.5(4)
C(23)-C(18)-C(19)	120.7(3)
C(23)-C(18)-N(2)	118.7(3)
C(19)-C(18)-N(2)	120.5(3)
C(20)-C(19)-C(18)	117.6(4)
C(20)-C(19)-C(24)	118.9(4)
C(18)-C(19)-C(24)	123.5(3)
C(21)-C(20)-C(19)	121.9(4)
C(20)-C(21)-C(22)	119.9(4)
C(21)-C(22)-C(23)	121.2(4)
C(22)-C(23)-C(18)	118.6(4)
C(22)-C(23)-C(27)	119.0(9)
C(18)-C(23)-C(27)	122.0(9)
C(19)-C(24)-C(25)	111.2(4)
C(19)-C(24)-C(26)	111.8(3)
C(25)-C(24)-C(26)	108.9(4)
C(23)-C(27)-C(28)	115.4(17)
C(23)-C(27)-C(29)	113.9(15)
C(28)-C(27)-C(29)	107.2(15)

Table A89. Crystal data and structure refinement for [(BDI_{DIPP})PbOTf] (58)

Identification code	may1507	
Empirical formula	C ₃₀ H ₄₁ F ₃ N ₂ O ₃ Pb S . 7/8(C ₇ H ₈)	
Formula weight	854.52	
Temperature	173(2) K	
Wavelength	0.71073 Å	
Crystal system	Triclinic	
Space group	P $\bar{1}$ (No.2)	
Unit cell dimensions	a = 12.9485(2) Å	a = 106.740(1)°.
	b = 24.6426(4) Å	b = 100.768(1)°.
	c = 25.1412(4) Å	g = 92.445(1)°.
Volume	7507.1(2) Å ³	
Z	8	
Density (calculated)	1.51 Mg/m ³	
Absorption coefficient	4.60 mm ⁻¹	
F(000)	3422	
Crystal size	0.25 x 0.20 x 0.10 mm ³	
Theta range for data collection	3.42 to 26.03°.	
Index ranges	-15 ≤ h ≤ 13, -30 ≤ k ≤ 29, -30 ≤ l ≤ 31	
Reflections collected	76006	
Independent reflections	29301 [R(int) = 0.057]	
Reflections with I > 2σ(I)	20304	
Completeness to theta = 26.03°	99.1 %	
Tmax. and Tmin.	0.4880 and 0.3678	
Refinement method	Full-matrix least-squares on F ²	
Data / restraints / parameters	29301 / 0 / 1581	
Goodness-of-fit on F ²	1.048	
Final R indices [I > 2σ(I)]	R1 = 0.056, wR2 = 0.107	
R indices (all data)	R1 = 0.099, wR2 = 0.123	
Largest diff. peak and hole	2.31 and -2.11 e.Å ⁻³ (near Pb)	
The asymmetric unit contains 4 units of the (L)Pb(OTf) polymeric chain , 3 toluene molecules in general positions, and one toluene molecule disordered over an inversion centre (for which the H atoms were omitted)		
Data collection KappaCCD , Program package WinGX , Abs correction MULTISCAN		
Refinement using SHELXL-97 , Drawing using ORTEP-3 for Windows (20% ellipsoids)		

Table A90. Atomic coordinates ($\times 10^4$) and equivalent isotropic displacement parameters ($\text{\AA}^2 \times 10^3$) for [(BDI_{DIPP})PbOTf] (**58**). U(eq) is defined as one third of the trace of the orthogonalized U^{ij} tensor.

	x	y	z	U(eq)
Pb(1)	3650(1)	589(1)	2845(1)	42(1)
Pb(2)	3904(1)	2494(1)	1379(1)	37(1)
Pb(3)	3867(1)	5447(1)	2549(1)	41(1)
Pb(4)	1870(1)	8037(1)	3133(1)	38(1)
S(1)	3902(2)	961(1)	1624(1)	50(1)
S(2)	4796(2)	3956(1)	1787(1)	46(1)
S(3)	2008(2)	6378(1)	3011(1)	54(1)
S(4)	2746(2)	9516(1)	3624(1)	46(1)
F(1)	4429(6)	-65(2)	1246(3)	86(2)
F(2)	4088(6)	365(3)	614(3)	99(2)
F(3)	5546(6)	580(3)	1220(3)	82(2)
F(4)	6491(5)	3560(2)	1469(2)	73(2)
F(5)	6710(5)	4442(2)	1957(3)	73(2)
F(6)	5873(5)	4195(2)	1089(2)	74(2)
F(7)	1146(6)	5557(2)	3295(3)	97(2)
F(8)	1484(6)	6355(3)	3964(3)	100(2)
F(9)	160(6)	6231(3)	3267(4)	114(3)
F(10)	2512(5)	9445(3)	4605(2)	84(2)
F(11)	3392(5)	10216(3)	4646(2)	91(2)
F(12)	1708(6)	10115(2)	4346(3)	81(2)
O(1)	4523(5)	1009(2)	2183(2)	53(2)
O(2)	4076(5)	1464(2)	1451(3)	58(2)
O(3)	2831(5)	722(3)	1522(3)	62(2)
O(4)	4152(5)	3527(2)	1298(3)	55(2)
O(5)	4430(5)	4515(2)	1884(3)	55(2)
O(6)	5072(5)	3771(2)	2281(2)	55(2)
O(7)	3038(5)	6223(2)	3225(3)	54(2)
O(8)	1934(5)	6984(2)	3181(3)	63(2)
O(9)	1574(6)	6081(3)	2433(3)	70(2)
O(10)	1787(4)	9133(2)	3353(2)	45(1)
O(11)	2825(5)	9996(2)	3406(3)	52(2)
O(12)	3688(5)	9235(3)	3694(3)	67(2)
N(1)	5253(5)	326(2)	3150(3)	35(2)
N(2)	4118(6)	1302(3)	3684(3)	44(2)

N(3)	2208(5)	2200(3)	877(3)	44(2)
N(4)	4308(5)	2111(3)	526(3)	40(2)
N(5)	4434(6)	5113(3)	3289(3)	46(2)
N(6)	5577(6)	5841(3)	2781(3)	39(2)
N(7)	743(6)	7691(3)	2272(3)	49(2)
N(8)	365(5)	7980(2)	3451(3)	40(2)
C(1)	5599(6)	375(3)	3692(4)	41(2)
C(2)	5269(7)	751(3)	4144(4)	42(2)
C(3)	4666(7)	1206(3)	4148(4)	45(2)
C(4)	6416(8)	-8(4)	3856(4)	55(2)
C(5)	4669(9)	1616(4)	4730(4)	65(3)
C(6)	5806(7)	26(3)	2723(3)	40(2)
C(7)	6675(7)	321(4)	2635(4)	48(2)
C(8)	7188(8)	40(4)	2208(4)	53(2)
C(9)	6836(9)	-511(5)	1877(4)	64(3)
C(10)	5971(8)	-792(4)	1976(4)	59(3)
C(11)	5446(7)	-532(3)	2395(4)	45(2)
C(12)	7086(7)	934(4)	2985(4)	52(2)
C(13)	8123(10)	969(5)	3399(5)	90(4)
C(14)	7222(10)	1314(5)	2620(5)	82(4)
C(15)	4527(8)	-853(4)	2498(5)	64(3)
C(16)	3590(9)	-985(5)	1997(5)	92(4)
C(17)	4841(10)	-1400(4)	2645(6)	91(4)
C(18)	3639(7)	1832(3)	3743(4)	48(2)
C(19)	2676(8)	1894(4)	3887(5)	67(3)
C(20)	2264(9)	2422(4)	3955(5)	72(3)
C(21)	2821(9)	2869(4)	3888(5)	68(3)
C(22)	3767(8)	2798(4)	3734(4)	57(3)
C(23)	4209(8)	2280(3)	3640(3)	46(2)
C(24)	2035(11)	1407(5)	3972(7)	102(5)
C(25)	1175(11)	1139(6)	3453(9)	146(8)
C(26)	1586(15)	1583(7)	4521(9)	180(10)
C(27)	5236(7)	2214(3)	3442(4)	48(2)
C(28)	6188(10)	2453(6)	3926(5)	99(4)
C(29)	5295(9)	2477(5)	2963(4)	73(3)
C(30)	4514(9)	429(4)	1151(4)	59(3)
C(31)	1977(8)	1743(4)	427(4)	52(2)
C(32)	2723(8)	1462(3)	137(4)	49(2)
C(33)	3770(8)	1636(4)	156(3)	46(2)
C(34)	825(8)	1499(4)	196(4)	67(3)

C(35)	4321(9)	1256(4)	-273(4)	68(3)
C(36)	1379(7)	2484(4)	1113(4)	51(2)
C(37)	1018(7)	2958(4)	951(4)	57(3)
C(38)	208(8)	3221(4)	1181(5)	68(3)
C(39)	-222(8)	3054(5)	1580(6)	79(4)
C(40)	154(8)	2592(4)	1743(5)	70(3)
C(41)	935(8)	2301(4)	1509(5)	59(3)
C(42)	1483(9)	3178(4)	526(4)	66(3)
C(43)	778(16)	2962(8)	-67(6)	178(10)
C(44)	1683(10)	3823(4)	709(6)	88(4)
C(45)	1329(8)	1803(4)	1711(5)	58(3)
C(46)	2055(9)	2017(4)	2295(4)	66(3)
C(47)	415(9)	1389(4)	1720(5)	81(3)
C(48)	5245(8)	2352(3)	410(3)	45(2)
C(49)	5132(8)	2731(4)	79(3)	48(2)
C(50)	6028(9)	2984(4)	-1(4)	61(3)
C(51)	7031(8)	2884(4)	224(4)	53(2)
C(52)	7132(8)	2510(4)	535(4)	51(2)
C(53)	6248(7)	2233(4)	634(3)	45(2)
C(54)	4051(9)	2835(4)	-197(4)	68(3)
C(55)	3954(10)	3460(5)	-138(5)	85(4)
C(56)	3731(11)	2479(5)	-827(5)	99(5)
C(57)	6422(8)	1842(4)	1000(4)	58(3)
C(58)	6866(10)	2195(5)	1630(5)	84(4)
C(59)	7142(10)	1391(5)	804(6)	98(4)
C(60)	6027(9)	4045(4)	1560(4)	58(3)
C(61)	5401(8)	4937(3)	3374(3)	47(2)
C(62)	6252(8)	5127(3)	3195(3)	47(2)
C(63)	6391(8)	5580(3)	2970(3)	45(2)
C(64)	5576(9)	4497(4)	3693(4)	64(3)
C(65)	7510(7)	5766(4)	2962(4)	54(2)
C(66)	3705(8)	5014(3)	3621(4)	50(2)
C(67)	3803(9)	5374(3)	4179(4)	59(3)
C(68)	3123(10)	5257(4)	4507(5)	77(4)
C(69)	2344(10)	4808(4)	4286(5)	79(4)
C(70)	2229(10)	4462(4)	3724(5)	77(4)
C(71)	2893(9)	4563(3)	3388(4)	56(3)
C(72)	4639(9)	5885(3)	4437(4)	62(3)
C(73)	5467(12)	5797(5)	4911(5)	103(5)
C(74)	4157(10)	6437(4)	4650(5)	83(4)

C(75)	2715(9)	4205(3)	2772(4)	58(3)
C(76)	1724(9)	4354(4)	2418(5)	73(3)
C(77)	2631(10)	3566(4)	2682(4)	71(3)
C(78)	5796(7)	6338(3)	2608(3)	37(2)
C(79)	5786(6)	6879(3)	3000(3)	37(2)
C(80)	6021(6)	7355(3)	2832(4)	41(2)
C(81)	6245(7)	7295(3)	2305(4)	44(2)
C(82)	6223(7)	6766(3)	1925(4)	44(2)
C(83)	5976(7)	6278(3)	2066(3)	40(2)
C(84)	5533(7)	6945(3)	3577(4)	44(2)
C(85)	6525(8)	7015(5)	4037(4)	70(3)
C(86)	4845(9)	7432(4)	3753(4)	63(3)
C(87)	5893(9)	5703(4)	1620(4)	56(3)
C(88)	4838(9)	5595(4)	1196(4)	66(3)
C(89)	6821(9)	5631(4)	1317(5)	72(3)
C(90)	1149(10)	6112(4)	3405(6)	77(4)
C(91)	-101(7)	7322(4)	2196(4)	51(2)
C(92)	-564(7)	7233(4)	2622(4)	59(3)
C(93)	-405(7)	7556(3)	3191(4)	45(2)
C(94)	-632(8)	6972(5)	1592(4)	77(3)
C(95)	-1167(7)	7398(4)	3534(4)	60(3)
C(96)	1092(7)	7799(4)	1797(4)	51(2)
C(97)	762(8)	8279(4)	1640(4)	62(3)
C(98)	1098(9)	8387(5)	1187(4)	70(3)
C(99)	1775(9)	8043(5)	904(4)	73(3)
C(100)	2102(8)	7590(5)	1072(4)	63(3)
C(101)	1770(7)	7451(4)	1523(4)	52(2)
C(102)	46(9)	8673(5)	1953(5)	72(3)
C(103)	305(12)	9297(5)	2008(6)	104(5)
C(104)	-1115(10)	8479(6)	1705(7)	134(6)
C(105)	2160(8)	6948(4)	1686(4)	57(3)
C(106)	2028(9)	6407(4)	1179(5)	79(3)
C(107)	3310(8)	7068(4)	2004(4)	67(3)
C(108)	310(6)	8375(3)	3984(3)	38(2)
C(109)	-277(7)	8849(3)	3976(4)	48(2)
C(110)	-316(8)	9234(3)	4496(5)	57(3)
C(111)	205(9)	9175(4)	4995(5)	67(3)
C(112)	790(8)	8723(4)	4996(4)	58(3)
C(113)	830(8)	8311(3)	4493(4)	47(2)
C(114)	-874(8)	8928(4)	3429(5)	64(3)

C(115)	-758(9)	9541(4)	3410(5)	71(3)
C(116)	-2048(9)	8718(5)	3298(7)	101(5)
C(117)	1445(8)	7796(4)	4513(4)	56(3)
C(118)	2633(8)	7973(5)	4669(4)	71(3)
C(119)	1108(11)	7499(4)	4913(5)	81(4)
C(120)	2584(9)	9845(4)	4348(4)	62(3)
C(1S)	9224(15)	4814(8)	1316(9)	136(6)
C(2S)	9657(13)	5262(7)	1145(7)	115(5)
C(3S)	9241(14)	5273(7)	634(8)	133(6)
C(4S)	8375(17)	4903(9)	175(9)	168(8)
C(5S)	8145(13)	4475(7)	438(7)	124(5)
C(6S)	8419(12)	4427(6)	905(6)	101(4)
C(7S)	9379(19)	4816(10)	1821(10)	206(10)
C(8S)	238(14)	5993(7)	5078(7)	118(5)
C(9S)	-459(15)	6389(8)	5228(8)	138(6)
C(10S)	-1533(15)	6317(8)	4908(8)	138(6)
C(11S)	-1959(17)	5812(8)	4450(8)	151(7)
C(12S)	-1219(17)	5392(9)	4310(9)	158(7)
C(13S)	-163(18)	5502(9)	4620(9)	164(7)
C(14S)	1267(19)	6068(10)	5477(10)	208(10)
C(15S)	-962(15)	3074(7)	3187(7)	120(5)
C(16S)	-235(17)	3521(9)	3309(8)	156(7)
C(17S)	-560(19)	4052(10)	3223(9)	170(8)
C(18S)	-1557(16)	4065(8)	2968(8)	144(6)
C(19S)	-2271(17)	3612(9)	2852(8)	153(7)
C(20S)	-1970(16)	3105(9)	2950(8)	149(7)
C(21S)	-595(14)	2525(7)	3286(8)	146(6)
C(22S)	464(15)	32(7)	534(7)	123(5)
C(23S)	1092(13)	-29(7)	147(7)	116(5)
C(24S)	659(17)	-68(8)	-430(9)	147(6)
C(25S)	1300(30)	-82(14)	-931(14)	127(11) occupancy 0.5

Table A91. Bond lengths [Å] and angles [deg] for [(BDI_{DIPP})PbOTf] (58)

Pb(1)-N(1)	2.263(6)
Pb(1)-N(2)	2.280(7)
Pb(1)-O(1)	2.591(6)
Pb(1)-O(11)'	2.624(5)
Pb(2)-N(4)	2.250(6)
Pb(2)-N(3)	2.289(7)
Pb(2)-O(2)	2.613(5)
Pb(2)-O(4)	2.622(6)
Pb(3)-N(5)	2.257(7)
Pb(3)-N(6)	2.278(7)
Pb(3)-O(7)	2.585(5)
Pb(3)-O(5)	2.642(5)
Pb(4)-N(8)	2.256(7)
Pb(4)-N(7)	2.278(7)
Pb(4)-O(10)	2.606(5)
Pb(4)-O(8)	2.636(6)
S(1)-O(3)	1.430(7)
S(1)-O(2)	1.449(6)
S(1)-O(1)	1.452(6)
S(1)-C(30)	1.817(10)
S(2)-O(6)	1.432(6)
S(2)-O(5)	1.446(6)
S(2)-O(4)	1.455(6)
S(2)-C(60)	1.815(10)
S(3)-O(9)	1.417(7)
S(3)-O(8)	1.443(6)
S(3)-O(7)	1.452(6)
S(3)-C(90)	1.837(11)
S(4)-O(12)	1.435(7)
S(4)-O(11)	1.447(6)
S(4)-O(10)	1.453(6)
S(4)-C(120)	1.823(10)
F(1)-C(30)	1.311(11)
F(2)-C(30)	1.320(11)
F(3)-C(30)	1.337(12)
F(4)-C(60)	1.342(10)

F(5)-C(60)	1.330(11)
F(6)-C(60)	1.323(11)
F(7)-C(90)	1.316(11)
F(8)-C(90)	1.335(14)
F(9)-C(90)	1.331(13)
F(10)-C(120)	1.335(11)
F(11)-C(120)	1.312(11)
F(12)-C(120)	1.339(12)
O(11)-Pb(1)''	2.624(5)
N(1)-C(1)	1.320(10)
N(1)-C(6)	1.445(10)
N(2)-C(3)	1.335(11)
N(2)-C(18)	1.452(10)
N(3)-C(31)	1.321(11)
N(3)-C(36)	1.436(11)
N(4)-C(33)	1.335(10)
N(4)-C(48)	1.441(11)
N(5)-C(61)	1.341(11)
N(5)-C(66)	1.429(11)
N(6)-C(63)	1.340(10)
N(6)-C(78)	1.447(9)
N(7)-C(91)	1.340(11)
N(7)-C(96)	1.441(12)
N(8)-C(93)	1.337(10)
N(8)-C(108)	1.427(9)
C(1)-C(2)	1.393(11)
C(1)-C(4)	1.525(11)
C(2)-C(3)	1.393(11)
C(3)-C(5)	1.519(12)
C(6)-C(11)	1.392(11)
C(6)-C(7)	1.399(12)
C(7)-C(8)	1.396(12)
C(7)-C(12)	1.526(12)
C(8)-C(9)	1.377(13)
C(9)-C(10)	1.390(14)
C(10)-C(11)	1.379(12)
C(11)-C(15)	1.502(13)
C(12)-C(14)	1.514(13)

C(12)-C(13)	1.521(14)
C(15)-C(16)	1.525(15)
C(15)-C(17)	1.547(13)
C(18)-C(19)	1.364(12)
C(18)-C(23)	1.412(12)
C(19)-C(20)	1.404(12)
C(19)-C(24)	1.517(14)
C(20)-C(21)	1.359(14)
C(21)-C(22)	1.356(13)
C(22)-C(23)	1.397(11)
C(23)-C(27)	1.503(12)
C(24)-C(25)	1.51(2)
C(24)-C(26)	1.55(2)
C(27)-C(28)	1.520(14)
C(27)-C(29)	1.535(12)
C(31)-C(32)	1.405(13)
C(31)-C(34)	1.524(13)
C(32)-C(33)	1.392(13)
C(33)-C(35)	1.521(12)
C(36)-C(41)	1.405(13)
C(36)-C(37)	1.412(12)
C(37)-C(38)	1.388(14)
C(37)-C(42)	1.533(14)
C(38)-C(39)	1.383(15)
C(39)-C(40)	1.393(14)
C(40)-C(41)	1.388(13)
C(41)-C(45)	1.530(13)
C(42)-C(44)	1.518(13)
C(42)-C(43)	1.526(15)
C(45)-C(46)	1.520(14)
C(45)-C(47)	1.537(13)
C(48)-C(53)	1.396(12)
C(48)-C(49)	1.414(11)
C(49)-C(50)	1.368(13)
C(49)-C(54)	1.509(13)
C(50)-C(51)	1.379(13)
C(51)-C(52)	1.367(12)
C(52)-C(53)	1.405(12)

C(53)-C(57)	1.507(12)
C(54)-C(55)	1.518(14)
C(54)-C(56)	1.540(15)
C(57)-C(59)	1.515(14)
C(57)-C(58)	1.555(14)
C(61)-C(62)	1.378(12)
C(61)-C(64)	1.526(11)
C(62)-C(63)	1.409(11)
C(63)-C(65)	1.507(13)
C(66)-C(67)	1.406(12)
C(66)-C(71)	1.408(13)
C(67)-C(68)	1.388(13)
C(67)-C(72)	1.525(14)
C(68)-C(69)	1.376(15)
C(69)-C(70)	1.402(14)
C(70)-C(71)	1.374(12)
C(71)-C(75)	1.513(12)
C(72)-C(74)	1.520(13)
C(72)-C(73)	1.521(15)
C(75)-C(77)	1.520(11)
C(75)-C(76)	1.543(14)
C(78)-C(83)	1.393(10)
C(78)-C(79)	1.414(10)
C(79)-C(80)	1.396(11)
C(79)-C(84)	1.511(11)
C(80)-C(81)	1.376(11)
C(81)-C(82)	1.372(11)
C(82)-C(83)	1.387(11)
C(83)-C(87)	1.519(11)
C(84)-C(85)	1.526(13)
C(84)-C(86)	1.538(11)
C(87)-C(88)	1.527(14)
C(87)-C(89)	1.530(13)
C(91)-C(92)	1.384(13)
C(91)-C(94)	1.524(12)
C(92)-C(93)	1.395(12)
C(93)-C(95)	1.531(12)
C(96)-C(101)	1.390(12)

C(96)-C(97)	1.408(13)
C(97)-C(98)	1.382(14)
C(97)-C(102)	1.527(13)
C(98)-C(99)	1.394(14)
C(99)-C(100)	1.361(14)
C(100)-C(101)	1.406(13)
C(101)-C(105)	1.494(13)
C(102)-C(104)	1.514(16)
C(102)-C(103)	1.521(16)
C(105)-C(107)	1.526(13)
C(105)-C(106)	1.532(12)
C(108)-C(113)	1.386(12)
C(108)-C(109)	1.425(11)
C(109)-C(110)	1.386(12)
C(109)-C(114)	1.515(14)
C(110)-C(111)	1.361(14)
C(111)-C(112)	1.374(13)
C(112)-C(113)	1.386(11)
C(113)-C(117)	1.535(12)
C(114)-C(115)	1.527(13)
C(114)-C(116)	1.529(14)
C(117)-C(119)	1.515(13)
C(117)-C(118)	1.527(14)
N(1)-Pb(1)-N(2)	82.2(2)
N(1)-Pb(1)-O(1)	87.2(2)
N(2)-Pb(1)-O(1)	101.4(2)
N(1)-Pb(1)-O(11)'	89.0(2)
N(2)-Pb(1)-O(11)'	87.0(2)
O(1)-Pb(1)-O(11)'	170.3(2)
N(4)-Pb(2)-N(3)	83.1(3)
N(4)-Pb(2)-O(2)	82.7(2)
N(3)-Pb(2)-O(2)	88.7(2)
N(4)-Pb(2)-O(4)	91.7(2)
N(3)-Pb(2)-O(4)	101.3(2)
O(2)-Pb(2)-O(4)	168.0(2)
N(5)-Pb(3)-N(6)	81.9(3)
N(5)-Pb(3)-O(7)	87.9(2)

N(6)-Pb(3)-O(7)	100.2(2)
N(5)-Pb(3)-O(5)	87.9(2)
N(6)-Pb(3)-O(5)	89.4(2)
O(7)-Pb(3)-O(5)	168.8(2)
N(8)-Pb(4)-N(7)	82.3(3)
N(8)-Pb(4)-O(10)	88.9(2)
N(7)-Pb(4)-O(10)	102.2(2)
N(8)-Pb(4)-O(8)	83.0(2)
N(7)-Pb(4)-O(8)	88.5(2)
O(10)-Pb(4)-O(8)	165.6(2)
O(3)-S(1)-O(2)	116.9(4)
O(3)-S(1)-O(1)	114.7(4)
O(2)-S(1)-O(1)	112.6(4)
O(3)-S(1)-C(30)	104.4(5)
O(2)-S(1)-C(30)	102.8(4)
O(1)-S(1)-C(30)	103.2(4)
O(6)-S(2)-O(5)	115.5(4)
O(6)-S(2)-O(4)	114.1(4)
O(5)-S(2)-O(4)	113.6(4)
O(6)-S(2)-C(60)	105.5(5)
O(5)-S(2)-C(60)	103.1(4)
O(4)-S(2)-C(60)	103.1(4)
O(9)-S(3)-O(8)	115.9(4)
O(9)-S(3)-O(7)	114.3(4)
O(8)-S(3)-O(7)	113.5(4)
O(9)-S(3)-C(90)	104.5(6)
O(8)-S(3)-C(90)	103.6(4)
O(7)-S(3)-C(90)	103.1(5)
O(12)-S(4)-O(11)	115.6(4)
O(12)-S(4)-O(10)	114.4(4)
O(11)-S(4)-O(10)	113.5(4)
O(12)-S(4)-C(120)	103.9(5)
O(11)-S(4)-C(120)	103.1(4)
O(10)-S(4)-C(120)	104.4(4)
S(1)-O(1)-Pb(1)	117.9(3)
S(1)-O(2)-Pb(2)	159.0(4)
S(2)-O(4)-Pb(2)	116.8(3)
S(2)-O(5)-Pb(3)	151.7(4)

S(3)-O(7)-Pb(3)	118.7(3)
S(3)-O(8)-Pb(4)	160.5(4)
S(4)-O(10)-Pb(4)	119.4(3)
S(4)-O(11)-Pb(1)"	153.5(4)
C(1)-N(1)-C(6)	121.1(6)
C(1)-N(1)-Pb(1)	120.9(5)
C(6)-N(1)-Pb(1)	117.3(5)
C(3)-N(2)-C(18)	118.9(7)
C(3)-N(2)-Pb(1)	121.0(5)
C(18)-N(2)-Pb(1)	119.0(6)
C(31)-N(3)-C(36)	120.2(8)
C(31)-N(3)-Pb(2)	122.1(6)
C(36)-N(3)-Pb(2)	117.1(5)
C(33)-N(4)-C(48)	119.8(7)
C(33)-N(4)-Pb(2)	121.5(6)
C(48)-N(4)-Pb(2)	118.3(5)
C(61)-N(5)-C(66)	119.4(7)
C(61)-N(5)-Pb(3)	120.8(5)
C(66)-N(5)-Pb(3)	119.3(6)
C(63)-N(6)-C(78)	118.6(7)
C(63)-N(6)-Pb(3)	123.1(5)
C(78)-N(6)-Pb(3)	117.1(5)
C(91)-N(7)-C(96)	121.3(8)
C(91)-N(7)-Pb(4)	121.2(6)
C(96)-N(7)-Pb(4)	116.4(5)
C(93)-N(8)-C(108)	120.1(7)
C(93)-N(8)-Pb(4)	122.1(5)
C(108)-N(8)-Pb(4)	117.4(5)
N(1)-C(1)-C(2)	125.3(7)
N(1)-C(1)-C(4)	119.4(7)
C(2)-C(1)-C(4)	115.3(7)
C(3)-C(2)-C(1)	129.4(8)
N(2)-C(3)-C(2)	124.7(8)
N(2)-C(3)-C(5)	119.7(8)
C(2)-C(3)-C(5)	115.6(8)
C(11)-C(6)-C(7)	121.7(8)
C(11)-C(6)-N(1)	120.1(8)
C(7)-C(6)-N(1)	118.1(7)

C(8)-C(7)-C(6)	118.3(8)
C(8)-C(7)-C(12)	118.7(9)
C(6)-C(7)-C(12)	123.0(8)
C(9)-C(8)-C(7)	120.7(10)
C(8)-C(9)-C(10)	119.5(9)
C(11)-C(10)-C(9)	121.7(9)
C(10)-C(11)-C(6)	118.0(9)
C(10)-C(11)-C(15)	120.3(8)
C(6)-C(11)-C(15)	121.7(8)
C(14)-C(12)-C(13)	109.1(9)
C(14)-C(12)-C(7)	112.8(8)
C(13)-C(12)-C(7)	112.2(8)
C(11)-C(15)-C(16)	111.3(9)
C(11)-C(15)-C(17)	111.9(9)
C(16)-C(15)-C(17)	111.3(9)
C(19)-C(18)-C(23)	121.5(8)
C(19)-C(18)-N(2)	121.4(8)
C(23)-C(18)-N(2)	117.0(7)
C(18)-C(19)-C(20)	119.1(9)
C(18)-C(19)-C(24)	121.9(8)
C(20)-C(19)-C(24)	119.0(9)
C(21)-C(20)-C(19)	120.7(9)
C(22)-C(21)-C(20)	119.5(8)
C(21)-C(22)-C(23)	122.9(9)
C(22)-C(23)-C(18)	116.2(9)
C(22)-C(23)-C(27)	121.0(8)
C(18)-C(23)-C(27)	122.9(7)
C(25)-C(24)-C(19)	110.2(13)
C(25)-C(24)-C(26)	111.7(13)
C(19)-C(24)-C(26)	113.3(12)
C(23)-C(27)-C(28)	112.3(8)
C(23)-C(27)-C(29)	113.0(8)
C(28)-C(27)-C(29)	109.7(9)
F(1)-C(30)-F(2)	109.1(9)
F(1)-C(30)-F(3)	106.9(8)
F(2)-C(30)-F(3)	106.6(9)
F(1)-C(30)-S(1)	111.6(7)
F(2)-C(30)-S(1)	111.0(7)

F(3)-C(30)-S(1)	111.5(7)
N(3)-C(31)-C(32)	124.5(9)
N(3)-C(31)-C(34)	118.8(9)
C(32)-C(31)-C(34)	116.6(8)
C(33)-C(32)-C(31)	130.8(8)
N(4)-C(33)-C(32)	123.9(8)
N(4)-C(33)-C(35)	118.8(8)
C(32)-C(33)-C(35)	117.3(8)
C(41)-C(36)-C(37)	119.9(9)
C(41)-C(36)-N(3)	120.6(8)
C(37)-C(36)-N(3)	119.5(9)
C(38)-C(37)-C(36)	118.3(10)
C(38)-C(37)-C(42)	119.7(9)
C(36)-C(37)-C(42)	121.9(9)
C(39)-C(38)-C(37)	122.5(10)
C(38)-C(39)-C(40)	118.5(10)
C(41)-C(40)-C(39)	121.1(10)
C(40)-C(41)-C(36)	119.6(9)
C(40)-C(41)-C(45)	118.8(9)
C(36)-C(41)-C(45)	121.5(8)
C(44)-C(42)-C(43)	110.2(10)
C(44)-C(42)-C(37)	112.7(9)
C(43)-C(42)-C(37)	111.1(10)
C(46)-C(45)-C(41)	110.9(8)
C(46)-C(45)-C(47)	110.1(9)
C(41)-C(45)-C(47)	112.2(8)
C(53)-C(48)-C(49)	120.2(8)
C(53)-C(48)-N(4)	121.2(7)
C(49)-C(48)-N(4)	118.6(8)
C(50)-C(49)-C(48)	118.3(9)
C(50)-C(49)-C(54)	121.0(9)
C(48)-C(49)-C(54)	120.7(9)
C(49)-C(50)-C(51)	123.1(9)
C(52)-C(51)-C(50)	118.2(9)
C(51)-C(52)-C(53)	122.0(9)
C(48)-C(53)-C(52)	118.3(8)
C(48)-C(53)-C(57)	122.7(8)
C(52)-C(53)-C(57)	118.9(8)

C(49)-C(54)-C(55)	112.6(9)
C(49)-C(54)-C(56)	112.2(9)
C(55)-C(54)-C(56)	110.0(8)
C(53)-C(57)-C(59)	113.1(8)
C(53)-C(57)-C(58)	110.2(8)
C(59)-C(57)-C(58)	110.2(9)
F(6)-C(60)-F(5)	107.8(8)
F(6)-C(60)-F(4)	108.6(7)
F(5)-C(60)-F(4)	106.8(8)
F(6)-C(60)-S(2)	111.6(7)
F(5)-C(60)-S(2)	111.3(6)
F(4)-C(60)-S(2)	110.5(7)
N(5)-C(61)-C(62)	124.7(7)
N(5)-C(61)-C(64)	117.9(8)
C(62)-C(61)-C(64)	117.4(8)
C(61)-C(62)-C(63)	130.9(8)
N(6)-C(63)-C(62)	122.1(9)
N(6)-C(63)-C(65)	121.4(7)
C(62)-C(63)-C(65)	116.4(8)
C(67)-C(66)-C(71)	120.6(8)
C(67)-C(66)-N(5)	119.4(8)
C(71)-C(66)-N(5)	120.0(7)
C(68)-C(67)-C(66)	118.9(9)
C(68)-C(67)-C(72)	119.0(8)
C(66)-C(67)-C(72)	122.1(8)
C(69)-C(68)-C(67)	120.8(10)
C(68)-C(69)-C(70)	120.1(9)
C(71)-C(70)-C(69)	120.7(10)
C(70)-C(71)-C(66)	118.9(9)
C(70)-C(71)-C(75)	119.7(9)
C(66)-C(71)-C(75)	121.3(8)
C(74)-C(72)-C(73)	110.1(9)
C(74)-C(72)-C(67)	112.1(9)
C(73)-C(72)-C(67)	111.5(8)
C(71)-C(75)-C(77)	114.3(8)
C(71)-C(75)-C(76)	110.9(8)
C(77)-C(75)-C(76)	109.3(9)
C(83)-C(78)-C(79)	121.8(7)

C(83)-C(78)-N(6)	120.5(7)
C(79)-C(78)-N(6)	117.7(7)
C(80)-C(79)-C(78)	117.1(7)
C(80)-C(79)-C(84)	120.9(7)
C(78)-C(79)-C(84)	121.9(7)
C(81)-C(80)-C(79)	120.9(7)
C(82)-C(81)-C(80)	121.0(7)
C(81)-C(82)-C(83)	120.5(8)
C(82)-C(83)-C(78)	118.5(7)
C(82)-C(83)-C(87)	118.8(7)
C(78)-C(83)-C(87)	122.6(7)
C(79)-C(84)-C(85)	112.3(7)
C(79)-C(84)-C(86)	112.7(7)
C(85)-C(84)-C(86)	110.5(8)
C(83)-C(87)-C(88)	110.3(7)
C(83)-C(87)-C(89)	113.2(8)
C(88)-C(87)-C(89)	111.2(8)
F(7)-C(90)-F(9)	108.4(10)
F(7)-C(90)-F(8)	108.6(11)
F(9)-C(90)-F(8)	107.5(10)
F(7)-C(90)-S(3)	110.4(8)
F(9)-C(90)-S(3)	111.2(9)
F(8)-C(90)-S(3)	110.6(8)
N(7)-C(91)-C(92)	125.6(8)
N(7)-C(91)-C(94)	118.7(9)
C(92)-C(91)-C(94)	115.7(9)
C(91)-C(92)-C(93)	129.3(9)
N(8)-C(93)-C(92)	124.5(8)
N(8)-C(93)-C(95)	119.0(8)
C(92)-C(93)-C(95)	116.5(8)
C(101)-C(96)-C(97)	121.7(9)
C(101)-C(96)-N(7)	120.3(9)
C(97)-C(96)-N(7)	117.9(8)
C(98)-C(97)-C(96)	118.3(9)
C(98)-C(97)-C(102)	119.8(10)
C(96)-C(97)-C(102)	121.9(10)
C(97)-C(98)-C(99)	121.0(10)
C(100)-C(99)-C(98)	119.6(10)

C(99)-C(100)-C(101)	122.0(10)
C(96)-C(101)-C(100)	117.4(9)
C(96)-C(101)-C(105)	123.3(9)
C(100)-C(101)-C(105)	119.3(8)
C(104)-C(102)-C(103)	111.6(10)
C(104)-C(102)-C(97)	112.3(10)
C(103)-C(102)-C(97)	113.5(10)
C(101)-C(105)-C(107)	111.8(8)
C(101)-C(105)-C(106)	113.1(8)
C(107)-C(105)-C(106)	109.6(8)
C(113)-C(108)-C(109)	120.7(7)
C(113)-C(108)-N(8)	121.6(7)
C(109)-C(108)-N(8)	117.8(8)
C(110)-C(109)-C(108)	117.3(9)
C(110)-C(109)-C(114)	120.4(8)
C(108)-C(109)-C(114)	122.2(7)
C(111)-C(110)-C(109)	122.0(9)
C(110)-C(111)-C(112)	120.1(9)
C(111)-C(112)-C(113)	120.8(10)
C(108)-C(113)-C(112)	119.0(8)
C(108)-C(113)-C(117)	121.6(7)
C(112)-C(113)-C(117)	119.3(9)
C(109)-C(114)-C(115)	113.5(8)
C(109)-C(114)-C(116)	112.8(10)
C(115)-C(114)-C(116)	109.0(8)
C(119)-C(117)-C(118)	111.3(9)
C(119)-C(117)-C(113)	111.9(8)
C(118)-C(117)-C(113)	110.6(8)
F(11)-C(120)-F(10)	107.9(9)
F(11)-C(120)-F(12)	108.2(9)
F(10)-C(120)-F(12)	109.2(9)
F(11)-C(120)-S(4)	111.5(7)
F(10)-C(120)-S(4)	109.5(7)
F(12)-C(120)-S(4)	110.5(7)

Symmetry transformations used to generate equivalent atoms:

' x,y-1,z " x,y+1,z

Appendix 6. References for appendices

1. Jana, A.; Roesky, H. W.; Schulzke, C.; Doring, A.; Back, T.; Pal, A.; Herbst-Irmer, R. *Inorg. Chem.* **2009**, *48*, 193.
2. Maksic, Z. B.; Kovacevic, B. *J. Chem. Soc.-Perkin Trans. 2* **1999**, 2623.
3. Jana, A.; Sarish, S. P.; Roesky, H. W.; Schulzke, C.; Döring, A.; John, M. *Organometallics* **2009**, *28*, 2563.
4. Yao, S.; Brym, M.; Merz, K.; Driess, M. *Organometallics* **2008**, *27*, 3601.
5. Ding, Y. Q.; Roesky, H. W.; Noltemeyer, M.; Schmidt, H. G.; Power, P. P. *Organometallics* **2001**, *20*, 1190.
6. Cordero, B.; Gomez, V.; Platero-Prats, A. E.; Reves, M.; Echeverria, J.; Cremades, E.; Barragan, F.; Alvarez, S. *Dalton. Trans.* **2008**, 2832.
7. Bondi, A. *J. Phys. Chem.* **1964**, *68*, 441.
8. Taylor, M. J.; Saunders, A. J.; Coles, M. P.; Fulton, J. R. *Organometallics* **2011**, *30*, 1334.
9. Breitmaier, E., *Structure Elucidation by NMR in Organic Chemistry: A Practical Guide*. John Wiley & Sons, Ltd.: West Sussex, England, 2002.
10. Ahmed, A.; Bragg, R. A.; Clayden, J.; Lai, L. W.; McCarthy, C.; Pink, J. H.; Westlund, N.; Yasin, S. A. *Tetrahedron* **1998**, *54*, 13277.